Trinity College Dublin
Coláiste na Tríonóide, Baile Átha Cliath
The University of Dublin

Claudin-5 expression at the Blood Brain Barrier and its therapeutic potential in neurological disease

A thesis submitted to the University of Dublin for the Degree of Doctor of Philosophy

by

Claire O'Connor

2023

Under the supervision of Prof. Matthew Campbell

Smurfit Institute of Genetics

Trinity College Dublin

Declaration

I declare that this thesis has not been submitted as an exercise for a degree at this or any other university and it is entirely my own work.

The work of the below individuals has been included in this research and is duly acknowledged in the text wherever included:

Dr. Chris Greene, Campbell lab, contributed to the physical characterisation of the *Cldn5*$^{fl/wt}$*xTie2Cre* model and carried out the IP injections for the KA model experiments.

Laurence Dion-Albert, Ménard lab, performed animal experiments including stereotaxic surgeries for the CSDS model.

I agree to deposit this thesis in the University's open access institutional repository or allow the library to do so on my behalf, subject to Irish Copyright Legislation and Trinity College Library conditions of use and acknowledgement.

I consent to the examiner retaining a copy of the thesis beyond the examining period, should they so wish (EU GDPR May 2018).

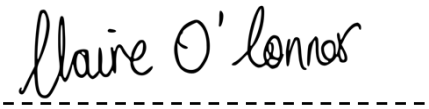

Claire O'Connor

Summary

Breakdown of the blood brain barrier's (BBB) integrity is a hallmark pathology in numerous neurological disorders. However, while research and therapeutic development has mostly focussed on neuronal function, the high prevalence of refractive cases noted for many neurological disorders has made it clear that other therapeutic targets should be explored. Therefore more recently, a greater focus has been put on BBB disruption as a cause or exacerbator of disease pathology and thus is being re-evaluated as a potential novel mechanism of action for therapeutic development. This dynamic barrier acts as a first line of defence. It is essential for the maintenance of the neuronal microenvironment, regulating ion and nutrient exchange between blood and brain, while simultaneously protecting the neural tissue from potentially damaging blood-borne components. Therefore restoration of BBB integrity provides a new pathway for innovative treatment design. While the BBB is a complex and dynamic structure with many synergistic components, to utilise a gene therapy-based approach to restore barrier function, a singular component is required that could effectively re-establish barrier integrity. Claudin-5, is the most highly expressed tight junction (TJ) protein of the BBB, which through knockout (KO) studies has shown a size selective loosening of the barrier and results in post-natal death (Nitta et al., 2003). These findings highlight claudin-5's essential role in the maintenance of BBB integrity. Interestingly, decreased levels of claudin-5 expression have been noted in either post mortem or surgically resected tissue from patients with major depressive disorder, schizophrenia or epilepsy (Greene et al., 2020; 2022). Therefore, claudin-5 shows promising potential as a therapeutic target. Thus, the overarching aims of this research is firstly, to further characterise claudin-5's relationship with BBB function and the underlying pathophysiology and endophenotypes that result from BBB disruption. Secondly, to develop a new gene therapy-based approach utilising claudin-5 overexpression to treat disorders with noted BBB disruption.

As the KO model results in a post-natal lethal phenotype, its use to further elucidate the underlying pathophysiology and endophenotypes as they would relate to neurological disease is limited. Therefore in Chapter 3, a claudin-5 heterozygote model was established, utilising the Tie2Cre system to ensure that claudin-5 expression was lost specifically in the endothelial cells (ECs) of the mice. The 50 % loss of claudin-5, resulted in a discontinuous pattern of claudin-5 expression in the vessels. While it did not cause significantly increased

permeability into the brain parenchyma, astrocytic gliosis was noted in the claudin-5 heterozygote cohort in comparison to the controls. Moreover, distinct deficits in learning and memory function, cognitive impairment and sensorimotor gating issues were noted in the claudin-5 heterozygote mice. To our knowledge, this is the first ever behavioural characterisation of a claudin-5 heterozygous mouse model.

The work described in Chapter 4, established a gene therapy-based approach to re-establish BBB integrity through the overexpression of claudin-5 specifically in ECs. Numerous optimisation strategies were examined and screened *in vitro*. At the plasmid level, strategies such as codon optimisation and promotor choice were utilised, while at the vector level different adeno-associated virus (AAV) serotypes were compared. It was determined that an AAV-9 viral vector containing a plasmid expressing native mouse claudin-5 under the control of an *Icam2* promoter was the most efficacious. It was shown *in vivo* to significantly overexpress claudin-5 through western blot (WB), reverse transcription polymerase chain reaction (RT-PCR) and immunohistochemistry (IHC). Moreover in healthy C57BL/6J mice, claudin-5 overexpression through AAV delivery was shown not to have any detrimental effect on normal animal behaviour.

Finally in Chapter 5, the therapeutic potential of this newly developed BBB restoring AAV was examined in four different mouse models. These four models were broken into two etiological cohorts. Firstly the *Cldn5*$^{fl/wt}$*xTie2Cre* model and the inducible claudin-5 knockdown (KD) model, act as a proof of concept, as all pathology noted in these models is directly associated with reduced claudin-5 expression. In these models, when the therapeutic AAV was administered into the hippocampus, it significantly improved learning and memory deficits, the aberrant grooming behaviour and rescued sensorimotor gating deficits. Moreover, for the inducible KD model, the survival time was also increased in the cohort treated with the therapeutic AAV. Overall these findings support the hypothesis that restoring claudin-5 expression at the barrier can restore function even when a distinct disease phenotype has developed. The second cohort, the chronic social defeat stress (CSDS) model and the kainic acid (KA) mouse model, are established models of disease, with complex etiology, induced by significant environmental stress or chemoconvulsant injury and thus are likely to be more predictive to the treatment efficacy in patients. However, in the CSDS model, no significant rescue effect was noted in susceptible mice following therapeutic AAV administration. In the KA model of epilepsy, those treated with

the therapeutic AAV had a lower cumulative seizure score and a longer latency to seizure onset compared to the control treated mice however across both treatment groups the seizure severity was similar. Acute central nervous system (CNS) inflammation was noted through IHC analysis of the astrocyte marker GFAP in the AAV treated controls. Overall it appears that claudin-5 overexpression may be a beneficial adjunct therapy in the treatment of complex neurological disorders.

Acknowledgements

To my supervisor Prof. Matthew Campbell, thank you for the opportunity to carry out this PhD.
Your support, encouragement and guidance over the last four years has helped me achieve more than I ever thought I could, and I will forever be grateful for the experience I have gained under your supervision.

To all the members of the Campbell lab, it has been a pleasure to work alongside so many brilliant people for the past four years. To Dr Chris Greene, thank you for sharing your knowledge and skills, for teaching me to do stereotaxic injections and the behavioural assays. To Dr Natalie Hudson and Dr Conor Delaney, thank you for keeping the lab running, for all the genotyping and ordering, for teaching and supporting me and most importantly for helping me with any, and every mouse emergency! To Dr Nicole Hanley, Avril Reddy, Kieva Byrne, and Jeff Henderson, it has been a pleasure to be PhD students together. You have all been a great source of support, advice and distraction, and the lab has been a wonderful place to work thanks to you all.

I would like to also thank the technical and administrative staff, Brenda, Philip, David and Rachel and CMU staff, particularly Ciaran, Charlie, Aoife and Monica for all their help over the course of my research in the genetics department.

To my wonderful friends, who have been ears to listen, shoulders to cry on and the most wonderful excuse to get out of the lab occasionally!! Thank you all for your support and understanding as well as all the laughs we have had along the way. I would like to particularly thank Cliodhna Congdon, Kate Horgan and Aoibhinn Dowdall who have gone above and beyond time and time again for me, especially when the PhD process was not smooth sailing.

To my Auntie Joan and my late Uncle Davy, who have always taken such an interest in everything I do, championed my success, and believed in me even when I didn’t. Thank you does not begin to cover it.

To Andy Hemeryck, who has been with me for the long haul, thank you for your patience, support, and encouragement… all while still not being totally sure of what I do beyond “claudin-5”! I love you.

To my Mum, Dad, and my sister Catherine, without whom, there would truly be no thesis to write acknowledgements for! Thank you seems too small an expression to acknowledge all you have done for me, for the love and support, not only in these last four years but for my whole life. I am so lucky to have you, I love you so much and I could not have done this without you.

Table of Contents

Figures:

Tables:

Abbreviations

AAV	Adeno-associated viral vector
ABC	ATP-binding cassette
AD	Alzheimer's disease
AGG	Aggressor
AJs	Adherens junctions
ALS	Amyotrophic lateral sclerosis
Amg	Amygdala
ANOVA	Analysis of variance
APS	Ammonium persulfate
AQP4	Aquaporin 4
AS	Audiogenic seizures
ASD	Anti-seizure drugs
BAs	Brodmann areas
BBB	Blood-brain barrier
BCA	Bicinchoninic acid
BCSFB	Blood-cerebrospinal fluid barrier
bEnd.3	Brain endothelial cell line (Mouse)
bTJ	Bicellular tight junction
BSA	Bovine serum albumin
CD31	Cluster of differentiation 31
Cldn5	Claudin-5
CMV	Cytomegalovirus
CNS	Central nervous system
CO	Codon optimised
CO_2	Carbon dioxide
COGs	Cost of goods
CSDS	Chronic social defeat stress model
CSF	Cerebrospinal fluid
CT	Cycle threshold
Da	Dalton
DAPI	4', 6-diamidino-2-phenylindole
dB	Decibel
DCE-MRI	Dynamic Contrast-Enhanced Magnetic Resonance Imaging
DH	Dorsal hippocampus

DISC1	*Disrupted-in-schizophrenia 1* gene
DMEM	Dulbecco's modified Eagle medium
DNA	Deoxyribonucleic acid
Dox	Doxycycline
EC	Endothelial cell
ECL	Extracellular loops
EDTA	Ethylenediaminetetraacetic acid
EEG	Electroencephalogram
EPM	Elevated plus maze
ELISA	Enzyme-linked immunosorbent assay
EV	Empty vector
FBS	Foetal bovine serum
FPI	Fluid percussion injury
FST	Forced swim test
Gd-DTPA	Gadolinium contrast agent
GFP	Green fluorescent protein
GLUT-1	Glucose transporter-1
GLUT-1 DS	GLUT-1 deficiency syndrome
GMP	Good Manufacturing Practices
GPCR	G-protein-coupled receptor
Hh	Hedgehog
HRP	Horseradish peroxidase
ICAM	Intercellular adhesion molecule
IF	Interstitial fluid
IHC	Immunohistochemistry
IH	Intrahippocampal
IP	Intraperitoneal
IV	Intravenous
KA	Kainic acid
KD	Knockdown
kDa	Kilodalton
KO	Knockout
Il-1β	Interlukin-1β
ISI	Intersession interval
ITR	Inverted terminal repeats
JAM	Junctional adhesion molecules

LB	Lysogeny broth
lPFC	Lateral prefrontal cortex
LPLD	Lipoprotein lipase deficiency
LSR	Lipolysis-stimulated lipoprotein receptor
MDD	Major depressive disorder
mPFC	Medial prefrontal cortex
MRI	Magnetic resonance imaging
MS	Multiple sclerosis
MSNs	Medium-sized spiny neurons
MW	Molecular weight
N	Native
NAbs	Neutralising antibodies
NAc	Nucleus accumbens
NAcc	Nucleus accumbens core
NAcs	Nucleus accumbens shell
NGS	Normal goat serum
NOR	Novel object recognition test
nfH_2O	nuclease free H_2O
NMDA	N-methyl-D-aspartate
NVU	Neurovascular unit
OCT	Optimal cutting temperature
OFT	Open field test
ORF	Open reading frame
P-gp	P-glycoprotein
PBS	Phosphate buffered saline
PCP	Phencyclidine
PCR	Polymerase chain reaction
PDGF	Platelet-derived growth factor
PDGFb	Platelet-derived growth factor-b
PFA	Paraformaldehyde
PVDF	Polyvinylidene difluoride
PFC	Prefrontal cortex
polyA	Polyadenylation
PPI	Pre-pulse inhibition
Ptch	Patched
PTE	Posttraumatic epilepsy

rAAV	Recombinant AAV
RAM	Radial arm maze
RES	Resilient
RNA	Ribonucleic acid
RPM	Revolutions per minute
RT	Room Temperature
RT-PCR	Reverse transcription polymerase chain reaction
rtTA	Reverse tetracycline controlled transactivator
SD	Standard deviation
SDS	Sodium dodecyl sulphate
SDS-PAGE	Sodium Dodecyl Sulphate Polyacrylamide Gel Electrophoresis
SEM	Standard Error of the mean
Shh	Sonic hedgehog
SI	Social interaction
SMA	Spinal muscular atrophy
Smo	Smoothened
SNP	Single nucleotide polymorphism
SS	stress-susceptible
TBI	Traumatic brain injury
TBS	Tris buffered saline
TBST	Tris buffered saline+Tween
TEMED	N, N, N', N'-tetramethyl ethylenediamine
TEER	Transendothelial electrical resistance
Tet	Tetracycline
TJs	Tight junctions
TLE	Temporal lobe epilepsy
TMB	Tetramethylbenzidine
TNF	Tumour necrosis factor
TRE	Tetracycline response element
tTJ	Tricellular tight junction
Wt	Wildtype
ZO	Zonula occludens
VCAM	Vascular cell adhesion molecule
VEGF	Vascular endothelial growth factor
VG	Viral genomes
VH	Ventral hippocampus

WAG/Rij	Wistar Albino Glaxo/Rijswijk rat
WB	Western Blot
22q11DS	22q11.2 deletion syndrome

Chapter 1. Introduction

1.1 The Neurovascular Unit and the Blood Brain Barrier

The central nervous system (CNS) which is comprised of both brain and spinal cord, controls vital processes such as cognition and the coordination of peripheral organ function. The principle component of the CNS is the neuron, a terminally differentiated, electrically excitable cell. For reliable neural signalling, through both chemical and electrical signals, the ionic microenvironment surrounding synapses must be maintained. The brain is one of the most energy demanding organs of the body, while accounting for only 2 % of bodily mass, it expends approximately 20 % of the body's energy production (Raichle and Gusnard, 2002). These significant metabolic and energy demands must be met while in turn protecting the brain from substances that may result in uncontrolled activation of inflammatory or neuronal responses in order to maintain the integrity of the delicate brain network. Due to the lack of adult neurogenesis to facilitate the replacement of damaged tissue, the brain is highly sensitive to damage, both from physical insult as well as to the passage of harmful blood-borne molecules.

Therefore there are three specialised multicellular barriers to form an interface between the blood and neural tissue with critical roles in maintaining CNS homeostasis. Firstly, the arachnoid barrier of the meninges, formed from the arachnoid epithelium at the interface between the blood and subarachnoid cerebrospinal fluid (CSF). Next the blood-cerebrospinal fluid barrier (BCSFB) of the choroid plexus, which is composed of the choroid plexus epithelium interfacing the blood and the ventricular CSF. Finally, the blood-brain barrier (BBB) which is made up of the cerebrovascular endothelial cells between blood and brain interstitial fluid (Abbott et al., 2004).

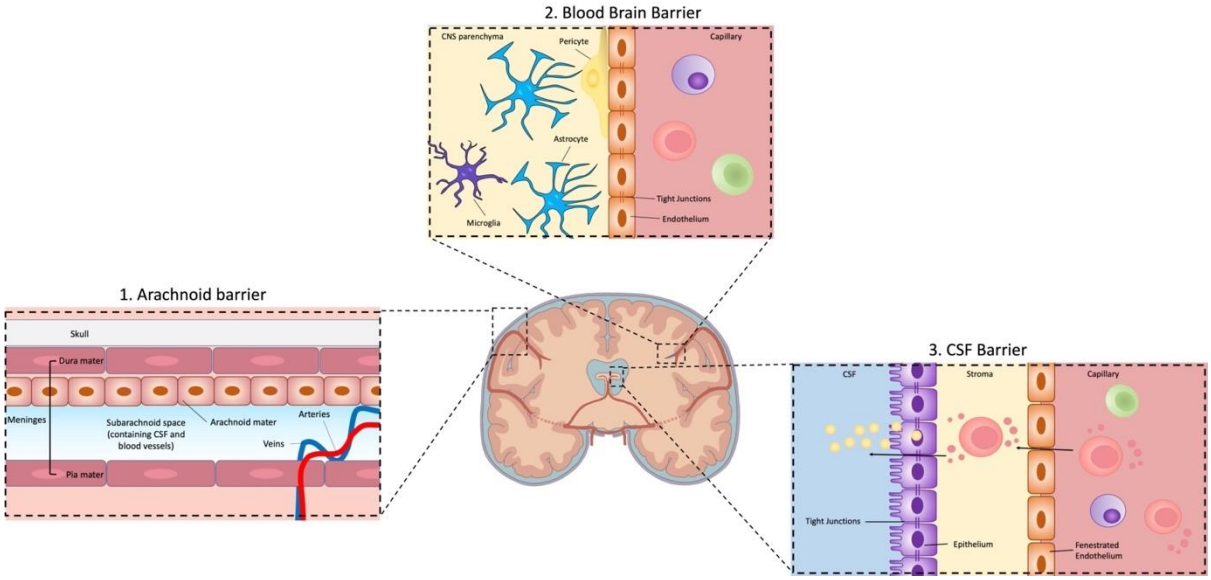

Figure.1.1 Barriers of the CNS

The three main specialised barriers of the central nervous system. (1) The arachnoid barrier, composed of the epithelium of the arachnoid layer of the meninges that encases the whole brain. (2) The blood-brain barrier, comprised of endothelial cells of the vasculature and whose properties are maintained by various cells of the NVU (3) The epithelial blood-CSF barrier (BCSFB) of the choroid plexus.

The arachnoid epithelium is an avascular membrane that underlies the dura and completely encloses the CNS (Abbott et al., 2010). Located below the cranium, this barrier separates the meningeal dura mater from the pia mater (Decimo et al., 2012) (Fig. 1.1.1). It is a multi-layered epithelium with tight junctions (TJs) between cells of the inner layer that form an effective seal. While the exact molecular composition of arachnoid TJs are still under investigation, claudin-11 has been noted in both rat and human brain (Brøchner et al., 2015; Anders and Goss., 1989). While the arachnoid epithelium does form the first of three barrier layers, its small surface area and avascular nature result in it having limited ability as a protective barrier and doesn't represent a significant surface for exchange between the peripheral blood and the brain (Kandel et al., 2000; Abbott et al., 2006)

The second barrier, is the BCSFB which is formed by epithelial cells of the choroid plexus (Abbott et al., 2006)(Fig. 1.1.3). The choroid plexus epithelium is located in the ventricles of the brain and is a highly vascularised tissue, which secretes CSF which fills the cerebral and spinal subarachnoid spaces. The CSF circulating the brain is also in contact with the previously mentioned arachnoid barrier of the meninges. CSF functions as a buffer, a means

of physical protection for both the brain and spinal cord against physical injury. Additionally, it helps to regulate cerebral blood flow, the homeostasis of the CNS microenvironment and molecular exchange with the brain. The vasculature of the choroid plexus is fenestrated, and so doesn't exhibit the same restricted paracellular transport that will be described later in the third and final barrier within the brain parenchyma (Zagórska-Świezy et al., 2008). However, the epithelial cells of the choroid plexus are polarised and express adherens junctions (AJs) basolaterally and TJs apically, together forming the BCSFB which prevents the entry of many harmful substances into the CSF (Hurley et al., 1981; Christensen et al., 2013).

Both the arachnoid barrier and the BCSFB act as secondary barriers, protecting the brain from peripheral circulating molecules, however, within the brain parenchyma itself, it is the vasculature that is specialised to form the most vital protective barrier. The BBB, the third and final barrier, is positioned along the blood vessels of the CNS. It is a highly selective and tightly regulated barrier, which reflects the brain's vital roles in cognitive function, in maintaining homeostasis and the strict coordination of peripheral organ function.

The BBB is important in controlling the exchange of ions and nutrients between the blood and brain and to protect neural tissue from potentially damaging blood-borne agents such as pathogens, immune cells and anaphylatoxins (Abbott et al., 2010). Moreover, to maintain the optimal ionic environment for neural function, the endothelium of the brain secretes approximately 200 ml of interstitial fluid per day (Hladky and Barrand, 2016). The human cerebral microvasculature has a combined surface area of 150-200 cm^2 /g of tissue, which would relate to approximately 15-20 m^2 per adult brain. This results in a dense mesh-like network of vessels that supply blood flow to all brain regions (Abbott et al., 2006). The vast extent of the vasculature is reflected in the close proximity noted between neurons and capillaries, a distance that never exceeds ~25 μm (Schlageter et al., 1999).

To regulate the flow of ions and solutes, while ensuring systemic influences do not disrupt optimum neuronal function, the BBB has developed a specialised vasculature. Lining the blood vessels of the CNS are endothelial cells (EC) which are the principal component of the BBB (Luissint et al.,2012), and separate the peripheral blood from the brain parenchyma. As such, ECs of the CNS have developed numerous specialisations, which make them distinct from the ECs of the periphery in a number of ways (Fig. 1.2)

The presence of specialised transport systems, which include the ABC (ATP-binding cassette) transporter family as well as BBB-specific transport proteins located on the luminal and/or abluminal membranes, control the influx and efflux of molecules across the barrier (Abbott et al., 2010). In addition to these transcellular transport systems, two other specialisations limit transcellular transport in the ECs of the CNS. Firstly, the absence of fenestrae, which are pores that allow rapid exchange of molecules between blood and tissue are noted. Secondly the low rate of absorptive transcytosis, which prevents transport of large hydrophilic molecules to the CNS are also noted in these cells. These together result in very limited transcellular transport (Saunders et al., 2012, Abbott et al., 2010; Obermeier et al.,2013). Paracellular transport, which is the flow of material between adjacent ECs, is restricted due to the enriched presence of TJs which create high electrical resistance between ECs (Keaney and Campbell., 2015). TJ particles of the CNS ECs associate with the protoplasmic membrane leaflets (P-face), whereas in the peripheral ECs, TJ strands associate with the extracellular fraction face (E-face) of the membrane bilayer (Liebner et al., 2000). The association with respective faces demonstrates the degree of barrier permeability and resistance (Lippoldt et al., 2000). Finally there is a significantly increased number of mitochondria in cerebrovascular ECs in comparison to ECs in muscle tissue, and therefore helps to facilitate higher energy expenditure (Oldendorf and Brown., 1975).

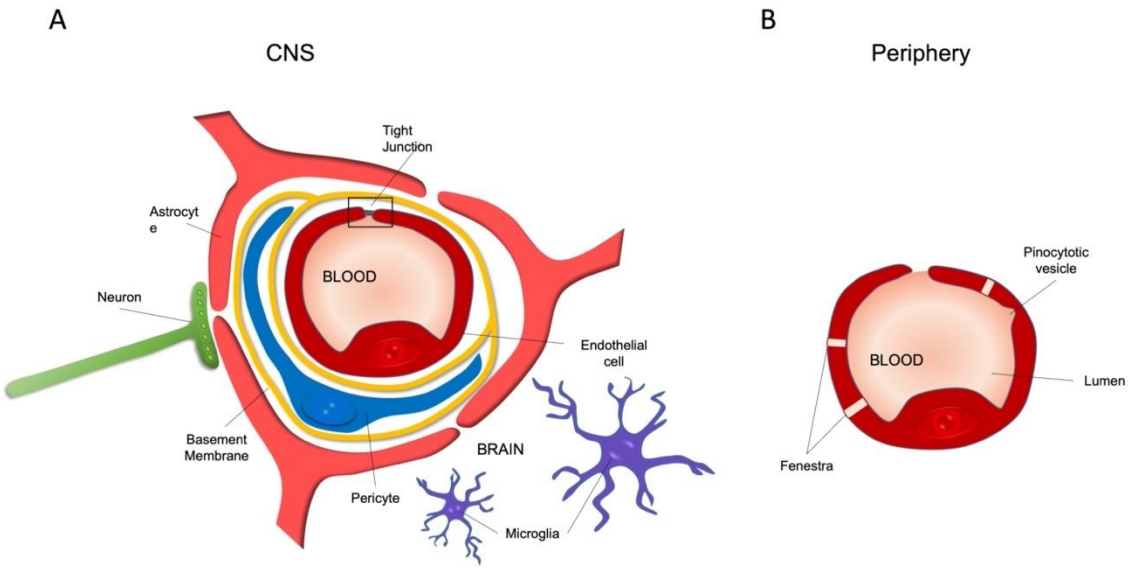

Figure 1.2 ECs of the CNS versus peripheral ECs

(A) ECs of the cerebrovasculature are encased by basement membrane, pericytes and astrocytes, which together through cooperative bidirectionally signalling maintain the BBB integrity. Movement of material from blood to brain and vice versa is restricted due to the presence of TJs

between ECs. (B) The ECs that comprise the peripheral vasculature do not have the same multicellular interactions. There is also an absence of TJs between ECs while there is an increased number of pinocytotic vesicles and fenestra which allows for the rapid exchange between blood and peripheral tissues.

The existence of a physical barrier between the CNS and the peripheral circulatory system was first identified through tracer dye-injection experiments by Paul Ehrlich and Edwin Goldmann. These seminal staining experiments noted a clear compartmentalisation of the blood and brain, with the water-soluble dyes injected into the vasculature resulting in all organs except the CNS being stained. The term "Blut-Hirnschranke" or blood brain barrier is often attributed to Lewandowsky's 1900 publication, however while essentially describing that the capillaries of the cerebrovascular did have specific restrictive properties to some compounds, the paper did not actually use the term itself (Lewandowsky., 1900). It wasn't until approximately 1918, that the term barrier was first used by Stern and finally in 1921 the full term blood–brain barrier (barrière hématoencéphalique) was coined (Stern and Gautier, 1918 ; Stern and Gautier, 1921). While it appears that very little credit was given for this work, this term has stood the test of time despite some potential confusion regarding the dynamics of this system and the mistaken assumption that it formed an absolute impediment in entry to the brain (Liddelow et al., 2011; Saunders et al., 2014)

The most seminal and cited papers in the discovery and characterisation of the BBB, are by Ehrlich's student Edwin Goldmann. In his investigation he compared the circulation of the dye trypan blue (960 Da) following either intravenous or intrathecal administration. He noted that dye injected intravenously did not stain the brain while in contrast, dye injected into the subarachnoid space, into the CSF through intrathecal administration resulted in strong staining of all nervous tissue (Goldmann (1909, 1913) reviewed by Liddelow., 2011; Saunders et al., 2014).

Further characterisation of the BBB went on to investigate a size-selective permeability of the BBB. While Ehrlich had noted several dyes injected intravenously could stain the CNS, it wasn't until the development of electron microscopy, that the size selective nature of the BBB could be accurately visualised and resolved. Through electron microscopy it was shown that in the capillaries of the cerebral cortex of mice, horseradish peroxidase (HRP) (40 kDa) administered intravenously, could reach up to, but not beyond the first TJ between adjacent ECs. This was repeated using smaller compounds, such as microperoxidase (1900

Da) and lanthanum (139 Da) (Brightman and Reese, 1969; Feder, 1971). While the physical barrier function of the BBB, provided by TJs, is the main obstacle to overcome, two other barriers exist to aid in the tightly regulated nature of this interface. Firstly, due to the limited permeability of the BBB, there is thus an increased dependence on active transport, which allows the BBB to regulate molecular traffic further through luminal or abluminal transport protein localisation (Hoshi et al., 2013; Liu et al., 2014). For example, the increased luminal expression of transendothelial glucose transporter, GLUT-1, allows for high glucose influx, that is necessary for cognitive function (Maher et al., 1994). Finally, a metabolic barrier is the last characteristic of this dynamic interface, through enriched abluminal efflux proteins, such as P-glycoprotein (P-gp), endogenous and exogenous toxins are removed or excluded from the brain parenchyma (Cecchelli et al., 2007).

Therefore, the third barrier that protects the CNS, the BBB, does so through a combination of physical, transport and metabolic barriers. Overall the CNS requires the specialised vasculature of the BBB, which regulates the flow of ions and solutes, while ensuring systemic influences do not disrupt optimum neuronal function. It is a dynamic barrier that can be modulated and regulated, in both physiology and pathology (Abbott et al., 2006)

1.2 The Neurovascular Unit:

Despite the unique nature of the morphology and functionality of the cerebral ECs, it has been shown through the famous quail-chick transplantation experiments that the properties of the BBB are not intrinsic (Stewart and Wiley.,1981). It is in fact the interactions between developing vascular tissue and the other components that make up what is known as the neurovascular unit (NVU), that are critical in the development of the BBB (Stewart and Wiley.,1981). Thus, the BBB cannot function independently, but instead requires complex co- operative interactions with the other cells of the NVU, both during development and in its maintenance**.** These interactions include both contact between the cell types as well as secreted soluble factors.

These other cell types that constitute the NVU are pericytes, astrocytes, microglia, neurons and interneurons as well as the non-cellular basement membrane as seen in Figure 1.3.

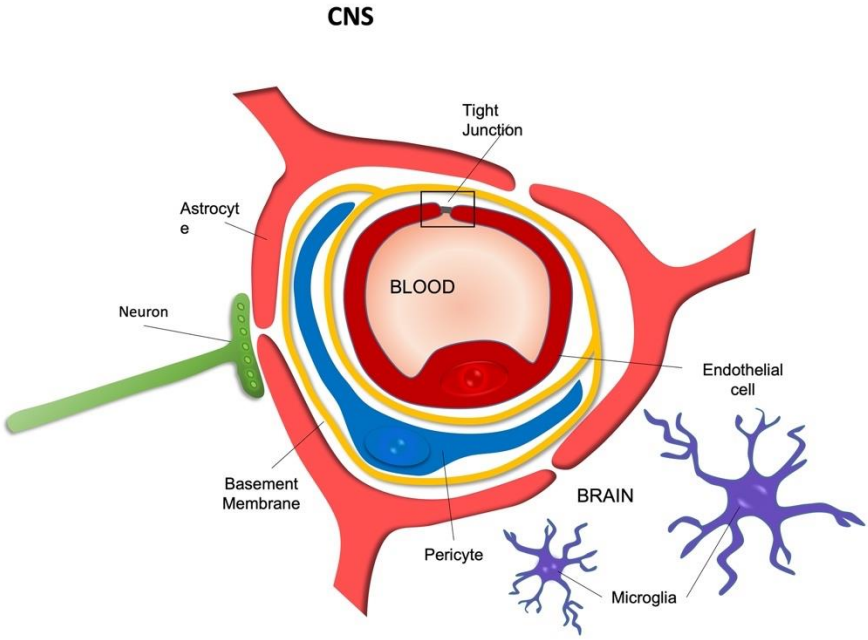

Figure 1.3 The neurovascular unit (NVU)

Complex network including endothelial cells, pericytes, astrocytes, microglia, interneurons and neurons, a complex composition of cell types that closely interact to form the NVU.

1.2.1 Endothelial cells:

As stated previously, the EC of the cerebrovascular have numerous specialisations, which limit both the transcellular and paracellular movement of material from blood to brain and vice versa. However as just discussed, these specialisations are not intrinsic, but rather a product of the overall CNS microenvironment, as was shown in the seminal work by Stewart and Wiley in 1981. As mentioned, paracellular transport is significantly limited due to the presence of TJs, which create the characteristically high transendothelial electrical resistance (TEER) between ECs and functions as a physical barrier. TEER values in peripheral capillaries are usually around 2-20 $\Omega \cdot cm^2$, however pure cultures of CNS ECs have noted TEER values up to 1800 $\Omega \cdot cm^2$ which can be enhanced further when co-cultured with other cells of the NVU, such as astrocytes and/or pericytes (Srinivasan et al., 2015). These junctional complexes are an essential feature of ECs of the CNS and will be discussed in detail in Section 1.3.

ECs are assembled into capillary tubes, with mature ECs of the CNS surrounded basolaterally by the basement membrane, a non-cellular matrix, which forms a continuous sleeve around the capillary. The basement membrane is composed of a heterogenous mix of proteins, with the key components including laminin, type IV collagen, perlecan and fibronectin, and which overall forms a layer that is between 20 and 200nm thick (LeBleu et al., 2007).

The basement membrane embeds the associated pericyte processes and obtains instructions from surrounding astrocyte end-feet. It has been shown through a conditional knockout mouse, that had a pericyte-specific deletion of laminin, that a small subset (10.7 %) of these mice had hydrocephalus, BBB breakdown as well as a loss of aquaporin 4 (AQP4) (Gautam et al., 2016). Currently, *in vitro* culture protocols for cerebrovascular EC types include the use of basement membrane components such as collagen IV or fibronectin. Overall, the basement membrane is necessary for vessel stability as well as supporting barrier function through the regulation of crosstalk between the cells of the NVU (Hallmann et al., 2005; Obermeier et al., 2013).

1.2.2 Pericytes:

Due to the close spatial relationship between the cell types of the NVU, it was difficult to determine the role each cell type plays in the development and maintenance of the BBB. However when the timing of the development of a functional BBB was analysed, through both the levels of protein expression that are specific to the BBB, such as TJ proteins and Glut-1, in addition to an examination of barrier function through the perfusion of tracer molecules, it was determined that the BBB forms during embryogenesis (Daneman et al., 2010). While astrocytes develop during the first postnatal week, pericyte recruitment to the nascent vessels occurs during embryogenesis. Therefore there is a clear temporal correlation between pericytes and the development of the BBB. Platelet-derived growth factor-b (PDGFb) receptor signalling is required for the accumulation of pericytes during angiogenesis. Null mutants (PDGFRb-/-) show increased BBB permeability and result in embryonic lethality, highlighting the importance of pericytes in the development and function of the BBB. Pericyte coverage is significantly higher in the cerebral vasculature in contrast to the periphery, with the extent of pericyte coverage showing a direct correlation with BBB permeability, the regions with the highest pericyte coverage showing the lowest permeability and vice versa (Armulik et al., 2010, Bell et al., 2010). While co-culturing EC

with pericytes has proven to enhance *in vitro* modelling of the BBB, with a significant decrease in permeability to tracer molecules, it was shown that treatment with either a transforming growth factor (TGF)-beta1 antibody or a TGF-beta type I receptor antagonist resulted in the loss of this enhanced BBB function. This finding indicates that pericytes support the development and maintenance of the BBB through TGF-beta signalling (Dohgu et al., 2005).

1.2.3 Astrocytes

Astrocytes are specialised glial cells. Glial cells have been noted as far back as the 19th century, by leading neuroscientists such as Rudolf Virchow, Santiago Ramón y Cajal and Pío del Río-Hortega (Jäkel and Dimou., 2017). During this period, the role of glial cells was thought to be as a glue, holding nerve tissue together. This idea is further reflected by its name, with glial cells being derived from the ancient Greek word for "glia" which translates to "glue" highlighting the idea that these were a glue-like cell. However, current research has shown that glial cells function expands to much more important roles than just as an adhesive within the brain. Firstly, glial cells constitute a significant cellular fraction of the brain, which can vary from 33-66 % of the total brain mass depending on the mammalian species in question (Azevedo et al., 2009; Herculano-Houzel, 2014). Of this, astrocytes are the most abundant fraction of glial cells in the adult brain (Kettenmann and Ransom, 2005).

Examination of the functional role of astrocytes has noted this glial cell type's broad utility in numerous aspects of brain physiology. Polarized astrocytic end-feet envelop the abluminal surface of cerebral ECs, covering more than 90 % of cerebral capillary surface area (Neuhaus, J., 1990; Abbott et al., 2006). These interactions between astrocytes and ECs of the cerebral vasculature are essential to regulate neurotransmitter levels as well as brain water volume and ion concentrations in order to maintain homeostasis of the neural microenvironment (Abbott et al., 2006). The most abundant water channel protein, aquaporin 4 (AQP4), is predominantly expressed in the astrocytic end-feet that encase the cerebral vessels. Additionally the ATP-sensitive potassium channel Kir4.1 and the gap junction protein connexin are highly enriched in these end-feet. Together these end-feet function as dynamic sites that control both water and ion flow (Abbott et al., 2006; Alvarez et al., 2013; Boulay et al., 2017) .

Interestingly, despite its important role in BBB function, for nearly the entire duration of embryonic BBB development, astrocytes are absent, appearing only at embryonic day 19 in mice. Astrocytes, while not required to induce the formation of BBB, have been shown to still be essential in its maturation and maintenance. Early studies have shown that astrocytes have an inductive influence, with their implantation in non-neural EC resulting in the expression of BBB properties (Janzer and Raff., 1987). Differences noted in the phenotype of various BBB transporters at different developmental stages, from embryonic to adult, suggests a gradual maturation of the BBB transporters (Braun et al., 1980). While brain EC lines retain many aspects of a BBB phenotype, this phenotype is typically reduced with more permeable TJs and a downregulation of transport systems (Krämer et al. 2001). These properties can however be upregulated by co-culture with glial cells, both up-regulation of TJ proteins and permeability (Dehouck et al. 1990; Rubin et al. 1991; Rist et al. 1997; Sobue et al. 1999) as well as the up- regulation of Glut-1 and P-gp transport systems (El Hafny et al. 1997; Bauer & Bauer, 2000).

Therefore, there is a common school of thought that astrocytes express numerous ligands that are suggested to be involved in BBB maintenance rather than development. Sonic hedgehog (Shh) is one such secretory factor which is primarily produced by astrocytes. Through its interactions with the Hedgehog (Hh) pathway, which involves the Shh ligand binding to Patched (Ptch), a cell surface receptor, which then allows for the G-coupled protein receptor Smoothened (Smo) to activate further downstream transcriptional changes, Shh has been shown to promote BBB maturation through the regulation of junctional proteins (Alvarez et al., 2011). Shh knockout mice have blood vessel of a normal density and number, however they have reduced TJ protein levels and are embryonically lethal (Alvarez et al., 2011). Moreover, mice with a conditional endothelial cell specific Smo deletion were shown to have poorer astrocyte recruitment in later developmental stages, as well as reduced TJ expression and reduced BBB integrity (Delaney and Campbell., 2017).

CNS ECs are also regulated by other astrocyte secreted factors such as Wnt. Astrocytes are one of the main sources of the Wnt ligand, which binds to Frizzled/LRP-5/6 receptor complexes on ECs to stabilise and activate cytosolic β-catenin (Hermann and ElAli, 2012; Zhou et al., 2014). The Wnt/ β-catenin signalling pathway has been shown to be fundamental to the vascularisation of the CNS as well as the formation and maturation of the BBB, as well as being essential in maintaining the integrity of the BBB in the adult brain

(Daneman et al., 2009; Liebner et al., 2008; Stenman et al., 2008; Wang et al., 2012). Through *in vivo* investigations, mice with Wnt7a, Wnt7b, or β-catenin targeted mutations, all supported the hypothesis that the Wnt signalling pathway is essential for both the formation and maintenance of the BBB. It was shown independently that without expression of these components, developing ECs are unable to adequately invade the embryonic CNS and lack the characteristic protein profile of a functioning BBB (Liebner et al., 2008; Stenman et al., 2008; Daneman et al., 2009). Moreover, the gain or loss of expression of Frizzled 4 resulted in a direct correlation in the gain or loss of BBB function, again supporting the idea that Wnt/ β-catenin pathway, which includes Frizzled is essential for barrier maintenance (Wang et al., 2012)

Astrocyte-derived trophic factors, such as vascular endothelial growth factor (VEGF), glial-derived neurotrophic factor and angiopoitein-1 all support the polarisation of ECs and aid in BBB maturation and maintenance (Abbott et al., 2006). Taken together, this data suggests that astrocytes play a key role in the maintenance of mature cerebrovascular integrity.

1.2.4 Microglia

The CNS had for a long time been considered immune privileged. While the CNS does have an immunological capacity that differs from most peripheral tissues, more recent evidence has shown it is capable, when necessary, of producing a powerful immune reaction. This response is dependent mostly on the resident immune cell of the CNS, the microglia. Microglia are, like astrocytes, another glia cell type, that in simple terms are the tissue-resident macrophages of the CNS, being both an immunocompetent and a phagocytic cell type.

Although microglia are a glial cell of the brain, they, unlike the other glial cell population, do not originate from ectodermal tissue. Instead they are derived from haematopoietic precursor cells that migrate from the embryonic yolk sac into the CNS parenchyma prior to vasuclogenesis (Alliot et al., 1999; Ginhoux et al., 2010).

As microgliogenesis and neurogenesis take place simultaneously in the developing CNS, it would indicate that some co-operative interaction is likely. The general migration of microglia into the parenchyma precedes EC sprouting, but as the microvasculature develops, there is a tight physical association between these vessels and the microglia,

indicating this interaction may be a possible mechanism in the formation of the BBB. The current model for neo-angiogenesis, is that vessel endothelium specialise into tip and stalk cells which supports the vascular networks expansion by a sprouting growth method. The tip cells extend filopodia to detect chemotactic growth factor gradients, which are formed by a mixture of different VEGF isoforms. Importantly, it has been shown that microglia express two transmembrane proteins that are essential for angiogenesis (Tie2 and NRP1). Thus the microglial interaction with the endothelial tip cells are essential to promote vascular anastomosis downstream of VEGF-mediated tip cell formation and sprout induction (Fantain et al., 2010).

While microglia have been shown to be involved in promoting angiogenesis during development, this is not the only function microglia have in CNS development. Microglia are also essential for synaptic pruning in the developing brain, which involves engulfing and eliminating synapses. Chemokines are a family of soluble and membrane-bound cytokines that perform an essential role in the mediation of neuron-microglia crosstalk in both the developing and mature brain. The fractalkine signalling pathway includes the chemokine receptor CX_3CR1 that is exclusively expressed on microglia and its ligand CX_3CL1 which is mainly expressed by neurons in brains under normal conditions. CX3CR1 null mice have been shown to have impaired synaptic pruning and increased dendritic spine densities in the hippocampus compared to controls. (Paolicelli et al., 2011).

Microglia are structurally characterised by a small cell body with fine ramified processes. They encompass a significant volume of the mature adult brain parenchyma, with the individual non-overlapping processes of each microglial cell constantly analysing the CNS environment for any issues or insults (Nimmerjahn et al., 2005; Cronk and Kipnis, 2013). It was thought that in the healthy brain, microglia reside in a dormant, inactive state. However, *in vivo* two-photon imaging in the neocortex of adult mice found that while conducting their homeostatic functions, the microglial cell bodies remain stationary but their processes are very motile, scanning the extracellular space and communicating directly with the other cells of the NVU including ECs, astrocytes and neurons (Davalos et al., 2005, Nimmerjahn et al., 2005). The bidirectional interactions between the various cells of the NVU and microglia ensures continuous immune surveillance and homeostasis in the healthy brain. Moreover, it ensures an immediate response to any insult or infection, with microglia actively migrating towards a site of damage in order to engulf and eliminate any

cell debris. In order to do this, microglia must change from their resting surveillance phenotype to one of two activated morphological states. In the M1 activated state, microglia release proinflammatory cytokines such as interlukin-1β (Il-1β) and tumour necrosis factor-α (TNF-α), while in the M2 activated state, microglia can diminish inflammation and promote tissue repair (Aguzzi et al., 2013).

1.3 Junctional complexes of the BBB

Limited paracellular permeability is one of the defining features of the BBB and is controlled mainly through two protein complexes, AJs and TJs (Greene and Campbell.,2016). AJs are ubiquitous structures of the vasculature, composed primarily of vascular endothelial (VE)-cadherin proteins that span the intercellular cleft and link to various catenin proteins in the cytoplasm of adjacent cells (Abbott et al., 2010). While their role in BBB function has not been fully defined, the cadherin–catenin system of the AJ have been noted to be important in maintaining both stability and cellular polarity. Moreover through interactions with cadherin proteins and the actin cytoskeleton, AJs can respond to stimuli and thus may contribute to the dynamic nature of this barrier. Due to the crosstalk between components of TJs and AJs, it has also been suggested that AJs are essential for TJ formation (Wolburg and Lippoldt 2002).

TJ's have two main functions. The first is to reduce the movement of polar solutes and ions through the intercellular space, helping to maintain the distinct molecular compositions of the microenvironments that the endothelial cellular sheets separate (Tsukita et al., 2001). The restricted flow of ions across the BBB results in high electrical resistance *in vivo* of approximately ~1800 $\Omega.cm^2$ (Butt et al., 1990; Abbott et al 2010). The second role of TJs is in the maintenance of cellular polarity. TJs restrict the movement of both membrane lipids and proteins between the apical and basolateral compartments of ECs, which result in the need for specific transporters to be present in the luminal and abluminal membranes. It is this differential expression of specific transporter proteins that results in EC polarity.

In contrast to AJs, which are present in all vascular beds, TJs are highly enriched in the endothelium of the cerebrovasculature. Through freeze fracture microscopy TJs have been defined as continuous networks of proteins, interacting both with proteins on the same EC or on the adjacent cells. These protein interactions are so tight that they are commonly

referred to as “kissing points” as they result in the near complete elimination of paracellular space (Tsukita et al., 2001). This in turn results in the limited movement of macromolecules, polar solutes and ions from blood to brain and vice versa. These dynamic structures that link the adjacent ECs are composed of a number of different transmembrane proteins and membrane-associated cytoplasmic proteins.

Membrane-associated cytoplasmic proteins, such as the zonula occludens (ZO), ZO-1, ZO-2 and ZO-3, proteins function as scaffolding proteins which connect the transmembrane proteins to the actin cytoskeleton and determine their spatial organisation and are therefore an essential component in barrier formation (Bazzoni et al., 2000; Zlokovic., 2008). Junctional adhesion molecules (JAM), which like ZO, have several isoforms are an additional protein that is present within the TJ structure. In addition to the bicellular TJ (bTJs) proteins, described above, at tricellular contacts, there are additional components expressed, namely tricellulin and lipolysis-stimulated lipoprotein receptor (LSR) which like the previously mentioned proteins have the potential to regulate paracellular permeability (Ikenouchi et al., 2005).

Transmembrane proteins include occludin and the claudins, both of which are tetra-spanning proteins (Haseloff et al.,2015). These proteins function as dimers, in which the two extracellular loops of each monomer interact with a counterpart on the neighbouring ECs, as can be seen in Figure 1.4 (Tsukita et al.,2001). Occludin was the first integral membrane protein of the TJ to be identified. Through ectopic overexpression experiments, occludin was shown to be capable of inducing the production of TJ-like structures (Furuse et al., 1996). However, further investigations showed cells lacking occludin were still capable of producing functional TJs, demonstrating that it is not essential for barrier formation (Saitou et al., 1998). Moreover, occludin knockout mice, while having a complex and impaired phenotype, still form intact TJs. Therefore other proteins are clearly necessary for TJ formation.

Further investigation led to the identification of the claudin family, of which there are 27 members (Furuse et al., 1998; Morita et al., 1999; Tsukita et al., 2001). All members are localised at TJs, however in different tissues different combinations of the various claudins are simultaneously expressed, for example in the liver claudin-1 and 2 are expressed while claudin-1, 3, 5, 11 and 12 expression were previously noted at the BBB (Morita et al,, 1999; Abbott et al., 2006). Moreover, even within an organ, the claudin expression pattern varies

between cell types with the lungs for example showing ubiquitous expression of claudin-4 and -7 while the expression of claudin-18 is unique to the alveolar epithelial cells (Schlingmann et al., 2015). It is these proteins that have been found to be the significant structural unit of the TJ, forming the backbone of the TJs through both homotypic and heterotypic interactions via their extracellular loops (Krause et al., 2008; Krause et al., 2009).

As stated, claudin-1, 3, 5, 11 and 12 expression were previously described at the mouse BBB. However more recent findings have noted a high cross-reactivity in claudin recognising antibodies which call into question the presence and function of claudin-12 and claudin-3 in the BBB. Through a claudin-12-lacZ-knock-in C57BL/6J mice, it was shown that the expression of claudin-12 was very low in brain endothelium and was mainly expressed in cells that typically lack TJs such as astrocytes and neurons. These claudin-12 knockout mice had an intact BBB which exhibited no signs of BBB dysfunction or neuroinflammation. Overall these findings would conclude that claudin-12 is not essential in establishing or maintaining BBB TJs integrity (Castro Dias et al., 2019). Interestingly, immunohistochemistry of claudin-12-lacZ-knock-in mouse brain sections using commercial claudin-12 antibodies resulted in false-positive immunoreactivity (Castro Dias et al., 2019). This was also noted recently in an investigation focussed on claudin-3, in which a claudin-3 knockout mouse resulted in positive immunoreactivity through immunohistochemical analysis and thus verifies that this positive result is nothing more than an artefact of antibody cross-reactivity. Through both bulk and single cell RNAseq as well as through RT-PCR, it has been shown that claudin-3 while expressed in the BCSFB and the choroid plexus, is not expressed by the endothelial cells of the BBB. These knockout mice also confirm that the absence of claudin-3 does not impair brain barrier function (Castro Dias et al., 2019b).

Due to these false positive artefacts recently observed in claudin recognising antibodies, the other claudins, such as claudin-1 and claudin-11 have also been examined. Immunohistochemical analysis revealed that, in both healthy human and mouse capillaries, claudin-11 is co-localized with claudin-5 in the brain. This finding was supported by mass spectrometry for total protein expression as well as through the use of siRNA knock-down, which both supported the finding that claudin-11 is expressed in the ECs of the BBB, and forms both cis- and trans-heterophilic dimers with claudin-5. Moreover, through *in vitro*

siRNA targeted knockdown of claudin-11 expression, increased permeability to FITC-Dextran further supports claudin-11's role in the maintenance of BBB function (Uchida et al., 2019).

These recent alterations to the assumed architecture and claudin composition of the TJs of the BBB aside, claudin-5 remains clearly the most essential for both the development and the maintenance of the BBB. Transcriptomic data has demonstrated claudin-5 to be enriched 500-fold at minimum in comparison to other members of the claudin family in brain endothelial cells (Daneman et al., 2010). Moreover, single-cell RNA sequencing has estimated that there are in excess of 10,000 claudin-5 mRNA transcripts per endothelial cell of the cerebrovasculature, a number which is roughly 10-fold greater than that of the housekeeper ß-actin (Daneman et al., 2010; Ohtsuki et al., 2008; Vanlandewijck et al., 2018).

In comparison to the occludin knockout experiments, the equivalent experiment for claudin-5 resulted in a size selective loosening of the BBB, allowing the extravasation of molecules that were less than 800Da in size (Nitta et al.,2003). The development and morphology of the vasculature remained intact, with both the structural and functional integrity of the vasculature maintained. Despite this, the necessity of claudin-5 is highlighted by the inviability of the knockouts, all of which die within 10 hours of birth (Nitta et al., 2003). Overall these simple knockout experiments clearly demonstrate that it is the claudins and not occludin that are both necessary and sufficient to form TJs. Therefore it is the claudins that will be a key target in any therapeutic aimed at modulating the BBB.

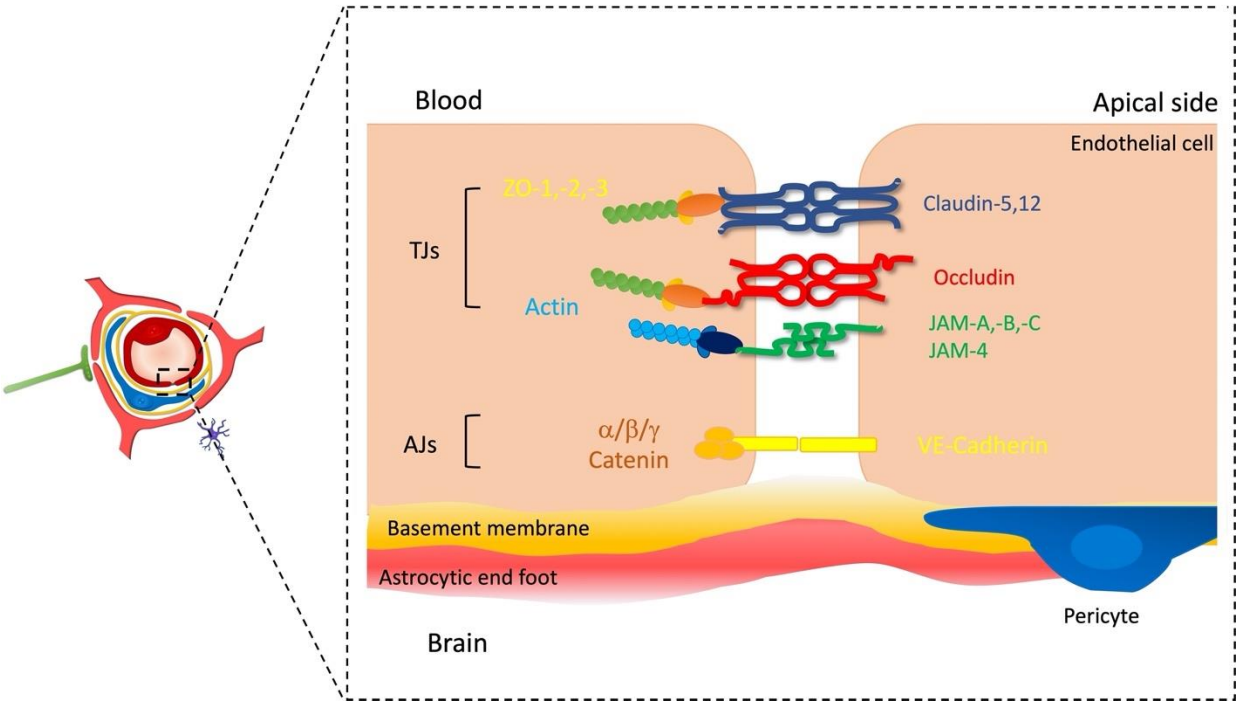

Figure 1.4 Junctional complexes of the BBB

TJ and AJ components creating a paracellular barrier between adjacent ECs, separating the blood and brain microenvironments. Claudin-5 and occludin are two of the major TJ components that are connected to the actin cytoskeleton by the ZO scaffolding protein family. VE-cadherin is an essential component of the AJs and the α/β/γ catenin proteins connect it to the actin cytoskeleton.

1.3.1 Claudin-5

The Claudin-5 (*Cldn5*) gene is located on chromosome 22 in humans and chromosome 16 in mice and is a member of the claudin multigene family, which contains 27 members. The protein product of this gene is a 23 kDa integral membrane protein, consisting of four transmembrane domains resulting in two extracellular loops (ECL) with an intracellular NH_2 terminus and a long COOH terminus (Fig. 1.5). This tetra-spanning protein functions as a dimer, in which the two extracellular loops of each monomer interact with a counterpart on the neighbouring ECs. Through this trans-interaction claudin-5 mechanically links the adjacent endothelial cells reducing the intercellular space to almost zero (Morita et al., 1999a; Tsukita and Furuse, 2000). In addition to its ability to form trans-interactions, claudin-5 can also form cis-interactions with claudins on the same cell (Gehne et al., 2017). These interactions can be homotypic or heterotypic and the strength of the interaction will depend on the claudins that are involved (Furuse et al., 1999).

Site directed mutagenesis of specific amino acids within the claudin-5 protein has allowed the functional role of the extracellular loops to be investigated and outlined. When transfected into TJ free MDCK cells, claudin-5 was noted to form a stable TJ network and with that came a selective decrease in permeability to ions (Wen et al., 2004). However, this decreased permeability was eradicated when cells were transfected with claudin-5 that had a mutation in one of its two conserved cystine residues located within the ECL1 (Wen et al., 2004). Therefore the ECL1 of claudin-5 possesses the ability to seal the barrier and so is essential for TJs to function. Mutations in conserved amino acid residues within the ECL2 have also negatively affected the function of claudin-5, in particular through their ability to form trans-interactions. While HEK cells transfected with wild-type claudin-5 note enrichment of claudin-5 at the cell- cell contact sites and the formation of TJs, both features are lost when transfected with claudin- 5 carrying specific mutations within the ECL2 (Piontek et al., 2008; Rossa et al., 2014)

Claudin-5 is expressed specifically in the EC layer of the brain, lung, liver, kidney and skin, with highest expression noted in both the brain and lungs (Daneman et al., 2010, Greene et al., 2019). In early foetal development, claudin-5 expression is dispersed in the cytoplasm of the EC. Between week 14 and week 18 of gestation, claudin-5 progresses from being discontinuously expressed along the interface of the neighbouring EC to eventually exhibiting a more continuous expression pattern (Virgintino et al. 2004). This expression persistently increases during post-natal development and is maintained by the signalling molecules secreted by the other components of the NVU, astrocytes and pericytes. Although other claudins are present within the TJs of the BBB, the expression level of claudin-5 at the mRNA level has been noted as being ~600 times higher to the other claudins (Ohtsuki et al.2008; Daneman et al. 2010).

There are several upstream signalling pathways that control claudin-5 expression both at the transcriptional and the post-translational level, examples of which include VEGF and Shh. VEGF is a powerful down-regulator of claudin-5 expression. In primary human brain microvascular EC cultures, VEGF-A was shown to specifically down-regulate claudin-5 at both the mRNA and protein level. This finding was mirrored *in vivo* in which mouse cerebral cortex had disrupted claudin-5 expression and overall BBB dysfunction following microinjection of VEGF-A (Argaw et al., 2009). Shh is a secretory protein primarily produced by astrocytes, that up-regulates the expression of claudin- 5. This increased

expression occurs when the Shh ligand binds to endothelial Patched homolog 1 receptor (Ptch), releasing the inhibitory effect of Smoothened (Smo) which results in the activation of GLI transcription on various downstream targets, including claudin-5 (Alvarez et al. 2011). In addition to the various signalling pathways that regulate the expression of claudin-5, due to the close and reciprocal relationship between the proteins of the TJ, claudin-5 is also regulated through the physical interactions it has with other proteins, such as the cytoplasmic scaffolding proteins ZO which determine the spatial organisation of claudin-5.

Claudin-5 protein has a relatively short half-life of 90 minutes (Mandel et al., 2012). As a vital component of TJs, it is essential that these dynamic structures are capable of continuous turnover and remodelling in a way that does not disrupt the BBB. A recent study has identified autophagy-mediated degradation of claudin-5 in TJ remodelling. Using MDCK cells that were transfected with claudin-5 tagged with YFP and TRQ, it was shown that claudin-5 is cross- over endocytosed into adjacent cells in large, double membrane vesicles (Gehne et al., 2017). Colocalisation of claudin-5 within these vesicles and the autophagosome markers confirm the autophagosomal pathways involvement in degradation. Cross-over endocytosis of claudin-5 relies on both the clathrin and caveolin pathways as well as claudin-claudin-interactions. As previously mentioned amino acid substitutions on ECL2 negatively affect claudin-5's ability to form both cis and trans interactions, and in addition have been shown to impair cross-over endocytosis, with weaker interactions resulting in less cross over endocytosis (Gehne et al., 2017).

The knockout models provide crucial information regarding the function of a protein *in vivo.* Claudin-5 deficient mice were shown to have a size selective loosening of the BBB, allowing the extravasation of molecules that were less than 800 Da in size while still limiting the entry of larger molecular weight molecules (Nitta et al., 2003). In this knockout experiment, development and morphology of the vasculature remained intact due to the other claudins present in the TJ, which ensured that both structural and functional integrity of the vasculature was maintained. Despite this, the necessity of claudin-5 is highlighted by the inviability of the knockouts, all of which die within 10 hours of birth (Nitta et al., 2003).

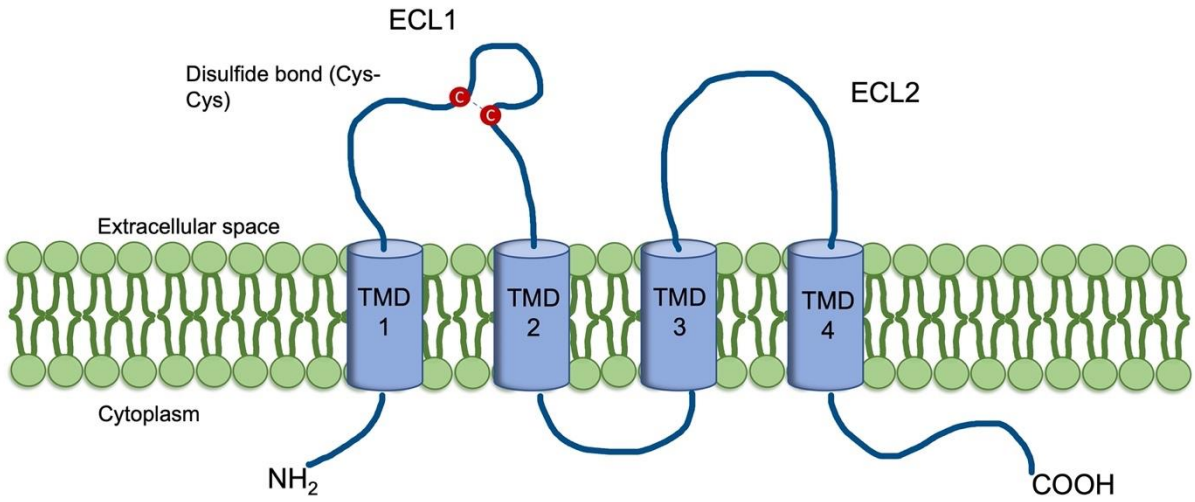

Figure 1.5 Claudin-5 structure

Claudin-5 protein contains four transmembrane domains (TMD) resulting in two extracellular loops (ECL) with an intracellular NH2 terminus and a long COOH terminus. ECL1, contains two highly conserved cysteine residues (C), and contains a disulphide bond.

1.4 Transport across the BBB

While the most essential role of the BBB is the barrier function, which regulates transport to the brain, it also in turn acts as one of the most significant obstructions to the pharmacokinetics to the brain. The BBB completely blocks the delivery of large-molecule neurotherapeutics as well as roughly 98 % of small-molecule drugs (Pardridge 2005; 2010). While there are currently a number of small molecule drug therapeutics on the market for some disorders such as depression, schizophrenia and epilepsy, the efficacy of these drugs remains inadequate. Moreover the BBB continues to act as a major roadblock in the development of new therapeutics for neurodegenerative diseases and brain cancer. Therefore understanding the various transport mechanisms across the BBB is essential for drug discovery and improving the treatment of CNS diseases (Cecchelli et al., 2007; Kuhnline Sloan et al., 2012).

Passive transcellular transport is generally limited to firstly, small gaseous molecules such as oxygen and carbon dioxide which can quickly diffuse through the brain endothelium and secondly small molecules such as ethanol and caffeine. Additionally small (<400 Da) lipophilic molecules, that contain fewer that 8-10 hydrogen bonds are simultaneously hydrophilic and lipophilic enough to ensure solubility in both water and through the

hydrophobic core of the lipid bilayer, allowing passive diffusion across the BBB (Pardridge, 2009) (Fig. 1.6.2). To regulate passive transport into the brain, efflux pumps are present, and can return any unwanted molecules back to the circulatory system.

However, as discussed previously, the energy needs of the brain are met by cerebral circulation and thus numerous transport systems are utilised to ensure these energy needs are met while protecting the brain from potential harm.

1.4.1 Paracellular pathway

The paracellular pathway describes the movement of material through the interendothelial space between the adjacent ECs that form the cerebrovasculature. The high electrical resistant TJ protein structures that are found within this interendothelial space, effectively eliminate this movement to all but the smallest solutes and ions (Fig. 1.6.1) (de Boer et al., 2003; Cecchelli et al., 2007; Abbott et al., 2010; Giacomini et al., 2010).

While the paracellular pathway is nearly impossible to penetrate, some entities can gain access to the brain by utilising specific mechanisms. An example of this is immune cell entry. Under inflammatory conditions leukocytes are able to cross the BBB into the brain. The movement of leukocytes across the BBB into the brain parenchyma is a multistep process which is controlled by the sequential interactions of adhesion and signalling molecules between the immune cells and the ECs of the BBB. This process begins the tethering of immune cells by the cell adhesion molecules, P- and E- selectin and their respective carbohydrate ligands. This tethering causes the immune cells to roll along the EC surface which reduces the immune cells speed and allows for the further recognition of chemokines on the surface of endothelial cells with their G-protein-coupled receptors (GPCRs). Activation of the GPCR results in activation of immune cell integrins, which cause significant conformational changes and leads to the total arrest of the leukocytes on the luminal surface of the ECs by binding them to endothelial adhesion molecules, vascular cell adhesion molecule 1 (Vcam-1) and intercellular adhesion molecule 1 (Icam-1). Following this, leukocytes polarise and crawl along the luminal surface of the EC to locate the endothelial junction and this allows for their diapedesis across the BBB. Under normal conditions, the healthy brain usually expresses leukocyte adhesion molecules at low levels,

however it has been noted under inflammatory conditions this expression is upregulated (Takeshita and Ransohoff, 2012; Marchetti and Engelhardt, 2020). (Fig. 1.6.5)

1.4.2 Transcellular pathway

As the paracellular pathway is extremely limited, the predominant pathway for the transport of proteins, carbohydrates and ions to the brain is the transcellular pathway. Passive transcellular transport, as discussed previously (Fig. 1.6.2) is also an extremely restricted mechanism, with only small (<400 Da) lipophilic molecules, that contain fewer that 8-10 hydrogen bonds, being capable of passive diffusion through the BBB. Therefore several active transport mechanisms are present, ensuring the remaining essentials are delivered to the brain. The various receptors that regulate these active transport mechanisms have also been a focus in the development of many new neurotherapeutic drugs, "hijacking" their transport systems to enhance delivery across the BBB.

The first active transcellular transport mechanism is carrier-meditated transport, which allows small polar molecules such as glucose, amino acids and ions to cross the BBB (Fig. 1.6.3). These carriers can range in specificity, with some limited to a single molecule, while others are multi-specific. This is an important transport mechanism as ion regulation is critical for optimal neuronal signalling and is maintained by carrier meditated transport proteins such as Na^+/K^+-ATPase pump on the abluminal membrane (Hawkins and Davis, 2005). Moreover the main energy source of the brain, glucose, is transported by glucose transporter-1 (GLUT-1), the principal cerebral hexose transporter. GLUT-1 is encoded by the SLC2A1 gene, which is notably enriched in the cerebrovascular ECs in comparison to the peripheral. A homozygous loss of SLC2A1 is embryonic lethal, highlighting its importance in brain health and function. Haploinsufficiency, in humans results in infantile onset neurodevelopmental disorder known as GLUT-1 deficiency syndrome (GLUT-1 DS) which is characterised by paediatric-onset epilepsy. There has recently been a debate however on how this deficiency is affecting the BBB. An earlier study in mice found that haploinsufficiency of the GLUT-1 transporter in brain ECs significantly damaged the BBB, with the $slc2a1^{+/-}$ mice displaying significant extravasation of serum proteins and expressed decreased TJs levels (Winkler et al., 2015). However the accuracy of these findings have been recently called into question when a GLUT-1 DS patient study did not note any significant increase in the level of serum proteins in the CSF, which would be expected if the integrity of the BBB was damaged (Tang et al., 2017). This finding has been

further supported with repeated animal experiments, which did not observe any BBB damage (Veys et al., 2020). This finding again highlights the importance of these carrier transport systems, which like the BBB itself, are vital to ensure healthy and functioning CNS (Tang and Monani., 2021).

The next form of active transcellular transport is active efflux, via ATP-binding cassette (ABC) transporters (Fig. 1.6.4). These ATP-dependant pumps are ubiquitous membrane-bound proteins that are expressed on the abluminal side of the ECs of the brain. They prevent the build-up of drugs, drug conjugates and xenobiotics in the brain through active efflux of these substances back into the blood. At the BBB, P-gp is a critically important efflux transporter. Due to its broad substrate specificity, it protects the brain from various neurotoxic compounds (Lin and Yamazaki, 2003). In humans P-gp is encoded by a single MDR1 gene but in mice there are two genes Mdr1a and Mdr1b. Both the Mdr1a and the Mdr1a/b knockout mouse models, while viable, fertile and appearing phenotypically normal, displayed a significantly elevated drug level in the brain and an overall greater sensitivity to various drugs (Schinkel et al., 1994; Schinkel et al., 1997). Thus while an important protective mechanism, active efflux and in particular P-gp, act as a major pharmacokinetic roadblock in brain targeted drug development.

Drugs that have been developed to act on the brain, such as anti-depressants and anti-seizure drugs are usually small and lipophilic, which means that they can easily cross the BBB by diffusion. However, these properties also make them likely P-gp substrates, with an estimated ~50 % of potential drug candidates on the market being substrates of this multidrug efflux transporter (Abbott et al., 2002). There is significant evidence to indicate elevated expression of efflux transporters, which includes P-gp, in the capillary ECs of surgically resected tissue from patients with medically intractable epilepsy (Tang et al., 2017). It has been hypothesised that in disorders such as epilepsy, where there is significant BBB damage, “a second line of defence” measure which includes the upregulation of P-gp, may be the reason for the significant pharmacoresistance that is noted in this disease, which affects ~30 % of patients (Löscher and Potschka, 2005; Löscher and Potschka., 2005b; Löscher and Schmidt, 2011; Löscher and Friedman., 2020).

The final two active transcellular transport methods are receptor-mediated transcytosis and adsorption mediated endocytic transport. Both allow for the transportation of proteins and peptides across the BBB. Receptor-mediated transcytosis allows for bidirectional trans-

endothelial transport of proteins and peptides like insulin from blood to brain as well as apolipoproteins which can be transported from brain to blood (Fig. 1.6.7). Adsorptive transcytosis allows plasma proteins like albumin to cross the BBB through the binding of the positively charged protein to the negatively charged phospholipid membrane (Fig. 1.6.6). It is estimated that ~10-15 % of all proteins in the NVU are transporters, which highlights the important role these transport mechanism play in maintaining the integrity of the NVU (Enerson and Drewes, 2006).

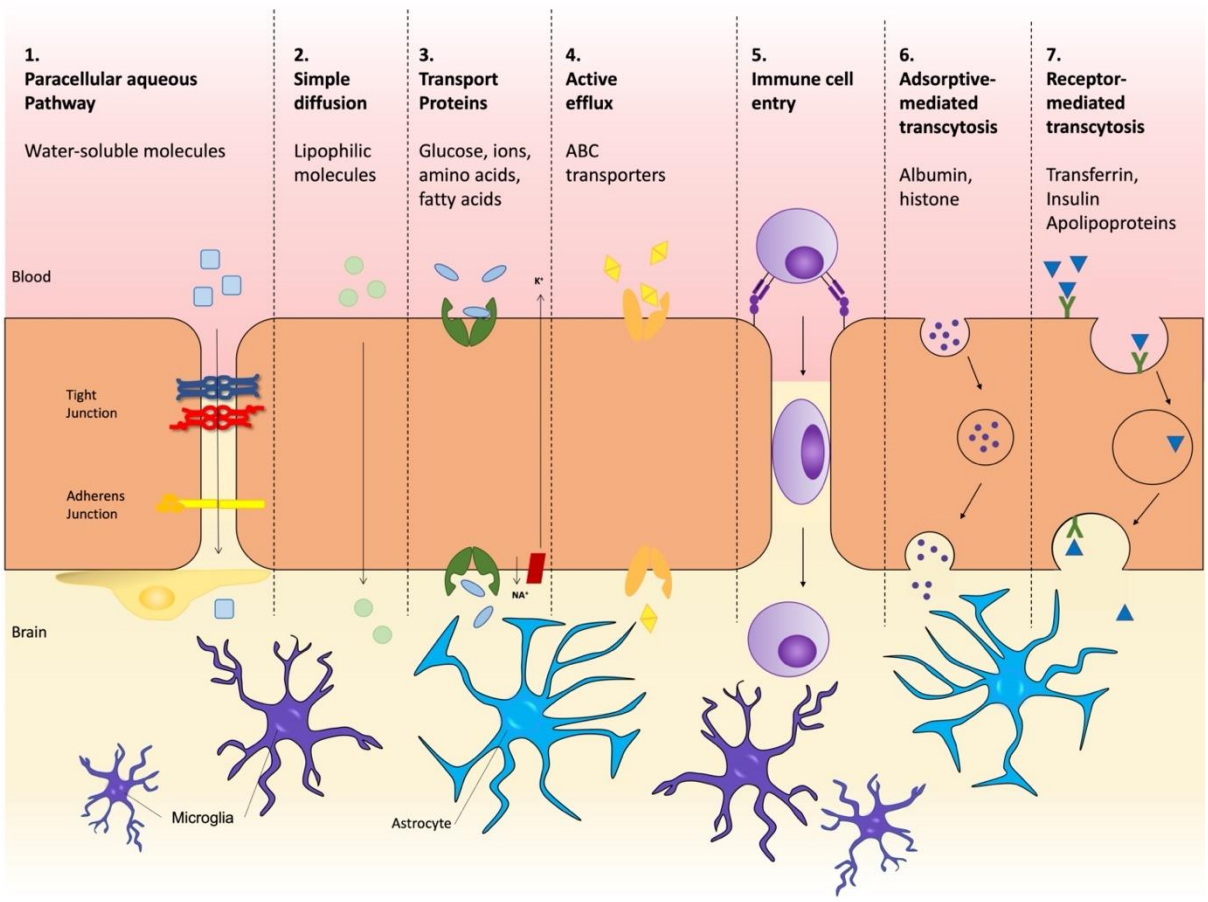

Figure 1.6 Transport mechanisms across the BBB

(1) paracellular pathway is restricted due to the presence of TJs which limit the free movement of solutes. (2) Simple diffusion allows small lipophilic molecules (<400 Da) that contain fewer than 8 hydrogen bonds to freely pass through the barrier. Gases such as O_2 and CO_2 can also freely diffuse through the barrier. (3) Transport proteins expressed on the luminal surface of the ECs facilitates the movement of essential components such as glucose, ions and amino acids into the brain. (4) Active efflux, through ATP-binding cassette (ABC) efflux transporters, actively reduce the entry of drugs into the brain parenchyma. (5) Immune cell entry occurs through the binding of the immune cell to a cell adhesion molecules and penetrating the CNS via either paracellular or transcellular pathway. (6) Adsorptive mediated transcytosis allows cationized plasma proteins like albumin to cross the BBB through the binding of the positively charged protein, to the negatively charged phospholipid membrane. This results in the internalisation and transcytosis of ligand across the EC barrier. (7) Receptor-mediated transcytosis requires binding the macromolecule ligand to a receptor, which results in endocytosis and transport of the receptor-macromolecule complex across the EC barrier within a vesicle where it is released into the brain parenchyma by exocytosis of the ligand. Large macromolecules such as insulin and transferrin utilise this method to cross the barrier.

1.5 BBB disruption and Disease

Clearly, the BBB is essential for the maintenance of the neural microenvironment, regulating the exchange of ions and nutrients between blood and brain while protecting neural tissue from potentially damaging blood-borne components. The critical importance of the BBB is highlighted by the severe pathology observed in diseases in which it is broken down.

The breakdown of the BBB results in changes to nearly all aspects of the NVU when compared to its healthy counterpart (Fig. 1.7). The principle component of the BBB, the ECs, frequently display degradation or shrinkage and the resulting reduced TJ protein expression can cause significant changes to the characteristically limited paracellular transport pathways (Sweeney et al., 2019; Obermeier et al., 2013; Knox et al., 2022). Moreover, this barrier dysfunction may further exacerbate the breakdown of these tightly regulated transport mechanisms, with alterations in expression or function of BBB-associated receptor mediated transcytosis and transport protein mechanisms like GLUT-1 also noted (Sweeney et al., 2019; Yang et al., 2020). Further to this, under pathological conditions ECs can increase leukocyte adhesion molecule expression which can lead to enhanced leukocyte extravasation into the brain, which again can enter into a positive feed-back loop in which BBB disruption can activate pathways which will further enhance barrier disruption (Brochard et al., 2009; Gerwien et al., 2016).

As the regulation and maintenance of the BBB is the result of a collaborative effort of numerous cell types, like ECs, these other cell types also show changes under the pathological state of BBB disruption (Fig. 1.7). Firstly, thinning of the non-cellular microvascular basement membrane has been noted in Alzheimer's disease (AD) patients with noted BBB disruption (Salloway et al., 2002). Moreover numerous studies have noted a reduction in both the number and coverage of pericytes as well as pericyte degeneration (Yang et al. 2020; Sengillo et al., 2013). Astrocytes under stress conditions have noted phenotypic alterations including swollen astrocytic end-feet and end-feet detachment from the microvasculature basement membrane (Obermeier et al., 2013; Garbuzova-Davis et al., 2007).

In AD alterations noted in both the structure and the permeability of the BBB are thought to play a critical role in the pathology of this disease (Bell and Zlokovic., 2009; Halliday et

al., 2016). Animal models of stroke and traumatic brain injury (TBI) have identified biphasic opening of the BBB and the downregulation of TJ proteins, which consequentially results in the extravasation of serum proteins (Baskaya et al., 1997; Knowland et al., 2014). As a hallmark pathology in numerous neurological conditions, the degree of the BBB disruption often demonstrates a clear correlation with the severity of the disorder. Epilepsy is a prime example of this, with the degree of BBB dysfunction correlating with seizure severity (van Vliet et al., 2007). Moreover the sheer extent of the vascular permeation in neuronal tissue may provide a simple mechanism to explain the complex and varied presentation noted in many psychiatric disorders. During BBB disruption numerous brain regions may be simultaneously affected and result in various cognitive and behavioural dysfunctions that are characteristic of disorders such a schizophrenia (Kealy et al., 2018). Overall, as the BBB clearly plays a vital protective role, its dysfunction will lead to disease. Therefore it should also be considered as a target when designing therapeutics for the aforementioned diseases.

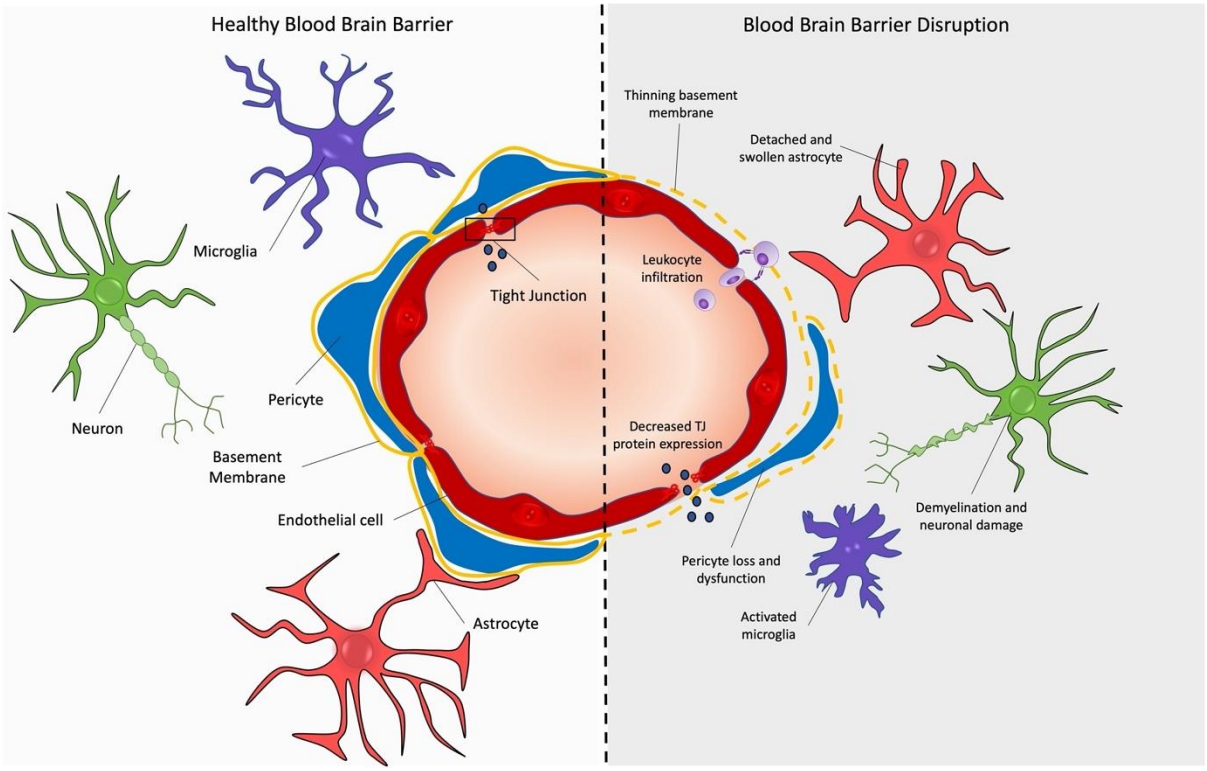

Figure 1.7 Schematic representation of the BBB in a healthy state and during breakdown

(A) A healthy, intact BBB is comprised of ECs encompassed by the basement membrane and pericytes. Astrocytic endfeet closely interact with the ECs and pericytes to maintain the BBB integrity. Microglia are inactive and functional healthy neurons are present and in close contact with the vasculature. (B) When there is BBB breakdown and disruption, the integrity of the barrier is affected in numerous ways. Clear hallmarks of BBB breakdown include several changes to ECs, including cell shrinkage, reduced TJ protein expression and changes to both paracellular and transcellular transport mechanisms which includes increased immune cell infiltration. Moreover pericyte loss or dysfunction is often noted as well as astrocytic endfeet becoming swollen or detached. Microglia morphology changes to its activated state and neurons can become demyelinated and damaged.

1.5.1 Epilepsy

Epilepsy is a chronic CNS disorder affecting approximately 1 % of the population. It is characterised by recurrent, spontaneous seizures caused by abnormal electrophysiological activity in the brain. The cause of these seizures is often unknown however brain insults such as TBI or stroke are often likely sources. In some cases however, it can have a strong genetic component with mutations predisposing an individual to epilepsy (Pitkänen et al., 2015).

The classification of seizures is based on where in the brain the seizure activity originated. There are three main categories, focal, generalised and unknown onset. The origin of a focal

seizure is restricted to one cerebral hemisphere whereas a generalised seizure originates in bilaterally distributed neuronal networks (Stafstrom and Carmant., 2015; Scheffer et al., 2017). Generalised seizures are further sub-characterised into absence, atonic, myoclonic and generalised tonic-clonic based on clinical manifestation. Absence seizures are characterised by staring and non-responsiveness, atonic seizures result in a sudden loss in muscle strength, myoclonic seizures note sudden involuntary movements, and finally, generalized tonic seizures result in the behaviour most commonly attributed to epilepsy, the bilateral convulsion of all limbs and associated loss of consciousness. Seizure type is generally determined through the use of electroencephalogram (EEG) and imaging studies as well as family and medical history, after which a treatment plan can be devised (Berg et al., 2010; Scheffer et al., 2017; Stafstrom and Carmant, 2015).

The epilepsy drug market value is forecast to reach an estimated US$6 Billion by 2024 and is currently almost exclusively made up of small molecule therapeutics that can regulate seizure activity (Grand View Research Report 2024)**.** However up to 30 % of patients continue to have seizures even after trying multiple anti-seizure drugs (ASDs). This refractive cohort represent up to 80 % of the costs associated with epilepsy treatment and more importantly, are a group of ~ 15 million people suffering with an uncontrolled disease (Perucca et al., 2007)

Epilepsy research has focussed mainly on neurons, and in particular ion channel dysfunction as the main underlying pathology affecting normal neuronal function (Han et al., 2017). While aberrant neural activity is the ultimate inducer of a seizure, recently other aspects of the NVU, such as the BBB, are being considered as additional causative factors in this disorder. As the BBB is vital in the maintenance of a homeostatic neural microenvironment, dysfunction in this protective layer could have significant consequences on neuronal excitability, and thus the possible generation of seizures. BBB dysfunction is a hallmark pathology of many neurological conditions, with the degree of BBB dysfunction often correlating with disease severity. This is clearly seen in epilepsy, where BBB dysfunction is one of the earliest events following status epilepticus and where seizure severity correlates with the degree of BBB dysfunction (Friedman 2011; van Vliet et al., 2007).

The induction of seizure activity through the artificial opening of the BBB using high-dose mannitol infusion has been show experimentally in animal models as well as clinically in

humans (Fieschi et al., 1980, Marchi et al., 2007). These findings provide a defined molecular etiology linking BBB disruption and seizure onset. However increasing BBB permeability does not instantly or consistently induce seizure activity. In clinical trials attempting to enhance the pharmacokinetics of chemotherapeutics through the transient osmotic opening of the BBB of patients with brain lymphomas, the most significant complication associated with the procedure noted was the incidence of seizures. However, different trials recorded significantly different incidence rates ranging from 4 % all the way to 50 % (Neuwelt et al., 1983, 1986; Roman-Goldstein et al., 1994). This finding highlights the heterogeneity and complexity of seizure development. Outlining the sequential events that would elucidate the relationship between seizure activity and BBB disruption has been difficult due to inconsistent and inconclusive data, resulting in the conclusion that BBB disruption is both a cause and consequence of seizure activity. Overall a "leaky" barrier contributes to the generation of seizures, leading to more seizures which trigger further barrier dysfunction leading to epilepsy progression (van Vliet et al., 2007; Marchi et al., 2007; Seiffert et al., 2004).

As previously mentioned, the TJ protein claudin-5 is a key regulator of BBB integrity. Studies utilising animal models of epilepsy have noted a reduced level of claudin-5 following seizure activity, indicating it as a precipitating factor in the subsequent disease progression of the model (Kim et al., 2015; Rempe et al., 2018). Additionally the inducible claudin-5 knockdown mouse model developed in the Campbell lab, has shown seizure activity and epileptogenesis following ~4 weeks of consistent claudin-5 suppression (Greene et al., 2018). The Campbell lab has also noted extensive disruption of claudin-5 levels with concomitant BBB disruption in human brain tissues resected from drug-resistant epilepsy patients (Greene et al., 2022). These findings support the hypothesis that the loss of claudin-5 increases the risk and severity of seizure activity.

1.5.2 Schizophrenia

Schizophrenia is a severe psychiatric disorder, characterised by altered cognitive abilities and in which hallucinations, delusions, irrational thought processes and behaviour, are the most commonly noted symptoms. Schizophrenia affects approximately 1 % of the population worldwide, with roughly 1.5 million newly diagnosed cases each year globally (WHO., 2016). The signs and symptoms of this disorder generally begin to appear in late adolescence or early adulthood. The symptoms of schizophrenia can be split into three

categories, positive, negative and cognitive. Symptoms that are classified as positive are those that are not seen in the general population. These symptoms are the ones most commonly associated with schizophrenia, in which the afflicted appear to have lost touch with reality. Symptoms include hallucinations, of which the main stimulus is auditory. In addition, delusions, as well as thought and movement disorders are all commonly noted. Negative symptoms are less conspicuous, associated with more withdrawn behaviour such as the "flat affect", which accurately describes the reduced emotional expression through facial expression or speech/voice tone (Gur, 2006). The severity of cognitive symptoms varies between patients, but symptoms are all the result of the reduced cognitive ability of the patient. Symptoms include issues with working memory, concentration and with executive functioning. These clinical symptoms make this disease extremely debilitating which is highlighted by the fact that the suicide rate is 13-fold greater in individuals suffering from schizophrenia in comparison to the general population (Saha et al., 2007). Overall, the average life expectancy of individuals with schizophrenia is 10 to 25 years less than normal, with meta-analysis suggesting up to 16,000 people die annually as a result of having to live with the condition (Voruganti et al., 2000; Leucht et al., 2009; Lieberman et al., 2005).

The genetics underlying the etiology of schizophrenia remains elusive however there is clearly a strong genetic component to this disorder. Twin studies have indicated there may be up to 80 % heritability of schizophrenia. Genetic studies have identified linkage between schizophrenia and chromosome 22, which suggests that this region may harbour major susceptible loci for this condition (Pulver 2000; Liu et al., 2002; Rees et al., 2014). This hypothesis is further supported by the fact that the highest known risk group for the development of schizophrenia, with a 30-fold increased risk, is a cohort of individuals with 22q11 deletion syndrome (22q11DS). 22q11DS is a genetic disorder otherwise known as velo-cardiofacial syndrome or Di-George Syndrome, that is the result of a micro-deletion within the chromosomal region 22q11.21.10-12. Additionally, a study carried out by Rees et al., 2014, noted that large duplications at 22q11.2, the reciprocal of the deletions in 22q11DS, are substantially less common in schizophrenia cases than in the general population. This duplication represents the first putative protective mutation identified for schizophrenia. These findings highlight the importance of the 22q11.2 region in the development of schizophrenia and have provided a more specific target for the identification of risk genes.

Within the deletion 22q11.2 region there are approximately 40 genes, which includes claudin-5. As claudin-5 is a dose-dependent gene, the haploinsufficiency caused by this deletion may have serious deleterious effects. As previously described, claudin-5 is a major component of TJs and therefore plays a key role in regulating BBB permeability and preventing any potential exogenous substances which could have a negative impact on neuronal activity (Fiorentino et al., 2016). Therefore claudin-5 may be a gene whose dysregulation shows a clear pathological effect that would correlate with the clinical symptoms of schizophrenia.

Further findings that support the hypothesis of an association between claudin-5 and schizophrenia development include the identification of a single nucleotide polymorphism (SNP) known as rs10314 located in the 3'-untranslated region of the claudin-5 gene, which through a transmission disequilibrium test showed a significant association with schizophrenia (Sun et al., 2004; Wu et al., 2010). This SNP has been shown to produce roughly half the amount of claudin-5 protein in comparison to the wild-type gene (Greene et al., 2018). Therefore individuals that carry this allele, must produce less claudin-5 protein. Through an inducible claudin-5 knock-down mouse model, the Campbell lab has noted a link between the gene-dosage effect of claudin-5 and the onset of schizophrenia-like characteristics in this model. This finding supports the hypothesis that in a 22q11DS cohort, the reduced level of claudin-5 expression that results from carrying both a low expression allele and being haploinsufficent, may predispose individuals to schizophrenia (Greene et al., 2018).

1.6 Animal models of neurological disorders

Animal models of disease are an essential preclinical tool to study the pathophysiology of diseases and associated mechanisms of injury, for the identification of potential drug targets, as well as a means to evaluate novel therapeutics for their safety profile, their pharmacokinetics, pharmacodynamics and importantly their efficacy *in vivo* (Singh et al., 2015; McGonigle and Ruggeri., 2014). The use of animal models allows for invasive investigations into the underlying structural and molecular changes that are caused by the disease and provide a means to test novel therapeutics.

However, modelling human neuropsychiatric and neurological disorders in animals is extremely challenging, due to the subjective nature of many key symptoms, the lack of biomarkers and objective diagnostic tests as well as the unknown underlying genetics (Jones et al., 2011; Nestler 2010). Therefore to be established as a strong model of a disease, the following three criteria must be considered. Firstly, construct validity refers to how the method utilised to develop the model relates to the natural development of the disease. Secondly, face validity describes the models ability to mimic the anatomical, neuropathological and behavioural features that are noted in the human disease. Finally, predictive validity represents the models ability to respond to treatments in a manner that may predict the treatment efficacy in patients.

1.6.1 Schizophrenia

There are four main mechanisms that have been utilised to develop models of schizophrenia, neurodevelopmental, pharmacological, lesion and genetic models.

1.6.1.1 Neurodevelopmental models

Neurodevelopmental models rely on the fact that while there is clearly a strong genetic contribution, environmental factors also have been noted to play an important role in the development of this neuropsychiatric disorder. Epidemiology of schizophrenia has noted compelling evidence that exposure to negative environmental insults as a neonate, either during gestation or during the perinatal period, increased the risk of schizophrenia development. A working hypothesis is that in individuals with a genetic predisposition, if exposed to an adverse environmental insult during this early developmental period, this insult could be the catalyst that results in an abnormal pattern of neuronal development and connectivity that will result in the pathological schizophrenia phenotype. One such environmental insult is post-weaning social isolation. Rodents are social creatures, with defined social structure and hierarchies when in a colony, all of which are essential for neurological development. When deprived of this sociability from this early stage (~21 days old), brain development is altered and this results in behavioural deficits in adulthood (Lapiz et al., 2003; Fone and Porkess, 2008). Behavioural changes include spontaneous locomotor hyperactivity, neophobia, sensorimotor gating deficits, cognitive impairments, and heightened anxiety (Valzelli, 1973; Heidbreder et al., 2000; Fone and Porkess, 2008). These behavioural phenotypes strongly resemble many of the main behavioural pathologies in

schizophrenia. This model has strong predictive validity as many of these symptoms can be reversed with anti-psychotic drugs (Fabricius et al., 2010a). It is known that chronic social stress can alter BBB integrity. Recently it has been shown that chronic childhood social isolation, in female but not male C57BL/6J mice induces many anxiety-like behaviours, and also results in decreased expression of Claudin-5 and increased BBB breakdown in the amygdala of the isolated female mice but not in the female group-housed mice (Wu et al., 2022).

1.6.1.2 Pharmacological models

Dysfunction of the glutamatergic system has been noted as a hallmark pathophysiological alteration in schizophrenia (Olney and Farber, 1995; Coyle et al., 2003). Clear pharmacological evidence to support the link between glutamate and the development of schizophrenia is evident in the finding that administration of phencyclidine (PCP), otherwise known as "angel dust", which is a non-competitive antagonist of the glutamatergic N-methyl-D-aspartate (NMDA) receptor, results in delusions and hallucinations in otherwise healthy individuals (Javitt and Zukin., 1991; Domino and Luby., 1981).

Therefore PCP has been utilised to develop a pharmacological rodent model of schizophrenia. Acute PCP administration has been shown to cause hyperlocomotion, social withdrawal as well as impairments of pre-pulse inhibition (PPI) in rodents. (Kalinichev *et al*., 2007; Sams-Dodd, 1995; Mansbach and Geyer, 1989). Chronic PCP administration in rodents (14 days) has been shown to reduce social interaction, which could be reversed with administration of clozapine but not haloperidol (Qiao *et al*., 2001). Additionally, locomotor sensitization to PCP, which refers to the hyperactive behaviour noted in mice previously exposed to PCP in response to an acute drug challenge, has been shown to be attenuated with treatment with anti-psychotic medications such as haloperidol and clozapine (Phillips *et al*., 2001). This together provides predictive validity for both the positive and negative symptoms of schizophrenia noted in this model.

Limitations to this model however are that many of the deficits induced by chronic PCP are not sustained, such as PPI deficits and reduced social behaviours which only persist for a certain amount of time following PCP withdrawal (Qiao *et al*., 2001; Martinez et al., 1999).

Therefore there are discrepancies in the findings between various studies which may be linked to the dose and timing of the PCP administration in the mouse model.

1.6.1.3 Lesion model

The next model is the neonatal ventral hippocampal lesion. This model is produced by bilateral intrahippocampal injections of ibotenic acid, an excitotoxin, into the ventral hippocampus of rodents on postnatal day 7 under anaesthesia with hypothermia (Lipska et al., 1993; Becker et al., 1999). The lesions must be bilateral in order to produce the full spectrum of behavioural changes (Chambers and Self, 2002). These long-term behavioural changes arise post-puberty overtime, which replicates the chronology of symptomology that is noted in human patients with schizophrenia, further supporting this model's face validity. Progressive development of these behavioural changes include impaired spatial learning and working memory which is noted around 25 days old, with deficits in social interaction noted around 35 days old. (Chambers et al., 1996; Sams-Dodd et al., 1997). However the full spectrum of deficits is not noted until around 56 days old, when hyper locomotor, PPI deficits and impairments in spatial working memory are noted. Moreover there are alterations to the architectural integrity of the developing medial prefrontal cortex (mPFC) and nucleus accumbens (NAc), both of which receive dense innervation from the hippocampus (Tseng et al., 2009). Adult ventral hippocampal lesioned rodents have a reduction in spine density and dendritic length of pyramidal neurones in both the mPFC and nucleus accumbens core (NAcc) medium spiny neurons. It appears that damage to the ventral hippocampus may trigger developmental alterations to other brain regions, particularly the PFC, which may also contribute to the changes in behaviour noted in this model. Finally the predictive validity in this model is generally good with antipsychotic drug administration in adulthood preventing some behavioural deficits (Sams-Dodd et al., 1997)

1.6.1.4 Genetic models

While twin studies have shown that there is no question that schizophrenia is predominately a genetic disorder, no single gene mutation has been identified that can completely account for this complex heterogenous disorder. In fact, a large genome wide analysis study has identified 108 risk loci for schizophrenia (Schizophrenia Working Group of the Psychiatric Genomics Consortium, 2014). It is thought that multiple susceptibility genes must act

synergistically, in addition to epigenetic processes and early-life negative environmental insults, which together, may lead to the development of schizophrenia. Therefore, any genetically manipulated mouse model constructed will have limited construct validity, due to the singular genomic changes but nevertheless they are still beneficial in research.

An example of this is the *disrupted-in-schizophrenia 1 (*DISC1) gene. DISC1 gene is one of the earliest genes implicated in risk of schizophrenia development, having been originally identified in a large Scottish family, which had a high incidence of mental illness including schizophrenia, which was associated with a balanced t(1;11)9q42.1;q14.3) chromosome translocation. DISC1 encodes a synaptic protein, that is expressed in early development and has been shown to impact many aspects of CNS function including synaptogenesis, neuronal migration and synaptic plasticity (Jaaro-Peled, 2009; Jonestone et al. 2011).

Development of a mouse model has been challenging due to the debate on the functional consequence of the t(1;11) on DISC1, whether the pathology linked to this mutation is due to haploinsufficiency or is a pathology due to a dominant negative effect of a truncated DISC1 protein. Therefore multiple different strains of transgenic DISC1 mutant models have been examined. In two models with truncated DISC1 protein expression, behaviours that are associated with schizophrenia pathology were noted including hyperactivity, despair, deficits in PPI, working memory deficits (female only) and reduced sociability (males only) (Hikida et al., 2007; Pletnikov et al., 2008).

Variability in behavioural and physical outcomes are noted in this model, which are dependent on the genetic manipulation utilised to create the model but overall there are overlapping phenotypes that support DISC1 link to schizophrenia and result in a model with sufficient face validity.

Model	Induction	Manifestations	Human relevance	Limitations with model	Effect noted on BBB
Neurodevelopmental					
Post-weaning social isolation	Socially isolated from ~21 days old .	Spontaneous locomotor hyperactivity, neophobia, sensorimotor gating deficits, cognitive impairments, and heightened anxiety.	Behaviours consistent with positive, negative and cognitive symptoms of schizophrenia.	Behavioural changes potentially reversed if overhandled during development (Weiss et al., 1999). Single housing is costly and impractical.	Decrease in Claudin-5 expression and increased BBB breakdown (Wu et al., 2022)
Pharmacological					
PCP-induced	Singular (acute) or multiple (chronic) systemic injection of PCP.	Acute: hyperlocomotion, social withdrawal as well as impairments of PPI in rodents. Chronic: reduce social interaction.	Behaviours consistent with positive and negative symptoms of schizophrenia.	Deficits induced by PCP are not sustained, only persist for a certain amount of time following PCP withdrawal. No gold standard dosing regimen established.	-
Lesion					
Neonatal ventral hippocampal lesion	Bilateral intrahippocampal injections of ibotenic acid into the ventral hippocampus on postnatal day 7 under anaesthesia with hypothermia.	Behavioural changes arise over time, post-puberty. Impaired spatial learning and working memory, decreased social interaction, hyper locomotor, PPI deficits.	Behaviours consistent with positive, negative and cognitive symptoms of schizophrenia.	Relatively high mortality rate. Time consuming to generate cohort. (Jones et al., 2011).	-
Genetic models					
DISC1-mutant	Model with truncated DISC1 protein expression	hyperactivity, despair, deficits in PPI, working memory deficits (female only) and reduced sociability (males only)	Behaviours consistent with positive, negative and cognitive symptoms of schizophrenia.	Limited construct validity due to the complex genetic heterogeneity of the disease.	-

Table 1.1 Summary of some of the commonly used models of schizophrenia and any noted effects on the BBB.

1.6.2 Epilepsy

While non-invasive technologies to study the human brain's structure and function have made significant progress, there are still significant limitations to our ability to examine certain details of physiology and molecular biology as it relates to disease. The complex etiology of epileptogenesis and seizure generation in epilepsy cannot be elucidated through human clinical studies alone. Therefore animal models of epilepsy have been essential for research. The most frequently used models of epilepsy and acute seizures are induced by chemoconvulsants, electrical stimulation, TBI or through genetic models.

1.6.2.1 Chemoconvulsants:

The most common chemoconvulsants used to induce recurrent spontaneous seizures in rodent models are kainic acid (KA) and pilocarpine. These models most closely resemble temporal lobe epilepsy (TLE). This model has strong construct validity, in that it mirrors what is noted in human patients, in which there is an initial precipitating injury, which affects the temporal lobe followed by a latent period after which spontaneous seizures occur. These seizures tend to be tonic-clonic seizures and there is also histopathological changes similar to what is noted in patients with TLE (Kandratavicius et al., 2013; Mathern et al., 2002). The precipitating injury in this case is status-epilepticus, which is defined as having a seizure lasting longer than 5 minutes or having more than 1 seizure within a 5 minute period without a return to consciousness between seizures, which can lead to permanent brain damage.

KA is an L-glutamate analog, which can be administered systemically or via intracerebral injection. Both routes of administration result in neuronal depolarisation and seizures. The KA model of TLE is described in more detail in section 5.1.3. KA causes more targeted hippocampal injuries, whereas pilocarpine result in a broader scope of injuries, with lesions in neocortical areas noted following the use of pilocarpine as the chemoconvulsant. This is not to its detriment however as damage to extra-hippocampal areas have also been noted in TLE. Pilocarpine is a muscarinic acetylcholine receptor agonist. Like with KA, both systemic or intracerebral injections of pilocarpine will result in seizures (Furtado et al., 2002; Turski et al., 1983). Strong face validity is noted in this model with structural damage and development of spontaneous recurrent seizures mirroring human complex partial

seizures (Cavalheiro et al., 1991). Moreover cognitive and memory deficits which are frequently noted in TLE patients have also been noted in the pilocarpine model (Pauli et al., 2006; Leite et al., 1990; Faure et al., 2014). Predictive validity has also been shown in this model as ASDs effective in treating complex partial seizures in patients have also been shown to stop seizures in the pilocarpine model (Leite et al., 1995). Chemoconvulsants appear to be a good animal model of epilepsy, with construct validity mirroring what is commonly noted in patients, as well as good face validity, where many of the neuropathological and behavioural changes are similar to patients with TLE. However, this model has not been completely clinically validated and does not appear to be a completely reliable for predicting the clinical response to all therapeutic strategies, therefore limiting its predictive validity. Although, overall it is a strong model for epilepsy.

1.6.2.2 Electrical stimulation:

The electrical stimulation model of seizures is beneficial as it replicates the epileptogenic features noted in seizure disorder but with low mortality of the model and with high reproducibility. Kindling, a seizure-induced plasticity phenomenon, that develops when repetitive after-discharges are induced by electrical stimulation within a specific brain region, results in a progressively increased susceptibility to seizures. Ultimately this results in the development of recurrent spontaneous seizures (Goddard et al., 1969).

As kindling is produced through repetitive after-discharges induced by electrical stimulation, this causes subtle but cumulative neuronal loss and cellular alterations in brain circuitry overtime, which eventually results in the development of spontaneous seizures (Sayin et al., 2003). Therefore, kindling may be a potent tool to study the mechanisms of epileptogenesis (Sutula., 2004; He et al., 2014). While being more time-consuming and laborious, it produces a robust and reproducible model to investigate the dynamics of epileptogenic processes (Sutula., 2004).

1.6.2.3 Brain pathology:

TBI is a leading cause of symptomatic epilepsies in adults. Approximately 20 % of all epilepsy cases are posttraumatic epilepsy (PTE), a condition which is classified as the

occurrence of recurrent spontaneous seizures more than 1 week post TBI (Pitkänen et al., 2006). As with chemoconvulsant models, in post-TBI PTE models, there is an initial precipitating injury, followed by a latent period after which spontaneous recurrent seizures emerge. Fluid percussion injury (FPI) is a commonly used strategy to generate a PTE model. A single incident of severe FPI is adequate to generate PTE (D'Ambrosio et al., 2004; Kharatishvili et al., 2006). In this model mossy fiber sprouting and hippocampal neuron loss are noted which correlates with the pathology that is noted in mesial TLE (Kharatishvili et al., 2006). However there are significant limitations to this PTE model. There are long latent periods and the yield of epileptic animals tends to be low. There is also significant heterogeneity in the nature of the TBI epilepsy models, which includes focal models of TBI, diffuse brain injury models and combined injury models. Thus, while mirroring the high heterogeneity noted in patients with TBI, no model fully recapitulates the full scope of the human disorder (Pitkänen et al., 2009).

1.6.2.4 Audiogenic seizures:

Audiogenic seizures (AS) are generalized seizures that are initiated by a high-intensity (110dB) acoustic stimulation (Garcia-Cairasco et al., 1993). The first audiogenic seizures were observed in the early 1920s in Pavlov's laboratory (Ross and Coleman., 2000). Since then many audiogenic strains have been developed including Genetically Epilepsy-Prone Rat, Wistar Albino Glaxo/Rijwijk rat (WAG/Rij) and the Wistar Audiogenic Sensitive Rat (Jobe et al., 1973; van Luijtelaar and Coenen., 1986; Marescaux et al., 1987). The inferior colliculus, a component of the midbrain that acts as the main auditory centre in the brain, is the most critical structure involved in the transduction of sensory to motor activity. Activation of this area is necessary for the initiation of AS (Garcia-Cairasco et al., 1993). In these models, a single acoustic stimulus is sufficient to trigger a reflex seizure. This generally initiates with wild running, which then progresses to a tonic-clonic seizure phase and postictal events are also common. While there are similarities among the different audiogenic strains, there are noted behavioural features that are strain-specific (Ross and Coleman., 2000).

A benefit to this model is that the audiogenic model of epilepsy, can be used to examine comorbidities that are associated with epilepsy. The WAG/Rij strain for example while being an audiogenic seizure model, is also a strong genetic model of absence seizures and

so can be used to examine both convulsive and nonconvulsive seizures (Coenen and Van Luijtelaar., 1987). Additionally, there are noted depressive-like symptoms in this strain. As depression is a common comorbidity in patients, the WAG/Rij strain may be a useful model to examine the comorbidity between absence epilepsy and depression (Kandratavicius et al., 2012). A significant limitation in this model however is the necessity of a trigger to evoke a seizure and the absence of any recurrent spontaneous seizures.

Model	**Induction**	**Manifestations**	**Human relevance**	**Issues with model**	**Effect noted on BBB**
Chemoconvulsants					
Kainic acid induced-SE and Pilocarpine induced-SE	Systemic or intrahippocampal injection of the chemoconvulsant	SE which mirrors the initial insult, followed by a latent period before the appearance of chronic seizures	Temporal lobe epilepsy (TLE)	Spontaneous seizures are variable in both severity and frequency. Not all of the neural damage is due to seizures	Enhanced permeability. (Lévesque and Avoli., 2013)
Electrical stimulation					
Kindling	Repeated after discharge induction by electrical stimulation	Initial kindling results in partial seizures which with continued induction progress into secondary generalisation and, eventually, spontaneous seizures	Due to more subtle but cumulative alterations, this model provides opportunity to investigate the dynamics of epileptogenic processes.	Time-consuming and expensive procedure	Enhanced permeability. (van Vliet et al., 2007)
Brain pathology					
Posttraumatic epilepsy	Fluid percussion injury	Long latency periods following insult, followed by generalised tonic-clonic seizures. Low frequency of PTE animals produced.	Post traumatic epilepsy (PTE)	Laborious induction with a long latency period.	Increased BBB permeability. (Tomkins et al., 2008)
Genetic models					
Audiogenic models	Acoustic stimulation in genetically prone rats (WAG/Rjj)	Wild running followed by generalised tonic-clonic seizures	TLE and Reflex epilepsy	No spontaneous recurrent seizures, model requires a trigger to evoke seizure.	No noted alterations.

Table 1.02. Summary of some of the most commonly used models of epilepsy and their noted effects on the BBB. (WAG/Rjj: Wistar Albino Glaxo/Rijwijk).

1.7 Gene therapy and Adeno-associated viral vector (AAV)

Gene therapy is a mechanism that operates by introducing genetic material into patients in order to alter gene or protein expression (Bulcha et al., 2021; Mendell et al., 2021). There are many attractive disease targets for this therapy, all with underlying genetic mutations resulting in the deficiency or malfunction of the proteins that are required for normal function. The potential in this market is astronomical, with the National Organization for Rare Disorders estimating that there are several hundred million patients worldwide with genetic disorders. Moreover, for more than 95 % of these patients, there are currently no effective therapeutics available (Mendell et al., 2021). While a few drug-based treatments do exist for some genetic disorders, these merely manage the symptoms and do not address the underlying genetic issue, and therefore they must be administered for the duration of the patients life. Therefore the aim of gene therapy is to treat the genetic disease at its source which, depending on the type of mutation causing the disorder, can be done in one of three ways. Firstly, a defective gene can be replaced with a functional copy. Secondly, a mutated version of a gene can be silenced, through mechanisms such as RNA interference. Lastly, a therapeutic gene can be introduced to overexpress a required protein.

Four decades of research has shown that adeno-associated viruses (AAVs) have strong potential as a vector for gene therapy. AAVs are derived wild-type AAVs which are small non-enveloped dependovirus from the *parvoviridae* family. As the name dependovirus would suggest, this virus replicates only in the presence of a helper virus, generally the adenovirus (Schaffer et al., 2008; Dayton et al., 2012). The wild type AAV is characterised by a single-stranded DNA genome of 4.7 kilobases that contains the viral genes rep and cap and flanked by two inverted terminal repeats (ITR)(Schaffer et al., 2008). Through alternative splicing and start codons, these two genes produce all the necessary viral proteins. The rep open reading frame (ORF) encodes four proteins that are required for viral assembly, transcriptional regulation of promoters, viral replication and for site specific integration, while the cap ORF produces the three structural proteins that form the viral capsid (Schaffer et al., 2008). To generate a recombinant AAV (rAAV) for gene delivery, the majority of the viral genome is removed, leaving only the two ITRs containing a replication origin and encapsidation signal. The rest of the genome is replaced with the therapeutic transgene and a promoter (Kwon and Schaffer 2008) (Fig. 1.8). As AAV lacks both *rep* and *cap*, it is incapable of replicating *in vivo*, even in the presence of a helper

virus. Therefore after administration to patients, AAVs remain a safe vector for long term transgene expression.

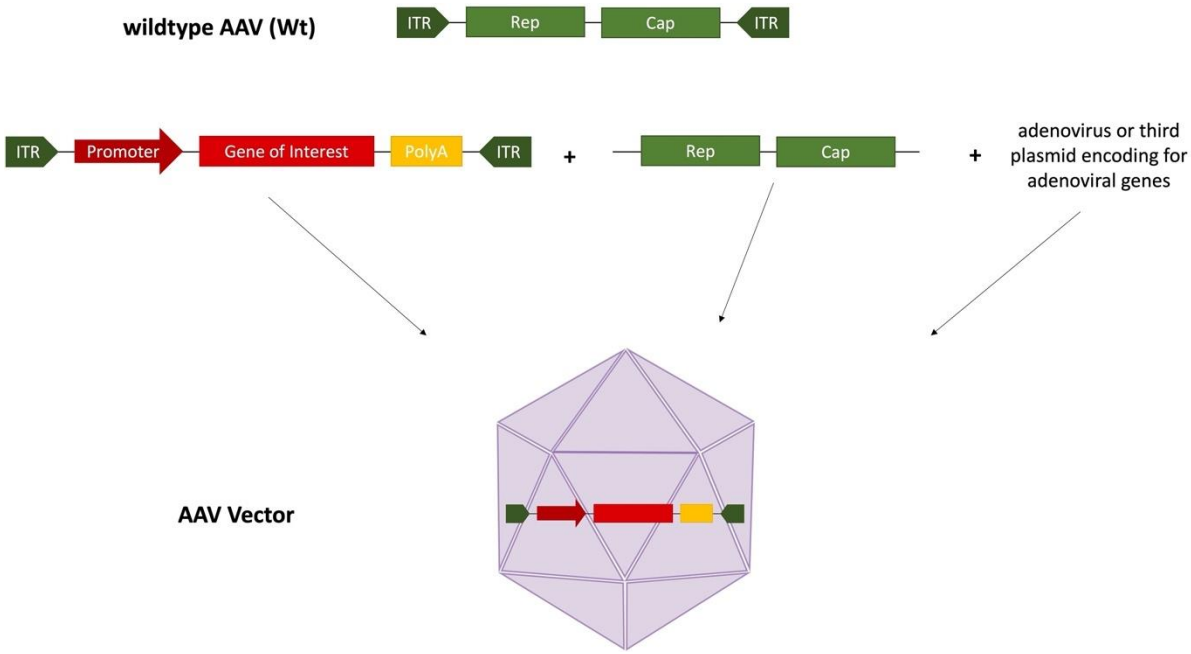

Figure 1.8. Schematic representation of wild-type AAV and recombinant AAV-derived vector system.

The wild type AAV contains 2 ORF, Rep (replication) and Cap (capsid), flanked by 2 inverted terminal repeats (ITR). In recombinant AAVs (rAAV), the viral genome is replaced with a synthetic expression cassette containing a promoter, transgene and a terminator such as a polyadenylation (polyA) sequence, flanked by the ITRs. Rep and Cap sequences are supplied as a plasmid in trans which will produce the viral capsid that packages the expression cassette.

Entry of the AAV vector begins when the virion capsid binds to receptors and co-receptors on the surface of the cell. This interaction is key to the tropism of the AAV which is an essential part of optimising gene therapy to specific cell types. This binding triggers endocytosis into endosomes. When released from endosomes, AAV virions are intracellularly trafficked to the nucleus where they are uncoated and the AAV genome is released. The single stranded genome is then through host-cell synthesis of the complementary strand, made into double stranded DNA. This DNA then undergoes transcription and the mRNA is transported from the nucleus for translation and expression of the transgene protein (Fig. 1.9). The AAV genome is maintained episomally in the nucleus (Li and Samulski., 2020).

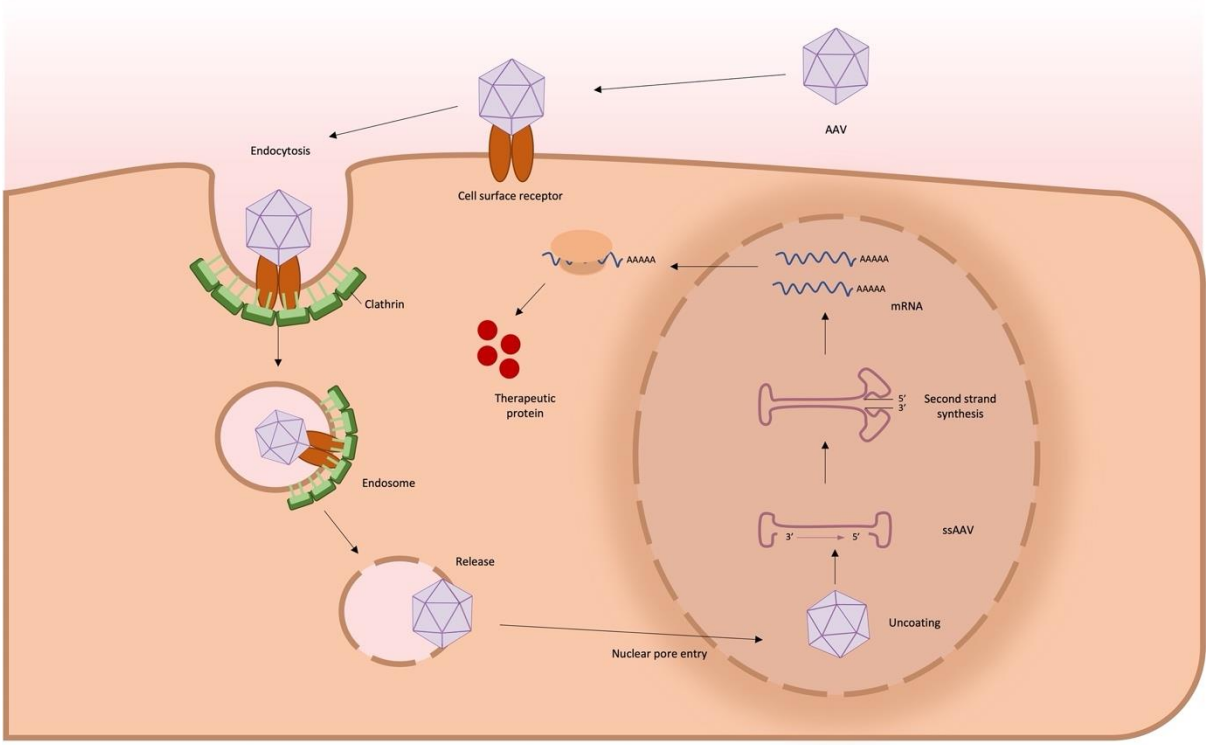

Figure 1.9. AAV vector transduction pathway.

Adeno-associated virus (AAV) vector virion capsid binds to receptors and co-receptors on the surface of cell. AAVs are endocytosed into endosomes within these cells. When released from endosomes, AAV virions are intracellularly trafficked to the nucleus. In the nucleus, AAV virions are uncoated and the AAV genome is released. The single stranded genome is then through host-cell synthesis of the complementary strand, made into double stranded DNA. dsDNA is then transcribed into mRNA and exported for translation and expression of the therapeutic transgene.

Many of the defining characteristics of AAVs make it an ideal candidate for gene therapy applications for the CNS. Firstly the wild-type virus appears to be non-pathogenic, with clinical trials to date noting low immunogenicity, making it an attractive vector for clinical gene therapy. Additionally its ability to transduce both dividing and non-dividing cells and to achieve long-term transgene expression is promising, particularly with regard to treatments designed for the CNS. This is because most cells of the CNS are post-mitotic and many chronic neurological diseases require long-term transgene expression (Weinberg et al., 2013).

However, as discussed above, the capsid serotype of the AAV can significantly influence the tropism of the virus to a particular cell or tissue type. To date, there are twelve human serotypes of AAV (AAV serotype 1 [AAV-1] to AAV-12) in addition to over 100 serotypes from nonhuman primates identified (Daya et al., 2008). While AAV2 is the most fully

characterised serotype, AAV9 has over recent years shown the most potential for gene therapy targeting the CNS. The discovery that AAV9 is capable of passage through the BBB both in neonatal and adult mice has provided an opportunity to administer AAV systemically with the possibility of widespread CNS expression (Foust et al., 2009., Zhang et al., 2011). Further investigations have confirmed intravenous (IV) injection of rAAV9 results in a dose-dependent and global transduction of the CNS in neonatal mice with gene expression maintained for up to 18 months post AAV administration (Miyake et al., 2011). Additionally, with the exception of AAV2, AAV9 is the only other serotype to have been approved by the FDA for a gene therapy. AAV9 is clinically enabled to treat the CNS disorder spinal muscular atrophy (SMA), which is a devastating neurodegenerative disease resulting from progressive loss of motor neurons.

Nevertheless, tropism of these natural serotypes may not allow specific transduction after systemic administration *in vivo*. There have been numerous techniques developed to modify the AAV capsid including, inserting phage-selected proteins to suppress their natural tropism and divert them to alternative cellular receptors peptides (White et al, 2004, 2008; Chen et al, 2009; Münch et al, 2013). However, screening of random AAV peptide libraries displayed within the AAV capsid either *in vitro* or *in vivo* has been very beneficial in improving transduction properties and cell specificity respectively (Müller et al, 2003; Michelfelder et al, 2007; Koerber et al, 2009; Deverman et al, 2016, Körbelin et al., 2016). An example of which is an AAV termed AAV-BR1, which is an AAV2 displaying the peptide NRGTEWD, which has been shown to achieve an improved transgene expression in both specificity and efficacy in ECs of the brain. Following a single IV injection, this vector was capable of transducing the BBB associated ECs across the entire CNS (Körbelin et al., 2016). Therefore the serotype of the viral vector is a key factor to consider when optimising the development of a gene therapy targeting the CNS.

Additional components that are important to consider when optimising an AAV vector are the promoter incorporated into the viral genome, the dosing regime and the administration route itself. Promoters can be viral or native to the host organism, and can control transgene expression either ubiquitously or in a tissue-specific manner. Therefore the choice of promoter in AAV development is a vital step to enhance targeted cell transduction and expression (Buck and Wijnholds., 2020). As mentioned the dosing regime is also important as dosages that are too low may result in inefficient transduction while dosages that are too

high may produce transduction related toxicities (Hinderer et al., 2018). In addition to the clinical benefit, from a manufacturing perspective, utilising a lower dosage is beneficial as the current production capacity of Good Manufacturing Practices (GMP) grade AAVs is typically capped at $\sim 5 \times 10^{13}$ viral particles/ml concentration (Naso et al., 2017). Therefore a key stage in developing a gene therapy is identifying the minimal dosage needed to achieve therapeutic significance.

While the challenge of efficient delivery of AAV vectors to the CNS are being addressed through altering serotypes of AAVs, the clinical experience with these designed AAV vectors is currently limited and cannot be fully relied on. Another key factor that will play an important role in determining efficacy of a gene therapy is through the choice of administration route. While many clinical trials utilise IV administration due to the technical ease of administration, this route does have a number of associated issues. These issues include viral tropism to non-target tissue and poor bio-distribution, in addition to the large doses that are required, which in itself has a two-fold issue. Firstly, larger doses bring an inherent risk of eliciting an immune response as well making the therapeutic more costly to manufacture per patient (Ronzitti et al., 2020). Other routes, such as intraparenchymal injection, while being a more technically difficult administration procedure, with inherent risk of damage or infection, allows for more efficient delivery and transduction within a focal region surrounding the injection site with significantly lower doses of the vector. Therefore understanding the limitations and benefits of these administration routes and how they may be relevant to the disease phenotype that is being targeted is essential in gene therapy development.

Finally, the considerations of serotype, dose and administration are important in developing a gene therapy in regards to transduction to the target tissue in the most efficient manner but these factors are also all crucial in regards to the issue of immunity. The majority of people have been exposed to some wild-type AAVs and so have developed an adaptive immunity against them, which includes neutralising antibodies (NAbs) and T cells. This pre-existing immunity could influence the efficacy and the safety of the gene therapy and may prevent re-administration (Naso et al., 2017; Vandamme et al., 2017). The prevalence of neutralising antibodies to AAV2, ranges anywhere from 30-60 % depending on the population being examined and has the ability to inhibit cell transduction (Calcedo et al.,

2009). Overall, to minimise immune response while achieving efficient gene transfer, viral design, dose and administration must all be carefully considered.

The first human gene therapy utilising AAV delivery was Glybera, which was approved in 2012, to treat lipoprotein lipase deficiency, a hereditary metabolic disorder (Gaudet et al., 2012; Watanabe et al., 2015). Currently, 75 % of all clinical trials are still at early phase, either phase 1 or phase 1/2. As many of the therapeutics are designed to target rare diseases, 64 % of all trials are combined phases, eg. phase 1/2 or phase 2/3. Moreover, there is a poor translation rate from phase 1 into phase 2 or 3. As of 2021, of the 23 late-stage trials, only two obtained FDA approval for commercialisation thus far, Luxturna utilising AAV2 for retinal dystrophy and Zolgensma utilising AAV9 for spinal muscular atrophy (SMA)(Au et al., 2022).

While progress is being made in this field of gene therapy, it is vital to be cognisant of the reality beyond academic research and be able to translate new therapeutics to clinical application with commercial feasibility. As previously mentioned, the first AAV delivery based gene therapy, Glybera, was approved in 2012. However it was withdrawn from the market in 2017 due to the rarity of the disease, the cost to the patient, and the expense to maintain therapeutic readiness overall resulted in the therapeutic being extremely challenging for the company to maintain on a commercial level. When Glybera was withdrawn from the market in 2017, only 31 people in the world had been treated with this therapeutic (Mendell et al., 2021).

Therefore, while there is many trials focussed on monogenic rare disorders, it is important that gene therapy does not stop there. There is a need to target more common disorders by identifying novel mechanisms of action which will allow gene therapy medicines to be designed to have broad utility in treating symptoms of disease.

1.8 Behavioural sequelae of BBB disruption

The behavioural consequences of BBB disruption are an important area of research in numerous neuropsychiatric disorders. Currently, many disorders, such as schizophrenia or major depressive disorder (MDD) are diagnosed solely on behavioural observations and

questionnaires, as there are still no reliable bio-markers or objective diagnostic tests. Moreover, it has been through the reverse engineering of drugs noted to be efficacious by clinical observation that have identified the molecular targets of the present leading classes of neurotherapeutic drugs (Berton and Nestler, 2006). Therefore understanding the neurobehavioral sequelae of BBB disruption and characterising it in disease models is essential in research, as even now behavioural outputs are still being heavily relied on in the clinic.

There is accumulating evidence that associates MDD with BBB disruption. The chronic social defeat stress (CSDS) model, is a model of depression that induces depression-like behaviour, which includes social avoidance and anhedonia in a subset of mice, known as stress-susceptible mice. Defeated mice that do not display this social avoidance in the social interaction test are considered "resilient". Menard et al., has shown that there is significantly reduced claudin-5 mRNA and protein expression as well as abnormal blood vessel morphology with discontinuous TJs in the nucleus accumbens (NAc) of the stress-susceptible (SS), mice but not resilient (RES) mice (Menard et al., 2017). Moreover, BBB integrity, examined through magnetic resonance imaging with gadolinium contrast agent (Gd-DTPA), showed significantly higher Gd-DTPA signalling in both the NAc and the hippocampus of the SS mice in comparison to both the RES mice and the unstressed control mice, indicating increased BBB leakiness in these regions. Both the reduced claudin-5 expression and the Gd-DTPA levels correlated with social avoidance behaviour. Additionally, in MDD patient post mortem samples, *Cldn5* mRNA expression was also significantly reduced in the NAc of unmedicated patients in comparison to healthy controls (Menard et al., 2017).

As described in section 1.5.2 schizophrenia, behaviourally manifests in a combination of what are described as positive and negative symptoms along with associated cognitive deficits. Most standard mouse models of schizophrenia resemble 'positive-like' symptoms of schizophrenia, but fewer present impaired social interactions, learning and memory deficits that are comparable to the negative and cognitive symptoms of schizophrenia. Interestingly, while investigating the effect of knocking down claudin-5 expression in mice Greene et al., noted many of these behavioural phenotypes (Greene et al., 2018). Through regional downregulation mediated through AAV-expressing claudin-5 shRNA, it was noted that a decrease in claudin-5 expression in the hippocampus resulted in memory deficits and

depression like symptoms. In mPFC even more significant issues were noted which included both recognition memory and working spatial memory deficits. Moreover, through an includible claudin-5 knockdown model which was genetically engineered to conditionally knockdown claudin-5 expression across all brain regions, a range of behavioural changes were noted including issues in learning and memory, elevated anxiety and depression related symptoms as well as significant deficits in acoustic PPI deficits, a behaviour that is strongly associated with schizophrenia. All three of these mouse models, showed increased leakage to circulating biotin. Together these findings support the hypothesis that BBB breakdown, through reduced claudin-5 expression, is a potential catalyst for the behavioural changes and development of neuropsychiatric symptoms (Greene et al., 2018). Moreover, 22q11DS patients, a cohort that is haploinsufficent for claudin-5, are one of the highest known risk groups for the development of schizophrenia.

Interestingly, given that most of the current medications on the market have been developed through serendipitous discovery rather than designed to target specific molecular components, both studies mentioned above have also noted that disorder specific medications alter claudin-5 expression. Chronic treatment with the anti-depressant, imipramine, was shown to normalise *Cldn5* mRNA expression in the NAc of the SS mice (Menard et al., 2017). Moreover Greene et al., examined anti-psychotic drugs including lithium, haloperidol and chlorpromazine, which all resulted in a dose-dependent increase in claudin-5 protein *in vitro* and similar result were also found *in vivo* in C57BL/6 mice (Greene et al., 2018). These findings present an interesting potential mode of action for these neurotherapeutics, showing that they are active in brain ECs and suggesting they have the potential to regulate BBB integrity. Furthermore it implies the significant potential claudin-5 may have as a specific therapeutic target for various neurological disorders.

1.9 Brain Atlas and Architecture

1.9.1 The Hippocampus

The hippocampus is located in the medial region of the temporal lobe and forms part of the limbic system. The limbic system is comprised of numerous structures which includes the cingulate gyrus, thalamus, hypothalamus, amygdala and hippocampus. The cytoarchitecture of the hippocampus was first describe by Ramón Y Cajal in 1901 with the

help of his student Lorente de Nó (Cajal., 1901; Nó 1934). Their pioneering work identified the subfields of the hippocampus, illustrating the distinct morphological properties of small pyramidal neurons in CA1, and large pyramidal neurons in CA3 and CA2 (with and without mossy fibers respectively). The name CA, is derived from "***C****ornu* ***A****mmonis*" meaning rams horn, which was how early neuroscience research described the hippocampus due to its curved cylindrical shape. The hippocampus, which includes CA1, CA2, CA3, CA4 and the dentate gyrus, is a easily identifiable area of the brain, where the cortex narrows into a single layer of densely packed neurons which form a tight U shape (Fig. 1.10).

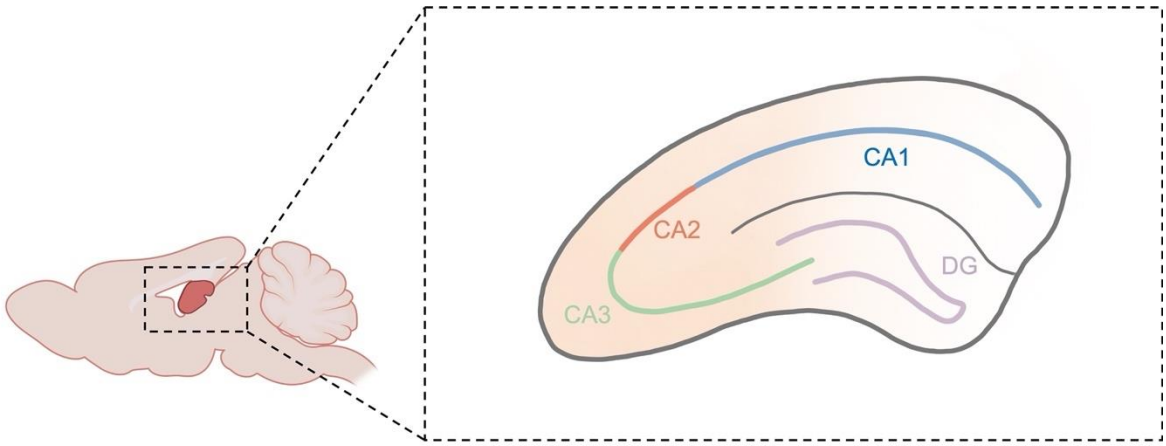

Figure 1.10. Location and basic structure of the hippocampus within a mouse brain.

There is a long standing association between memory and the hippocampus. The ground breaking case of Henry Gustav Molaison (HM), is one of the most clear examples. HM was a patient who developed anterograde amnesia following a bilateral medial temporal lobe surgical resection which was carried out in an attempt to treat his refractive epilepsy (Scoville & Milner, 1957). The hippocampus has also been associated with emotion processing, as it has been shown to exert strong regulatory control of the hypothalamic-pituitary-adrenal axis, which controls the level of cortisol (Dedovic et al., 2009). Moreover, decreased hippocampal volumes as well as hippocampal dysfunction are associated with numerous psychological disorders that have a strong affective component to the pathology (Bonne et al., 2008; Frey et al., 2007).

Interestingly, the hippocampus can be divided further, into dorsal and ventral, which in primates is referred to as anterior and posterior. While both regions have a similar

composition, they have different neural circuitry and different gene expression, and it has long been debated that the functions that are accredited to the hippocampus may also be divided within these regions. This idea was first suggested in 1998 by Moser and Moser, who hypothesised that the hippocampus does not act as a unitary structure but that the dorsal and ventral sections have different functional roles (Moser and Moser., 1998). This idea was based on 3-fold evidence. This was based firstly on the observation that the circuitry of the dorsal hippocampus (DH) and ventral hippocampus (VH) are distinct, with each section having a distinctive pattern of efferent connections (Swanson & Cowan, 1977). Secondly, behavioural assays, such as the Morris water maze, indicated that only DH was implicated in spatial working memory. Lesions affecting as little as 25 % of the DH increased the escape latency on the water maze but additional damage to the VH region did not exacerbate the deficit. Lesions that were restricted to the VH did not have any effect on this behaviour (Moser et al., 1995). Finally, it has been shown that VH but not DH lesions affect emotional behaviour and stress response. In a cold-restraint stress test, lesions to the VH but not the DH increase the severity of gastric stress ulcers, and this finding indicates that the VH is part of a coping system (Henke, 1990). It is thought that VH modifications alter fear conditioning by depriving the amygdala of hippocampal information. The amygdala has a clear role in mediating fear memory and only obtains direct hippocampal input though the VH circuitry (Maren & Fanselow, 1995). Overall the evidence indicates that the DH is involved in navigation and related spatial memory, whereas in contrast the VH influences stress responses and emotional behaviours.

In addition to the functional differences between the regions of the hippocampus, genomic evidence further supports the hypothesis of heterogeneity of the DH and VH. Through a systematic, high-resolution analysis of a genome-wide expression digital library known as Allen Brain Atlas, (Lein et al. 2007), multiple studies have been conducted to examine expression in the hippocampus of C57BL/6 mice. Analysis revealed robust dorsal/ventral molecular heterogeneity with a large cohort of genes having robust regionalised hippocampal expression (Dong et al., 2009; Thompson et al., 2008). Moreover, the gene expression noted in the dorsal hippocampus correlates with the cortical regions that are implicated in information processing, whereas genes noted to be expressed in the ventral hippocampus are associated with other regions of the limbic system that regulate emotion and stress, such as the amygdala. The correlation between gene expression and behavioural function support the hypothesis of heterogeneity within the hippocampus.

1.9.2 The medial Prefrontal Cortex (mPFC)

The significance of the prefrontal cortex (PFC) and an insight into its function was greatly enhanced through the serendipitous discovery of Phineas Gage, who in 1848, suffered a terrible accident when an iron-tamping rod pierced his ventromedial PFC. While miraculously surviving this terrible injury, he changed forever, from a once a respectable family man into a short-tempered and irrational one.

Anatomically, the PFC is the cerebral cortex, covering the anterior part of the frontal lobe. Based on cytoarchitecture and topographical criteria of the Brodmann areas (BAs), the PFC in humans includes BA8 to 14 and BA44 to 47. Moreover, the PFC can be further subdivided into two general areas based on neuroanatomical connections and functions, the medial prefrontal cortex (mPFC) and the lateral prefrontal cortex (lPFC). The mPFC has reciprocal connections with brain regions such as the amygdala, hippocampus and temporal visual association areas, which are associated with behaviours such as emotional processing, memory and higher-order sensory processing respectively. Humans require a plethora of higher cognitive skills to perform executive functions. Executive functions are defined as the involvement of multifactorial higher-order cognitive processes that enable a person to perform independent, purposive and goal-directed behaviour. The mPFC plays an important regulatory role in numerous cognitive functions, including attention, inhibitory control, habit formation and memory. The highly interconnected nature of the mPFC to other important regulatory brain regions appears to allow it to exert top-down executive control over various cognitive domains and stimuli.

Considerable knowledge of individual PFC subdivision functions have been attained by evaluating humans with brain damage, as well as rodent models with precise lesions, and have been essential for investigating distinct structure–function relationships within the PFC through behavioural testing. Behavioural features that have been noted in patients with lesions in the PFC include problem-solving, inhibitory control, decision-making, working memory and the ability to maintain sustained attention and cope with novelty (Anderson et al., 1999; Bechara & Damasio., 2000; Yuan & Raz., 2014). Most interestingly, it was noted that patients with early-onset prefrontal damage had a behavioural phenotype that manifested similarly to psychopathy (Anderson et al 1999).

1.9.3 The Nucleus Accumbens

Another target of increasing interest is the nucleus accumbens (NAc), which has been extensively examined as a key brain region mediating a variety of behaviours including reward processing and stress response. The NAc is thought to be one of the most essential elements in a network known as the brain reward system, a multilevel organisation of extensively interconnected brain regions and multiple neurotransmitter systems. In addition to the NAc, this system includes other subcortical mesolimbic structures such as the ventral tegmental area (VTA) and amygdala (Amg), in addition to several mesocorticolimbic regions, such as the hippocampus and PFC as well as motor function-related cortical areas (Koob et al., 2010). The NAc is a round but dorsally flattened structure, situated parallel to the midline, anterior to the posterior border of the anterior commissure. Its boundaries are still not fully elucidated but is thought to go into two areas of the motor system, the putamen and the caudate nucleus. It is also a major component of the ventral striatum and so, an essential part of the limbic system. Moreover, the NAc has an extensive system of connections with numerous brain regions. These include projections from the cortical areas of the limbic system, such as the mPFC and both the dorsal and ventral hippocampus respectively. Additionally, the NAc also projects to the brain stem areas that are involved in motor function. This localisation and connectivity of the NAc between the motor and limbic areas supports the NAcs essential role in the brain reward system, with its connections enabling coordination of limbic and motor functions.

The NAc can be subdivided into the shell (NAcs) and the core (NAcc) which show distinct morphological, immunohistochemical and connectivity differences. The predominant neurons in the NAc are small and medium-sized spiny neurons (MSNs) (Meredith et al., 1992). Of these, the GABAergic neurons with dopaminergic and glutamatergic synapses on dendritic spines are the most common (Gangarossa et al., 2013; Jones et al., 1980). However characteristic differences have been noted between the shell and core of the NAc which include the levels of neurotransmitters released and receptors expressed. These observations suggest a functional differentiation between the two parts of NAc. Functional analysis studies support the hypothesis that the NAc is involved in a multitude of behaviours that are essential for survival. These behaviours include general locomotor activity, in addition to feeding behaviour and sexual motivation (Kelly et al., 1975; Roberts et al., 2012; Kelley et al., 2005; Everitt., 1990). As it has been clearly highlighted above, the NAc is an essential component of the reward system in the brain and so it is unsurprising that modulation of

motivation and incentivised learning have also shown a clear association with the NAc (Di Chiara., 1995). However, these behaviours have been more specifically linked with the NAcc or NAcs. The NAcc has been shown to mediate spatial learning, as well as conditioned response and impulsive choices (Maldonado-Irizarry and Kelley 1995; Parkinson et al., 2000; Cardinal and Cheung., 2005). The NAcs is involved in feeding behaviour and drug relapse (van der Plasse et al., 2012; Bossert et al., 2006). While the function of the NAc is clearly associated with brain reward responses and addiction, there is a growing body of evidence that also indicates an important role in some neurological disorders, such as depression and schizophrenia. Current research is suggesting that this association may be due to the breakdown of the extensive connections between important brain regions in addition to the deterioration of the neuroplasticity mechanisms of the NAc.

Chapter 2. Material and Methods

2.1 Cell Culture Methods

All cell cultures were maintained in a humidified Sterile Cycle CO_2 incubator (Hepa Class 100, ThermoScientific) at 37 °C in the presence of 5 % CO_2. Cell culture procedures were all carried out in a laminar flow cabinet (Holten LaminAir Model 1.2, Thermo Electron Corporation). Cells were visualised using an inverted light microscope (Olympus CK30).

2.1.1 bEnd.3 cell culture

The mouse brain endothelial cells line, bEnd.3 (American Type Culture Collection, [ATCC] CRL-2299), was cultured in T75 flasks in Dulbecco's Modified Eagle Medium (DMEM) GlutaMAX™ media supplemented with 10 % Fetal Bovine Serum (FBS). To subculture the cells when sufficiently confluent, the media was aspirated, and the cells were gently washed in 1X phosphate-buffered saline (PBS) to remove any residual media. The PBS was removed, and the cells were incubated in trypsin-EDTA in the incubator at 37 °C for ~8 min until the cells detached from the flask. Detachment was ensured by observing cells using the inverted microscope before continuing with subculture. Media was added to deactivate the trypsin and the resulting cell suspension was then centrifuged at 1,000 RPM for 5 min. Supernatant was discarded and the cell pellet was resuspended in fresh media and divided into new flasks. Cells were subcultured once a week and replenished every 2-3 days with fresh media.

2.1.2 HeLA cell culture

The human cervical epithelial cell line, HeLa [ATCC] was cultured in T75 flasks in DMEM GlutaMAX™ supplemented with 10 % FBS and 1 % penicillin/streptomycin (P/S). Cells were sub-cultured and maintained identically to the bEnd.3 cell line (Section 2.1.1).

2.1.3 Cell counting

Adherent cells were trypsinised as described above and centrifuged at 1,000 RPM for 5 min. Following centrifugation, the cell pellet was resuspended in 1 ml of fresh growth media. An aliquot was diluted 1:2 with Trypan Blue (Sigma) and 10 µl was pipetted into a LUNA cell counting slide (Logos Biosystems) Luna™ Automated Cell Counter (Logos

Biosystems). Focus was adjusted and the cell counter determined the total number of viable and dead cells as well as the number of viable cells/ml.

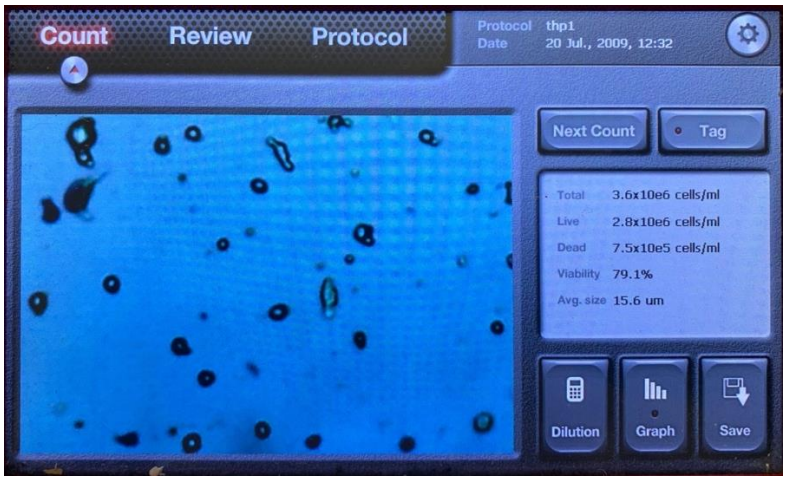

Figure 2.1 Automated Cell Counter display with automated read-out of viable cells.

2.1.4 Cryopreservation of cells

Following trypsinisation and centrifugation, the cell pellet was resuspended in 1 ml of freezing media, which was fresh growth media containing 50 % FBS and 10 % DMSO (Sigma). Cells were diluted to approximately $2x10^6$ cells/ml before being placed in a cryotube and then placed in a isopropanol-filled Mr Frosty (Thermo Scientific) and stored at -80 °C for 24 hour (hr). Cryotubes were then placed in liquid nitrogen for long term storage.

To remove from cryopreservation, cells were rapidly thawed by incubating the cryovials in a water bath at 37 °C. Once thawed sufficiently, cells were decanted into 10 ml of growth media to dilute the cytotoxic DMSO. Cells were centrifuged as previously described, supernatant was discarded and the cell pellet was resuspended in growth media and seeded into one T75 flask.

2.1.5 Construction of claudin-5 plasmid constructs

Eight plasmids were constructed by ATUM (USA). Each non inducible plasmid construct had the same backbone which included a kanamycin resistance gene, P-amp promoter for the Kanamycin resistance gene, the inverted terminal repeats (ITRs) derived from the AAV2 vector, the origin of replication, the polyadenylation signal as well as the gene of

interest insert, Claudin-5 (Fig. 2.2). The plasmids varied in regards to the claudin-5 gene insert, which was either human or mouse derived. In addition, both native and codon optimised versions of each species were examined. Finally, each plasmid gene expression was examined under one of two different promoters, intercellular adhesion molecule 2 (*Icam2*) or claudin-5 (*Cldn5*). Relevant control plasmids, such as the empty vector plasmid, which contains the backbone of the construct without the gene insert, or the green fluorescent protein (GFP) producing plasmid which the claudin-5 gene was replaced with a GFP gene, were also produced by ATUM.

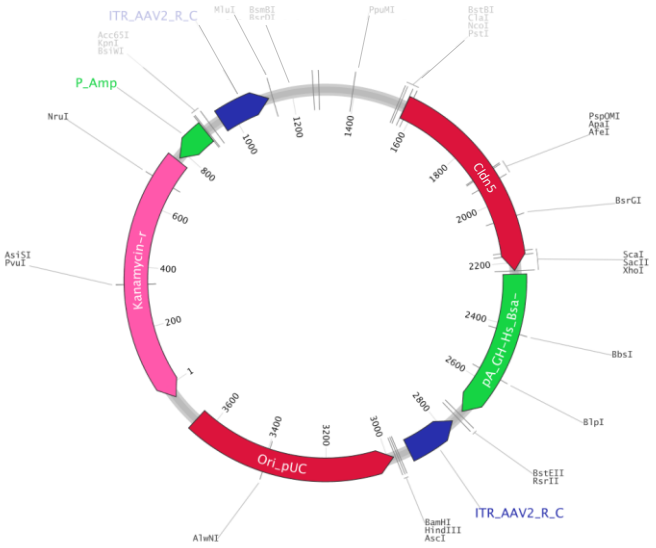

Figure 2.2 Representative plasmid map of the claudin-5 construct.

Design of the claudin-5 plasmid backbone, which includes all components, the kanamycin resistance gene, P-amp promoter for the Kanamycin resistance gene, the ITRs derived from the AAV2 vector, the origin of replication, the polyadenylation signal as well as the gene of interest insert, Claudin-5. Gene of interest arrow in this map relates to both gene of interest and the promoter driving expression. Plasmid is 3792bp.

The inducible plasmids were constructed with the same components as before, Kanamycin resistance gene, the ITRs derived from the AAV2 vector, the origin of replication, the polyadenylation signal as well as the gene of interest insert, Claudin-5. However, it also contained tetO repeats upstream of a cytomegalovirus (CMV) minimal promoter, which together form the tetracycline response element (TRE) (Fig. 2.3; 2.5A). Claudin-5 is under the control of the TRE and so can only be expressed in the presence of tetracycline (Tet) or its derivative doxycycline, as the reverse tetracycline controlled transactivator (rtTA)

protein can only bind to the operator if it is also bound by Tet. Therefore in this case the presence of doxycycline activates expression. Plasmids were again designed and constructed by ATUM.

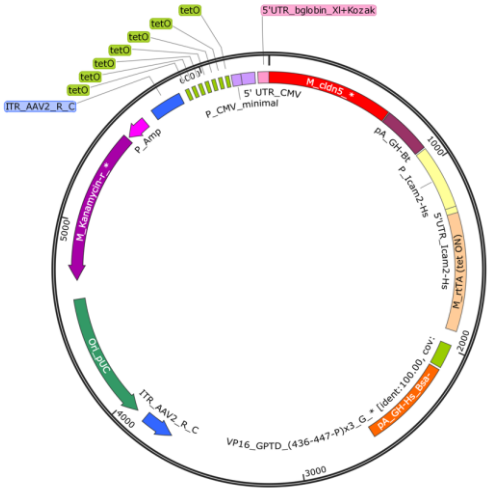

Figure 2.3 Representative plasmid map of the inducible claudin-5 plasmid construct.

Plasmid backbone, includes all basic components, the kanamycin resistance gene, the ITRs derived from the AAV2 vector, the origin of replication, the polyadenylation signal as well as the gene of interest insert, Claudin-5. In addition to control inducible expression, the inclusion of the tetracycline response element, composed of tetO repeats and CMV promoter which controls the gene of interest, claudin-5 expression. Plasmid is 6334bp.

2.1.6 Transformation

2.1.6.1 Preparation:

Lysogeny broth (LB) media (10 g NaCl+10 g tryptone+ 5 g yeast extract+ H_2O to 1 litre) and LB Agar (10 g NaCl+ 10 g tryptone+ 5 g yeast extract+ 15 g Agar+ H_2O to 1 litre) were prepared and then autoclaved at 121 °C for 20 min. Kanamycin sulfate 1000x stock solution (50 mg/ml) was also prepared. When the LB agar had cooled to approximately 60 °C, in a sterile hood, the kanamycin was added and then the culture plates were poured. Once dry, the plates were stored upside down at 4 °C until needed.

2.1.6.2 Transformation Method:

All work was carried out using filter tips and under a working Bunsen burner to maintain a sterile environment. Competent cells were thawed on ice. Agar plates were removed from the fridge and warmed to room temperature (RT). 1 µl of plasmid DNA was added to 30 µl

of competent cells and mixed gently by flicking the tube with your finger a few times. The DNA and cell mixture was incubated on ice for 30 min, followed by a heat shock at 42 ^{o}C for 45 seconds and then incubated on ice for another 2 min. LB media was warmed to 37 °C. 970 µl of pre-warmed LB media was added to the tube, mixed and incubate at 37 ^{o}C for 1 hr in a shaking incubator. 50 µl of sample was plated onto LB agar plates. These plates were then incubated upside down overnight at 37 °C.

2.1.6.3 Mini Prep:

Single colonies on culture plates were observed the next day. 5 ml of LB media and 5 µl of 50 µg/ml of Kanamycin were added into 30 ml universal tubes. Two separate colonies per plasmid plate were picked using a sterile pipette tip and then dropped into LB solution. Mini preps were then placed in shaking incubator overnight at 37 °C at 200 rpm.

2.1.6.4 Maxi Prep:

Following the overnight incubation in the shaker, the mini prep was then transferred into a 1L Erlenmeyer flask containing 250 ml of autoclaved LB media and 250 µl of 50 mg/ml Kanamycin. The maxi preps were then kept in the shaking incubator overnight at 37 °C at 200 rpm.

2.1.6.5 Glycerol Stock:

Following the maxi prep, glycerol stocks were prepared. 500 µl of the overnight culture was added to 500 µl of 50 % glycerol in a 2 ml cryovial and gently mix. The glycerol stock tube was then stored at -80 °C.

2.1.6.6 Plasmid Isolation:

Plasmids were isolated using the Qiagen HiSpeed® Plasmid Maxi Kit and protocol was conducted as manufactures instructions (Qiagen).

2.1.7 Transfection of plasmid DNA

Cells were prepared for subculture as described above (Section 2.1.1; 2.1.2). The cell pellet was resuspended in 1 ml of fresh growth media and an aliquot was removed for cell counting (as described above, section 2.1.3). $2.5x10^{5}$ cells were seeded onto a 12 well plate

and were placed in the incubator. 24 hrs later the cells were transfected using Lipofectamine® 2000 transfection reagent (ThermoFisher Scientific).

For transfection of plasmid DNA, a ratio of 3 µl of Lipofectamine® 2000 was used for 1 µg of DNA. 500 ng/ml of plasmid DNA was diluted in 100µl of OptiMEM reduced serum media and incubated at RT for 5 min. At the same time, in a separate Eppendorf tube, 1.5 µl of Lipofectamine 2000 was diluted in 100 µl of OptiMEM and incubated at RT for 5 min. Following this, the diluted plasmid DNA and Lipofectamine® 2000 were mixed together and incubated at RT for 20 min to allow for complex formation. After 20 min, 200 µl of the complexes were dropwise pipetted onto the sub-confluent cells and mixed by gently rocking the plate back and forth. The cells were then incubated at 37 °C for a set time period post transfection before they were assayed for transgene expression.

2.1.8 MTS Cell Viability assay

The CellTiter 96® AQueous One Solution Cell Proliferation Assay (Promega) was used to measure cell viability in *in vitro* experiments. $1x10^4$ cells/well were seeded onto 96-well plates in 100 µl of culture media and grown to confluence at 37 °C in 5 % CO2. Cells were then treated with experimental treatment and left to incubate for the required timepoints. Following this, media was replaced with 100 µl of fresh growth media and 20 µl/well of the MTS Reagent, (3-(4,5-Dimethylthiazol-2-yl)-5-(3-carboxymethoxyphenyl)-2-(4-sulfophenyl)-2H-tetrazolium, was added to each well and left to incubate for 1-4 hr at 37 °C in 5 % CO_2.

The absorbance of each well was read at 490 nm using a microplate spectrophotometer (Multiskan™ FC Microplate Photometer, Thermo Scientific). The blank absorbance value of a cell-free well was subtracted from all other readings and the percentage of viable cells was calculated.

2.2 *In vivo* techniques

2.2.1 Animal experiments

All experiments involving the use of C57BL/6J, inducible claudin-5 knockdown and *Cldn5$^{fl/wt}$xTie2Cre* mice were assessed and approved by an internal ethics committee in Trinity College Dublin prior to all experimentation. All studies conducted in the Smurfit Institute of Genetics in TCD adhere to the principles laid out by the internal ethics

committee at TCD and all relevant national licences were obtained prior to commencement of all studies. All mice were bred on-site in the Specific Pathogen Free (SPF) unit at the Smurfit Institute of Genetics in TCD. The CSDS model work was carried out by members of the Ménard Lab, in the CERVO Brain Research Centre. All mouse procedures were performed in accordance with the Canadian Council on Animal Care as well as animal care and use committee of Université Laval.

2.2.2 Injectable anaesthetics

Mice were anaesthetised with a mixture of Ketamine (10 mg/ml) and Sedastart (0.025 mg/ml). Anaesthetic was administered via intraperitoneal injection (IP) at a dose of 100 µl/10g using a 30-gauge needle. Mice were monitored until they were unconscious. To reverse anaesthetic, mice were injected with Sedastop (0.1 mg/ml) and were kept in a heated incubator until conscious and moving freely.

2.2.3 AAV production

Following screening of all the plasmids *in vitro*, the most efficient inducible construct, the *Icam2* promoter with the native mouse claudin5 gene, was incorporated into AAV-9 vector. An equivalent control construct was also generated, replacing the claudin-5 insert with a GFP gene. Both AAV-9 viruses were then generated using a triple transfection system in a stably transfected HEK293 cell line for the generation of high-titre viruses (SignaGen).

A non-inducible version of the construct was incorporated into an both an AAV-9 vector and an AAV-BR1 vector. Again both were generated using a triple transfection system in a stably transfected HEK293 cell line for the generation of high-titre viruses (SignaGen).

2.2.4 Stereotaxic injection

C57/BL6J/ *Cldn5*$^{fl/wt}$*xTie2Cre*/ inducible claudin5 knockdown mice (8–12 weeks old) were anaesthetized using Ketamine/Sedastart mixture (Ketamine 10 mg/ml, Sedastart 0.025 mg/ml), administered via IP injection at a dose of 100 µl/10g and monitored until unconscious. The fur within the surgical field was shaved off and the animal was placed in the stereotaxic frame. The ear bars were positioned into the ear sockets and the jaw was placed into the mouth guard ensuring the head remained fixed during surgery. A ~2cm incision was made using a scalpel blade, anterior to posterior along the sagittal suture. The

scalp was peeled to the side open the field of vision providing access to the skull. Surgical spears were used to stem any bleeding. Bregma was identified and using the stereotaxic frame, the dorsal hippocampus (co-ordinates: A/P = − 2.0 mm; M/L = ± 1.55 mm; D/ V = + 2.0 mm) or the mPFC (coordinates: A/P = + 1.9 mm; M/L = ± 0.4 mm; D/V = - 2.5 mm) were identified. Burr holes were made using a surgical drill (Mason Technology Ltd) above the dorsal hippocampus or mPFC on both hemispheres. A Hamilton syringe was loaded with the relevant AAV and the needle was lowered slowly into the hippocampus. Once the needle had reached the correct co-ordinates, it was left for 2 min to allow the area to stabilise to minimise reflux. The volume of AAV injected was 1.5 µl and was injected at a rate of 0.2 µl per min. Once complete, the needle was again left in place for 2 min to again minimise reflux. The procedure was repeated in the other hemisphere. The incision site was then sutured and anaesthesia was reversed with an IP injection of Sedastop (0.1 mg/ml). Mice were then placed into an incubator until fully recovered. All mice were given 7 days of recovery before any experiments began.

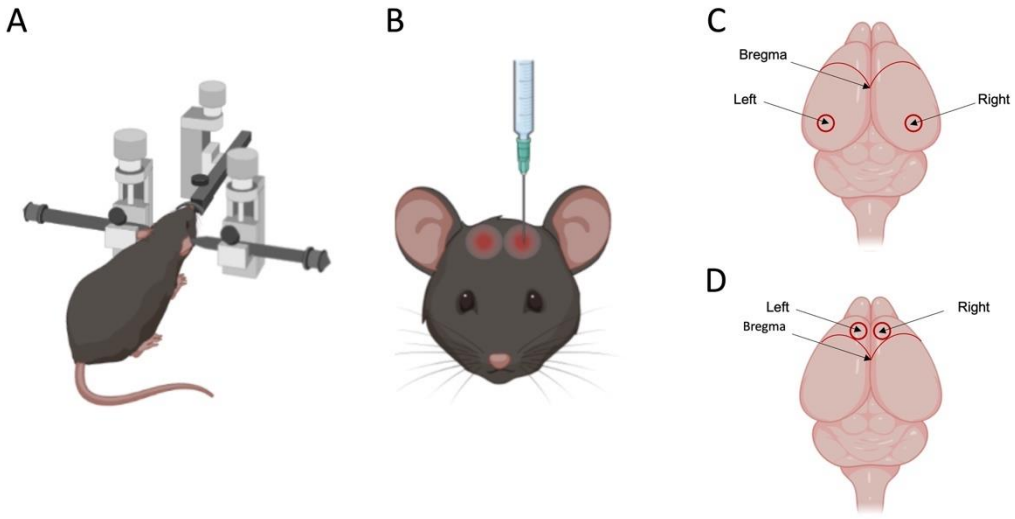

Figure 2.4 Schematic of stereotaxic injection protocol

(A) Animal correctly placed into the stereotaxic frame, with ear bars positioned into the ear sockets and the jaw placed into the mouth guard to ensure the head remained fixed during surgery. **(B)** Bilateral injection of AAV into the mouse. **(C)** Bregma was identified and using the stereotaxic frame, the dorsal hippocampus was identified. **(D)** Bregma was identified and using the stereotaxic frame, the mPFC was identified. Images adapted from BioRender.

2.2.5. Intravenous injection of AAV

Mice were confined to a 50 ml tube with a cork in each end to prevent escape and to keep the mouse secure. The tail was controlled by placing through the guide hole of the cork. Tail veins were warmed with heated pad and made clearly visible by positioning a lamp underneath the tail. A 28-gauge needle was attached to a 1 ml syringe, and each mouse was injected with $4x10^{10}$ viral genomes (VG)/ml of respective therapeutic AAV or control AAV. Light pressure was applied to the site of injection to stem bleeding and then mouse was returned to its home cage.

2.2.6 Kainic acid administration

C56BL/6J mice were injected systemically, through an IP injection, with a sub-seizure threshold dose of KA at 10 mg/kg. Standard seizure induction dose is 15 mg/kg KA. Mice were observed and video-recorded for 2 hr. Seizure severity was recorded according to the Racine scale: 0: no change in behaviour; 1: immobility; 2: head nodding; 3: forelimb clonus; 4: forelimb clonus with rearing and falling; 5: wild running and jumping often followed by generalised tonic-clonic activity and loss of postural tone. Mice were scored using the video recordings while blinded to the genotypes and treatments.

2.2.7 Doxycycline administration

Both the inducible plasmid and inducible AAV, as well as the inducible claudin-5 knockdown mouse model involve the use of the Tet-On system.

The tetO repeats upstream of the CMV minimal promoter, form the tetracycline response element (TRE). TRE controlled genes can only be expressed in the presence of tetracycline (Tet) or its derivative doxycycline (Dox), as the reverse tetracycline controlled transactivator (rtTA) protein can only bind to the operator if it is also bound by Tet. Therefore in this case the presence of doxycycline activates expression. The inducible plasmid construct, as described in section 2.1.5, has either claudin-5 or GFP under the control of TRE, and therefore are only expressed when Dox is present in the environment (Fig. 2.5A).

For *in vitro* work, following transfection with the inducible plasmid construct, cells were treated with the standard Dox treatment concentration of 1 µg/ml, unless otherwise stated. Moreover in the *in vivo* work, 1 week after the bilateral intrahippocampal injection of the inducible AAV, Dox was administered to the drinking water (2 mg/ml in 2 % sucrose solution). Dox water was changed every three days.

Additionally, the use of an the inducible claudin-5 knockdown model is described in section 5.1.1. This model, using the same Tet-On system that is described above, the presence of Dox activates the expression of an shRNA which targets claudin-5 and so silences gene expression. Again, for *in vivo* work Dox was administered through the drinking water at 2 mg/ml in 2 % sucrose solution, with the treatment water being changed every three days (Fig. 2.5B).\

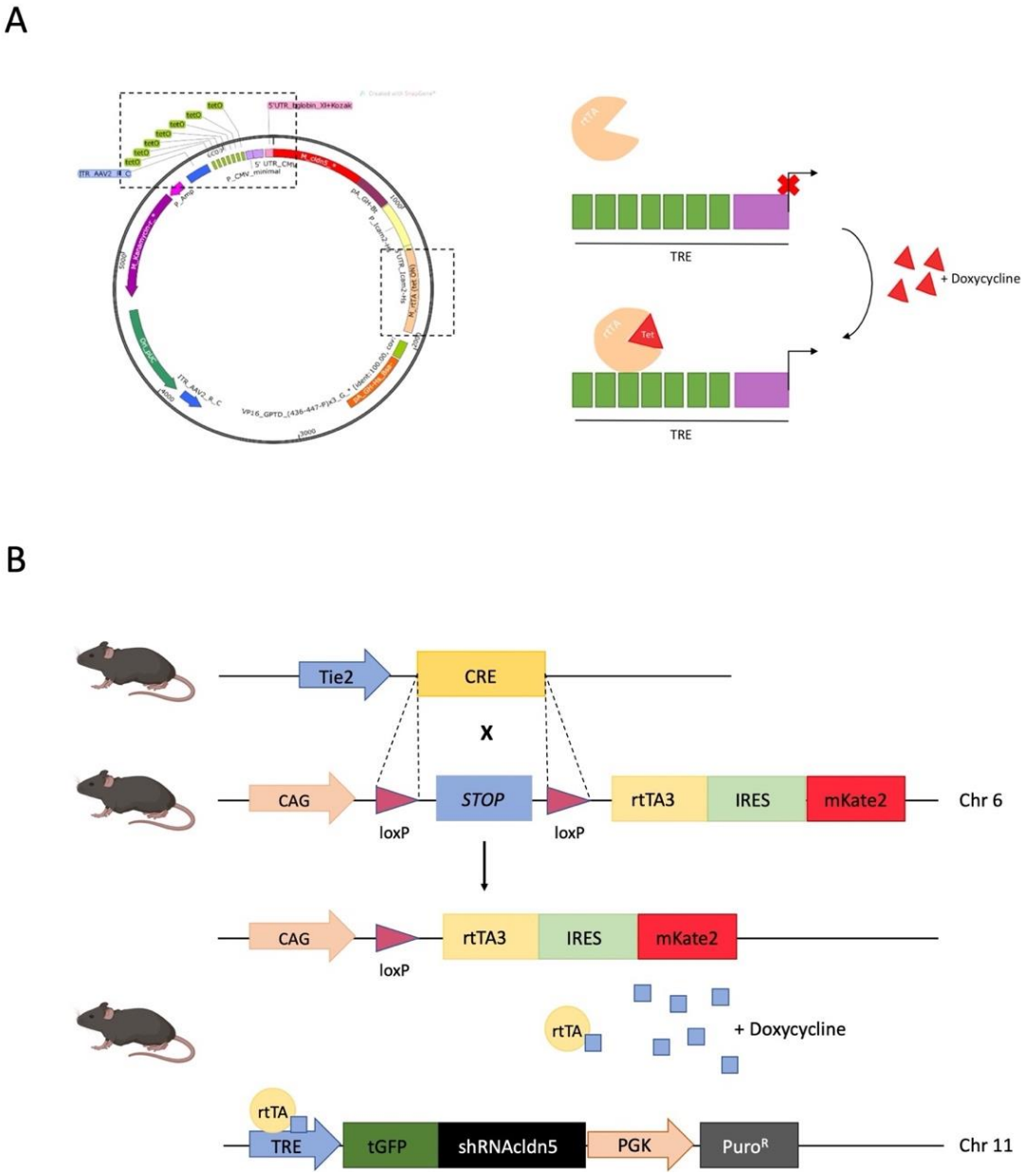

Figure 2.5 Doxycyline treatment

Use of Doxycyline to (A) up-regulate (B) or down-regulate the expression of Claudin-5 using the Tet-On system.

2.2.8 Submandibular blood collection

Following anaesthesia mice were held in the non-dominant hand, with the loose skin around the ears and shoulders restrained tightly in a “scruff”, so all skin around the face and neck is taut. The submandibular vein was punctured with a 18 gauge needle (Fisher Scientific), using a quick piercing motion in which only the tip of the needle shallowly enters the vessel.

The immediate blood flow was collected in a Eppendorf tube. For this experiment a single large volume was required before the mice were sacrificed by cervical dislocation and brain tissue was collected.

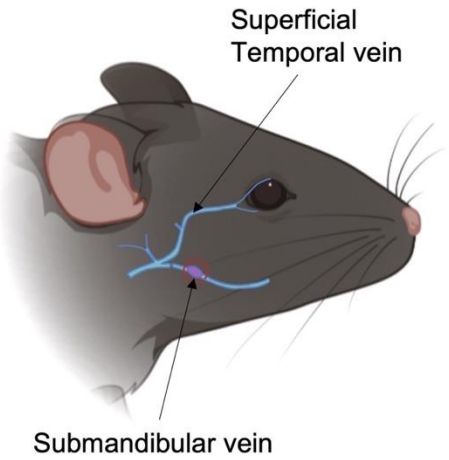

Figure 2.6 Submandibular puncture

Schematic of vasculature and location for blood collection.

2.2.9 Perfusion of tracer molecules

The extent of BBB permeability was assessed by perfusion of tracer molecules. *Cldn5*$^{fl/wt}$*xTie2Cre* mice were injected IV with 2 mg/ml of EZ-LinkTM Sulfo-NHS- Biotin (600 Da). Biotin was left to circulate for 10 min, after which the mouse was sacrificed. Following tracer molecule perfusion, brains were dissected and placed in 4 % paraformaldehyde (PFA, pH 7.4) overnight at 4 °C for cryosectioning.

2.2.10 Brain Removal

Before dissection all instruments and bench surface were cleaned with 70 % alcohol. Animals were killed by CO_2 asphyxiation followed by cervical dislocation to verify death. With blunt scissors the head was removed from the rest of body, after which the head was held by the ears and the skin was cut and pealed back to reveal skull. Any remaining vertebrae were cut away after which on medial lateral plane at the base of the skull a horizontal cut was made on either side of the skull. Next the skull was cut into at the base along the midline just beneath the cerebellum. Using fine scissors pressure was applied up the midline in the skull towards the nose. It is important to keep the scissors pointing upwards top avoid damaging the brain. Both sides of the skull were then peeled away using forceps. The brain was then released from the skull by cutting at the nose just in front of the

olfactory bulbs. The brain was then gently removed by allowing it to free fall onto a petri dish. A forceps was used to cut away remaining meninges. The extracted brain was then placed in one of various fixatives that will be discussed below depending on downstream assay.

2.3 Analytical Techniques

2.3.1 RNA extraction

RNA was extracted from bEnd.3 cells samples using the E.Z.N.A total RNA Kit I, with protocol conducted as instructed in kit (Omega Bio-Tek). In summary, once all treatment timepoints had been reached, growth media was removed and cells were washed once with PBS to remove any residual media. PBS was discarded, and cells were lysed by adding 350 µl of TRK Lysis Buffer to each well followed by scraping the well with the pipette tip as well as pipetting up and down several times to disrupt and homogenise the cell monolayer. 350 µl of 70 % ethanol was added to the cells and vortexed. Next, 700 µl of the sample was transferred to a HiBind® RNA Mini Column and centrifuged at 10,000 g for 1 min. The filtrate was discarded and 500 µl of RNA Wash Buffer I was added to the column and centrifuged at 10,000 g for 30 seconds. Again, filtrate was discarded and 500 µl of RNA Wash Buffer II was added to the column and centrifuged at 10,000 g for 1 min. This step was repeated, after which the column was spun at maximum speed for 2 min to dry the column. The column was transferred to a new 1.5 ml Eppendorf tube and 60µl of nuclease-free H_2O (nfH_2O) was added directly to the column and again was centrifuged at maximum speed for 2 min. To increase RNA yield the eluent was added onto the column again and the centrifugation step was repeated. The concentration of RNA was measured using the Nanodrop Spectrophotometer ND-1000 (Thermo Scientific) and RNA was store at -80 °C until required.

2.3.2 cDNA synthesis

cDNA synthesis was carried out using the High-Capacity cDNA Reverse Transcription Kit (Applied Biosystems). A final concentration of 100 ng of RNA was used per cDNA reaction, with nfH_2O bringing the total volume up to 10µl. The cDNA reaction was prepared according to Table 2.1. 10 µl of master mix was added to each reaction tube containing 100 ng RNA. The cDNA synthesis programme was as follows: 25 °C for 10 min, 37 °C for 2 hr, and 85 °C for 5 min and held at 4 °C. cDNA synthesis was carried out using a Miometra T3000 Thermocycler.

cDNA Master Mix	Total Volume 10µl
10X RT Buffer	2 µl
25X dNTP	0.8 µl
10X RT Random Primers	2 µl
Multiscribe RT	1 µl
Nuclease free H_2O	4.2 µl

Table 2.1 Reagents of master mix per cDNA reaction.

2.3.3 Reverse Transcription Polymerase Chain Reaction (RT-PCR)

RT-PCR was carried out using the SensiFAST SYBR Hi-ROX Kit (Bioline). A master mix was prepared as follows per sample: 5 µl SYBR Green mix, 0.5 µl Forward and Reverse primer mix (10 µM) (primer sequences used indicated in Table 2.2) and 2 µl nfH2O. 7.5 µl of this master mix was added to each well of a MicroAMP® Fast 96-Well Reaction Plate (Applied Biosystems). The cDNA samples were diluted 1 in 20 and 2.5 µl of this was added to their respective wells in triplicate. Control wells were created by replacing the cDNA content with additional nfH20. The MicroAmp® Optical Adhesive Film was then fixed to the top of the plate, centrifuged for a few seconds and placed into the Step-One Plus™ Real-Time PCR instrument (Applied Biosystems). RT-PCR reaction occurred through the following steps: 95 °C x 10 min, (95 °C x15 seconds, 60 °C x1 min) x 40 cycles. A melt-curve analysis stage was included when using new primers: 95 °C x15 seconds, 60 °C x 1 min, 95°C x 15 seconds.

Data analysis was carried out using the delta cycle threshold (CT) method to quantify changes in mRNA levels between treatment groups. CT values from each sample's gene of interest were normalised to that of the housekeeping gene to generate the delta CT (ΔCT) value for each well. Following this, control ΔCT values were averaged and subtracted from all sample ΔCT values to generate delta delta Ct (ΔΔCT) values for each samples gene of interest. Gene expression was calculated and presented as a fold-change, relative to untreated controls by calculating $2^{(-\Delta\Delta CT)}$. Statistical analysis was performed using the one-way ANOVA and Tukey's Multiple Comparison Test or two-sided unpaired t-test, results reaching significance if $p<0.05$. All data was analysed and graphed using the GraphPad Prism software.

Primer Target	Direction	Sequence 5'-3'
β-actin	Forward	GGGAAATCGTGCGTGACAT
	Reverse	GTGATGACCTGGCCGTCAG
Claudin-5 (*Cldn5*)	Forward	TTTCTTCTATGCGCAGTTGG
	Reverse	GCAGTTTGGTGCCTACTTCA
ZO-1 (*Tjp1*)	Forward	CCACCTCTGTCCAGCTCTTC
	Reverse	CACCGGAGTGATGGTTTTCT
Occludin (*Ocln*)	Forward	ACAGTCCAATGGCCTACTCC
	Reverse	ACTTCAGGCACCAGAGGTGT
Tricellulin (*Marveld2*)	Forward	CTGAGAATCTGGGTGTGGT
	Reverse	ACGAGTACGAAGGGGGTCTT
Lsr	Forward	AGTAATACACTCCACTGTC
	Reverse	CAGGAGAATCACCATCACAGGAA
Icam1	Forward	TGTCAGCCACCATGCCTTAG
	Reverse	CAGCTTGCACGACCCTTCTA
Vcam1	Forward	GAAGCCGGTCACAGTCAAGT
	Reverse	CCTCGCTGGAACAGGTCATT
Gfap	Forward	AGCCCTGCCAGCTCTCCCTTAG
	Reverse	AAGGTGTGGCTGAAATGCGCG
Iba1	Forward	GGATTTGCAGGGAGGAAAAG
	Reverse	TGGGATCATCGAGGAATTG
Ccl2	Forward	CACTCACCTGCTGCTACTCA
	Reverse	GCTTGGTGACAAAAACTACAGC
Mmp2	Forward	CCCCATGAAGCCTTGTTTA
	Reverse	CAGTGGACATAGCGGTCTCG
Rage	Forward	ACATGTGTGTCTGAGGGAAGC
	Reverse	AGCTCTGACCGCAGTGTAAAG
Cd68	Forward	CCAATTCAGGGTGGAAGAAA
	Reverse	TTGCATTTCCACAGCAGAAG
Il-34	Forward	CGTACAGCGGAGCCTCATGGAT
	Reverse	CAGCTCGCAGTCCTGCCATTTT
Sarm1	Forward	TCACCCGCAAGAGGTTCTTT
	Reverse	TCAAGCTTCTCAGGCCAGTC

Table 2.2. RT-PCR primer sequences. Primer sequences were obtained using the NCBI Primer-BLAST resource (Ye et al., 2012)

2.3.4 Western Blot

2.3.4.1 Protein extraction

Protein was extracted from cells when the timepoint of treatment was reached using 1X RIPA lysis buffer (50mM Tris, pH 8.0, 0.5M NaCl, 0.1 % sodium dodecyl sulphate (SDS), 0.5 % deoxycholate, 1 % NP40) with a protease inhibitor tablet (1P) (1 tablet/10 ml; Roche). 200 µl of RIPA+1P was added to each well of the 12 well plates and placed on ice for 10 min. Then per well, the sample was removed by scraping the well with the pipette tip as well as pipetting up and down several times to lyse and homogenise the cell monolayer, placed in separate 1.5 ml Eppendorf tubes and centrifuged at 12,000 rpm for 15 min. The supernatant was transferred to a new Eppendorf tube and stored at -20 °C until ready to use. Protein quantification was performed using the Pierce® BCA Assay Kit (as described below section 2.3.4.2)

2.3.4.2 Bicinchoninic acid (BCA) assay for protein quantification

BCA assay to quantify protein was performed using the Pierce BCA Protein Assay kit (ThermoFisher Scientific). Standards were prepared according to kit instructions. The working reagent was prepared by mixing reagents A:B at a 50:1 ratio. 5µl of either the standard or the sample was added to each well of a 96 well plate followed by 200 µl of the working reagent. The plate was covered with adhesive film, mixed and then incubated at 37ºC for 30 min.

Following the incubation, the absorbance of each sample was measured at 562 nm using a Multiskan™ FC plate reader (Thermo Scientific). A standard curve of BSA standards was plotted as absorbance vs concentration (µg/ml). The protein concentration of each sample was then extrapolated from the standard curve.

2.3.4.3 Protein sample preparation

For each protein sample, 10 µg was required and was calculated based on the concentrations determined by the BCA assay using the following equation:

Protein concentration = X µg/µl: 10 / (X * 1000) = number of µl required for 10 µg

For each sample, the final volume was 20 µl, with a total volume of protein up to 16 µl using dH_2O, as 4 µl of 5X sample buffer (Thermo Scientific) was also added to the sample.

The samples were then heated at 95 °C for 5-10 min to denature the protein. Before loading into gel, samples were cooled to RT.

2.3.4.4 Sodium Dodecyl Sulphate Polyacrylamide Gel Electrophoresis (SDS-PAGE)

The Dual Mini Slab kit (Atto) was used for SDS-PAGE and set up according to the manufacturer's instructions. Resolving and stacking gels were prepared according to Table 2.3, allowing approximately 20 min between gel preparations for gel polymerisation. 6ml of resolving gel was poured into the gel plate leaving enough space for the well comb plus 1 cm. Roughly 2 ml of 70 % ethanol was then gently added on top to provide air-free conditions for polymerisation and to remove any bubbles that may have formed in the unset gel. The gel was left at RT to polymerise. Once set, the ethanol was poured off and dried before the stacking gel was poured on top filling the remaining gel plate, the comb added and again allowed to set at RT. Once set, the rubber gasket was removed, and the gel was placed into an ATTO gel electrophoresis rig filled with 1X running buffer (10X: 250 mM Tris, 1.92 mM Glycine, 0.1% SDS, 1000 ml dH_2O (pH 8.6)). Gels were fixed in place with spacers and the inner chamber was then filled with 1X running buffer before combs were slowly removed.

The first well of each gel was filled with 2.5µl of Prime Step pre-stained protein ladder (BioLegend) which acts as a molecular weight standard, after which all remaining wells were loaded with 20 µl of the protein sample (preparation described above in section 2.3.4.3). Gels were run firstly at a low voltage of 80V for 20 min for the separating gel and then a higher voltage of 140V, until there was significant separation of bands of the protein ladder.

12 % Resolving Gel		**4 % Stacking Gel**	
H_20	6.6ml	H_20	6.8ml
1.5M Tris	5ml	0.5M Tris	1.67ml
30 % Acrylamide	8ml	30 % Acrylamide	1.33ml
10 % SDS	200 µl	10 % SDS	100 µl
10 % APS	200 µl	10 % APS	100 µl
TEMED	20 µl	TEMED	10 µl

Table 2.3. Resolving and stacking gel components and quantities required for SDS-PAGE. (Ammonium Persulfate (APS); N,N,N'-tetramethylethylene diamine (TEMED). 10 % APS

made up fresh each day in dH_2O. Gel components added in the order as they appear in the table to prevent early polymerisation.

2.3.4.5 Semi Dry Transfer

The semi-dry transfer method was used to transfer protein from gels to Polyvinylidene fluoride (PVDF) membranes (Merck Millipore). PVDF membranes first required activation in methanol, and the gel(s) were equilibrated in cold transfer buffer. Additionally, 4 layers of filter paper, the PVDF membrane, the gel and 4 more layers of filter paper were all soaked in transfer buffer before being stacked in this order in the transfer rig. The protein transfer was run at a constant 12V for 2 hr. After completed transfer, PVDF membranes were removed from the gel-filter paper sandwich and rinsed with dH_2O to remove any gel debris. Membranes were then incubated in methanol for 5 min and allowed to air-dry on dry filter paper to enhance protein binding to the membrane and reduce noise. The dried PVDF membrane was stained with Ponceau S solution (Sigma) to visualise successful protein transfer. The membrane was then washed 3-4 times with 1X Tris buffered saline/ 0.1 % Tween-20 (TBST), to wash away any unspecific binding.

2.3.4.6 Antibody Incubation

All washing, incubating and equilibration steps were performed on a benchtop orbital shaker. Membranes were cut into sections to separate the various proteins under investigation. Membranes were incubated in methanol for 5 min, equilibrated in TBST and blocked for 1hr at RT in 5 % w/v non-fat dried milk (Marvel) or 5 % BSA in TBST.
Blocked membranes were washed for 5 min in TBST three times, and then each specific section was placed into its relevant primary antibody. Blots were incubated overnight (16 hr) in primary antibody (diluted in TBST with 1 % w/v BSA, and primary antibody as described in full in Table 2.4) at 4 °C.

Primary Antibody	Dilution	Supplier
β-actin	1:4000	Abcam (ab8227)
Claudin-5	1:1000	Invitrogen

Table 2.4. Primary Antibodies for Western Blot analysis. Dilutions were made up in TBS containing 1 % w/v BSA.

Following overnight incubation, membranes were washed 3 times for 5 min each in 1X TBST. Membranes were incubated with horse-radish peroxidase (HRP) conjugated goat

anti-rabbit secondary antibody (1:2000) for 2 hours at RT. The membrane was washed a further 4 times in 1X TBST.

2.3.4.7 Enhanced chemiluminescence (ECL) And Densitometry

Membranes were visualised using the C-DiGit (LI-COR) scanner. To detect bound HRP-conjugated secondary antibody, blots were incubated in Strong Enhanced Chemiluminescence (ECL) Substrate (Advansta). Equal volumes of WesternBright ECL Luminol/enhancer solution and Peroxide Chemiluminescent solution were made up and incubated for 2 min. Membranes were then placed into the mixture and incubated for a further 2 min before being transferred directly, face down, onto the C-DiGit. These were scanned for 12 min using the high sensitivity method to visualise protein expression.

Densitometric analysis using Image studio lite software (LI-COR) was carried out to measure the expression levels of the proteins. Expression levels of the genes of interest were standardised to levels of the house-keeping gene, β-actin. Densitometry was expressed as a fold change relative to the untreated control. All densitometry was performed between samples run on the same SDS-PAGE gel and transferred onto the same membrane. Statistical analysis was performed using one-way ANOVA and Tukey's Multiple Comparison Test or Dunnett post-test results reaching significance if $p<0.05$.

2.3.5 Cryopreservation and Cryosectioning of Mouse Tissue

Cryopreservation is required to prevent the formation of ice crystals that form from water within tissues when frozen. Ice crystals formation disrupts cell membranes and creates holes within cells resulting in "swiss cheese" artifacts. Unless otherwise stated, all steps were carried out at 4 °C. Mouse brain hemispheres were dissected and immersion fixed in 4 % PFA for overnight. After this, the tissues were washed four times in ice-cold 1X PBS for 5 min. Tissues were then placed in a sucrose gradient (10 %, 20 %, 30 % sucrose in PBS (w/v)) until the tissue sunk. The tissue was then placed in plastic cryomolds filled with Optimal Cutting Temperature (OCT) compound, and then snap frozen in dry ice/methanol slurry. Following this, brains were equilibrated at -20 ^{o}C overnight. 12 μm thick sections of each hemisphere were prepared using a Leica CM1950 cryostat, placing sections on polylysine slides which were then stored at – 20^{o}C.

For brains in which TJ proteins were the focus of the immunohistochemical analysis, they were snap frozen directly by the OCT immersion- dry ice/methanol slurry method described above, after which they were post-fixed in methanol at 4 ^{o}C for 10 min and then stored at -20 ^{o}C.

2.3.6 Tissue Preparation and Vibratome sectioning

Mouse brain tissue was fixed in 4 % PFA overnight. Following overnight incubation, tissue was washed in PBS x3 to remove any excess fixative. Tissue was embedded in 40 °C 4 % agarose. Once solidified excess agarose was trimmed away and agarose block was glued to the metal plate of the vibratome. 200μm sections were cut and placed into a PBS filled 12 well plate. To stain, the PBS was replaced with Dapi (1:5,000; Hoescht; diluted in 1X PBS) for 2 min at RT, followed by 3 x 5 min 1X PBS washes. Sections were then placed onto polylysine adhesion slides (Thermo Scientific) and a coverslip was mounted using Aqua poly/mount (Polysciences, Inc). Vibratome sections were examined and images taken using the Olympus microscope using the cell sense software.

2.3.7 Immunohistochemistry

Mouse brain cryosections (12 μm thick) were warmed to RT for 30 min prior to staining. Mouse brain sections were encircled with a PAP pen, rinsed with PBS and then blocked and permeabilised with block buffer (5 % NGS, 0.5 % Triton X-100 in 1X PBS) for 1hr at RT. Blocking buffer was removed and sections were incubated with primary antibodies at 4°C overnight (Table 2.5). After overnight incubation, slides were washed 3 times for 5 min in 1X PBS and then incubated with fluorescently labelled secondary antibodies for 2 hr at RT (Table 2.6). Subsequently, slides were washed 3 times for 5 min in 1X PBS, after which the slides were counterstained with Dapi (1:5,000; Hoescht 33258; in 1X PBS) for 1 min at RT. Slides were then washed 3 more times in 1X PBS**,** dried and a coverslip was mounted using Aqua polymount (Polysciences, Inc). Images were taken using the Zeiss LSM 710 confocal laser scanning microscope.

Primary Antibody	Dilution	Supplier
Rat anti-CD31	1:100	BD Biosciences
Mouse anti-GFAP	1:200	Sigma
Rabbit anti-IBA1	1:200	Wako (019-19741)
Rabbit anti-NeuN	1:200	Abcam (ab177487)
Rabbit anti-Cldn5	1:250	Invitrogen
Secondary Antibody	**Dilution**	**Supplier**
Goat anti-rabbit Cy3	1:500	Abcam (ab6939)
Goat anti-mouse Cy3	1:500	Invitrogen (A10521)
Goat anti-rat Cy3	1:500	Abcam (ab150160
Goat anti-rabbit Alexa flour 488	1:500	Invitrogen
Goat anti-mouse Alexa flour 488	1:500	Biosciences (A11001)

Table 2.5. Primary and Secondary antibodies used for Immunohistochemical analysis. Dilutions were made up in 1 % NGS.

Isolectin-IB4 Alexa Fluor 488 or Isolectin-IB4 Alexa Fluor 596 was used at a dilution of 1:200 to stain blood vessels in the brain. To stain for Sulfo NHS-Biotin, sections were incubated with Cy3-conjugated streptavidin at a 1:200 dilution overnight at 4°C.

2.3.8 Image Acquisition and Analysis

All immunohistochemistry images were obtained using the ZEN Black Edition (Zeiss) software and a Zeiss LSM 710 confocal laser scanning microscope. Acquisition settings, such as laser intensity, gain and pinhole diameter were each kept identical within experiments for each combination of staining carried out. Images were exported as .czi files and imported into ImageJ (National Institutes of Health, Rockville, MD, USA) using the BioFormats plugin.

To quantify changes in gene expression, the pixel intensity threshold was set across all images and integrated pixel intensity values between the control and treated groups were compared. Quantification was expressed as integrated density/expressing the data as integrated pixel intensity fold change.

2.3.9 Enzyme-linked immunosorbent assay (ELISA)

Following the blood extraction using the submandibular puncture method described in section 2.2.8, samples were allowed to clot for 30 mins at RT prior to centrifugation for 20 min at 1000x g. The serum fraction was then collected and aliquoted and stored at -80 °C until required for assays.

Serum S100β levels were quantified using the Mouse S100β (protein S100β) Elisa Kit (AssayGenie) as per the manufacturer's instructions. All reagent and standard preparation was carried out according to the manufacturing instructions. S100β standards were prepared by using the stock solution at 5000 pg/ml and performing serial 2-fold dilutions of this stock using sample dilution buffer. The plates were precoated, removing the necessity of overnight incubation of the capture antibody. Test samples were diluted 1/2 with sample dilution buffer. The plate was washed twice with the kit's wash buffer before beginning. Excess wash buffer was removed by shaking over a sink and blotting against paper towels, which was carried out following every wash step in this protocol. 100 µl of each standard and sample was added to the designated well of the 96 well plate, recording their positions on the 96 well plate. The plate was sealed with a cover and incubated at 37 °C for 90 min. Following this incubation the cover was removed, the liquid aspirated from the plate and the plate washed twice with the wash buffer. Without touching the sides of the well, 100 µl of biotin-labelled antibody working solution was added to the bottom of each well. The plate was then resealed with a new cover and incubated at 37 °C for 60 min. After this, the cover was removed and the plate was washed 3 times with the wash buffer. 100 µl of SABC working solution was then added to each well, the plate was covered and incubated at 37 °C for 30 mins. Following this incubation, the plate was washed 5 times with wash buffer. 90 µl of tetramethylbenzidine (TMB) substrate was then added to each well, the plate was again covered and incubated at 37° C for 20 min in the dark. Once a strong blue colour developed in the most concentrated standard wells, while the less concentrated wells showed a much weaker colour change, the reaction was terminated by adding 50 µl of stop solution into each well and mixing it thoroughly. The colour should immediately change from blue to yellow. The O.D. absorbance was measured immediately on the Multiskan™ FC Microplate Photometer (ThermoScientific) at 450 nm. Values were blank corrected using blank control standard and pg/ml concentrations were determined using a standard

curve. Analysis was performed in GraphPad Prism 9.0, using 4-parameter logistic (4PL) non-linear regression to generate the standard curve utilised for concentration interpolation.

2.3.10 Statistical Analysis

All statistical analyses were performed in GraphPad Prism 9.4. Two-group data were analysed by two-sided unpaired t-test, experiments with greater than two groups were analysed by one or two-way ANOVA, with post-tests for multiple comparisons as indicated in figure legends. Correlations were evaluated with Pearson's correlation coefficient. Survival analysis was analysed using a Log-rank (Mantel-Cox) test to compare the survival distribution between treatment groups. In all cases, $p < 0.05$ was considered significant, and error bars are presented as the standard error of the mean.

2.4 Behavioural Assays

2.4.1 General information and test schedule

To prevent any behavioural outputs that were caused by stress or anxiety, mice were habituated to both the investigator and the testing room, by being brought into the room and handled for approximately 5 min per day for 1 week prior to the behavioural testing. Except where stated, mice had free access to food and water throughout the testing schedule. Before each trial, mice were taken from their holding room to the testing room approximately 30 min before testing began to allow them to habituate to their surroundings. All behavioural experiments were performed during the light phase and all apparatus cleaned with 70 % ethanol before use and between trials, except where stated. Statistical analysis was carried out using Prism 9.4 for Mac (GraphPad Software, Inc., U.S.A.) and $P < 0.05$ was taken as being statistically significant.

The test schedules for the various groups which underwent behavioural trials:

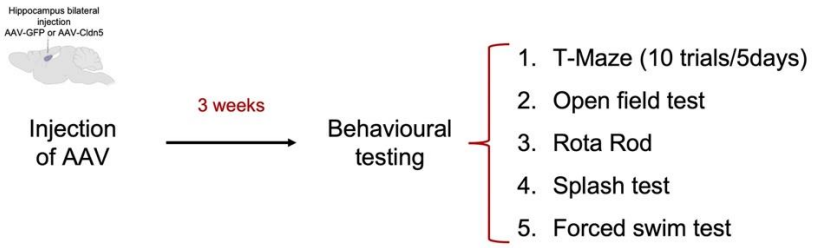

Figure 2.7 Timeline and test schedule for C57BL/6J mice bilaterally intrahippocampally injected with claudin-5 over-expression AAV or relevant GFP control.

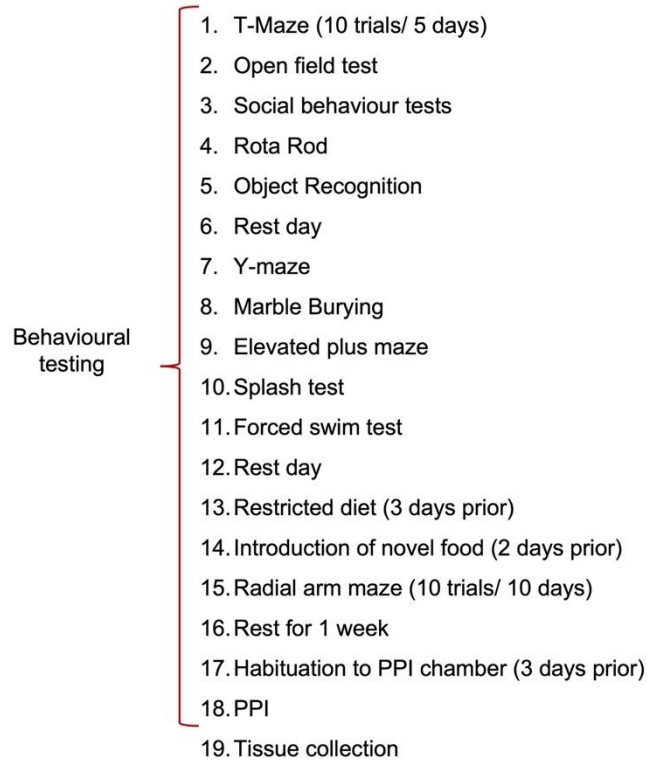

Figure 2.8 Test schedule for the behavioural characterisation of the *Cldn5*$^{fl/wt}$*xTie2Cre* model.

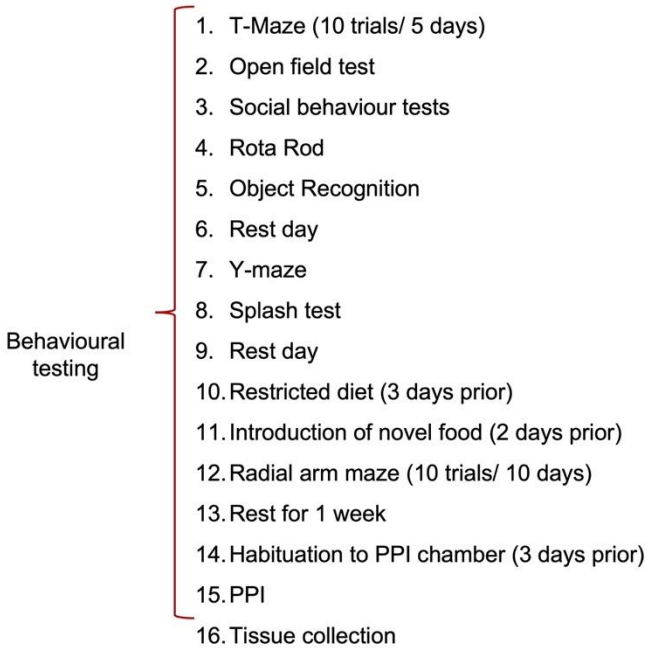

Figure 2.9 Test schedule for the behavioural characterisation of the aged *Cldn5*$^{fl/wt}$*xTie2Cre* model.

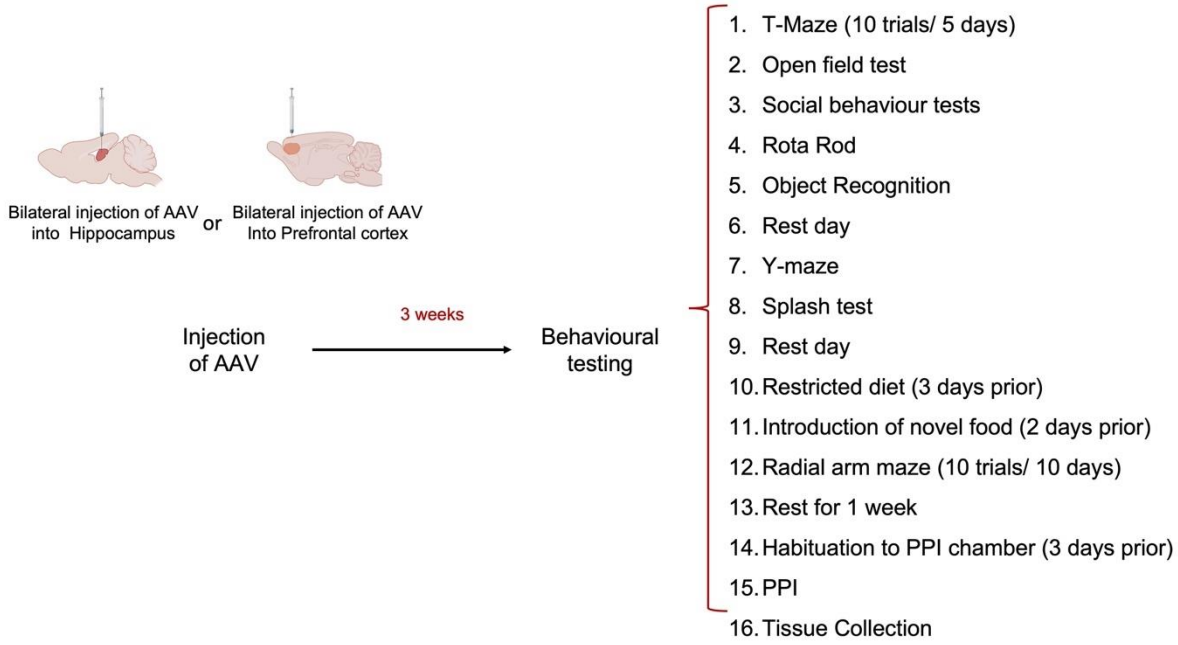

Figure 2.10 Timeline and test schedule for *Cldn5*$^{fl/wt}$*xTie2Cre* mice bilaterally injected into the hippocampus or PFC with claudin-5 over-expression AAV or relevant GFP control.

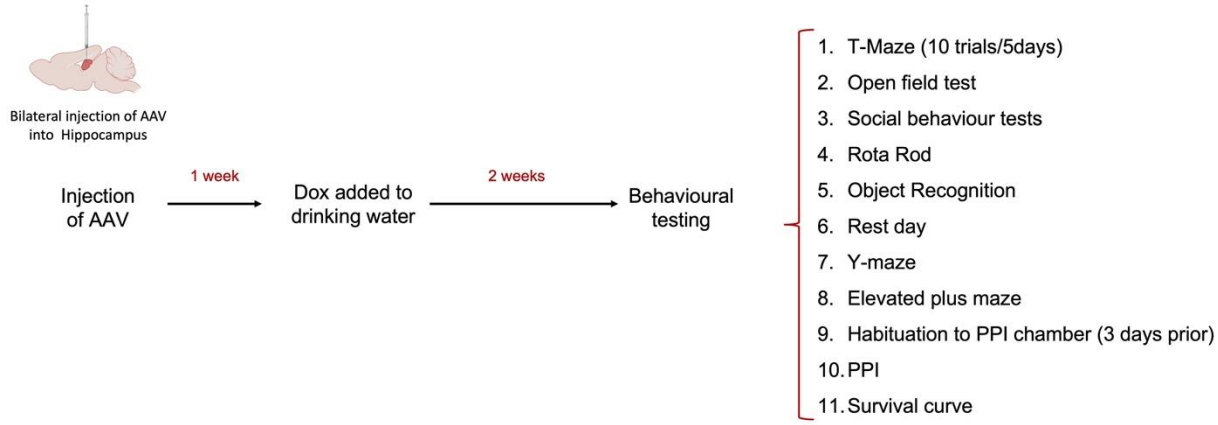

Figure 2.11. Timeline and test schedule for the doxycycline inducible claudin-5 knockdown mouse after a bilateral stereotaxic injection with therapeutic or control AAV.

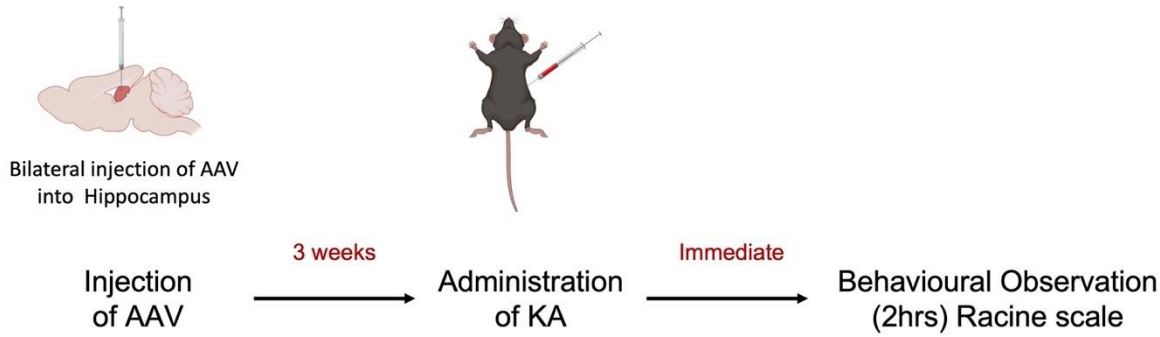

Figure 2.12. Timeline and test schedule for AAV injected C57BL/6J following Kainic acid IP administration

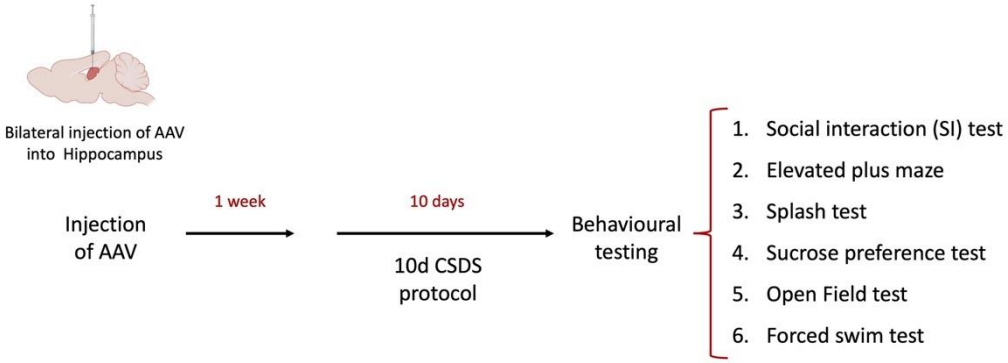

Figure 2.13. Timeline and test schedule for CSDS model injected bilaterally into the hippocampus with therapeutic or control AAV.

2.4.2 T-maze

The alternating T-Maze paradigm (Deacon and Rawlins, 2006) was used to examine working spatial memory. The T-maze, as its name suggests, is an enclosed apparatus in the form of a T (three arms 30 x 10 cm; wall height 20 cm) (Fig. 2.14). No previous habituation to the maze was required as the novelty of the maze is the driving factor for exploration of the maze.

Each mouse underwent 10 sessions with each session comprising of two trials. One session was performed in the morning and another in the afternoon over a 5 day period. Each mouse was placed individually into the base of start arm of the Perspex T-Maze, with a guillotine door that prevents them from accessing the maze. During the first trial in each session, a

Perspex divider was included to encourage the selection of one arm over the other. This central partition is a modification to the apparatus which has enhanced the consistency and reliability of alternation results (Deacon and Rawlins, 2006).

The trial began when the guillotine door in the start arm was removed and a stopwatch was started simultaneously. The clock was stopped when the mouse entered one of the arms. An arm entry was defined as the point when the entire mouse, including its tail, was in the arm. The guillotine door was then placed at the entrance of the arm to stop the mouse from re-entering the start arm. The name of the arm selected (A or B) and the time taken to complete the trial was noted by the experimenter. The guillotine door to the start arm was replaced and the mouse was returned to the start arm for the second trial. Before starting the second trial, the T-maze apparatus was reset, the guillotine door in the arm chosen in the first trial was removed and the central divider between the two choice arms was removed. However, the apparatus was not cleaned between trials, as olfactory cues should be used by the mice to make a choice on this task (Deacon & Rawlins, 2006). The second trial again started when the guillotine door for the start arm was removed and ended when the mouse entered one of the two arms completely, again using a stopwatch to note time taken to complete the task. Both time and the arm entered were again noted. The mouse was then returned to its home cage.

The premise of this experiment is that when 2 trials are carried out in quick succession, the mouse will usually choose the arm not visited before, indicating memory of the first choice, which is defined as “spontaneous alternation”. This behaviour is a reflection on an animals need to explore their environment in order to find any available resources such as food, water, mates or shelter. Importantly, animals do not need to be deprived of these ahead of the experiment to show alternation behaviour, thus being defined as “spontaneous”.

Each mouse was scored for each session using a binary system: 1 for alternating between the arms; and 0 for visiting the same arm twice in a session. The time taken to enter an arm on the second trial of each session was also analysed as a response time. Each experimental group was compared to its relevant control group via unpaired t-tests or one-way ANOVA when greater than two groups were to be analysed.

Figure 2.14. T-maze apparatus

The T-maze apparatus, which consists of 2 arms that form a T shape, utilises spontaneous alternation behaviour to assess short term working memory. Alternate arms are noted as A or B.

2.4.3 Open field test

The open field test provides a unique opportunity to assess a multitude of behaviours, including novel environment exploration, general locomotor activity, and provide an initial examination for anxiety-related behaviour (Bailey and Crawley, 2009).

Mice were placed individually into a Perspex open field arena (30 x 30 x 21 cm) and allowed to freely explore for 10 min (Fig. 2.15). The mice were tracked using a computerised tracking system (ANY-Maze, Version 4.99m, Stoelting Co., U.S.A.) on a Hewlett-Packard ProBook running Windows 8.1. This automatically records a large amount of information for each trial, including distance, average speed, time spent in the two zones (outer perimeter and centre zone) and time spent freezing. The experimenter observing the test also used "hot keys" to record the time spent rearing and grooming during the 10 min test. Each experimental group was compared to its relevant control group via unpaired t-tests or one- or two-way ANOVA when greater than two groups were to be analysed.

Figure 2.15. Open Field Test apparatus

Open field allows for the examination of behaviours such as environment exploration, general locomotor activity, and anxiety-related behaviour.

2.4.4 Social behaviour tests

Crawley's sociability and preference for social novelty protocol was used to examine social behaviour (Kaidanovich-Beilin et al., 2011). The apparatus used was a plastic arena (38 x 43 x 18 cm) divided into three areas by Perspex dividers. The central start zone was empty but circular dome-shaped transparent plastic housing containers (diameter 15 cm; height 9 cm) that had several air holes drilled around their circumference, were placed in the two other zones (Fig. 2.16).

For this protocol, each mouse carried out one session, which was broken down into three distinct trials, habituation trial, social preference trial and social novelty trial. In the habituation trial, mice were placed individually into the central start zone and allowed to freely explore the empty apparatus for 5 min. For the social preference trial, an unfamiliar mouse was firstly placed into one of the two housing containers. The mouse being tested was then placed in the start zone and allowed to explore the apparatus freely for 10 min. Before starting the social novelty trial, another unfamiliar mouse was then placed into the

previously empty housing container. The apparatus now contains two occupied housing containers, one containing a familiar mouse from the social preference trial and the other containing a novel mouse. As with the previous trial, for the social novelty trial, the mouse being tested was placed in the start zone and allowed to explore the apparatus for 10 min. At the end of the session, all mice were returned to their respective home cages. Before all trials the apparatus was cleaned with 70 % ethanol. In the social preference and social novelty trials, the mice were tracked using a computerised tracking system (ANY- Maze, Version 4.99m, Stoelting Co., U.S.A.) on a Hewlett-Packard ProBook running Windows 8.1.

The specificity in the design of this experiment is in the subject mouse having complete choice in this test. The unfamiliar mice are enclosed in containers so it is only the subject mouse that can move freely. There is no physical contact between the mice, which prevents fighting or any aggressive behaviours but still allows for sensory interactions through sight, sound and smell. These interactions are at the discretion of the subject mouse, which can initiate or terminate any interactions and has complete choice between the unfamiliar mouse versus empty chamber in the social preference trial or between the familiar versus novel mice in the social novelty trial. The time (in seconds) spent in the area around each housing container was noted and a social interaction index was calculated for each trial. For the social preference trial, the social interaction index was calculated as:

$$\text{Social interaction index}_{\text{Preference}} = \frac{\text{Time}_{\text{Mouse}} - \text{Time}_{\text{Empty}}}{\text{Time}_{\text{Mouse}} + \text{Time}_{\text{Empty}}}$$

with $\text{Time}_{\text{Mouse}}$ being the time spent in the zone surrounding the unfamiliar mouse and $\text{Time}_{\text{Empty}}$ being the time spent in the zone surrounding the empty housing container.

For the social novelty trial, the social interaction index was calculated as:

$$\text{Social interaction index}_{\text{Novelty}} = \frac{\text{Time}_{\text{Novel}} - \text{Time}_{\text{Familiar}}}{\text{Time}_{\text{Novel}} + \text{Time}_{\text{Familiar}}}$$

with $Time_{Novel}$ being the time spent in the zone surrounding the novel mouse and $Time_{Familiar}$ being the time spent in the zone surrounding the familiar mouse from the previous social preference trial.

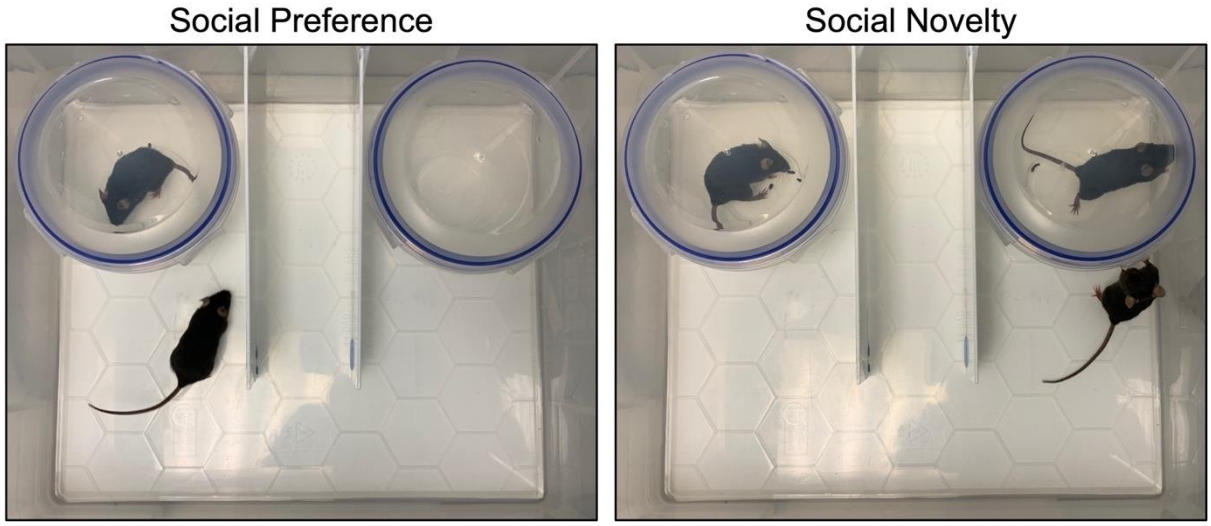

Figure 2.16. Social behaviours test apparatus

(A) Sociability was examined using the social preference task. Mice were free to explore the arena containing one empty cage versus a cage with an unfamiliar mouse. Time taken exploring these two options allows the social interaction index to be calculated. (B) Sociability was further examined using the social novelty task in which mice were free to explore an arena containing a cage with a familiar mouse, from the social preference trial and a cage containing a new unfamiliar mouse.

2.4.5 Rotarod

Motor co-ordination was assessed using the Rotarod (Deacon, 2013). All mice from a singular cage carried out the Rotarod task together to reduce anxiety in performing the trial.

The Rotarod (Ugo Basile, Italy) was started at a constant speed of 4 rotations per min (rpm) and each mouse from the cage was placed on a lane in the Rotarod. Once all the mice were in position, the Rotarod was started and it was set to accelerate from 4 to 60 rpm over a 3 min period. As mice fell from their lane, two measures were noted, firstly the time at which the mouse fell and secondly the acceleration (rpm) at the time at which the mouse fell.

Each experimental group was compared to its relevant control group via an unpaired t-test or one-way ANOVA when greater than two groups were to be analysed. The Rotarod was cleaned with 70 % ethanol between each trial and reset to 4 rpm for the next cage.

2.4.6 Novel Object recognition:

Long-term recognition memory was examined using the novel object recognition task (Leger et al., 2013). This test was carried out in a plastic rectangular arena (38 x 43 x 18 cm). Three Lego structures were used for all mice. While each structure was similarly sized, each was constructed from building blocks of different shapes and colours making them 3 clear and distinct entities, with animals showing no preference for one over the others.

The task consisted of two 3 min sessions:

1. The Familiarisation session: Two objects were positioned at two fixed locations within the testing arena.
2. The Test session: One of the objects from the familiarisation session was positioned in the same location as before (familiar object) and the second object is replaced with a third object (novel object).

Before starting the trial, the test mouse was placed in the arena facing the wall and positioned equidistant from the two objects. The timer was immediately started when the mouse left the tunnel. The mice were tracked using a computerised tracking system (ANY-Maze, Version 4.99m, Stoelting Co., U.S.A.) on a Hewlett-Packard ProBook running Windows 8.1, counting the number of nose contacts with each object and time spent around each object (Fig. 2.17).

There was an intersession interval (ISI) of 3 hr, during which time the mouse was returned to its home cage. The arena and all objects were cleaned with 70 % ethanol between all sessions. After Object recognition task was complete, data from the tracking system was analysed and each mouse's performance was examined by calculating their discrimination index during the test session. Discrimination index is calculated as:

$$\text{Discrimination index} = \frac{\text{Nose contacts}_{\text{Novel}} - \text{Nose contacts}_{\text{Familiar}}}{\text{Nose contacts}_{\text{Novel}} + \text{Nose contacts}_{\text{Familiar}}}$$

$\text{Nose contacts}_{\text{Novel}}$ representing the number of nose contacts with the novel object and $\text{Nose contacts}_{\text{Familiar}}$ representing the number of nose contacts with the familiar object from the familiarisation session.

Preference for a novel object corresponds to a positive value in the Discrimination index and negative values are associated with a preference for the familiar object. Values around 0 indicate that the mouse showed no preference for one object over the other. In normal mice, the expected behaviour would be a preference to the novel object. Each experimental group was compared to its relevant control group via an unpaired *t*-test or via ANOVA when greater than two groups were to be analysed.

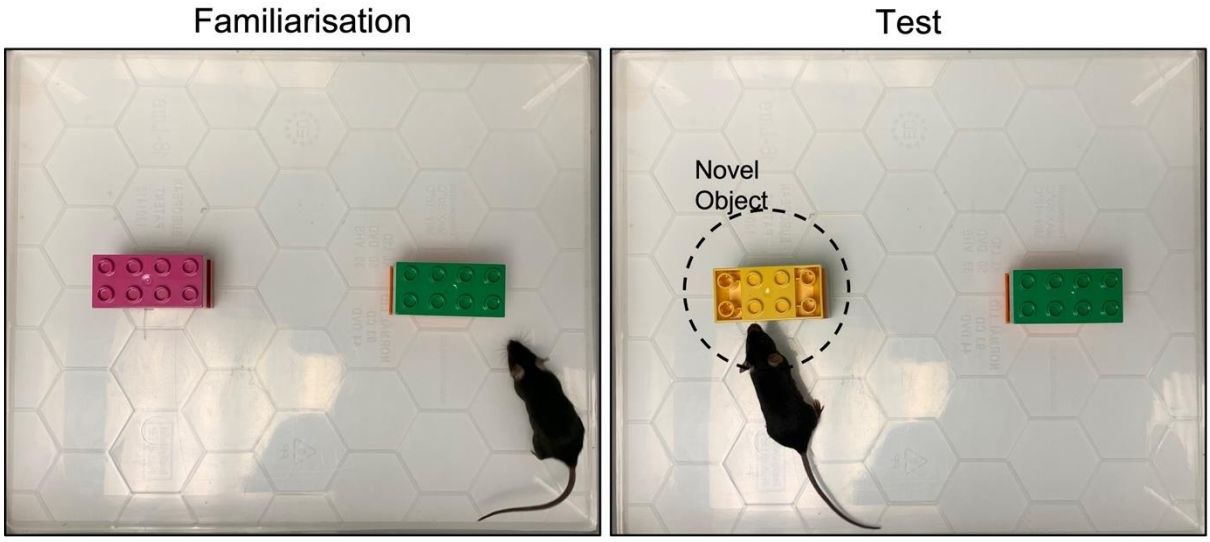

Figure 2.17. Novel object recognition task apparatus

Learning and memory was assayed using the novel object recognition task, which examines long-term, non-spatial recognition memory over a two-trial test period.

2.4.7 Y-maze

Spontaneous alternation on a Y-Maze was used to examine working spatial memory (Maurice et al., 1994, Kraeuter et al., 2019). Mice were placed individually in the centre zone of a Perspex Y- Maze (three 30 x 5 cm joined by a 20 cm diameter central area; bounded by wall 15 cm high) and allowed to freely explore the apparatus for 8 min (Fig. 2.18).

Arm entries were counted both by the experimenter as well as being logged by a computerised tracking system (ANY-Maze, Version 4.99m, Stoelting Co., U.S.A.) on a Hewlett-Packard ProBook running Windows 8.1. An arm entry was defined as all four paws entering into an arm, which are clearly defined by the slots which support the guillotine

doors that can be used with this apparatus. Arm entries was recorded in the order in which they occurred. Spontaneous alternation was assessed after the experiment was over; a successful alternation being defined as the mouse entering all three arms of the Y-Maze over any 4-arm entry span (e.g. if the mouse entered the arms in the order 1, 3, 1, 3, 2, 3 then it would count as two alternations out of a possible three as seen below:

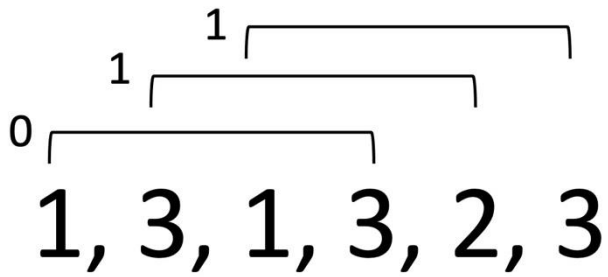

Errors were counted if the mouse exited an arm and then re-entered that arm before entering either of the other two arms. Each experimental group was compared to its relevant control group via an unpaired *t*-test or via one or two-way ANOVA when greater than two groups were to be analysed.

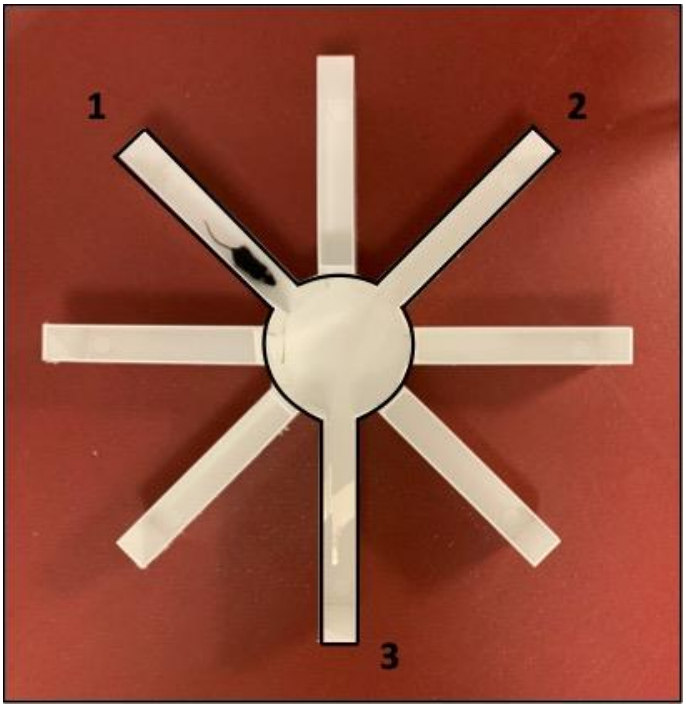

Figure 2.18. Y-maze apparatus with open arms 1-3 noted

The Y-maze apparatus, which consists of 3 arms that form a Y shape, utilises spontaneous alternation behaviour to assess short term working memory.

2.4.8 Marble Burying

Anxiety behaviour was examined using a marble burying assay (Thomas et al., 2009). This task takes advantage of the fact that when under stress, mice exhibit burying behaviour, commonly referred to as "defensive burying", which refers to the animals attempt to displace bedding material in an attempt to cover an object (Pinel and Treit 1978)

A clean cage (27 x 16.5 x 12cm) was prepared by filling it with 4.5cm of clean loose chip bedding followed by gently overlaying 20 glass marbles of the same colour (15mm diameter) in a equidistant arrangement (Fig. 2.19). Mice were free to explore the cage for the full duration of the trial which was 30 min in total. The number of marbles buried, which was defined as greater than 50 % of the marble covered by bedding material, was recorded. Each experimental group was compared to its relevant control group via an unpaired *t*-test.

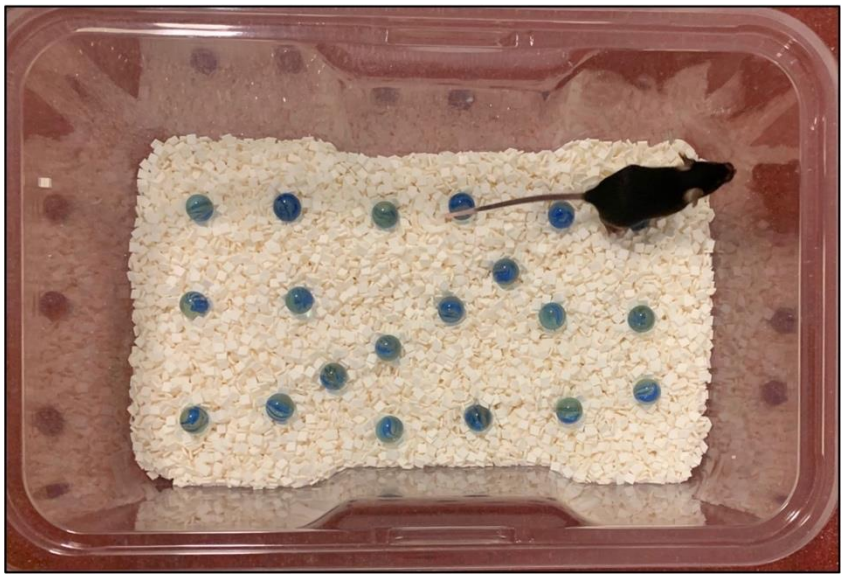

Figure 2.19. Marble burying apparatus

Anxiety and obsessive-compulsive disorder (OCD) like behaviours were examined using the marble burying assay which consists of a clean cage with 20 habituated glass marbles overlaying the bedding.

2.4.9 Elevated plus maze

Anxiety-like behaviour was examined using the elevated plus maze (Komada et al., 2008). The test is based on the balance between natural aversion of mice for open and elevated areas and their natural spontaneous exploratory behaviour when in a novel environment.

Individual mice were placed in the centre zone of a Perspex elevated plus maze (four 30 x 5 cm arms; two open arms and two closed arms with wall height = 20 cm; apparatus raised on Perspex legs to a height of 40 cm) and allowed to freely explore the apparatus for 10 min (Fig. 2.20).

Arm entries were logged by a computerised tracking system (ANY-Maze, Version 4.99m, Stoelting Co., U.S.A.) on a Hewlett-Packard ProBook running Windows 8.1 with the total closed arm entries and open arm entries being taken for analysis.

The open and closed arms are thought to stimulate the same exploratory drive, therefore a noted avoidance of the open arms would indicate a higher level of anxiety in these animals (Rodgers and Dalvi, 1997). Levels of anxiety-like behaviour were analysed by comparing the number of entries into the open arms between the groups. Each experimental group was compared to its relevant control group via an unpaired *t*-test or via one-way ANOVA when greater than two groups were to be analysed.

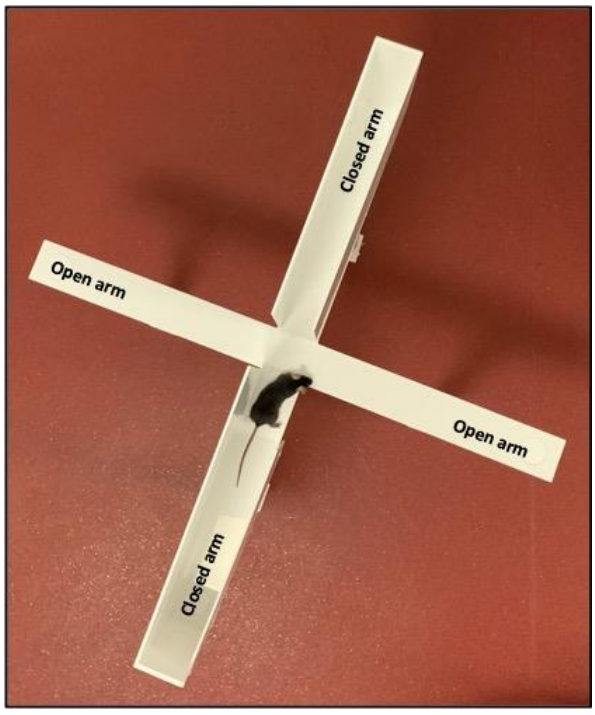

Figure 2.20. The elevated plus maze apparatus

Anxiety-related behaviour was assessed using this apparatus which consists of an elevated 4-armed maze containing two open and two closed arms.

2.4.10 Splash test

Induced grooming behaviour was examined through the splash test (Yalcin et al., 2005). The trial was conducted for each mouse individually in their home cage, with their cage mates stored temporarily in a separate cage. The mouse was sprayed on its dorsal side with a 10 % sucrose solution and a 5 min timer was started. At the end of the trial, the mouse was moved to the temporary holding cage with its cage mates and the next mouse was placed in the home cage for the splash test.

Video recordings were made of the entire trial, including the spraying procedure. The videos were then analysed by an experimenter who was blind to the experimental condition looking at two measures. Firstly, latency to begin grooming was measured. This is the time (seconds) taken for the mouse to initiate any form of grooming behaviour. Secondly, the total grooming time was calculated, the total time (seconds) that the mouse engaged in any form of grooming behaviour. Each experimental group was compared to its relevant control group via an unpaired *t*- test or via one or two-way ANOVA when greater than two groups were to be analysed.

2.4.11 Forced swim test

Depression-like behaviour was assessed using the forced swim test (Can et al., 2012). A large transparent plastic beaker (diameter 17 cm; height 21 cm) was filled with lukewarm water (20-21 °C). The water level was 15cm from the bottom and marked on the beaker, to ensure water levels were kept consistent across all mice in the experiment. These dimensions were selected as mice were not able to touch the bottom of the tank with their feet or tails, nor were they able to escape from the tank. This apparatus set up thus renders a situation in which "behavioural despair" is induced, in which the animal loses hope to escape the stressful environment.

Mice were very slowly placed individually into the water and a timer was started the moment the mouse's tail was released. Mice were allowed to swim for 6 min and then were lifted from the water and dried off with paper towel. To prevent hypothermia, mice were then placed under a heating lamp to fully dry before being returned to the home cage.

The whole trial, from the start when the mouse is gently placed into the apparatus until the completion of the 6 min swimming period were video recorded. The videos were then analysed by an experimenter who was blind to the experimental condition, recording the total time (in seconds) each mouse spent engaged in escape behaviour during the final 4 min of the swimming period. Only the last 4 min of the trial are analysed as most mice are very active at the start of this trial, which can obscure potential differences between treatment groups (Can et al., 2012). Additionally, specific criterion regarding escape behaviour must be set out before analysing video data. Mice readily float in water with some small movement to maintain balance and keep their heads above the water level, these movements as well as momentum from previous escape behaviour attempts should not be counted as genuine escape behaviour.

Time spent engaged in escape behaviour was subtracted from the total time (240 seconds) to give the time spent immobile. Each experimental group was compared to its relevant control group via an unpaired *t*-test or via one or two-way ANOVA when greater than two groups were to be analysed.

2.4.12 Radial arm maze

Both working and reference memory were examined using the 8-armed radial arm maze (Crusio et al., 1993). Mice were placed on a restricted diet for three days prior to the start of the test and remained on this diet until all testing was complete to encourage the pursuit of the food rewards. Each mouse was weighed before the start of the restriction, and weight was monitored throughout the trial, ensuring mice maintained approximately 90 % of its free-feeding weight throughout. Adding small chow pieces inside the cage rather than large pieces in the hopper, ensures that firstly, one animal cannot monopolise the food but also ensures ease of access, as without the normal weight of the diet pinning down the ration, animals can often have difficulty eating from the hopper (Deacon and Rawlins 2006).

Mice were familiarised with the food reward (chocolate flavoured cereal, Aldi, Ireland) for two days before the test by introducing a small amount into their cage. Habituating the mice to the taste of the reward eliminates hyponeophagia, as mice are wary of eating anything new or while in a novel environment. The standard radial arm maze protocol consisted of one trial per day over 10 days. Mice were habituated to the Perspex radial arm maze (eight 30 x 5 cm joined by a 20 cm diameter central area; bounded by wall 15 cm high) one day

before testing. Mice were placed in the maze with their cage mates and allowed to freely explore the apparatus in groups for 5 min. Habituation to the maze in groups was done to minimise any anxiety effects that may affect learning in the radial arm maze.

On test days, the radial arm maze was baited with four food rewards. These were each placed into four of the eight arms, leaving four empty arms. Baited arms were pseudorandomly assigned for each mouse before the experiment started. The food rewards were put into recessed food wells so that mice could not see whether a food reward was present or not until they had travelled down the arm to directly check the well. The radial arm maze was cleaned with 70 % ethanol between all trials as well as after the food rewards had been added to minimise olfactory cues.

For each trial, mice were individually placed in the central start zone of the radial arm maze and allowed to explore the maze until they had consumed all four of the food rewards or until the trial had run for 15 min (Fig. 2.21). At the end of the trial, mice were returned to their home cage. All trials were recorded using the computerised tracking system ANY-Maze (Version 4.99m, Stoelting Co., U.S.A. on a Hewlett-Packard ProBook running Windows 8.1) with the number of arm entries, average speed and trial duration being measured. Working memory errors were noted when a mouse entered an arm that it had already entered during that trial. Reference memory errors were noted when a mouse entered an arm that does not contain a food reward. The first two trials were considered as training trials and were not included in the statistical analysis of the task (Crusio et al., 1993). Each experimental group was compared to its relevant control group via repeated measures ANOVAs for data obtain over the total experiment. Some measures were analysed on a trial-by-trial basis via unpaired t-test.

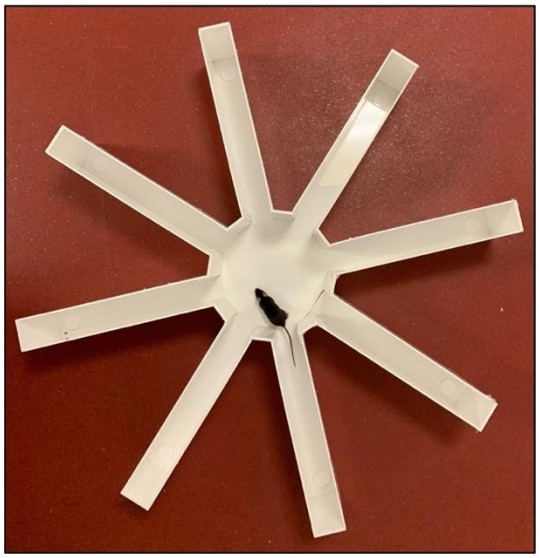

Figure 2.21. The radial arm maze apparatus

Both short and long-term memory can be examined using the radial arm maze, which consists of 8 potentially baited arms.

2.4.13 Pre-pulse inhibition (PPI) of the acoustic startle response

Sensorimotor gating was examined by prepulse inhibition (PPI) of the acoustic startle response. The PPI apparatus consisted of a soundproof PPI chamber with a weighing scale positioned in the centre of the chamber beside a loudspeaker. Mice were individually contained in a holding chamber which was placed on the scale.

Each mouse was given two days to habituate to the PPI apparatus, by being placed in the holding chamber within the soundproof PPI chamber for 10 min each day with a constant white noise background, 65 decibels (dB). Before the beginning of the experiment, all instruments were calibrated and startle stimulus (71, 77, 83, 100, 110, 120 dB) were set. The animal holding chamber was cleaned with 70 % ethanol between trials and allowed to airdry. PPI was divided into 3 stages. The first stage is a 2 min habituation with a constant white noise background of 65dB. The next stage is the presentation of random combinations of prepulse (71, 77, 83 dB) and pulse (100, 110 and 120 dB) intensities to habituate the animals to the startle stimulus. Finally, 10 blocks of random combinations of prepulse alone, pulse alone, prepulse plus pulse and no stimulus trials are conducted. The startle stimulus were presented as 20ms bursts of white noise with a 100ms interstimulus interval, which is time between production of prepulse and pulse stimuli.

The PPI program was written in MATLAB and the sound files were generated in Microsoft Visual Studios. Raw data was exported from MATLAB to Excel. Excel files for each block were then loaded into MATLAB and the data were averaged across the 10 blocks for each prepulse, pulse, prepulse plus pulse and no stimulus trial and PPI was calculated as:

$$\%PPI = 100\ x \quad \frac{pulse - (prepulse + pulse)}{pulse\ alone}$$

2.4.14 Social interaction (SI) test

SI testing was carried out under red-light conditions (Golden et al., 2011; Hodes et al., 2014). SI testing is broken into 2 trials, each lasting 2.5 min. The first trial is without the aggressive mouse (AGG) present. To begin the trial mice were placed in a Plexiglas open-field arena (42 cm × 42 cm × 42 cm, Nationwide Plastics), which contained a small empty wire animal cage at one end of the arena. All movement was monitored and recorded automatically using a tracking system Ethovision 11.0 Noldus Information Technology). This measures both locomotion and the exploratory behaviour of the mouse and provides a baseline behaviour for comparison. After this trial, the animal is removed from the open field arena and the arena is cleaned with 70 % ethanol. A novel social target, the AGG, is placed into the wire animal cage that is located within the open field. Next the mouse under observation is placed back into the arena and its exploratory behaviour is again monitored and recorded, with the time spent in the interaction and corner zones and the overall locomotion being compared to the first trial. The SI ratio is calculated by dividing the time spent in the interaction zone when the AGG is present by the time spent in the interaction zone when the AGG is absent. Mice that have an SI ratio below 1 are designated as stress-susceptible (SS) and mice that have an SI ration above 1 are noted to be resilient (RES). The SI ratio was calculated as:

$$\text{SI ratio} = \frac{\text{Time in interaction zone (AGG } \mathbf{present}\text{)}}{\text{Time in interaction zone (AGG } \mathbf{absent}\text{)}}$$

2.4.15 Sucrose preference test:

Anhedonia describes the inability to experience pleasure from rewarding activities and is a hallmark symptom of depression. Anhedonia is evaluated in mice using the sucrose preference task. In this assay, the water bottle from the home cage was removed and replaced with two 50-mL conical tubes with sipper tops filled with normal water for a 24h habituation period. Next, the water in one of the 50-mL conical tubes was replaced with a 1 % sucrose solution. Both tubes were weighed, and mice were allowed to drink *ad libitum* for a 24 hr period. After the 24 hr assay, tubes were reweighed and switched. Mice were allowed to drink *ad libitum* for another 24 hr period, which avoids place preference from affecting the results. After the completion of the 48 hr assay period, both tubes were reweighed. Sucrose preference was calculated by dividing the total amount of sucrose consumed by the total amount of fluid consumed over the 48 hr period of sucrose availability. Anhedonia is defined as a reduction in sucrose preference ratio relative to a control group in the preference test. Sucrose preference can be calculated as:

$$\text{Sucrose preference} = \frac{\text{Volume of sucrose consumed}}{\text{Total volume of fluid consumed}}$$

2.4.16 CSDS model

The CSDS protocol requires both the aggressor mouse as well as the mouse under investigation. CD-1 mice are used as the aggressor and were screened for aggressive behaviour during inter-male social interaction for 3 consecutive days utilising criteria describe in depth in Golden et al, 2011 and Golden et al.,2016. The CD-1 aggressor (AGG) was housed on one side of the clear perforated Plexiglas divider (0.6 cm × 45.7 cm × 15.2 cm, Nationwide Plastics) in the social defeat cage (26.7 cm width × 48.3 cm depth × 15.2 cm height, Allentown Inc) 24 hr before the start of the social defeat protocol. The mice under investigation were C57BL/6 J mice, and were subjected to physical interactions with an unfamiliar AGG for a 10 min period once a day for 10 consecutive days. After every social defeat interaction the experimental mouse is moved and house in the opposite side of the social defeat cage divider for the next 24 hr period. This allows for sensory contact between the experimental mouse and the AGG mouse without any physical interaction. Unstressed control mice were housed 2 per cage, one on

either side of the social defeat cage divider and rotated each day, but are not exposed to the AGG mice. After the 10 day protocol, following the last social defeat session, experimental mice are housed singularly for 24 hr before undergoing the social interaction test to identify if they are susceptible or resilient (Hodes at al., 2014; Golden et al., 2011).

Chapter 3. Characterisation of the *Cldn5$^{fl/wt}$xTie2Cre* mice

3.1 Introduction:

3.1.1 Animal models of disease

Animal models of disease are a valuable preclinical tool with which to investigate the pathophysiology of diseases and associated mechanisms of injury, for the identification of potential drug targets as well as to evaluate novel therapeutics for their safety profile, their pharmacokinetics and pharmacodynamics and importantly their efficacy *in vivo* (Singh et al., 2021; McGonigle and Ruggeri., 2014).

Animal models of disease offer a more rapid platform to monitor disease progression in comparison to humans. Moreover despite the advent of non-invasive technologies to study the human brain's structure and function, the ability to examine certain details of the physiology and molecular biology as it relates to disease remains significantly limited. The use of animal models provides the ability to invasively investigate the underlying structural and molecular changes that are caused by the disease and test novel therapeutics, in a way that would be unethical with human patients (Winship et al., 2019). Moreover, safety and efficacy parameters established in animal models are an essential step during the initial phases of drug development, the results of which may determine the drugs approval for translation into human clinical trials and may also help to predict the clinical outcomes (Singh & Seed., 2021).

However, modelling human neuropsychiatric disorders in animals is an extremely challenging task, due to the subjective nature of many key symptoms, the lack of biomarkers and objective diagnostic tests as well as the unknown underlying genetics (Jones et al., 2011; Nestler 2010). Therefore, to be established as a strong model of a disease, there are three criteria all models must meet in order to be a good representative of a certain disease model. Firstly, construct validity refers to how the method utilised to develop the model relates to the natural development of the disease. For Mendelian disorders, caused by a single gene mutation, this would be as simple as knocking out the gene of interest to simply recapitulate the molecular etiological process in mice. However, most neurological disorders have complex genetic architecture with no single disease-causing genes established. Secondly, face validity describes the model's ability to mimic the anatomical, neuropathological and behavioural features that are noted in the human disease. Finally,

predictive validity represents the models ability to respond to treatments in a manner that may predict the treatment efficacy in patients. In regard to neuropsychiatric disorders however this final validity is limited, as the assays developed to measure efficacy were designed to identify drugs that acted similarly to those found serendipitously, rather than being validated by an accurate pathophysiological model (Jones et al., 2011). Therefore current animal models have significant limitations, that range from weak validation to poor predictive power for therapeutic efficacy in human clinical trials. But their value in further elucidating the underlying mechanisms of neurological disorders cannot be undervalued, as progress in understanding pathophysiology are still highly dependent on specific animal models of disease.

While neuropsychiatric disorders like schizophrenia and neurological disorders like epilepsy have complex genetic architecture and environmental influences, animal models with single gene manipulations are unlikely to replicate the full syndrome. However, this approach is designed to characterise the relationship between individual genes and the underlying pathophysiology and specific endophenotypes of the disorder and may help to identify potential biomarkers that have therapeutic relevance.

Claudin-5, is our major gene of interest. Claudin-5 is located within the region of chromosome deleted in 22q11DS, individuals with a substantially increased risk of developing schizophrenia and psychosis. Furthermore, as recently reported by Greene et al., claudin-5 protein levels are significantly disrupted in surgically resected tissue from patients with temporal lobe epilepsy, with the tissue showing a decrease in the both the pattern and intensity of claudin-5 staining relative to the endothelial cell marker cluster of differentiation 31 (CD31) (Greene et al., 2022). Claudin-5, is the most highly expressed TJ component at the BBB, present at greater levels than other claudins and tight junction components. Single-cell RNA sequencing results conclude that there are over 10,000 *Cldn5* mRNA transcripts per cell in brain capillaries, which is ~10- fold more than the number of the housekeeper beta actin transcripts (Daneman et al., 2010; Vanlandewijck et al., 2018). Overall, this indicates claudin-5 plays a vital role in BBB maintenance. Moreover, the BBB itself plays a vital role in protecting the brain while maintaining the optimum microenvironment for neuronal signalling. BBB disruption is a hallmark pathology in numerous neurological disorders, with the degree of disruption often demonstrating clear correlation with the severity of the disorder, as is seen in epilepsy, where seizure severity

often correlates with the extent of BBB disruption (van Vliet et al, 2015). Therefore, claudin-5 seems to be an important gene to target, to characterise its relationship with BBB function and the underlying pathophysiology and endophenotypes that result from its disruption.

A full claudin-5 knockout (KO) mouse model has already been investigated by Nitta et al. The development and morphology of blood vessels in these claudin-5 deficit mice was normal. However, a size selective loosening of the BBB, for molecules that were less than 800 Da was noted through tracer experiments, as well as through dynamic contrast-enhanced magnetic resonance imaging (DCE-MRI) analysis (Nitta et al., 2003). Therefore, claudin-5 shows promising potential as a therapeutic target to regulate the permeability of the BBB and therefore may be key in the development of new gene therapy-based approaches for disorders with noted BBB disruption. However, in the Nitta et al investigation, the claudin-5 KO mice all died within 10 hr of birth. Therefore, to further investigate the effect of reduced claudin-5 expression in the brain and how this may relate to neurological disorders, a new claudin-5 heterozygote model was established, the *Cldn5*$^{fl/wt}$*xTie2Cre* mouse model.

3.1.2 The *Cldn5*$^{fl/wt}$*xTie2Cre* mouse model:

The *Cldn5*-LoxP mice was acquired from the Betsholtz Lab at the Uppsala University in Sweden. The *Cldn5*-LoxP mouse has loxP inserts flanking the claudin-5 gene. This mouse is effectively wild-type in the absence of Cre. The *Cldn5*-LoxP mice were then crossed with another strain, the Tie2Cre mice, which express Cre recombinase under the control of the Tie2 endothelial cell specific promoter. This ensures that the activity of the Cre recombinase was found almost exclusively in the ECs of Cre positive mice. This enzyme in combination with the loxP sites forms a recombination system which results in the excision of the DNA found between the loxP sites, which in this model, includes the claudin-5 gene.

The Cre-loxP system, results in constitutive expression. Tie2Cre+; Cldn5$^{fl/wt}$ mice results in claudin-5 heterozygotes, specifically in ECs. This constitutive expression, occurs intracellularly as soon as Cre expression is activated. Therefore these mice develop in a claudin-5 deficient environment.

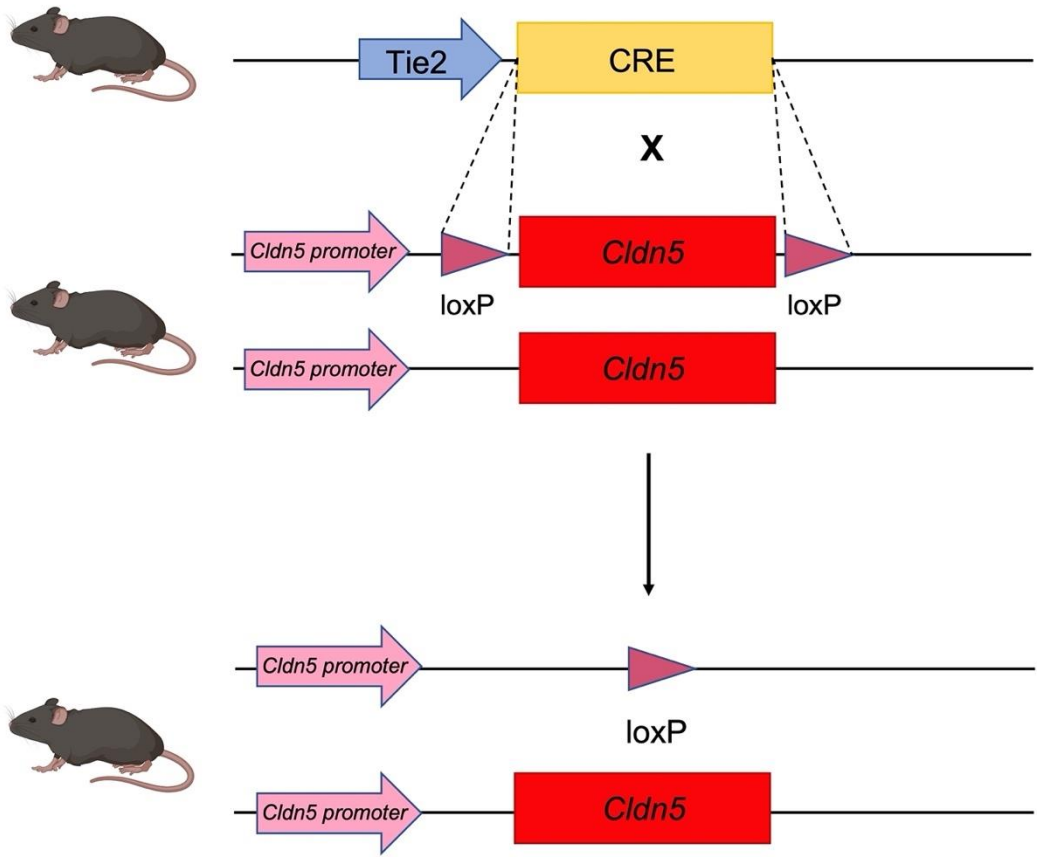

Figure 3.1. The *Cldn5*$^{fl/wt}$*xTie2Cre* mouse model

The *Cldn5*$^{fl/wt}$*xTie2Cre* mouse model was generated by crossing the new *Cldn5*-LoxP mouse with the Tie2Cre mouse. Utilising the loxP system, the cross ensures all Cre positive animals have only one copy of the claudin-5 allele and so produces ~ 50 % less claudin-5 mRNA and protein.

The aim of this chapter is to further characterise claudin-5's relationship with BBB function and the underlying pathophysiology and endophenotypes that result from its disruption.

3.2 Objectives:

- To quantify the level of claudin-5 expression in the *Cldn5*$^{fl/wt}$*xTie2Cre* model
- To determine the physical effects this loss of claudin-5 has on this model.
- To assess how a decrease in claudin-5 expression affects symptomatology through behavioural characterisation.
- To examine the effect of aging on this model.

3.3 Results:

3.3.1 Physical characterisation of *Cldn5$^{fl/wt}$xTie2Cre* mice shows a distinct and significant knockdown of Claudin-5 expression.

Given that a full claudin-5 knockout mouse die before adulthood, to further elucidate the role of claudin-5 in the development of neurological disease, the *Cldn5$^{fl/wt}$xTie2Cre* mouse line was generated. The first aim of this chapter is to physically characterise this model. This was necessary to firstly determine if one chromosomal copy of the *Cldn5* gene was successfully excised by the Cre induced recombination and additionally, to examine if any dosage related effects were observed due to this haploinsufficiency. Examining *Cldn5* mRNA expression levels obtained from microvasculature alone or whole brain samples showed an approximate 50 % loss of claudin-5 expression (Fig. 3.2 A, B). A similar reduction was noted at the protein level using immunohistochemical analysis of isolates microvessels from these mice (Fig. 3.2 C). This loss of claudin-5 did not cause any notable change at a macroscopic level with both the claudin-5 heterozygote *Cre+Cldn5$^{fl/wt}$* mice showing no obvious physical differences compared to the *Cre-Cldn5$^{fl/wt}$* controls (Fig. 3.3).

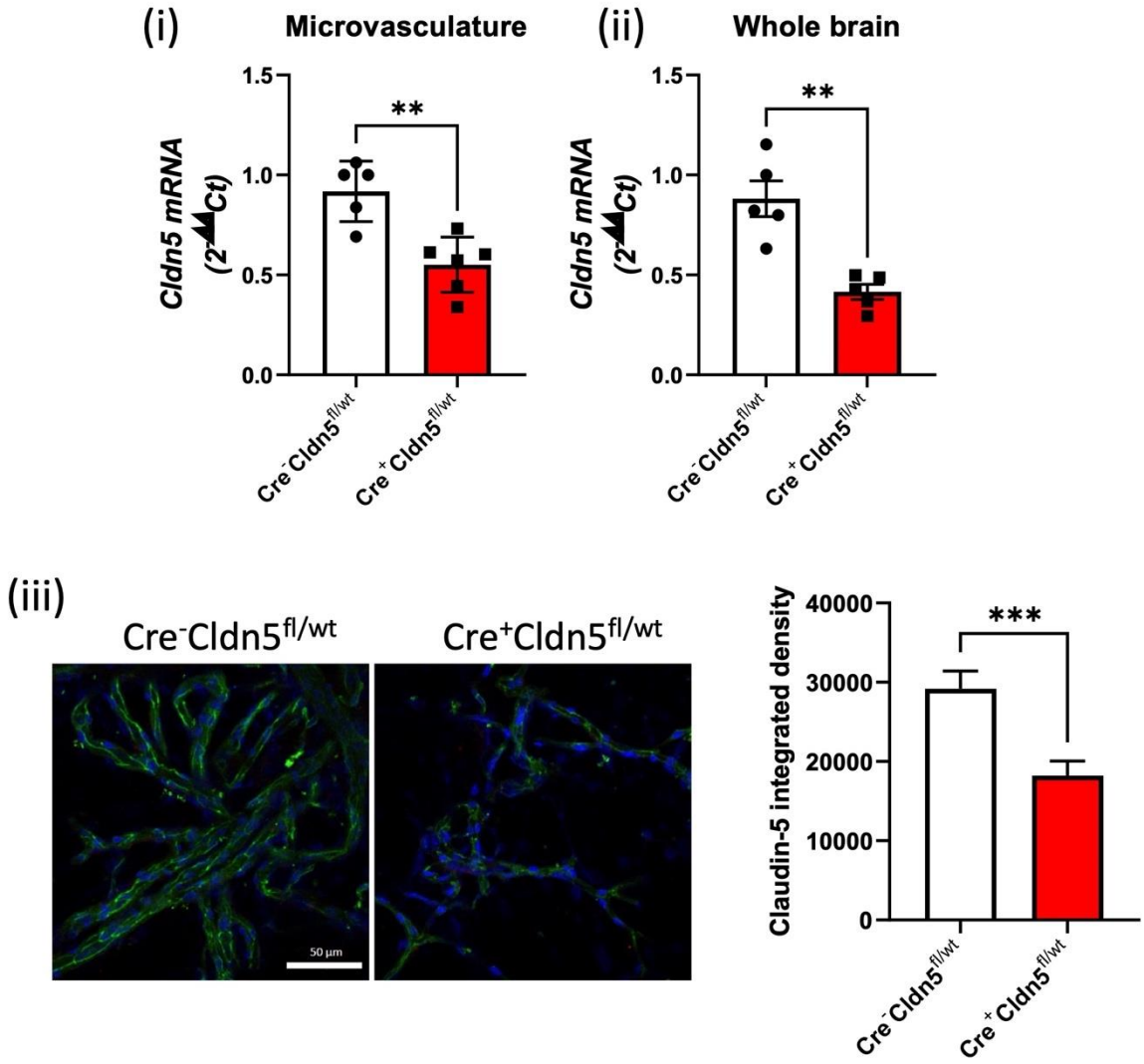

Figure 3.2. Initial physical characterisation of the *Cldn5*$^{fl/wt}$*xTie2Cre* mouse model

Cldn5 transcript levels were significantly decreased in (i) isolated microvasculature (**$p = 0.0023$) and (ii) whole brain (**$p = 0.0014$) of the *Cre+Cldn5*$^{fl/wt}$ mice in comparison to the *Cre-Cldn5*$^{fl/wt}$ controls. (iii) This decrease in claudin-5 expression was also noted through IHC analysis of the microvasculature. All data are means ± SEM; each data point represents one animal. Statistical analysis was carried out using two-sided unpaired t-test. *$p < 0.05$ Scale bar – 50 µm. Work carried out by Dr Chris Greene (Greene et al., 2022).

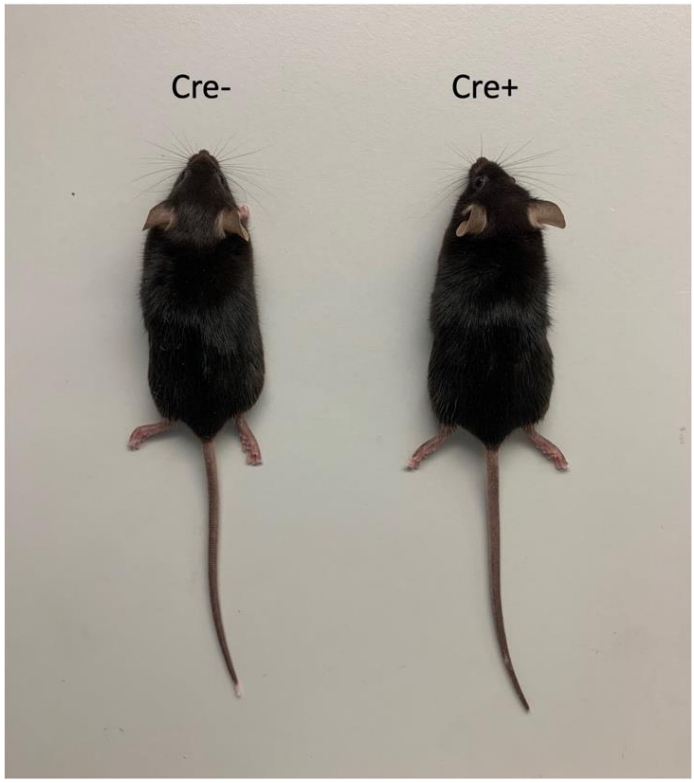

Figure 3.3. No macroscopic differences noted between the claudin-5 heterozygote mice and controls.

Cre+Cldn5$^{fl/wt}$ mice developed normally with no macroscopic differences noted in comparison to their *Cre-Cldn5*$^{fl/wt}$ littermates.

To further characterise this model, with evidence that there is a ~ 50 % reduction in claudin-5 in both the microvasculature and whole brain, specific regions of the brain were then examined. The brain regions chosen were the hippocampus, the PFC and the NAc. The hippocampus, which includes the CA1, CA3 and dentate gyrus (DG), is an easily identifiable area of the brain with distinct morphological properties of small pyramidal neurons in CA1, and large pyramidal neurons in CA3. Due to these clear morphological areas it was possible to examine each region using IHC analysis to examine claudin-5 protein levels in addition to examining the mRNA transcript level of the whole hippocampal structure through RT-PCR analysis. RT-PCR analysis of hippocampal tissue revealed a 50% reduction in *Cldn5* mRNA in the *Cre+Cldn5*$^{fl/wt}$ mice in comparison to the *Cre-Cldn5*$^{fl/wt}$ control littermates (** $p = 0.0022$) (Fig. 3.4). More specifically, IHC analysis of hippocampal subregions revealed a significant reduction in claudin-5 expression in the (iii) dentate gyrus (** $p = 0.0013$) (iv) the CA1 (* $p = 0.0393$) and (v) the CA3 (* $p = 0.0221$) (Fig. 3.4). In addition to the intensity of the claudin-5 (green) staining relative to CD31

(red), the patterning of the claudin-5 staining was discontinuous (Fig.3.4; Fig 3.7). RT-PCR analysis of PFC tissue indicates that the claudin-5 heterozygote *Cre+Cldn5*$^{fl/wt}$ mice express at least 50 % less mRNA in comparison to the *Cre-Cldn5*$^{fl/wt}$ control littermates (**** p = <0.0001). Moreover IHC analysis supported this finding with significant reduction in the level of claudin-5 expression noted within the PFC (** p = 0.0015) (Fig. 3.5). The final region analysed, the NAc, again supported the finding that *Cre+Cldn5*$^{fl/wt}$ mice express over 50 % less mRNA and protein in comparison to the *Cre-Cldn5*$^{fl/wt}$ control littermates (**** p = <0.0001) (Fig. 3.6).

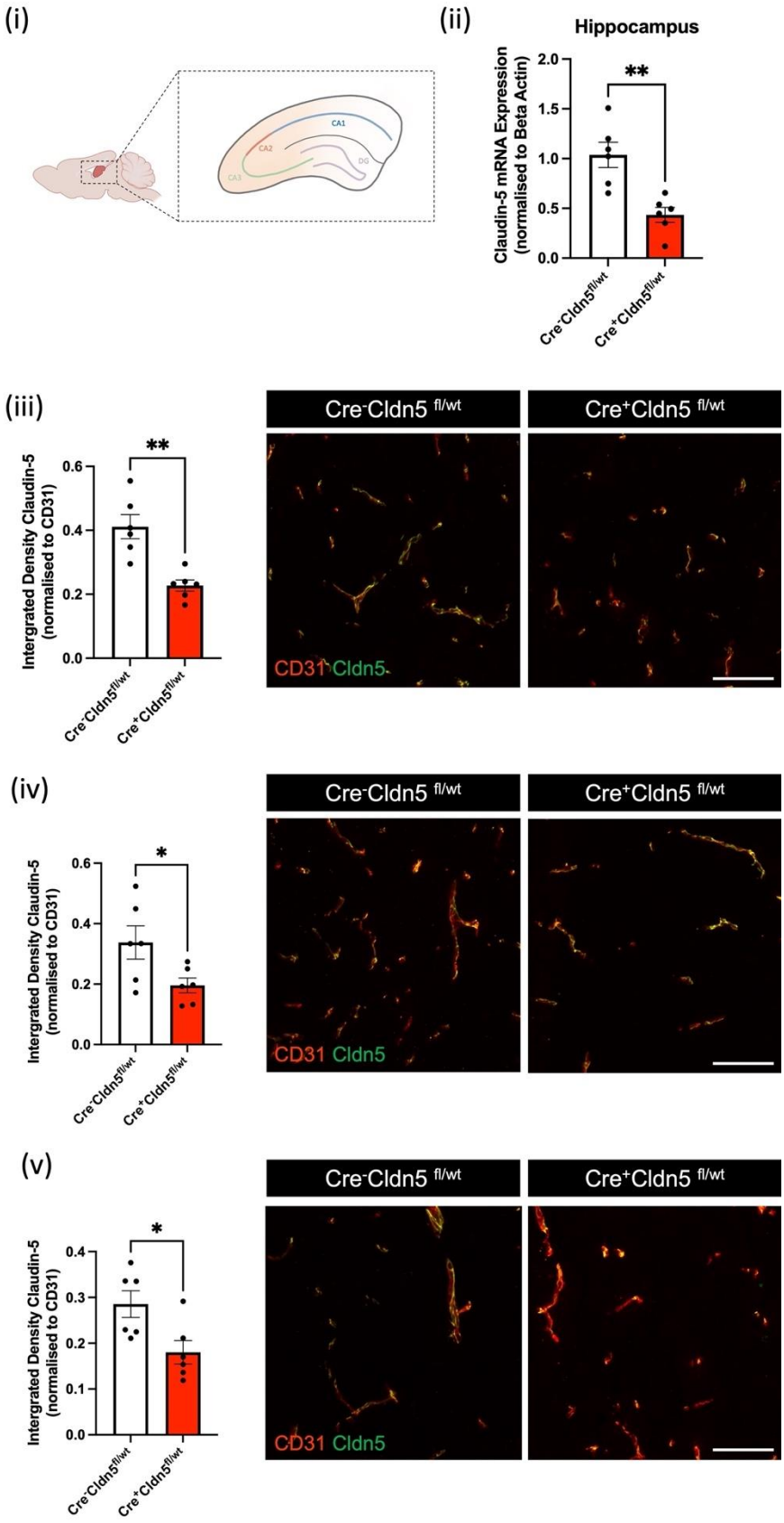

Figure 3.4 RT-PCR and IHC analysis of claudin-5 expression level in the hippocampus.

(i) Schematic of the hippocampus, showing location within the brain and the specific structures within the hippocampus including the dentate gyrus (DG), the CA1 and CA3 regions. (ii) RT-PCR analysis of hippocampal tissue shows *Cre+Cldn5*$^{fl/wt}$ mice express ~ 50 % less mRNA in comparison to the *Cre-Cldn5*$^{fl/wt}$ control littermates (** p = 0.0022). IHC analysis of claudin-5 expression (green) in comparison to CD31 (red) within hippocampal regions show a significant reduction in claudin-5 expression in the (iii) DG (** p = 0.0013) (iv) the CA1 (* p = 0.0393) and (v) the CA3 (** p = 0.0069). A discontinuous staining pattern of claudin-5 is also noted. Scale bar – 100 µm. Statistical analysis was carried out using two-sided unpaired t-test. All data are means ± SEM; each data point represents one animal, n = 6 per group.

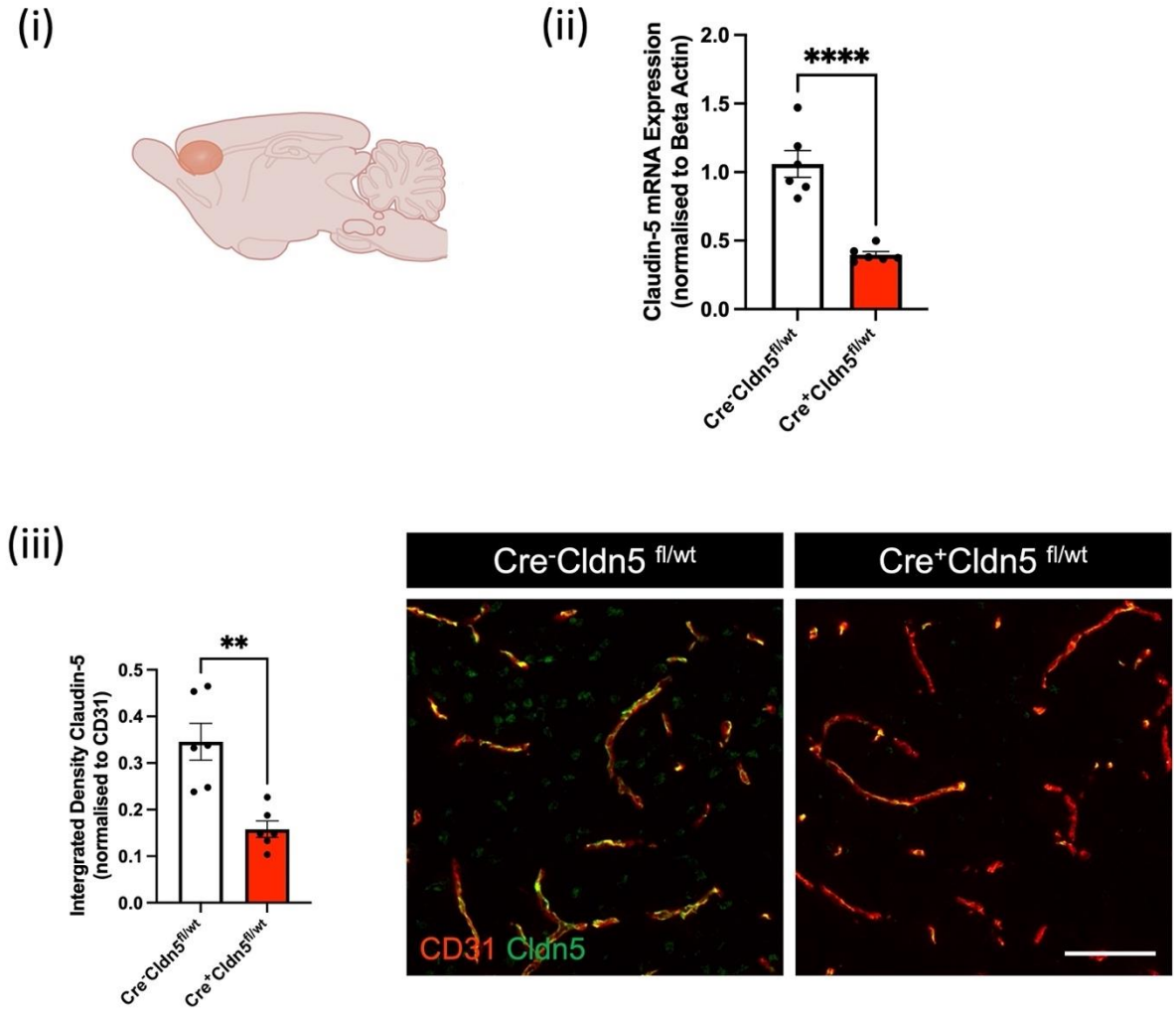

Figure 3.5. RT-PCR and IHC analysis of claudin-5 expression level in prefrontal cortex (PFC)

(i) Schematic of the brain showing location of PFC (ii) RT-PCR analysis of prefrontal cortical tissue dissected from brain shows *Cre+Cldn5*$^{fl/wt}$ mice express over 50 % less mRNA in comparison to the *Cre-Cldn5*$^{fl/wt}$ control littermates (**** p = <0.0001) (iii) IHC analysis shows a significant reduction of claudin-5 (green) expression, relative to the microvessel marker CD31 (red) within the PFC (** p = 0.0015). Scale bar – 100 µm. Statistical analysis was carried out using two-sided unpaired t-test. All data are means ± SEM; each data point represents one animal, n = 6 per group.

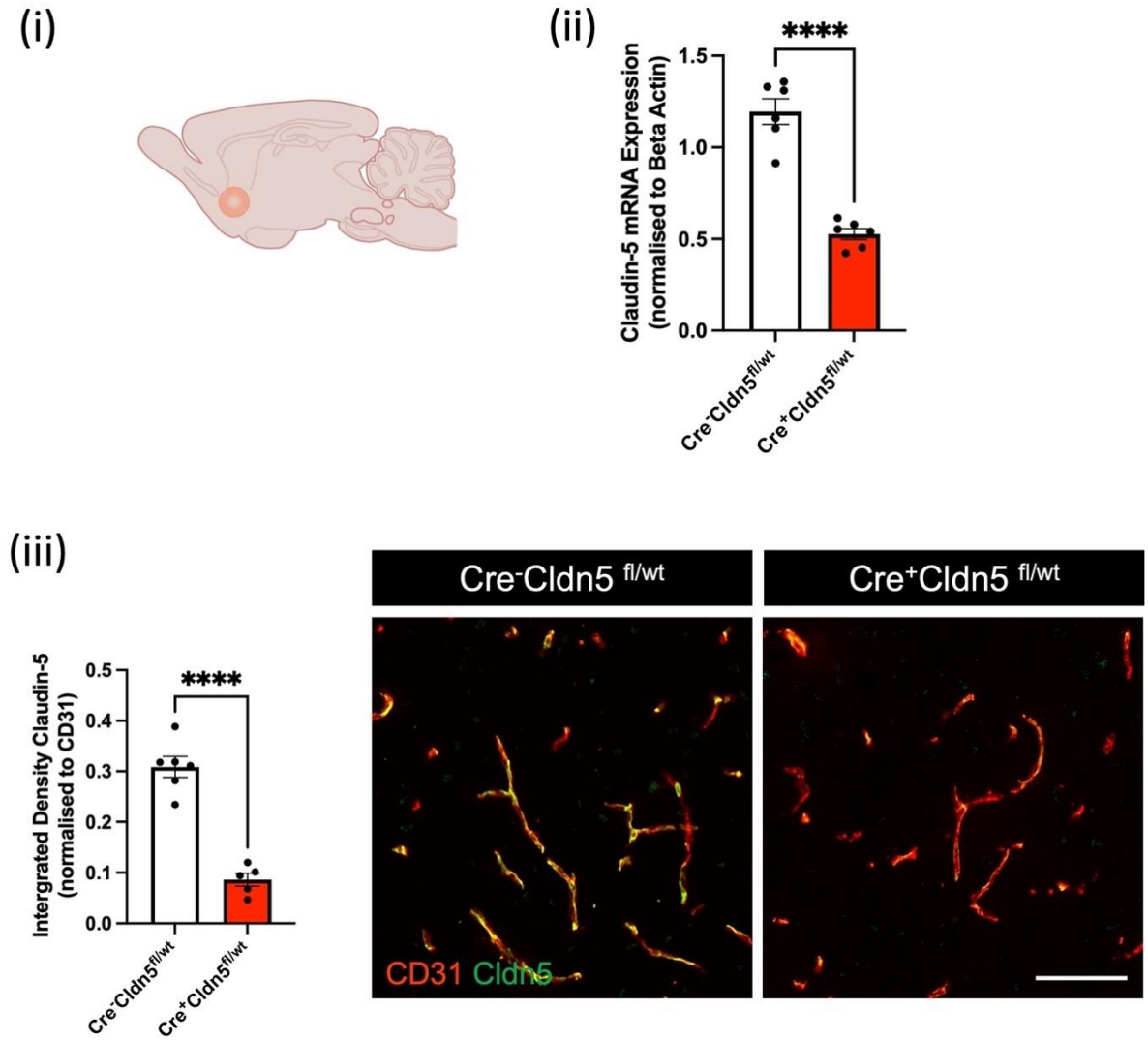

Figure 3.6. RT-PCR and IHC analysis of claudin-5 expression level in nucleus accumbens (NAc)

(i) Schematic of the brain showing location of NAc (ii) RT-PCR analysis of tissue dissected from NAc shows *Cre+Cldn5*$^{fl/wt}$ mice express over 50 % less mRNA in comparison to the *Cre-Cldn5*$^{fl/wt}$ control littermates (**** p = <0.0001) (iii) IHC analysis examining claudin-5 expression (green) in comparison to CD31 (red) shows a significant reduction in the level of claudin-5 expression within the NAc (**** p = <0.0001). Scale bar – 100 µm. Statistical analysis was carried out using two-sided unpaired t-test. All data are means ± SEM; each data point represents one animal, n = 6 per group.

A distinct decrease in both the pattern and intensity of claudin-5 protein expression can been seen clearly in the microvessels of *Cre+Cldn5*$^{fl/wt}$, in comparison to *Cre-Cldn5*$^{fl/wt}$ control littermates (Fig. 3.4 - 3.7). However, examining BBB permeability through the functional screen of tracer analysis showed no significant leakage of biotin in the claudin-5 heterozygote mice in comparison to the *Cre-Cldn5*$^{fl/wt}$ controls. Despite this, through

Image J analysis a non-significant trend for an increase in biotin leakage in the claudin-5 heterozygote mice was noted (Fig. 3.8).

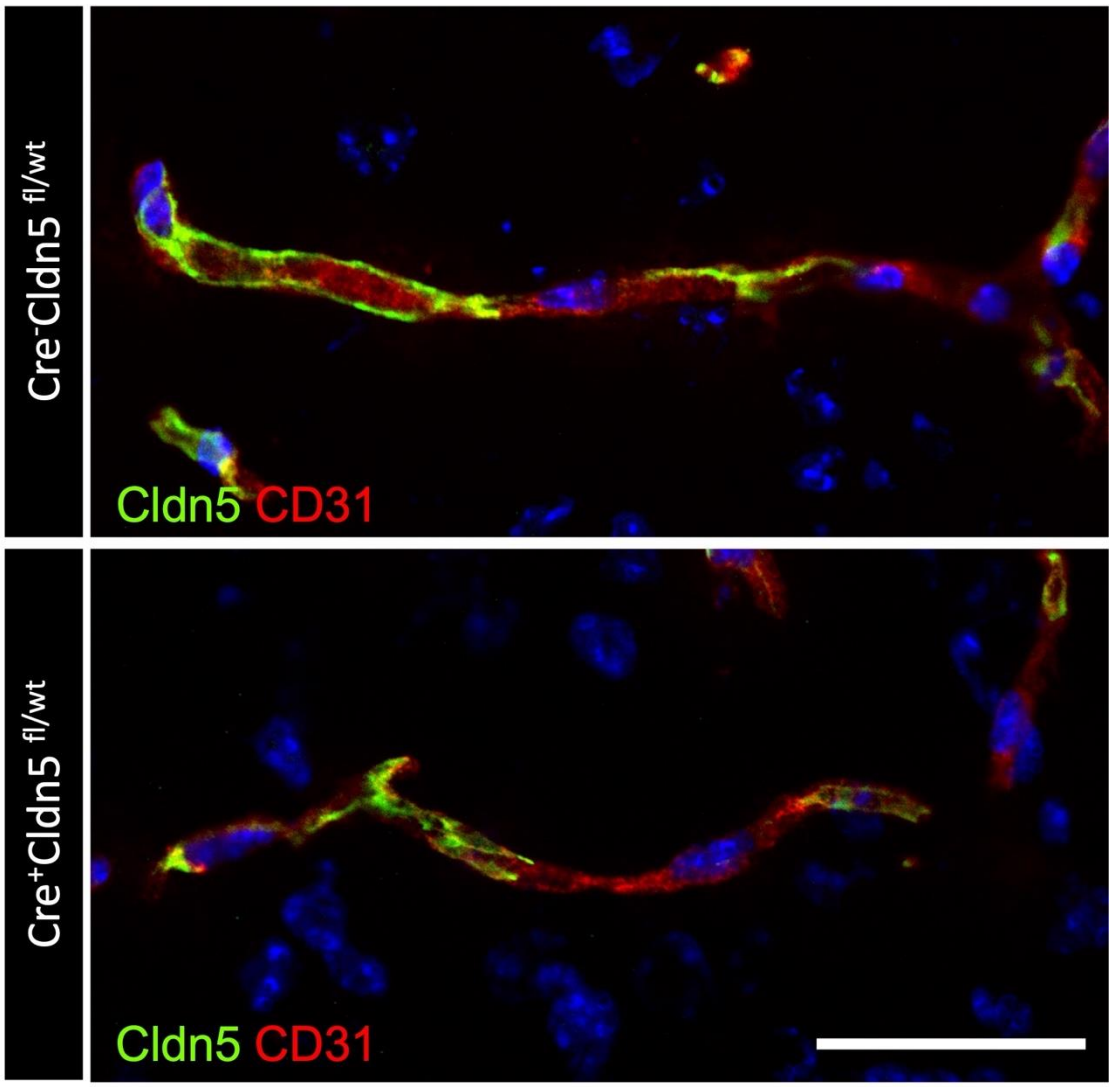

Figure 3.7. IHC analysis of claudin-5 expression in a vessel

Immunohistochemical analysis of claudin-5 (green) and CD31 (red) in a vessel within the brains of $Cldn5^{fl/wt}$ x Tie2Cre mice in the hippocampus. Cellular nuclei stained with 4′,6-diamidino-2-phenylindole (DAPI, blue). Scale bar – 50 μm.

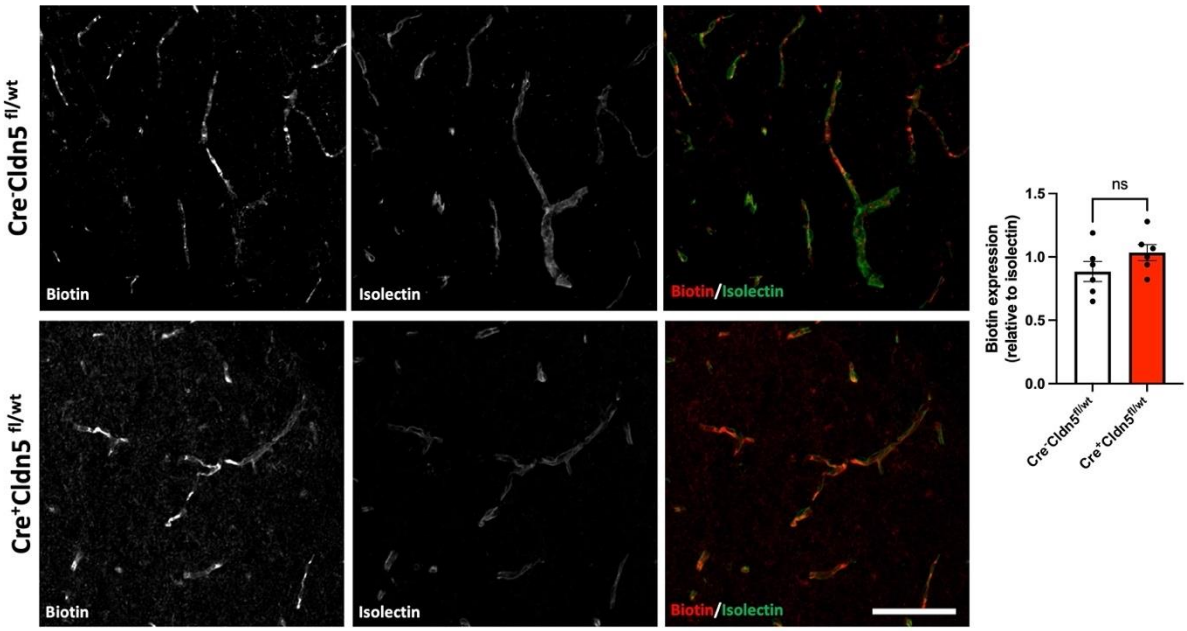

Figure 3.8. IHC analysis of Sulfo-NHS biotin leakage in *Cldn5*$^{fl/wt}$*xTie2Cre* mouse model

Quantification of biotin (red) staining relative to isolectin (green) staining was carried out in *ImageJ.* Statistical analysis carried out by two-sided unpaired t-test (ns p = 0.1154). Scale bar – 50 μm. All data are means ± SEM; each data point represents one animal, n = 6 per group

Astrogliosis is noted in the claudin-5 heterozygote mice with IHC analysis of astrocyte marker GFAP revealing significantly increased staining in the CA1, CA3 and DG regions of the hippocampus in *Cre+Cldn5*$^{fl/wt}$ in comparison to the *Cre-Cldn5*$^{fl/wt}$ control littermates (Fig. 3.9). No significant changes in microglial expression or any discernible structural changes are noted with the level of microglial marker IBA1 remaining similar between the two cohorts. Both show ramified microglial structures, a resting form of microglia noted by the long branching processes and small cellular body, that are indicated by the arrows (Fig. 3.10).

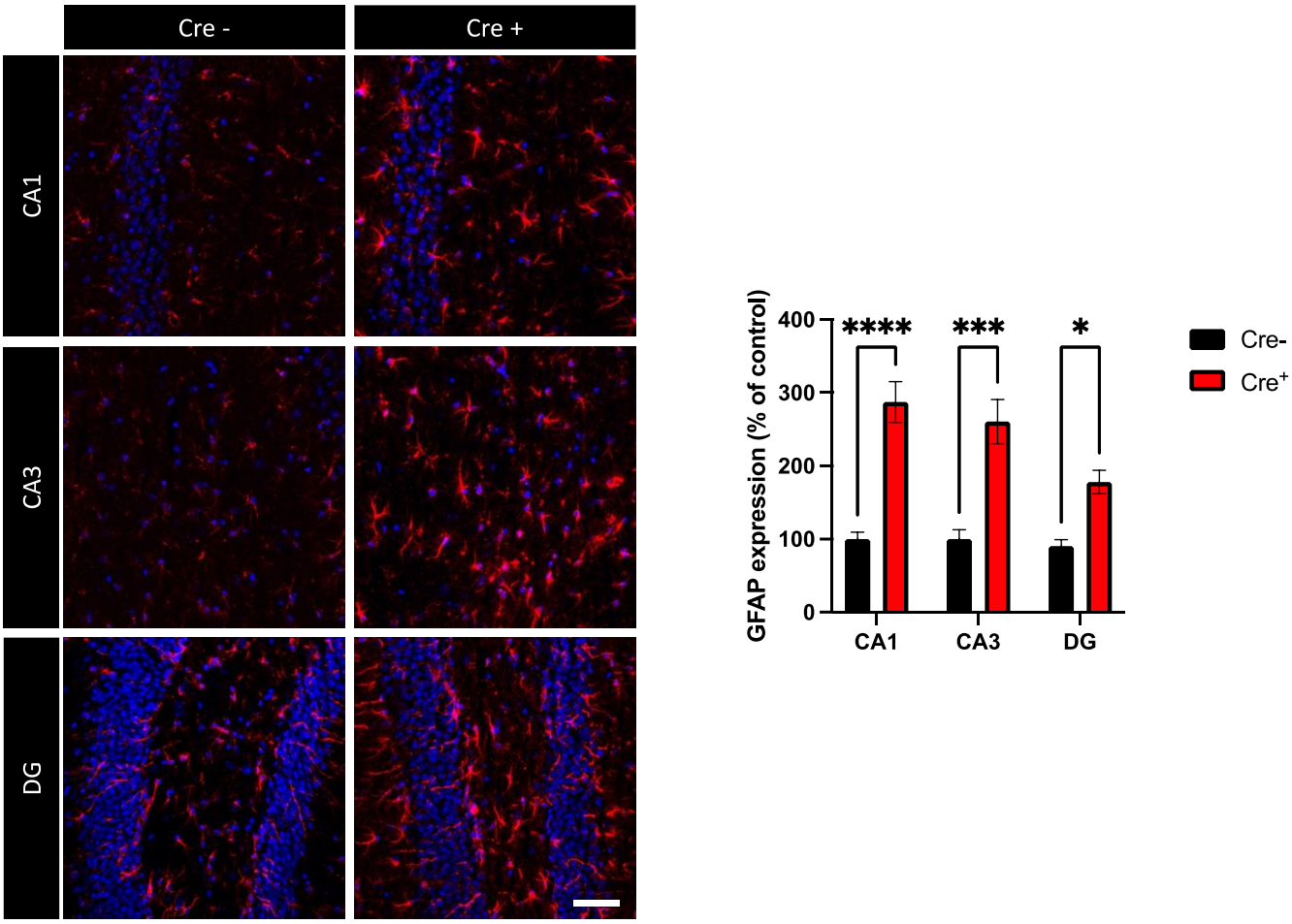

Figure 3.9. IHC analysis of GFAP in the CA1, CA3 and DG regions of the hippocampus of *Cldn5*$^{fl/wt}$*xTie2Cre* mice

IHC analysis of GFAP (red) in the CA1, CA3 and dentate gyrus (DG) regions of the hippocampus of *Cldn5*$^{fl/wt}$*xTie2Cre* mice. Cellular nuclei stained with DAPI (blue). Quantification of GFAP levels was carried out using *ImageJ*. Scale bar 50 μm. *P<0.05 by two-way ANOVA with Tukey's post-test. All data are means ± SEM with n = 6 mice per group.

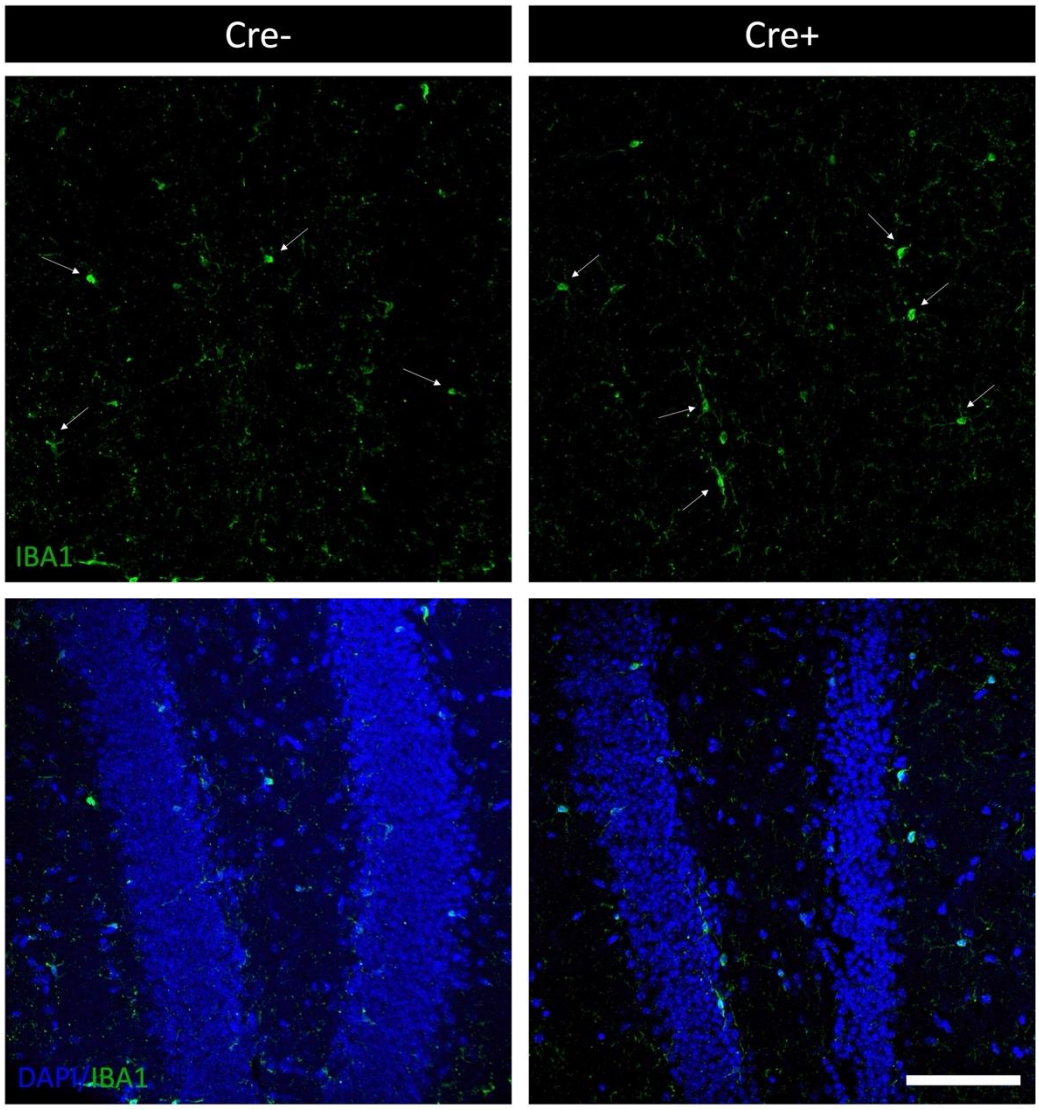

Figure 3.10. IHC analysis of IBA1 staining in *Cldn5$^{fl/wt}$ xTie2Cre* mice.

IHC analysis of IBA1 (green) in the brains of *Cre-Cldn5$^{fl/wt}$* controls compared to Cldn5 heterozygote *Cre+Cldn5$^{fl/wt}$* mice in the DG region of the hippocampus. Cellular nuclei stained with DAPI (blue). Scale bar 50 μm. Arrows indicating clear microglia structures.

Heatmap analysis illustrating mRNA expression level changes of key junctional proteins and inflammatory markers in hippocampal tissue taken from *Cre-Cldn5$^{fl/wt}$* control mice and *Cre+Cldn5$^{fl/wt}$* heterozygote mice (Fig. 3.11). BBB disruption is a hallmark pathology in numerous neurological conditions, which often co-insides with altered inflammatory processes. The *Cre+Cldn5$^{fl/wt}$* mice are haploinsufficent for a key TJ component required to maintain BBB integrity. Therefore investigating if this haploinsufficiency affects the

other key junctional proteins or elicits any changes in inflammatory responses is an important part of the physical characterisation of the *Cldn5*$^{fl/wt}$ *xTie2Cre* model.

An approximate 50 % loss in *Cldn5* expression is again noted in this analysis. This loss of the most highly expressed and essential component of the TJs does not however affect any of the remaining TJ proteins analysed, all remaining within their normal range of expression (Fig. 3.11). A non-significant increase in tricellulin (*Marveld2*) expression was noted ($p = 0.0671$). Important markers of both cell adhesion as well as inflammation are *Icam1* and *Vcam1*. Both play important roles in the maintenance of BBB integrity, but also act as markers of inflammation. Under inflammatory conditions, their expression would be expected to be upregulated by proinflammatory cytokines (Huang et al., 2021). However, in the transcript analysis of the *Cldn5*$^{fl/wt}$*xTie2Cre* mice, no significant changes are noted between the *Cre+Cldn5*$^{fl/wt}$ and *Cre-Cldn5*$^{fl/wt}$ controls. A significant increase in *Gfap* expression was observed in the *Cre+Cldn5*$^{fl/wt}$ mice, which further supports the IHC finding of elevated astrogliosis observed previously (Fig. 3.9). Astrocytes have an important role in the maintenance and regulation of the BBB, and are capable of producing both pro- and anti-inflammatory mediators which can have a significant effect on BBB permeability (Farfara et al., 2019). No change in *Iba1* expression is observed, again supporting the previous IHC findings (Fig. 3.10). Moreover, other markers of inflammation such as *Rage*, *Mmp-2* and *Il-34* remain unchanged between the two cohorts. Interestingly, the chemokine, *Ccl2* and the macrophage marker *Cd68* were both decreased in the *Cre+Cldn5*$^{fl/wt}$ cohort. This suggests that a 50 % loss of claudin-5 does not cause sufficient disruption to BBB integrity to allow for increased immune cell infiltration. However a more in-depth analysis with other inflammatory molecules and immune cell markers would be required to obtain a definitive assessment. Finally, *Sarm1* was also significantly downregulated in the *Cre+Cldn5*$^{fl/wt}$ mice. As a Toll/IL-1 Receptor (TIR) adaptor, Sarm1 plays an important role in mediating immune responses, but also has a novel role in the induction of neuronal axon degeneration following injury (Gibbons et al., 2022). Interestingly, loss of *Sarm1* function has been shown to be neuroprotective in mice (Osterloh et al., 2012) and so this reduced expression in *Cre+Cldn5*$^{fl/wt}$ mice may potentially be a protective mechanism in this *Cldn5*$^{fl/wt}$ *xTie2Cre* model (Fig. 3.11).

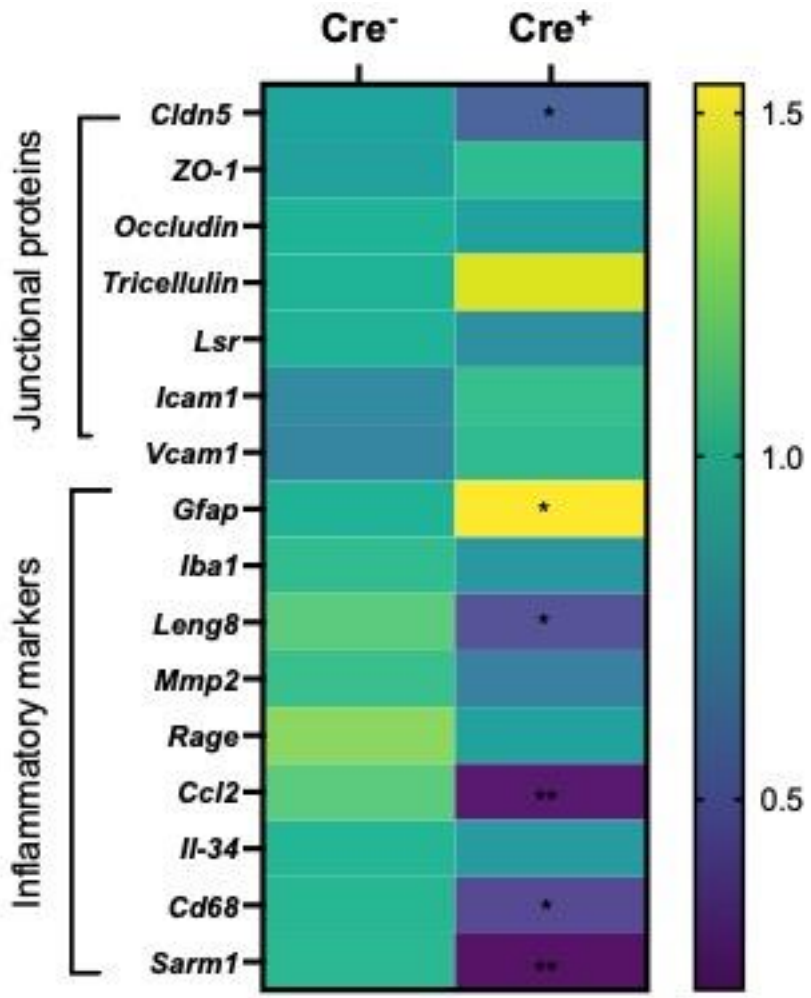

Figure 3.11. RT-PCR analysis of junctional and inflammatory markers in *Cldn5$^{fl/wt}$xTie2Cre* mice

RT-PCR revealed changes in the claudin-5 heterozygote *Cre+Cldn5$^{fl/wt}$* when compared to the *Cre-Cldn5$^{fl/wt}$* littermate controls of gene expression related to junctional proteins and inflammatory markers. mRNA expression levels were normalised to β-actin. *P<0.05 two-sided unpaired t-test. All data are means ± SEM with n = 6 per group.

3.3.2 Behavioural characterisation of the *Cldn5$^{fl/wt}$xTie2Cre* mice:

In many disorders with noted BBB disruption, such as schizophrenia and epilepsy, there are clear and noted behavioural characteristics. However, these are complex, multifactorial disorders, in which many biological pathways are disrupted. The second aim of this chapter was to determine the behavioural effects of an endothelial-specific 50% knockdown of claudin-5 expression. For this purpose, a behavioural dataset was generated. Behaviour assays was broken down into a few different categories; learning and memory, anxiety, locomotor and sensorimotor gating.

3.3.2.1 Learning and memory tasks:

Learning and memory capacity were examined through both spatial and non-spatial trials which included the Y-maze and T-maze, the novel object recognition test as well as the radial arm maze.

Both the Y-Maze and T-Maze are used to assess working spatial memory by exploiting spontaneous alternation behaviour. Spontaneous alternation behaviour describes the animals need to explore their environment in search of resources, which results in the tendency to alternate their search routes in consecutive trials without any training or reinforcement. Spatial memory relates to the ability to record and recover spatial information, to recall the location of an object or occurrence of an event. Working memory, also known as short term memory, is where information is retained temporarily and utilised during the completion of a task.

In the Y-maze, successful spontaneous alternation is defined as the mouse entering all three arms of the Y-Maze over any 4-arm entry span (Fig.3.12 A). No differences were noted between the groups alternation scores, however a non-significant trend for an increased side-bias in *Cre+Cldn5*$^{fl/wt}$ mice was noted in the Y-maze ($p = 0.0513$) (Fig.3.12 (i;ii)). This may explain why we do not see a difference in alternation scores between cohorts, as mice with a side-preference have the potential to outperform controls just by preferentially turning in the one direction in the Y-maze, and so it can be difficult to identify memory errors. However, *Cre+Cldn5*$^{fl/wt}$ mice committed significantly more errors, which is defined as re-entering the same arm it had just left. When mice are examined individually, specific expression of *Cldn5* mRNA was found to be reduced in mice that made more errors in the Y-maze (Fig. 3.12 A (iii)). Spontaneous alternation, which in the T-maze is simply going into alternate arms, as well as the time taken to complete the trial were not significantly different between the two groups (Fig. 3.13).

Long-term recognition memory was assessed using the novel object recognition task. A preference for a novel object would result in a discrimination index with a positive value, while negative values are associated with a preference for the familiar object. Values around 0 suggest that there was no preference for one object over the other. No significant difference in the discrimination index was noted between the claudin-5 heterozygote

Cre+Cldn5$^{fl/wt}$ group and *Cre-Cldn5*$^{fl/wt}$ control group, with the preference values varying equally within each group (Fig. 3.14).

The radial arm maze is a 10 day protocol on a restricted diet (see section 2.4.12). As with the Y-maze, the radial arm maze shows a significant increase in the number of errors made by the *Cre+Cldn5*$^{fl/wt}$ group in comparison to the *Cre-Cldn5*$^{fl/wt}$ group (Fig. 3.15 A (ii). Errors are defined as a mouse re-entering an arm it has just been in, before it has entered any of the other arms in the maze. As mice have exploratory behaviour in which they want to exhaust an environment of any resources, re-entering an arm that has a noted lack of resources, indicates an issue with their short-term spatial memory. The radial arm maze is beneficial as it allows numerous forms of memory to be analysed at the same time, allowing for both short-term "working" memory as well as long term "reference" memory to be examined. Working memory errors were counted when a mouse entered a baited arm that it had already visited during that trial. Across the trial, the number of working memory errors made by the *Cre-Cldn5*$^{fl/wt}$ control group was lower in comparison to the claudin-5 heterozygote *Cre+Cldn5*$^{fl/wt}$ group, with statistically significant differences noted on day 6, 8 and 10 (Fig. 3.15 A (i)). Reference memory errors, reflecting long-term storage of food reward locations, were counted when a mouse entered a non-baited arm. Again, across nearly the whole duration of the 10-day trial, the *Cre-Cldn5*$^{fl/wt}$ control mice made fewer errors in comparison to the *Cre+Cldn5*$^{fl/wt}$ group, with statistically significant differences noted on days 6, 8, 9 and 10 (Fig. 3.15 A (iii)).

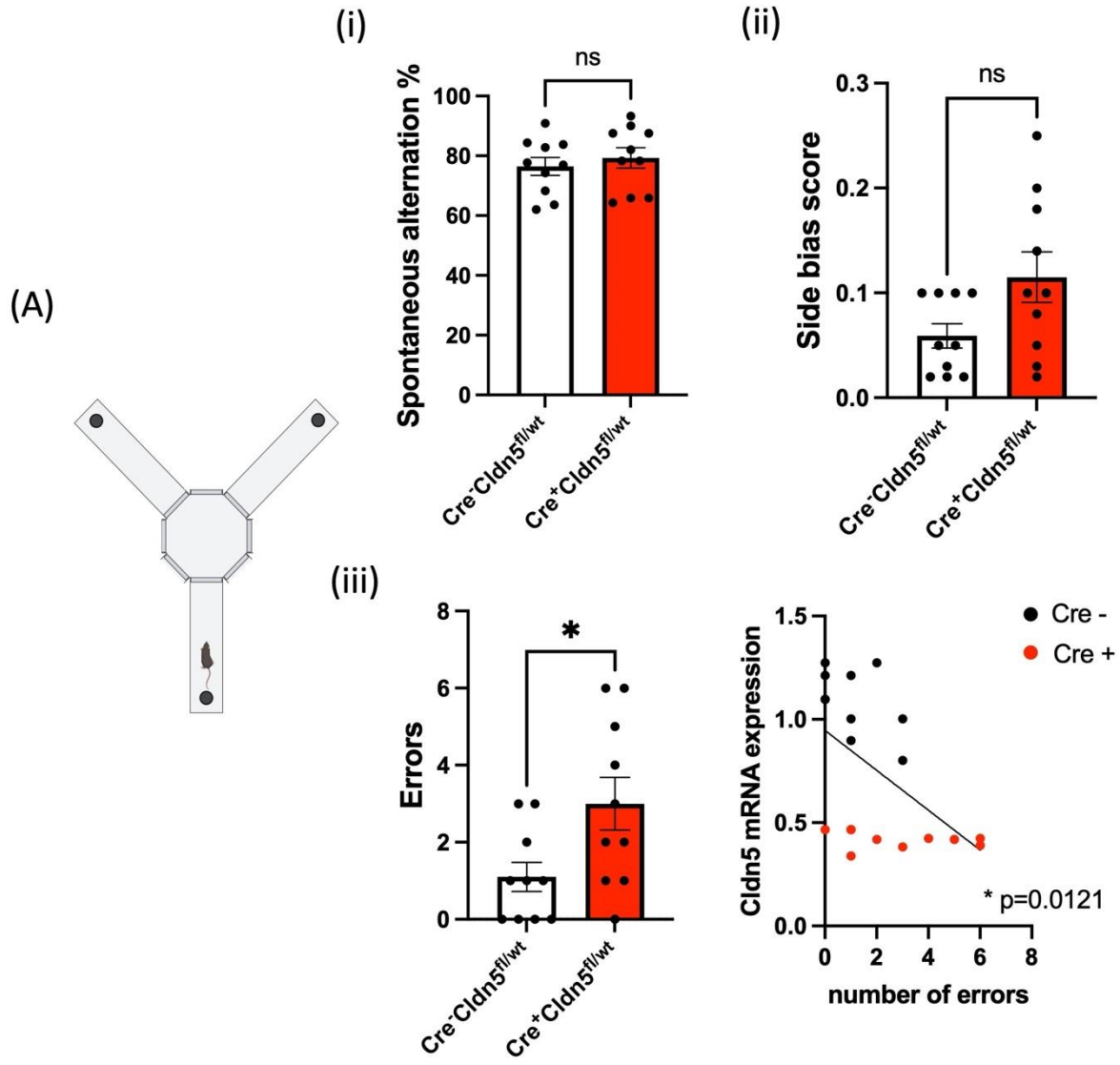

Figure 3.12. Learning and memory function analysed via the Y-maze.

(A) Schematic of the Y-maze. (i) No differences noted between the groups alternation scores. (ii) A non-significant trend for an increased side-bias in *Cre+Cldn5*$^{fl/wt}$ mice was noted (p = 0.0513) (iii) A significant number of errors were made by the *Cre+Cldn5*$^{fl/wt}$ mice in comparison to the *Cre-Cldn5*$^{fl/wt}$ controls (* p = 0.0243). The *Cldn5* mRNA expression level, normalized to β-actin, showed a negative correlation with the number of errors made in the Y-maze (* p = 0.0121; r = -0.5271). *P<0.05 by two-sided unpaired t-test. Correlations were evaluated with Pearson's correlation coefficient. All data are means ± SEM; each data point represents one animal, with n = 10 per group. Schematic created with BioRender.

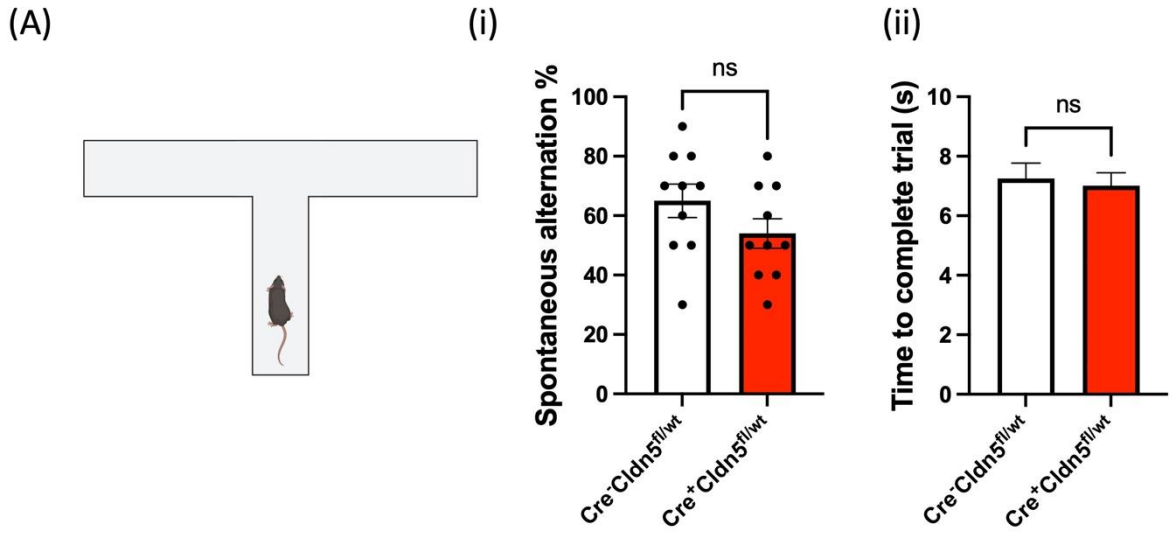

Figure 3.13. Learning and memory function analysed via the T-maze

(A) Schematic of the T-maze. (i) Neither spontaneous alternation or (ii) the time to complete the trial were significantly different. Not significant by two-sided unpaired t-test. All data are means ± SEM; each data point represents one animal, with n = 10 per group. Schematic created with BioRender.

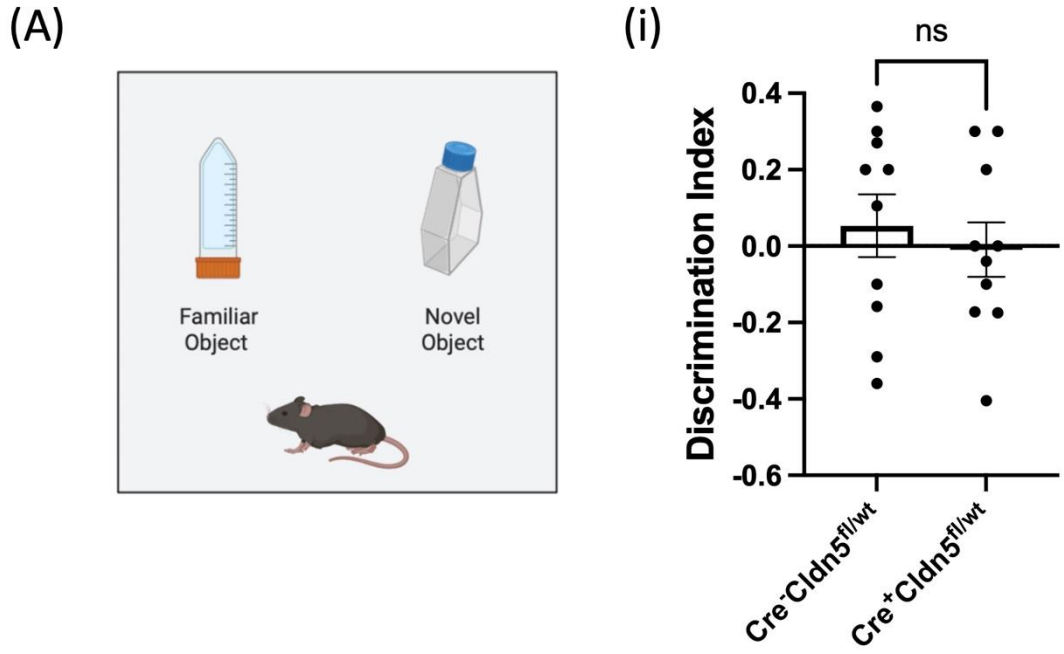

Figure 3.14. Learning and memory analysed via novel object recognition task.

(A) Schematic of the Novel object recognition apparatus. (i) No significant difference in the discrimination index was noted between the claudin-5 heterozygote group and the littermate controls. Not significant by two-sided unpaired t-test. All data are means ± SEM; each data point represents one animal, with n = 10 per group. Schematic created with BioRender.

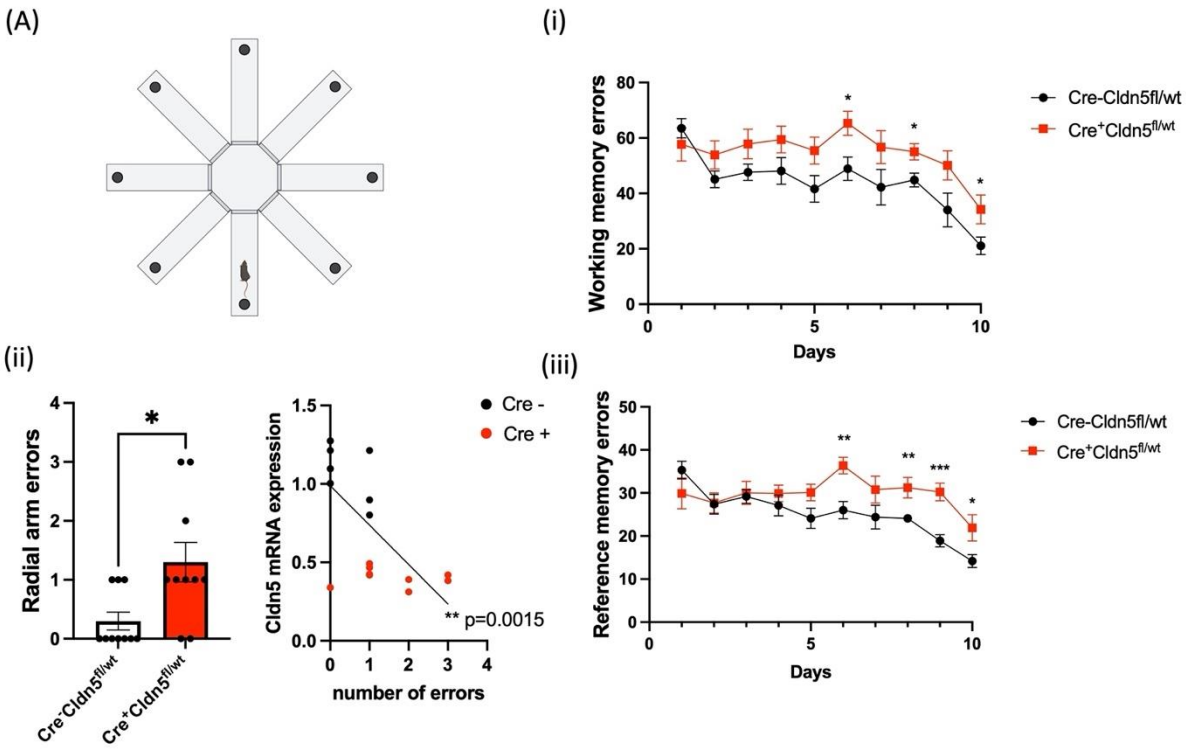

Figure 3.15. Learning and memory analysed via the radial arm maze.

(A) Schematic of the Radial arm maze apparatus. (i) A significant difference between the *Cre+Cldn5*$^{fl/wt}$ mice in comparison to the *Cre-Cldn5*$^{fl/wt}$ controls in both the number of working memory errors and (iii) reference memory errors made. (ii) A significant number of errors made by the *Cre+Cldn5*$^{fl/wt}$ mice in comparison to the *Cre-Cldn5*$^{fl/wt}$ controls (* p = 0.0142 r = -0.6745). The *Cldn5* mRNA expression level showed a negative correlation with the number of errors made in the radial arm maze. *Cldn5* mRNA expression level was normalized to β-actin. *P<0.05 by two-sided unpaired t-test. Correlations were evaluated with Pearson's correlation coefficient. All data are means ± SEM; each data point represents one animal, with n = 10 per group. Schematic created with BioRender.

3.3.2.2 Anxiety assays:

Anxiety and depressive-related behaviour was examined through a number of different assays. In the splash test (Section 2.4.10), a 10 % sucrose solution was squirted on the dorsal coat of a mouse in its home cage. The sucrose solution dirties the coat and induces grooming behaviour. While there was no significant difference in total time spent grooming, the *Cre+Cldn5*$^{fl/wt}$ group neglected coat grooming when compared to the *Cre-Cldn5*$^{fl/wt}$ controls as shown by the increased latency (Fig. 3.16). Correlation data shows a negative correlation with the lower level of *Cldn5* mRNA expression resulting in a longer latency to begin grooming (Fig. 3.16(ii)).

Social behaviour was assessed using the social preference and social novelty tasks. For the social preference trial, the mouse being tested was placed in the start zone and allowed to explore the apparatus, which contains one empty housing container and one with an unfamiliar mouse in it, for 10 min. There was a significant difference between the two cohorts, with the *Cre+Cldn5*$^{fl/wt}$ mice having a reduced preference for social interaction (Fig. 3.17 A(i)). While the correlation data was not significant, it still showed a clear trend for increased *Cldn5* mRNA expression being associated with a high social interaction index score again supporting the finding that reduced claudin-5 expression is causing this reduced preference for social interaction. For the social novelty trial, the apparatus is the same except that both housing containers have mice in them, one containing a familiar mouse from the social preference trial and the other containing a novel mouse. In this trial there was no significant difference in the social interaction index noted between groups (Fig. 3.17 B(i)).

The open field test provides a unique opportunity to assess a multitude of behaviours, including novel environment exploration, general locomotor activity as well as anxiety-related behaviours. Behaviours such as total time grooming, the latency to begin grooming, freezing and the time spent in the two zones of the field, are good indicators of anxiety-like behaviour. No significant change in the time spent in the inner and outer zones, the time spent freezing or in the total time spent grooming was noted between cohorts (Fig. 3.18). However, as was seen in the splash test, the latency to begin grooming and the average grooming episode were both significantly increased in the *Cre+Cldn5*$^{fl/wt}$ claudin-5 heterozygote group in comparison to the *Cre-Cldn5*$^{fl/wt}$ control group (Fig. 3.18 (ii; iii)). These findings are supported by the correlation data, both which show significant correlation supporting the results that reduced *Cldn5* mRNA expression results in an increased latency to begin grooming (Fig. 3.18). The remaining anxiety and depression assays of the forced swim test, the elevated plus maze and marble burying did not yield any significant results (Fig. 3.19).

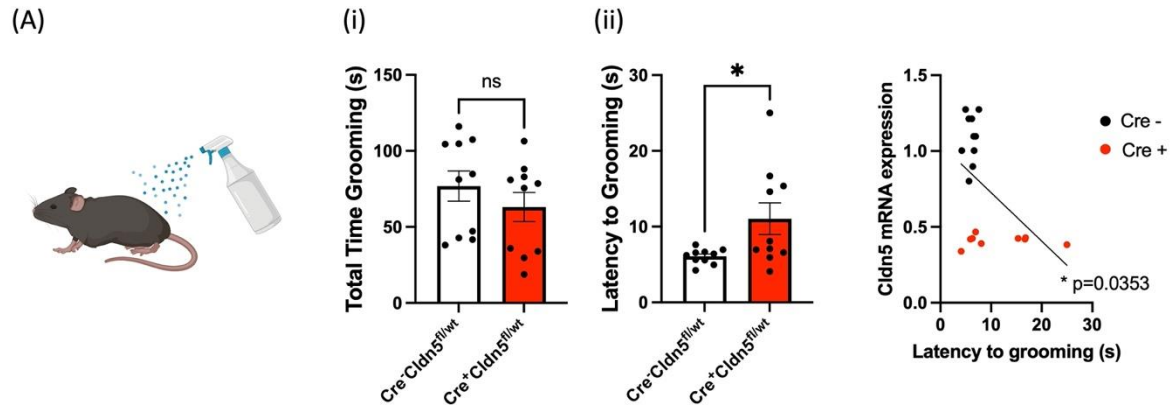

Figure 3.16. Anxiety analysed via the splash test.

(A) Schematic of the splash test procedure. (i) No significant difference between the *Cre+Cldn5*$^{fl/wt}$ mice in comparison to the *Cre-Cldn5*$^{fl/wt}$ controls in the total time spent grooming following the sucrose spray (ii) The latency to begin grooming behaviour is significantly increased in the *Cre+Cldn5*$^{fl/wt}$ mice in comparison to the *Cre-Cldn5*$^{fl/wt}$ group (* p = 0.0305; r = -0.4851). Correlation data shows a negative correlation between mice with a lower level of *Cldn5* mRNA expression and a longer latency to begin grooming (* p = 0.0353). *Cldn5* mRNA expression level was normalized to β-actin. *P<0.05 by two-sided unpaired t-test. Correlations were evaluated with Pearson's correlation coefficient. All data are means ± SEM; each data point represents one animal, with n = 10 per group. Schematic created with BioRender.

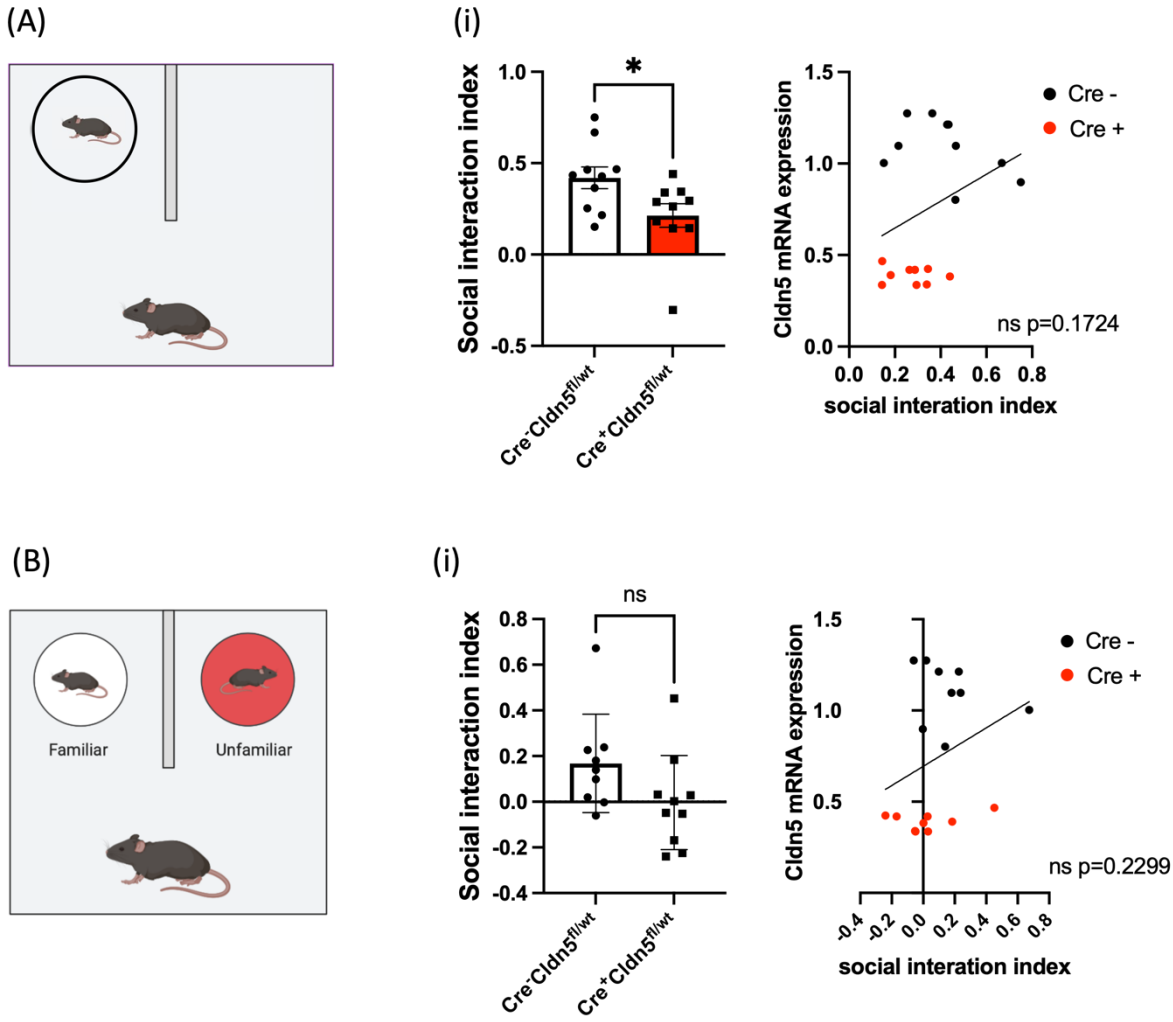

Figure 3.17. Anxiety analysed via the social behaviour tests.

(A) Schematic of the social preference test. (i) A significantly decreased preference for social interaction is noted in the *Cre+Cldn5*$^{fl/wt}$ mice in comparison to the *Cre-Cldn5*$^{fl/wt}$ controls (* p = 0.0309). Correlation data shows, while not significant, that a higher level of *Cldn5* mRNA expression is associated with a higher social interaction index score (p = 0.1723; r = 0.3265). (B) Schematic of the social novelty test. (i) No significant difference is noted in the social interaction index score for novelty between the *Cre+Cldn5*$^{fl/wt}$ mice in comparison to the *Cre-Cldn5*$^{fl/wt}$ group. Correlation data did not observe anything of significance (p = 0.2299; r = 0.2979). *Cldn5* mRNA expression level was normalized to β-actin. *P<0.05 by two-sided unpaired t-test. Correlations were evaluated with Pearson's correlation coefficient. All data are means ± SEM; each data point represents one animal, with n = 10 per group. Schematic created with BioRender.

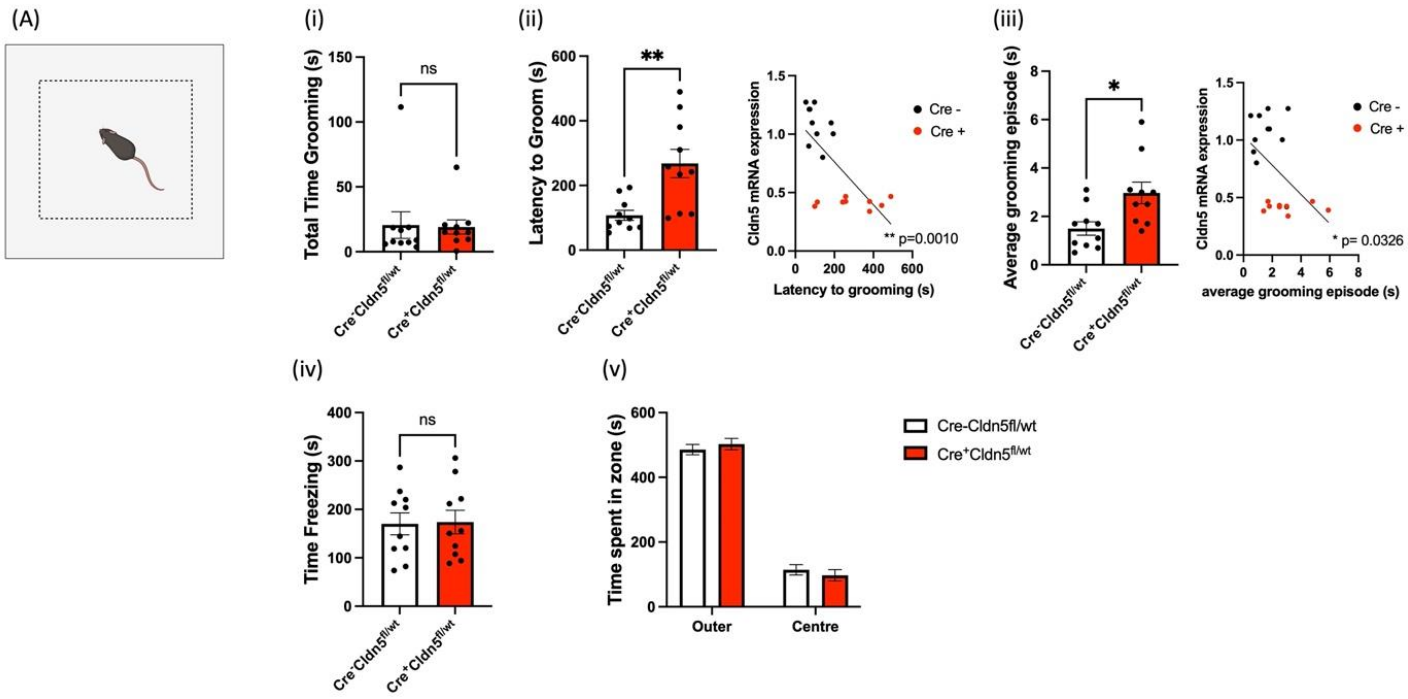

Figure 3.18. Anxiety analysed via the open field test.

(A) Schematic of the open field test apparatus (i) No significant differences noted in the total time spent grooming between the cohorts. (ii) The latency to begin grooming and (iii) the time of an average grooming episode were both significantly increased in the *Cre+Cldn5*$^{fl/wt}$ mice in comparison to the *Cre-Cldn5*$^{fl/wt}$ control group. The correlation data supports these results, indicating that mice with reduced *Cldn5* mRNA expression took longer to initiate grooming behaviour ($p = 0.0010$; $r = -0.6926$) but had longer grooming episodes ($p = 0.0326$; $r = -0.4790$). (iv) The time spent freezing and (v) the time spent in the different zones of the open field showed no differences of note between the groups. *Cldn5* mRNA expression level was normalized to β-actin. *P<0.05 by two-sided unpaired t-test. Correlations were evaluated with Pearson's correlation coefficient. All data are means ± SEM; each data point represents one animal, with n = 10 per group. Schematic created with BioRender.

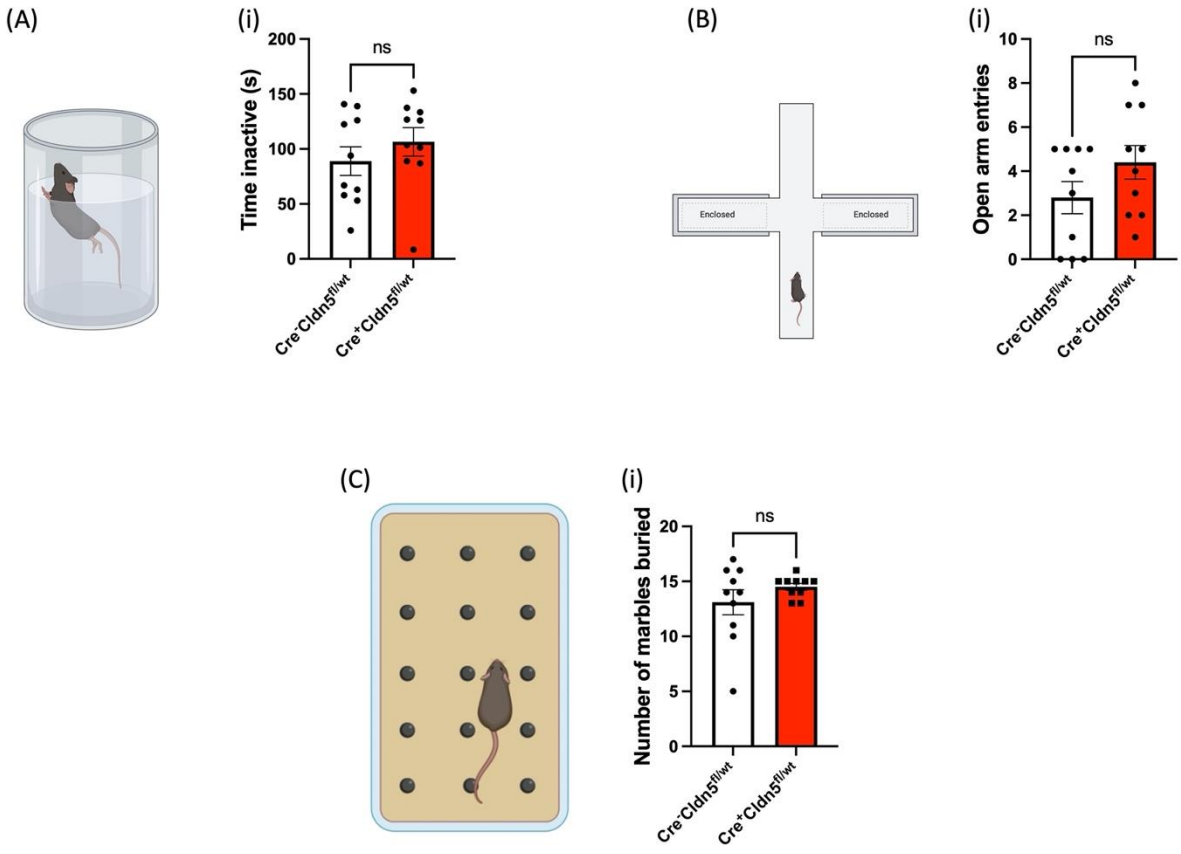

Figure 3.19. Anxiety analysed via forced swim, elevated plus maze and marble burying tests.

(A) Schematic of the forced swim test. (i) No significant differences noted in the total time spent inactive between the cohorts. (B) Schematic of the elevated plus maze (i) No significant differences noted in the time spent in the open arms of the maze between the cohorts. (C) Schematic of the marble burying assay (i) No significant differences noted in the total number of marbles buried between the cohorts. *P<0.05 by two-sided unpaired t-test. All data are means ± SEM; each data point represents one animal, with n = 10 per group. Schematics created with BioRender.

3.3.2.3 Locomotor trials:

No locomotor differences were noted between the claudin-5 heterozygote *Cre+Cldn5*$^{fl/wt}$ mice and their littermates controls in three different locomotor assays utilised, the open field test, the rotarod as well as the radial arm maze. This is important to note as it shows that any other behavioural outputs such as memory or anxiety deficits noted previously are not due to locomotor issues (Fig. 3.20).

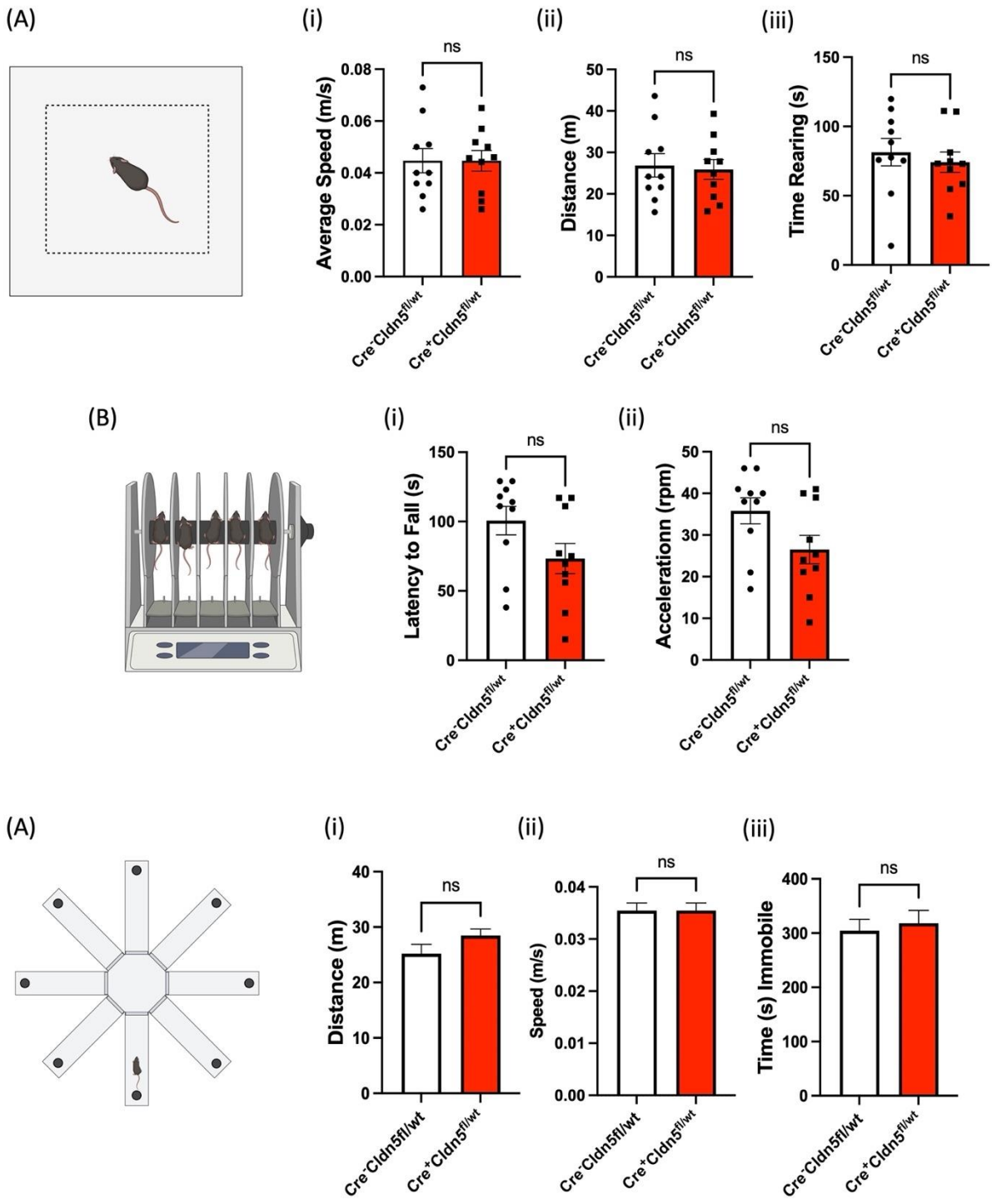

Figure 3.20. Locomotor assays.

(A) Schematic of the open field test. (i) No significant differences noted in the average speed, (ii) distance travelled or (iii) time spent rearing between the cohorts. (B) Schematic of the rotarod (i) No significant differences noted in the latency to fall or (ii) the acceleration speed at time of fall between the cohorts. (C) Schematic of the radial arm maze (i) No significant differences noted in the distance travelled, (ii) the average speed or (iii) the time spent immobile between the cohorts. *P<0.05 by two-sided unpaired t-test. All data are means ± SEM; each data point represents one animal, with n = 10 per group. Schematics created with BioRender.

3.3.2.4 Sensorimotor gating assay:

Acoustic PPI is a sensorimotor gating phenomenon that is preserved across species and has previously been shown to strongly associate with many neurological disorders, such as schizophrenia. PPI describes the ability of a non-startling "prepulse" stimulus, such as in this case a lower decibel (dB) sound to inhibit the response to a subsequent "pulse" startling stimulus, which in this case is a larger dB sound level. Mice were assessed for PPI at 71, 77, 83 dB prepulse sound levels with 100, 110 and 120 dB pulse sound levels. *Cre+Cldn5*$^{fl/wt}$ mice displayed a significantly reduced acoustic PPI response with a 77 dB prepulse at a 110 dB pulse and a 77 and 83 dB prepulse at a 120 dB pulse (Fig. 3.21(ii;iii). Significant positive correlation is noted between these prepulse-pulse combinations and *Cldn5* mRNA expression. Both cohorts showed similar startle responses at 100, 110 and 120 dB indicating that these deficits in PPI are not just a result of an impaired startle response or due to impaired hearing (Fig. 3.21(i)).

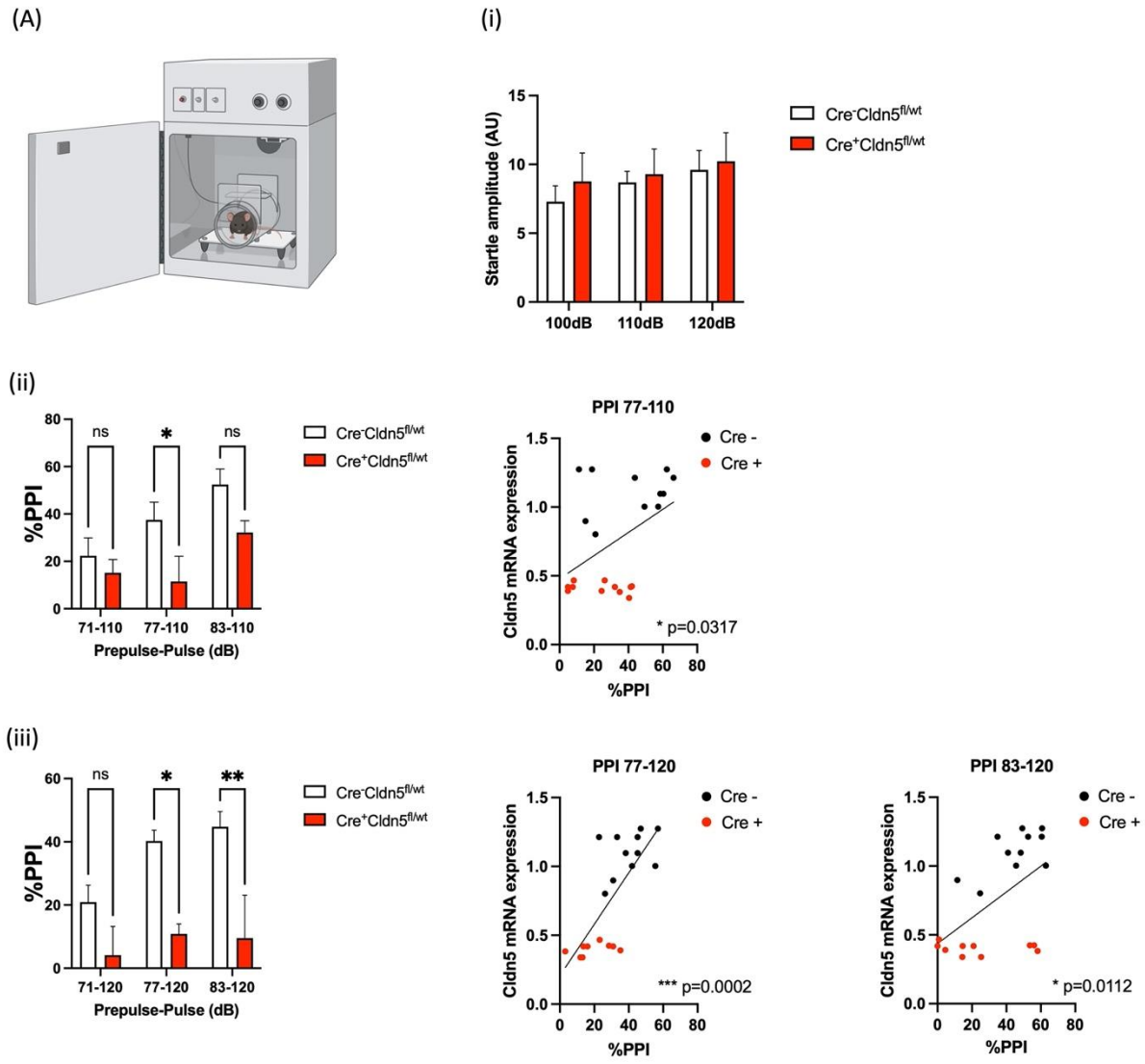

Figure 3.21. Sensorimotor gating deficits in *Cldn5*$^{fl/wt}$*xTie2Cre* mice.

(A) Schematic of PPI chamber. (i) Analysis of startle amplitude at 100, 110 and 120 dB pulse sound levels. Examining acoustic prepulse inhibition at 71, 77 and 83 dB prepulse sound levels (ii) 110 dB (iii) 120 dB pulse sound levels. Correlation data shows that (ii) 77-110 dB ($p = 0.0317$; $r = 0.4588$) (iii) 77-120 dB ($p = 0.0002$; $r = 0.7445$) and 83-120 dB ($p = 0.0112$; $r = 0.5419$) prepulse-pulse combinations, mice with a higher level of *Cldn5* mRNA expression had higher % PPI response. *Cldn5* mRNA expression level was normalized to β-actin. *P<0.05, **P<0.01 by two-way ANOVA with Bonferroni post-test. All data are means ± SEM; each data point represents one animal, with n = 10 per group. Schematic created with BioRender.

3.3.3 Characterisation of the aged *Cldn5$^{fl/wt}$xTie2Cre* model:

Cldn5$^{fl/wt}$xTie2Cre mice were aged to 50 weeks old in order to examine the effects of aging on this model. Behavioural characterisation of the mice was carried out after which mice underwent a submandibular puncture procedure to obtain blood samples for serum and then were sacrificed and tissue taken for analysis.

3.3.3.1 Physical characterisation the aged *Cldn5$^{fl/wt}$xTie2Cre* model:

S100β is a calcium binding protein that is expressed mainly by astrocytes in the brain parenchyma. Under normal conditions, when the BBB is intact, S100β levels in peripheral circulation are low. Thus the level of serum S100β has been a useful biomarker to measure the integrity of the BBB, with increased S100β levels in peripheral circulation indicating disruption of the BBB (Marchi et al., 2004). While there have been some conflicting results, due to issues such as cohort size and previous exposure to neurotherapeutics, overall, there is an accumulation of evidence that S100β levels are elevated in untreated patients with neurological disorders such as schizophrenia and MDD (Schroeter et al., 2008, Zhang et al., 2010). Higher levels of serum S100β reflect a higher degree of BBB disruption, however, in this analysis of the aged *Cldn5$^{fl/wt}$xTie2Cre* model, no significant difference in level of S100β was noted between the aged *Cre+Cldn5$^{fl/wt}$* and the age matched *Cre-Cldn5$^{fl/wt}$* control mice ($p=0.2229$) (Fig. 3.22).

Heatmap analysis illustrating changes in mRNA expression level for key junctional proteins and inflammatory markers in hippocampal tissue taken from aged *Cldn5$^{fl/wt}$xTie2Cre* mice (Fig. 3.23). In comparison to what was noted in the younger cohort, the 50 % loss of claudin-5 expression does appear to be affecting some of the remaining TJ proteins analysed. A significant decrease in ZO-1 (*Tjp1*), *Lsr* and *Vcam1* expression was noted in the aged *Cre+Cldn5$^{fl/wt}$* in comparison to the age matched *Cre-Cldn5$^{fl/wt}$* controls. As before there was a non-significant increase in tricellulin (*Marveld2*) expression observed ($p = 0.0728$). The significant increase in *Gfap* expression that was noted in the younger *Cre+Cldn5$^{fl/wt}$* cohort is again observed in the aged *Cre+Cldn5$^{fl/wt}$* cohort, but this time a non-significant increase in the expression of the microglial marker *Iba1* is also noted. The majority of the inflammatory markers observed no significant change, with only *Cd68* and *Sarm1* showing a significant decrease in expression in the *Cre+Cldn5$^{fl/wt}$* group.

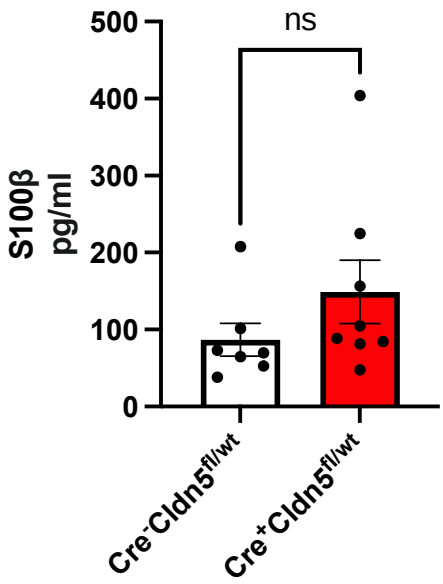

Figure 3.22. ELISA analysis of serum S100β in aged *Cldn5$^{fl/wt}$xTie2Cre* mice

ELISA analysis of serum S100β in aged *Cre+Cldn5$^{fl/wt}$* mice compared the *Cre-Cldn5$^{fl/wt}$* controls. Statistical analysis carried out by two-sided unpaired t-test (ns p =0.2229). All data are means ± SEM; each data point represents one animal, with n = 7 *Cre-Cldn5$^{fl/wt}$* group, n=8 *Cre+Cldn5$^{fl/wt}$* group.

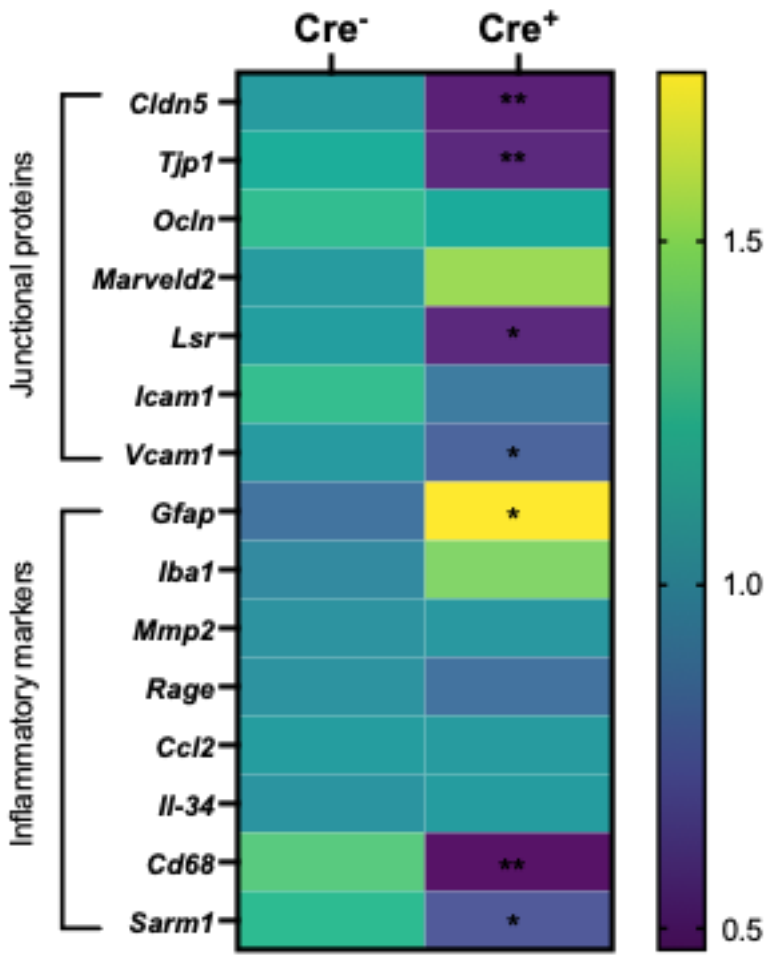

Figure 3.23 RT-PCR analysis of junctional and inflammatory markers in aged *Cldn5$^{fl/wt}$xTie2Cre* mice

RT-PCR revealed changes in the aged *Cre+Cldn5$^{fl/wt}$*claudin-5 heterozygote mice when compared to the aged matched *Cre-Cldn5$^{fl/wt}$* controls of gene expression related to junctional proteins and inflammatory markers. mRNA expression levels were normalized to β-actin. *P<0.05 by two-sided unpaired t-test. All data are means ± SEM, with n = 7 *Cre-Cldn5$^{fl/wt}$* group, n=8 *Cre+Cldn5$^{fl/wt}$* group.

3.3.3.2 Behavioural characterisation the aged *Cldn5$^{fl/wt}$xTie2Cre* model:

3.3.3.2.1 Learning and memory assays:

Learning and memory capacity were again examined through both spatial and non-spatial trials which included the Y-maze and T-maze, the novel object recognition test as well as the radial arm maze.

Unlike in the young mice, in the Y-maze, a significant difference was noted between the groups alternation scores. The *Cre+Cldn5*$^{fl/wt}$ mice showed a significant lower spontaneous alternation % score in comparison to the age-matched *Cre-Cldn5*$^{fl/wt}$ controls (Fig. 3.24 (i)). Interesting the non-significant trend for an increased side-bias in *Cre+Cldn5*$^{fl/wt}$ mice was still noted in the Y-maze (Fig. 3.24 (iii)). The errors made in the Y-Maze, which is defined as re-entering the same arm it had just left, is still significantly higher in the *Cre+Cldn5*$^{fl/wt}$ mice in comparison to the control cohort. The lower level of *Cldn5* mRNA expression level showed a significant negative correlation, indicating that the increased the number of errors made in the Y-maze is associated with the lower level of claudin-5 expression. Spontaneous alternation, on the T-maze however remains unchanged between the two groups as does the time taken for the mice to complete the trial (Fig. 3.25 A (i; ii)).

The results from the radial arm maze remain similar to what was noted for the younger cohort of mice. Significant errors are noted in both short-term "working" memory and long term "reference" memory. Across nearly the whole duration of the 10-day trial, the number of both working and reference memory errors made by the *Cre-Cldn5*$^{fl/wt}$ age matched control group was lower in comparison to the claudin-5 heterozygote *Cre+Cldn5*$^{fl/wt}$ group, with statistically significant differences noted on day 7, 8 and 10 (Fig. 3.24 B (ii)). Moreover, errors made in the radial arm maze, defined as a mouse re-entering an arm it has just been in before it has entered any of the other arms in the maze, also showed significant differences between cohorts (Fig. 3.24 B (i)). As mice have exploratory behaviour in which they want to exhaust an environment of any resources, re-entering an arm that has a noted lack of resources, indicates an issue with their short-term spatial memory.

Long-term recognition memory was again assessed using the novel object recognition task. As the mean discrimination index values for each group are around 0, this suggests that there was no preference for one object over the other (Fig. 3.25 (i)).

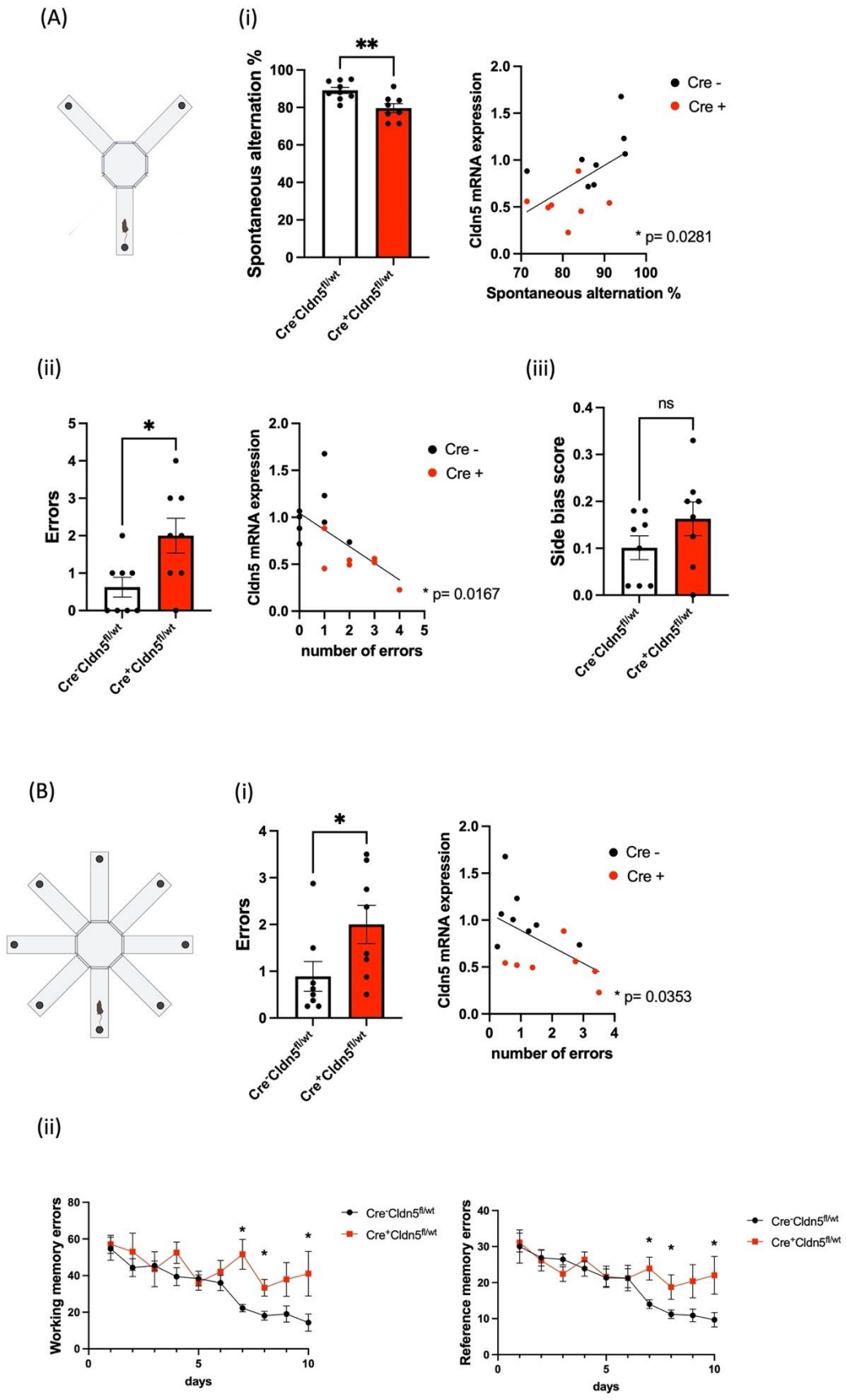

Figure 3.24. Learning and memory function in aged *Cldn5*$^{fl/wt}$*xTie2Cre* mice analysed via the Y-maze and radial arm maze

(A) Schematic of the Y-maze. (i) A significant difference is noted between the groups alternation scores. A higher spontaneous alteration score correlates with mice with higher *Cldn5* mRNA expression ($p = 0.0281$; $r = 0.5652$) (ii) A significantly higher number of errors were made by the *Cre+Cldn5*$^{fl/wt}$ mice in comparison to the *Cre-Cldn5*$^{fl/wt}$ controls. A negative correlation is observed between the *Cldn5* mRNA expression level and the number of errors made in the Y-maze ($p = 0.0167$; $r = -0.6057$). (iii) A non-significant trend for an increased side-bias was noted in *Cre+Cldn5*$^{fl/wt}$ mice. (B) Schematic of the radial arm maze apparatus. (i) Significantly more errors were made by the *Cre+Cldn5*$^{fl/wt}$ mice in comparison to the *Cre-Cldn5*$^{fl/wt}$ controls. The level of *Cldn5* mRNA expression displays a negative correlation with the number of errors made in the radial arm maze ($p = 0.0353$; $r = -0.5458$). (ii) A significant difference is noted between the *Cre+Cldn5*$^{fl/wt}$ mice compared to the *Cre-Cldn5*$^{fl/wt}$ controls in both the number of working memory and reference memory errors made. *Cldn5* mRNA expression level was normalized to β-actin. *P<0.05 by two-sided unpaired t-test. Correlations were evaluated with Pearson's correlation coefficient. All data are means ± SEM; each data point represents one animal, with n = 8 per group. Schematics created with BioRender.

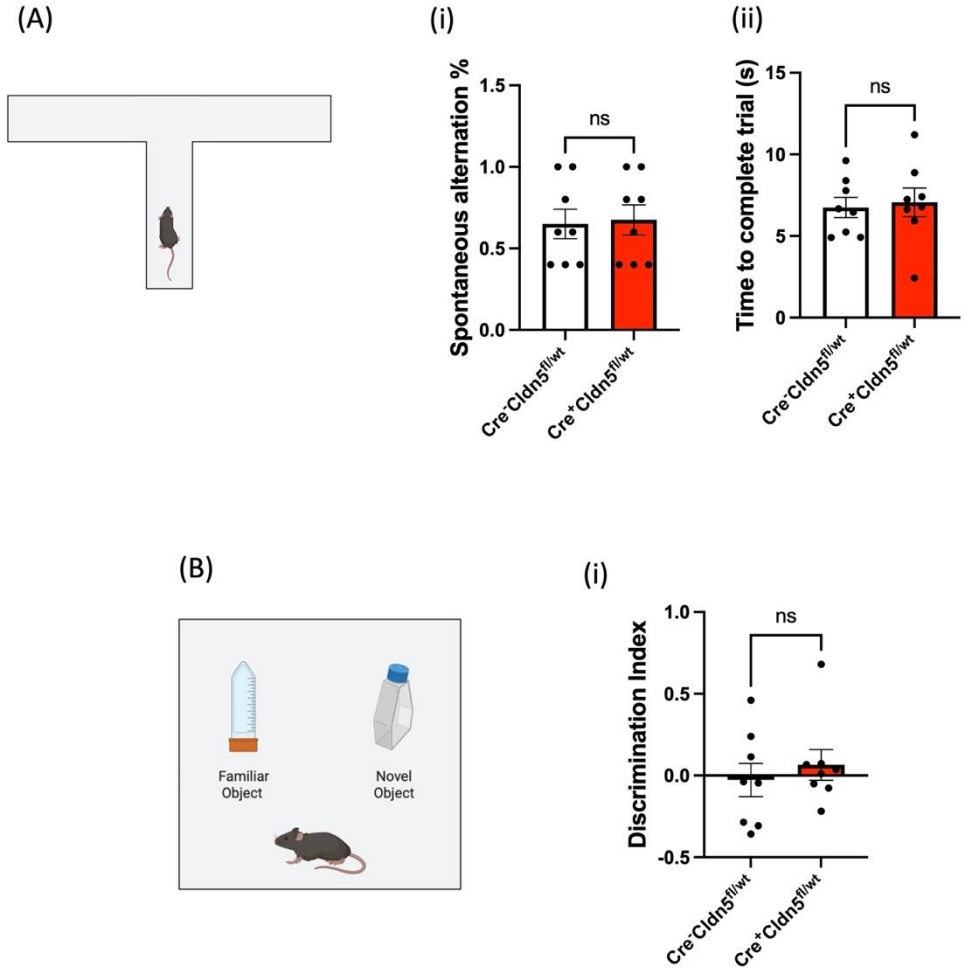

Figure 3.25. Learning and memory function in aged *Cldn5*$^{fl/wt}$*xTie2Cre* mice analysed via the T-maze and novel object recognition task

(A) Schematic of the T-maze. (i) Neither spontaneous alternation nor (ii) the time to complete the trial were significantly different. (B) Schematic of the novel object recognition apparatus. (i) No significant difference in the discrimination index was noted between the *Cre+Cldn5*$^{fl/wt}$ claudin-5 heterozygote group and the *Cre-Cldn5*$^{fl/wt}$ littermate controls. Not significant by two-sided unpaired

t-test. All data are means ± SEM; each data point represents one animal, with n = 8 per group. Schematics created with BioRender.

3.3.3.2.2 Anxiety assays:

Anxiety and depressive behaviour was measured through the splash test, the social behaviour tests as well as the open field test.

As was seen in the characterisation of the younger *Cldn5$^{fl/wt}$xTie2Cre* mice, there was no discernible difference noted between the claudin-5 heterozygote *Cre+Cldn5$^{fl/wt}$* mice and the control group in the splash test (Fig. 3.26 A). The latency to begin grooming too shows no significant difference between groups, however there is still a clear trend indicating that the loss of claudin-5 is associated with a longer latency to groom, which is supported by the correlation data (Fig. 3.26 A (ii))

Social behaviour was assessed using the social preference and social novelty tasks. As before, the social preference trial measures sociability by allowing the test mouse to freely explore the apparatus which contains one empty housing container and one with an unfamiliar mouse in it, with the time spent with each being measured (Fig. 3.26 B). As in the original characterisation, a significant difference was noted between the two cohorts, with the *Cre+Cldn5$^{fl/wt}$* mice having a significantly reduced preference for social interaction (Fig. 3.26 B (i)). For the social novelty trial, there was again no significant difference in the social interaction index scores observed between the two groups (Fig. 3.26 C (i)).

The open field test was again utilised to examine a number of anxiety and depressive-related behaviours. The time spent in the different zones, as well as the total time spent grooming and the latency to groom all showed no significant differences between groups (Fig. 3.27 A (ii; iii; iv)). The time spent freezing, while not significant, suggests that the claudin-5 heterozygote *Cre+Cldn5$^{fl/wt}$* mice spent less time freezing in place (Fig. 3.27 A (i)). Finally, while the other grooming behaviours showed no significant changes, the average grooming episode was significantly higher in the *Cre+Cldn5$^{fl/wt}$* claudin-5 heterozygote mice (Fig. 3.27 A (v)).

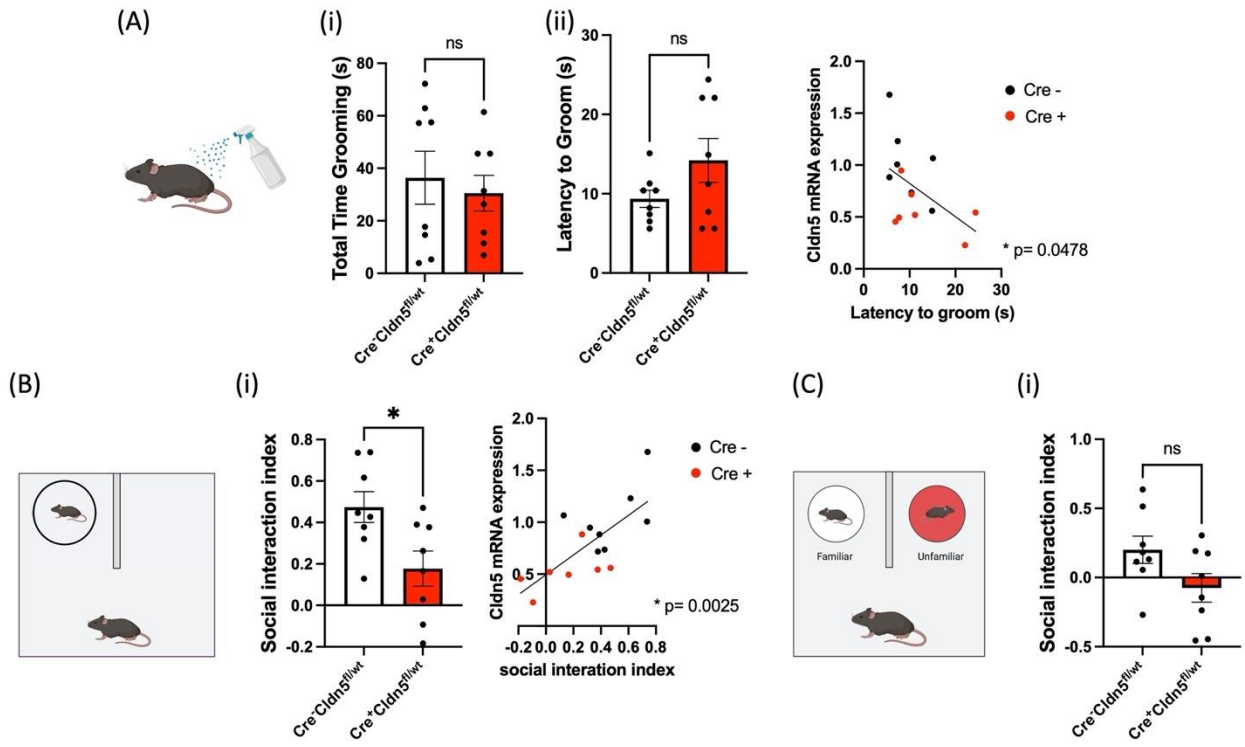

Figure 3.26. Anxiety in aged *Cldn5*$^{fl/wt}$*xTie2Cre* mice analysed via splash test and social behaviour tests.

(A) Schematic of the splash test procedure. (i) No significant difference between the *Cre+Cldn5*$^{fl/wt}$ mice in comparison to the *Cre-Cldn5*$^{fl/wt}$ controls in the total time spent grooming following the sucrose spray (ii) The latency to begin grooming behaviour while not significant, is still increased in the *Cre+Cldn5*$^{fl/wt}$ mice in comparison to the *Cre-Cldn5*$^{fl/wt}$ group. Correlation data shows a significant negative correlation with mice with a lower level of *Cldn5* mRNA expression exhibiting a longer latency to begin grooming (* p = 0.0478; r = -0.5183) (B) Schematic of the social preference test. (i) A significantly decreased preference for social interaction is noted in the *Cre+Cldn5*$^{fl/wt}$ mice in comparison to the *Cre-Cldn5*$^{fl/wt}$ controls, with significant correlation noted between a higher level of *Cldn5* mRNA expression and a higher social interaction index score (p = 0.0025; r = 0.7196). (C) Schematic of the social novelty test. (i) No significant difference is noted in the social interaction index score between the *Cre+Cldn5*$^{fl/wt}$ mice in comparison to the *Cre-Cldn5*$^{fl/wt}$ group. *Cldn5* mRNA expression level was normalized to β-actin. *P<0.05 by two-sided unpaired t-test. Correlations were evaluated with Pearson's correlation coefficient. All data are means ± SEM; each data point represents one animal, with n = 8 per group. Schematics created with BioRender.

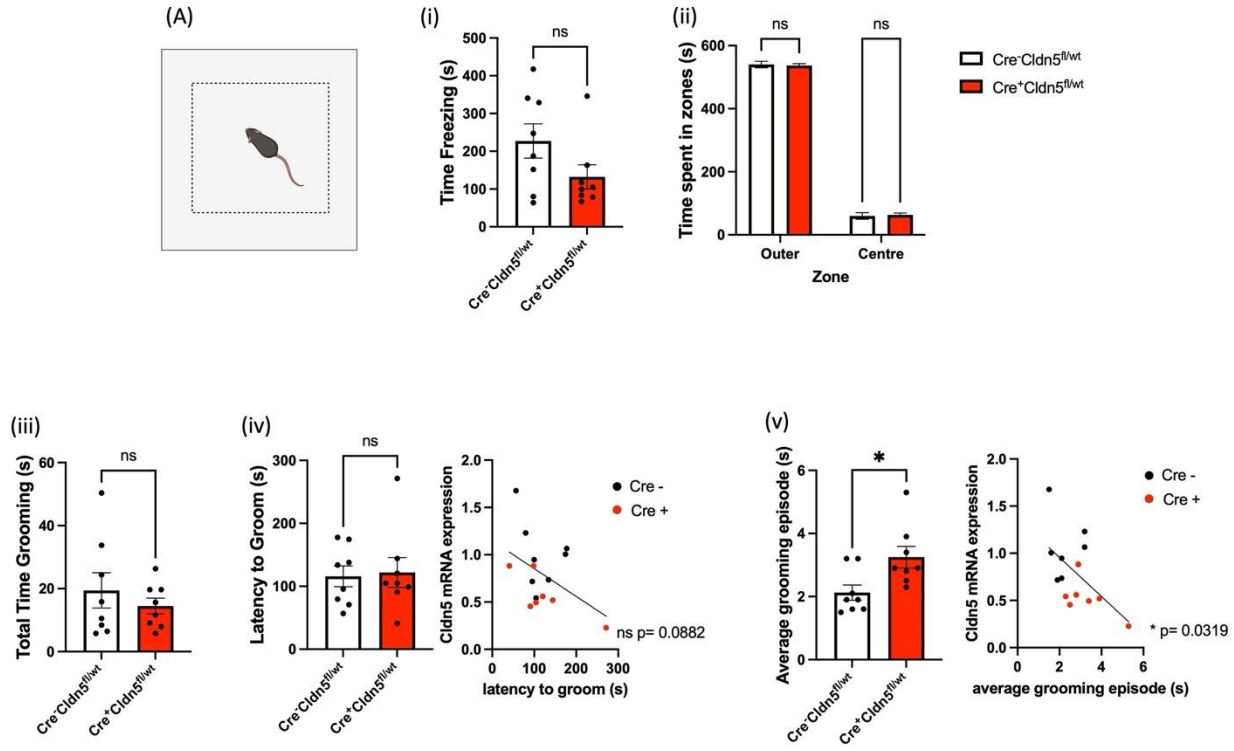

Figure 3.27. Anxiety in aged *Cldn5$^{fl/wt}$xTie2Cre* mice analysed via the open field test

(A) Schematic of the open field test apparatus (i) Non significant trend indicating *Cre+Cldn5$^{fl/wt}$* mice spent less time freezing. (ii) However, no differences were noted in the time spent across the different zones of the open field. (iii) Neither the time spent grooming and (iv) the latency to groom showed any significant differences between groups. (v) The average grooming episode of the *Cre+Cldn5$^{fl/wt}$* mice were significantly longer, which is supported through the correlation data comparing *Cldn5* mRNA expression with the average grooming episode duration ($p = 0.0319$; $r = -0.5546$). *Cldn5* mRNA expression level was normalized to β-actin. *P<0.05 by two-sided unpaired t-test compared to *Cre-Cldn5$^{fl/wt}$* control littermates. Correlations were evaluated with Pearson's correlation coefficient. All data are means ± SEM; each data point represents one animal, with n = 8 per group. Schematic created with BioRender.

3.3.3.2.3 Locomotor activity:

Locomotor activity was assessed by the open field test, the rotarod and radial arm maze, analysing behaviours such as speed and distance travelled, as well the time spent rearing. Neither the open field test or the radial arm maze noted any significant differences in regards to the speed at which these animals moved or the distance they travelled (Fig. 3.28 A; C). However the rotarod did show a substantial change in the latency to fall and thus in turn the acceleration rate at which the mice fell (Fig. 3.28 B). In this assay, the claudin-5 heterozygote *Cre+Cldn5$^{fl/wt}$* mice maintained their balance and movement on the revolving rod for longer than the controls.

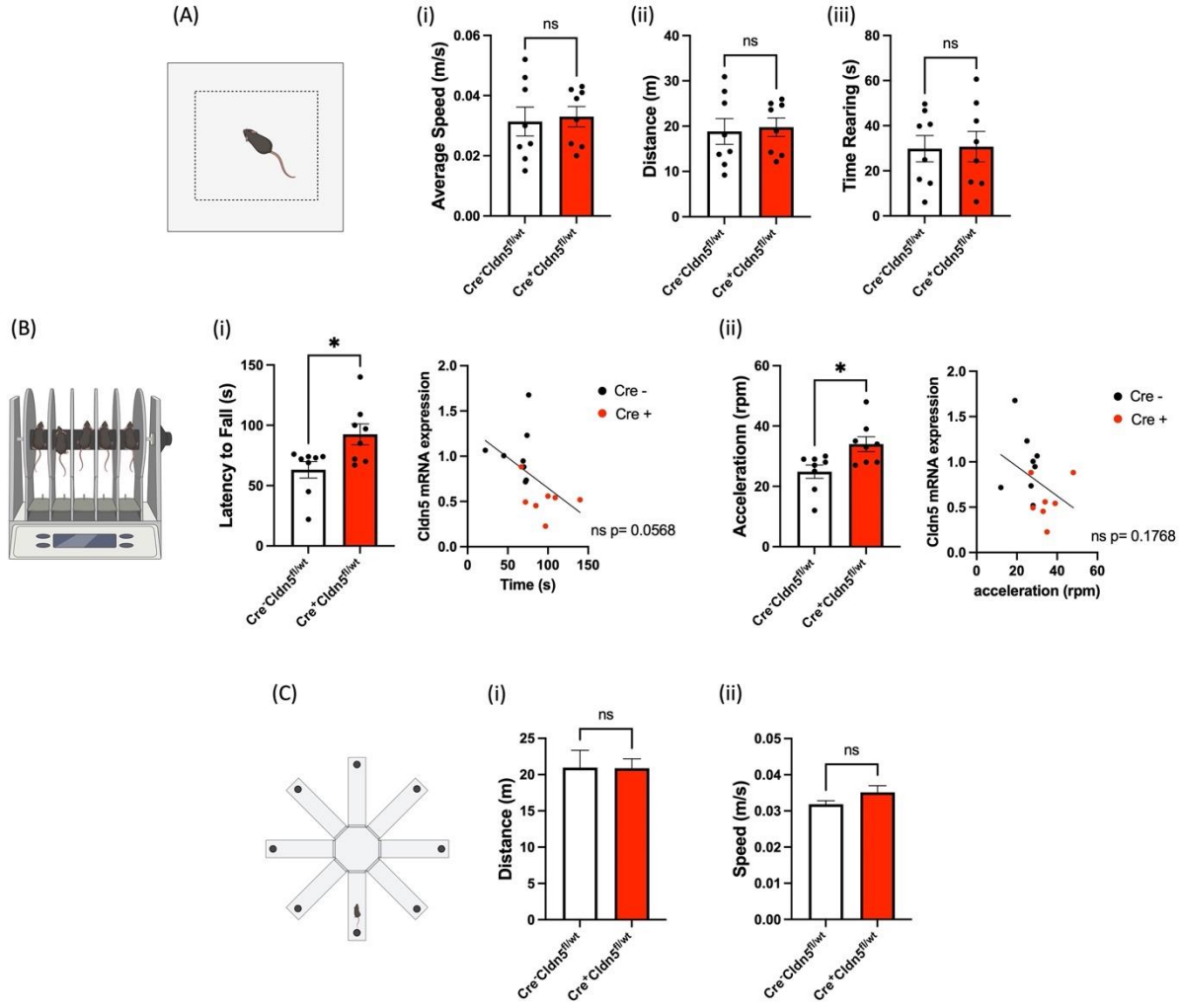

Figure 3.28 Locomotor ability in aged *Cldn5*$^{fl/wt}$*xTie2Cre* mice

(A) Schematic of the open field test. No significant differences noted in (i) the average speed, (ii) distance travelled or (iii) time spent rearing between the cohorts. (B) Schematic of the rotarod. Significant increase in both (i) latency to fall or (ii) the acceleration speed at time of fall noted in claudin-5 heterozygote *Cre+Cldn5*$^{fl/wt}$ mice compared to the age matched controls. (C) Schematic of the radial arm maze. No significant differences noted in (i) the distance travelled or (ii) the average speed. *Cldn5* mRNA expression level was normalized to β-actin. *P<0.05 by two-sided unpaired t-test. Correlations were evaluated with Pearson's correlation coefficient. All data are means ± SEM with n = 8 per group. Schematics created with BioRender.

3.3.3.2.4 Sensorimotor gating

To investigate the sensorimotor gating phenomenon mice were assessed for PPI at 71, 77, 83 dB prepulse sound levels with 100, 110 and 120 dB pulse sound levels. *Cre+Cldn5*$^{fl/wt}$ mice displayed a significantly reduced acoustic PPI response with a 77 and 83 dB prepulse at a 120 dB pulse (Fig. 3.29 (ii)). Correlation data for both support the finding that reduced

claudin-5 expression is associated with a reduced PPI response and thus indicates a potential sensorimotor gating deficit in these mice (Fig. 3.29).

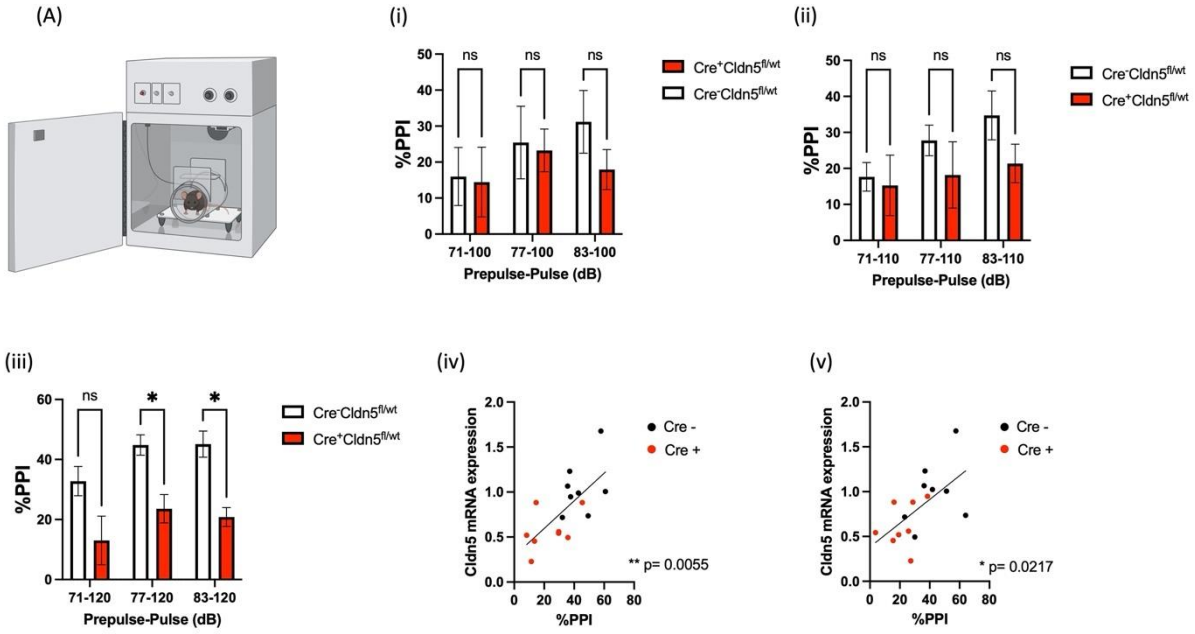

Figure 3.29. Sensorimotor gating deficits in aged *Cldn5*$^{fl/wt}$*xTie2Cre* mice.

(A) Schematic of PPI chamber. Examining acoustic prepulse inhibition at 71, 77 and 83db prepulse sound levels (i) 100 dB (ii) 110 dB and (iii) 120dB pulse sound levels. Correlation data for the significant findings (iv) % PPI response at 77-120 dB ($p = 0.0055$; $r = 0.6839$) (v) % PPI response at 83-120dB ($p = 0.0217$; $r = 0.5965$). *Cldn5* mRNA expression level was normalized to β-actin. *P<0.05, by two-way ANOVA with Bonferroni post-test. Correlations were evaluated with Pearson's correlation coefficient. All data are means ± SEM; each data point represents one animal, with n = 8 per group. Schematic created with BioRender.

3.5 Discussion:

Cldn5$^{fl/wt}$*xTie2Cre* mouse model was generated from crossing a *Cldn5*-LoxP mouse with a Tie2Cre mouse. The resulting *Cre+Cldn5*$^{fl/wt}$ mice are claudin-5 heterozygotes and so express 50 % less claudin-5 mRNA and protein. *Cre-Cldn5*$^{fl/wt}$ cohort are essentially wild-type mice expressing the normal level of claudin-5 mRNA and protein and so function as the control group.

Altering gene dosage in a subset of genes in our genome, either by duplication or deletion will cause a phenotypic effect and so these genes are known as dosage sensitive genes. A copy number change in such genes often results in disease (Rice and McLysaght., 2017).

Through research into 22q11DS, a chromosomal abnormality deletion syndrome within a region that the claudin-5 gene is located, it has been shown that claudin-5 is a dosage sensitive gene. An association between schizophrenia in 22q11DS patients and a variant in the claudin-5 gene which results in 75 % less claudin-5 expression had been noted (Greene et al., 2018; Guo et al., 2020). Moreover, a duplication in this region appears to have a protective effect, with this reciprocal copy number variant (CNV) being significantly less common in patients with schizophrenia in comparison to the general population (Rees et al., 2014). Overall, claudin-5 is a dosage sensitive gene with notable deleterious or protective effects. Thus the generation of a mouse model that is haploinsufficent must be fully characterised both physically and behaviourally to understand its potential as a mouse model of disease.

In regards to the physical characterisation, no macroscopic changes were noted between the claudin-5 heterozygote mice and the control group (Fig. 3.3). Despite this, it was shown that at both the microvasculature and whole brain level, the claudin-5 heterozygote mice did indeed produce 50 % less claudin-5 (Fig. 3.2). Region-specific regulation and dysregulation of claudin-5 expression in CNS disorders such as schizophrenia and MDD have been recently highlighted (Greene et al., 2018; Menard et al., 2017). Reduced claudin-5 expression has been noted in the PFC and hippocampus grey matter of schizophrenic patients in comparison to controls, while no changes were noted in hippocampus white matter or the orbitofrontal cortex (Nishiura et al., 2017; Greene et al., 2020). Moreover, site-specific suppression of claudin-5 in either the hippocampus or mPFC resulted in localized BBB disruption and schizophrenia-like behavioural changes in mice (Greene et al., 2018). Moreover, it has been shown that in patients with MDD, claudin-5 expression is also decreased, but in an entirely different region of the brain than was noted in patients with schizophrenia. From post mortem studies of MDD patients, claudin-5 expression is reduced in the NAc but not in the PFC or hippocampus. This loss of claudin-5 in the NAc is also noted in the CSDS model and site-specific suppression of claudin-5 in the NAc of mice also results in a depression-like phenotype (Menard et al., 2017). Overall these findings indicate that claudin-5 expression is altered in a brain region-selective manner in both schizophrenia and MDD. Therefore it was essential to further examine regionality of claudin-5 expression in the brain, with a focus on 3 major regions of the brain, the hippocampus, the PFC and the NAc. Through RT-PCR and IHC analysis, there was a

significant decrease in claudin-5 expression in the hippocampus (Fig. 3.4), the PFC (Fig. 3.5) and NAc (Fig. 3.6).

Examining claudin-5 expression at the vessel level showed a decrease in both the pattern and intensity of claudin-5 staining, relative to the endothelial cell marker CD31 (Fig. 3.7). This discontinuous pattern of claudin-5 immunoreactivity has also been observed in the resected tissue from patients with epilepsy, suggesting that claudin-5 disruption and associated BBB dysfunction are key drivers in the epilepsy pathology (Greene et al., 2022). Therefore noting similar patterns of claudin-5 staining in this model is suggestive that similar hyper-permeability may be noted in these mice. However, functional analysis examining the permeability of the BBB through a tracer experiment did not display a significant increase in permeability to Sulfo-NHS-biotin in the claudin-5 heterozygote cohort in comparison to their littermate controls (Fig. 3.8).

At the NVU level, other important cell types were examined. Through IHC analysis, increased expression of the astrocyte marker Glial fibrillary acidic protein (GFAP) was noted in the DG, CA1 and CA3 regions of the hippocampus of the *Cre+Cldn5*$^{fl/wt}$ cohort in comparison to the *Cre-Cldn5*$^{fl/wt}$ controls (Fig. 3.9). This indicates that there is astrocytic gliosis in the claudin-5 heterozygote cohort in comparison to the controls. However no changes were noted in microglial expression, with IBA1 staining remaining similar between the two mouse groups (Fig. 3.10).

Transcript analysis, via RT-PCR revealed numerous changes in the *Cre+Cldn5*$^{fl/wt}$ claudin-5 heterozygote mice compared to the *Cre-Cldn5*$^{fl/wt}$ control mice for gene expression related to BBB integrity and inflammatory responses (Fig. 3.11). In numerous neurological disorders, in addition to BBB disruption, CNS inflammation is a frequently noted co-morbidity, with each pathology potentially exacerbating the other. For example, inflammatory processes in the CNS enhance neuronal excitability, which is associated with alterations in BBB integrity in animal models of epilepsy (Vezzani & Friedman, 2011). It is known that a loss of BBB integrity can allow infiltration of immune cells and inflammatory molecules into brain parenchyma which can lead to a positive feedback loop of further BBB disruption through glial activation. Therefore it was necessary, as part of the physical characterisation of the *Cldn5*$^{fl/wt}$*xTie2Cre* model, to determine if a 50% loss of

claudin-5 at the BBB was sufficient to result in alterations to other junctional proteins as well as inflammatory markers.

In regards to the other important components of the TJs, this loss of *Cldn5* expression in the *Cre+Cldn5*$^{fl/wt}$ mice, did not cause any significant changes to their expression. The transcript levels of bTJs components occludin (*Ocln*) and ZO-1(*Tjp1*) were both comparable between cohorts. At the tTJs, while *Lsr* expressed was unchanged, the level of tricellulin (*Marveld2*) expression in the *Cre+Cldn5*$^{fl/wt}$ claudin-5 heterozygote mice was elevated, although not to a statistically significant level ($p = 0.0671$). Taken together these findings suggest that there is no other junctional component that is playing a compensatory role for the loss of claudin-5 at the level of the BBB. *Icam1* and *Vcam1* are adhesion molecules expressed on ECs which help to maintain BBB integrity. However, under inflammatory conditions, proinflammatory cytokines can upregulate expression of adhesive molecules such as *Icam1* and *Vcam1*. This activation can result in gap formation or junctional weakening of EC–cell interactions, which facilitates leukocyte transendothelial migration into the CNS (Huang et al., 2021). Therefore changes in expression of either of these genes can provide insight into changes to barrier integrity or potential changes in inflammatory responses. However, in this characterisation no significant changes were observed for either *Icam1* or *Vcam1* expression between the *Cre+Cldn5*$^{fl/wt}$ and *Cre-Cldn5*$^{fl/wt}$ controls.

The CNS immune system in itself is represented by glia cells such as astrocytes and microglia.

A significant increase in the expression of the astrocyte marker, *Gfap* was noted in the *Cre+Cldn5*$^{fl/wt}$ cohort, supporting the finding noted through IHC analysis (Fig. 3.9), of astrocytic gliosis in this cohort. Astrocytic gliosis refers to the reactive astrocytic response to a brain injury or insult (Sofroniew and Vinters., 2010). Moreover, depending on what has prompted the response, astrocytes can produce pro- or anti-inflammatory mediators which can have a significant effect on BBB permeability and leukocyte infiltration (Farfara et al., 2019). No change in *Iba1* expression is observed, again supporting the previous IHC findings that no significant microglial activation is noted in this model (Fig. 3.10). Moreover, other markers of inflammation such as *Rage* and *Mmp-2* remain unchanged between the two cohorts. The chemokine, *Ccl2* and the macrophage marker *Cd68* were both decreased in the *Cre+Cldn5*$^{fl/wt}$ cohort. This suggests that a 50 % loss of claudin-5 does not

cause sufficient disruption to BBB integrity to allow for increased immune cell infiltration. However a more in-depth analysis with other inflammatory makers such as *Tnf-α*, *Il-1β*, *Il-6*, *Tgf-β* and Vegf will be necessary to obtain a more definitive assessment of the changes that are occurring in the *Cldn5*$^{fl/wt}$*xTie2Cre* model. Finally, *Sarm1* was also significantly downregulated in the *Cre+Cldn5*$^{fl/wt}$ mice. As a Toll/IL-1 Receptor (TIR) adaptor, Sarm1 plays an important role in mediating immune responses, but also has a novel role in the induction of neuronal axon degeneration following injury (Gibbons et al., 2022). Interestingly, loss of *Sarm1* function has been shown to be neuroprotective in mice (Osterloh et al., 2012) and so this reduced expression in *Cre+Cldn5*$^{fl/wt}$ mice may potentially be acting as a protective mechanism in this *Cldn5*$^{fl/wt}$*xTie2Cre* model (Fig. 3.11).

As the overarching aim of this chapter was to fully characterise this claudin-5 heterozygote model, an essential component is to outline the neurobehavioral sequelae of claudin-5 loss and TJ disruption. There are relatively no neurobiological abnormalities that have been classified with certainty as a unique hallmark and biomarker of common neurological disorders like MDD or schizophrenia. Due to this, these disorders still rely solely on behavioural observations and questionnaires for diagnosis. Therefore, in animal models, the behavioural features that may potentially mirror that of the human disorder are necessary for face validity of the model. Therefore to assess how a 50 % decrease in claudin-5 expression specifically in the ECs affects symptomatology, a behavioural dataset was generated. Mice were subjected to a series of behavioural assays designed to identify impairments in several domains such as learning and memory, depression and anxiety, locomotor and sensorimotor gating.

Importantly, before beginning to discuss the behavioural trials themselves, it is essential to discuss the methods used to handle the mice. There are a number of external environmental influences that may affect trial outcomes. A most notable one is the handling stress. The traditional approach is to lift mice at the base of the tail, a method known as “tail handling”. However, this approach has consistently been shown to cause adverse effects. Elevated stress and anxiety in mice has been shown to suppress exploratory behaviour, can impair ability to learn and overall can impair the reliability of the results (Gouveia and Hurst., 2017). Handling stress is a well-recognised source of variation that can result in failure to replicate phenotypes between experiments (Mandillo et al., 2008; Crabbe et al., 1999). Despite this, this aversive handling technique has remained a consistent method to handle

mice. However, other methods, such as the tunnel handling method have more recently been encouraged. Tunnel handling is considered an important refinement in animal research and is encouraged by the National Centre for the Replacement, Refinement and Reduction of animals in research. This method utilises a tunnel that is kept within the home cage, which in itself has been shown to be beneficial as a source of enrichment for mice (Moons et al., 2004). There are now many studies that support the use of tunnel handling as it has been shown to reduce anxiety. This in turn allows the mice to complete the trials with more robust and accurate results. Therefore in these trials, in addition to handler and environment habituation, tunnel handling was utilised across all behavioural trials to ensure robust and reliable results as well as improving the welfare for the test subjects.

The Y-maze examines learning and memory through spontaneous alternation behaviour that is generally exhibited in mice. No differences were noted between the cohorts alternation scores, however a non-significant trend for an increased side-bias was noted in claudin-5 heterozygote mice. Firstly a side-bias, in which mice will preferentially turn in one particular direction, is often noted in mice with a damaged or resected hippocampus (Deacon and Rawlins, 2006). Secondly, this potential side-bias may explain the similar alternation scores between cohorts. It can be difficult to clearly identify memory errors, as mice with a side-preference have the potential to out-perform control mice by preferentially turning in the one direction. However, through a different memory error measure, which was defined as re-entering the same arm it had just left, there were a significant increase in the number of errors made by the claudin-5 heterozygote mice. A negative correlation was noted when examining *Cldn5* mRNA expression levels and the number of errors made in the Y-maze indicating that reduced claudin-5 resulted in more errors (Fig. 3.12). Learning and memory function was further examined through the radial arm maze. This 10-day baited protocol on a restricted diet permits various components of memory to be examined. For both short (working) and long (reference) term memory, there is clear and significant differences noted between the claudin-5 heterozygote mice and their control littermates (Fig. 3.13). Additionally, the number of errors was significantly higher in the claudin-5 heterozygote mice in comparison to the control mice, with again correlation data clearly indicating that 50 % loss of claudin-5 is associated with an increased number of errors. This data together indicates that claudin-5 heterozygosity resulted in issues with learning and memory function.

The ability to interact with others, either cooperatively or competitively, is a fundamental skill that is crucial for both survival and reproduction. Mus musculus is a social species that participates in high levels of reciprocal social interactions, that includes cooperative behaviours such as communal nesting, mating and parenting as well as competitive behaviours such as territorial scent marking and fighting. Social interactions between two mice typically occurs through two phases. The first is the appetitive phase, which reflects the mouses desire to satisfy a biological need and is characterised by approaching and investigating the new individual via touch and smell. This is then followed by the consummatory phase which, depending on factors such as gender and familiarity of the two mice, may result in a variety of goal-directed behaviours such as mating or fighting (Anderson 2016; Chen and Hong 2018). The three-chamber paradigm test, otherwise known as "Crawley's sociability and preference for social novelty protocol" allows for two important but separate aspects of social behaviour to be examined. The first "sociability", reflects social motivation. As mice are a social species, healthy mice should display a tendency to approach and spend time with the unfamiliar mouse rather than spending time alone in the centre chamber or the identical empty chamber. Preference for novelty, reflects social memory. Mice have an innate tendency to prefer a novel social stimulus in comparison to a familiar one and so this assay measures the mouses ability to discriminate between two mice and recognise which is familiar and which is novel (Thor and Holloway., 1982; Netser et al., 2017).

In the analysis of the *Cldn5*$^{fl/wt}$*xTie2Cre* model there was a significant decrease in preference for social interaction in the claudin-5 heterozygote mice. The correlation data, while not significant, does appear to support the finding that lower levels of claudin-5 expression results in a low social interaction index score. No significant differences were noted between the control mice and the claudin-5 heterozygote mice in regards to social novelty measures (Fig. 3.17). However, while the control mice showed a distinct preference for the novel interaction, as would be expected, the claudin-5 heterozygote mice show a social interaction index score that is close to zero, indicating they showed no preference for either the familiar or novel mouse (Fig. 3.17). Numerous neuropsychiatric disorders have clear characteristic deficits in social behaviour and social recognition including schizophrenia, depression, autism and obsessive-compulsive disorders (OCD).

Social behaviour, is a multi-step information process requiring multimodal sensory inputs that through a social decision-making network are transformed into appropriate behavioural outputs. This social decision-making network is thought to consist of the mPFC, anterior cingulate cortex, amygdala and the hippocampus (Tanimizu et al., 2017; Xu et al., 2021). The hippocampus is thought to be at the centre of this neural circuit, acting as a connector hub. The hippocampus is essential for encoding declarative memory, the archive of knowledge on who, what, where and when. Therefore the hippocampus plays an essential role in forming the relational memory that is essential for both flexible cognition and social behaviour, both of which are needed for a diverse range of tasks such as navigation, decision making, social discourse and establishing and maintaining social bonds (Rubin et al., 2014). Moreover, the CA2 region of the hippocampus has been shown to be essential for social recognition memory (Hitti and Siegelbaum 2014). Therefore loss of claudin-5 expression at the BBB is clearly negatively affecting this social decision making circuit, with a significantly reduced preference for social interaction and no notable preference for novelty. While the change in preference for social interaction is a likely indicator of heighted anxiety, the discernible lack of preference for novelty supports the previous findings in the Y-maze and radial arm maze, which indicate clear issues with memory formation, in this case social recognition memory.

Self-grooming is an innate behaviour seen across most animal species and is an important component in mouse behaviour, taking up between 30-50 % of their waking time (Kalueff et al., 2007). In mice there is a general pattern to self-grooming behaviour known as cephalocaudal progression. This behavioural sequence can be broken down into four distinct phases. It starts with paw licking followed by nose and face wash, then head wash to body wash and fur licking and finishes with tail licking and wash (Kalueff et al., 2004). Once the first phase begins, the remaining sequential pattern is continued to completion approximately 15 % of the time (Kalueff et al., 2007). The remainder of the time, more flexible sequences of grooming are noted. Self-grooming is a complex behaviour with multiple brain regions involved in its regulation, such as the limbic circuitry which includes the amygdala and hypothalamus (Kalueff et al., 2016). Therefore examining mouse self-grooming behaviour in research provides more than just a direct comparison to aberrant grooming behaviour in human disease but should be really used to examine the models ability to carry out complex repetitive, self-directed and sequentially patterned behaviours. Claudin-5 heterozygote mice took longer to initiate grooming behaviours, with increased

latency to begin grooming observed in regards to both spontaneous grooming behaviour that was examined via the open field test (OFT) as well as in forced grooming behaviour analysed through the splash test. Moreover, in the spontaneous grooming in the OFT protocol, the average grooming episode in the claudin-5 heterozygote mice was significantly longer than that of the control mice. Manipulation of the dopamine levels in the brain, through lesions of the dopamine-containing nigrostriatal tract, administration of dopaminergic drugs, as well as via a DA1-deficient mutant model, have all been shown to induce aberrant grooming behaviour (Cromwell and Berridge., 1996; Berridge and Whishaw 1992; Berridge and Aldridge 2000; Cromwell et al., 1998). Potentially the loss of claudin-5 expression at the BBB is disrupting the neural microenvironment, altering the dopamine levels and overall negatively affecting synaptic signalling that is required for these complex motor functions. However, further research into this behaviour may be necessary, as only gross measures of time, including total time spent grooming and the latency to begin grooming were examined. Examining the frequency at which mice correctly carried out the cephalocaudal sequential pattern correctly, may give more insight into the full extent of potential neurological deficits.

Finally sensorimotor gating was examined in the *Cldn5*$^{fl/wt}$*xTie2Cre* model through PPI. Sensorimotor gating refers to the regulation of sensory information as it is transmitted to motor outputs. As sensory information is processed, some level of filtering, known as "gating" is needed before inducing any motor output. Therefore, put simply it is the ability of a sensory event to suppress a motor response. PPI is a form of startle plasticity, in which a non-startling stimulus preceding an intense startling stimulus within 500ms, will inhibit a startle response (Graham 1975; Hoffman and Ison 1980). The underlying mechanism of this inhibition is thought to mirror the normal filtering process of incoming sensory stimuli (Geyer and Braff 1987). PPI response level therefore should signify an operational measure of sensorimotor gating.

PPI response is reduced in schizophrenic patients, as first reported in 1978 (Braff et al., 1978). Since then however reduced PPI response been shown in other neuropsychiatric and neurodevelopmental disorders including OCD, Tourette's syndrome, Huntington's disease, bipolar patients in a manic episode and autism in adults (Swerdlow et al. 1993; Swerdlow et al. 2001; Swerdlow et al. 1995; Perry et al. 2001; Perry et al. 2007). Interestingly in regards to our research into reduced claudin-5 expression, patients with 22q11DS have also

shown distinct deficits in PPI (Sobin et al., 2005). While the central symptoms in each of these disorders is different, each feature a common gating deficit, which may be broken into one of three deficit domains, sensory, motor or cognitive. Deficits in sensory gating has been well characterised in schizophrenia, while motor gating deficits are noted in Huntington's and Tourette's, and cognitive gating deficits are noted in OCD (Braff et al., 2001; Hoenig et al., 2005). As PPI is preserved across species, it has emerged as a widely translational tool in both preclinical neuropharmacological and genetic research, allowing the integrity of basic neural circuits in genetic mouse models to be examined in addition to screening new therapeutic agents.

PPI can be examined through various parameters such as acoustic, tactile and light stimulus. In this study acoustic startle response was used to assess PPI deficits in the *Cldn5*$^{fl/wt}$*xTie2Cre* mouse model. PPI of the acoustic startle response was tested at three non-startling "prepulse" sound levels of 71, 77 and 83 dB in combination with 3 startling "pulse" sound levels of 100, 110 and 120 dB. In comparison to the control mice, the claudin-5 heterozygote mice had significantly reduced acoustic PPI response at 77 dB prepulse with 110 dB pulse and at 77 dB and 83 dB prepulse with 120 dB pulse (Fig. 3.21). Correlation data of *Cldn5* mRNA expression and PPI response showed a clear positive correlation between claudin-5 expression and higher PPI % responses. Moreover examining the acoustic startle amplitude, showed that startle responses were similar between the claudin-5 heterozygote cohort and their littermate controls, indicating that no hearing impairments in the claudin-5 heterozygote model is causing the reduced PPI response. Overall these findings provide conclusive evidence that there is a distinct sensorimotor gating deficit in mice that are deficient in claudin-5 at the BBB. A summary of the behavioural dataset generated for the *Cldn5*$^{fl/wt}$*xTie2Cre* model, highlighting the behavioural changes that are caused by a 50% loss of claudin-5 can be seen in Fig. 3.30.

Further characterisation of *Cldn5*$^{fl/wt}$*xTie2Cre* mouse model was carried out by examining physical and behavioural changes in an aged version of this model. Characterisation of an aged model is beneficial in order to identify any progressive or enhanced pathological phenotypes. Moreover, in this claudin-5 haploinsufficent model, there are a number of factors that incentivise further investigation into the ramifications of aging on this dosage sensitive TJ-component. This is due firstly, to the noted changes in BBB that are associated with healthy aging. It has been shown that there is an age-dependant loss of BBB integrity

in the hippocampus, even in those that show no distinct cognitive impairment (Montagne et al., 2015). Moreover in aged mice, the hallmarks of diminished BBB integrity, which include increased immunoglobulin (IgG) leakage into the brain parenchyma, reduced TJ protein expression and a reduction in pericyte coverage, has been noted when compared to a younger cohort (Yang et al., 2020; Elahy et al., 2015). However, while there is a certain level of BBB disruption that is associated with aging, these hallmarks of BBB breakdown appear exacerbated in age associated neurodegenerative disorders. BBB disruption is a key characteristic in several neurodegenerative disease including Alzheimer's disease (AD), amyotrophic lateral sclerosis (ALS) and multiple sclerosis (MS) (Sweeney et al., 2018). An increase in BBB permeability is commonly noted in post-mortem AD patients with noted reduction of TJ proteins (Sweeney et al., 2018; Bake et al., 2009). Additionally, a distinct loss of claudin-5 expression has been noted in both mouse models of AD as well as in aged mice (Zhu et al., 2022). Taken together, these findings suggest that there is a close association between aging and a loss of claudin-5 expression and ultimately damage to the integrity of the BBB. Moreover, claudin-5 has been shown to cycle in a distinct circadian rhythm and is regulated by the essential circadian clock transcription factor, BMAL-1. Loss of BMAL-1 function has been shown to block claudin-5 cycling, which in turn affects EC expression and overall results in a loss of barrier integrity (Hudson et al., 2019). Importantly, it has also been established that BMAL1-mediated circadian rhythm is notably dysregulated in aging cohorts (Wyse and Coogan., 2010; Kondratov, et al., 2006). Therefore there is the potential that in this model, further claudin-5 downregulation may occur which has the potential to further exacerbate the previously described phenotype.

The Y-maze and the radial arm maze were again utilised to examine learning and memory ability of the aged *Cldn5*$^{fl/wt}$*xTie2Cre*. A significantly reduced spontaneous alternation score was noted in the claudin-5 heterozygous mice, which had not been noted in the previous characterisation of the model. This was potentially due to the increased side bias noted in the heterozygous mic, however in this aged model the presence of a non-significant side bias is still noted. As before, there was an increase in the number of errors made by the claudin-5 heterozygous mice. The correlation data utilising *Cldn5* mRNA levels supports both significant behaviour findings, that lower claudin-5 level results in a lower spontaneous alternation score but a higher number of repeat entry errors (Fig. 3.24 A). The radial arm maze analysis provides similar results to what had been noted in the characterisation of the younger cohort. The number of repeat entry errors was significantly

higher in the claudin-5 heterozygote mice in comparison to the control mice, which is again supported by the correlation data (Fig. 3.24 B (i)). Moreover the claudin-5 heterozygous mice, committed significantly more working and reference memory errors in comparison to the control cohort on days 7, 8 and 10 of the trial (Fig. 3.24 B (ii)). Across these learning and memory trials, while deficits are still clearly present in the claudin-5 heterozygote cohort, no substantial changes due to age are noted. The social interaction behaviour that was noted in the original characterisation did not change with age. The reduced preference for social interaction but no preference or aversion to novelty was still noted in this aged model (Fig. 3.26 B (i;ii)). The neglect of grooming behaviour that had been noted in the original characterisation of *Cldn5*$^{fl/wt}$*xTie2Cre* mouse model is no longer seen in the aged cohort. The aberrant grooming in the claudin-5 heterozygous cohort is thought to potentially be associated with disrupted neuronal signalling which results in the inability to complete complex sequential patterns and a loss of motor skills. In the characterisation of the aged cohort however, the significant difference is no longer noted between the claudin-5 heterozygote mice and the controls (Fig. 3.26 A; 3.27 A (iii;iv)). Rather than due to the effect of age on the knockdown mice, this may be due more to gradual impairments in the healthy cohort as they age, which results in a less significant difference between the cohorts. Locomotor skills were examined during both characterisations to ensure no mobility issues could potentially confound the results. While in the young *Cldn5*$^{fl/wt}$*xTie2Cre* model no locomotor deficits were noted, in the aged model an increased latency to fall from the rotarod was noted in the aged claudin-5 heterozygous mice (Fig. 3.28 B). In comparison to the age matched control mice, the aged claudin-5 deficient mice had significantly reduced acoustic PPI response at 77 dB and 83 dB prepulse with 120 dB pulse (Fig. 3.29). Correlation data of *Cldn5* mRNA expression and PPI response showed a clear positive correlation between claudin-5 expression and higher PPI % responses (Fig. 3.29 (iv;v)). The sensorimotor gating deficits noted have not deteriorated further with age. Overall these findings suggest that aging does not causes any further exacerbation on the behavioural deficits noted in the *Cldn5*$^{fl/wt}$*xTie2Cre* mouse model. A summary of all aged *Cldn5*$^{fl/wt}$*xTie2Cre* behavioural outputs can be seen in Fig. 3.31.

3.6 Summary:

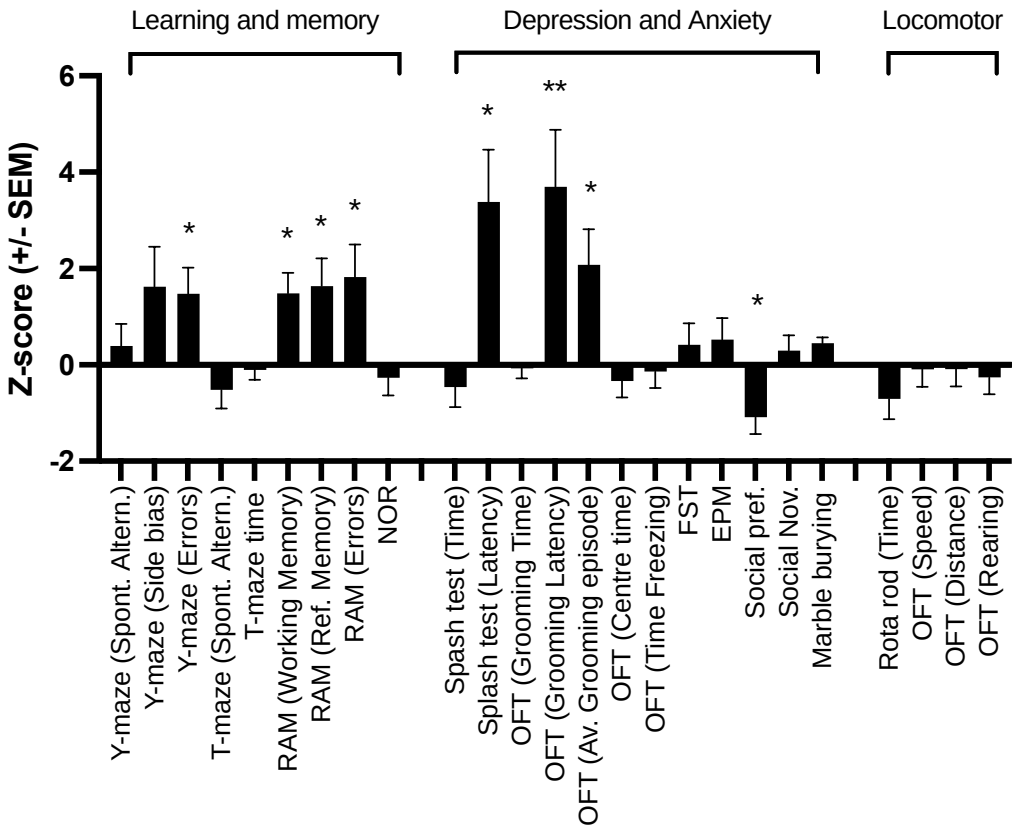

Figure 3.30 Summary of the behavioural dataset generated for the *Cldn5*$^{fl/wt}$*xTie2Cre* mice.

Data is expressed as Z-scores ± SEM. A positive Z-scores indicates the behaviour is above the average expected behavioural output and a negative Z-score signifies that the behaviour is below the expected behavioural output.

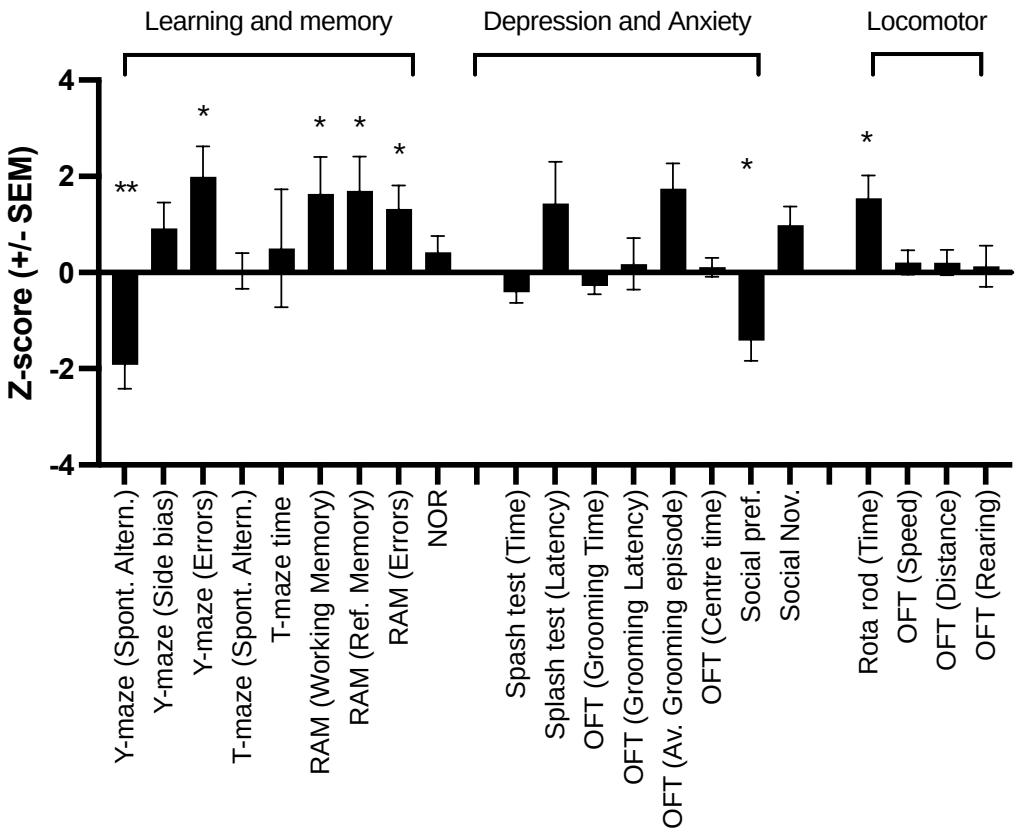

Figure 3.31 Summary of the behavioural dataset generated for the aged *Cldn5$^{fl/wt}$xTie2Cre* mice.

Data is expressed as Z-scores ± SEM. A positive Z-scores indicates the behaviour is above the average expected behavioural output and a negative Z-score signifies that the behaviour is below the expected behavioural output.

3.7 Conclusion:

- To our knowledge, this is the first ever behavioural characterisation of a claudin-5 heterozygous mouse model.
- This characterization has shown that a 50 % loss of claudin-5 is sufficient to result in negative behavioural phenotypes which includes issues with memory and elevated anxiety and sensorimotor gating deficits.

Chapter 4. Developing an AAV vector based gene therapy approach to overexpress claudin-5 specifically in ECs of the CNS.

4.1 Introduction:

As was discussed in detail in chapter 3, there is a large body of work which shows a clear link between decreased claudin-5 expression, BBB disruption and neurological disorders. Importantly, it has also been shown that in disorders with BBB disruption, such as epilepsy, if the barrier integrity is restored, the disease pathology can be attenuated. In the inducible claudin-5 knockdown model which will be described in detail in chapter 5, section 5.1.1, a severe pathology has been noted which includes seizures and death after 5 weeks of claudin-5 suppression (Greene et al., 2018). However it has also been shown that the reversal of claudin-5 suppression rescues the seizure phenotype. Mice put on doxycycline (Dox) for 4 weeks showed significant seizure activity as scored by the Racine scale and also significant astrogliosis in the hippocampus. These disease phenotypes were resolved following the removal of Dox for 2 weeks and the rescue was maintained, as noted in a 3 month follow up examination (Greene et al., 2022). Overall these findings showed that restoring claudin-5 expression at the barrier can restore function even when a clear and significant disease phenotype has developed.

Moreover, dynamic contrast enhanced MRI (DCE-MRI) imaging of patients with pharmacoresistant epilepsy conducted pre-surgical resection of epileptogenic tissue showed numerous sites of gadolinium extravasation, a finding that is drastically different to the age matched controls (Greene et al., 2022). Interestingly, findings from the lab has discovered in follow-up DCE-MRI imaging, two of the patients post-surgical resection noted a distinct reduction in gadolinium extravasation and overall clear rescue of BBB integrity (data unpublished).

ALK5 is an important signalling component of the TGFβ pathway. RepSox, a potent ALK5 inhibitor has also been shown to be an effective regulator of claudin-5 expression (Roudnicky et al., 2020). It is capable of inducing *Cldn5* mRNA expression and enhancing barrier properties *in vitro.* Moreover, its therapeutic effect has been further demonstrated, as when administered into a mouse model of epilepsy it sufficiently reduced seizures induced by intrahippocampal administration of KA. In addition to reducing seizure activity,

other rescue effects noted include attenuated BBB leakiness and reducing neural activity and astrogliosis. These findings suggest that RepSox, by restoring the level of claudin-5 in brain ECs, helps to stabilise the barrier integrity and prevent seizure activity (Greene et al., 2022). Moreover, as was also previously discussed in Section 1.8, several current neurotherapeutic drugs on the market that target disorders with BBB disruption such as MDD and schizophrenia, which include the anti-depressant, imipramine and the anti-psychotic drugs lithium, haloperidol and chlorpromazine have all been shown to normalise claudin-5 expression levels in *in vivo* studies (Menard et al., 2017; Greene et al., 2018). These findings further support the hypothesis that resolving barrier integrity through the restoration of claudin-5 expression in the ECs may rescue barrier function and reduce disease pathology.

While gene therapy has until now focussed on monogenic and usually rare disorders, it has become clear that this focus needs to pivot to include more common disorders. This pivot is essential, as monogenic rare diseases alone have a limited market and the cost of developing them cannot scale up to be commercially viable. This is due to two major contributing factors. Firstly, the cohort size for rare disorders is clearly limited. Additionally, the most common administration route in clinical trials is systemic (Au et al., 2021). This choice of administration route is often due to the disease in question, with disorders such as lysosomal storage disease requiring high systemic dosing. However, disease pathology for many disorders can be localised to a more specific target tissue. Despite this, often systemic administration is still chosen as the route of administration in a clinical trial solely because it is the least invasive and technically easiest method for clinicians. But this pathway requires a large dose to be effective. All of these factors drive the cost of goods (COGs) upwards (Fig. 4.1). Therefore it is essential to examine techniques to treat patients with local delivery and with a lower dose of the viral vector. This could drive down the overall COGs but also open up the potential of gene therapy to more common disorders that also have limited therapeutic options available currently. To develop gene therapies for more common diseases such as epilepsy, identifying a novel mechanism of action, such as the loss of claudin-5 expression at the BBB, is essential.

Therefore the central theme of this chapter is to develop a gene therapy based approach to treat refractive epilepsy and other neurological disorders with noted reduction in claudin-5 expression. To achieve this, the overarching aim is to design an AAV vector that is capable

of specifically expressing high levels of claudin-5 expression in the cerebrovascular endothelium.

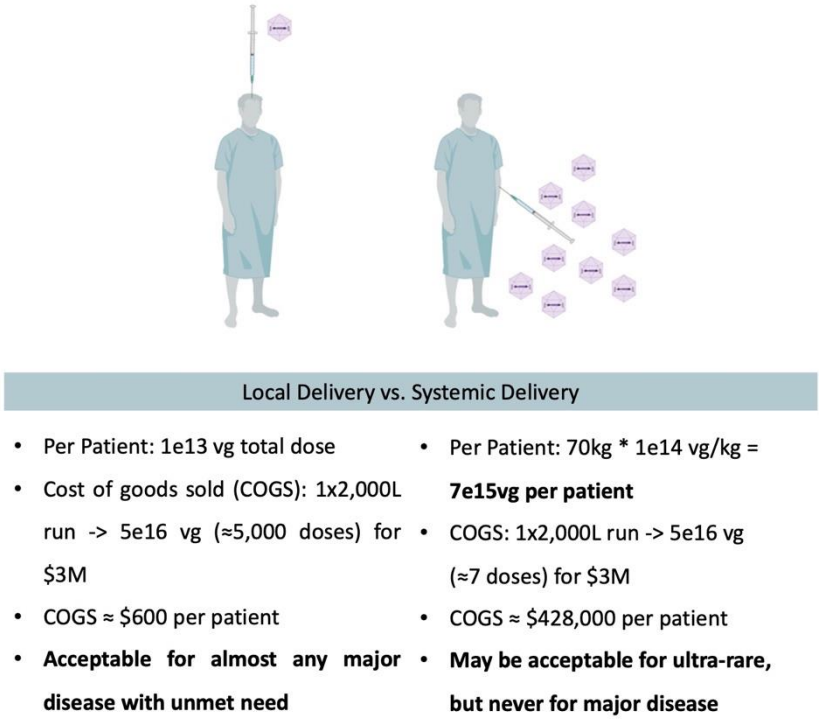

Figure 4.1 Example of delivery routes affecting COGs for gene therapy development. Schematic created with BioRender. Example based on standard dosages (Au et al., 2021).

4.2 Objectives:

- Carry out *in vitro* characterisation of the various plasmids and identify what components result in the most efficient upregulation of claudin-5 expression.
- Characterise the resulting AAV *in vivo* examining aspects such as administration route, dosage and toxicity.
- Behaviourally characterise the effect of overexpression of claudin-5 *in vivo.*

4.3 Results:

4.3.1 Screening plasmids *in vitro* to assess efficacy of claudin-5 expression induction

4.3.1.1 Screening non-inducible claudin-5 plasmids *in vitro*

Initial development of the gene therapy based approach starts with the design and optimisation of the gene expression vector that will later be incorporated into an AAV vector. Plasmids were designed by Dr. Chris Greene. The gene of interest for our new gene therapy is the most enriched TJ protein and one that is notably downregulated in numerous neurological disorders, claudin-5. Therefore each plasmid contains a claudin-5 gene. However, while all plasmids carried a claudin-5 gene, between plasmids there are numerous sources of variation, most notably the use of either the human (H) or mouse (M) versions of the claudin-5 gene. Additionally screening to compare the native (N) version of each gene to a codon optimised (CO) version was undertaken (Fig. 4.2). Moreover, the effect of different promoters driving expression was investigated, comparing the endogenous claudin-5 promoter to the EC specific promoter *Icam2*. Plasmids were screened *in vitro* in the mouse brain EC line, bEnd.3 cells. Initial screening was used to investigate any changes to claudin-5 expression over time, at 24 hr and 48 hr.

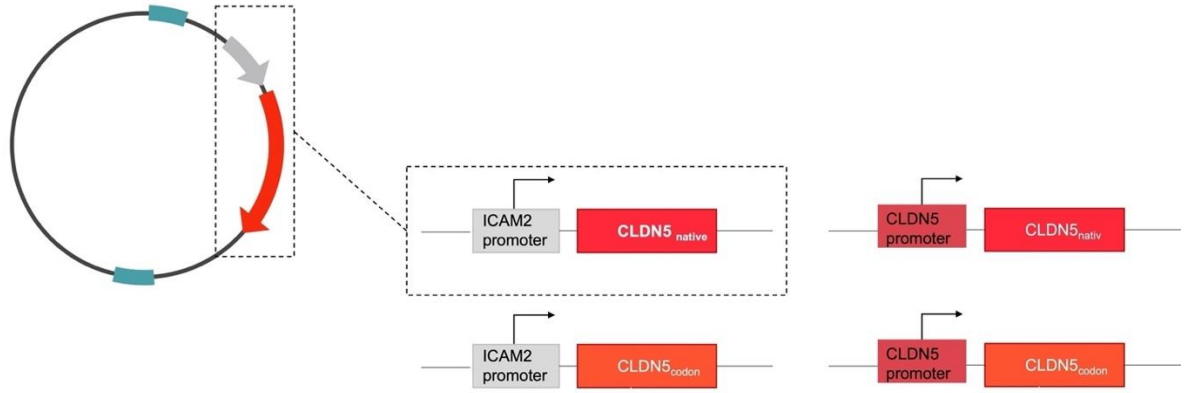

Figure 4.2. Non-Inducible Plasmid Maps

Plasmid map represent the various plasmids used. Each plasmid contains a *Cldn5* gene. Between plasmids, this gene varied in a number of ways. Firstly, the gene was either human or mouse. Secondly, the gene could either be the native or the codon optimised version. Lastly the gene was under the control of one of two possible promoters, either the endogenous *Cldn5* or the *Icam2* promoter.

The first screen compared two plasmids with the native mouse claudin-5 gene insert under the control of either the *Icam2* promoter or the claudin-5 promoter. In this case the *Icam2* promoter plasmid (*Icam2-Cldn5*(N.M)) was more successful, as after 48 hr there was a significant increase in claudin-5 expression in both the RNA and protein screens (Fig. 4.3 A; C). The claudin-5 promoter (*Cldn5-Cldn5*(N.M)) in comparison, while resulting in some increased RNA expression 48 hr post transfection, showed no significant change at the protein level (Fig. 4.3 B). Through RT-PCR analysis the effect of the claudin-5 plasmid transfection on the other junctional components was examined. In comparison to the empty vector (EV) treated cells, the *Icam2-Cldn5*(N.M) plasmid resulted in an increase in occludin expression only. However the *Cldn5-Cldn5*(N.M) plasmid significantly increased the expression of ZO-1, occludin and Lsr, even more so than the claudin-5 expression itself (Fig. 4.3 C). Overall, transfection with the *Cldn5-Cldn5*(N.M) plasmid resulted a less successful overexpression of claudin-5 and resulted in more off target changes in gene expression.

Next, two plasmids containing native human claudin-5 gene were compared, again examining expression changes driven by the *Icam2* promoter to the *Cldn5* promoter. In this case the *Icam2* promoter plasmid (*Icam2-CLDN5*(N.H)) resulted in a significant increase in the RNA expression levels of claudin-5, with again the protein levels mirroring the expression changes but not significantly (Fig. 4.4 A;C). The claudin-5 promoter version of the plasmid (*Cldn5-CLDN5*(N.H)) actually resulted in an overall very poor level of expression at the protein level and resulted in only off target gene expression changes at the transcriptional level (Fig. 4.4 B;C) .

Optimising expression was further examined by investigating the effect of utilising CO versions of the claudin-5 genes in the plasmid design. Therefore, four more plasmids were designed with the CO versions of the mouse or human claudin-5 gene under the control of either the *Icam2* or the *Cldn5* promoter. In comparison to the *Icam2-Cldn5*(N.M) plasmid used in (Fig. 4.3 A;C), the codon optimised version (*Icam2-Cldn5*(CO.M)) resulted in poorer results overall, with an increase in claudin-5 at the transcriptional level but no changes noted at the protein level (Fig. 4.5 A;C).

Codon optimisation of the claudin-5 driven plasmid (*Cldn5-Cldn5*(CO.M)) however did result in improved expression from what had been observed with the *Cldn5-Cldn5*(N.M) plasmid (Fig. 4.3C). The *Cldn5-Cldn5*(CO.M) version yielded much higher transcriptional

expression of claudin-5 (Fig. 4.5 C). Codon optimisation of the human claudin-5 plasmids also noted improvement from what had been noted in the native screens (Fig. 4.5 vs 4.4). Transfection with the *Icam2-CLDN5*(CO.H) plasmid resulted in significant increase in claudin-5 expression at both the transcriptional and translational level (Fig. 4.5 D;F). The *Cldn5-CLDN5*(CO.H) plasmid resulted in significant increase in claudin-5 RNA expression, however this was not seen at the protein level examined through Western blot (Fig. 4.5 E;F). Across the board, codon optimisation appeared to be result in fewer off target effects. (Fig. 4.5 C;F).

Overall, the *Icam2* promoter appears to generally result in a much higher level of expression in comparison to the endogenous *Cldn5* promoter. Additionally, while codon optimisation is generally carried out to enhance expression, in this case, while it did appear to help reduce off-target effects, the overall level of claudin-5 expression did not appear to significantly change, particularly in the plasmids whose expression was controlled by the *Icam2* promoter. To verify this observation, a final screen was carried out to directly examine and compare the efficacy of the CO plasmids in comparison to their native counterparts. Through this final screen it is clear that firstly, the *Icam2* promoter overall resulted in a consistently higher level of claudin-5 expression at 48 hr in comparison to the endogenous *Cldn5* promoter at both the transcriptional and translational level (Fig. 4.6 A (i;ii)). Moreover, while the CO plasmids had reduced off-target gene expression, it had not successfully increased the level of claudin-5 expression in comparison to the native versions. Consistently the native plasmids resulted in equally if not better levels of expression (Fig. 4.6).

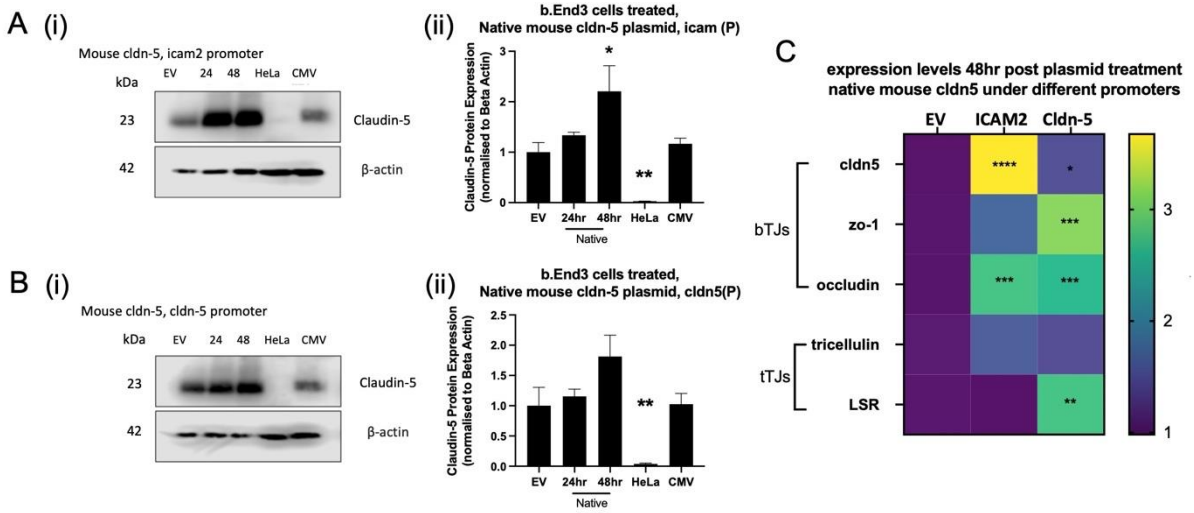

Figure 4.3. Changes in protein and RNA expression in bEnd.3 cells following transfection with plasmid containing the native mouse claudin-5 gene under *Cldn5* or *Icam2* promoter

A. (i) Western blot and (ii) densitometric analysis of claudin-5 protein expression in bEnd.3 cells transfected for 24 or 48 hr with *Icam2-Cldn5*(N.M) plasmid. B. (i) Western blot and (ii) densitometric analysis of claudin-5 protein expression in bEnd.3 cells transfected for 24 or 48 hr with *Cldn5-Cldn5*(N.M) plasmid C. RT-PCR data of important bTJ and tTJs components revealed transfection resulted in a significant increase in *Cldn5* mRNA expression compared to the empty vector (EV) control, with the *Icam2-Cldn5*(N.M) promoter plasmid being the most successful. Transfection with the *Cldn5-Cldn5*(N.M) plasmid resulted in more off target changes in gene expression. All control samples were taken 24 hr post transfection with plasmid of interest. HeLa samples act as the negative control. CMV-*Cldn5* functions as the positive control. Results expressed as mean ± SEM. Unless otherwise stated, the results were non-significant. *P<0.05 by one-way ANOVA and Tukey's post-test. n=2 per transfection.

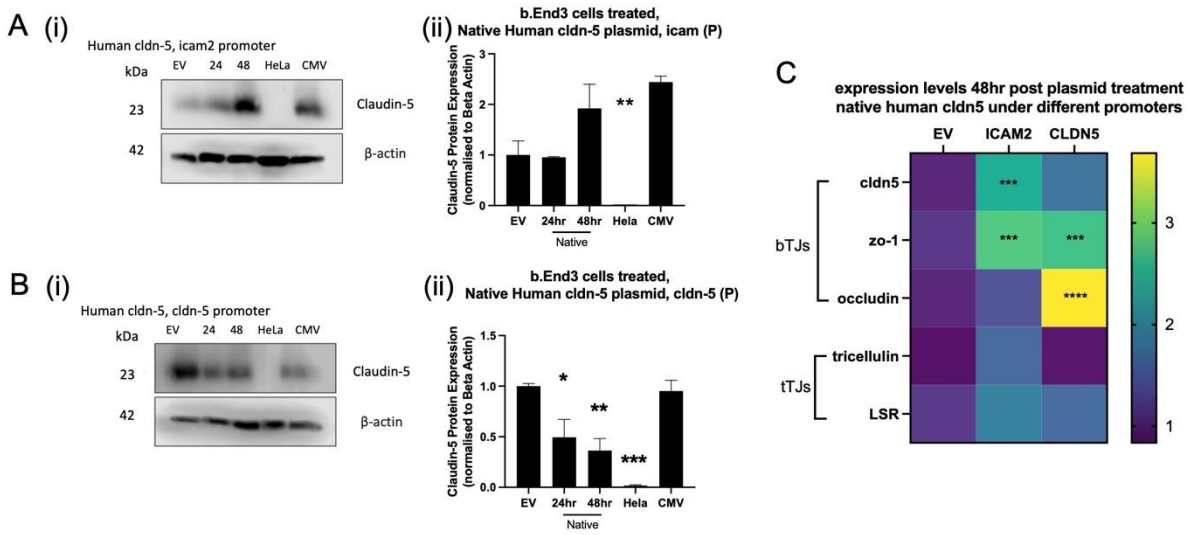

Figure 4.4. Changes in protein and RNA expression in bEnd.3 cells following transfection with plasmid containing the native human claudin-5 gene under *Cldn5* or *Icam2* promoter

A. (i) Western blot and (ii) densitometric analysis of claudin-5 protein expression in bEnd.3 cells transfected for 24 or 48hr with *Icam2-CLDN5*(N.H) plasmid. B. (i) Western blot and (ii) densitometric analysis of claudin-5 protein expression in bEnd.3 cells transfected for 24 or 48 hr with *Cldn5-CLDN5*(N.H) plasmid. C. RT-PCR data revealed transfection resulted in a significant increase in *Cldn5* mRNA expression compared to the EV control with the *Icam2-CLDN5*(N.H) plasmid only. Transfection with the *Cldn5-CLDN5*(N.H) plasmid resulted in only off-target changes in gene expression. All control samples were taken 24 hr post transfection with plasmid of interest. HeLa acts as the negative control. CMV-*Cldn5* functions as the positive control. Results expressed as mean ± SEM. Unless otherwise stated, the results were non-significant. *P<0.05 by one-way ANOVA and Tukey's post-test. n=2 per transfection.

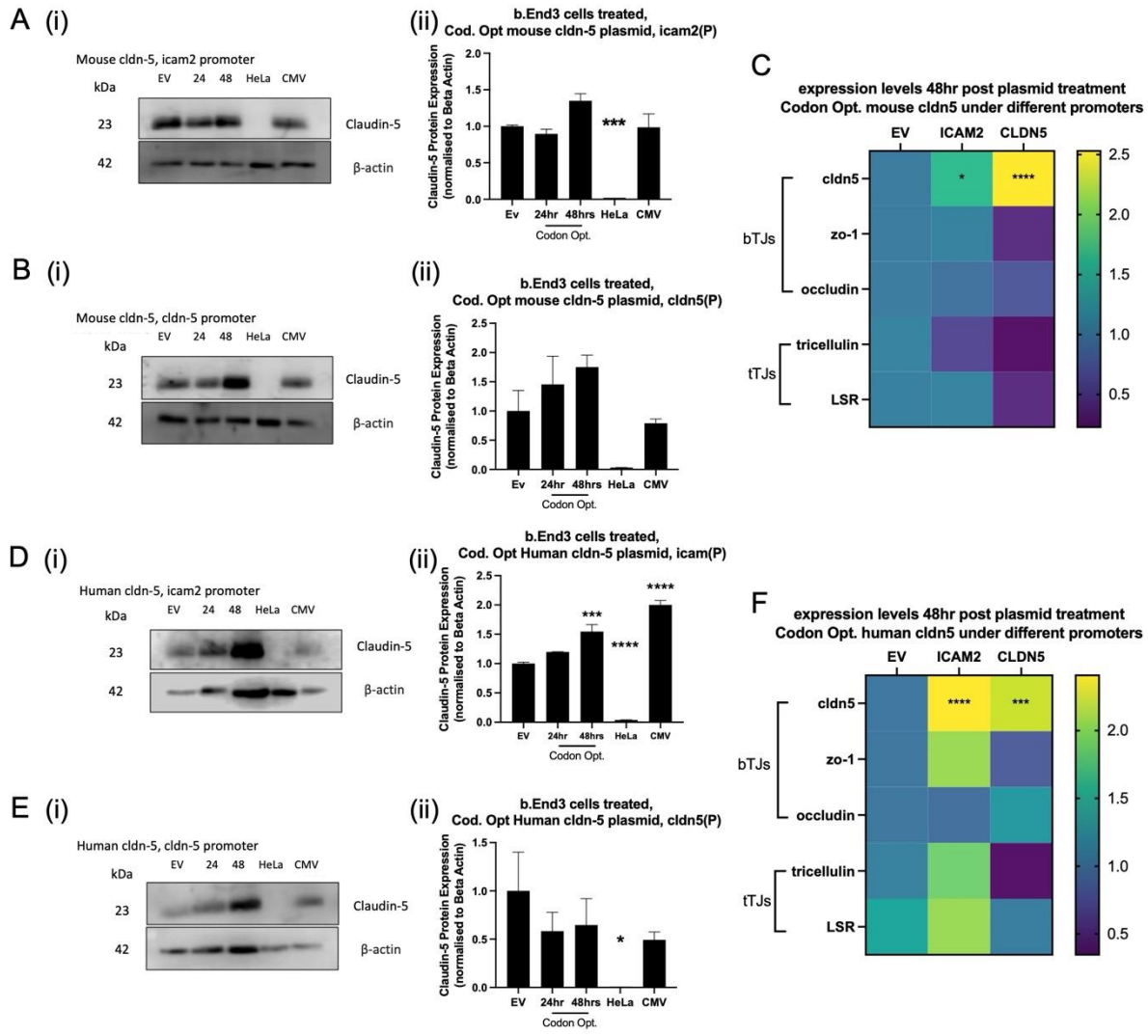

Figure 4.5 Changes in protein and RNA expression in bEnd.3 cells following transfection with plasmid containing the codon optimised mouse or human claudin-5 gene under *Cldn5* or *Icam2* promoter

A. (i) Western blot and (ii) densitometric analysis of claudin-5 protein expression in bEnd.3 cells transfected for 24 or 48 hr with *Icam2*-*Cldn5*(CO.M) plasmid. B. (i) Western blot and (ii) densitometric analysis of claudin-5 protein expression in bEnd.3 cells transfected for 24 or 48 hr with *Cldn5*-*Cldn5*(CO.M) plasmid. C. RT-PCR data revealed transfection resulted in a significant increase in *Cldn5* mRNA expression compared to the EV control for both plasmids, with a higher level of *Cldn5* expression noted from the *Cldn5*-*Cldn5*(CO.M) plasmid transfection. Neither resulted in any off target changes in gene expression. D. (i) Western blot and (ii) densitometric analysis of claudin-5 protein expression in bEnd.3 cells transfected for 24 or 48 hr with *Icam2*-*CLDN5*(CO.H) plasmid. E. (i) Western blot and (ii) densitometric analysis of claudin-5 protein expression in bEnd.3 cells transfected for 24 or 48 hr with *Cldn5*-*CLDN5*(CO.H) plasmid. F. RT-PCR data revealed transfection resulted in a significant increase in *Cldn5* mRNA expression compared to the EV control with both the *Icam2*-*CLDN5*(CO.H) and *Cldn5*-*CLDN5*(CO.H) plasmid with no off target gene expression changes. All control samples were taken 24 hr post transfection with plasmid of interest. HeLa samples act as the negative control. CMV-*Cldn5* functions as the positive control. Results expressed as mean ± SEM. Unless otherwise stated, the results were non-significant. *P<0.05 by one-way ANOVA and Tukey's post-test. n=2 per transfection.

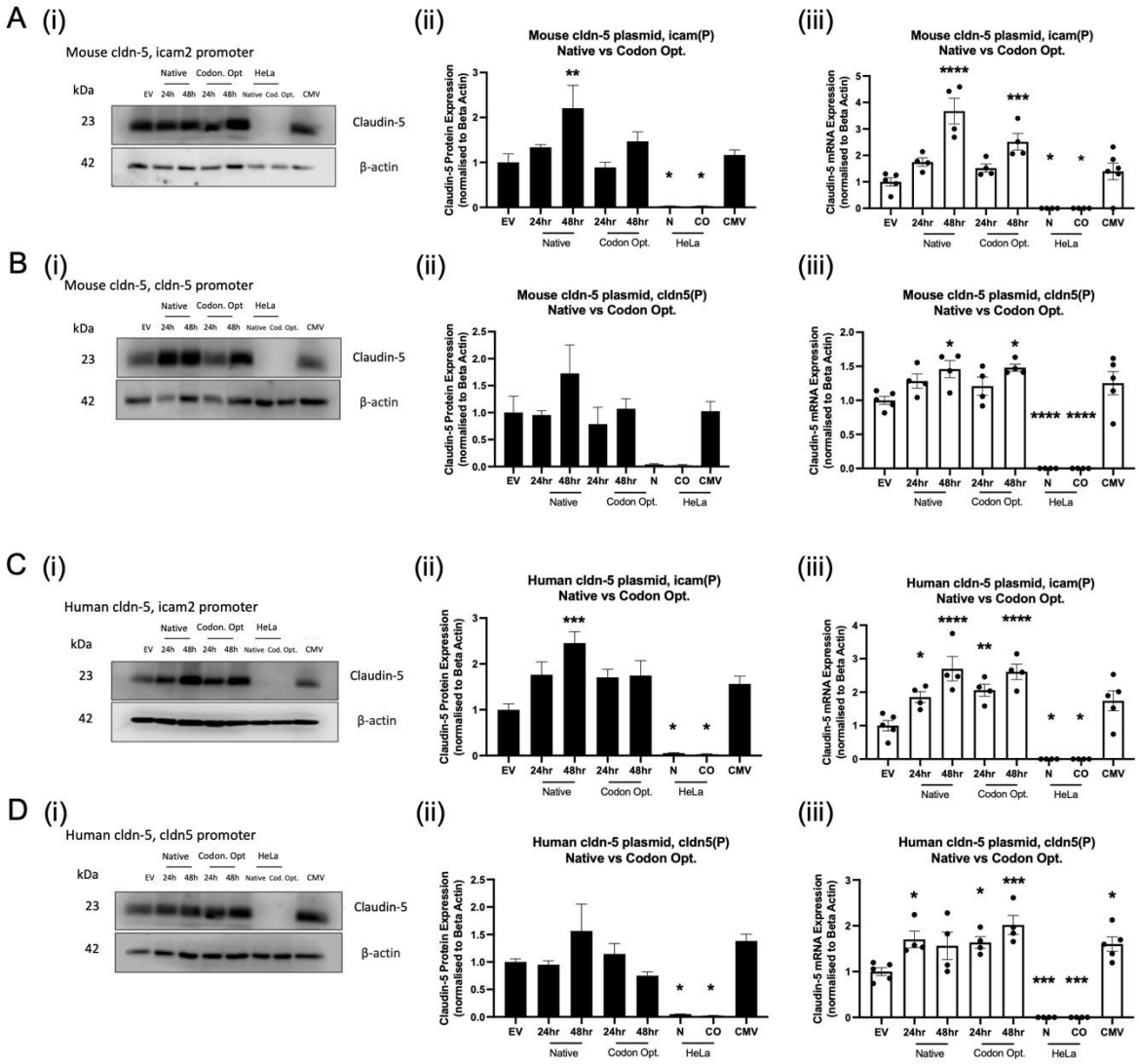

Figure 4.6 Changes in protein and RNA expression in bEnd.3 cells following plasmid transfections comparing efficacy of native gene expression to the codon optimised gene expression

A. (i) Western blot and (ii) densitometric analysis of claudin-5 protein expression, comparing efficacy of native mouse *Cldn5* gene to the codon optimised version, both under the control of the *Icam2* promoter 24 or 48 hr post-transfection. (iii) 2^-ΔΔCt values of *Cldn5* mRNA expression. **B. (i)** Western blot and (ii) densitometric analysis of claudin-5 protein expression, comparing efficacy of native mouse *Cldn5* gene to the codon optimised version, both under the control of the *Cldn5* promoter 24 or 48 hr post-transfection. (iii) 2^-ΔΔCt values of *Cldn5* mRNA expression. **C (i)** Western blot and (ii) densitometric analysis of claudin-5 protein expression, comparing efficacy of native human *CLDN5* gene to the codon optimised version, both under the control of the *Icam2* promoter 24 or 48 hr post-transfection. (iii) 2^-ΔΔCt values of *Cldn5* mRNA expression. **D. (i)** Western blot and (ii) densitometric analysis of claudin-5 protein expression, comparing efficacy of native human *CLDN5* gene to the codon optimised version, both under the control of the *Cldn5* promoter 24 or 48hr post-transfection . (iii) 2^-ΔΔCt values of *Cldn5* mRNA expression. All control samples were taken 24 hr post transfection with plasmid of interest. HeLa samples act as the negative control. CMV-*Cldn5* functions as the positive control. Results expressed as mean ± SEM. Unless otherwise stated, the results were non-significant. *P<0.05 by one-way ANOVA and Tukey's post-test. n=2 per transfection.

4.2.1.2 Screening inducible claudin-5 plasmids *in vitro*

The introduction of additional control elements into the vector is a necessary step when the aim is to move this towards therapeutic relevancy in the clinic. The inclusion of the Tet-inducible system was designed in a way that not only allows for temporal control but additionally due to the arrangement of the promoters ahead of an essential element of the Tet-on system, the reverse tetracycline controlled transactivator (rtTA), it should also ensure more cell specific expression.

In this screen, only the mouse claudin-5 gene was incorporated into plasmids. Furthermore, due to the clear success in driving expression in the previous non-inducible plasmid screens, the *Icam2* promoter was utilised in the plasmid design and became the focus of further investigation. As with the previous plasmid screens, the point of variability was the use of the CO version of the gene in comparison to the native version of the gene. An additional control was added into this screen with the inclusion of a control plasmid, which contains the green fluorescent protein (GFP) gene under the control of either the *Icam2* promoter.

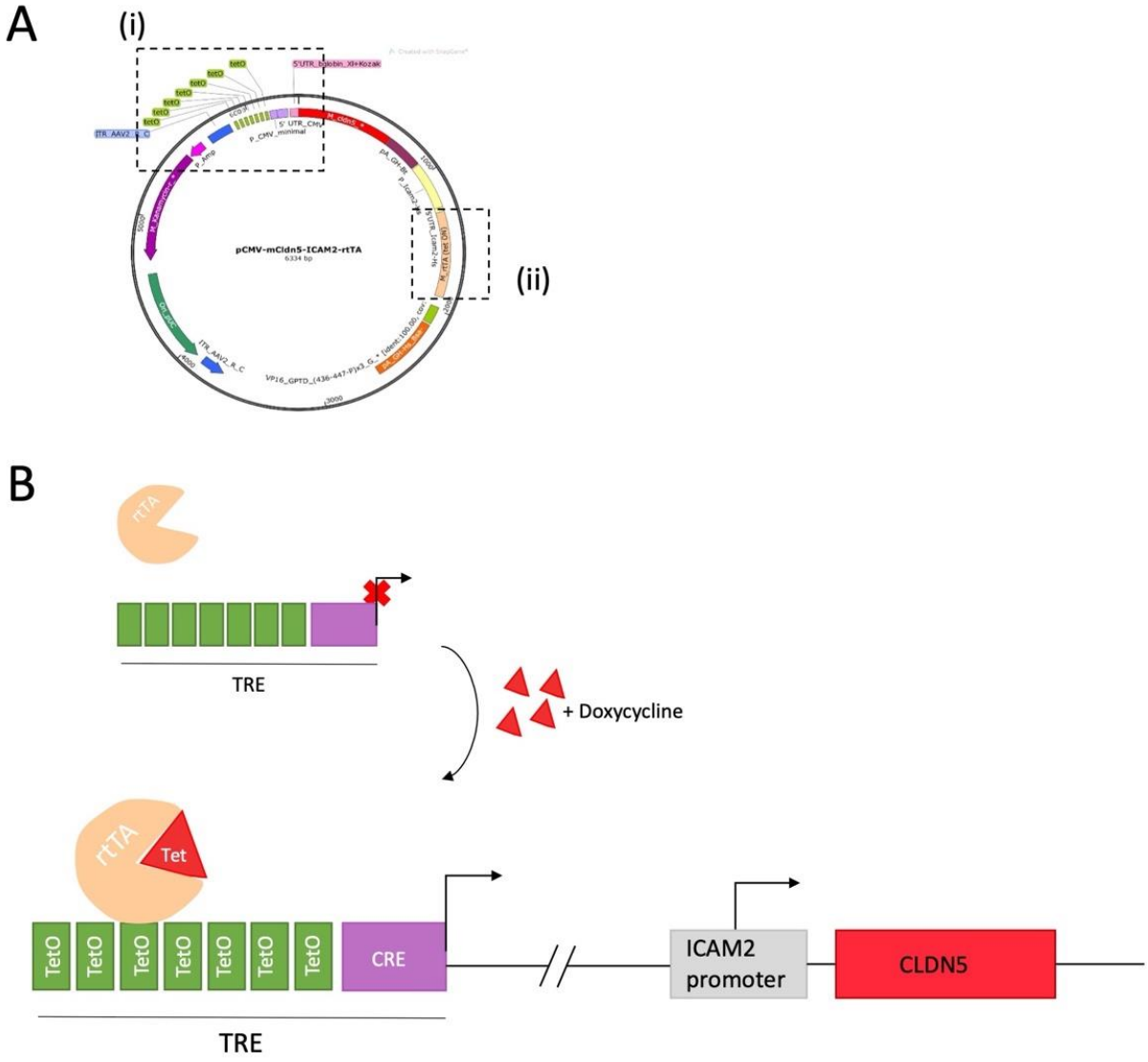

Figure 4.7. Inducible Plasmid Map and the Tet-On system

(A) Representative plasmid map for the inducible plasmids. (i) location of the inducible tetracycline response element (TRE) within the plasmid. (ii) location of the gene of interest, *Cldn5*. For each plasmid, the backbone was the same, containing a Tet-On system which controls the gene of interests expression. (B) The inducible Tet-On system, contains tetO repeats upstream of a cytomegalovirus (CMV) minimal promoter, which together form the TRE. *Cldn5* is under the control of the TRE and so can only be expressed in the presence of tetracycline (Tet) or its derivative doxycycline (Dox), as the rtTA protein can only bind to the operator if it is also bound by Tet. Therefore in this case the presence of doxycycline activates expression.

bEnd.3 cells were transfected with the doxycycline (Dox) inducible plasmid. 24 hr following transfection, cells were treated with (1 µg/ml) of Dox. Both inducible plasmids displayed clear induction of claudin-5 overexpression following Dox treatment in comparison to the control plasmid, a Dox inducible plasmid with the *Icam2* promoter

driving GFP expression. However, as was seen in the non-inducible screens, the native plasmid did overall result in a much higher level of overexpression in comparison to the CO version (Fig. 4.8 A;B).

The inducibility of the plasmids over time was investigated, comparing the expression levels of claudin-5 in bEnd.3 cells transfected with the control or the plasmid of interest, followed by either treatment with Dox or no treatment (DMEM media). While there is clear upregulation of claudin-5 expression following treatment with Dox, it is important to note that this inducible expression system may not be maintaining tight control on gene expression. Indications of a "leaky" expression system can clearly be seen when comparing the control plasmid to the claudin-5 plasmid when neither have been treated with Dox. While both untreated, there is still increased claudin-5 expression in bEnd.3 cells transfected with the claudin-5 plasmid in comparison to the control (Fig. 4.9 A).

Another important factor to examine when using an inducible expression system is the ability to reverse the effect of the inducible system. The effect of treating transfected bEnd.3 cells with Dox for 24 hr followed by the removal of the treatment along a series of timepoints was examined. Changes in claudin-5 expression was compared to both the control plasmid and the claudin-5 plasmid being treated with Dox for those same timepoints (Fig. 4.10). The results for both protein and mRNA expression following treatment with the inducible plasmid carrying the native claudin-5 plasmid were similar. Firstly, the Dox treated controls showed a low level of expression, providing a baseline level of claudin-5 expression in bEnd.3 cells. This expression however significantly increases both at the protein and mRNA levels in claudin-5 plasmid transfected cells treated with Dox, with the consistent finding of the most significant expression seen 48hrs post Dox treatment (Fig. 4.10). Finally, following the removal of Dox the level of claudin-5 expression quickly reverts to low level that is more similar to the control samples (Fig. 4.10 A). The level of claudin-5 expression that results from transfection with the CO plasmid and treatment with Dox is low in comparison to the native plasmid. While the control samples retain a low level of expression that is comparable to the controls in the native plasmid screen, the transfected and Dox treated cells did not result in any major increase in expression at the protein or mRNA level. While a significant increase in expression is noted at the transcriptional level, this was found when treatments were compared to the 24 hr control sample, which in itself is significantly different to the other control samples of later

timepoints (Fig. 4.10 B). While the reversible treatment group showed a trend towards decreasing expression with time following drug withdrawal, its expression levels as with the Dox treated group, are all within the control expression range and so not realistically significant in comparison to the results with the native plasmid (Fig. 4.10 A versus B).

Examining the reversibility of plasmid expression over time was then carried out, firstly treating cells with Dox for set time periods ranging from 24 hr-72 hr followed by removal of this treatment for a range of time periods again between 24 hr and 72 hr. Both the native (Fig. 4.11A) and the CO (Fig. 4.11 B) plasmids were examined. The native plasmid clearly produced significantly higher levels of *Cldn5* mRNA expression in comparison to the CO plasmid transfection. For the native plasmid, RT-PCR analysis details the clear effect of the treatments on bEnd.3 cell expression. The control samples (GFP) show little expression regardless of Dox treatment while treatment with Dox on the inducible claudin-5 samples result in a statistically significant increase in expression. Samples that were taken off Dox show much lower levels of expression in comparison to the Dox treated samples, demonstrating reversibility along a range of timepoints. Following the removal from Dox the claudin-5 expression levels reduce to a comparable level to the control samples (Fig. 4.11A). An important finding to note is again the issue of leakiness within this inducible system. When comparing the expression at the level of transcription, in the untreated group, the control GFP and the native plasmid should show the same level of expression. However as seen in Fig.4.11 A, there is a statistically significant increase in expression of the native plasmid without treatment. Comparing the expression level of the untreated claudin-5 with its counterpart in the treated group however, there is a substantially higher level of expression in the treated group. Therefore this system while certainly inducible, shows indications that there may be issues with the control of its expression.

All previous experiments had been carried out using the standard Dox treatment concentration of 1 μg/ml. To fully characterise the inducibility of this plasmid an investigation into the effect of Dox concentration on the efficacy of induction was carried out. Following transfection with either the native or codon optimised plasmid, cells were treated with Dox at a range of concentrations 0.1 μg/ml, 0.5 μg/ml, 1 μg/ml and 2 μg/ml. While the level of protein expression appears comparable between the native claudin-5 plasmid and the vector carrying the CO gene, through densitometric analysis the native

plasmid resulted in higher claudin-5 expression over both time and dose and moreover resulted in much higher claudin-5 expression with RT-PCR analysis in comparison to the CO construct (Fig. 4.12). For the native plasmid transcriptional data indicated that at both 24 hr and 48 hr, at all concentrations assessed there was increased expression. This indicates that the inducible system is highly sensitive to the Dox effector molecule. This expression is reduced by the 72 hr timepoint. The high mRNA levels noted translates to high protein expression with a later timepoint, with both the 48 hr and 72 hr timepoints showing higher expression.

Overall the plasmid construct containing the native claudin-5 gene under the control of the *Icam2* promoter resulted in overall better overexpression of claudin-5 at the mRNA and protein level, as verified through RT-PCR and WB analysis respectively. Clear inducibility and reversibility was demonstrated with the presence or absence of the effector, Dox. While the inducible target gene overexpression was achieved, results demonstrate that there may be leaky expression in the inducible expression system.

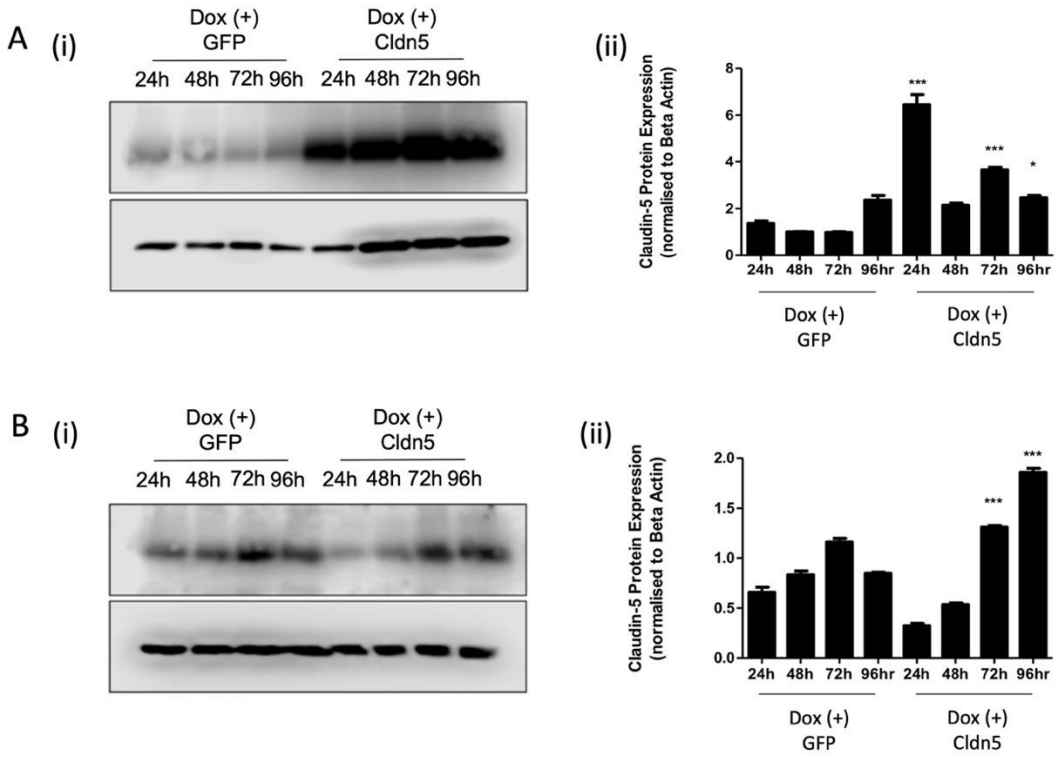

Figure 4.8. Western blot and densitometric analysis of protein expression levels of claudin-5 in bEnd.3 cells transfected with doxycycline inducible plasmids.

A. (i) Western blot and (ii) densitometric analysis of bEnd.3 cells transfected with inducible native claudin-5 plasmid from 24 to 96 hr, showing clear induction of claudin-5 overexpression in

transfected cells following Dox treatment. B. (i) Western blot and (ii) densitometric analysis of bEnd.3 cells transfected with inducible codon optimised claudin-5 plasmid from 24 to 96 hr, showing induction of claudin-5 overexpression in transfected cells following Dox treatment. Results expressed as ± SEM. Unless otherwise stated, the results were non-significant. *** P<0.001 by ANOVA with Dunnett post-test. n=2 per transfection.

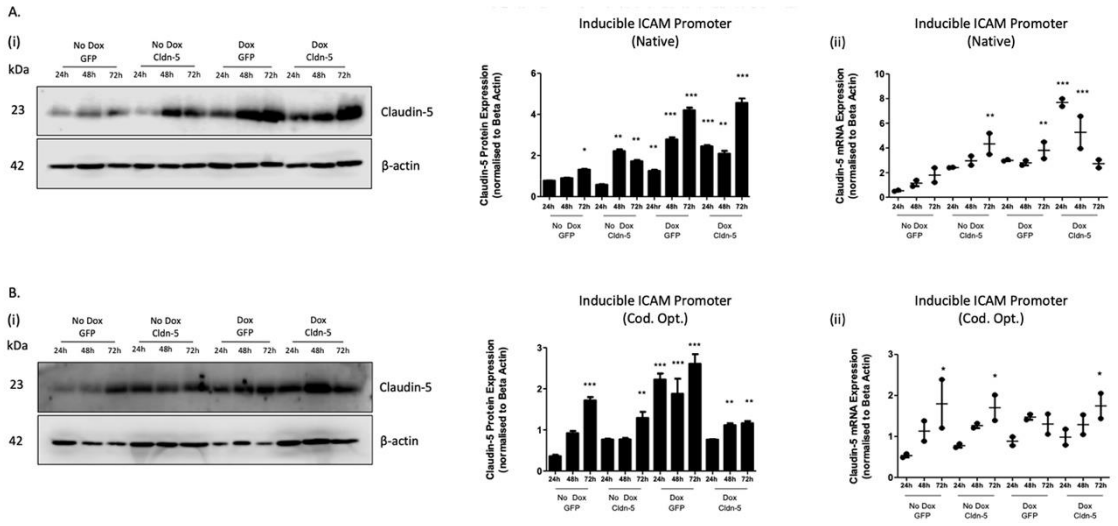

Figure 4.9. Change in claudin-5 protein and mRNA expression following doxycycline inducible plasmid transfection and treatment with doxycycline over time

A.(i) Western blot shows claudin-5 expression in bEnd.3 cells transfected with plasmid containing native *Cldn5* gene following treatment with or without Dox treatment over a series of timepoints from 24-72hr. Densitometry analysis normalised to β-actin. (ii) Graph represents 2^-ΔΔCt of bEnd.3 cells following the same treatment. B.(i) Western blot shows claudin-5 expression in bEnd.3 cells transfected with plasmid containing CO *Cldn5* gene following treatment with or without Dox treatment over a series of timepoints from 24-72 hr. bEnd.3 cells transfected with plasmid containing GFP gene following treatment with or without Dox treatment over a series of timepoints from 24-72hr used as a control. Densitometry analysis normalised to β-actin. (ii) Graph represents 2^-ΔΔCt of bEnd.3 cells following the same treatment. Results expressed as ± SEM. *** P<0.001 by ANOVA with Dunnett post-test. n=2 per transfection.

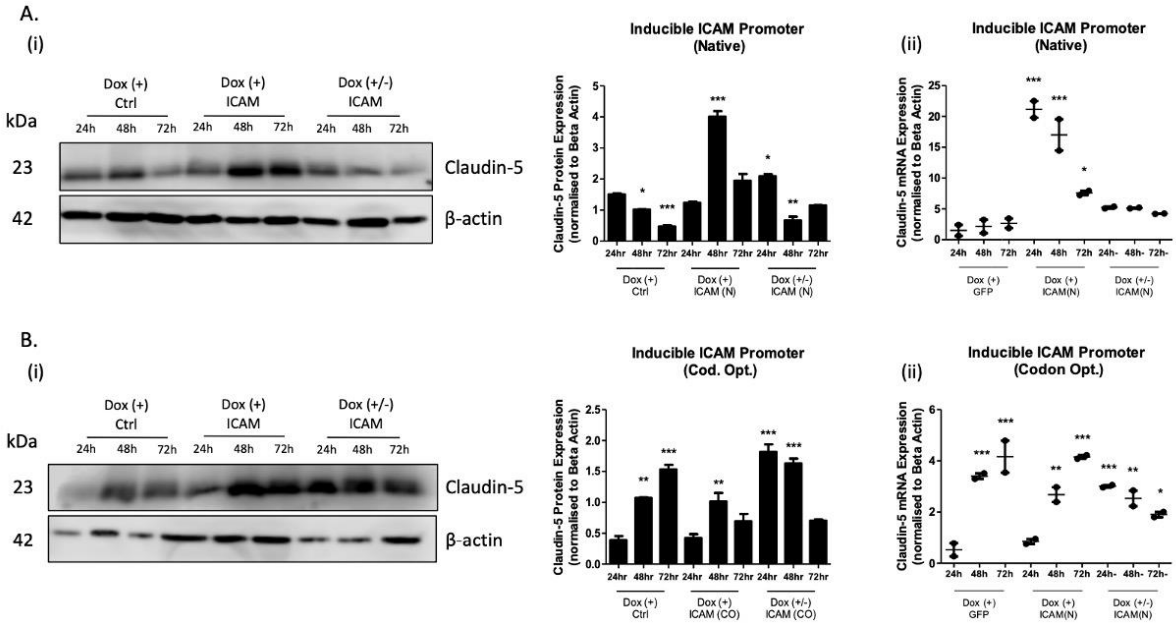

Figure 4.10. Determining reversibility of claudin-5 expression following removal of doxycycline treatment

bEnd3 cells were transfected with plasmid containing native claudin-5 (A) or CO claudin-5 (B) followed by treatment with Dox (+) for varying periods of time compared to GFP control plasmid. To assess reversibility bEnd3 transfected cells were treated with Dox for 24 h and then subsequently dox removed (+/) and claudin-5 expression levels analysed 24-48 h after dox removal **(i)**Western blot and densitometric analysis determining claudin-5 expression levels normalised to β-actin. **(ii)** Transcript analysis representing claudin-5 changes expressed as 2^-ΔΔCt of bEnd.3 cells following the same treatment as (i). Results expressed as ± SEM. *** P<0.001 by ANOVA with Dunnett post-test. n=2 per transfection.

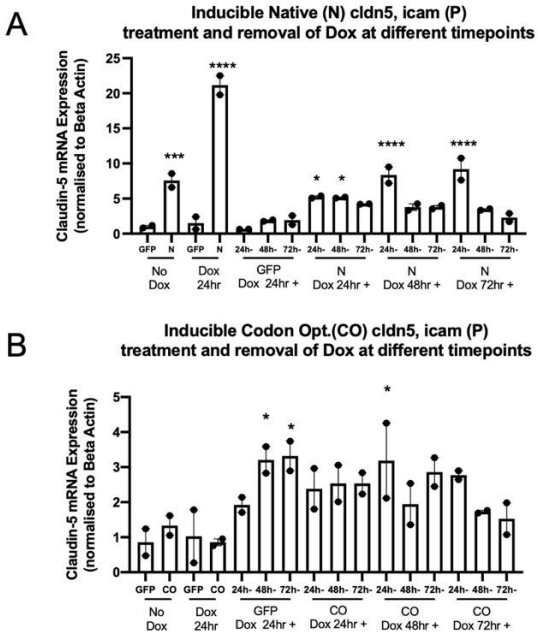

Figure 4.11. Determining reversibility of claudin-5 expression following removal of doxycycline treatment over time

A. *Cldn5* mRNA expression in bEnd.3 cells transfected with plasmid containing native (N) *Cldn5* gene following treatment and withdrawal of Dox for varying time periods (24-72hrs). Graph represents 2^-ΔΔCt. B. *Cldn5* mRNA expression in bEnd.3 cells transfected with plasmid containing codon optimised (CO) *Cldn5* gene following treatment and withdrawal of Dox for varying time periods (24-72hrs). Results expressed as ± SEM. *** P<0.001 by ANOVA with Dunnett post-test. n=2 per transfection.

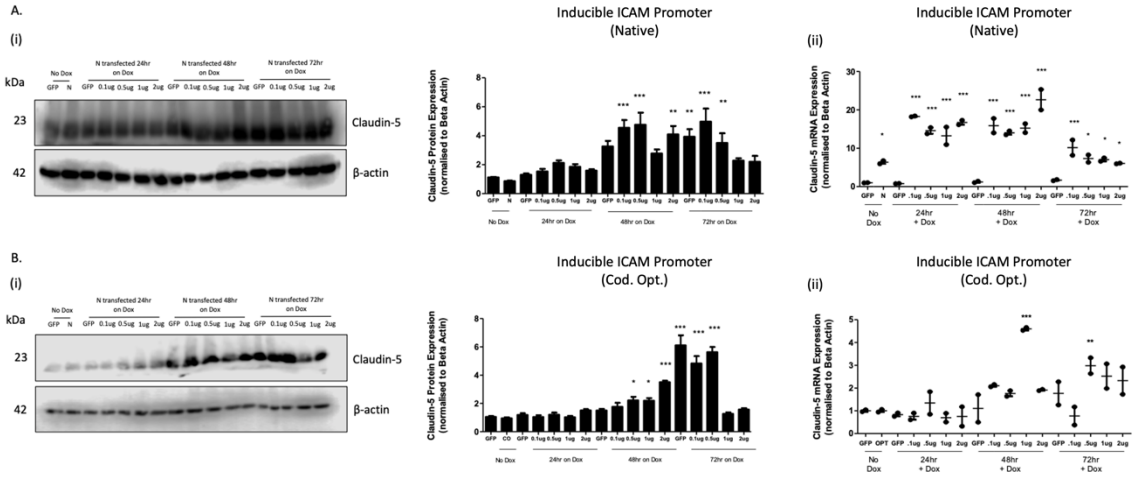

Figure 4.12. Change in claudin-5 protein and mRNA expression following doxycycline inducible plasmid transfection and treatment with doxycycline at different concentrations.

A. (i) Western blot shows claudin-5 expression in N plasmid transfected bEnd.3 cells following Dox treatment at a range of concentrations. Densitometry analysis normalised to β-actin **(ii)** Graph represents 2^-ΔΔCt of bEnd.3 cells following the same treatment. **B. (i)** Western blot shows claudin-5 expression in CO plasmid transfected bEnd.3 cells following treatment with Dox treatment at a range of concentrations. Densitometry analysis normalised to β-actin. **(ii)** Graph represents 2^-ΔΔCt of bEnd.3 cells following the same treatment. Dox concentration treatments were 0.1μg/ml, 0.5μg/ml, 1 μg/ml and 2 μg/ml. Results expressed as ± SEM. *** P<0.001 by ANOVA with Dunnett post-test. n=2 per transfection.

4.3.2 Screening inducible AAV *in vivo*

4.3.2.1 Investigating Delivery method for AAV:

Having fully characterised the plasmids effect *in vitro*, the next step was to generate the inducible claudin-5 overexpression AAV. Thus, the inducible plasmids, either containing the *Icam2-Cldn5*(N.M) plasmid or the relative GFP control plasmid, were incorporated in to respective AAV-9 vectors by SignaGen (USA). As before the gene insert, either claudin-5 or GFP is under the control of the Tet-On inducible CMV minimal promoter and the

expression of the rtTA component of the Tet-On system is controlled by the *Icam2* promoter.

Two methods of AAV delivery were under investigation, intrahippocampal (IH) and intravenous (IV) administration. Mice receiving an IH injection received a dose of $2x10^{10}$ VG/ml of the control AAV (GFP-AAV) while the IV injected mice received a dose of $4x10^{10}$ VG/ml. Following AAV administration, all mice were left for one week to allow the mice that had undergone an IH injection to recover. After this the IH or IV mice were then further divided into groups, either the untreated group (no Dox added to water) or the treated group (Dox added to their water). Mice were left on their respective treatments for 3 weeks before they were sacrificed for tissue collection.

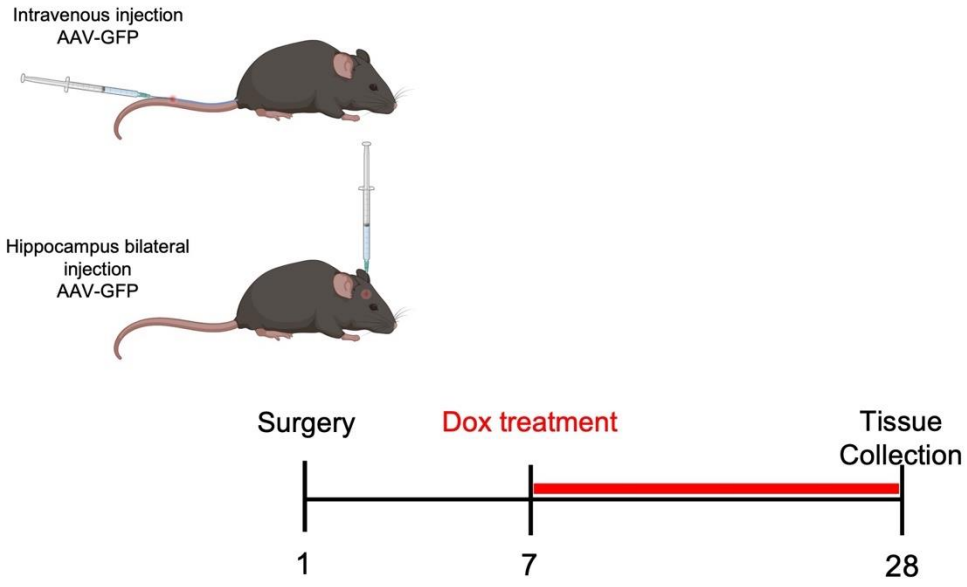

Figure 4.13. Timeline of experiment for investigating the optimum delivery method of the AAV**.**

AAV was administered by either IH or IV injection. 1 week later, Dox was added to the treatment groups drinking water, the untreated controls were left on normal water. Delivery of Dox activates the Dox inducible AAV and initiates gene expression. Mice are sacrificed following three weeks of Dox treatment and brains and peripheral tissues were taken for characterisation. Schematic created with BioRender.

Analysis of GFP expression was carried out by IHC of PFA fixed tissue of mice sacrificed 3 weeks post IH or IV injection of the AAV. Brain sections were analysed for the expression of GFP, Isolectin and DAPI post-IH injection (Fig. 4.14 A) or post-IV injection (Fig. 4.14 B). Intrahippocampally injected mice show very clear and strong expression of GFP

following 3 weeks of Dox treatment. However no GFP expression was noted in the mice intravenously injected with the AAV and put on Dox for 3 weeks.

AAVs have known tropisms for specific tissues. AAV9, has clear neuronal tropism but this is not exclusive. Tropism to other peripheral tissues such as lung, liver and heart has also been noted for this serotype (Wu, et al., 2006; Zincarelli, et al., 2008). Therefore to further determine the most successful administration route, it was essential to verify no-off target tissues were being inadvertently transduced instead of the target brain ECs. IHC analysis of GFP expression was carried out on peripheral tissues of the lung, liver, heart and eye of mice IH or IV injected with the AAV-GFP and placed on Dox for 3 weeks. Peripheral tissue sections of both IH and IV mice were analysed for GFP, Isolectin and DAPI following 3 weeks of Dox treatment (Fig. 4.15). No notable expression of GFP was observed in either administration groups.

To examine the efficacy of the inducible system *in vivo* brain tissue was obtained from cohorts of mice that were administered the AAV-GFP via IH injection comparing one group administered Dox in their water supply (treated group) to another which remained on normal water (untreated group). In the treatment group, strong GFP expression is noted following the 3 weeks of Dox treatment. Comparing this expression to the untreated group, which shows no GFP expression, clearly indicates that the AAV is functioning in a highly inducible manner (Fig. 4.16). While target gene overexpression was achieved, there also appeared to be off target expression which would indicate a leaky inducible system as was noted in the *in vitro* screens of the inducible plasmid (Fig. 4.9 A (ii)). The design of the inducible system with the use of the EC specific promoter *Icam2* should ensure that all expression remains endothelial specific, however cells which are clearly not vasculature are expressing GFP as denoted by the arrow in (Fig. 4.17). Moreover, while there are noted issues regarding the transduction cell specificity of this AAV, it is also expressing the relevant protein at an extremely high level, as can been seen through both IHC analysis (Fig. 4.14 A) as well as with the naked eye, in which GFP expression could be clearly seen during the dissection of the brain (Fig. 4.18). This level of expression is so potent that it may have the potential to cause alterations in the sensitive NVU microenvironment. Astrogliosis is also observed in brain sections of the high dose treated mice, with elevated levels of GFAP expression noted in the DG region of the hippocampus (Fig. 4.19).

Overall, it was determined that the best route for AAV administration was through a local, IH injection. This coupled with the Dox treatment resulted in successful induction of GFP. However, while having determined the optimum route of administration, the dose used clearly required additional examination. This high dose, yielded excessive expression which firstly does not have the EC specificity for which it was designed. Moreover this high level of expression appears to have activated inflammatory responses within the CNS. Overall, this indicates a need to carry out a dose curve to determine if a lower dose of the AAV can yield significant expression of the viral gene of interest, without causing any negative effects with the NVU.

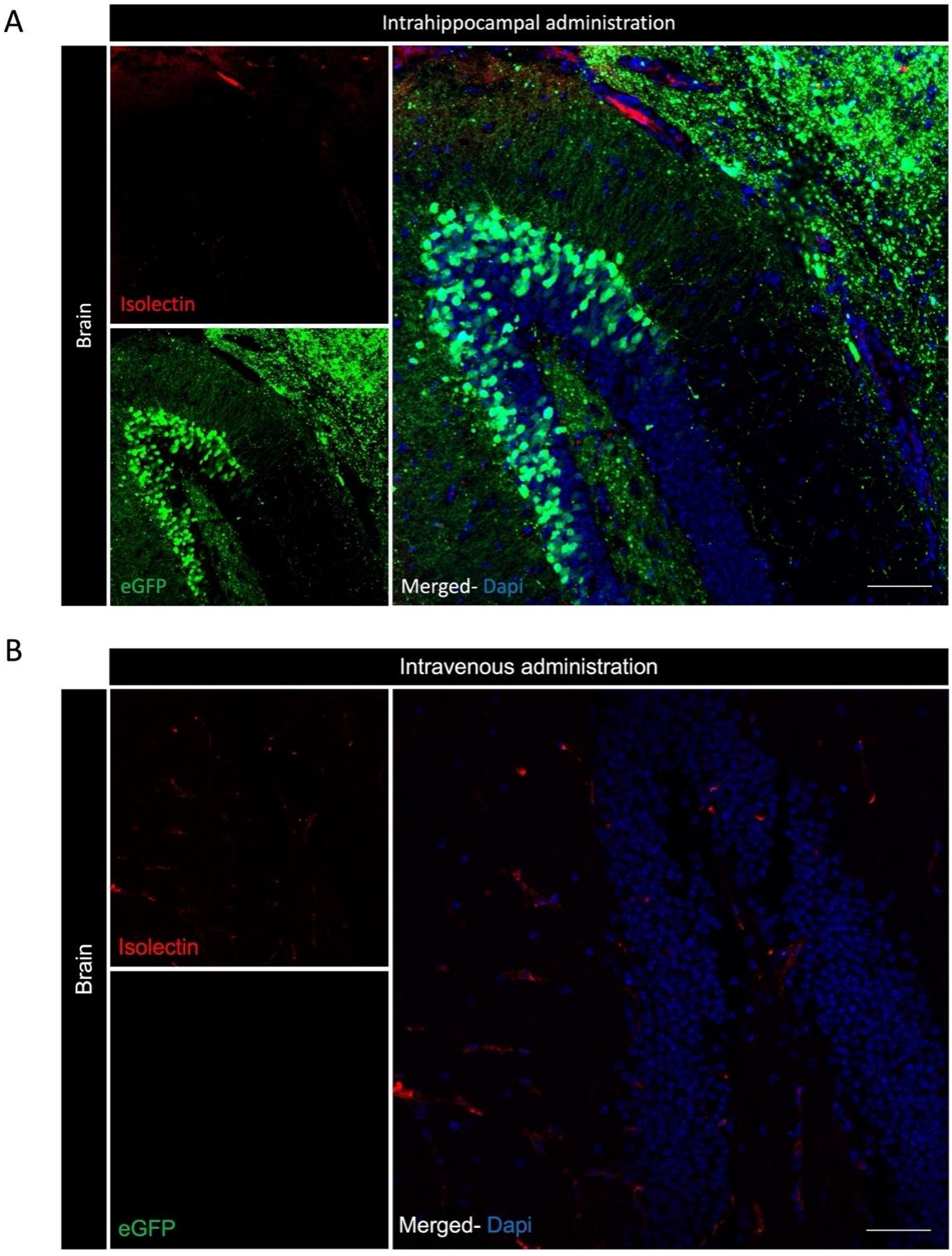

Figure 4.14. AAV-GFP expression following IH or IV AAV administration.

(A) Clear GFP expression in the DG region of the hippocampus following IH administration of AAV. (B) No GFP expression in the dentate gyrus region of the hippocampus following IV administration of AAV. Isolectin used as a vessel marker (red) and Dapi for cell nuclei. Scale bar = 100 μm.

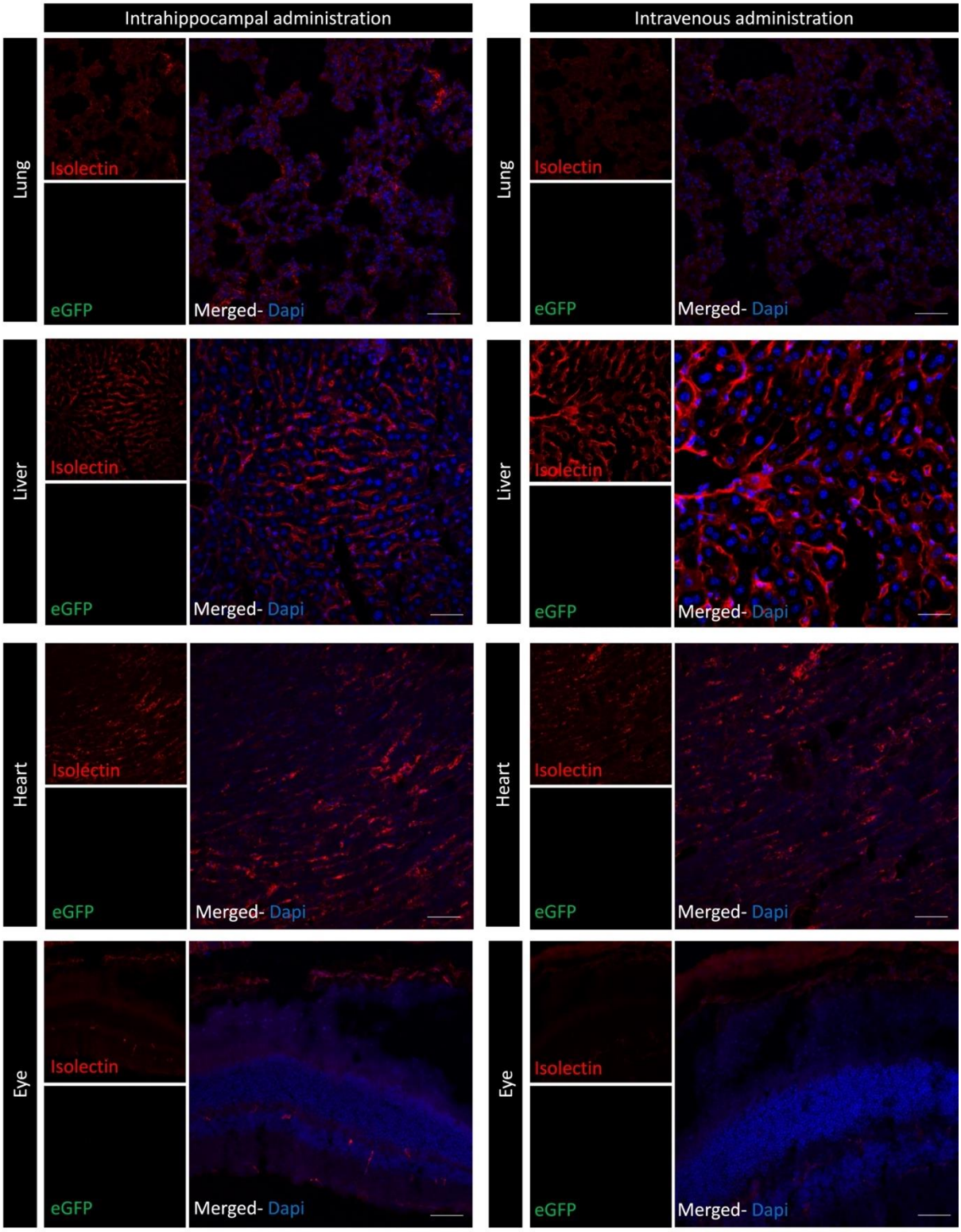

Figure 4.15 IHC analysis of peripheral tissues following IH vs IV administration of AAV-GFP.

Across 4 main peripheral tissues, the lung, liver, heart and eye, no endogenous GFP (eGFP) expression is noted in either the IH or IV administered cohorts. Vessel maker isolectin (red), eGFP (green) and cell nuclei stained with DAPI (blue). Scale bar = 100 μm.

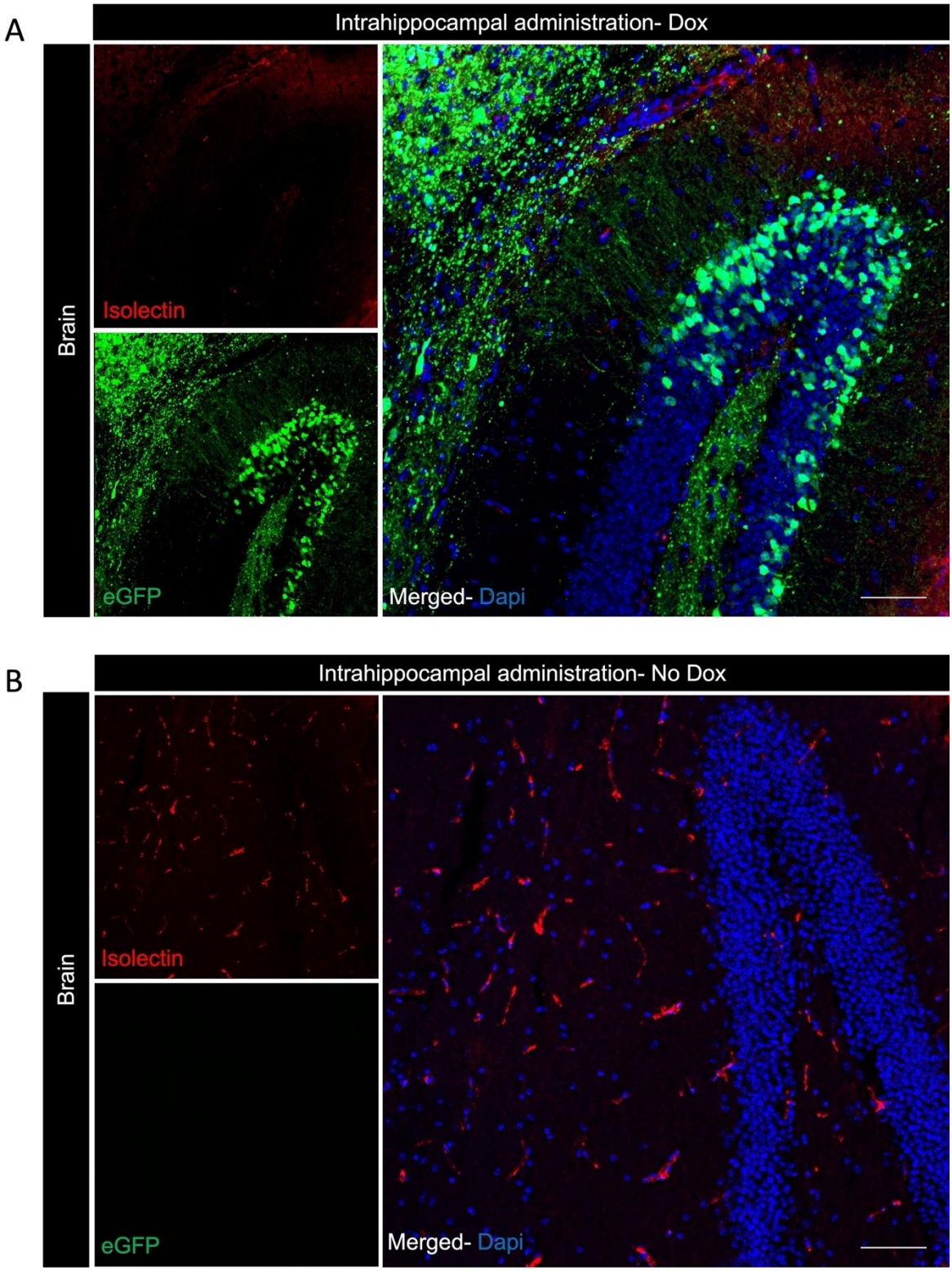

Figure 4.16. AAV-GFP expression examining inducibility of the virus with doxycycline.

(A) Clear GFP expression in the DG region of the hippocampus following IH administration of AAV and Dox treatment for 3 weeks. (B) No GFP expression in the DG region of the hippocampus following IH administration of AAV but no Dox treatment. Co-stained for isolectin (red) and DAPI (blue). Scale bar = 100 μm.

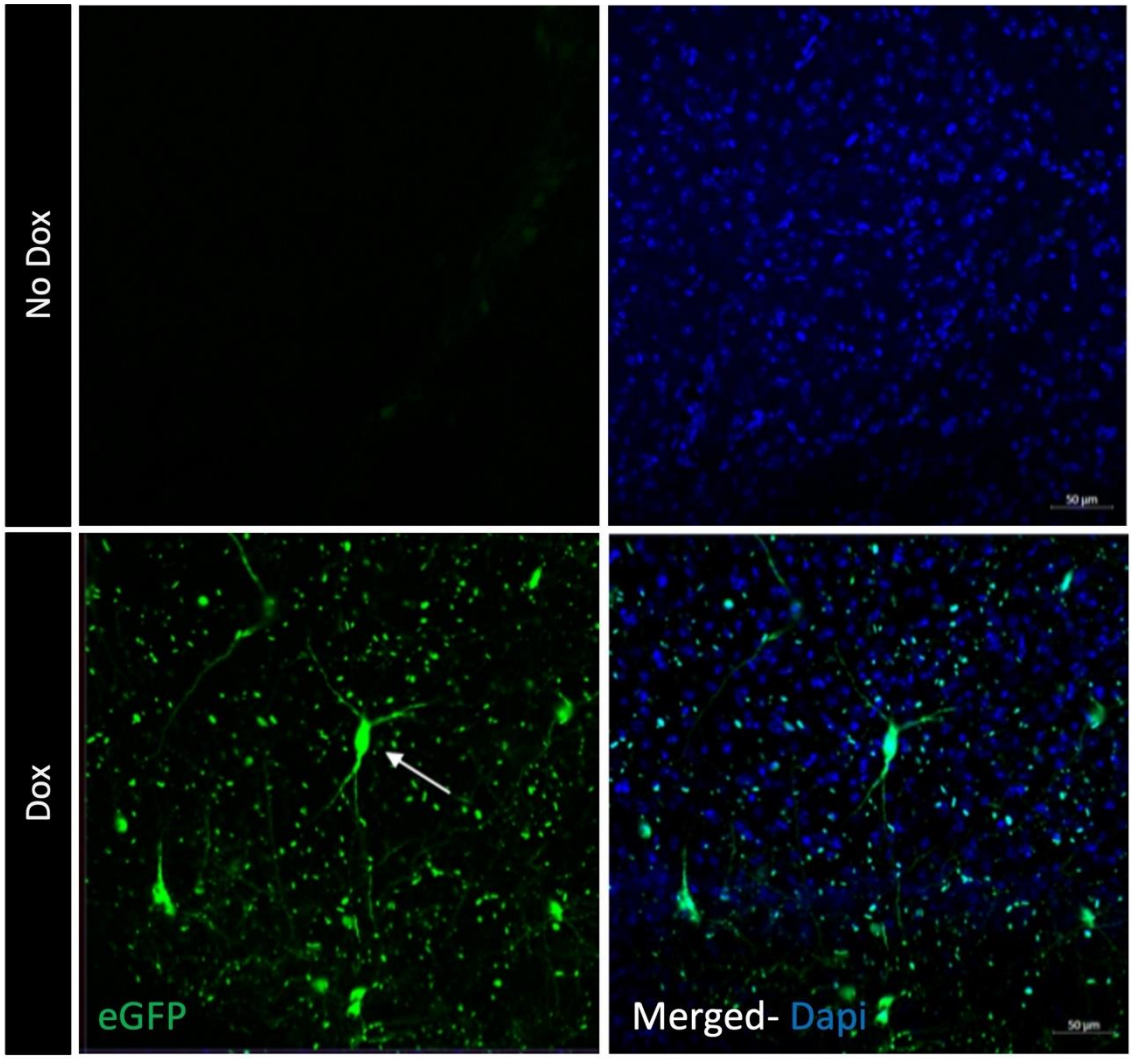

Figure 4.17. Unspecific transduction of AAV-GFP

IHC analysis of brain sections following transduction of AAV9-GFP and treatment with Dox indicates issue with inducible expression system. GFP expression indicates the cells transduced with the AAV. Arrow points to non-endothelial cell expressing GFP. Cell nuclei are stained with DAPI. Scale bar = 50 µm.

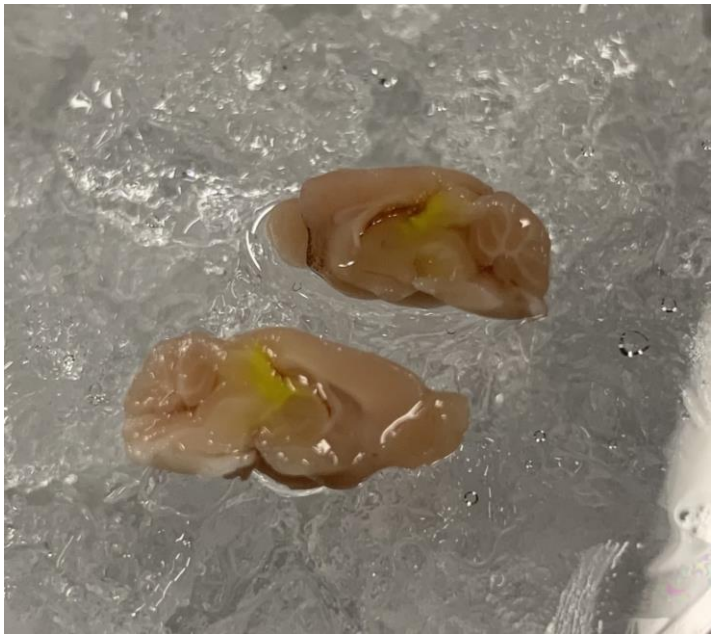

Figure 4.18 Potent expression of GFP following IH administration and Dox treatment.

Brain immediately after removal and dissection of the 2 hemispheres through a sagittal cut shows clear and extremely potent level of GFP expression in the hippocampal region of the brain, that can been seen by eye.

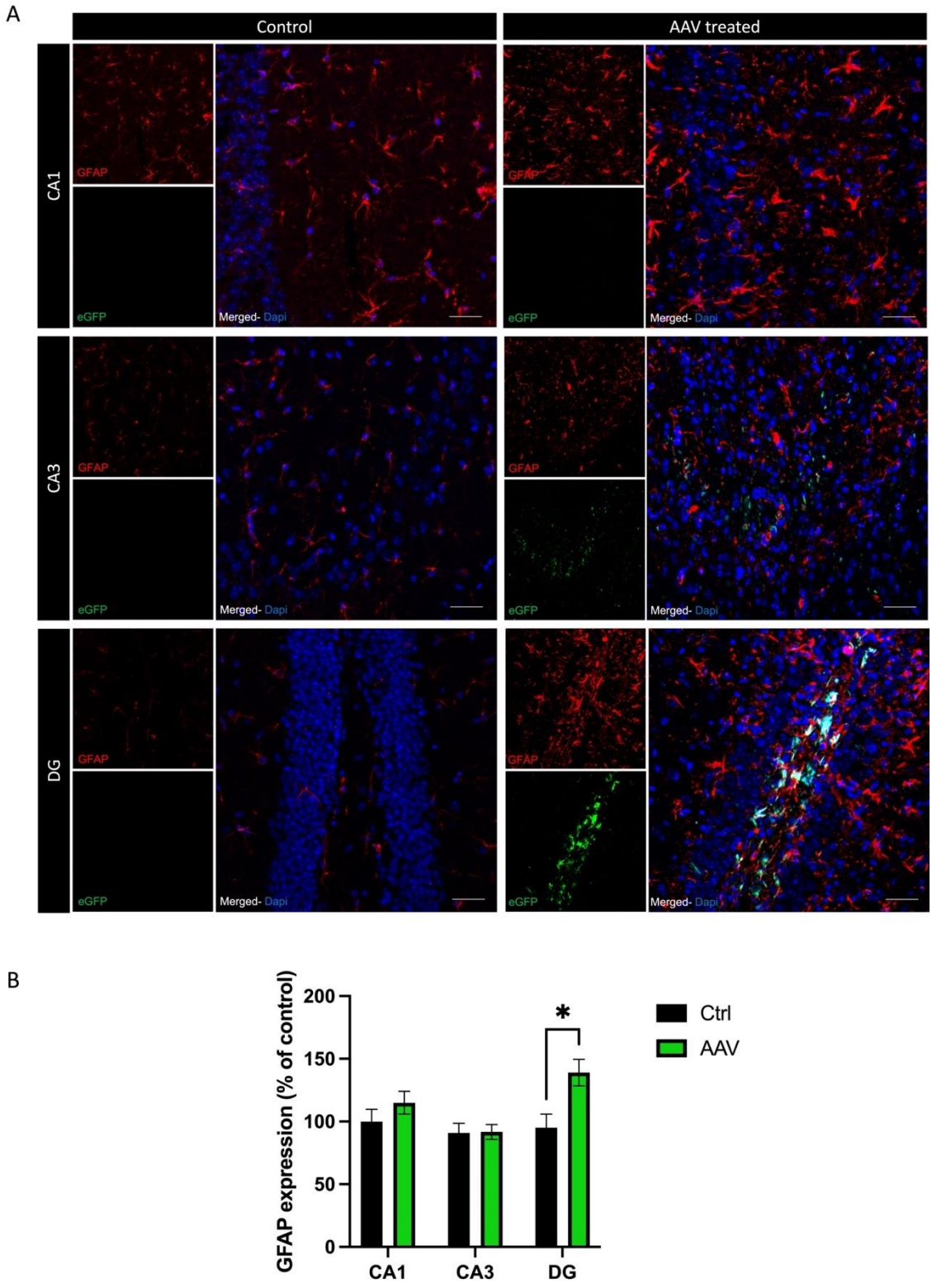

Figure 4.19 Astrogliosis in the dentate gyrus region of the hippocampus post AAV IH administration.

(A) IHC analysis of GFAP (red), eGFP (green) and DAPI (blue) showing clear elevated GFAP expression in the DG region of the hippocampus. (B) ImageJ analysis of GFAP expression changes. Scale bar = 100 μm. Results expressed as mean ± SEM. *P<0.05 by one-way ANOVA and Tukey's post-test. n=4 per group.

4.3.2.2 Optimising AAV Dose:

The high dose of the inducible AAV9-GFP, yielded excessive and non-specific expression which overall appeared to induce an inflammatory responses within the CNS. Therefore conducting a dose curve analysis to determine if a lower dose of the AAV can yield significant expression of the viral gene of interest, without causing any negative effects with the NVU was a necessary step in this characterisation. Examining the effect of different concentrations on transduction efficiency was carried out using three different dose groups of the AAV9 GFP, high ($2x10^{10}$VG/ml), medium ($5x10^{9}$ VG/ml) and low ($1x10^{9}$ VG/ml) doses, as well as a saline injected control. Mice were bilaterally injected intrahippocampally and following a week of recovery, were put on Dox for 3 weeks (Fig. 4.20).

In high dose AAV-injected mice there is an extremely significant level of GFP protein expression that appears to be to be expressed throughout the hippocampal tissue rather than co-localising with the vasculature (Fig. 4.21). Both medium and low dose treated brains show a dose dependant decrease in the level of GFP expression that appears to be more vascularly expressed but still not exclusively (Fig. 4.21). Imaging of the whole hippocampus at a lower magnification provided an overview of the full hippocampal region. This gave a clear and distinct display of dosage effect. High magnification images may have distorted the overall level of expression that was being achieved in the hippocampus, therefore a wider scope of the overall affect was important when examining the dose curve (Fig. 4.22). Finally, an ELISA was carried out to examine any potential detrimental effect the AAV was having at the various doses on the integrity of the BBB. S100β is an astrocytic protein that is used as a peripheral reporter of BBB disruption (Bargerstock et al., 2014). As it is derived from an intracranial source when a certain concentration of this marker appears in peripherally circulating blood, this is an indication of BBB disruption. When comparing the GFP expressing AAV to the therapeutic claudin-5 expressing vector, the GFP control virus does appear to result in higher S100β circulating serum levels, that is dose dependant, indicating that the high levels of GFP expression are actually damaging the BBB. The claudin-5 expressing AAV however does not seem to yield the same issue. This may be due to the high levels of GFP being toxic in the brain, rather than the viral load itself being too high (Fig. 4.23).

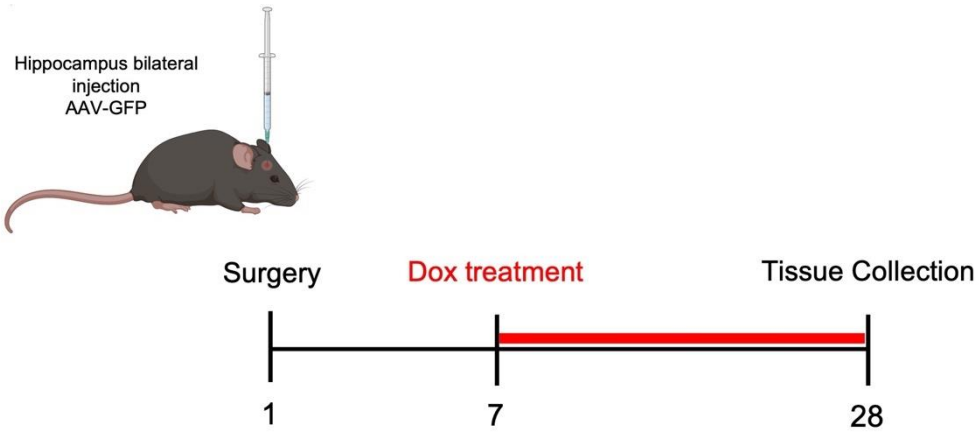

Figure 4.20. Timeline of experiment investigating the optimum dose required for strong AAV expression.

Optimising the titre of the AAV vector required to achieve high transduction efficiency while minimising off-target effects and toxicity is a necessary step in AAV *in vivo* characterization. Mice were injected on day 1 with AAV9-GFP at three different doses. On day 7 mice were given Dox supplemented in their drinking water or normal water for controls. At day 28 mice were sacrificed and tissue collected. Schematic created with BioRender.

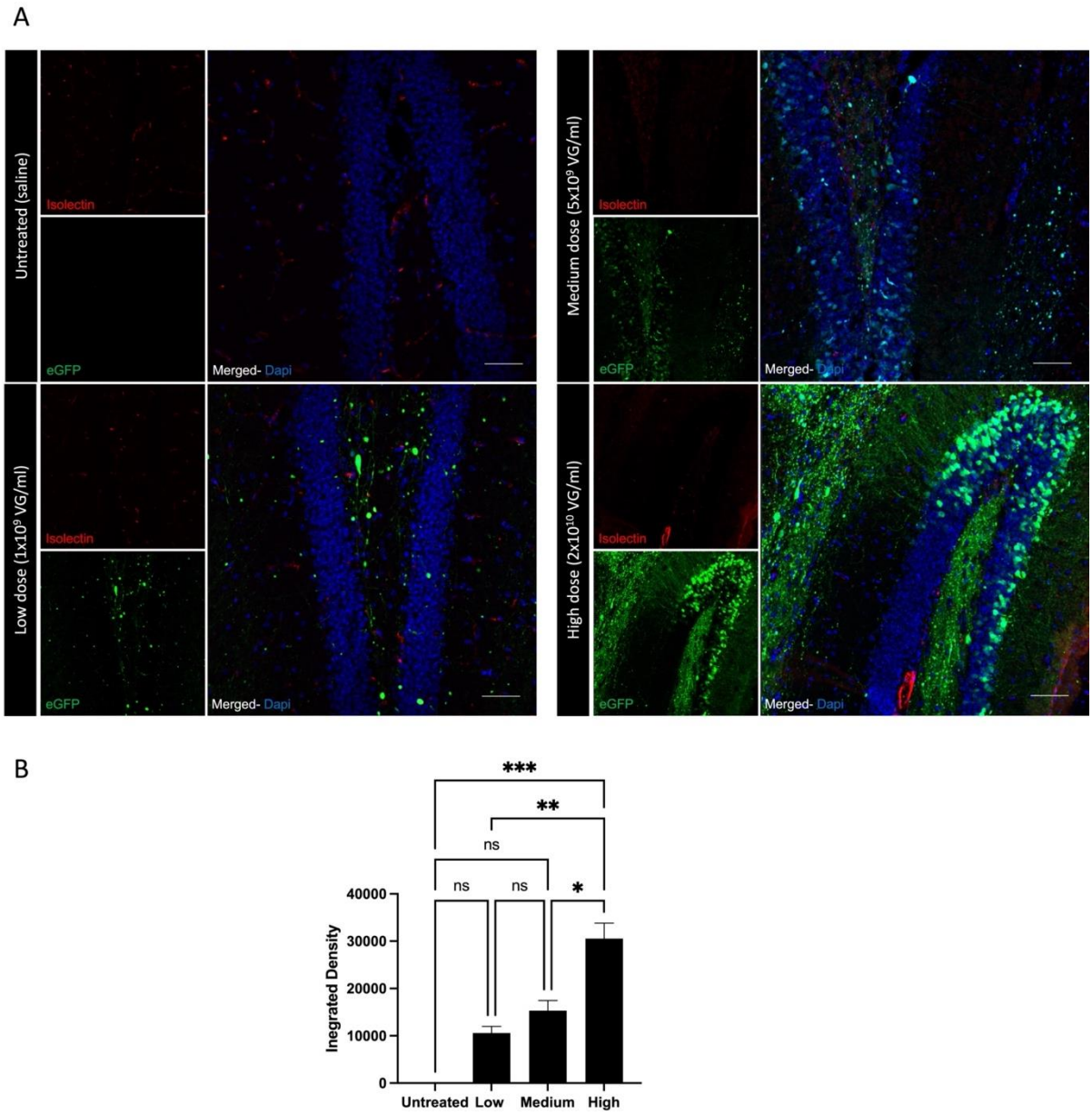

Figure 4.21 Dose curve analysis for inducible AAV9-GFP.

A. IHC analysis of GFP expression in untreated mice compared to low, medium and high dose AAV9-GFP injected mice. GFP expression (green), co-stained with vessel marker isolectin (red) and cell nuclei stained using DAPI (blue) B. ImageJ analysis of IHC GFP staining. Scale bar = 100 μm. Results expressed as mean ± SEM. *P<0.05 by one-way ANOVA and Tukey's post-test. n=4 per treatment group.

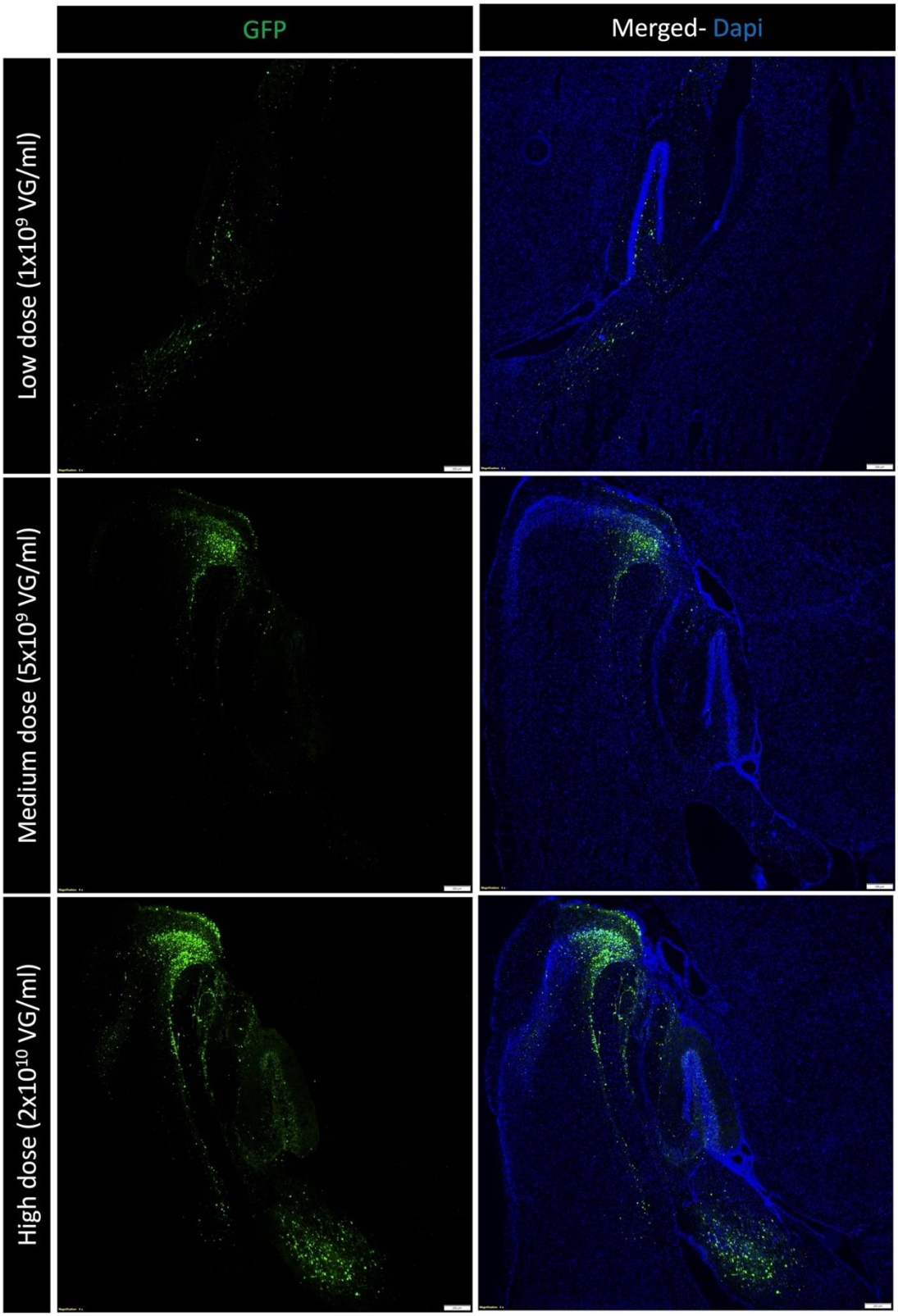

Figure 4.22 Dose curve analysis for inducible AAV9-GFP visualising the full hippocampus.

IHC analysis of GFP expression (green) in low, medium and high dose AAV9-GFP IH injected mice. Co-stained with DAPI (blue) to stain for cellular nuclei, which provides clear visualisation of the hippocampus and its subregions identified by their distinct nuclear staining patterns. Scale bar= 200μm.

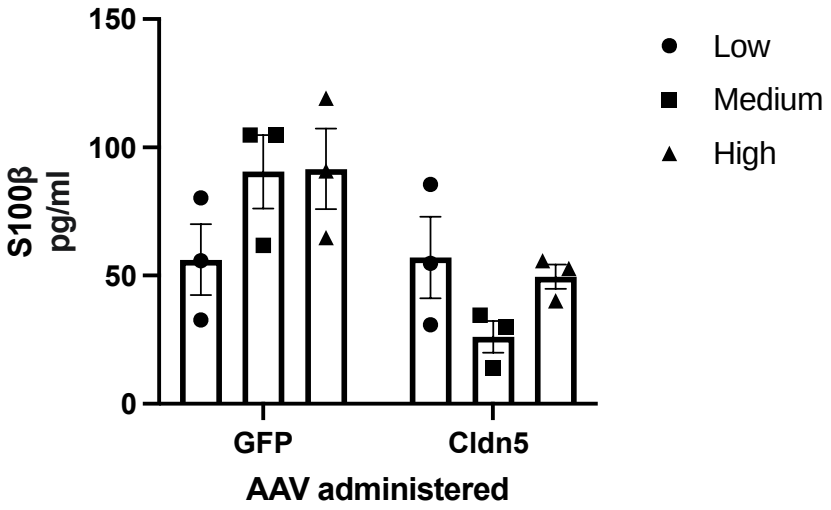

Figure. 4.23 S100β levels in the serum of peripherally circulating blood following AAV9 GFP or AAV9-Cldn5 injection at varying doses.

ELISA examining S100β levels in the serum of peripherally circulating blood. Results expressed as mean ± SEM. The results were non-significant by one-way ANOVA and Tukey's post-test. n=3 per treatment group.

4.3.2.3 Determining AAV transduction capacity:

To further characterise the AAV *in vivo,* analysis of transduction capacity was carried out through IHC of the mouse brain following bilateral IH injection of high dose ($2x10^{10}$VG/ml) AAV9-GFP under the control of the *Icam2* promotor after one week of Dox administration. 200μm sections were consecutively taken along the coronal plane. IH injection site was at position anterior/posterior (AP): -2. Through IHC analysis of GFP expression, the AAV was shown to be capable of transducing cells within the AP:-1.4 section, which is 600 μm from the injection site in the anterior direction. Cells were transduced to position AP:-3, which is 1000 μm in the posterior position (Fig. 4.24).

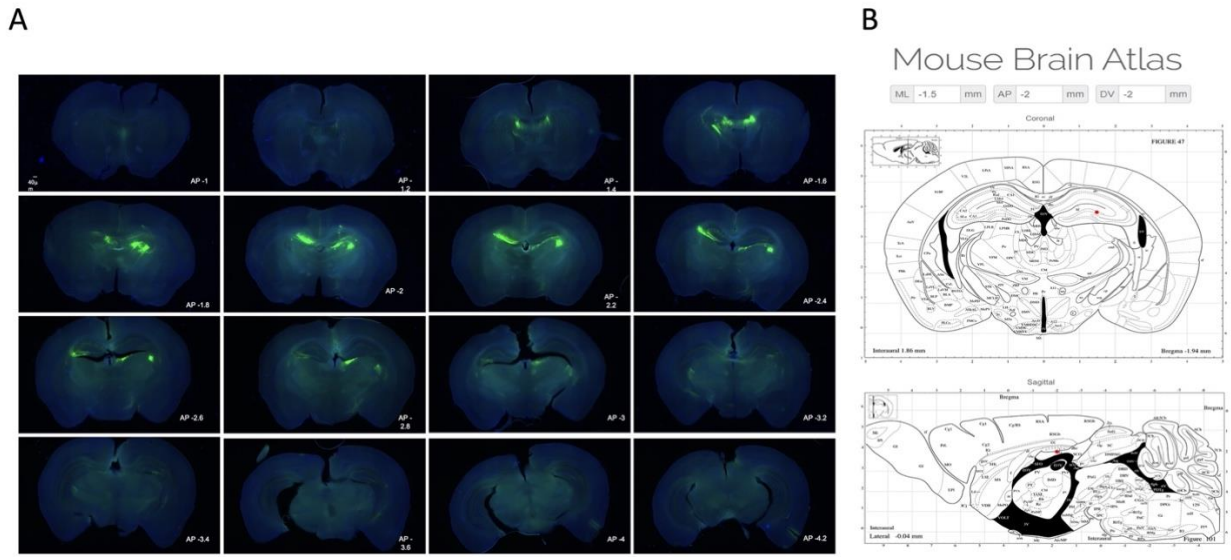

Figure 4.24 Transduction capacity of AAV9-GFP

Transduction capacity of AAV analysed through IHC. Co-ordinates are determined according to bregma (0.0). (B) The mouse brain atlas visually represents the co-ordinates of the IH injection. Medial-Lateral (ML)+/- 1.5, Anterior-Posterior (AP) -2 and Dorsal-Ventral (DV) -2. (A) Sections were taken along the coronal plane and so their labelled co-ordinates are based on their location along the AP axis**.** Green staining identifies the GFP expressing AAV and its transduction capacity throughout the brain. Cell nuclei are stained with DAPI (blue). Scale bar = 40μm Brain atlas (Paxinos and Franklin., 2001)

4.3.3 Characterising non-inducible AAV *in vitro*

The results in section 4.3.2 showed that the inducible AAV, while producing strong overexpression of the viral protein, resulted in uncontrolled and non-EC specific expression. These factors do not meet the requirements for the design of a new BBB restoring AAV. Therefore, a new AAV, utilising the non-inducible plasmid that was originally screened in section 4.3.1, (Fig. 4.3 A) was made. The non-inducible plasmid, which contains the native mouse claudin-5 gene under the control of the *Icam2* promoter was incorporated into an AAV-9 vector and separately into an AAV-BR1 vector by SignaGen. AAV-BR1 is a recently developed AAV serotype that has shown strong specificity and long-lasting transduction efficiency in brain ECs when administered intravenously (Körbelin et al., 2016).

Next, the mouse brain EC line bEnd.3 cells were transfected with either AAV-9 (Fig. 4.25) or AAV-BR1(Fig. 4.26) at various doses. Claudin-5 expression was then examined via WB and RT-PCR. Examining the toxicity of the various doses of the AAV were also examined

by doing an MTS assay on transfected cells. Across both the AAV-9 and AAV-BR1 screens, no significant change in expression was noted either at the transcription or translation level. No viability issues was noted either (Fig. 4.25; Fig. 4.26).

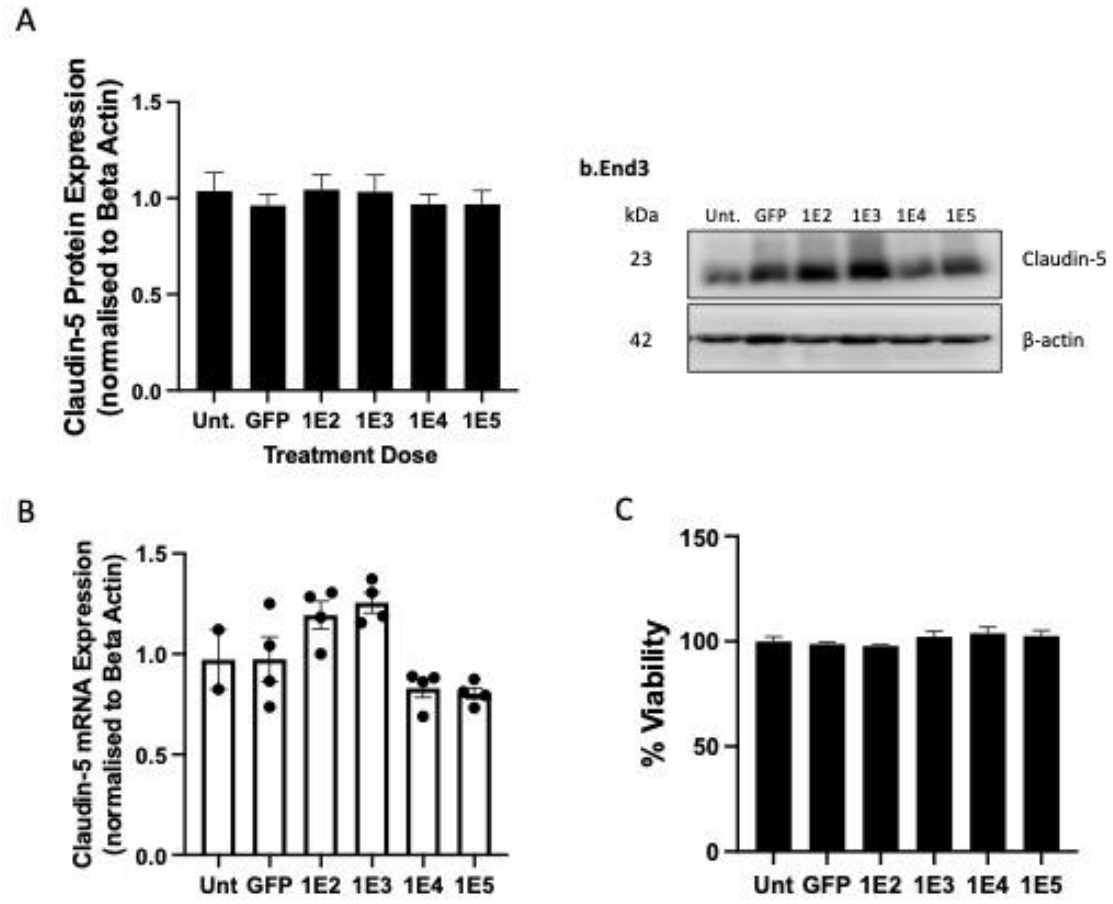

Figure 4.25 *in vitro* screen of non-inducible AAV-9-*Cldn5*

A. Western blot and densitometric analysis of claudin-5 protein expression examining effect of AAV-9 transfection at various doses. **B.** 2^-ΔΔCt values of *Cldn5* RNA expression following AAV-9 transfection at various doses. **C.** MTS assay examining viability of cells following transfection with AAV-9 at various doses.1E(number) denotes the dosage of $1x10^{N}$VG/ml. Results expressed as mean ± SEM. Unless otherwise stated, the results were non-significant by one-way ANOVA and Tukey's post-test. n=2 for each untreated control, n = 4 for each AAV dosage group

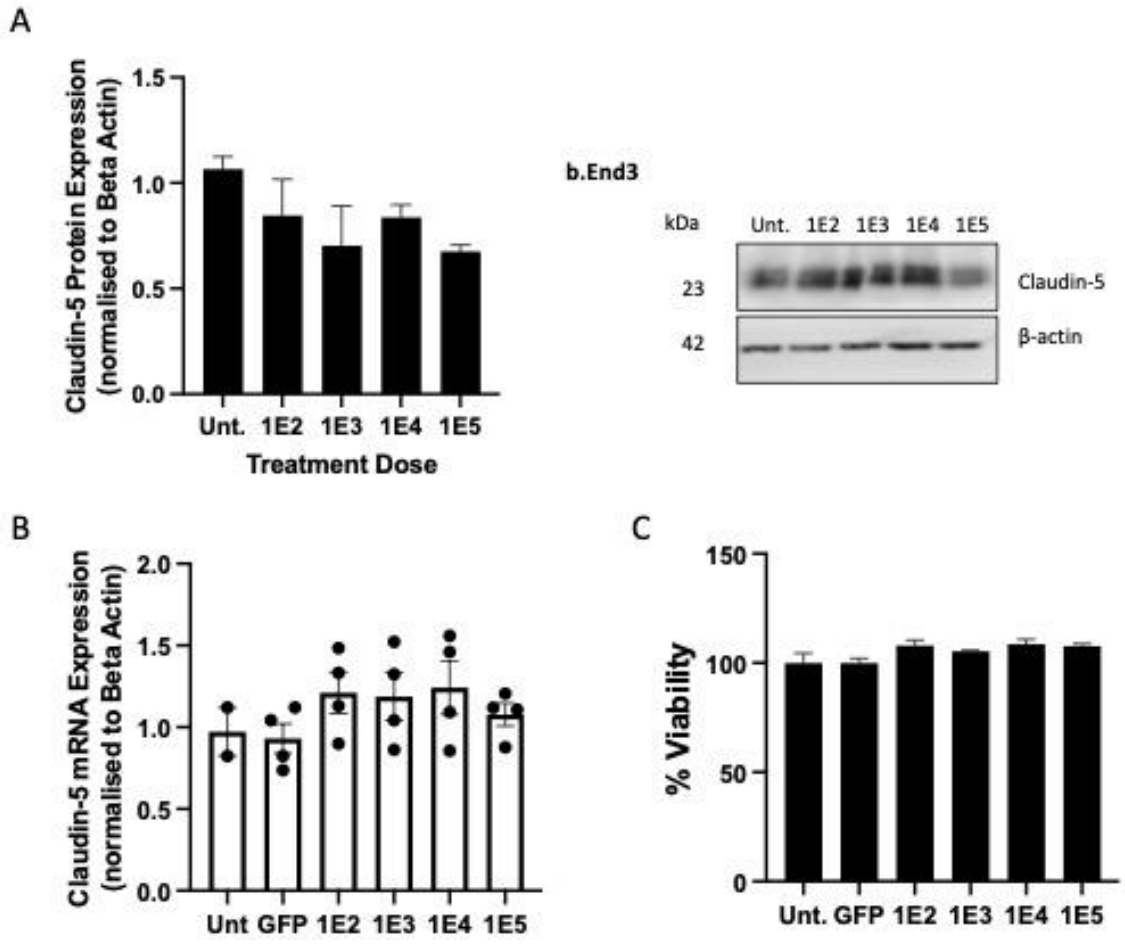

Figure. 4.26 *in vitro* screen of non-inducible AAV-BR1-*Cldn5*

A. Western blot and densitometric analysis of claudin-5 protein expression examining effect of AAV-BR1 transfection at various doses. **B.** 2^-ΔΔCt values of *Cldn5* RNA expression following AAV-BR1 transfection at various doses. **C.** MTS assay examining viability of cells following transfection with AAV-BR1 at various doses. 1E(number) denotes the dosage of $1x10^{N}$VG/ml. Results expressed as mean ± SEM. Unless otherwise stated, the results were non-significant by one-way ANOVA and Tukey's post-test. n = 2 for each untreated control n = 4 for each AAV dosage group.

4.3.4 Characterising non-inducible AAV *in vivo*

While *in vitro* analysis had not provided much insight into the efficacy of the AAV, further work was carried out *in vivo*, as although no difference had been seen in cells the same might not be true for mice. As before, two routes of AAV administration were examined, IH and IV administration. In this case, AAV-9 was examined for both route of administration as well as a dose curve, while when investigating the AAV-BR1 virus, administration route was the focus. In regards to the administration route, C57BL/6J mice

undergoing an IH injection, received a dose of $2x10^{10}$ VG/ml, while the IV injected mice received a dose of $4x10^{10}$ VG/ml. For the dose curve, the $2x10^{10}$ VG/ml dose was classified as the high dose, and this was compared to a medium dose of $5x10^{9}$ VG/ml, as well as a low dose of $1x10^{9}$ VG/ml. This investigation again was carried out using the GFP version of the AAV. Following AAV administration, mice were left for 3 weeks before they were sacrificed for tissue collection (Fig. 4.27).

Figure 4.27. Timeline for administration and collection of tissue for the characterisation of non-inducible AAV-9 or AAV-BR1. Schematic created with BioRender.

IHC analysis of GFP expression was carried out on PFA fixed tissue of mice sacrificed 3 weeks post IH or IV injection of the AAV-9 or AAV-BR1. To focus on AAV-9 first, brain sections were co-stained for GFP, isolectin and DAPI post-IH injection (Fig. 4.28 A) or post-IV injection (Fig. 4.28 B). While there was no noted GFP expression in the brain sections of the IV injected mice, there was GFP staining noted in the IH injected mice. Its expression in comparison to the inducible AAV is significantly lower. The inducible system utilised a CMV promoter within its system, while the non-inducible system relies solely on the *Icam2* promoter. *Icam2* being an EC specific promoter is therefore going to have a lower expression efficacy than the CMV promoter. However, the reduced expression does co-inside with much more specific expression, with the GFP staining clearly co-localising with

the vascular marker, isolectin (Fig. 4.33). Again, following IV administration of AAV-9, peripheral tissues were also examined to verify no-off target tissues were being inadvertently targeted instead of the brain. No GFP expression was noted in any peripheral tissue from either the IH or IV AAV-9 administered groups (Fig. 4.29). This also verifies that the lack of GFP expression in the brain noted from IV administration, is more likely to be due to an inadequate dose of the AAV rather than peripheral tissues monopolising the AAV. Next AAV-BR1 was examined. No GFP expression was noted in either the IH or the IV administered groups (Fig. 4.30 A;B). Moreover, no GFP expression was noted in the peripheral tissues of both IH and IV AAV-BR1 injected mice (Fig. 4.31). Simultaneously, a dose curve of the AAV-9 vector was carried out to examine GFP expression. It was noted that only the high dose of $2x10^{10}$ VG/ml was sufficient to achieve GFP expression following IH administration (Fig. 4.32).

Following this, another cohort of mice were bilaterally IH injected with the claudin-5 version of the AAV-9 vector at the high dose to examine the expression change. This achieved stronger results than the GFP version of the virus. When ImageJ analysis was used to quantify the difference in IHC staining, a significant increase in claudin-5 expression was noted in the brain sections that had been intrahippocampally injected with the AAV-9-*Cldn5* virus (Fig. 4.34). Moreover, tissue collected following 3 weeks transduction after IH AAV administration, was used to quantify claudin-5 RNA and protein expression in the hippocampus. Both at the transcriptional and translation level, hippocampal tissue that had received the claudin-5 overexpression AAV noted a significant increase in claudin-5 expression (Fig. 4.35).

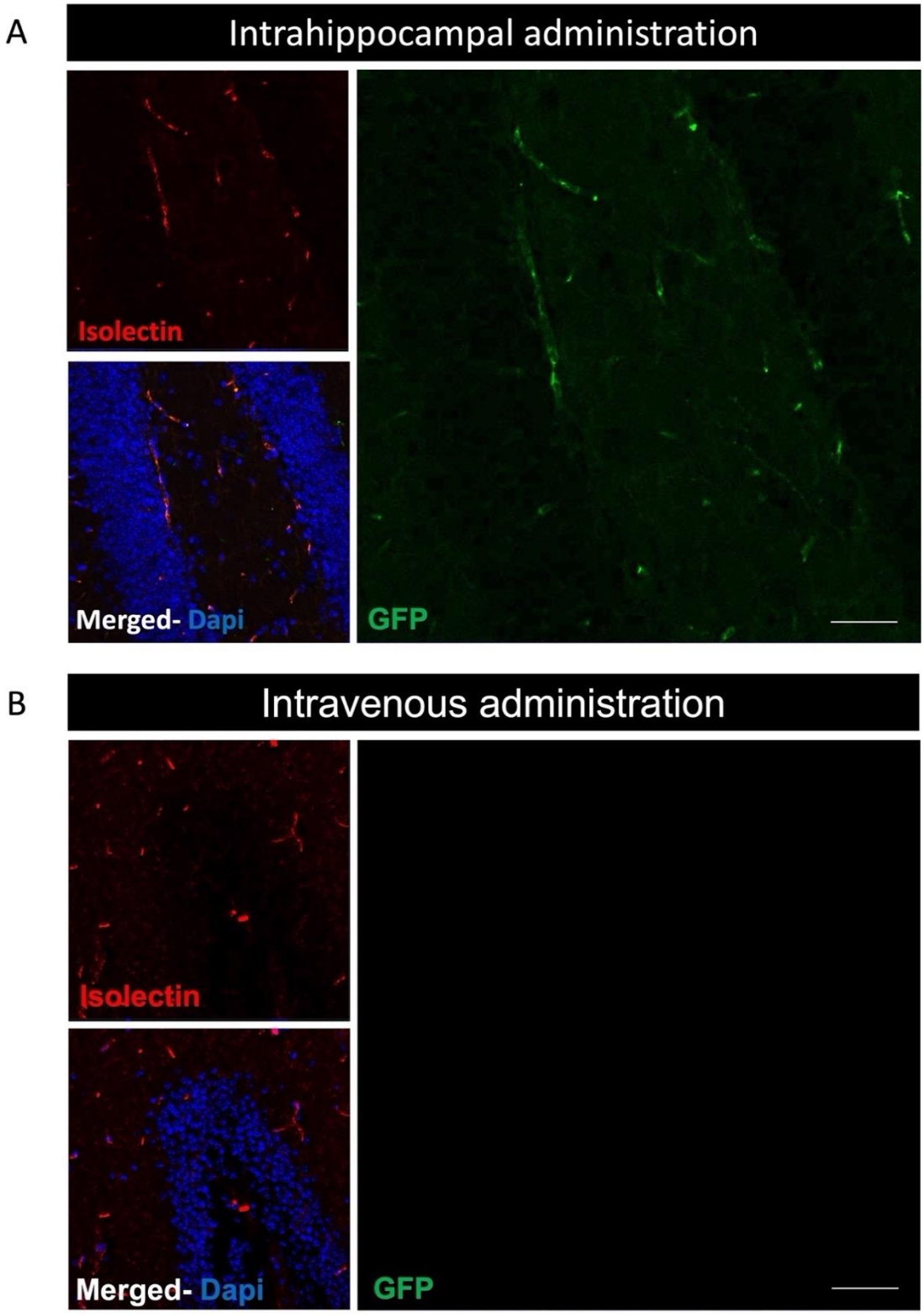

Figure 4.28. AAV-9-GFP expression following IH or IV AAV administration.

(A) GFP (green) expression in the DG region of the hippocampus following IH administration of AAV. Specific expression in the vasculature is observed by co-staining with vessel marker isolectin (red) (B) No GFP expression in the DG region of the hippocampus following IV administration of AAV. DAPI (blue) stains cellular nuclei, providing clear visualisation of the DG region of the hippocampus. Scale bar = 100 μm.

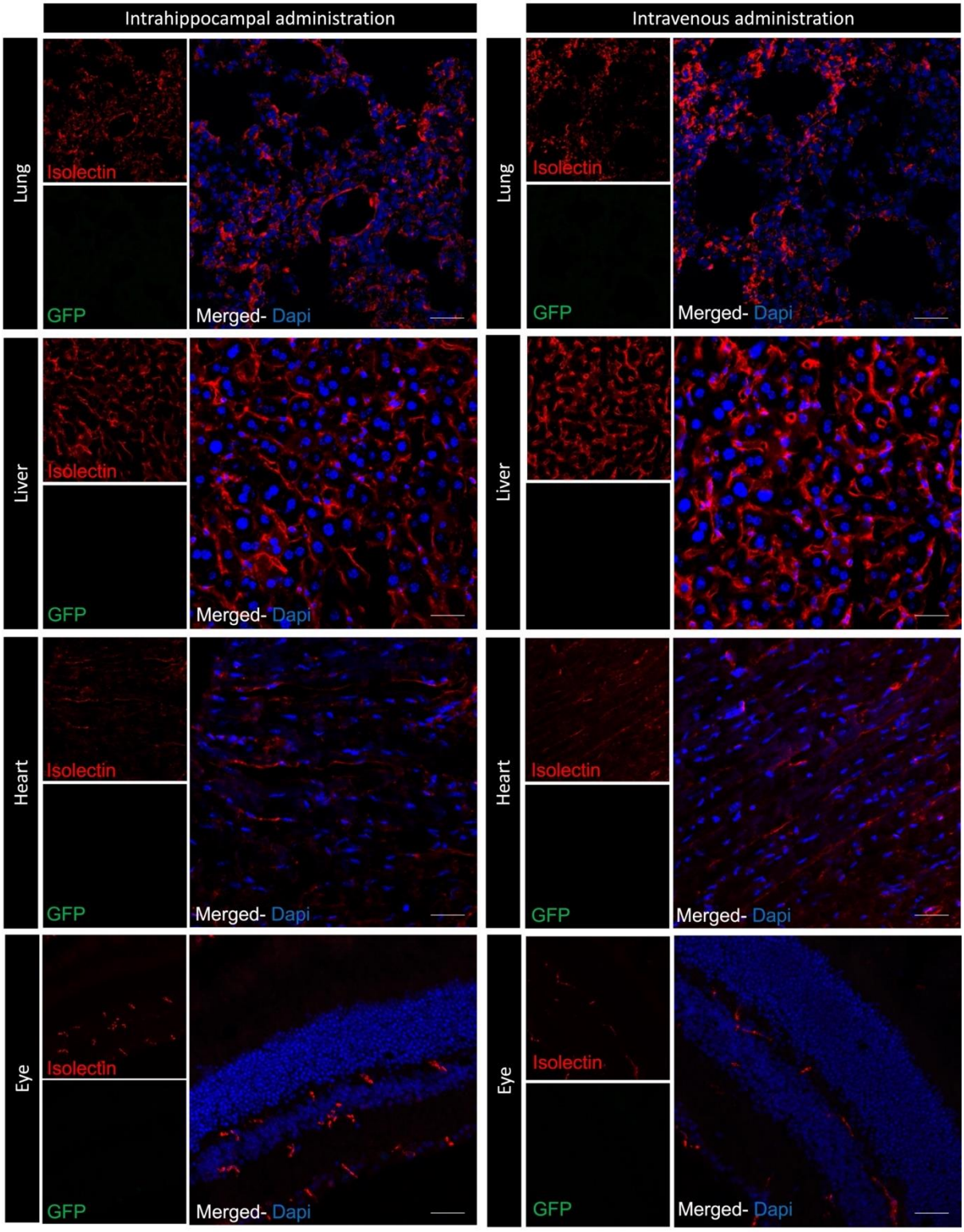

Figure 4.29 IHC analysis of peripheral tissues following IH vs IV administration of AAV-9-GFP.

Across 4 main peripheral tissues, the lungs, liver, heart and eye, no GFP (green) expression is noted in either the IH or IV administered cohort. Isolectin (red), DAPI (blue). Scale bar = 100 μm.

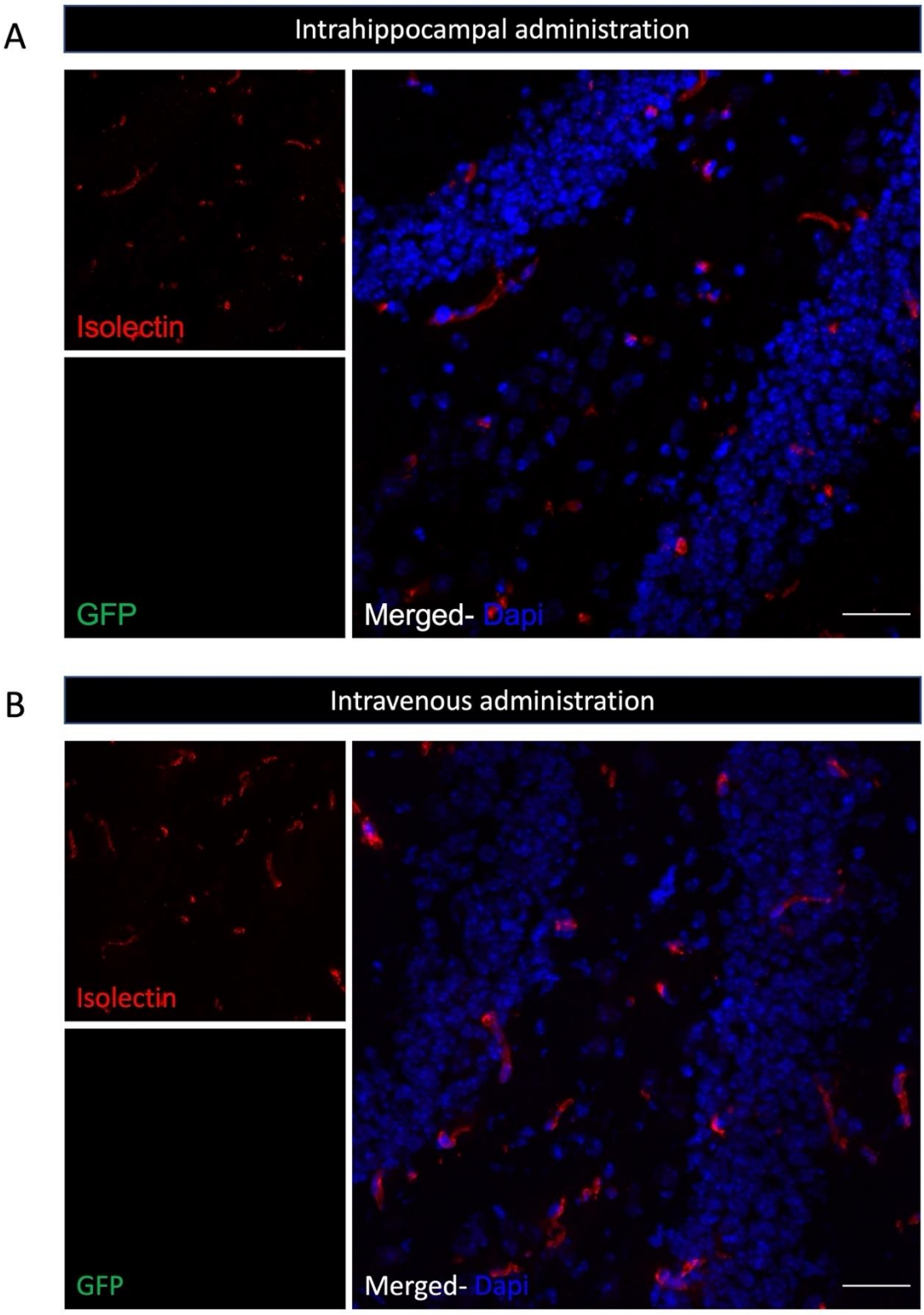

Figure 4.30 AAV-BR1-GFP expression following IH or IV AAV administration.

(A) No GFP (green) expression in the DG region of the hippocampus following IH administration of AAV. (B) No GFP expression in the DG region of the hippocampus following IV administration of AAV. Vasculature stained with isolectin (red), cell nuclei stained with DAPI (blue). Scale bar = 100 μm.

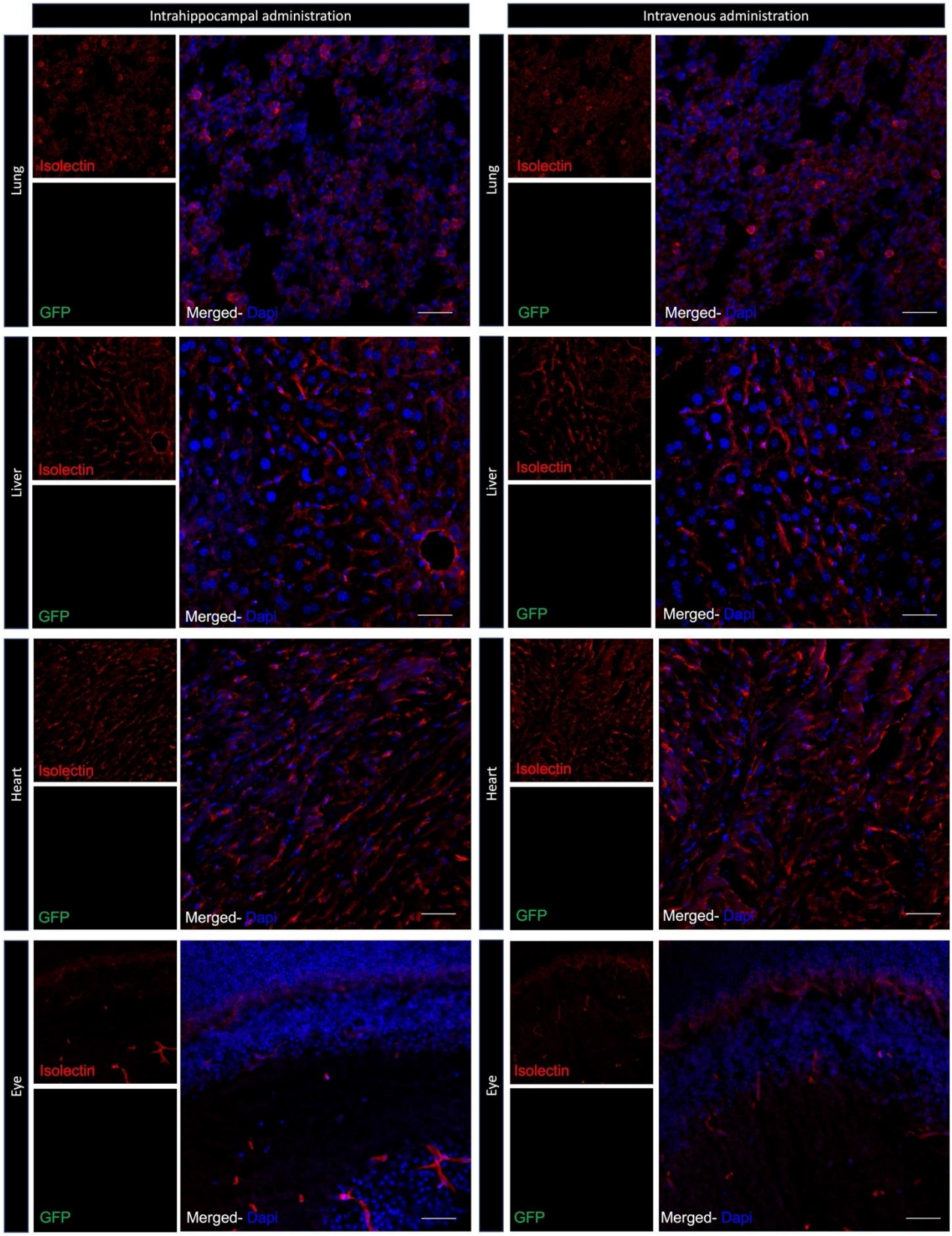

Figure 4.31 IHC analysis of peripheral tissues following IH vs IV administration of AAV-BR1-GFP.

Across 4 main peripheral tissues, the lungs, liver, heart and eye, no GFP (green) expression is noted in either the IH or IV administered cohort. Vasculature stained with isolectin (red), cell nuclei stained with DAPI (blue). Scale bar = 100 μm.

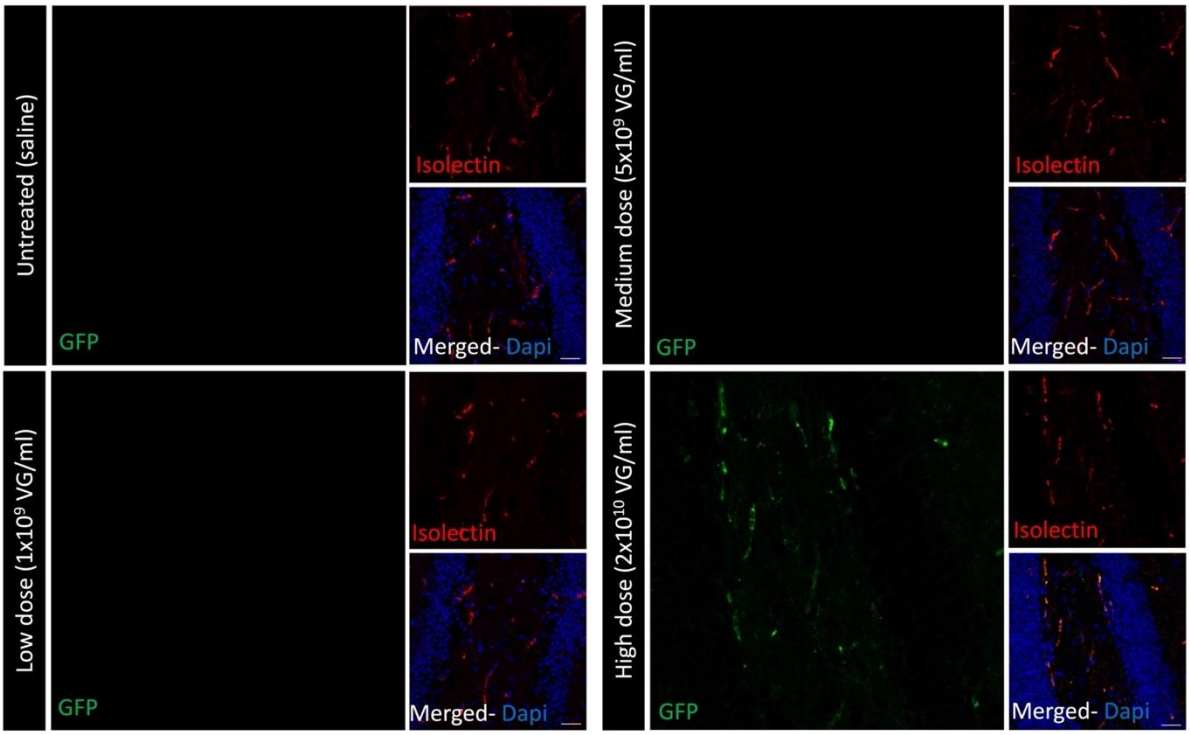

Figure 4.32. Dose curve analysis for non-inducible AAV9-GFP.

A. IHC analysis of GFP (green) expression in untreated (saline injected) mice compared to low, medium and high dose AAV9-GFP injected mice. Vasculature stained with isolectin (red), cell nuclei stained with DAPI (blue). Scale bar = 100 μm.

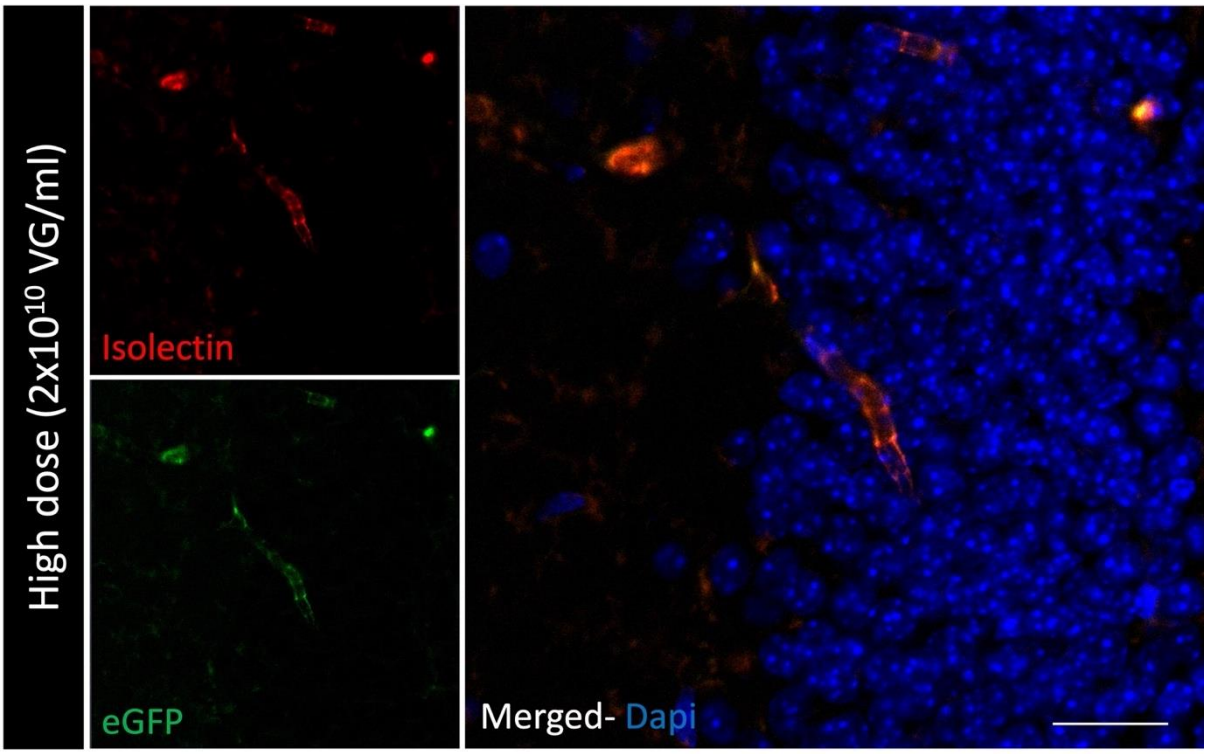

Figure 4.33. AAV-9-GFP expression showing specific transduction in vasculature.

(A) GFP expression in the DG region of the hippocampus following IH administration of AAV showing specific expression in vasculature with good co-staining with Isolectin (red). Cell nuclei stained with DAPI (blue). Scale bar = 50 μm.

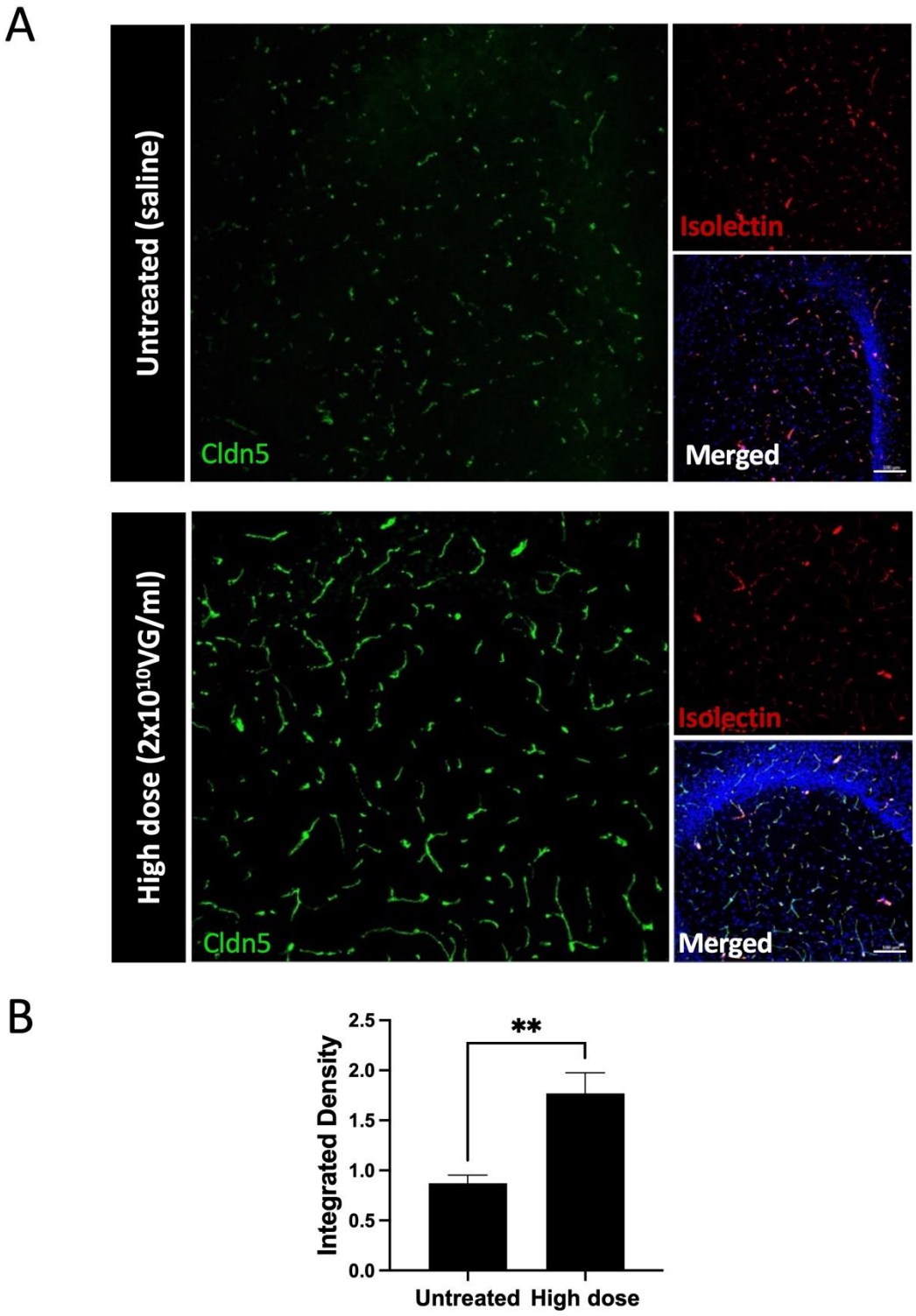

Figure 4.34 IHC analysis of claudin-5 overexpression using AAV-9 vector

(A) Immunohistochemical analysis of claudin-5 expression (green), co-stained with vessel marker isolectin (red) and cell nuclei stained by DAPI (blue). (B) ImageJ analysis comparing untreated to high dose of AAV-9 expressing claudin-5. Scale bar = 100 μm. Results expressed as mean ± SEM. *P<0.05 by one-way ANOVA and Tukey's post-test. n=4 per treatment group.

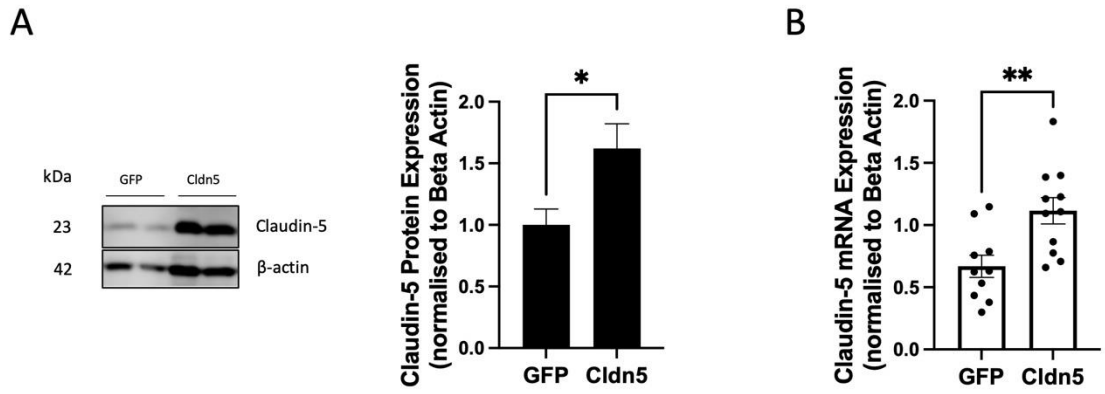

Figure 4.35 Protein and transcript analysis of claudin-5 overexpression using AAV-9

A. Representative Western blot and densitometric analysis of claudin-5 protein expression examining effect of AAV-9 transduction compared to the control AAV-GFP. B. 2^-ΔΔCt values of *Cldn5* mRNA expression following AAV-9 transduction. Results expressed as mean ± SEM. *P<0.05 by two-sided unpaired t-test. n=10 for each treatment group.

4.3.5 Behavioural characterisation of AAV in C57BL/6J mice

The loss of claudin-5 expression has been shown to cause significant behavioural deficits (Greene et al., 2018). As this TJ protein is a dose dependant gene, it is important to also verify that negative behavioural outputs do not occur if the protein is overexpressed. Therefore before beginning any investigation into the rescue effect of claudin-5 overexpression as a gene therapy based approach, it was important to firstly verify that no determinantal effects on behaviour are noted when claudin-5 is overexpressed in control animals.

C57BL/6J mice were bilaterally stereotaxically injected with either the control GFP-AAV or with the therapeutic Cldn5-AAV. Behavioural assays were carried out 3 weeks post AAV administration. Following behavioural trials, mice were sacrificed and tissue was taken to verify the overexpression of claudin-5 (Fig. 4.36). Behaviour assays were broken into three main areas to investigate. Firstly learning and memory ability were analysed by the T-maze which utilises spontaneous alternation behaviour to examine memory. No differences were noted in this assay, with the duration to trial completion and the spontaneous alternation score for both treatment groups remaining similar (Fig. 4.37).

Anxiety were assessed through the splash test, the forced swim test and the open field test. In the splash test, both the latency to groom and the total time spend grooming was similar

between treatment groups (Fig. 4.38 A). The time spent immobile, in which the mice do not exhibit any escape behaviour, was also not significantly different between the groups (Fig. 4.38 B). Additionally none of the behavioural assays measured in the open field test, which includes total time spent grooming, freezing or the time spent in the two different zones in the open field noted any significant changes between cohorts (Fig. 4.38 C).

Finally locomotor ability was also assessed through the open field test. Examining the distance the mice travelled and the average speed at which the mice moved indicated that no locomotor issues were noted between the treatment groups. Moreover the time spent rearing, showed no differences of note between the cohorts (Fig. 4.39 A). Finally, the rotarod provided a final insight into the locomotor ability of both cohorts. Again, the latency to fall and the acceleration at which they fell was similar between groups and so no discernible issues with locomotor ability were noted (Fig. 4.39 B). Overall significantly increasing claudin-5 expression in the hippocampus did not cause any detrimental effects on behaviour.

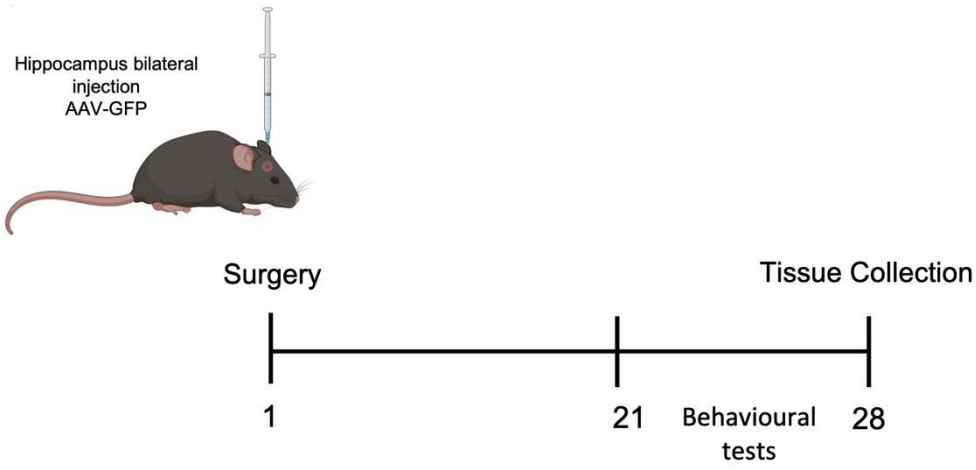

Figure 4.36 Timeline for AAV-9-*Cldn5* characterisation

Timeline for administration of AAV, followed by recovery and transduction period after which behavioural test were carried out and collection of tissue for the characterisation of the non-inducible claudin-5 overexpression AAV. Schematic created with BioRender.

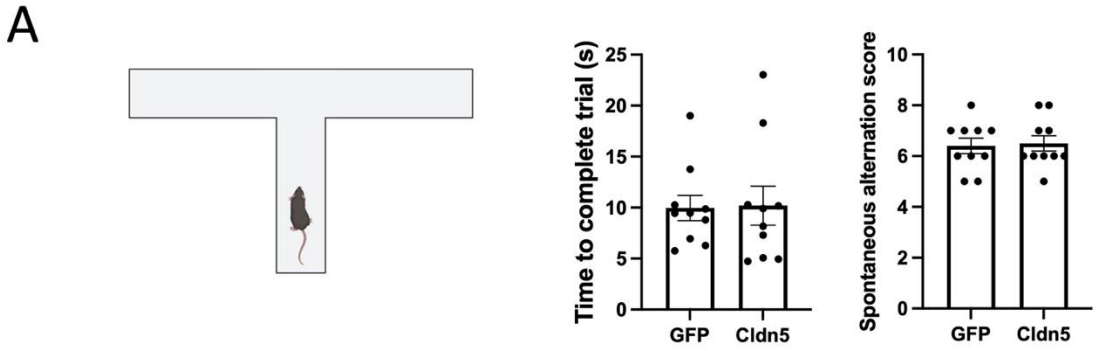

Figure 4.37. Analysis of claudin-5 overexpression on learning and memory function

(A) Schematic of the T-maze. No differences noted between the groups time to complete the trial or their alternation scores. No significant results by two-sided unpaired t-test. All data are means ± SEM with n = 10 per group. Schematic created with BioRender.

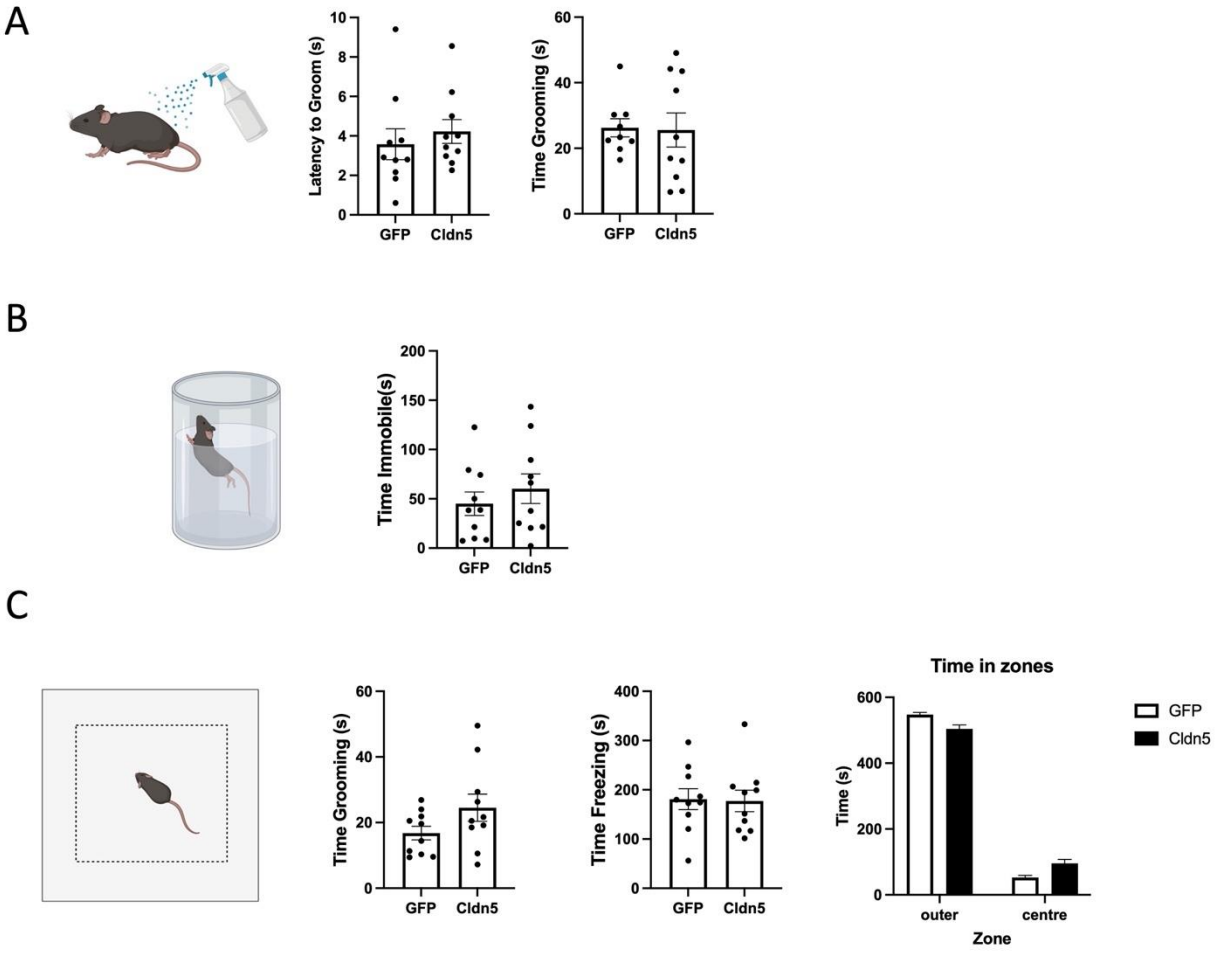

Figure 4.38. Analysis of claudin-5 overexpression on anxiety

(A) Schematic of the splash test procedure. No significant difference between the Cldn5-AAV treated mice in comparison to the GFP-AAV controls in both the latency to begin grooming and the total time spent grooming following the sucrose spray (B) No difference noted in the time spent immobile in the forced swim test. (C) No differences between the claudin-5 overexpression AAV treated mice in comparison to the GFP treated controls noted in time spent grooming, time freezing or the time in the zones of the open field. No significant results by two-sided unpaired t-test. All data are means ± SEM with n = 10 per group. Schematics created with BioRender.

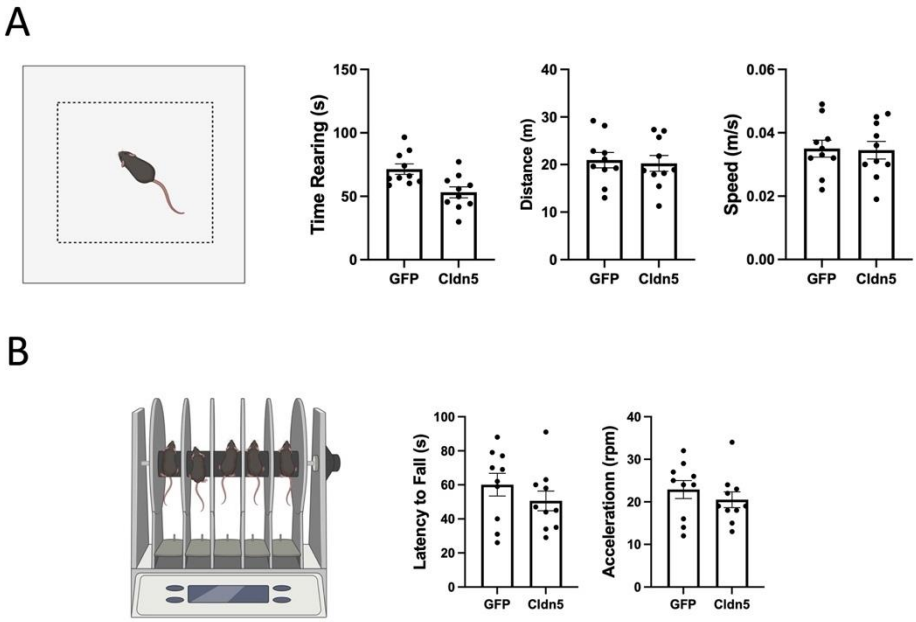

Figure 4.39. Analysis of claudin-5 overexpression on locomotor ability

(A) Schematic of the open field test. No significant differences noted in the time spent rearing, the distance travelled or the average speed between the cohorts. (B) Schematic of the Rotarod. No significant differences noted in the latency to fall or the acceleration speed at time of fall between the cohorts. No significant results by two-sided unpaired t-test. All data are means ± SEM with n = 10 per group. Schematics created with BioRender.

4.4 Discussion:

4.4.1 Screening non-inducible claudin-5 plasmids *in vitro*:

To develop and optimise an AAV based gene therapy that is capable of overexpressing claudin-5 in the ECs of the CNS, it was essential to begin this work from the ground up, by optimising the gene cassette first. Various components of the gene cassette can be adapted and optimised, including the promoter and version of the transgene used. These factors can affect potency and expression pattern which overall may affect the dose of the AAV

required. The safety and efficacy of AAVs are closely linked with the dose of the viral vector and thus optimising expression allows lower doses to achieve a therapeutic outcome.

In a recent meta-analysis of clinical trials, of 106 disclosed promoters, over half used one of three different ubiquitous promoters, either CBA, CMV or CAG, with the latter two being heavily used in CNS targeting therapies (Au et al., 2021). The heavy reliance of these promoters is realistically due to each having a strong history of high efficiency. However, more tissue-specific promoters are beginning to be used to achieve more specific expression into the target tissue. While these tissue specific promoters show great promise, their translation to clinical trials has been slow. The first neurone-specific NSE promoter, was utilised to deliver glutamic acid decarboxylase (GAD) in Parkinson's patients in a clinical trial in 2005 and has taken 16 years to progress to phase 2 (MEIRAGTX., 2018; Carvalho J., 2020). Previous work in the lab had attempted to design an AAV to upregulate claudin-5, with the claudin-5 gene under the direct control of a CMV promoter. While this successfully upregulated the expression of claudin-5, it resulted in excessive and non-specific expression of claudin-5 in the brain which in turn resulted in neuroinflammation and astrogliosis. As mentioned, the CMV promotor is a heavily utilised promoter in gene therapy development due to its ability to drive high levels of gene expression constitutively in all cell types. Therefore it was necessary to utilise a different promoter to achieve a more refined and target-specific transgene expression. Two different promoters were examined for this purpose, the endogenous claudin-5 (*Cldn5*) promoter and the intercellular adhesion molecule 2 (*Icam2*) promoter. Firstly, the claudin-5 promoter was selected for screening as it is the natural promoter for the gene of interest. As the claudin-5 gene is specifically expressed in the EC layer of numerous tissues of the body, including the brain, lung and liver, it should show a much higher specificity in expression in comparison to a constitutive promoter like CMV. This is also the case for the expression of the *Icam2* promoter, which in adult tissue is restricted to vascular ECs (Cowan et al., 1998). The use of either of these tissue specific promoters in the construct should ensure that overexpression of claudin-5 is specific to the target cell type, the ECs of the BBB. Increasing the specificity of the expression profile will be beneficial to reduce any off target effects. The inclusion of a cell specific promoter adds an additional level of control and safety that is essential when developing a therapeutic delivery system.

Another method to optimise expression of a gene cassette is through codon optimisation. Due to redundancy within the genetic code, a codon usage bias, which as the name suggests is the unequal use of different codons, has been observed in many different organisms from unicellular organisms right up to complex multicellular organisms like humans. It is thought that this bias is a method to optimise translation efficiency, by favouring codons that have higher tRNA levels (Ikemura., 1985; dos Reis et al., 2004; Waldman et al., 2010). Codon optimisation is a method to resynthesise genes so that their codons are more appropriate for the desired expression host. Therefore, we examined both the native (N) versions of both human derived and mouse derived claudin-5 genes compared to versions that were codon optimised (CO).

Each plasmid was transfected into the mouse brain EC bEnd.3 cell line for 24 and 48 hr periods. Their resulting expression levels were compared to both an empty vector (EV) plasmid and a CMV promoter plasmid. The EV is a plasmid vector that contains the contents of the plasmid without the gene of interest. It firstly provides information regarding the general protein expression level of the cell. Furthermore it provides information regarding the effect the plasmid has on the viability of the cell, if the transfection rather than the overexpression of the gene is causing an issue with viability. Hence, this is the control that will be used to determine any significant changes in expression from plasmid transfection. Additionally each plasmid was also transfected into HeLa cells as a negative control. Plasmids rely on the host machinery to make additional copies. HeLa cells are an epithelial cell line and a claudin-5 null cell, meaning they lack the ability to produce the associated gene product (Daugherty et al., 2007). Thus, HeLa cells act as a strong negative control in this experiment, in a two-fold manner. Firstly, they intrinsically do not produce claudin-5 protein and so the expression level should be null. Additionally as plasmid expression is driven by an endothelial cell specific promoter, no claudin-5 expression should be observed in this epithelial cell line following transfection.

The native mouse-claudin-5 plasmid driven by the *Icam2* promoter (*Icam2-Cldn5*(N.M)), showed a significant increase at both the mRNA and protein level 48 hr post transfection. The same plasmid driven by the *Cldn5* promoter (*Cldn5-Cldn5*(N.M)) by comparison resulted in less of an increase in expression of claudin-5 at 48hrs, although increases in other TJ proteins ZO-1, occludin and Lsr at the transcriptional level was observed (Fig. 4.3). The native human claudin-5 plasmids resulted in poorer expression levels in

comparison to the mouse claudin-5 plasmids but again the *Icam2* promoter driven plasmid (*Icam2*-*CLDN5*(N.H)) resulted in higher expression levels of the two (Fig. 4.4). The codon optimised version of the mouse claudin-5 plasmid at the protein level showed no significant changes in expression in comparison to the EV control, but at the transcriptional level, *Cldn5*-*Cldn5*(CO.M) plasmid had significantly improved expression in comparison to the native version with more specific upregulation of claudin-5 alone. This more specific upregulation of claudin-5 was also noted in the *Icam2*-*Cldn5*(CO.M) plasmid but the overall increase in expression was less efficient when compared to the native plasmid, *Icam2*-*Cldn5*(N.M) (Fig. 4.5 C; Fig. 4.6 A, B). The codon optimised version of the human-claudin-5 plasmids also resulted in significant increases in both the protein and mRNA levels at 48 hr post transfection, again with the *Icam2*-*CLDN5*(CO.H) plasmid resulting in higher expression of claudin-5 in comparison to the endogenous promoter, *Cldn5*-*CLDN5*(CO.H) (Fig. 4.5 D, E).

Overall, through the various individual screens of the plasmids, RT-PCR analysis indicated that both the *Cldn5* and the *Icam2* promoters worked well at the transcriptional level, often leading to significantly increased levels of *Cldn5* mRNA expression after 48 hr. However at the protein level, only the native mouse and the codon optimised human plasmids, both driven by the *Icam2* promoter, resulted in significant increases in claudin-5 expression 48 hr after transfection. The *Icam2* promoter generally resulted in higher expression in comparison to the *Cldn5* promoter with fewer off target changes in TJ expression.

Directly comparing the native genes to their codon optimised counterparts found that, while RT-PCR analysis noted relatively equal levels of claudin-5 expression at the transcriptional level, the results of the WB demonstrated that the native plasmids in each case resulted in higher expression than the codon optimised version (Fig. 4.6). The native plasmid not only result in higher expression in comparison to the codon optimised plasmids, but in each case also led to higher expression in comparison to the positive control, the plasmid construct carrying *CLDN5* driven by the CMV promoter. CMV as a constitutive promoter, drives constant and high levels of claudin-5 expression in all relevant cell types (Fig. 4.6). When comparing the effect of the claudin-5 gene derived from different species, both the human and the mouse claudin-5 genes resulted in similar expression profiles for both the codon optimised version of the gene as well as the native form. There was no notable species specificity in expression observed, as both the mouse and human derived claudin-5 gene,

when transfected in the mouse brain ECs, produced similar changes in claudin-5 expression. Overall, gene expression that was driven by the *Icam2* promoter resulted in better expression, with generally the native constructs resulting in higher expression of claudin-5 in comparison to the codon optimised version.

4.4.2 Screening inducible claudin-5 plasmids *in vitro*:

Further development of this plasmid construct was carried out by redesigning it to include a tetracycline inducible expression system. Using the results from section 4.3.1.1, two new inducible plasmids were designed**.** Each construct carried a mouse claudin-5 gene which was either the native version or codon optimised version, with the *Icam2* promoter driving expression as well as a GFP control plasmid with either promoter for comparison.

While the *Icam2* promoter is still driving expression, it is now part of the Tet-On system. The EC specific promoter is located upstream of the reverse tetracycline-controlled transactivator (rtTA) driving its expression. The claudin-5 transgene is situated downstream of a set of tetO repeats and a CMV minimal promoter, that together form the tetracycline response element (TRE). If the Dox effector is present, the Dox bound rtTA will only then be capable of binding to the tetO sequence in the TRE of the target transgene and allow for transcription (Fig. 4.7). The key aspect to consider when analysing inducible plasmid constructs was the inducibility of the plasmid, and how factors such as exposure time and concentration of the effector molecule Dox would effect this induction. The initial screen of inducibility demonstrated clear induction of expression for each plasmid following treatment with Dox (Fig. 4.8). bEnd.3 cells transfected with the plasmid carrying the native claudin-5 insert resulted in higher expression in comparison to the vector carrying the codon optimised version. There was strong expression noted both at 24 and 48 hr, with a possible peak in expression levels recorded at the 48hr timepoint that was observed through WB and RT-PCR (Fig. 4.10)

The general standard Dox treatment concentration *in vitro* was 1 μg/ml. However in order to fully characterise the inducibility of this plasmid investigating the effect of Dox concentration on the efficacy of induction was carried out using additional concentrations of 0.1 μg/ml, 0.5 μg/ml and 2 μg/ml. Comparing the CO to the native, as with all previous findings, the native plasmid was more successful, resulting in much higher expression in both WB and RT-PCR analysis (Fig. 4.12). For the native plasmid, transcriptional data

indicated that at both 24 hr and 48 hr there was increased expression at all concentrations. This demonstrates that the inducible system is highly sensitive to the Dox effector molecule. This expression reduces by the 72 hr timepoint as has been seen previously (Fig. 4.10). The high mRNA levels noted translate to high protein expression at a later timepoint, with both the 48 hr and 72 hr timepoints showing higher expression (Fig. 4.12).

Additionally, examining the reversibility of expression following the withdrawal of the effector molecule is also essential. The use of an inducible expression system is beneficial to control when and where a transgene is expressed, therefore being capable of reverting expression with the removal of the effector is important to verify. Results are consistent across RT-PCR and WB, following transfection with the inducible plasmid carrying the native claudin-5 insert (Fig. 4.10). Firstly, from WB and RT-PCR analysis the Dox treated controls show low level of claudin-5 expression, indicating the normal level of claudin-5 expression in bEnd.3 cells. This expression however significantly increases after 48 hr on Dox treatment. Finally, following the removal of Dox, the level of claudin-5 expression quickly reverts to a low level that is more consistent with the control samples (Fig. 4.10). The native plasmid overall results in a much higher expression in comparison to the codon optimised version.

4.4.3 A leaky inducible expression system:

This analysis has shown that the tetracycline dependent expression system is clearly inducible following treatment with Dox over time. Moreover, it is highly sensitive, activating expression over a range of effector concentrations and expression is reversible when Dox is removed. However, a key issue was also observed through these inducible screens, a leakiness within the expression system. Through the various screens that were carried out, in the untreated group, it was consistently noted that the native claudin-5 plasmid resulted in higher claudin-5 expression in comparison to the control GFP plasmid (Fig. 4.9; 4.11- 4.12 A(ii)). If the inducible expression system was under tight control it would be expected that when untreated, both plasmids should result in the same level of expression. This is not the case, with a statistically significant difference in the claudin-5 expression level noted between the control and native claudin-5 plasmid transfected cells when they are untreated. Therefore, despite the lack of the Dox effector, the plasmid must still be actively producing the gene product (Fig. 4.11 A.(ii)).

The Tet system, is a highly accepted system for engineered gene expression control, that enables modulation of target gene transcription. However, it appears that the system has a tendency to activate transcription even in the absence of tetracycline, resulting in leaky target gene expression (Roney et al., 2016). There are numerous components within the Tet-On system that may be the source of the background expression. Firstly, the rtTA upon the addition of the tetracycline derivative Dox, undergoes a conformational change that increases its affinity for its DNA binding site and enhances the recruitment of the machinery required for transcription. However it has been found that the rtTA protein retains some affinity for its DNA binding site in the absence of inducer which could result in leaky transcription of target genes. Nevertheless, the rtTA is one of the most investigated and modified components of the system. The Tet-On system is derived from the original Tet-Off system through the molecular manipulation of the rtTA and continued work to improve this activation system has focussed on transactivator manipulation, attempting to either reduce residual DNA binding in the non-induced state or through the enhancement of activation in the induced state (Roney et al., 2016). Therefore it is unlikely to be this component of the system.

The other main component that may be causing the leaky expression is the TRE, which is made up by several TetO repeats upstream of a minimal promoter. The Tet-On system depends critically on the choice of minimal promoters. In the AAV designed for this project, the widely used CMV promoter was included in the TRE. It is likely that activation of this minimal promoter is the source of the intrinsic background activity. There are numerous characteristics of the promoter that may influence background expression. Firstly this expression may be intrinsic activity of the promoter due to the presence of hidden binding sites for transcription factors. Secondly, rtTA independent expression is often caused by the presence of enhancers (Loew et al., 2010). Uncontrolled expression can also be due to the accessibility of the promoter, determined by epigenetics parameters. Overall, the non-specific expression of the target gene is likely due to activation of the TRE in the absence of the Dox bound rtTA.

4.4.4 Screening inducible AAV *in vivo*:

Following the *in vitro* screening of the various plasmids, the *Icam2-Cldn5*(N.M) plasmid was chosen to translate into *in vivo* work. An AAV9 vector was generated by Signagen, incorporating the chosen inducible plasmid for an *in vivo* work-up. As discussed in Chapter

1, section 1.7, AAVs are a favoured vector for *in vivo* gene transfer for numerous reasons and have been clinically enabled with recent FDA approval for two AAV based gene therapies. Characterisation of the AAV was carried out *in vivo*, optimising both the route of administration as well as the dose required. The inducibility and persistence of AAV gene expression was examined in addition to its transduction capacity.

To characterise the AAV *in vivo*, determining the optimum administration route for AAV delivery is essential. Safety and efficacy are generally the main factors that must be considered when choosing an injection route (Jin et al., 2015). Many clinical trials opt for the systemic route due to its technical ease of administration, being both a fast and relatively non-invasive method of administration. However, factors such as the high systemic dosing required to achieve therapeutic efficacy, the potential off target effects and inflammatory risks, as well as the cost of these therapeutics, suggest that other administration routes should be considered. Investigating more local administrations routes, especially in regards to disorders that are localised to the CNS may have some benefits. Therefore two methods of AAV delivery were under investigation in this work, the intrahippocampal (IH) and intravenous (IV) routes of administration. Mice receiving an IH injection received a dose of $2x10^{10}$ VG/ml of the control AAV-GFP, while the IV injected mice received a higher dose of $4x10^{10}$ VG/ml. One week after administration, Dox was added to the water supply for 3 weeks before mice were culled and tissue was collected (Fig. 4.13). In IH injected mice, strong endogenous GFP expression in the hippocampus was noted following 3 weeks on Dox. In comparison, mice that were injected IV showed no GFP expression within the brain following the same 3 week treatment timeline (Fig. 4.14). Moreover, no GFP expression was noted in any peripheral tissue following either administration route (Fig. 4.15).

AAV9 has been shown to be capable of crossing the BBB following systemic injection (Foust et al., 2009). Thus it is not the vectors inability to cross the barrier that is the cause of the lack of GFP expression noted in the brain of the IV injected mice. The absence of any GFP expression in the brain as well as in any peripheral tissues, would indicate that the systemic dose, at $4x10^{10}$ VG/ml, was too low. While it is a larger dose than the $2x10^{10}$ VG/ml that was administered locally via IH injection which yielded a very successful result, the IV dose at $4x10^{10}$ VG/ml based on the literature, is a low systemic dose. It is generally

suggested that AAV vector titres used for IV administration should be within the 10^{12}-10^{13} VG/ml range (Stoica et al., 2013; Shibata et al., 2017).

As mentioned previously, progressively increasing the dosage to achieve therapeutic efficacy is not a viable strategy due to a number of limiting factors. Firstly, dosages that are too high may produce transduction related toxicities (Hinderer et al., 2018). Moreover, ectopic expression of the transgene in peripheral tissues may lead to unwanted side effects. AAV9, while capable of transducing cells within the CNS, shows no strong preferential tropism to any one tissue in particular. AAV9, while having neuronal tropism, has also been shown to have tropism to peripheral tissues such as lung, liver and heart. (Wu, et al., 2006; Zincarelli, et al., 2008). While non-target expression may be limited by a cell-type-specific promoter (Dashkoff et al., 2016), in this case the vector contains an EC specific promoter, *Icam2*. While *Icam2* is EC specific, its expression is not limited to the vasculature of the BBB, but is broadly expressed throughout body. The claudin-5 gene is expressed in numerous tissues including the lung, liver and kidney (Greene et al., 2019). Being a dose dependent gene, overexpression of claudin-5 systemically could have serious off-target effects on peripheral tissues if administered systemically. Additionally, the efficacy of systemic administration may be limited by the presence of neutralising antibodies, which have been noted in commonly used animal models (Rapti et al., 2012). Thus there is the possibility that regardless of the dose used, through IV administration there could be a generalised inhibition of gene transfer, limiting its efficacy *in vivo*. Finally, as previously discussed the route of administration chosen could have a major effect on the pharmacoeconomic value of the AAV produced. Therefore while a non-invasive vector delivery route for the neural tissue would be advantageous, in this case, the high dose that may be required, in addition to the risk of off-target effects suggest that IH-injection is a better route of administration for this particular AAV.

As with the *in vitro* work, when working with the inducible system, it is important to verify the inducibility of the system. Using the same timeline as in the delivery investigation, mice that were intrahippocampally injected with AAV-GFP, were either the untreated control group and supplied normal “no Dox” water, or the treatment group with Dox added to the drinking water. The control mice that receive no Dox show no GFP expression in the hippocampus, which indicates that the AAV is acting in an inducible manner (Fig. 4.16). When treated with Dox, GFP overexpression was achieved in the target cells of the

vasculature. However there also appeared to be off-target expression, which supports the potential for a leaky inducible system, as was discussed in the *in vitro* screens of the inducible plasmid (Fig. 4.11 A(ii)). The design of the inducible system with the use of the EC specific promoter *Icam2* should ensure that all expression remains endothelial specific, however cells which are clearly not vasculature are expressing GFP as denoted by the arrow in Fig. 4.17. The cell structure suggest a glial origin, such as microglia. The reasons for the non-specific expression of the target gene are, as discussed previously, likely due to activation of the TRE in the absence of the Dox bound rtTA.

Importantly, while the high dose resulted in notably strong GFP expression in IHC analysis, the potency of the virus was unprecedented, with GFP expression clearly seen with the naked eye during the tissue collection and dissection protocol (Fig. 4.18). With this finding, it is unsurprising to note that astrogliosis is noted in the hippocampal region of the brain following administration with high dose AAV (Fig. 4.19). Astrocytes play a vital role in the maintenance of the BBB and changes in their morphology and function, referred to as reactive astrogliosis, are highly associated with disruption in the homeostasis of the NVU (Sofroniew and Vinters., 2010). High levels of GFAP staining, a marker for astrocytes, is noted in both the CA1 and DG regions of the hippocampus in AAV treated brains. Moreover Image J analysis shows a statistically significant difference in the GFAP staining in the DG region of the hippocampus between the control saline-injected brains and those that received a high dose of the GFP expressing AAV. Reactive astrogliosis is a neuroinflammatory response which highlights the need for a more precise and controlled upregulation of gene expression if this is to become a realistic treatment option.

The transduction efficiency of an AAV depends on viral concentration. While IH-injection of $2x10^{10}$ VG/ml of AAV-GFP resulted in successful expression, this expression was excessive and non-specific. Therefore examining the effect of different concentrations on transduction efficiency was carried out using 3 different dose groups, high ($2x10^{10}$VG/ml), medium ($5x10^{9}$ VG/ml) and low ($1x10^{9}$ VG/ml). Investigations were carried out using AAV-GFP. In each case, mice were bilaterally injected intrahippocampally and following a week of recovery, were put on Dox for 3 weeks (Fig. 4.20). The high dose, as seen before, results in a significant elevation of GFP expression that appears to be to be expressed throughout the hippocampal tissue rather than co-localising with the vasculature. The expression profile for both the medium and low dose was significantly less than the high

dose treatment, with the concentration of AAV administered correlating with the expression profile, verifying that transduction efficiency depends on viral concentration. However, even at the low dose, the GFP expression does not appear to be exclusively expressed within the vasculature (Fig. 4.21).

To further characterise the AAV *in vivo*, analysis of transduction capacity was carried out through IHC of the mouse brain following bilateral IH injection of high dose ($2x10^{10}$VG/ml) AAV-GFP after three weeks on Dox. Through IHC analysis of GFP expression, the AAV was shown to be capable of transducing cells 600 µm away from the injection site at the AP and 1000 µm towards the posterior with GFP expression noted in the AP (Fig. 4.24). As the target for this gene therapy is the cerebrovasculature which forms the BBB, achieving a global transduction of the AAV throughout the brain from bilateral injection would be beneficial in the practical development of this as a therapeutic option. This is a promising result, however, as seen previously the dose used may be eliciting an neuroinflammatory response. Overall, these findings conclude that it will be necessary to design a more precise claudin-5 vector.

4.4.5 Screening non-inducible AAV *in vivo*:

Due to the structural set up of the inducible plasmid backbone, the *Icam2* promoter is upstream of the rtTA, while the CMV promoter is upstream of the GFP gene. Therefore, while the *Icam2* promoter is still controlling overall gene expression, the CMV promoter is directly involved in GFP expression and so while being an excellent promoter with high transduction efficiency, it is not sufficiently specific. Thus to simplify this plasmid structure, in order to ensure EC specific expression, the non-inducible *Icam2-Cldn5*(N.M) plasmid backbone was utilised and incorporated into either AAV-9 or AAV-BR1 for further analysis. AAV-9 has been shown to have tropism to the CNS as well as being capable of crossing the BBB following systemic injection (Foust et al., 2009). AAV-BR1 is a more recently developed AAV serotype, an AAV2 viral vector displaying a capsid variant which has displayed an unprecedented degree of specificity and long- lasting transduction efficiency for brain microvasculature ECs (Körbelin et al., 2016).

However, in this case, the AAV-BR1 administered either IH or IV did not result in any notable transduction, with no GFP staining noted in either brain sections or in peripheral tissues. Due to the degree of specificity this AAV has been shown to have towards the ECs

of the BBB, the lack of GFP expression in the peripheral tissues is unsurprising. However, the lack of GFP expression in the brain was disappointing. Previous work has shown impressive transduction following either local or IV administration of AAV-BR1 (Ivanova et al., 2022). While the dose that was used in those experiments was higher than what was utilised in these current experiments, ultimately, this is unlikely the whole issue. The promoter previously utilised while examining the efficacy of AAV-BR1 was either a CAG or CMV promoter, while in this investigation, an *Icam2* promoter was used. As can been seen within this research itself, when comparing the difference in expression of the AAV-9 inducible to non-inducible vectors, there is a considerable difference in the level of expression that is solely due to the strength of different promoters. Interestingly, previous work has shown that when administered IV, the virus targets the vasculature, but when administered locally neurons are the main target of the AAV-BR1 vector (Ivanova et al., 2022). Therefore, while the AAV-BR1 vector is an excellently designed new AAV serotype for targeting the BBB, the need for peripheral administration at high doses in order to specifically target the ECs of the BBB, does not fit into gene therapy design that is the aim of this project. The overarching aim is to target locally and with lower doses to achieve a financially viable therapy option for common neurological disorders. For disorders such as epilepsy, which often has a focal region that is damaged, local administration may be sufficient to treat, rather than the global effect the IV administration route generally obtains.

The AAV-9 vector on the other hand, when administrated locally, did result in GFP expression, which showed much higher specificity to the brain microvasculature ECs, as seen via the counterstaining with isolectin (Fig. 4.28A; 4.33). Hippocampal tissue taken from mice injected with AAV-9-*GFP* or AAV-9-*Cldn5* showed significant increase in claudin-5 mRNA and protein level expression relative to the GFP control treated group (Fig. 4.35).

4.4.6 Behavioural characterisation of AAV induced claudin-5 overexpression:

Claudin-5 is a dose dependant gene, therefore before examining its potential rescue effect in various disease models, it was essential to determine that overexpression of claudin-5 in the cerebrovasculature does not in itself cause any detrimental effects. Therefore, characterisation of normal C57BL/6J mice behaviour was conducted following IH injection of either the control GFP-AAV or the therapeutic Cldn5-AAV. As before, mice were

bilaterally intrahippocampally injected with the relevant AAV at a dose of $2x10^{10}$ VG/ml. Three weeks post-surgery behavioural assays were conducted and once complete tissue was collected for analysis (Fig. 4.36).

Behaviour assays were divided into 3 main areas of investigation. The first was learning and memory, which was analysed via the T-maze which utilises spontaneous alternation behaviour to examine if subjects have a functioning spatial working memory. No issues with working memory were noted as both treatment groups completed the trial in similar times and with similar spontaneous alternation scores (Fig. 4.37).

The next area of investigation is in anxiety related behaviour, which was assessed through the splash test, the forced swim test and the open field test. Across all three assays there were no significant differences noted between the treatment groups, again indicating that claudin-5 overexpression has no adverse effect on anxiety or depression related behaviour. (Fig. 4.38). Finally the locomotor skills were also assessed through the open field test and rotarod test. Factors such as the distance travelled and the average speed as well as latency to fall displayed no discernible issues with locomotor ability. This indicates that a significant increase in claudin-5 expression in the hippocampus does not cause any locomotor issues (Fig. 4.39).

Overall, these findings indicate that the claudin-5 overexpression AAV, does not have a toxic effect, with no detrimental effects on mouse behaviour. Therefore the next step will be to examine the rescue potential it has in models of disease, which is the subject of Chapter 5.

4.5 Conclusions:

- From *in vitro* screening the plasmid containing the native mouse claudin-5 gene under the control of the *Icam2* promoter, (*Icam2-Cldn5*(N.M)), resulted in the most efficacious upregulation of expression.
- From *in vivo* characterisation, the non-inducible AAV-9 vector, administered at the high dose of $2x10^{10}$ VG/ml via IH injection resulted in the most efficient claudin-5 overexpression specifically in the cerebrovasculature.
- Overexpression of claudin-5 in the hippocampus did not cause any negative behavioural outputs in normal C57BL/6J mice.

Chapter 5. Rescue potential of newly generated claudin-5 overexpression AAV

5.1 Introduction:

BBB breakdown and its association with numerous neurological disorders has been extensively discussed in previous sections of this thesis. Moreover, from the work described in Chapter 3, in addition to the various published work in this field, including the work of Nitta et al., 2003, Greene et al., 2018; 2022 and Menard et al., 2017, there is a undeniable association between BBB breakdown, the loss of claudin-5 expression and the neurobehavioral sequelae that is associated with disorders such as schizophrenia, epilepsy and MDD. Additionally, the work described in Chapter 4 has established a gene therapy based approach to re-establish BBB integrity through the overexpression of claudin-5 in ECs specifically. Therefore, the next step in the development of this gene therapy based approach, is to examine the AAV's rescue potential, *in vivo,* in animal models of disease. As discussed previously, animal models of disease are an essential preclinical tool to evaluate novel therapeutics for their safety profile, their pharmacokinetics, pharmacodynamics and importantly their efficacy *in vivo* (Singh et al., 2015; McGonigle and Ruggeri., 2014). Therefore a number of models were administered this newly established gene therapy to determine its potential efficacy.

The four models used to examine the claudin-5 overexpression AAVs rescue potential can be broken into two different cohorts. The first includes the *Cldn5*$^{fl/wt}$*xTie2Cre* mouse model and the inducible claudin-5 knockdown mouse model. Both of these models have noted behavioural deficits that are the direct result of a loss of claudin-5 expression. These are proof of concept models, to show that restoring claudin-5 expression at the level of the BBB can resolve the barrier's function and rescue the pathological phenotype. The second two models are the KA-induced epilepsy model and the CSDS model of MDD. Both of these models are established and accepted models of their respective diseases. Examining the rescue potential of claudin-5 overexpression in these models is essential. As these models are established models of disease, they have been validated and proven to mirror many aspects of their representative disorder. The method utilised to develop the model relates to the natural development of the disease, the model mimics the anatomical, neuropathological and behavioural features that are noted in the human disease and most importantly for this

work, the model has the ability to respond to treatments in a manner that may be predictive to the treatment efficacy in patients.

Details of each model used in the examination of AAV rescue potential are described below:

5.1.1 The Inducible Claudin-5 Knockdown Mouse model:

To further investigate the role of claudin-5 in BBB function, the generation of an inducible knockdown (KD) model was required. An inducible KD model, allows both cell type-specific and time-specific KD of gene expression, thus avoiding the inviability issue while beneficially adding an additional level of control to the investigation. Previous work in the Campbell lab generated such a model (Greene et al., 2018). Inducible KD mice were generated, through a complex strategy of knock-in genes and crosses. As can be seen in Figure 5.1, a gene containing a doxycycline-inducible claudin-5 160 shRNA was knocked-in at the Col1a1 locus on chromosome 11, while on chromosome 6, at the Rosa26 locus, a CAG-lox-stop-lox-rtTA3-IRESmKate2 (CLR3K) allele was knocked in. Knock-in mice were then crossed with another strain expressing Cre recombinase under the control of the Tie2 EC specific promoter. This ensured that the activity of the Cre recombinase was found only in the ECs of Cre positive mice. This enzyme in combination with the loxP sites forms a recombination system which results in the excision of the DNA found between the loxP sites, which in this model, includes a stop codon. The removal of the stop codon, allows the reverse tetracycline-controlled transactivator (rtTA) to be transcribed. In the presence of its effector, tetracycline or the tetracycline derivative, doxycycline (Dox), the rtTA is activated and can then activate the transcription of genes under the control of the tetracycline-responsive promoter element (TRE) (Das et al., 2016). Thus, when the induction of expression of the shRNA is required, this engineered inducible knockdown mouse must simply be supplied with doxycycline in their drinking water. The claudin-5 targeted shRNA transcribed is then processed into siRNA, which results in the degradation of *Cldn5* mRNA and overall results in the RNAi mediated silencing of claudin-5 in the ECs of this inducible knockdown mouse model (Davison and McCray., 2011).

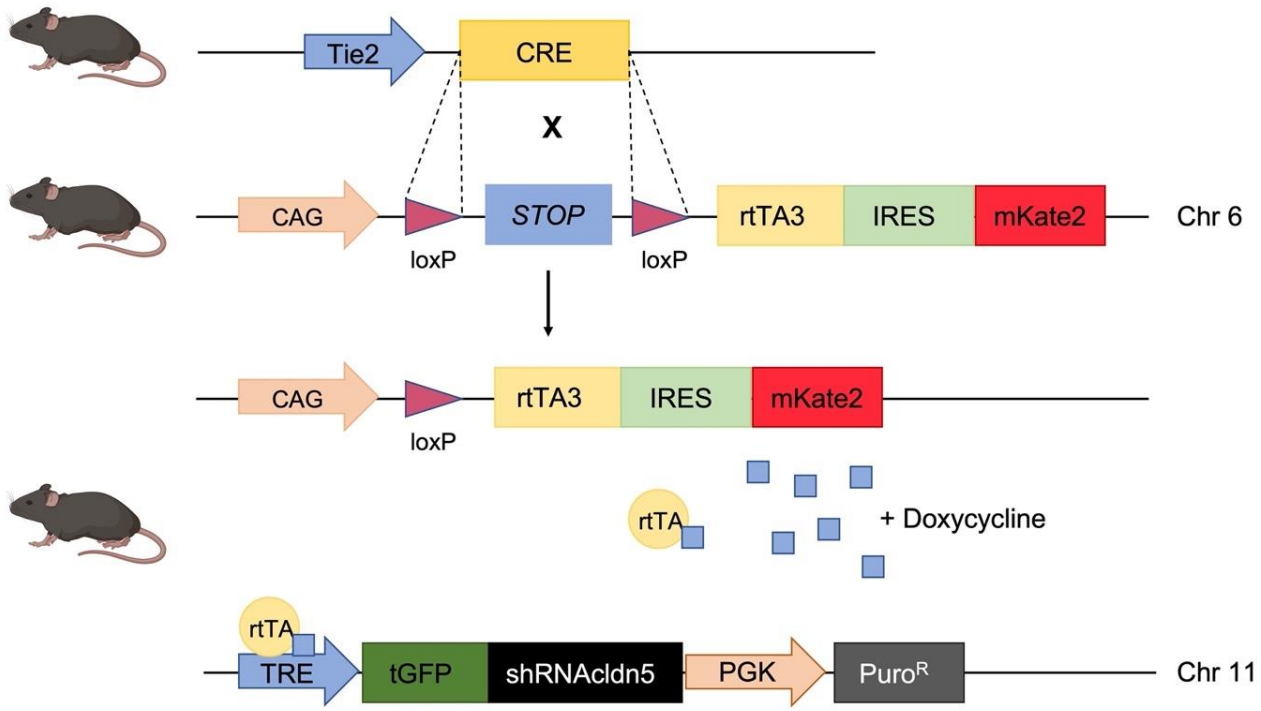

Figure 5.1. Doxycycline inducible knockdown system.

The inducible claudin-5160xTie2Cre mice were generated, through a complex strategy of knock-in genes, at chromosomes 6 and 11 followed by crossing with a Tie2Cre mouse. The cross ensures that the RNAi mediated silencing of claudin-5 is specific to ECs of Cre positive mice. shRNA and rtTA expression is verified by the GFP and mKate2reporters. The puromycin resistance gene ($Puro^R$) is incorporated for cloning of shRNA vectors. (Greene et al., 2018)

5.1.2 The *Cldn5$^{fl/wt}$xTie2Cre* Mouse model:

The genetics of *Cldn5$^{fl/wt}$xTie2Cre* mice has been described in detail on section 3.1.2. In summary utilising the Cre-loxP system, mice that are Tie2Cre+ are EC specific claudin-5 heterozygotes.

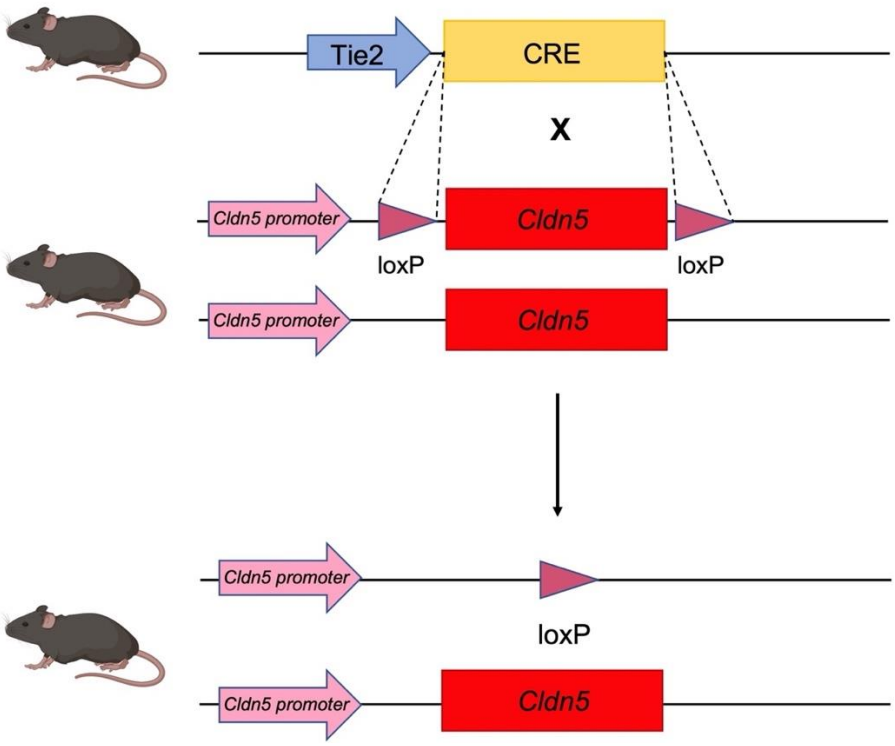

Figure 5.2. The *Cldn5*$^{fl/wt}$*xTie2Cre* mouse model.
The *Cldn5*$^{fl/wt}$*xTie2Cre* mouse model was generated by crossing the new *Cldn5*-LoxP mouse with the Tie2Cre mouse. Utilising the loxP system, the cross ensures all Cre positive animals have only one copy of the claudin-5 allele and so produces ~ 50 % less claudin-5 mRNA and protein.

5.1.3 Kainic Acid Model for Temporal Lobe epilepsy

While no experimental animal model reproduces all the features of temporal lobe epilepsy (TLE), some models have been extensively used in epilepsy research due to their high level of similarity to human epilepsy. One of these models is the KA model of TLE, that was originally discovered by Ben-Ari (Ben-Ari and Lagowska, 1978; Ben-Ari et al., 1979). The KA model of TLE has become one of the most established animal models of epilepsy and has greatly contributed to the understanding of the molecular, cellular and pharmacological mechanisms underlying epileptogenesis, which is the sequence of events that convert a normal neural network into hyperexcitable one.

The initial studies carried out by Ben-Ari showed that an intra-amygdaloid injection of KA resulted in seizure activity and the development of neuropathological lesions in the CA3 region of the dorsal hippocampus that are comparable to those noted in patients with TLE. Importantly, this model is also characterised by a latent period that ensues the initial precipitating injury, in this case status epilepticus, until the development of recurrent

spontaneous seizures, as is seen also in the human condition. Status epilepticus, the injury driven by the KA administration, is a prolonged, continuous seizure that lasts longer than 5 minutes, or having two or more sequential seizures without recovery between episodes, which may lead to permanent brain damage or death.

KA is a cyclic analogue of L-glutamate and an agonist of ionotropic KA receptors. It was first identified and isolated in the 1950s from red algae (Digenea simplex) and originally utilised as an ascaricide, to treat a parasitic disease ascariasis (Murakami et al., 1953). However when it was noted that it could cause prolonged excitatory responses in cortical neurons in rats, the potential for KA in neurological research as an analog for glutamate became clear (Shinozaki and Konishi, 1970). Glutamate is a principal excitatory amino acid transmitter in the CNS and binds to numerous ionotropic receptors such as NMDA receptors, AMPA receptors, and kainate receptors. KA is capable of binding to kainate receptors, and thus could induce robust depolarization and neuronal cell death via repression of presynaptic GABA release and activation of postsynaptic glutamatergic neurons, which is a central pathology noted in TLE (Bloss and Hunter, 2010; Vincent and Mulle, 2009).

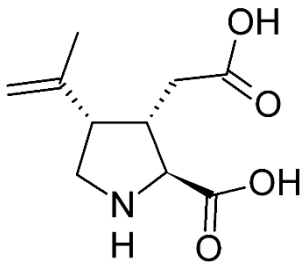

Figure 5.3. Chemical structure of KA

The KA model is a robust model that can be reproduced in a variety of species, through various administration routes, systemic, intrahippocampal or intra-amygdaloid administrations (Levesque and Avoli 2013). Doses range from 10-30 mg/kg for systemic injection or 0.1-0.5 µg for intracerebral injection. For this thesis the model was utilised through a systemic route. Seizures were induced by an IP injection of 10mg/kg KA. Seizure severity was recorded according to the Racine scale: 0: no change in behaviour; 1: immobility; 2: head nodding; 3: forelimb clonus; 4: forelimb clonus with rearing and

falling; 5: wild running and jumping often followed by generalised tonic-clonic activity and loss of postural tone.

5.1.4 Chronic Social Defeat Stress (CSDS) Model:

MDD is the most prominent cause of disability and the most common mood disorder worldwide (Menard et al., 2017; Kessler et al., 2005). Chronic social stress is a key contributor to the prevalence of mood disorders and suicide attempts in cohorts of individuals that have been subjected to bullying (Meltzer et al., 2011). Similarly in rodents, CSDS is an established method of creating a mouse model of depression. This method induces a depression-like phenotype that includes social withdrawal and anhedonia, in a subset of mice, which can be reversed with chronic anti-depressant treatment. This subset of mice are characterised as susceptible (SS) mice. Those that do not develop the depression-associated behaviours are known as resilient (RES) mice, further mimicking outcomes noted in humans, in which not every individual that experiences trauma or bullying will develop depression. Interestingly, CSDS also induces changes in metabolism in mice which is noted by weight gain and insulin and leptin resistance, which again is consistent to homeostatic abnormalities in MDD patients.

CSDS protocol requires an aggressor, in this case a CD-1 mouse. Mice under investigation, in this case C57Bl/6 J mice, are subjected to physical interactions with an unfamiliar CD-1 aggressor mouse 10 min per day, over 10 consecutive days. Following these social defeat sessions, the C57Bl/6 J mouse is removed and housed on the opposite side of the social defeat cage divider, which allows for sensory but not physical contact. Following the 10 day protocol, 24 hr after the final social defeat, mice undergo the social interaction test to determine if they are susceptible or resilient.

5.2 Objectives:

- Characterisation of the rescue effect of claudin-5 overexpression in the hippocampus of *Cldn5*$^{fl/wt}$*xTie2Cre* mice.
- Characterisation of the rescue effect of claudin-5 overexpression in the PFC of *Cldn5*$^{fl/wt}$*xTie2Cre* mice.
- Characterisation of the rescue effect of claudin-5 overexpression in the hippocampus of the inducible knockdown claudin-5 mouse model.

- Characterisation of the rescue effect of claudin-5 overexpression in the hippocampus of MDD model, CSDS mice.
- Characterisation of the rescue effect of claudin-5 overexpression in the hippocampus of KA-induced epilepsy model.

5.3 Results

Clear behavioural deficits were noted in the *Cldn5$^{fl/wt}$xTie2Cre*, due to the 50 % loss of claudin-5 expression in the cerebrovasculature, as describe in Chapter 3. Chapter 4 detailed the design and optimisation of the AAV vector gene therapy to overexpress claudin-5 specifically at the level of ECs and so can specifically upregulate expression of claudin-5 at the vasculature of the brain. Therefore the next step, and the overarching aim of this chapter, was to determine if overexpression of claudin-5 can attenuate the behavioural deficits in models of disease.

5.3.1 Characterisation of rescue potential in *Cldn5$^{fl/wt}$xTie2Cre* mice following AAV administration into the hippocampus.

The *Cldn5$^{fl/wt}$xTie2Cre* mice were divided into four groups, with both the claudin-5 heterozygote *Cre+Cldn5$^{fl/wt}$* mice as well as the *Cre-Cldn5$^{fl/wt}$* control mice each receiving either the control GFP version of the AAV (GFP-AAV) or the therapeutically relevant claudin-5 overexpression AAV (Cldn5-AAV). To determine the potential rescue effect of the therapeutic AAV on the behavioural issues noted in the *Cldn5$^{fl/wt}$xTie2Cre* model, a behavioural dataset was generated following targeted upregulation of claudin-5 *in vivo* in the hippocampus.

All mice underwent stereotaxic surgery, with the relevant control or therapeutic AAV being bilaterally, intrahippocampally injected. Allowing 3 weeks for recovery and AAV transduction, all mice then underwent a series of behavioural trials, the timetable of which are outlined in section 2.4.1. When all behaviour assays were complete mice were sacrificed and tissue was collected for analysis and claudin-5 quantification (Fig. 5.4)

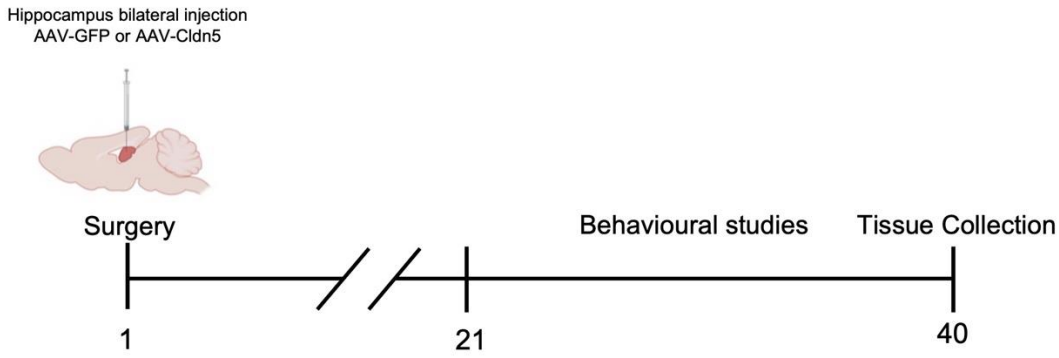

Figure 5.4. Timeline for characterisation of rescue potential of claudin-5 overexpression AAV in hippocampus of *Cldn5$^{fl/wt}$xTie2Cre* mice.

Timeline depicting bilateral intrahippocampal injection of AAV followed 3 weeks later by behavioural characterisation. Mice were sacrificed and tissue taken when all behaviour trials were completed. Schematic created with BioRender.

As there were clear deficits noted in memory function of the *Cldn5$^{fl/wt}$xTie2Cre* mice, various behavioural tests were carried out to examine the effect of the overexpression claudin-5 AAV on the *Cre+Cldn5$^{fl/wt}$* claudin-5 heterozygote mice. Firstly, spontaneous alternation on the Y-maze was again used to examine working spatial memory. There were significant differences in spontaneous alternation noted between the treatment groups in the *Cre+Cldn5$^{fl/wt}$* mice with the GFP-AAV control mice showing a significantly lower spontaneous alternation in comparison to those that received the Cldn5-AAV treatment. The correlation data between the two *Cre+Cldn5$^{fl/wt}$* groups again indicates that the level of claudin-5 being expressed is associated with a high spontaneous alternation score ($p = 0.0398$; $r = 0.5984$) (Fig. 5.5. A (i)). Additionally the number of errors made was significantly higher in the *Cre+Cldn5$^{fl/wt}$* GFP-AAV treated group in comparison to the *Cre-Cldn5$^{fl/wt}$* GFP-AAV group and the *Cre+Cldn5$^{fl/wt}$* Cldn5-AAV cohort. The *Cre+Cldn5$^{fl/wt}$* Cldn5-AAV treated mice, committed fewer errors in the maze and finished the test with a result that is much more comparable to the *Cre-Cldn5$^{fl/wt}$* control groups, which would indicate the claudin-5 overexpression AAV is indeed having a positive effect on memory function (Fig. 5.5. A (ii)). The number of arm entries remained similar between the groups (Fig. 5.5. A (iii)).

The radial arm maze was again utilised to further examine various aspects of the *Cldn5$^{fl/wt}$xTie2Cre* model's memory that had noted impairments in the original

characterisation. In the radial arm maze the *Cre-Cldn5*$^{fl/wt}$ mice that received either AAV treatment, GFP-AAV or Cldn5-AAV, produced very similar results across the duration of the 10 day trial in regards to both their working and reference memory (Fig. 5.5). This in turn shows that in healthy subjects, no adverse effects are being caused by the control or treatment gene therapy. However in the *Cre+Cldn5*$^{fl/wt}$ mice there were numerous days that showed a significant difference between the treatment groups. Examining reference memory, within the *Cre+Cldn5*$^{fl/wt}$ groups, significant differences are noted between the two treatment groups, on day 3 as well as from day 6 onwards to the completion of the trial on day 10 (Fig. 5.5 B (iii)). Reference memory, emulates long-term memory therefore these errors reflect an inability to retain memory regarding the location of the food rewards in this trial resulting in mice entering the incorrect arms in their search. Overtime these errors should reduce, as is seen in the *Cre-Cldn5*$^{fl/wt}$ control mice (Fig. 5.5 B (ii)). This is also seen in the *Cre+Cldn5*$^{fl/wt}$ mice that received the therapeutic Cldn5-AAV further supporting the rescue potential of this gene therapy (Fig. 5.5 B (ii;iii)).

Working memory, which reflects short term memory, is counted when a mouse enters an arm it has already investigated during the trial. As with the reference memory, no discernible differences were noted between treatment groups in the *Cre-Cldn5*$^{fl/wt}$ mice. However in the *Cre+Cldn5*$^{fl/wt}$ mice there are significant differences were noted between the two treatment groups from day 7 to 10, again further supporting the hypothesis that these memory issues can be resolved if claudin-5 expression in the BBB is restored. Further support for this hypothesis is seen in Fig. 5.5 B (iv;v) with the lower levels of *Cldn5* mRNA expression in the hippocampus showing a significant negative correlation with the number of working memory errors made during the trial ($p = 0.0280$; $r = -0.6304$).

In the characterisation of the *Cldn5*$^{fl/wt}$*xTie2Cre* mouse model, one of the most notable changes in behaviour that is associated with anxiety was in grooming behaviour. There was a significant neglect in both forced and spontaneous grooming, noted through the splash test and open field test. Following claudin-5 overexpression in the hippocampus through AAV administration, the claudin-5 heterozygote *Cre+Cldn5*$^{fl/wt}$ mice showed a latency that is comparable with both *Cre-Cldn5*$^{fl/wt}$ control treatment groups. Moreover, the *Cre+Cldn5*$^{fl/wt}$ mice that were treated with the control GFP-AAV continued to exhibit a significant neglect to initiate grooming behaviour compared to the control mice that received either treatment option (Fig. 5.6 A (ii)). Correlation data again indicates that the

increased latency to groom shows an association with decreased claudin-5 expression ($p = 0.0234$; $r = -0.4810$) (Fig. 5.6 A (iii)). This same finding is seen for the open field test in regards to spontaneous grooming behaviour ($p = 0.0002$; $r = -0.7210$) (Fig. 5.6 C (ii)). Additionally, another behaviour associated with increased anxiety is the reduced preference for social interaction, which was measured in the social preference task. The *Cre+Cldn5*$^{fl/wt}$ mice that received the control GFP-AAV continues to show a decreased preference for social interaction, while the *Cre+Cldn5*$^{fl/wt}$ that were administered the therapeutic Cldn5-AAV showed a trend towards an increased social interaction index score (Fig. 5.6 B (i)).

Distinct deficits in sensorimotor gating had been noted in the *Cldn5*$^{fl/wt}$*xTie2Cre* mouse model, with a significant decrease in PPI response at the 77-110 dB, 77-120 dB and 83-120 dB prepulse-pulse combinations (Fig. 3.21 (ii;iii)). Mice were again assessed for PPI response at 71, 77, 83 dB prepulse sound levels with 100, 110 and 120 dB pulse sound levels. Following therapeutic overexpression of claudin-5 in the *Cre+Cldn5*$^{fl/wt}$ mice there was a significant improvement of this PPI response, with a significant difference noted in the *Cre+Cldn5*$^{fl/wt}$ mice that were treated with the therapeutic Cldn5-AAV over the cohort that received the control GFP-AAV vector at 83-120db pre-pulse pulse (Fig. 5.8 (ii)). The *Cre+Cldn5*$^{fl/wt}$ Cldn5-AAV treated mice show a PPI response that is much more comparable to the *Cre-Cldn5*$^{fl/wt}$ control mice (Fig. 5.8 (i) vs (ii)).

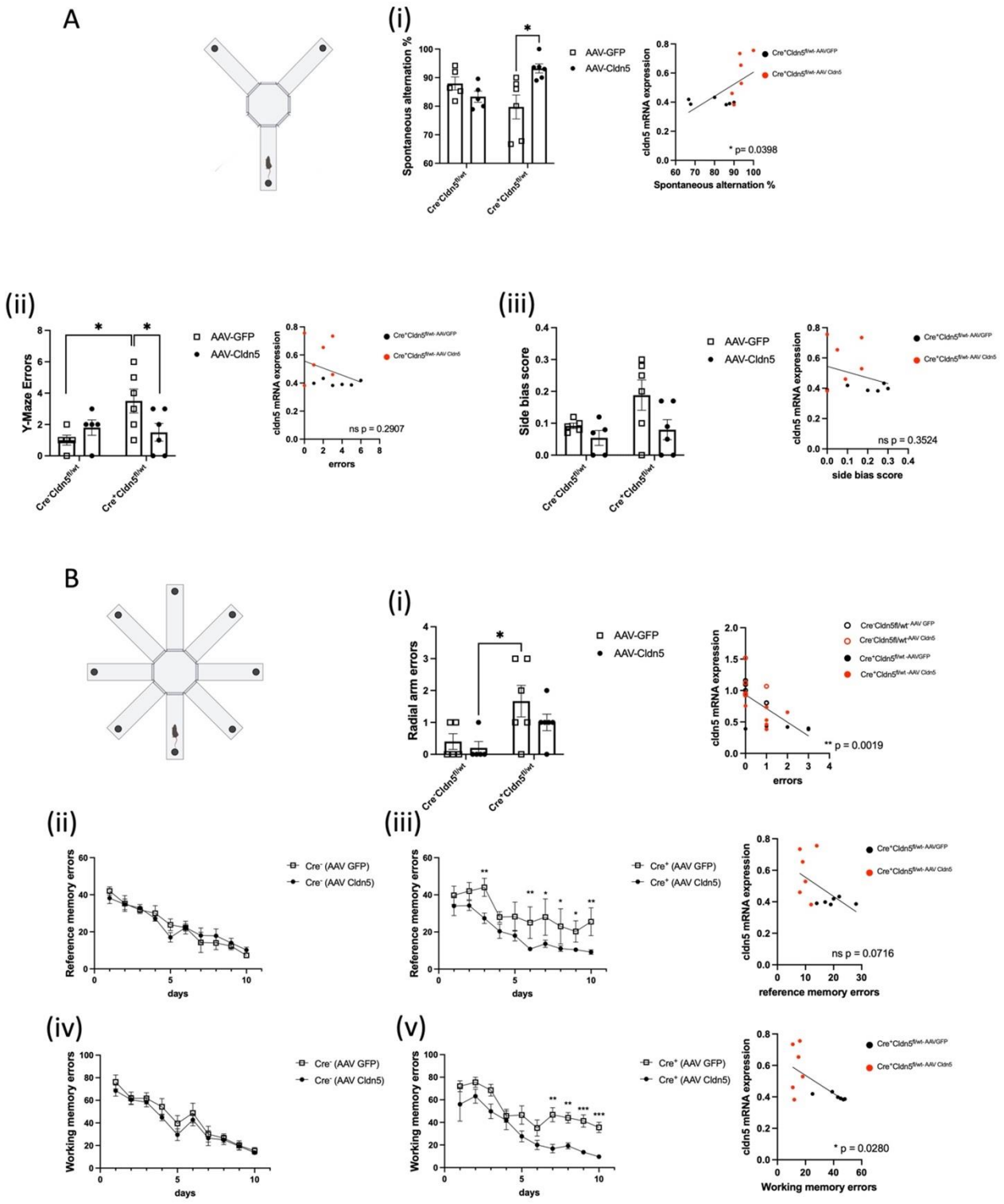

Figure 5.5. Improvement in learning and memory ability noted following intrahippocampal administration of the claudin-5 overexpression AAV in *Cldn5$^{fl/wt}$xTie2Cre* model

The rescue potential of the AAV IH administered to the *Cldn5$^{fl/wt}$xTie2Cre* model. Learning and memory deficits that had previously been noted in this model were rescued following treatment with Cldn5-AAV. *P<0.05 by two-way ANOVA and Tukey's post-test. Correlations were evaluated with Pearson's correlation coefficient. All data are means ± SEM with n=5 per *Cre-Cldn5$^{fl/wt}$* group, n = 6 per *Cre+Cldn5$^{fl/wt}$* group. Schematics created with BioRender.

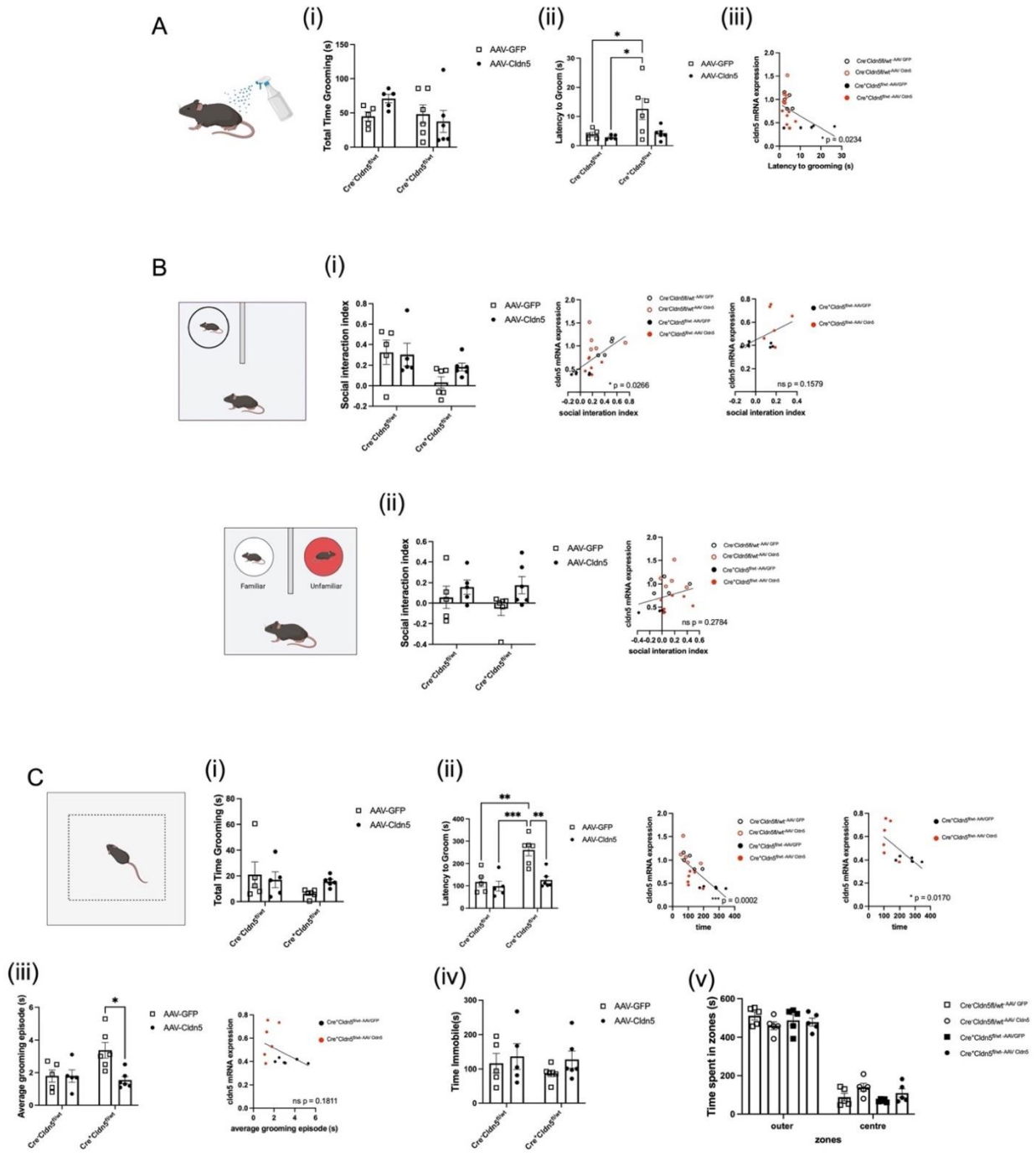

Figure 5.6. Reduced anxiety related behaviours noted following intrahippocampal administration of the claudin-5 overexpression AAV in *Cldn5$^{fl/wt}$xTie2Cre* model

The rescue potential of the therapeutic AAV IH administered to the *Cldn5$^{fl/wt}$xTie2Cre* model. (A) Shorter latency to groom in the *Cre+Cldn5$^{fl/wt}$* mice treated with the Cldn5-AAV (B) (i) *Cre+Cldn5$^{fl/wt}$* mice treated with Cldn5-AAV show a non-significant increase in preference for social interaction in comparison to the control treated ones (C) *Cre+Cldn5$^{fl/wt}$* mice treated with Cldn5-AAV display grooming behaviour that is more comparable to *Cre-Cldn5$^{fl/wt}$* mice in comparison to the *Cre+Cldn5$^{fl/wt}$*; GFP-AAV treated cohort. *P<0.05 by two-way ANOVA and Tukey's post-test. Correlations were evaluated with Pearson's correlation coefficient. All data are means ± SEM with n=5 per *Cre-Cldn5$^{fl/wt}$* group, n = 6 per *Cre+Cldn5$^{fl/wt}$* group. Schematics created with BioRender.

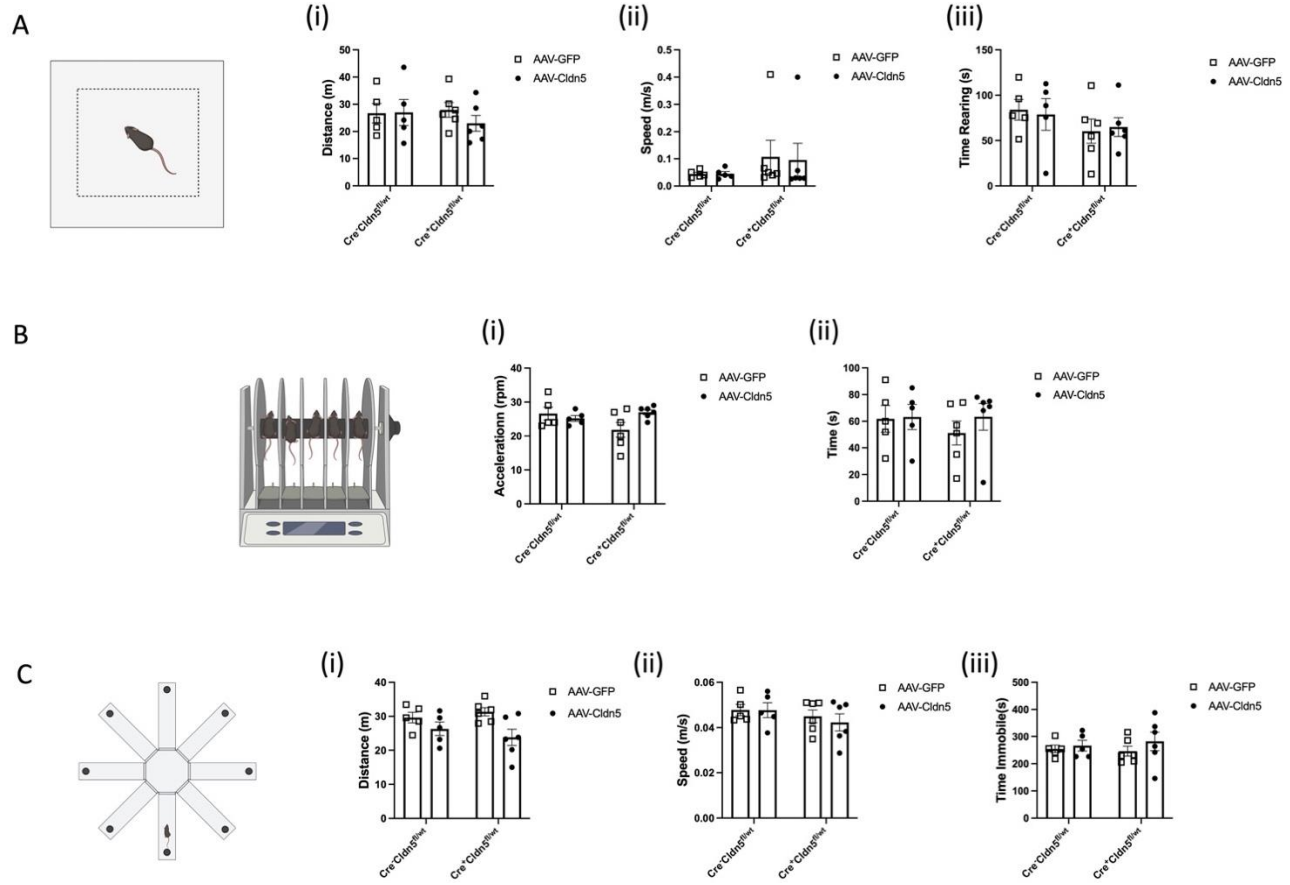

Figure 5.7. No change in locomotor activity noted following intrahippocampal administration of the claudin-5 overexpression AAV in *Cldn5*$^{fl/wt}$*xTie2Cre model*

Locomotor activity remained normal regardless of treatment *P<0.05 by two-way ANOVA and Tukey's post-test. Correlations were evaluated with Pearson's correlation coefficient. All data are means ± SEM with n=5 per *Cre-Cldn5*$^{fl/wt}$ group; n = 6 per *Cre+Cldn5*$^{fl/wt}$ group. Schematics created with BioRender.

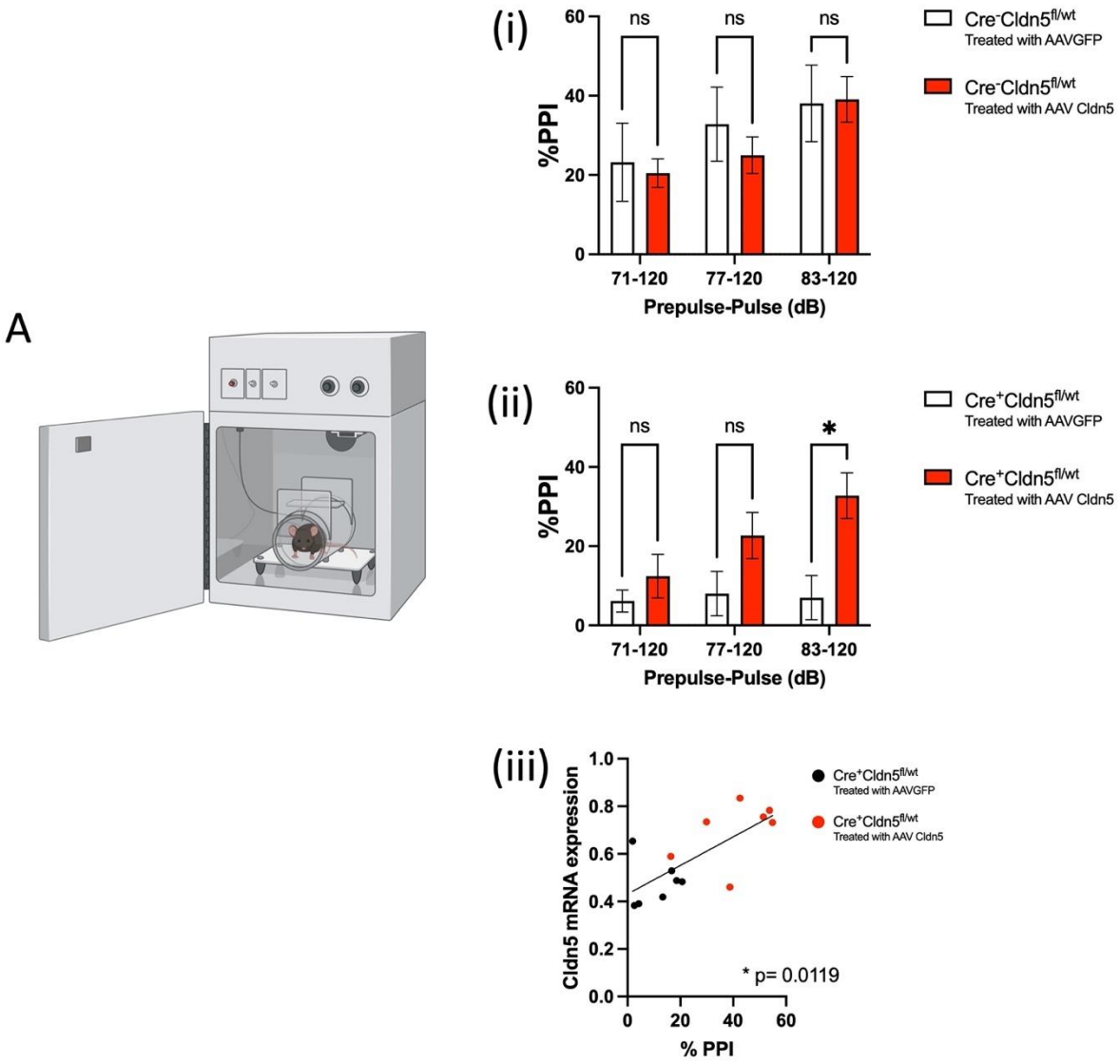

Figure 5.8. Improved sensorimotor gating noted following intrahippocampal administration of the claudin-5 overexpression AAV in *Cldn5$^{fl/wt}$xTie2Cre* model

The rescue potential of the AAV intrahippocampally administered to the hippocampus of *Cldn5$^{fl/wt}$xTie2Cre* model examining sensorimotor gating. (A) PPI apparatus (i) *Cre-Cldn5$^{fl/wt}$* showed no difference in PPI response regardless of AAV treatment (ii) *Cre+Cldn5$^{fl/wt}$* mice that were treated with the control GFP-AAV displayed a significantly reduced acoustic PPI response with a pre-pulse/pulse combination of 83dB-120dB in comparison to those treated with the Cldn5-AAV, showing rescue effect. (iii) Correlation data ($p = 0.0119$; $r = 0.6040$) *P<0.05 by two-way ANOVA and Tukey's post-test. Correlations were evaluated with Pearson's correlation coefficient. All data are means ± SEM with n=7 per *Cre-Cldn5$^{fl/wt}$* group; n = 7 per *Cre+Cldn5$^{fl/wt}$* group. Schematic created with BioRender.

5.3.2 Characterisation of rescue potential in *Cldn5$^{fl/wt}$xTie2Cre* mice following AAV administration into the medial prefrontal cortex.

Section 5.3.1 has shown a distinct rescue effect of the claudin-5 overexpression AAV when administered into the hippocampal region of the brain. Therefore the next step was to examine the potential rescue effect this BBB restoring AAV may have in a different region of the brain. The mPFC was selected as the next targeted brain region for examination. Previous work by Greene et al., had shown that suppression of claudin-5 in the mPFC resulted in profound behavioural changes, with distinct impairments in various forms of memory (Greene et al., 2018). As described in section 1.9.2 the mPFC is involved in memory function, as well as emotional processing and high-order cognitive processes. Taken together, this region showed strong potential as a target for claudin-5 overexpression in a gene therapy-based approach. As before the *Cldn5$^{fl/wt}$xTie2Cre* mice were divided into four groups, with both the claudin-5 heterozygote, *Cre+Cldn5$^{fl/wt}$* mice, as well as the *Cre-Cldn5$^{fl/wt}$* control mice each receiving either the control GFP version of the AAV (GFP-AAV) or the therapeutically relevant claudin-5 overexpression AAV (Cldn5-AAV). To determine the potential rescue effect of the therapeutic AAV on the behavioural issues noted in the *Cldn5$^{fl/wt}$xTie2Cre* model, a behavioural dataset was generated following targeted upregulation of claudin-5 *in vivo* in the mPFC.

All mice underwent stereotaxic surgery, with the relevant control or therapeutic AAV being bilaterally injected into the mPFC. Following 3 weeks for recovery and AAV transduction all mice underwent a series of behavioural trials, the timetable of which are outlined in section 2.4.1. When all behaviour assays were complete mice were sacrificed and tissue was collected for analysis and claudin-5 quantification (Fig. 5.9)

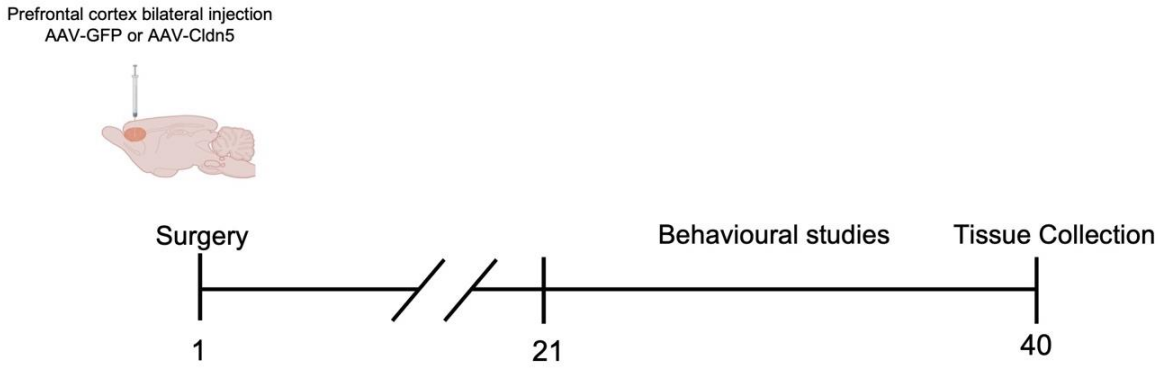

Figure 5.9. Timeline for characterisation of rescue potential of claudin-5 overexpression AAV in mPFC of *Cldn5*$^{fl/wt}$*xTie2Cre* mice.

Timeline depicting bilateral prefrontal cortex injection of AAV followed 3 weeks later by behavioural characterisation. Mice were sacrificed and tissue taken when all behaviour trials were completed. Schematic created with BioRender.

To examine the effect of the Cldn5-AAV in the mPFC in the *Cre+Cldn5*$^{fl/wt}$ claudin-5 heterozygote mice, the same assays were utilised as in section 5.3.1. the Y-maze and the radial arm maze. The Y-maze noted no differences in spontaneous alternation (Fig. 5.10 A (i)). The number of errors remained significantly higher in the *Cre+Cldn5*$^{fl/wt}$ mice that were treated with the control GFP-AAV, however in this case the therapeutic Cldn5-AAV does not appear to have any significant rescue effect (Fig. 5.10 A (ii)). Finally, no noted side bias was observed in these mice (Fig. 510 A (iii)).

The radial arm maze was utilised to further examine the potential rescue effect the BBB restoring AAV had when administered to the mPFC. As was noted in the Y-maze, the *Cre+Cldn5*$^{fl/wt}$ cohort treated with the GFP-AAV committed the most errors in the trials, but those that were treated with the Cldn5-AAV also committed a higher number of errors in comparison to either *Cre-Cldn5*$^{fl/wt}$ control group (Fig. 5.10 B (i)). In regards to both reference and working memory errors, as before the *Cre-Cldn5*$^{fl/wt}$ mice that received either AAV treatment produced very similar results across the duration of the 10 day trial (Fig. 5.10 B (ii; iv)). Comparing reference memory errors within the *Cre+Cldn5*$^{fl/wt}$ groups, showed no significant differences between treatment groups (Fig. 5.10 B (iii)). This result, when compared to the hippocampally injected cohort shows poor rescue of the reference memory deficits that are noted in this model (Fig. 5.5 B (iii)). In regards to the working memory errors committed by the *Cre+Cldn5*$^{fl/wt}$ mice, significant differences are noted

between the two treatment groups, on day 7 and 8 (Fig. 5.10 B (v)). This rescue is minimal in comparison to what was noted in the hippocampally injected mice (Fig. 5.5 B (v)).

Forced grooming behaviour analysed through the splash test did not show any significant differences in any cohort (Fig. 5.11 A). Spontaneous grooming showed a significant difference in the total time spent grooming between the *Cre+Cldn5*$^{fl/wt}$ treatment groups, with the control AAV treated cohort showing a longer latency to begin grooming but when doing so, the total time that was spent grooming was significantly higher than the therapeutic Cldn5-AAV cohort (Fig. 5.11 C (i;ii)). Neither of the social behaviour tasks noted any discernible differences. A decreased social interaction score had been noted in the characterisation of this model. While this trend can still be seen in the *Cre+Cldn5*$^{fl/wt}$ mice compared to the *Cre-Cldn5*$^{fl/wt}$ controls, there is no differences noted between the AAV treatment groups (Fig. 5.11 B (i)). The lack of behavioural changes between treatment groups are not due to any mobility issues which was verified through open field test, radial arm maze and rotarod (Fig. 5.12).

Sensorimotor gating deficits had been noted in the model and some rescue had noted with AAV treatment overexpressing claudin-5 in hippocampus. A similar result was obtained through the same AAV treatment in the mPFC. Mice were again assessed for PPI response at 71, 77, 83 dB prepulse sound levels with 100, 110 and 120 dB pulse sound levels. Following therapeutic overexpression of claudin-5 in the mPFC of *Cre+Cldn5*$^{fl/wt}$ mice there is a significant improvement of this PPI response, with a significant difference noted in the *Cre+Cldn5*$^{fl/wt}$ mice that were treated with the Cldn5-AAV over the cohort that received the GFP-AAV control at 83-120db pre-pulse pulse (Fig. 5.13 (ii))

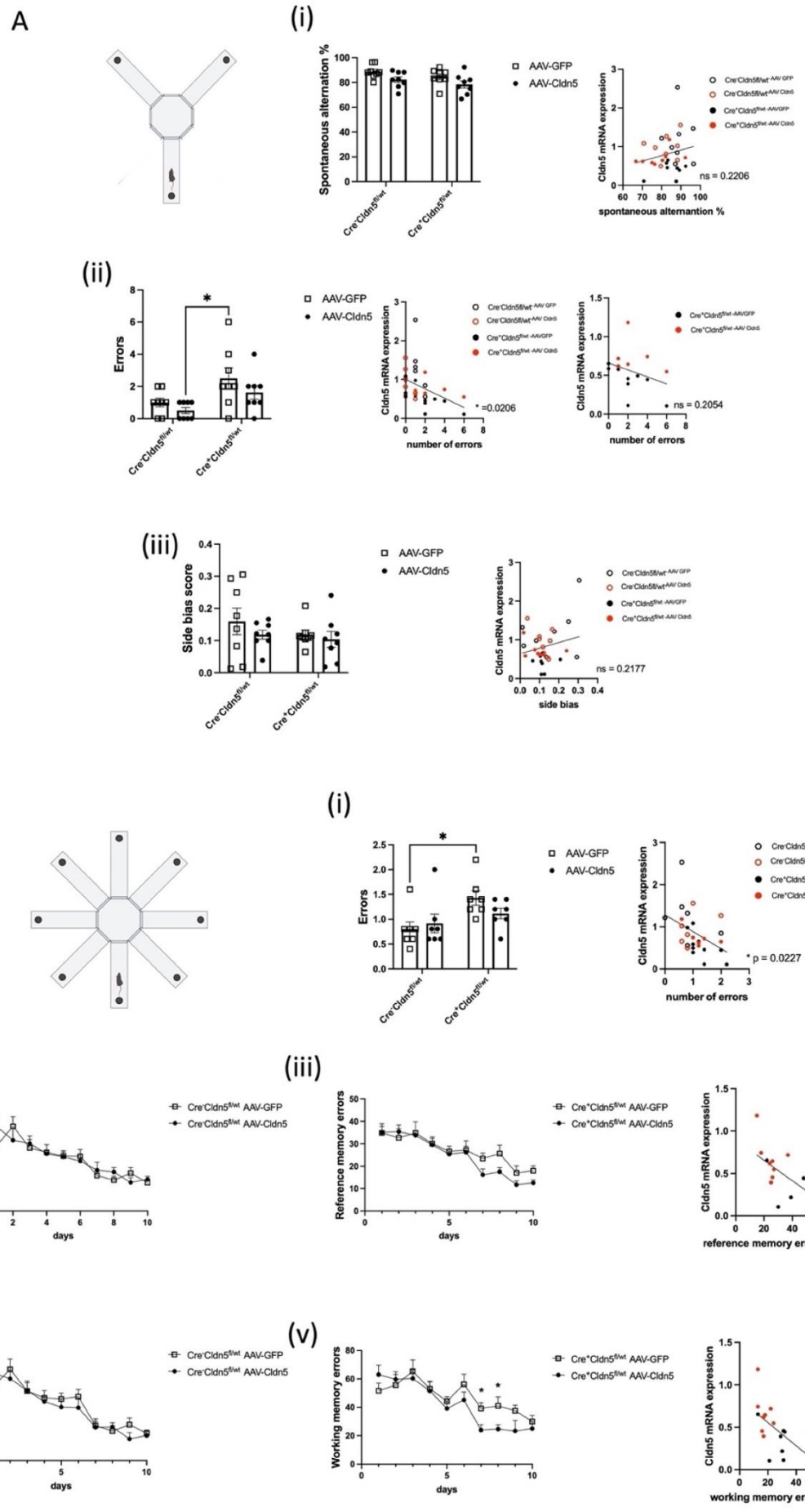
A
(i)
Spontaneous alternation %
AAV-GFP
AAV-Cldn5
Cre-Cldn5fl/wt
Cre+Cldn5fl/wt
Cldn5 mRNA expression
ns = 0.2206
spontaneous alternantion %
(ii)
Errors
*
*=0.0206
number of errors
ns = 0.2054
(iii)
Side bias score
ns = 0.2177
side bias
B
(i)
* p = 0.0227
(ii)
Reference memory errors
days
(iii)
* = 0.0237
reference memory errors day 8
(iv)
Working memory errors
(v)
ns = 0.0515
working memory errors day 8

Figure 5.10. No significant rescue of the learning and memory deficits following bilateral administration of AAV into the mPFC of *Cldn5$^{fl/wt}$xTie2Cre* model

Learning and memory function was analysed via the (A) Y-maze and (B) radial arm maze. No significant differences in behaviour were observed between *Cre+Cldn5$^{fl/wt}$* mice treated with the Cldn5-AAV or the GFP-AAV. This suggests that claudin-5 overexpression in the mPFC does not have a therapeutic effect on the memory deficits observed in the *Cldn5$^{fl/wt}$xTie2Cre* mice. *P<0.05 by two-way ANOVA and Tukey's post-test. Correlations were evaluated with Pearson's correlation coefficient. All data are means ± SEM with n=8 per group. Schematics created with BioRender.

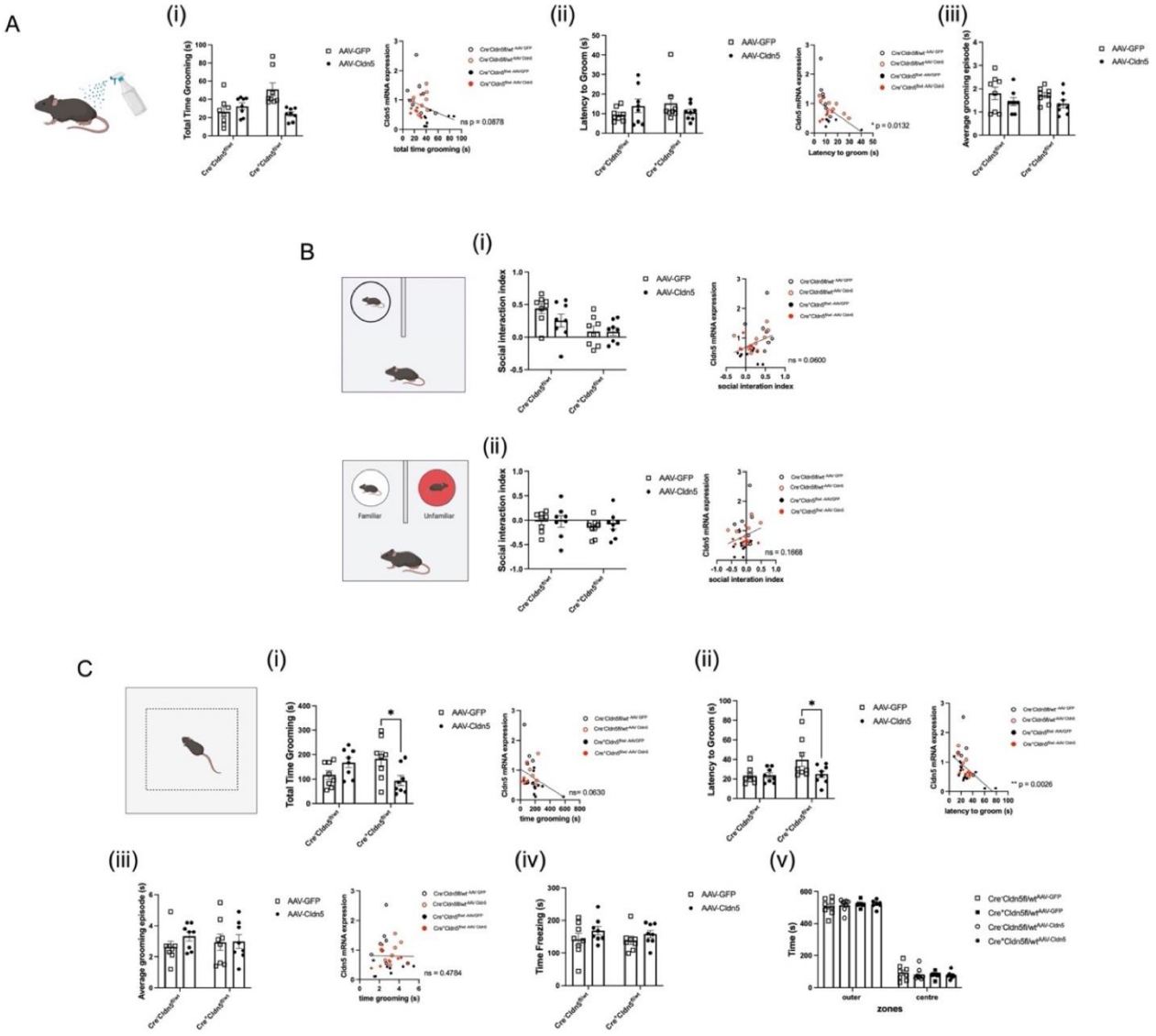

Figure 5.11. No significant rescue of the anxiety-associated behaviours following bilateral administration of AAV into the mPFC of *Cldn5$^{fl/wt}$xTie2Cre* model

Anxiety-associated behaviours were analysed via the (A) splash test, (B) the social behaviours tests and (C) the open field test. (B (i)) No significant rescue of the anxiety-associated reduced preference for social interaction in the *Cldn5$^{fl/wt}$xTie2Cre* model was noted following Cldn5-AAV treatment in the mPFC but (A;C) some potential improvement in grooming behaviour was noted. *P<0.05 by

two-way ANOVA and Tukey's post-test. Correlations were evaluated with Pearson's correlation coefficient. All data are means ± SEM with n=8 per group. Schematics created with BioRender.

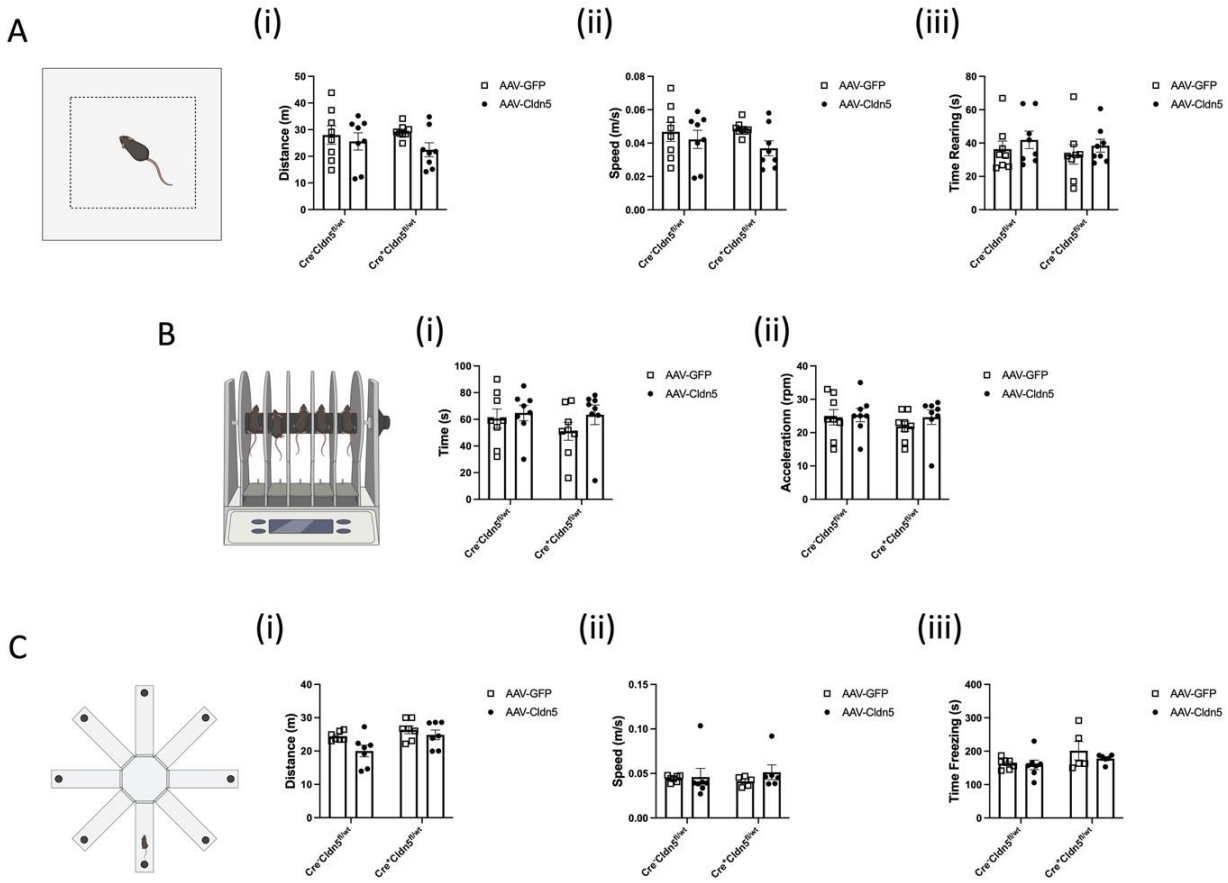

Figure 5.12. No change in locomotor activity noted following administration of the claudin-5 overexpression AAV in the mPFC of *Cldn5$^{fl/wt}$xTie2Cre* model

Locomotor activity remained normal regardless of treatment. *P<0.05 by two-way ANOVA and Tukey's post-test. All data are means ± SEM with n=8 per group. Schematics created with BioRender.

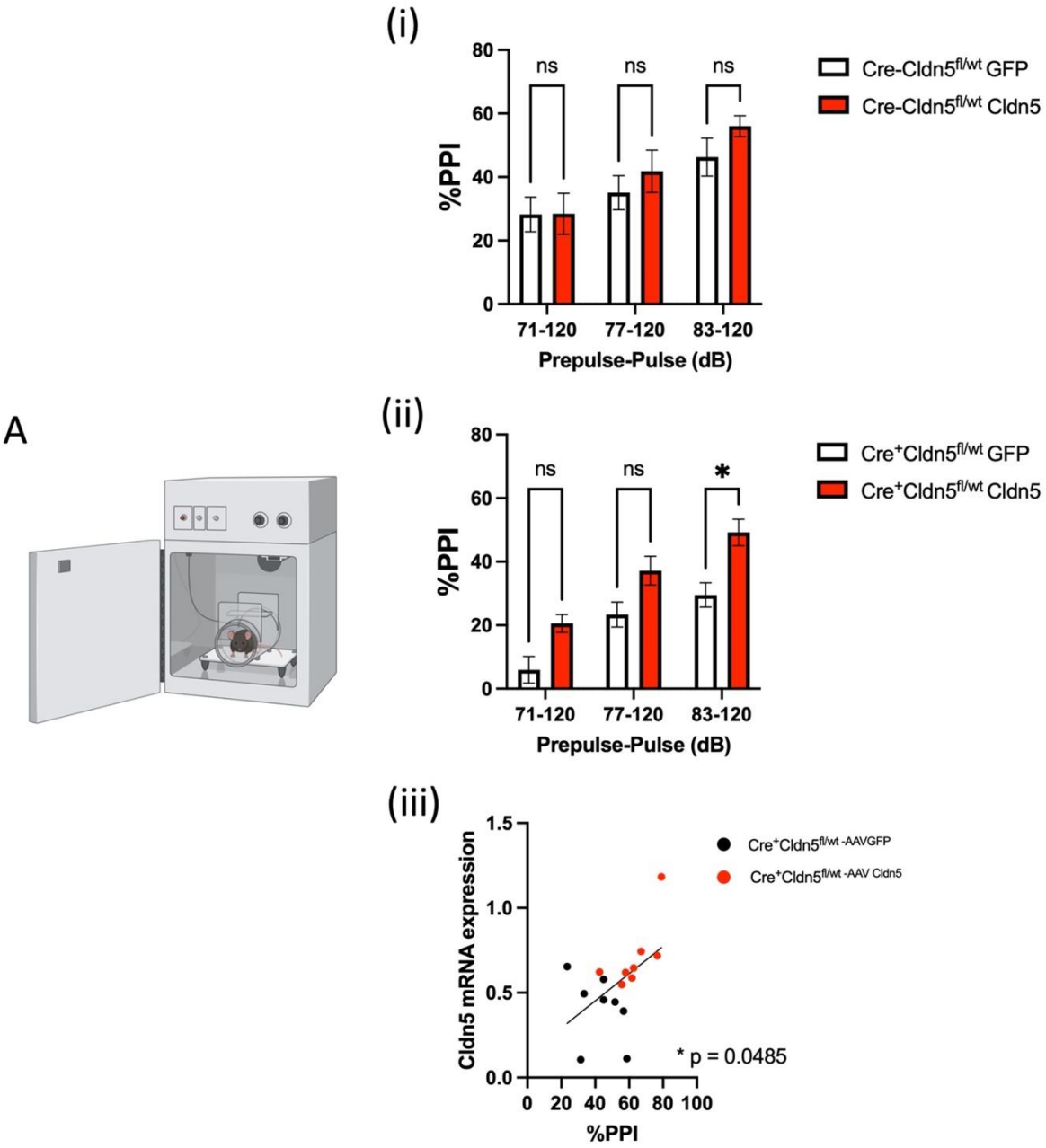

Figure 5.13. Improved sensorimotor gating noted following administration of the claudin-5 overexpression AAV in the mPFC of *Cldn5$^{fl/wt}$xTie2Cre* model

Cre+Cldn5$^{fl/wt}$ mice that were treated with the GFP-AAV displayed a continued deficit in PPI response at 83-120 dB prepulse pulse while the Cldn5-AAV treated cohort showed improvement, more comparable to the control *Cre-Cldn5$^{fl/wt}$* result. *P<0.05 by two-way ANOVA and Tukey's post-test. Correlations were evaluated with Pearson's correlation coefficient. All data are means ± SEM with n=8 per group. Schematic created with BioRender.

5.3.3 Characterising the rescue potential of the AAV in the doxycycline inducible claudin-5 knockdown mouse.

In the previous *Cldn5$^{fl/wt}$xTie2Cre* model, the *Cre+Cldn5$^{fl/wt}$* mouse is constitutively haploinsufficent for claudin-5 and so development and maintenance of its BBB has been carried out in claudin-5 deficient background. These mice while having behavioural deficits, have a normal lifespan with no extreme pathological phenotype. However the inducible claudin-5 knockdown mice, which were established in the Campbell lab a number of years ago, have been shown to, in conjunction with behavioural deficits, also develop seizures and die following persistent knockdown of claudin-5 (Greene et al., 2018). These mice are essentially wild-type mice with normal levels of claudin-5 until doxycycline is introduced into their diet. The overall greater loss of claudin-5 expression that is observed in this model, in comparison to the *Cldn5$^{fl/wt}$xTie2Cre* model, in addition to the sudden change from sufficient to deficient expression of claudin-5, are together likely to be contributing factors in their more severe symptoms and shorter lifespan. The inducible knockdown model, is a second model in which the noted pathogenesis is the direct result of claudin-5 knockdown. Therefore this model, in conjunction with the previous, act as a proof of concept that restoring claudin-5 expression can resolve function.

The inducible claudin-5 knockdown mouse were bilaterally intrahippocampally injected with the claudin-5 overexpression AAV or the control GFP-AAV. 1 week after surgery doxycycline was added to the drinking water. Following two weeks of doxycycline administration mice were subjected to a range of behavioural tasks to examine learning and memory, anxiety and depression, locomotor activity and sensorimotor behaviour. After all behavioural trials were complete a survival curve was carried out. A survival curve required the observation of the mice every day to do welfare checks and to note any loss of life. (Fig. 5.14).

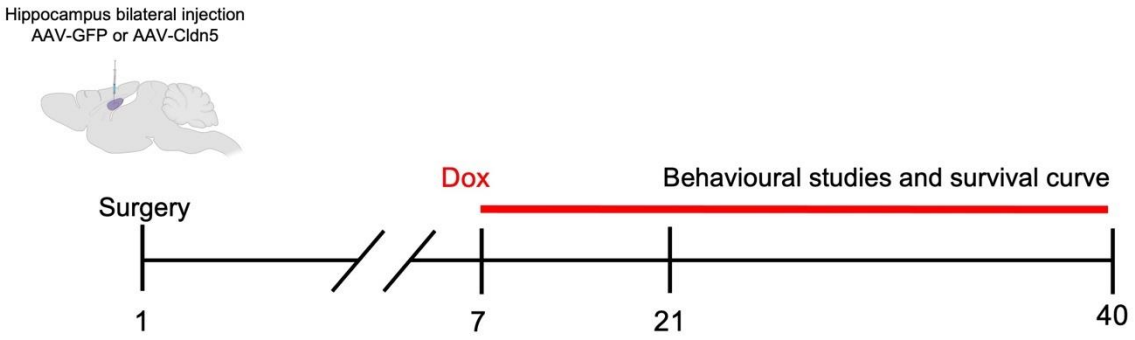

Figure 5.14 Timeline of treatment and behavioural characterisation of inducible claudin-5 knockdown model.

Timeline depicting bilateral intrahippocampal injection of AAV. 1-week post-surgery Dox treatment was added water supply. Following 2 weeks of Dox treatment behavioural characterisation was carried out. Mice were then observed until death for survival curve. Schematic created with BioRender.

Numerous impairments in learning and memory were noted in these mice, with sufficient rescue noted in those treated with the claudin-5 overexpression AAV. Claudin-5 knockdown (Cre+) mice treated with the control GFP-AAV committed significantly more errors in the Y-maze in comparison to the control (Cre-) mice or the Cre+ mice that were treated with the Cldn5-AAV (Fig. 5.15 (ii)). A non-significant increase in side bias is also seen in the Cre+ GFP-AAV injected mice which may have impaired the spontaneous alternation behaviour in this trial (Fig. 5.15 (iii)). Additionally, on the T-maze the Cre+ GFP-AAV injected mice showed significant impairments in comparison to both Cre- treatment cohorts and the Cre+ mice injected with the Cldn5-AAV (Fig. 5.15 B (i)).

Social interactions measured in the social behaviours tests did not detect any significant differences between treatment groups, regardless of genotype (Fig. 5.16 A;B). No increased level of anxiety was noted across the elevated plus maze (EPM) in which similar number of entries into open arms were observed for all four cohorts (Fig. 5.15 C). The total time spent grooming was, however, significantly reduced as well as a distinct neglect for coat grooming as measured through latency to groom during the trial is noted in the Cre+ mice that were treated with the control GFP-AAV. The Cre+ mice that were treated with the therapeutic Cldn5-AAV showed distinct rescue from this behaviour, with behavioural outputs similar to the Cre- control mice treated with either the control or therapeutic AAV (Fig. 5.16 D (iii;iv)). There was also a significant decrease in the amount of exploratory

behaviour noted in the Cre+ GFP-AAV mice, as noted through the reduced rearing behaviour noted in the open field test (Fig. 5.16 D (ii)).

Both the Cre- controls and the Cre+ claudin-5 knockdown mice regardless of treatment completed the locomotor-related tasks with no differences noted in distance travelled or average speed on the open field test (Fig. 5.17 A (i;ii). Moreover, all four cohorts performance were similar on the rotarod (Fig. 5.17 B).

Clear sensorimotor gating deficits had been noted in the model during its characterisation (Greene et al., 2018). Claudin-5 knockdown mice exhibited a distinctly reduced acoustic PPI response with a 77-110 dB, 77-120 dB and 83-120 dB prepulse-pulse combinations. Moreover both the Cre- controls and the Cre+ knockdown mice had shown comparable startle responses at 100, 110 and 120 dB which verified these deficits in PPI are not due to impaired hearing (Greene et al., 2018). Thus following AAV administration the four cohorts were analysed for PPI response, as before they were assessed for PPI at 71, 77, 83 dB prepulse sound levels with 100, 110 and 120 dB pulse sound levels. The Cre+ knockdown mice that were treated with the control GFP-AAV continued to show distinct deficits at the same prepulse-pulse combinations that were seen in the original characterisation, when compared to the Cre- controls of either AAV treatment. However, the Cre+ mice that had been treated with the Cldn5-AAV displayed a higher PPI response that was no longer significantly different from either of the Cre- control treated cohorts (Fig. 5.18). This again provides strong support that there is therapeutic relevance for the claudin-5 overexpression AAV.

As mentioned previously, the persistent knockdown of claudin-5 in this model does result in seizure development and death following 4-5 weeks of claudin-5 suppression. In the 48 hr before death, the claudin-5 knockdown mice all display a similar pathological phenotype, which included seizures, hyperactivity followed by notable immobility as well as refraining from food and water consumption. A clear rescue effect was noted, in which Cre+ knockdown mice treated with the therapeutic Cldn5-AAV survived for longer than those that received the control AAV (* $p=0.0268$) (Fig. 5.19).

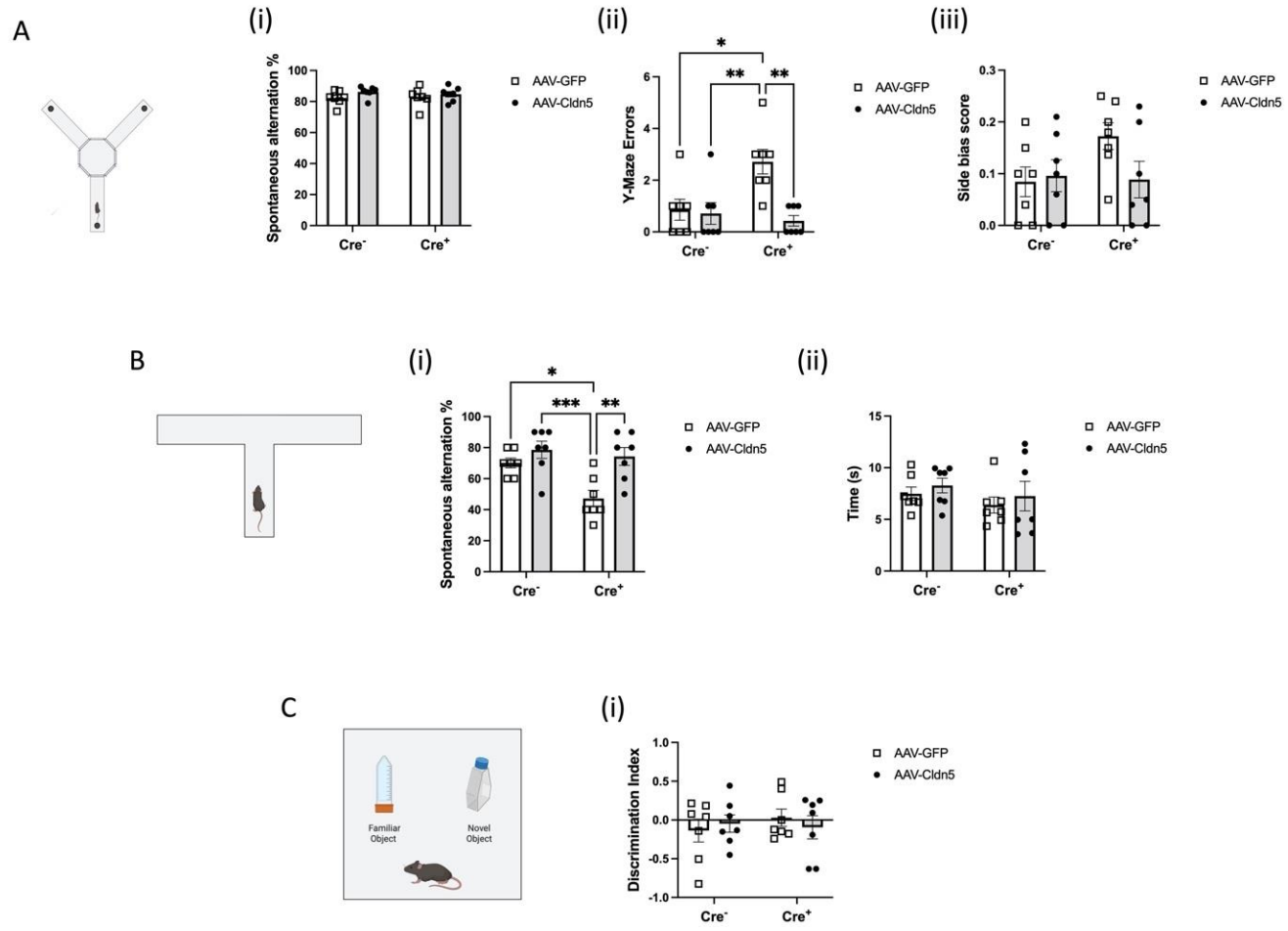

Figure. 5.15 Rescue of learning and memory impairments in inducible KD model following intrahippocampal administration of the claudin-5 overexpression AAV

(A) Schematic of Y-maze (i) no changes in spontaneous alternation (ii) significant number of errors noted in Cre+ mice treated with control GFP-AAV but not the therapeutic Cldn5-AAV (iii) non-significant trend for an increased side bias in the Cre+ control treated mice in comparison to both Cre- groups and Cre+ mice treated with Cldn5-AAV. (B) Schematic of the T-maze (i) significantly reduced spontaneous alternation on the T-Maze in Cre+ control treated mice in comparison to all other cohorts. (ii) no differences in the time to complete the trial. (C) novel object recognition trial noted no differences. *P<0.05 by two-way ANOVA and Tukey's post-test. All data are means ± SEM with n=7 per group. Schematics created with BioRender.

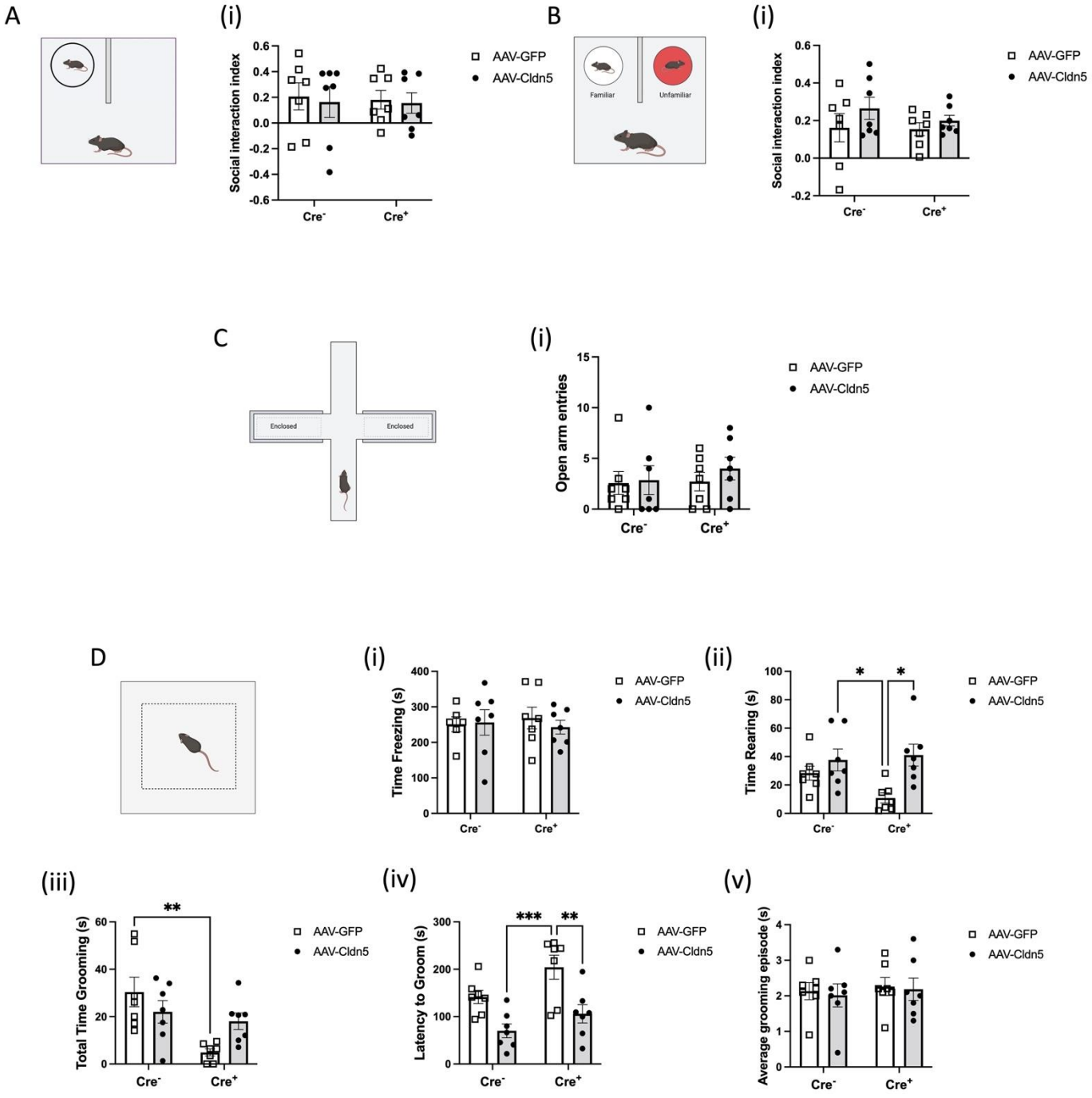

Figure 5.16 Rescue of anxiety-like behaviours in inducible KD model following intrahippocampal administration of the claudin-5 overexpression AAV

(A) Schematic of social preference task (i) no differences noted between Cre- and Cre+, or between treatment groups in social preference. (B) Schematic of social novelty task (i) no differences noted no differences noted between Cre- and Cre+, or between treatment groups in preference for novelty. (C) Schematic of elevated plus maze. (i) All cohorts completed trial with a similar number of open arm entries. (D) Schematic of open field test apparatus. No differences noted in time spent freezing or the average grooming episode (i; v) but significant changes in the GFP-AAV treated claudin-5 knockdown Cre+ mice for time spent rearing, time spent grooming and the latency to begin grooming behaviour (ii; iii; iv). *P<0.05 by two-way ANOVA and Tukey's post-test. All data are means ± SEM with n=7 per treatment group. Schematics created with BioRender.

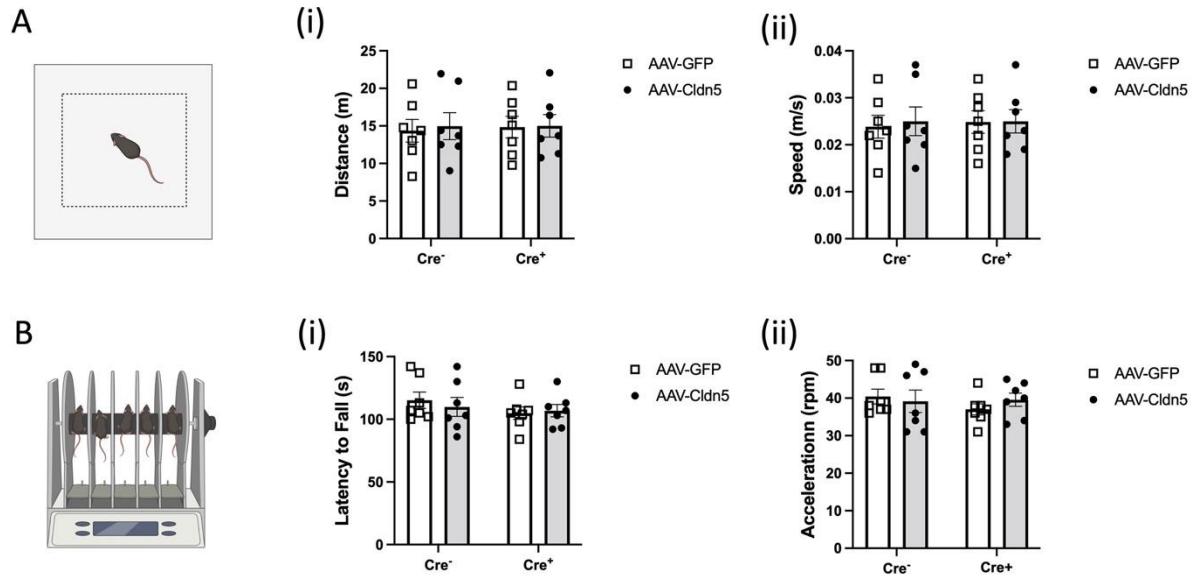

Figure 5.17. No change in locomotor ability in inducible KD model following intrahippocampal administration of the claudin-5 overexpression AAV

(A) Schematic of the open field test apparatus. No differences noted in (i) average distance travelled and (ii) average speed. (B) No differences noted in (i) latency to fall or (ii) the acceleration regardless of treatment type or genotype. *P<0.05 by two-way ANOVA and Tukey's post-test. All data are means ± SEM with n=7 per treatment group. Schematic created with BioRender.

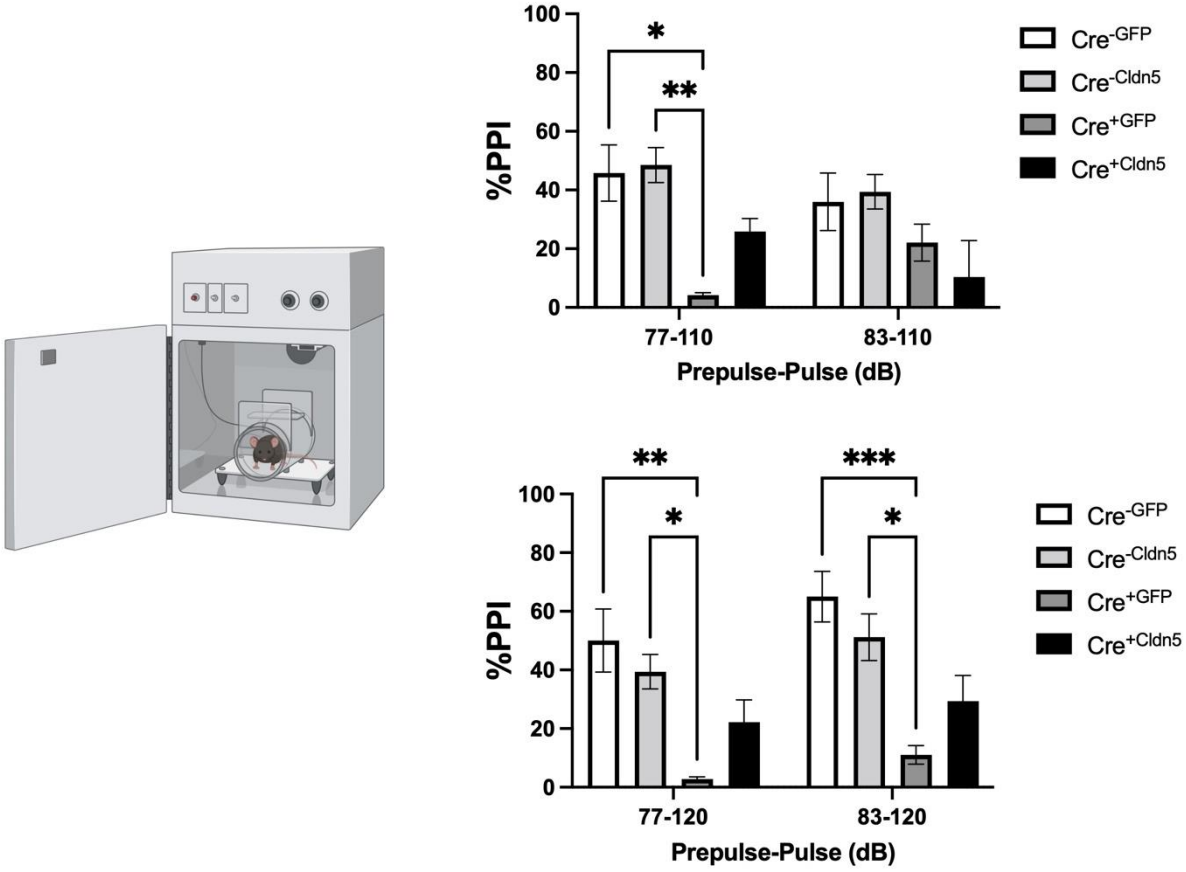

Figure 5.18. Improved sensorimotor gating noted in inducible claudin-5 KD model following intrahippocampal administration of the claudin-5 overexpression AAV

Claudin-5 knockdown (Cre+) mice treated with the control GFP-AAV displayed a significantly reduced acoustic PPI response with a pre-pulse/pulse combination at 77-110, 77-120 and 83dB-120dB in comparison to those treated with the Cldn5-AAV. *P<0.05, **P<0.01 by two-way ANOVA and Tukey's post-test. All data are means ± SEM with n=7 per treatment group. Schematic created with BioRender.

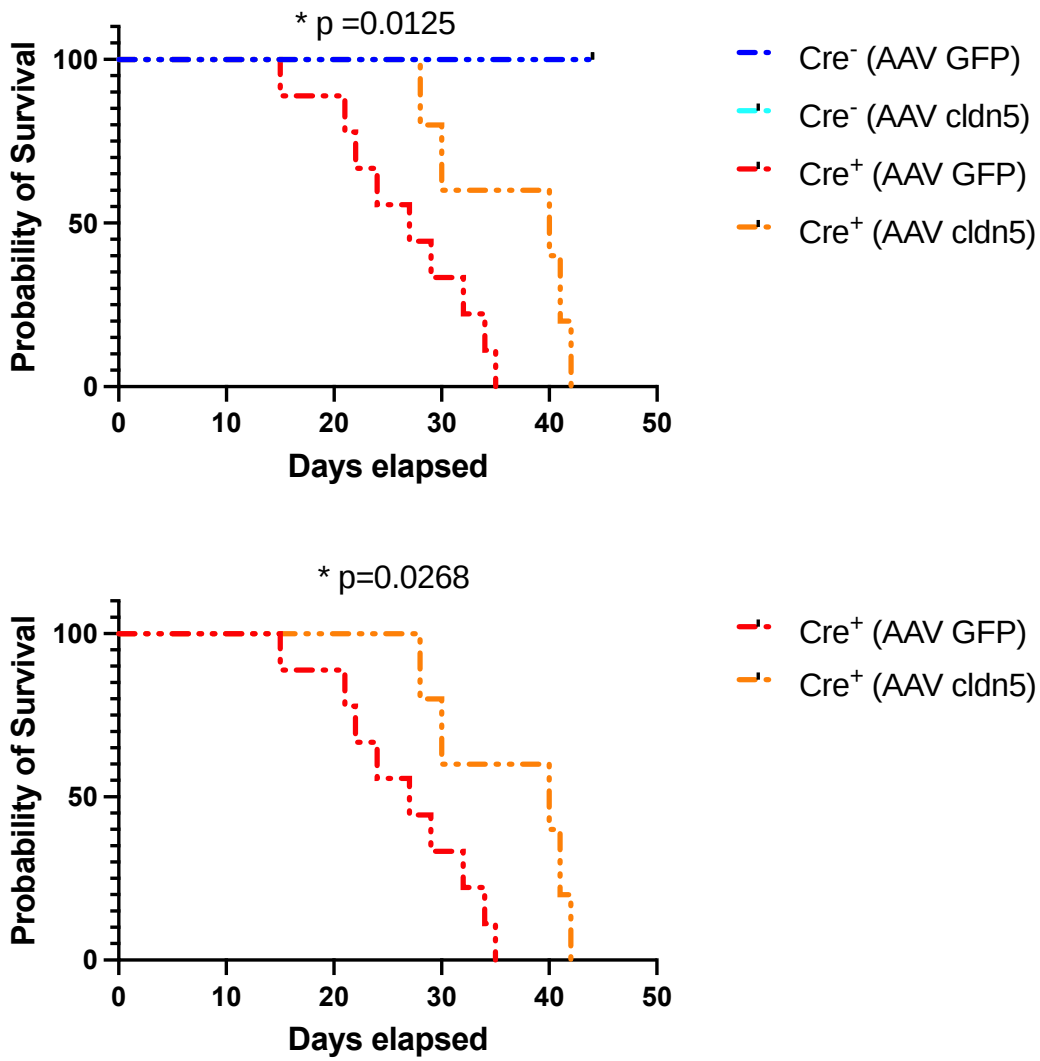

Figure 5.19. Survival curve in claudin-5 knockdown mice treated with the claudin-5 overexpression AAV.

Survival analysis of the claudin-5 knockdown (Cre+) and its relative control (Cre-), either treated with the therapeutic Cldn5-AAV or the control GFP-AAV. Cre+ mice that were treated with the control gene therapy all died within 35 days with a median survival of 27days, while those that were treated with the therapeutic AAV had a median survival of 40 days with all dying within 42 days. *P<0.05 by Log-rank Mantel-Cox test. n=7 per treatment group.

5.3.4 Characterising the rescue potential of the AAV in the Chronic Social Defeat Stress (CSDS) model of depression.

The CSDS model is a mouse model of depression. This work was carried out in collaboration with Laurence Dion-Albert and the Menard Lab, Department of Psychiatry and Neuroscience, Université Laval and CERVO Brain Research, Canada, who have established this model in their lab. The claudin-5 overexpression AAV and control GFP vector were sent to the Menard lab. All mice underwent stereotaxic surgery, with the relevant control or therapeutic AAV being bilaterally, intrahippocampally injected. Following 1 week of recovery all mice underwent the 10 day CSDS protocol after which mice were assessed for social avoidance in the social interaction (SI) test. This test allows the cohorts to be broken into susceptible and resilient groups. Once the groups have been assigned, all undergo a series of behavioural studies to investigate any potential rescue effect from the AAV. The control mice in this case are those that underwent IH administration of the relevant AAV but were not put through the CSDS protocol and so act as an unstressed control (Fig. 5.20).

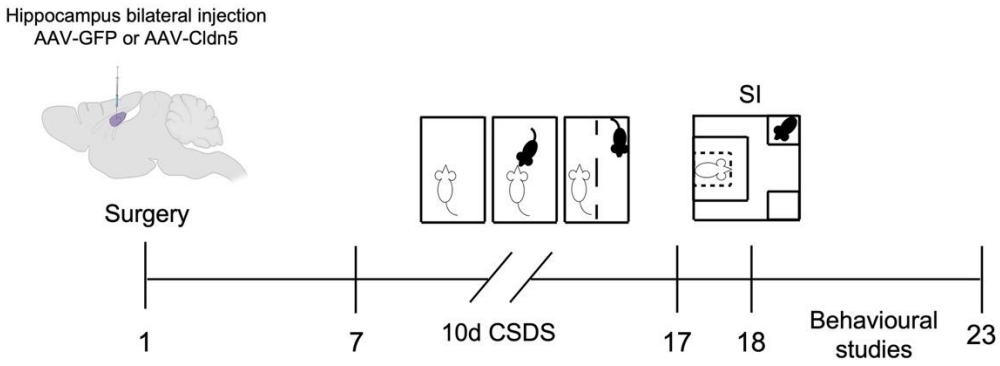

Figure 5.20. Timeline of AAV treatment followed by CSDS protocol and behavioural studies. Schematic created with BioRender.

SI ratio is calculated by dividing the time spent in the interaction zone when the aggressor (AGG) was present by the time spent in the interaction zone when the AGG was absent. Mice that obtain an SI ratio that was less than 1 were designated stress-susceptible (SS) mice while those over 1 were classified as resilient (RES). The percentage of mice that show a resilient phenotype following CSDS protocol is ~30–40 % (Golden et al., 2011).

While the numbers are small in this pilot study, there does appear to be more RES mice in the Cldn5-AAV treated cohort (n=5, compared to RES mice treated with GFP-AAV n=3, or SS mice n=3 each per treatment group) (Fig. 5.21 A).

However, no differences in behaviour are noted between the SS and RES or between AAV treatment groups. Cldn5-AAV had no noted rescue effect on anxiety-related behaviours as assessed with the elevated plus maze (Fig. 5.21 B) or the open field tests (Fig. 5.21 E). Stressed mice treated with Cldn5-AAV spent equal time grooming in the splash test (Fig. 5.21 C), did not display anhedonia as examined with the sucrose preference test (Fig. 5.21 D) and spent a similar amount of time immobile in the forced swim test (Fig. 5.21 F) as those that had been treated with the GFP-AAV. Overall no rescue effect noted following intrahippocampal administration of the claudin-5 overexpression AAV in this mouse model of depression.

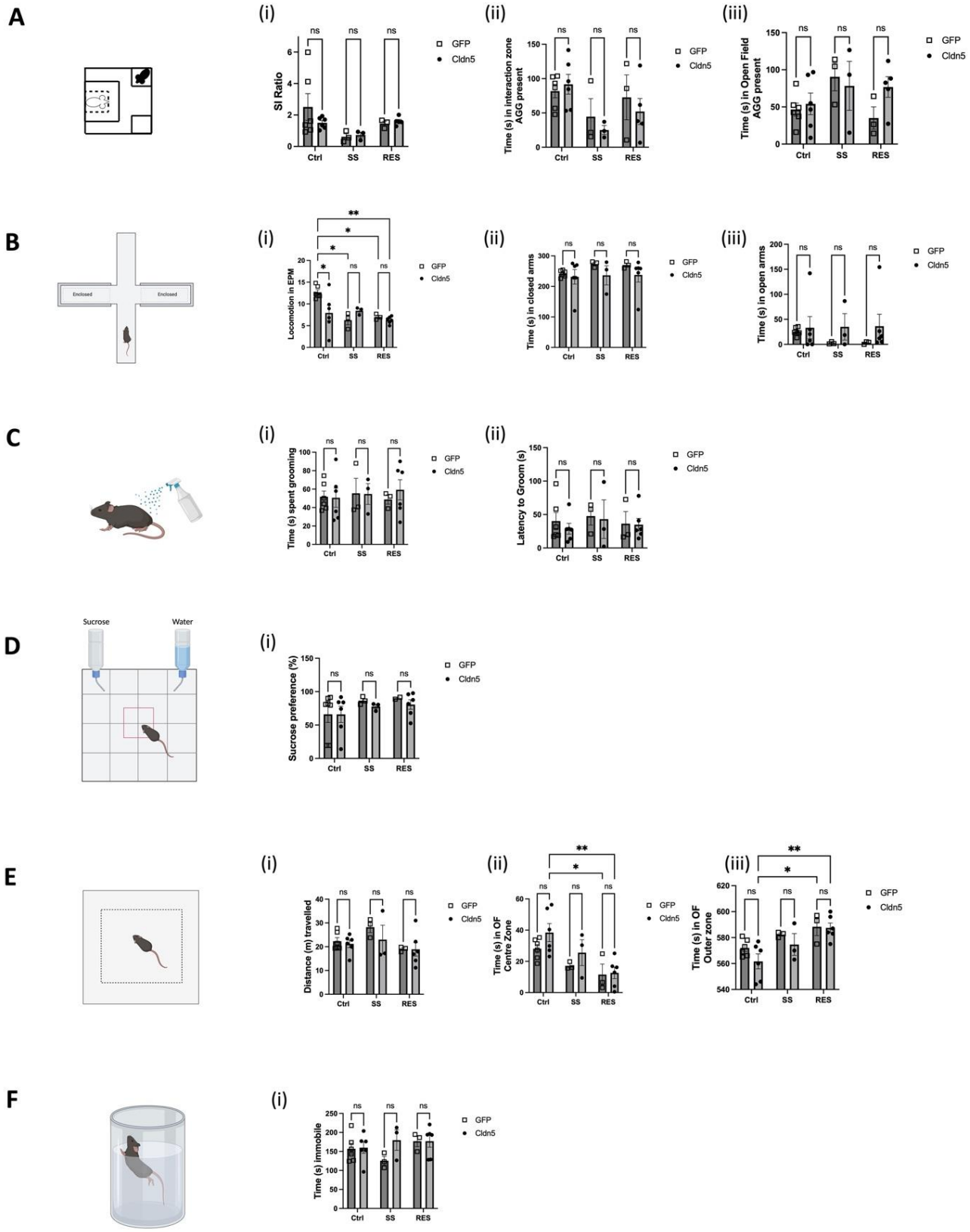

Figure 5.21. Behavioural analysis of the CSDS model following treatment with claudin-5 overexpression AAV.

(A) Schematic of social interaction apparatus. (i) SI ratio for the unstressed controls, the SS and RES cohorts injected with GFP-AAV or Cldn5-AAV. (ii) time in interaction zone when AGG

present for each cohort injected with GFP-AAV or Cldn5-AAV. (iii) time spent in the open field when AGG present for each cohort injected with GFP-AAV or Cldn5-AAV.

(B) Schematic of elevated plus maze (EPM) apparatus. (i) Locomotion in the EPM for the unstressed controls, the SS and RES cohorts injected with GFP-AAV or Cldn5-AAV. (ii) time spent in closed arms of the EPM for each cohort injected with GFP-AAV or Cldn5-AAV. (iii) time spent in open arms of the EPM for each cohort injected with GFP-AAV or Cldn5-AAV.

(C) Schematic of splash test. (i) time spent grooming for the unstressed controls, the SS and RES cohorts injected with GFP-AAV or Cldn5-AAV. (ii) latency to begin grooming for each cohort injected with GFP-AAV or Cldn5-AAV.

(D) Schematic of sucrose preference test. (i) sucrose preference for the unstressed controls, the SS and RES cohorts injected with GFP-AAV or Cldn5-AAV.

(E) Schematic of open field test. (i) distance travelled for the unstressed controls, the SS and RES cohorts injected with GFP-AAV or Cldn5-AAV. (ii) Time spent in centre of the open field each cohort injected with GFP-AAV or Cldn5-AAV. (iii) Time spent in outer of the open field each cohort injected with GFP-AAV or Cldn5-AAV.

(F) Schematic of forced swim test. (i) time spent immobile for the unstressed controls, the SS and RES cohorts injected with GFP-AAV or Cldn5-AAV.No significant therapeutic effect was noted between treatment groups

*P<0.05 by two-way ANOVA and Tukey's post-test. Schematics created with BioRender.

5.3.5 Characterising the rescue potential of the AAV in the Kainic Acid (KA) model of Epilepsy.

C57BL/6J mice bilaterally intrahippocampally injected with either the control GFP version of the AAV or the therapeutically relevant claudin-5 overexpression AAV. 3 weeks post AAV administration mice were IP injected with a mildly-convulsant dose of KA. All mice were observed and video recorded for 2 hr to measure seizure activity based on the Racine scale. After this both control and claudin-5 mice were divided into timeline groups, one group were then sacrificed at the 3 hr post KA timepoint, while the other group were left 48 hr post KA administration before they were sacrificed for tissue collection (Fig. 5.22).

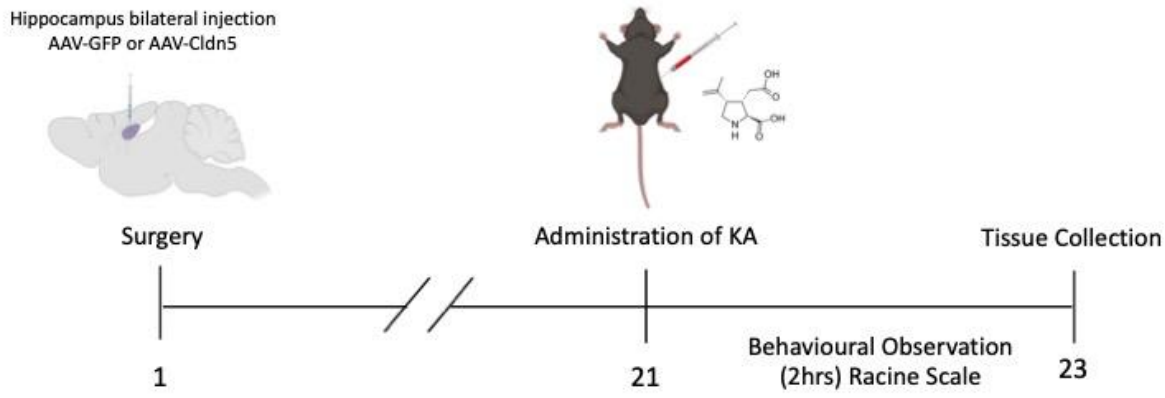

Figure 5.22. Timeline of treatment and seizure induction in KA model of epilepsy. Schematic created with BioRender.

Mice treated with the claudin-5 overexpression AAV had a lower cumulative seizure score in comparison to those treated with the GFP expressing AAV (Fig. 5.23 A (i)). Moreover, claudin-5 overexpression in the hippocampus appeared to non-significantly increase the latency to seizure onset, thus acting in a protective fashion ($p = 0.0512$)(Fig. 5.23 A (iii)). Finally it appears that the Cldn5-AAV treatment non-significantly reduced the overall seizure severity (Fig. 5.23 A (ii)).

Elevated neuronal activity is noted in mice 3 hr post KA administration that had been previously treated with the control GFP-AAV virus. A non-significant increase in cFos staining is notable in the control mice at the 3 hr timepoint when compared to those treated with the therapeutic claudin-5 overexpression virus at the same timepoint (Fig. 5.24). NeuN staining is also non-significantly higher in the control treated mice in comparison to the therapeutic vector (Fig. 5.25) Mice that were treated with GFP-AAV showed some initial increased inflammation in the brain, as noted through an increase in IHC staining for GFAP when compared at the acute 3 hr timepoint, this however had equalised with continued high levels of GFAP expression at the 48 hr timepoint (Fig. 5.26). Moreover, IBA1 staining remained elevated but equal between the two cohorts (Fig. 5.27).

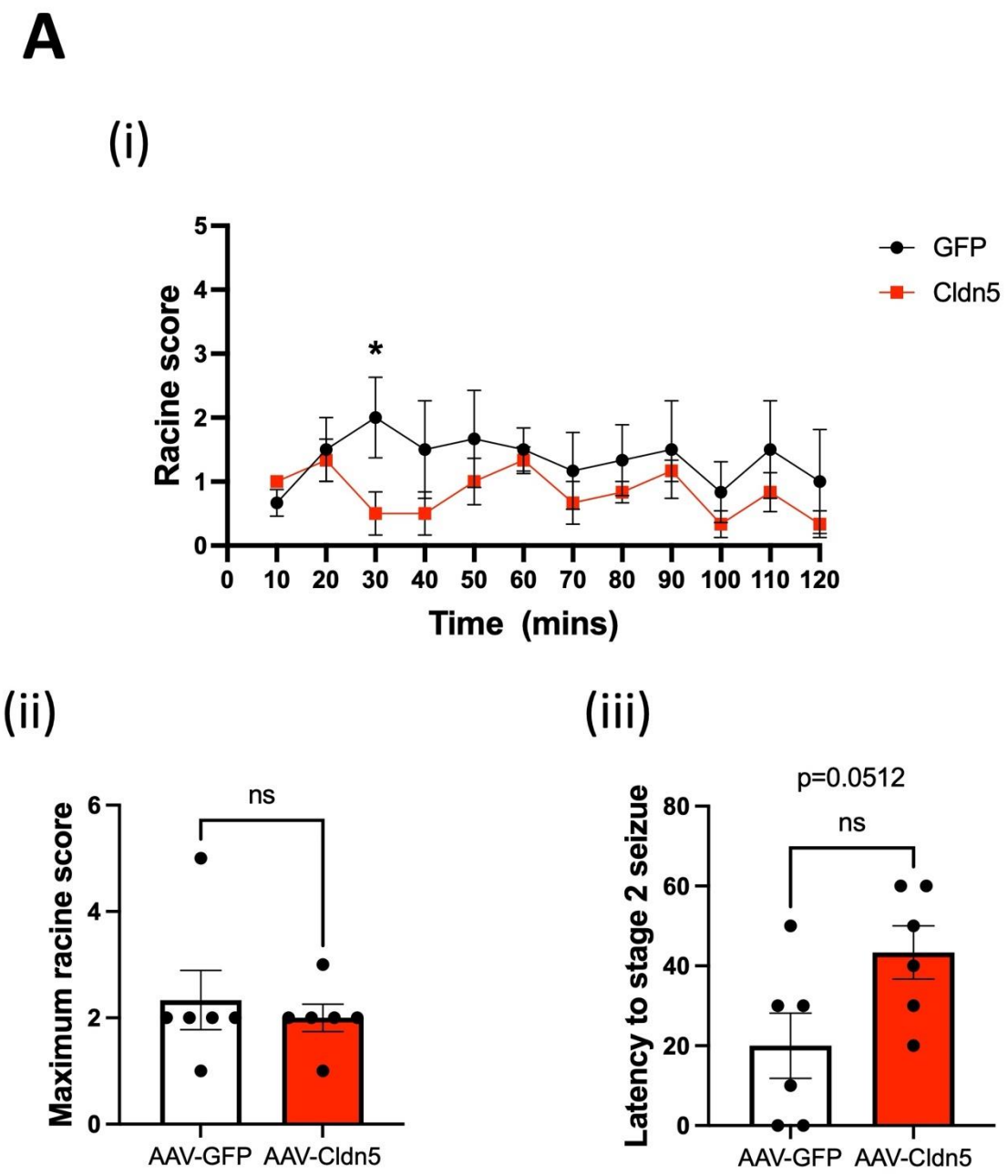

Figure 5.23. Reduced Racine score following intrahippocampal administration of the claudin-5 overexpression AAV.

(A) (i) Reduced Racine score over time in mice treated with the claudin5 overexpression AAV (*p= 0.0366) at 20-30 mins post KA (ii) Non-significant difference in maximum Racine score between treatment groups post injection of KA (iii) Non-significant increase in latency to stage 2 of the Racine scale in mice treated with Cldn5-AAV. Racine scale 1: immobility, 2: head nodding, 3: forelimb clonus, 4: forelimb clonus with rearing and falling, 5: wild running and jumping often followed by generalised tonic-clonic activity and loss of postural tone. *P<0.05 by two-sided unpaired t-test. n=6 per treatment group.

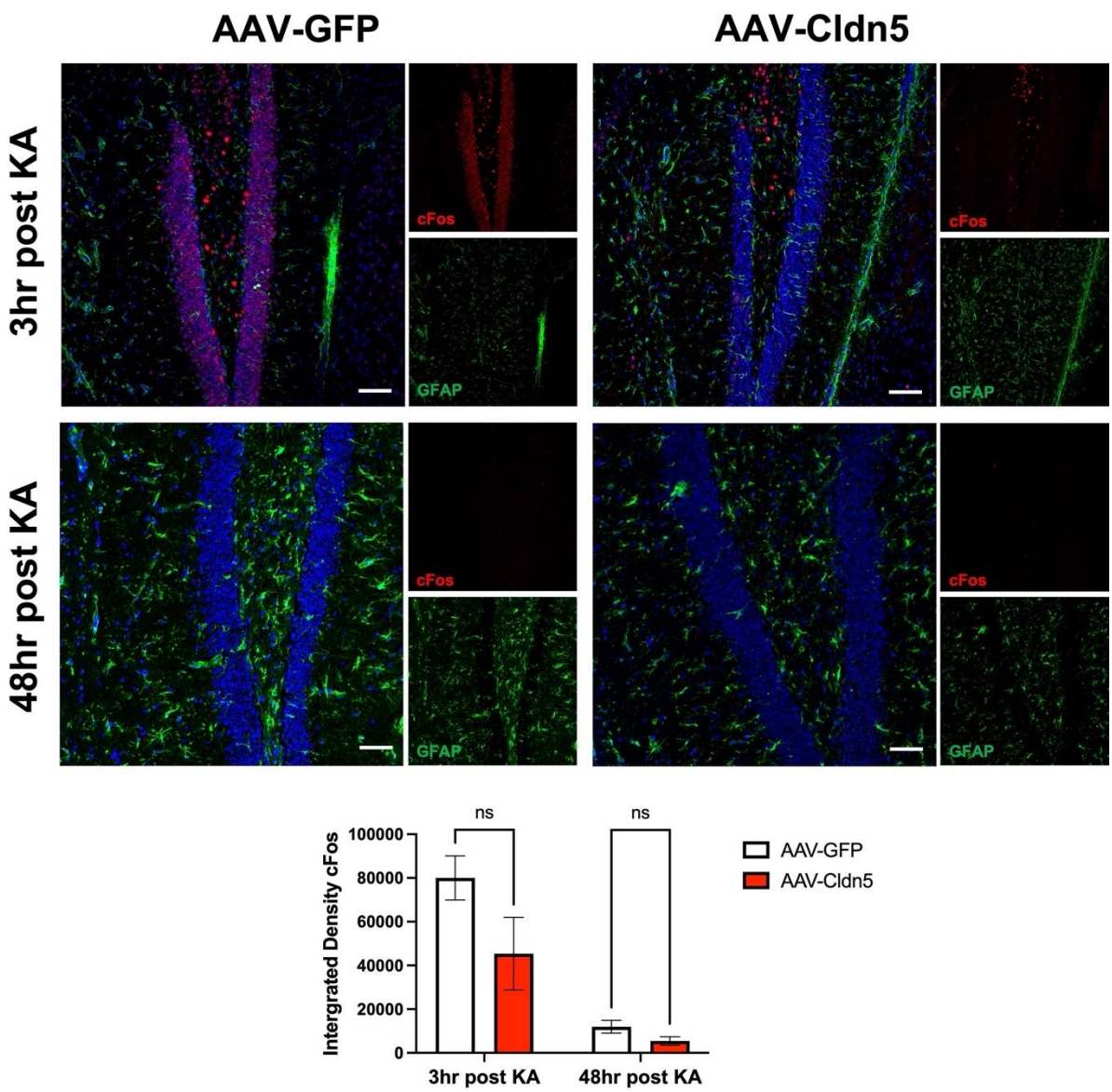

Figure 5.24 Immunohistochemical analysis of cFos expression in mice post KA administration at set timepoints

Immunohistochemical analysis examining cFos expression (red) and GFAP (green) within the DG region of hippocampus as noted through DAPI (blue) staining of the cell nuclei. (A) Mice 3 hr post KA injection that had been treated with GFP-AAV showed the highest cFos expression. Higher levels noted at 3 hr post KA in comparison to 48 hr (B) ImageJ analysis of cFos expression. Scale bar – 100 μm. Statistical analysis was carried out using two way ANOVA and Tukey's post-test comparing GFP-AAV treated mice to Cldn5-AAV treated mice at set timepoints. All data are means ± SEM with n = 6 all groups

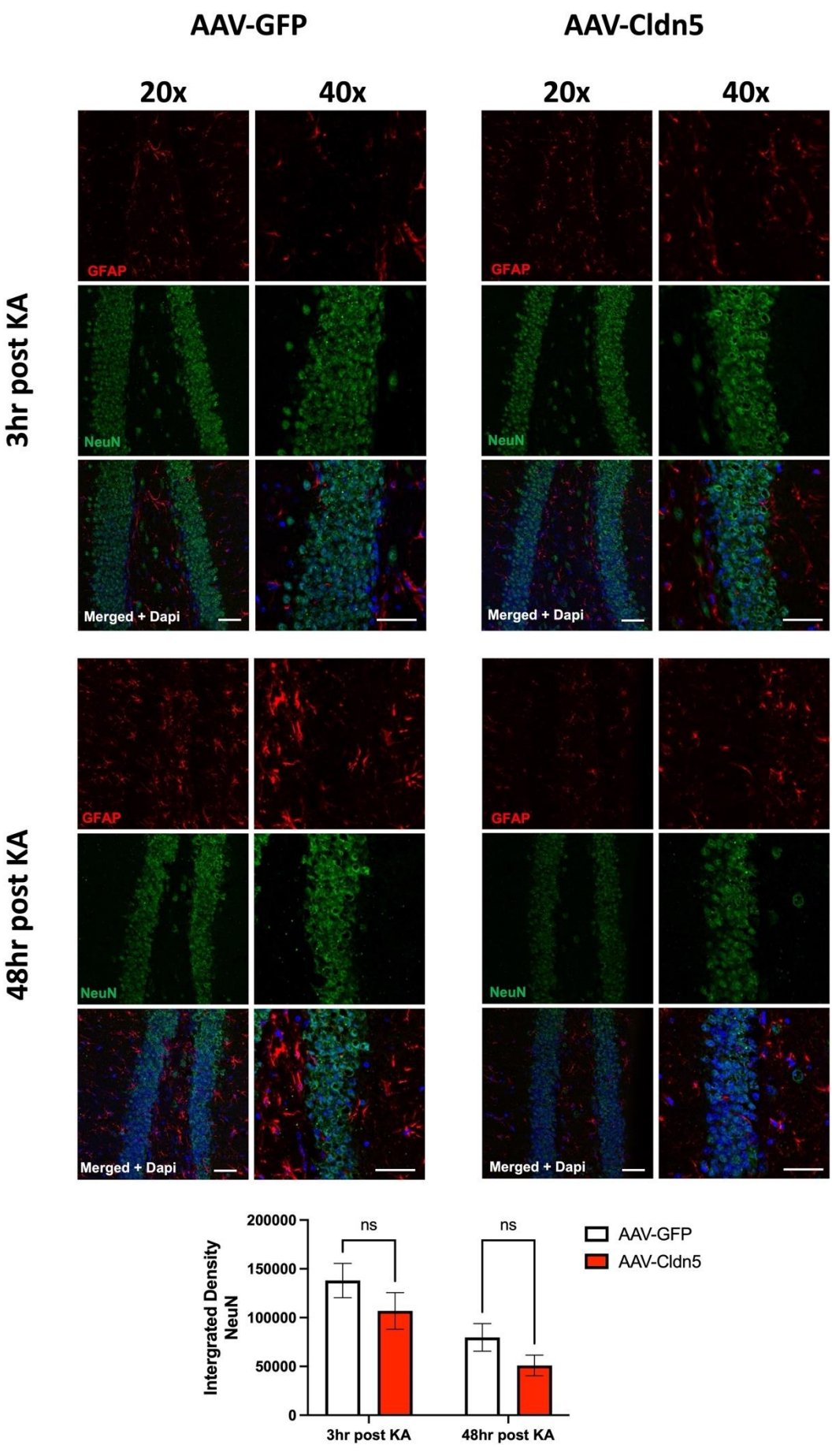
AAV-GFP
AAV-Cldn5
20x
40x
20x
40x
3hr post KA
48hr post KA
GFAP
NeuN
Merged + Dapi
Intergrated Density NeuN
200000
150000
100000
50000
0
ns
ns
AAV-GFP
AAV-Cldn5
3hr post KA
48hr post KA

Figure 5.25 Immunohistochemical analysis of NeuN expression in mice post KA administration at set timepoints.

Immunohistochemical analysis examining GFAP (red) and NeuN (green) in the hippocampal DG as noted through DAPI (blue) staining of the cell nuclei. Acute time points following IP administration of KA in AAV injected mice. Scale bars, 100 μm for 20X images; 50 μm for 40X images. Statistical analysis was carried out using two way ANOVA and Tukey's post-test comparing GFP-AAV treated mice to Cldn5-AAV treated mice at set timepoints. All data are means ± SEM with n = 6 all groups

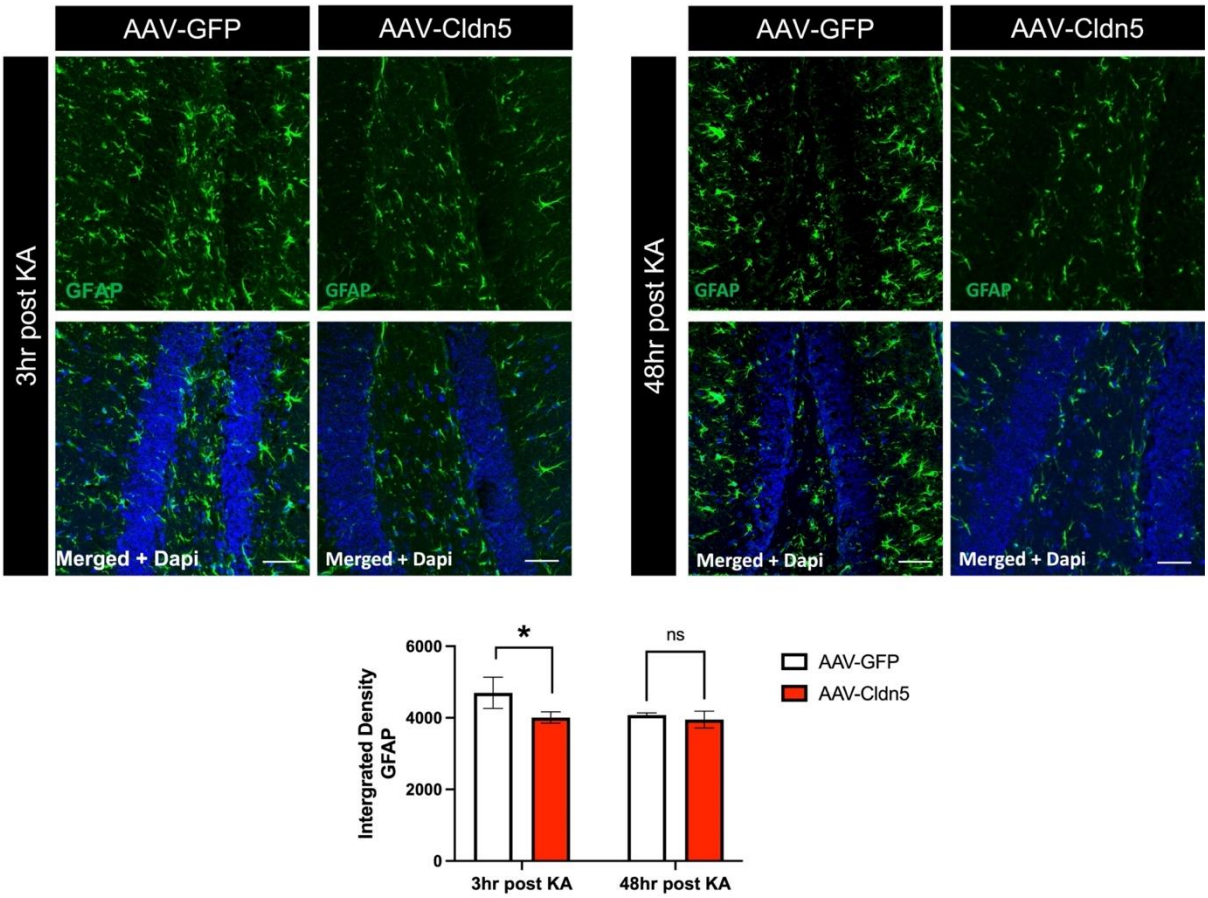

Figure 5.26 Immunohistochemical analysis of GFAP expression in mice post KA administration at set timepoints.

Immunohistochemical analysis examining GFAP (green) in the hippocampal DG visualised via DAPI (blue) staining of the cell nuclei. Acute time points following intraperitoneal administration of KA in AAV treated mice. Scale bars, 100 μm. Statistical analysis was carried out using two way ANOVA and Tukey's post-test comparing GFP-AAV treated mice to Cldn5-AAV treated mice at set timepoints. All data are means ± SEM with n = 6 all groups

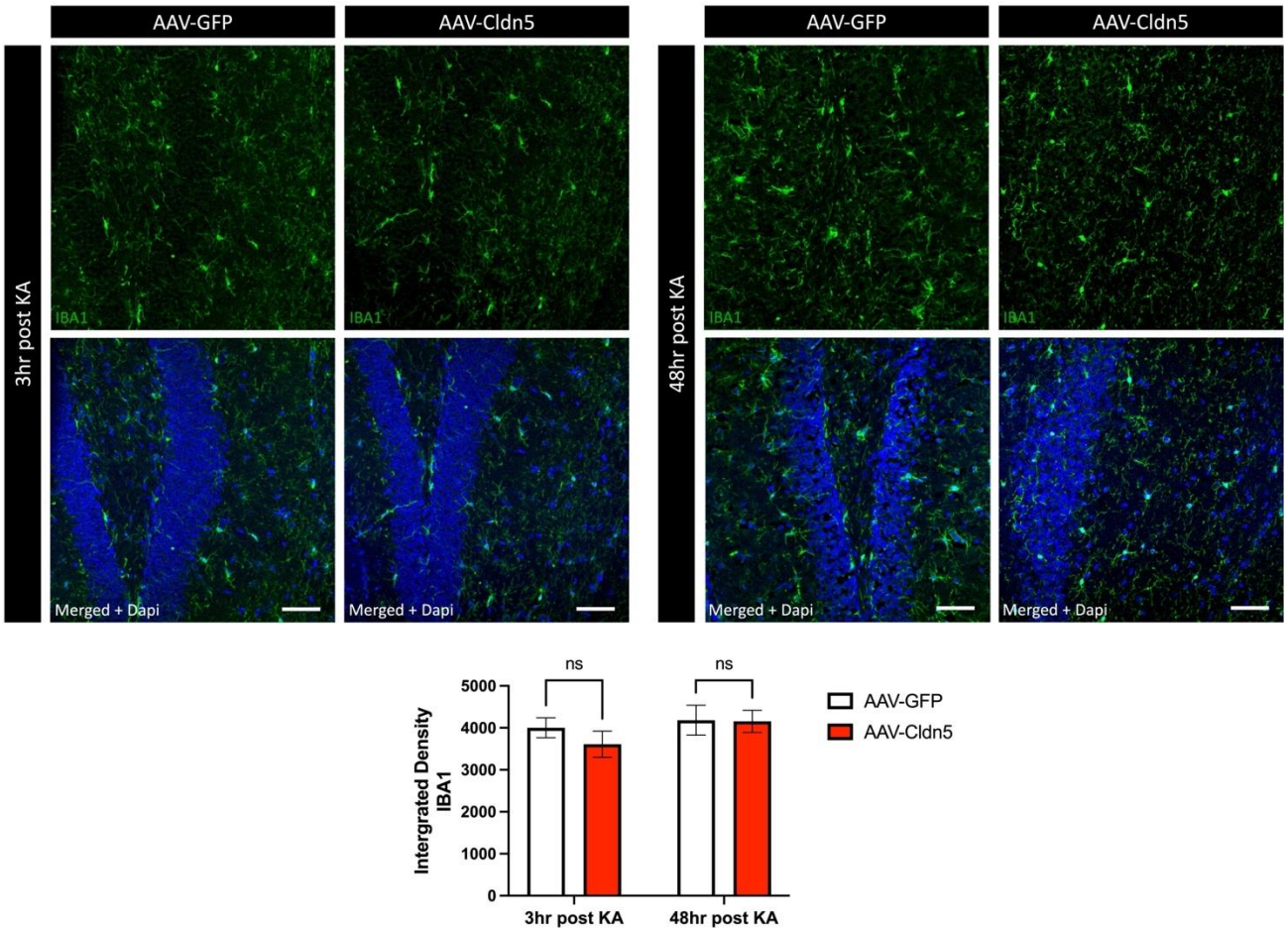

Figure 5.27 Immunohistochemical analysis of IBA1 expression in mice post KA administration at set timepoints.

Immunohistochemical analysis examining IBA1 (green) in the hippocampal DG visualised via DAPI (blue) staining of the cell nuclei. Acute time points following intraperitoneal administration of KA in AAV treated mice. Scale bars, 100 μm. Statistical analysis was carried out using two way ANOVA and Tukey's post-test comparing GFP-AAV treated mice to Cldn5-AAV treated mice at set timepoints. All data are means ± SEM with n = 6 all groups

5.4 Discussion:

We examined four different models to determine if claudin-5 overexpression at the level of the BBB could have the potential to attenuate the noted pathologies. However, these four models should be examined as two separate groups. Firstly the *Cldn5$^{fl/wt}$xTie2Cre* mice and the inducible claudin-5 KD model, both show distinct behavioural pathology, with the latter also showing seizure development and death. These pathologies are directly associated with loss of claudin-5 expression. Therefore together, these models being treated with the claudin-5 overexpression AAV act as a proof of concept, that resolving the barrier can restore function.

However, most of the relevant disorders, such as schizophrenia, epilepsy and MDD are all complex, multifactorial disorders. While each has shown a distinct link to claudin-5 downregulation, it is not the only factor that contributes to the disease. The models that were examined over the course of this research, the CSDS model and the KA model are both well-established and accepted models of their respective diseases of MDD and epilepsy. These models have been validated and proven to mirror many aspects of the relevant disease. This includes the method utilised to develop the model, which mirrors the natural development of the disease, such as stress or status epilepticus. The models mimic the anatomical, neuropathological and behavioural features that are noted in the patients, which are complex and affect numerous cell signalling pathways and cell types. Importantly, these models also generally have the ability to respond to treatments in a manner that is likely to be predictive to the treatment efficacy in patients. Overall, determining a rescue effect in these models is crucial to prove therapeutic relevance.

Thus to start with the proof of concept element to this research. Can restoration of claudin-5 attenuate the noted pathologies? In the characterisation of the rescue potential of the claudin-5 overexpressing AAV in the *Cldn5$^{fl/wt}$xTie2Cre* model, the answer is yes. This BBB restoring AAV was shown, when administered into the hippocampus, to significantly improve learning and memory deficits that had been noted in this model (Fig. 5.5). It also improved the aberrant grooming behaviour that had been noted (Fig. 5.6) and rescued sensorimotor gating deficits (Fig. 5.8). Interestingly, this same effective rescue was not as clearly seen when the AAV was administered into the mPFC. A summary of the behavioural dataset, displayed as Z-scores to signify the deviation of behaviour from the expected

behaviour noted in the control mice can be seen for both the hippocampus (Fig. 5.28) and mPFC (Fig. 5.29). Both the hippocampus and the mPFC have been shown to have essential roles in learning, memory and spatial processing, which allow for flexible cognition and thus the ability to carry out complex behaviours such as navigation, exploration, decision making and social interaction (Rubin et al., 2014). The mPFC, the hippocampus as well as other structures such as the anterior cingulate cortex and the amygdala have been shown to form a neural network that is involved in learning and memory processes such as fear conditioning and social recognition (Feder et al., 2009; Tanimizu et al., 2017). However, within this circuit, it appears that the hippocampus may play a more central role, acting as a connector hub, integrating information from numerous other brain regions and generating memory (Tanimizu et al., 2017). In comparison, the mPFC, while being an essential region for the consolidation of memory, does not appear to act in the same manner. This may potentially explain why significant rescue is noted following the local restoration of the BBB via claudin-5 overexpression in the hippocampus but not as significantly in the mPFC. As a central hub, connecting many brain regions and integrating all information, the hippocampus appears to be a better region to target to improve function.

To further this proof of concept, an examination of the inducible claudin-5 KD model was carried out. This model, has a normal level of claudin-5 expression until the induction of claudin-5 KD through RNA interference (RNAi). Therefore unlike the previous *Cldn5*$^{fl/wt}$*xTie2Cre* model, which developed in a claudin-5 deficient environment and thus has a controlled and constant 50 % loss of claudin-5, the inducible model goes from a normal, 100 % level of claudin-5 expression to a sudden and persistent loss of claudin-5 that is likely to be significantly more than a 50 % loss of the TJ protein over time. Thus overall it results in a more severe phenotype. While similar behavioural issues are noted, there is the additional pathologies of seizures and death with persistent knockdown. Thus this model is a larger challenge for the AAV based gene therapy approach. Following administration of the gene therapy there was noted rescue of some of the behavioural issues. Memory deficits, as measured through both the Y- and T-mazes, were rescued with the knockdown Cre+ mice treated with the Cldn5-AAV behaving more similarly to the control Cre- mice. The aberrant grooming behaviour was also rescued following treatment with the Cldn5-AAV. PPI response was improved, with only the Cre+ knockdown mice that were given the GFP-AAV showing a significantly reduced PPI response, while those treated with the Cldn5-AAV had an improved response. Finally, the survival time was also increased in

the cohort treated with the therapeutic Cldn5-AAV. Overall, it appears the RNAi mechanism in these mice outcompetes the therapeutic Cldn5-AAV in the end and reduces the claudin-5 level to a point that makes the mice inviable. However, this still provides evidence that maintaining a certain level of claudin-5 expression at the level of the BBB can help function. As a dose dependent gene, if claudin-5 expression can be maintained at a certain threshold, it may have the potential to attenuate symptoms of a disease.

Examining the potential therapeutic effect of claudin-5 overexpression was then carried out in established models of disease, which are, due to the methods used to develop the disorder, more complex, with many potential disease contributing components. Multifactorial disorders are thought to have many small contributing factors which together increase the risk of disease development. Diseases like MDD and schizophrenia have a clear heritable element but do not function like Mendelian disorders. Therefore there is clearly a disease burden threshold that must be reached through a combination of contributing genetic and environmental factors. Starting with the CSDS model, an interesting aspect to this model is its ability to recapitulate an aspect of neurological disorders that few other models do, which is variance within its population. In this model following the CSDS protocol, mice either show SS or RES phenotypes. When investigated, it was found that at the NAc the SS mice had a significantly lower level of claudin-5 expression in comparison to both the unstressed controls and also the RES mice. At the hippocampus however, the transcriptional loss of claudin-5 was seen in both SS and RES compared to the controls. Interestingly, at the translational level in the RES mice, the claudin-5 level was higher than in the SS. This together indicates some compensation and indicates that claudin-5 is protective (Menard et al., 2017). Therefore, IH administration of the claudin-5 overexpression AAV could potentially act in a protective manner. However, in this study no significant rescue effect was noted. This may be due to the AAV not having rescue potential in this more complex disorder but other factors may have effected this result. Firstly, the region in which the AAV was administered may not have been the ideal target area for notable change. As stated earlier, it is the NAc that has the most distinct expressional difference between the RES and SS and potentially this area would have been better to target in order to observe significant behavioural rescue. However a crucial element, that may be potentially confounding the results, is that the depression phenotype wasn't strong enough in this small cohort that was acting as a pilot study. This model has shown distinct behavioural changes associated with anxiety and depression, however in this case there was few significant changes noted

between the unstressed control group and stressed mouse groups regardless of treatment. Finally, while behaviourally no changes were noted between viral treatment groups, it should be noted that in this small study there was an increased number of RES mice in the cohort that had been injected with the Cldn5-AAV. Increasing the level of claudin-5 expression before undergoing the chronic stress may have protected vulnerable individuals from the SS phenotype. Larger numbers would be required to verify this hypothesis.

A second established model of disease, the KA model of epilepsy was utilised to investigate the potential of the claudin-5 overexpression AAV. This model, which utilises a chemoconvulsant to induce a status epilepticus injury, is a strong and validated model of epilepsy. The previous work of Greene et al., has provided significant evidence that the level of claudin-5 expression in the microvasculature ECs of the CNS play a significant role in the risk of seizure development. Not only does KA-induced seizures reduce claudin-5 expression, but additionally the *Cldn5*$^{fl/wt}$*xTie2Cre* model, which is haploinsufficent for claudin-5, has an increased vulnerability to seizure induction (Greene et al., 2022). Overall, the idea of a positive-feedback loop, in which loss of claudin-5 expression is both cause and consequence of seizures is undeniable. These findings again provide evidence that there is a threshold to claudin-5 expression which is protective to pathologenesis. However, if expression goes below threshold, either through genetics or injury, seizures occur. Therefore utilising the gene therapy based approach to restore claudin-5 levels at the BBB to a level that is above this threshold, has the potential to restore the protective function of the BBB and resolve the pathology. In this pilot investigation into the rescue effect the claudin-5 overexpression AAV, C57BL/6J mice 3 weeks previously administered the gene therapy, were treated with a mildly convulsive dose of KA. It was found that those treated with the Cldn5-AAV had a lower cumulative seizure score examined across a 2 hr time period (Fig. 5.23 A(i)). Moreover the latency to seizure onset was longer in comparison to the control treated mice (Fig. 5.23 A(iii)). However, across both treatment groups the seizure severity was similar (Fig. 5.23 A(ii)). This may be due to the mildly convulsive KA dose, which produced overall mild symptoms with few mice exceeding stage 3 on the Racine scale. If repeated, mice could be administered stronger doses which may show more notable rescue. Additionally, hallmark features of the KA model, such as the acute induction of cFos appeared more extreme in the control treated mice in comparison to those treated with the Cldn5-AAV (Fig. 5.24). Moreover there appeared to be potential granule cell dispersion in the DG region in GFP treated mice (Fig. 5.25) Acute CNS inflammation was

noted through IHC analysis of the astrocyte marker GFAP (Fig. 5.26) but the microglial marker IBA1 remained similar through both timepoint and treatment.

Overall these findings indicate that maintenance of claudin-5 expression at the BBB can restore its function, which can resolve some pathologies. However, in complex diseases such as MDD, schizophrenia and epilepsy, there are many factors at play. It appears that this concept of resolving barrier function through the overexpression of claudin-5 is still a viable and beneficial avenue to investigate in regards to the development of a gene therapy based approach to treat neurological disorders. However, objectively it may need to be looked at as an adjunct therapy. Most neurological disorders have at least 100 years of research behind them, and after that degree of investigation, it is clear that there is realistically no all-inclusive solution. Therefore for a complex problem, complex and co-operative solutions are required. For example, this claudin-5 overexpression gene therapy, in conjunction with the gold-standard clinical and pharmacological approaches may improve the current efficacy of clinical outcomes. For example in the treatment of epilepsy, 30 % of cases are refractory. Interestingly, in these cases when the tissue has been surgically resected as a last resort treatment option, there has been notably increased levels of drug efflux transporters such as P-gp noted in the ECs of the cerebrovasculature (Tang et al., 2017). It is likely that any anti-seizure drugs (ASDs) entering the brain are immediately getting pumped back out into peripheral circulation, aiding in this high number of refractive cases. But there is a line of thought that this high level of P-gp expression is acting as a second line of defence due to the loss of barrier integrity. Therefore if barrier function could be resolved with this BBB restoring gene therapy approach, there would be no need for this second line of defence and thus efflux transporter pump expression should normalise. This would allow adequate levels of ASDs to enter the brain and reduce the number of refractive cases which at present is a common and expensive issue. This drug resistant issue is a universal problem for most neurological disorders, as along with ASDs, anti-psychotics and anti-depressants currently have limited success. This is due to a multitude of issues, including intolerable side-effects, which again may be due to the high doses required to overcome BBB issues. The increased function and expression of P-gp is also not exclusive to epilepsy, with similar findings noted in schizophrenic patients (Hoosain et al., 2015).

5.5 Conclusions:

- Overexpression of claudin-5 in the hippocampus of *Cldn5$^{fl/wt}$xTie2Cre* mice and the inducible claudin-5 KD mice resulted in improved learning and memory function and reduced aberrant grooming behaviour and sensorimotor gating deficits. Increased survival time for the inducible claudin-5 KD mice.
- When administered to the mPFC of *Cldn5$^{fl/wt}$xTie2Cre* mice the claudin-5 overexpression AAV did not show the same effective rescue.
- No significant rescue noted in the CSDS model but some improvement noted in the KA model of epilepsy.
- Overall this gene therapy based approach to overexpress claudin-5 within regions of the brain may have strong potential as an adjunct therapy.

5.6 Summary:

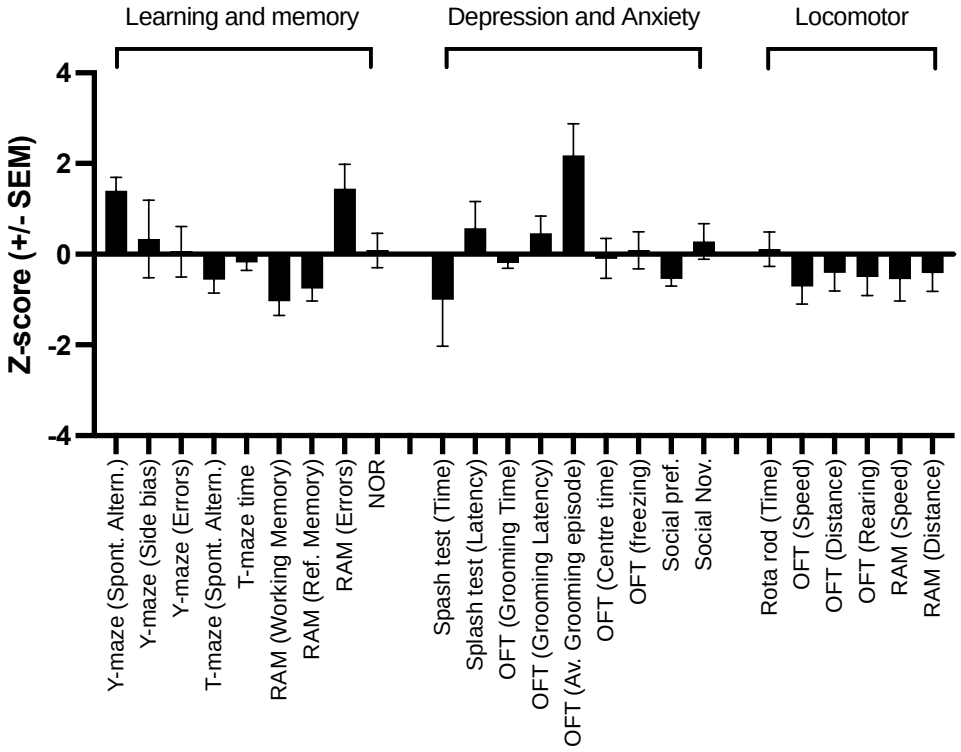

Figure 5.28. Summary of the behavioural dataset generated for the *Cldn5$^{fl/wt}$xTie2Cre* mice following AAV claudin-5 overexpression in the hippocampus.

Data is expressed as Z-scores ± SEM. A positive Z-scores indicates the behaviour is above the average expected behavioural output and a negative Z-score signifies that the behaviour is below the expected behavioural output.

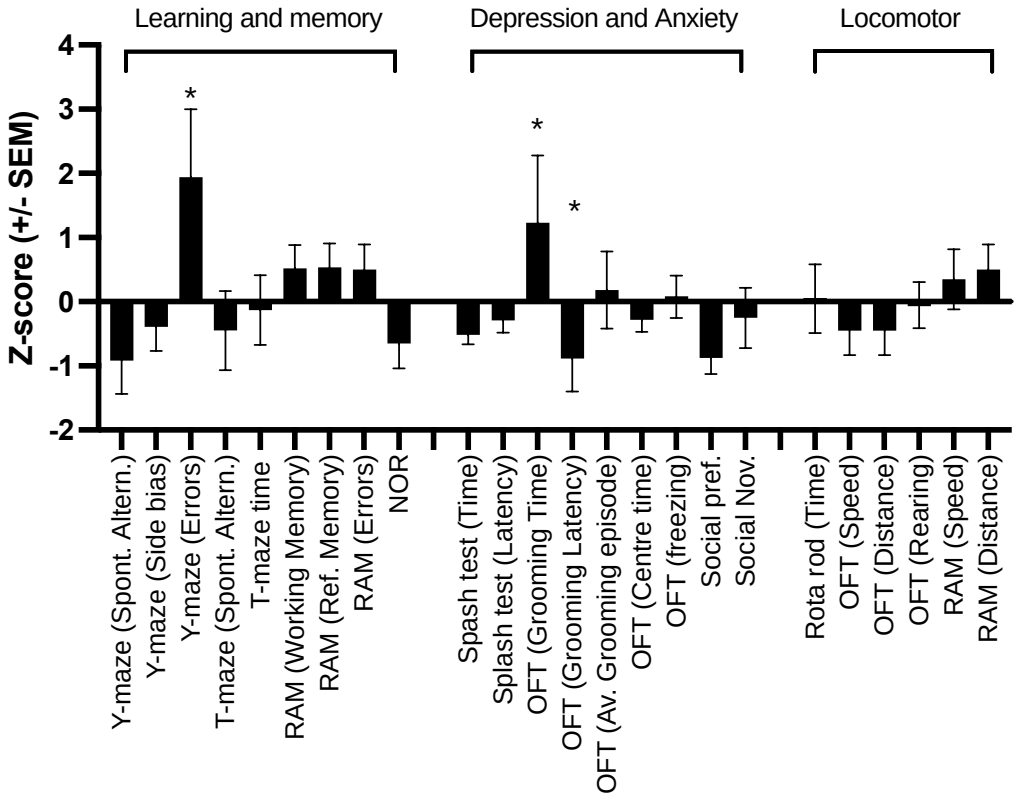

Figure 5.29. Summary of the behavioural dataset generated for the *Cldn5*$^{fl/wt}$*xTie2Cre* mice following AAV claudin-5 overexpression in the mPFC.

Data is expressed as Z-scores ± SEM. A positive Z-scores indicates the behaviour is above the average expected behavioural output and a negative Z-score signifies that the behaviour is below the expected behavioural output.

Assay	*Cldn5*$^{fl/wt}$ *xTie2Cre* model	AAV rescue - Hippocampus	AAV rescue – PFC
Learning and memory assays			
Y-maze (Spont. Altern.)	-	↑	-
Y-maze (Side bias)	ns ↑	↓	-
Y-maze (Errors)	↑	↓	ns↓
T-maze (Spont. Altern.)	-	-	-
T-maze (Time)	-	-	-
RAM (Working Memory)	↑	↓	-
RAM (Ref. Memory)	↑	↓	-
RAM (Errors)	↑	ns↓	-
NOR	-	-	-
Depression and anxiety assays			
Splash test (Time)	-	-	-
Splash test (Latency)	↑	↓	-
OFT (Grooming Time)	-	-	↓
OFT (Grooming Latency)	↑	↓	↓
OFT (Av. Grooming episode)	↑	↓	-
OFT (Centre time)	-	-	-
OFT (Time freezing)	-	-	-
FST	-		
EPM	-		
Social Preference	↓	ns ↑	-
Social Novelty	-	-	-
Marble burying	-		
Locomotor			
Rotarod (time)	-	-	-
OFT (Speed)	-	-	-
OFT (Distance)	-	-	-
OFT (Rearing)	-	-	-
RAM (Speed)	-	-	-
RAM (Distance)	-	-	-
Sensorimotor gating			
PPI	↓	↑	↑

Table 5.1. Summary of *Cldn5*$^{fl/wt}$ *xTie2Cre* behavioural outputs and changes that are obtained following AAV derived/directed claudin-5 overexpression in distinct regions of the brain.

Radial arm maze (RAM), novel object recognition (NOR), open field test (OFT), forced swim test (FST), elevated plus maze (EPM) and prepulse inhibition (PPI).

Chapter 6. General Discussion and Future directions

Neurological disorders are estimated to affect roughly 1 in 4 individuals worldwide, and in spite of the prevalence of these disorders and the extensive research that has been carried out in this field, the efficacy of treatment remains severely limited (Greene et al., 2020). Due to the lack of reliable and specific biomarkers, as well as a continued reliance on behavioural observations to make a clinical diagnosis, many individuals remain undiagnosed or misdiagnosed (Nobis et al., 2020). Adding to this, despite the availability of pharmacological and psychological therapies, it is estimated that only one third of people utilise these treatment options (Greene et al., 2020). Of those that do receive treatment, there are further obstacles that include intolerable side-effects or being refractive to treatment. Unfortunately, intolerable side-effects are commonly reported for many routinely used anti-depressants and anti-psychotics, which generally results in poor medication compliance and reduced usage (Leucht et al., 2009). Moreover, the prevalence of patients that do not respond to treatment, known as the refractive cohort, is notably high for these common neurological disorders. Treatment resistance or symptom recurrence is estimated to be around 30 % of all epilepsy patients, 30-50 % of all MDD patients and approximately 34 % of schizophrenic patients (Kwan et al., 2011; Fava and Davidson, 1996, Krishnan and Nestler, 2008; Potkin et al., 2020). These common disorders, with high refractive cohorts, place an extremely high economic burden on society, with the economic burden of schizophrenia estimated to be US$343.2 billion and MDD to be US$326.2 billion for the US alone, while globally the estimated cost burden of epilepsy is $119.27 billion (Kadakia et al., 2022; Greenberg et al., 2021; Begley et al., 2022). In fact, mental health disorders as a whole have been estimated to cost approximately US$6 trillion by 2030 (The Lancet Global Health., 2020). Research into the mechanisms behind these disorders has mainly focussed on neuronal function, while many neurotherapeutics have been developed through the reverse engineering of drugs previously observed to be clinically efficacious (Berton and Nestler, 2006). The limited efficacy, high prevalence of refractive cohorts and the economic burden of these diseases, taken together, highlight the clear need for the identification of novel mechanisms of action that are associated with these diseases, in order to develop new and innovative therapies.

Dysfunction of the BBB is a newly recognised mechanism of action that has strong therapeutic relevance in neurotherapeutic development. This dynamic barrier acts as a first

line of defence. It is essential for the maintenance of the neuronal microenvironment, regulating ion and nutrient exchange between blood and brain, while simultaneously protecting the neural tissue from potentially damaging blood-borne components. There is accumulating evidence that BBB disruption is a hallmark pathology in numerous neurological disorders and can proceed and/or exacerbate the symptoms of these disorders. Thus BBB disruption may be seen as both a cause and consequence of the disease. Therefore restoration of BBB integrity may have strong potential as a novel mechanism of action for innovative treatment design. The BBB is however a complex and dynamic structure composed of many synergistic components, so the first question will be what component should be specifically targeted. Claudin-5, is a TJ protein of the BBB. It is so highly expressed in the ECs of the BBB that it is estimated to be 10-fold higher than the housekeeper, beta-actin (Daneman et al., 2010; Ohtsuki et al., 2008; Vanlandewijck et al., 2018). KO studies have shown a size selective loosening of the barrier and results in post-natal death (Nitta et al., 2003). Taken together, this data supports claudin-5's essential role in BBB maintenance. Moreover, decreased levels of claudin-5 expression have been noted in either post-mortem or surgically resected tissue from patients with either MDD, schizophrenia or epilepsy (Greene et al., 2020; 2022). Therefore, claudin-5 shows promising potential as a therapeutic target. Thus, the overarching aim of this thesis was to further characterise claudin-5's relationship with BBB function and the underlying pathophysiology and endophenotypes that result from its disruption, as well as to utilise it to develop a new gene therapy-based approach to treat disorders with noted BBB disruption.

KO mouse models are generally extremely useful in order to identify the role certain genes play in an overall system. However, while the seminal work by Nitta et al using a claudin-5 KO model provided great insight into the size selective changes to barrier function that results from the loss of claudin-5 expression, all mice died within 10 hr of birth (Nitta et al., 2003). Therefore the continued use of this KO model for further characterisation is limited. Thus in chapter 3, a claudin-5 heterozygote model was established, utilising the Tie2Cre system to ensure that claudin-5 expression was lost specifically in the ECs of the mice. The 50 % loss of claudin-5, was shown both specifically in the vasculature, as well as within key brain regions, and resulted in a discontinuous pattern of claudin-5 expression in the vessels, similar to what has been noted in the resected tissue from patients with epilepsy (Greene et al., 2022). While it did not cause significant permeability into the brain, astrocytic gliosis was noted in the claudin-5 heterozygote cohort in comparison to the

controls. Moreover, distinct deficits in learning and memory function, cognitive impairment and sensorimotor gating issues were noted in the claudin-5 heterozygous mice. Many of these behavioural deficits can be associated with neurological disorders such as schizophrenia. To our knowledge, this is the first ever behavioural characterisation of a claudin-5 heterozygous mouse model. Of note for future work, examining sex differences as part of this models characterisation will be important. In this characterisation, both male and female mice were utilised. However, there is accumulating epidemiological data indicating that there are significant sex differences in regards to prevalence, clinical symptoms and age of onset of disorders like MDD and schizophrenia. Reduced claudin-5 expression has been noted in patients with schizophrenia, a study which included both male and female patients, but sex was not a factor considered in the analysis of the results (Greene et al., 2020). In MDD, however, through sex-specific analysis it was shown that there were clear gender differences, with claudin-5 loss noted in the NAc of men but in the PFC of women (Menard et al., 2017; Dudek et al., 2020; Dion-Albert et al., 2022). This finding highlights the importance of further examination of this work, and in fact all neurological disorder research, in a sex specific manner. These findings may provide further insights into why male and female patients with the same disorder exhibit different clinical symptoms, as well as display different efficacy and side effects following treatment (Hoekstra et al., 2021). Overall there is compelling evidence that sex differences are an important variable in mental health research and thus in order to further develop our understanding of claudin-5 and the role it plays in these disorders, it will be essential to further characterise this model in a sex-specific manner.

The work described in Chapter 4, established a gene therapy based approach to re-establish BBB integrity through the overexpression of claudin-5 specifically in ECs. Gene therapy has exponential potential in therapeutic development. However, for too long focus has remained on monogenic disorders, which for the most part are rare. While progress has been made, the cost of goods and the rarity of some of these disorders has made translating these new therapeutics into clinical application commercially infeasible. The prime example being the first approved human AAV based gene therapy, Glybera. Glybera was both approved and withdrawn from the market within a 5 year period, having only treated 31 people, due to the expense on both patient and company (Mendell et al., 2021). Therefore utilising this technology to treat more prevalent disorders with a clear genetic mechanism of action will be crucial to push this field forward. One of the major cost limiting aspects to

gene therapy thus far is the use of large systemic doses. Therefore, utilising a local delivery approach and thus a lower dose of the vector may be a method to pivot gene therapy innovation towards more common disorders. In utilising lower doses, many more patients can be treated from a singular batch of AAV produced, driving down the cost of goods per patient. There are clear limitations to this as a therapeutic option, including the limited transduction of the viral vector to specific brain regions as well a more invasive treatment approach when compared to systemic administration. However, based on current standard of care, in which there are such large cohorts of refractive patients that have no treatment options available, or in the case of epilepsy where surgical resection of brain tissue is the last resort, local injection of gene therapy may be a welcome alternative.

Examining the rescue effect of this new claudin-5 overexpression gene therapy was then examined in four different mouse models. These four models were broken into two etiological cohorts. Firstly the *Cldn5*$^{fl/wt}$*xTie2Cre* model and the inducible claudin-5 knockdown model, act as a proof of concept as all pathology noted in these models is directly associated with reduced claudin-5 expression. The second cohort, the CSDS model and the KA mouse model, are established models of disease with more complex etiology than just reduced claudin-5 expression, and thus were more predictive to the treatment efficacy in patients. In the *Cldn5*$^{fl/wt}$*xTie2Cre* model and the inducible claudin-5 knockdown model, when the therapeutic AAV was administered into the hippocampus, it significantly improved learning and memory deficits, the aberrant grooming behaviour and rescued sensorimotor gating deficits. Moreover, for the inducible KD model, the survival time was also increased in the cohort treated with the therapeutic AAV. Overall these findings support what has been shown in previous studies (Greene et al., 2022), that restoring claudin-5 expression at the barrier can restore function even when a distinct disease phenotype has developed. Therefore, it appears likely that below the normal level of claudin-5 expression, there is a certain threshold level of claudin-5 expression that is required to maintain BBB integrity and support normal neuronal function. Once below this minimum threshold however, the homeostasis of the neuronal microenvironment changes and will result in physiological and behavioural changes. As described previously, establishing a strong model of disease can be difficult, as the method used to develop the model should relate to the natural development of the disease. As many of these disorders are known to have strong genetic and environmental contributions, a potentially interesting future direction for the *Cldn5*$^{fl/wt}$*xTie2Cre* model would be to utilise it in conjunction with

an environmental stressor. Environmental stressors include post-weaning social isolation protocol for schizophrenia models and chronic social defeat stress protocol for MDD models. Using an environmental stressor in a mouse that is already genetically vulnerable may further exacerbate any underlying pathology and allows for further investigation into the environmental and genetic contributions to neurological disease development and progression. Overall, this may create a model with stronger construct validity, that has the potential to be a strong model of disease. Additionally, in regards to the gene therapy administration method, future studies should examine the potential for enhancing efficacy through multiple injection sites. These initial rescue experiments validated that overexpression of claudin-5 within the hippocampal region resulted in an improved outcome in comparison to the mPFC targeted cohort. However, executing complex higher order behaviours such as self-grooming, social behaviour and memory consolidation requires a complex neural circuit that comprises multiple brain regions, including the hippocampus, the mPFC and the NAc. Moreover, all three of these regions have been associated with a distinct loss of claudin-5 expression and associated disordered behaviour (Greene et al., 2018; Menard et al., 2017; Dion-Albert et al., 2022). Therefore, future research should examine the potential to improve therapeutic efficacy by targeting multiple brain regions with this gene therapy.

Examining the potential therapeutic effect of claudin-5 overexpression was then carried out in established models of disease, the CSDS and the KA model, which are, due to the methods used to develop the disorder, more complex with many potential disease contributing components. For the CSDS, no significant rescue effect was noted. While this may be due to the overexpression of claudin-5 within the hippocampus not being sufficient to rescue the more complex disease phenotype, it may also be due to the fact that the incorrect brain region was targeted. As described previously, claudin-5 loss has been noted in the NAc of men but in the PFC of women (Menard et al., 2017; Dudek et al., 2020; Dion-Albert et al., 2022). Therefore a potential future study should be carried out, injecting these brain regions in a sex specific manner with larger numbers in each trial to examine if the lack of rescue effect is due to claudin-5 being insufficient to rescue pathology or if more specific brain regions are required to achieve therapeutic potential. In the second established model of disease, the KA model of epilepsy, it was found that those treated with the Cldn5-AAV had a lower cumulative seizure score examined across a 2 hr time period. Additionally, the latency to seizure onset was longer than the control treated mice, but

across both treatment groups the seizure severity was similar. Hallmark features of the KA model, such as the acute induction of cFos appeared more extreme in the control treated mice in comparison to those treated with the Cldn5-AAV. Acute CNS inflammation was noted through IHC analysis of the astrocyte marker GFAP in the GFP-AAV treated controls, but the microglial marker IBA1 remained similar through both timepoint and treatment. As mice were treated with a mildly convulsive KA dose, it produced overall milder symptoms with few mice exceeding stage 3 on the Racine scale. For future examination, mice could be administered a stronger KA dose, which may produce a more distinct pathology and may also give clearer insight into the potential of this AAV for therapeutic rescue.

In summary, the work described in Chapter 3, supports the current published literature and research, that there is a undeniable association between loss of claudin-5 expression and the neurobehavioral sequelae that is associated with neurological disorders such as schizophrenia and MDD. Moreover, the work described in Chapter 4 developed a gene therapy based approach to re-establish BBB integrity through the overexpression of claudin-5 in ECs specifically. Finally the work described in Chapter 5 provided evidence that maintaining a certain minimum threshold of claudin-5 can attenuate pathology. However for more complex models, while still being a viable avenue for therapeutic development, it may need to be approached as an adjunct therapy. As discussed many of these neurological disorders have high refractive cohorts. High level of P-gp efflux transporter expression has been noted in many neurological disorders and the idea that increased P-gp expression is acting as a second line of defence due to the loss of barrier integrity is becoming a popular line of thinking (Tang et al., 2017; Hoosain et al., 2015). However, while trying to protect the brain, this mechanism may be playing a role in the reduced efficacy of current therapeutics, by reducing the bioavailability of medication in the brain. Therefore if the primary barrier function could be resolved with this BBB restoring gene therapy, this second line of defence would no longer be required and efflux transporter expression should normalise. This in turn would resolve the pharmacodynamic issues noted for the current therapeutics and reduce the number of refractive cases. Therefore an interesting future direction for investigation would include, examining the P-gp expression level in the *Cldn5*$^{fl/wt}$*xTie2Cre* model. Determining the level of P-gp expression in claudin-5 heterozygotes as well as evaluating any changes in expression following treatment with the claudin-5 overexpressing AAV will give further insight into

the potential this gene therapy has to treat the refractive cohort of neurological disease. Additionally to further examine its use as an adjunct therapy, mouse models of disease such as the CSDS model, in which behaviour pathology is reversed by chronic antidepressant treatment, could be utilised to examine if the latency to treatment efficacy and the dosage of antidepressant required can be reduced if utilised in parallel with this gene therapy. Overall, developing a gene therapy based approach to restore claudin-5 expression at the BBB, in order to re-establish barrier function appears to be a promising step in the development of a novel and improved method to treat neurological disorders.

References

Abbott, N. J. (2004). Evidence for bulk flow of brain interstitial fluid: significance for physiology and pathology. *Neurochemistry International*, *45*(4), 545–552. https://doi.org/10.1016/j.neuint.2003.11.006

Abbott, N. J., Khan, E. U., Rollinson, C. M. S., Reichel, A., Janigro, D., Dombrowski, S. M., Dobbie, M. S., & Begley, D. J. (2002). Drug resistance in epilepsy: the role of the blood-brain barrier. *Novartis Foundation Symposium*, *243*, 38–47; discussion 47-53, 180–185.

Abbott, N. J., Patabendige, A. A. K., Dolman, D. E. M., Yusof, S. R., & Begley, D. J. (2010). Structure and function of the blood-brain barrier. *Neurobiology of Disease*, *37*(1), 13–25. https://doi.org/10.1016/j.nbd.2009.07.030

Abbott, N. J., Rönnbäck, L., & Hansson, E. (2006). Astrocyte–endothelial interactions at the blood–brain barrier. *Nature Reviews Neuroscience*, *7*(1), 41–53. https://doi.org/10.1038/nrn1824

Aguzzi, A., Barres, B. A., & Bennett, M. L. (2013). Microglia: scapegoat, saboteur, or something else? *Science (New York, N.Y.)*, *339*(6116), 156–161. https://doi.org/10.1126/science.1227901

Alliot, F., Godin, I., & Pessac, B. (1999). Microglia derive from progenitors, originating from the yolk sac, and which proliferate in the brain. *Brain Research. Developmental Brain Research*, *117*(2), 145–152. https://doi.org/10.1016/s0165-3806(99)00113-3

Alvarez, J. I., Dodelet-Devillers, A., Kebir, H., Ifergan, I., Fabre, P. J., Terouz, S., Sabbagh, M., Wosik, K., Bourbonnière, L., Bernard, M., van Horssen, J., de Vries, H. E., Charron, F., & Prat, A. (2011). The Hedgehog pathway promotes blood-brain barrier integrity and CNS immune quiescence. *Science (New York, N.Y.)*, *334*(6063), 1727–1731. https://doi.org/10.1126/science.1206936

Alvarez, J. I., Katayama, T., & Prat, A. (2013). Glial influence on the blood brain barrier. *Glia*, *61*(12), 1939–1958. https://doi.org/10.1002/glia.22575

Anders, J. J., & Goss, G. (1989). Morphological changes in the junctional complex of cells in the arachnoid layer of the rat after cold injury. *Cell and Tissue Research*, *256*(2), 303–307. https://doi.org/10.1007/BF00218887

Anderson, D. J. (2016). Circuit modules linking internal states and social behaviour in flies and mice. *Nature Reviews. Neuroscience*, *17*(11), 692–704. https://doi.org/10.1038/nrn.2016.125

Anderson, S. W., Bechara, A., Damasio, H., Tranel, D., & Damasio, A. R. (1999). Impairment of social and moral behavior related to early damage in human prefrontal cortex. *Nature Neuroscience*, *2*(11), 1032–1037. https://doi.org/10.1038/14833

Argaw, A. T., Gurfein, B. T., Zhang, Y., Zameer, A., & John, G. R. (2009). VEGF-mediated disruption of endothelial CLN-5 promotes blood-brain barrier breakdown. *Proceedings of the National Academy of Sciences*, *106*(6), 1977–1982. https://doi.org/10.1073/pnas.0808698106

Armulik, A., Genové, G., Mäe, M., Nisancioglu, M. H., Wallgard, E., Niaudet, C., He, L., Norlin, J., Lindblom, P., Strittmatter, K., Johansson, B. R., & Betsholtz, C. (2010). Pericytes regulate the blood–brain barrier. *Nature*, *468*, 557. https://doi.org/10.1038/nature09522

Arnold, T., & Betsholtz, C. (2013). Correction: The importance of microglia in the development of the vasculature in the central nervous system. *Vascular Cell*, *5*(1), 12. https://doi.org/10.1186/2045-824X-5-12

Au, H. K. E., Isalan, M., & Mielcarek, M. (2021). Gene Therapy Advances: A Meta-Analysis of AAV Usage in Clinical Settings. *Frontiers in Medicine*, *8*, 809118. https://doi.org/10.3389/fmed.2021.809118

Azevedo, F. A. C., Carvalho, L. R. B., Grinberg, L. T., Farfel, J. M., Ferretti, R. E. L., Leite, R. E. P., Jacob Filho, W., Lent, R., & Herculano-Houzel, S. (2009). Equal numbers of neuronal and nonneuronal cells make the human brain an isometrically scaled-up primate brain. *The Journal of Comparative Neurology*, *513*(5), 532–541. https://doi.org/10.1002/cne.21974

Bailey, K. R., & Crawley, J. N. (2009). *Anxiety-Related Behaviors in Mice*.

Bake, S., Friedman, J. A., & Sohrabji, F. (2009). Reproductive age-related changes in the blood brain barrier: expression of IgG and tight junction proteins. *Microvascular Research*, *78*(3), 413–424. https://doi.org/10.1016/j.mvr.2009.06.009

Bargerstock, E., Puvenna, V., Iffland, P., Falcone, T., Hossain, M., Vetter, S., Man, S., Dickstein, L., Marchi, N., Ghosh, C., Carvalho-Tavares, J., & Janigro, D. (2014). Is peripheral immunity regulated by blood-brain barrier permeability changes? *PloS One*, *9*(7), e101477. https://doi.org/10.1371/journal.pone.0101477

Başkaya, M. K., Rao, A. M., Doğan, A., Donaldson, D., & Dempsey, R. J. (1997). The biphasic opening of the blood-brain barrier in the cortex and hippocampus after traumatic brain injury in rats. *Neuroscience Letters*, *226*(1), 33–36. https://doi.org/10.1016/s0304-3940(97)00239-5

Bauer, H.-C., & Bauer, H. (2000). Neural Induction of the Blood–Brain Barrier: Still an Enigma. *Cellular and Molecular Neurobiology*, *20*(1), 13–28. https://doi.org/10.1023/A:1006939825857

Bayassi-Jakowicka, M., Lietzau, G., Czuba, E., Steliga, A., Waśkow, M., & Kowiański, P. (2021). Neuroplasticity and multilevel system of connections determine the integrative role of nucleus accumbens in the brain reward system. In *International Journal of Molecular Sciences* (Vol. 22, Issue 18). MDPI. https://doi.org/10.3390/ijms22189806

Bazzoni, G., Martinez-Estrada, O. M., Orsenigo, F., Cordenonsi, M., Citi, S., & Dejana, E. (2000). Interaction of junctional adhesion molecule with the tight junction components ZO-1, cingulin, and occludin. *The Journal of Biological Chemistry*, *275*(27), 20520–20526. https://doi.org/10.1074/jbc.M905251199

Bechara, A., Tranel, D., & Damasio, H. (2000). Characterization of the decision-making deficit of patients with ventromedial prefrontal cortex lesions. *Brain*, *123*(11), 2189–2202. https://doi.org/10.1093/brain/123.11.2189

Becker, A., Grecksch, G., Bernstein, H. G., Höllt, V., & Bogerts, B. (1999). Social behaviour in rats lesioned with ibotenic acid in the hippocampus: quantitative and qualitative analysis. *Psychopharmacology*, *144*(4), 333–338. https://doi.org/10.1007/s002130051015

Begley, C., Wagner, R. G., Abraham, A., Beghi, E., Newton, C., Kwon, C., Labiner, D., & Winkler, A. S. (2022). The global cost of epilepsy: A systematic review and extrapolation. *Epilepsia*, *63*(4), 892–903. https://doi.org/10.1111/epi.17165

Bell, R. D., & Zlokovic, B. v. (2009). Neurovascular mechanisms and blood-brain barrier disorder in Alzheimer's disease. *Acta Neuropathologica*, *118*(1), 103–113. https://doi.org/10.1007/s00401-009-0522-3

Bell, R. D., Winkler, E. A., Sagare, A. P., Singh, I., LaRue, B., Deane, R., & Zlokovic, B. v. (2010). Pericytes control key neurovascular functions and neuronal phenotype in the adult brain and during brain aging. *Neuron*, *68*(3), 409–427. https://doi.org/10.1016/j.neuron.2010.09.043

Ben-Ari, Y., & Lagowska, J. (1978). [Epileptogenic action of intra-amygdaloid injection of kainic acid]. *Comptes Rendus Hebdomadaires Des Seances de l'Academie Des Sciences. Serie D: Sciences Naturelles*, *287*(8), 813–816.

Ben-Ari, Y., Lagowska, J., Tremblay, E., & le Gal La Salle, G. (1979). A new model of focal status epilepticus: intra-amygdaloid application of kainic acid elicits repetitive secondarily generalized convulsive seizures. *Brain Research*, *163*(1), 176–179. https://doi.org/10.1016/0006-8993(79)90163-x

Berg, A. T., Berkovic, S. F., Brodie, M. J., Buchhalter, J., Cross, J. H., van Emde Boas, W., Engel, J., French, J., Glauser, T. A., Mathern, G. W., Moshé, S. L., Nordli, D., Plouin, P., & Scheffer, I. E. (2010). Revised terminology and concepts for organization of seizures and epilepsies: Report of the ILAE Commission on Classification and Terminology, 2005-2009. *Epilepsia*, *51*(4), 676–685. https://doi.org/10.1111/j.1528-1167.2010.02522.x

Berridge, K. C., & Aldridge, J. W. (2000). Super-stereotypy I: enhancement of a complex movement sequence by systemic dopamine D1 agonists. *Synapse (New York, N.Y.)*, *37*(3), 194–204. https://doi.org/10.1002/1098-2396(20000901)37:3<194::AID-SYN3>3.0.CO;2-A

Berridge, K. C., & Whishaw, I. Q. (1992). Cortex, striatum and cerebellum: control of serial order in a grooming sequence. *Experimental Brain Research*, *90*(2), 275–290. https://doi.org/10.1007/BF00227239

Berton, O., & Nestler, E. J. (2006). New approaches to antidepressant drug discovery: beyond monoamines. *Nature Reviews Neuroscience*, *7*(2), 137–151. https://doi.org/10.1038/nrn1846

Bloss, E. B., & Hunter, R. G. (2010). Hippocampal kainate receptors. *Vitamins and Hormones*, *82*, 167–184. https://doi.org/10.1016/S0083-6729(10)82009-6

Bonfanti, L., & Peretto, P. (2011). Adult neurogenesis in mammals--a theme with many variations. *The European Journal of Neuroscience*, *34*(6), 930–950. https://doi.org/10.1111/j.1460-9568.2011.07832.x

Bonne, O., Vythilingam, M., Inagaki, M., Wood, S., Neumeister, A., Nugent, A. C., Snow, J., Luckenbaugh, D. A., Bain, E. E., Drevets, W. C., & Charney, D. S. (2008). Reduced posterior hippocampal volume in posttraumatic stress disorder. *The Journal of Clinical Psychiatry*, *69*(7), 1087–1091. https://doi.org/10.4088/jcp.v69n0707

Bossert, J. M., Gray, S. M., Lu, L., & Shaham, Y. (2006). Activation of group II metabotropic glutamate receptors in the nucleus accumbens shell attenuates context-induced relapse to heroin seeking. *Neuropsychopharmacology : Official Publication of the American College of Neuropsychopharmacology*, *31*(10), 2197–2209. https://doi.org/10.1038/sj.npp.1300977

Boulay, A.-C., Saubaméa, B., Adam, N., Chasseigneaux, S., Mazaré, N., Gilbert, A., Bahin, M., Bastianelli, L., Blugeon, C., Perrin, S., Pouch, J., Ducos, B., le Crom, S., Genovesio, A., Chrétien, F., Declèves, X., Laplanche, J.-L., & Cohen-Salmon, M. (2017). Translation in astrocyte distal processes sets molecular heterogeneity at the gliovascular interface. *Cell Discovery*, *3*(1), 17005. https://doi.org/10.1038/celldisc.2017.5

Braff, D. L., Geyer, M. A., & Swerdlow, N. R. (2001). Human studies of prepulse inhibition of startle: normal subjects, patient groups, and pharmacological studies. *Psychopharmacology*, *156*(2–3), 234–258. https://doi.org/10.1007/s002130100810

Braff, D., Stone, C., Callaway, E., Geyer, M., Glick, I., & Bali, L. (1978). Prestimulus effects on human startle reflex in normals and schizophrenics. *Psychophysiology*, *15*(4), 339–343. https://doi.org/10.1111/j.1469-8986.1978.tb01390.x

Braun, L. D., Cornford, E. M., & Oldendorf, W. H. (1980). Newborn Rabbit Blood-Brain Barrier Is Selectively Permeable and Differs Substantially from the Adult. *Journal of Neurochemistry*, *34*(1), 147–152. https://doi.org/10.1111/j.1471-4159.1980.tb04633.x

Brightman, M. W., & Reese, T. S. (1969). Junctions between intimately apposed cell membranes in the vertebrate brain. *The Journal of Cell Biology*, *40*(3), 648–677. https://doi.org/10.1083/jcb.40.3.648

Brochard, V., Combadière, B., Prigent, A., Laouar, Y., Perrin, A., Beray-Berthat, V., Bonduelle, O., Alvarez-Fischer, D., Callebert, J., Launay, J.-M., Duyckaerts, C., Flavell, R. A., Hirsch, E. C., & Hunot, S. (2009). Infiltration of CD4+ lymphocytes into the brain contributes to neurodegeneration in a mouse model of Parkinson disease. *The Journal of Clinical Investigation*, *119*(1), 182–192. https://doi.org/10.1172/JCI36470

Brøchner, C. B., Holst, C. B., & Møllgård, K. (2015). Outer brain barriers in rat and human development. *Frontiers in Neuroscience*, *9*, 75. https://doi.org/10.3389/fnins.2015.00075

Buck, T. M., & Wijnholds, J. (2020). Recombinant Adeno-Associated Viral Vectors (rAAV)-Vector Elements in Ocular Gene Therapy Clinical Trials and Transgene Expression and Bioactivity Assays. *International Journal of Molecular Sciences*, *21*(12). https://doi.org/10.3390/ijms21124197

Bulcha, J. T., Wang, Y., Ma, H., Tai, P. W. L., & Gao, G. (2021). Viral vector platforms within the gene therapy landscape. *Signal Transduction and Targeted Therapy*, *6*(1), 53. https://doi.org/10.1038/s41392-021-00487-6

Butt, A. M., Jones, H. C., & Abbott, N. J. (1990). Electrical resistance across the blood-brain barrier in anaesthetized rats: a developmental study. *The Journal of Physiology*, *429*, 47–62. https://doi.org/10.1113/jphysiol.1990.sp018243

Cajal SR. (1901). Significación probable de las células de axón corto. . *Trab Lab Investig Biol.* , 151–157.

Calcedo, R., Vandenberghe, L. H., Gao, G., Lin, J., & Wilson, J. M. (2009). Worldwide epidemiology of neutralizing antibodies to adeno-associated viruses. *The Journal of Infectious Diseases*, *199*(3), 381–390. https://doi.org/10.1086/595830

Can, A., Dao, D. T., Arad, M., Terrillion, C. E., Piantadosi, S. C., & Gould, T. D. (2012). The mouse forced swim test. *Journal of Visualized Experiments : JoVE*, *59*, e3638. https://doi.org/10.3791/3638

Cardinal, R. N., & Cheung, T. H. C. (2005). Nucleus accumbens core lesions retard instrumental learning and performance with delayed reinforcement in the rat. *BMC Neuroscience*, *6*, 9. https://doi.org/10.1186/1471-2202-6-9

Carvalho J. *RE: MeiraGTx Planning to Launch New Trial of AAV-GAD in Parkinson's Patients*, New York, NY: (2020).

Castro Dias, M., Coisne, C., Baden, P., Enzmann, G., Garrett, L., Becker, L., Hölter, S. M., Hrabě de Angelis, M., Deutsch, U., & Engelhardt, B. (2019). Claudin-12 is not required for blood–brain barrier tight junction function. *Fluids and Barriers of the CNS*, *16*(1), 30. https://doi.org/10.1186/s12987-019-0150-9

Castro Dias, M., Coisne, C., Lazarevic, I., Baden, P., Hata, M., Iwamoto, N., Francisco, D. M. F., Vanlandewijck, M., He, L., Baier, F. A., Stroka, D., Bruggmann, R., Lyck, R., Enzmann, G., Deutsch, U., Betsholtz, C., Furuse, M., Tsukita, S., & Engelhardt, B. (2019b). Claudin-3-deficient C57BL/6J mice display intact brain barriers. *Scientific Reports*, *9*(1), 203. https://doi.org/10.1038/s41598-018-36731-3

Castro Dias, M., Mapunda, J. A., Vladymyrov, M., & Engelhardt, B. (2019). Structure and Junctional Complexes of Endothelial, Epithelial and Glial Brain Barriers. *International Journal of Molecular Sciences*, *20*(21). https://doi.org/10.3390/ijms20215372

Cavalheiro, E. A., Leite, J. P., Bortolotto, Z. A., Turski, W. A., Ikonomidou, C., & Turski, L. (n.d.). Long-term effects of pilocarpine in rats: structural damage of the brain triggers kindling and spontaneous recurrent seizures. *Epilepsia*, *32*(6), 778–782. https://doi.org/10.1111/j.1528-1157.1991.tb05533.x

Cecchelli, R., Berezowski, V., Lundquist, S., Culot, M., Renftel, M., Dehouck, M.-P., & Fenart, L. (2007). Modelling of the blood-brain barrier in drug discovery and development. *Nature Reviews. Drug Discovery*, *6*(8), 650–661. https://doi.org/10.1038/nrd2368

Chambers, R. A., & Self, D. W. (2002). Motivational responses to natural and drug rewards in rats with neonatal ventral hippocampal lesions: an animal model of dual diagnosis schizophrenia. *Neuropsychopharmacology : Official Publication of the American College of Neuropsychopharmacology*, *27*(6), 889–905. https://doi.org/10.1016/S0893-133X(02)00365-2

Chambers, R. A., Moore, J., McEvoy, J. P., & Levin, E. D. (1996). Cognitive effects of neonatal hippocampal lesions in a rat model of schizophrenia. *Neuropsychopharmacology : Official Publication of the American College of Neuropsychopharmacology*, *15*(6), 587–594. https://doi.org/10.1016/S0893-133X(96)00132-7

Chen, P., & Hong, W. (2018). Neural Circuit Mechanisms of Social Behavior. *Neuron*, *98*(1), 16–30. https://doi.org/10.1016/j.neuron.2018.02.026

Chen, Y. H., Chang, M., & Davidson, B. L. (2009). Molecular signatures of disease brain endothelia provide new sites for CNS-directed enzyme therapy. *Nature Medicine*, *15*(10), 1215–1218. https://doi.org/10.1038/nm.2025

Chiba, H., Ichikawa-Tomikawa, N., Imura, T., & Sugimoto, K. (2021). The region-selective regulation of endothelial claudin-5 expression and signaling in brain health and disorders. *Journal of Cellular Physiology*, *236*(10), 7134–7143. https://doi.org/10.1002/jcp.30357

Christensen, I. B., Gyldenholm, T., Damkier, H. H., & Praetorius, J. (2013). Polarization of membrane associated proteins in the choroid plexus epithelium from normal and slc4a10 knockout mice. *Frontiers in Physiology*, *4*, 344. https://doi.org/10.3389/fphys.2013.00344

Coenen, A. M., & van Luijtelaar, E. L. (1987). The WAG/Rij rat model for absence epilepsy: age and sex factors. *Epilepsy Research*, *1*(5), 297–301. https://doi.org/10.1016/0920-1211(87)90005-2

Cowan, P. J., Tsang, D., Pedic, C. M., Abbott, L. R., Shinkel, T. A., d'Apice, A. J., & Pearse, M. J. (1998). The human ICAM-2 promoter is endothelial cell-specific in vitro and in vivo and contains critical Sp1 and GATA binding sites. *The Journal of Biological Chemistry*, *273*(19), 11737–11744. https://doi.org/10.1074/jbc.273.19.11737

Coyle, J. T., Tsai, G., & Goff, D. (2003). Converging evidence of NMDA receptor hypofunction in the pathophysiology of schizophrenia. *Annals of the New York Academy of Sciences*, *1003*, 318–327. https://doi.org/10.1196/annals.1300.020

Crabbe, J. C., Wahlsten, D., & Dudek, B. C. (1999). Genetics of mouse behavior: interactions with laboratory environment. *Science (New York, N.Y.)*, *284*(5420), 1670–1672. https://doi.org/10.1126/science.284.5420.1670

Cromwell, H. C., & Berridge, K. C. (1996). Implementation of Action Sequences by a Neostriatal Site: A Lesion Mapping Study of Grooming Syntax. *The Journal of Neuroscience*, *16*(10), 3444–3458. https://doi.org/10.1523/JNEUROSCI.16-10-03444.1996

Cromwell, H. C., Berridge, K. C., Drago, J., & Levine, M. S. (1998). Action sequencing is impaired in D1A-deficient mutant mice. *The European Journal of Neuroscience*, *10*(7), 2426–2432. https://doi.org/10.1046/j.1460-9568.1998.00250.x

Cronk, J. C., & Kipnis, J. (2013). Microglia - the brain's busy bees. *F1000prime Reports*, *5*, 53. https://doi.org/10.12703/P5-53

Crusio, W. E., Schwegler, H., & Brust, I. (1993). Covariations between hippocampal mossy fibres and working and reference memory in spatial and non-spatial radial maze tasks in mice. *The European Journal of Neuroscience*, *5*(10), 1413–1420. https://doi.org/10.1111/j.1460-9568.1993.tb00927.x

D'Ambrosio, R., Fairbanks, J. P., Fender, J. S., Born, D. E., Doyle, D. L., & Miller, J. W. (2004). Post-traumatic epilepsy following fluid percussion injury in the rat. *Brain : A Journal of Neurology*, *127*(Pt 2), 304–314. https://doi.org/10.1093/brain/awh038

da Fonseca, A. C. C., Matias, D., Garcia, C., Amaral, R., Geraldo, L. H., Freitas, C., & Lima, F. R. S. (2014). The impact of microglial activation on blood-brain barrier in brain diseases. *Frontiers in Cellular Neuroscience*, *8*, 362. https://doi.org/10.3389/fncel.2014.00362

Daneman, R., Agalliu, D., Zhou, L., Kuhnert, F., Kuo, C. J., & Barres, B. A. (2009). Wnt/beta-catenin signaling is required for CNS, but not non-CNS, angiogenesis. *Proceedings of the National Academy of Sciences of the United States of America*, *106*(2), 641–646. https://doi.org/10.1073/pnas.0805165106

Daneman, R., Zhou, L., Agalliu, D., Cahoy, J. D., Kaushal, A., & Barres, B. A. (2010). The mouse blood-brain barrier transcriptome: a new resource for understanding the development and function of brain endothelial cells. *PloS One*, *5*(10), e13741. https://doi.org/10.1371/journal.pone.0013741

Das, A. T., Tenenbaum, L., & Berkhout, B. (2016). Tet-On Systems For Doxycycline-inducible Gene Expression. *Current Gene Therapy*, *16*(3), 156–167. https://doi.org/10.2174/1566523216666160524144041

Dashkoff, J., Lerner, E. P., Truong, N., Klickstein, J. A., Fan, Z., Mu, D., Maguire, C. A., Hyman, B. T., & Hudry, E. (2016). Tailored transgene expression to specific cell types in the central nervous system after peripheral injection with AAV9. *Molecular Therapy. Methods & Clinical Development*, *3*, 16081. https://doi.org/10.1038/mtm.2016.81

Daugherty, B. L., Ward, C., Smith, T., Ritzenthaler, J. D., & Koval, M. (2007). Regulation of Heterotypic Claudin Compatibility. *Journal of Biological Chemistry*, *282*(41), 30005–30013. https://doi.org/10.1074/jbc.M703547200

Davalos, D., Grutzendler, J., Yang, G., Kim, J. v, Zuo, Y., Jung, S., Littman, D. R., Dustin, M. L., & Gan, W.-B. (2005). ATP mediates rapid microglial response to local brain injury in vivo. *Nature Neuroscience*, *8*(6), 752–758. https://doi.org/10.1038/nn1472

David, Y., Cacheaux, L. P., Ivens, S., Lapilover, E., Heinemann, U., Kaufer, D., & Friedman, A. (2009). Astrocytic dysfunction in epileptogenesis: consequence of altered potassium and glutamate homeostasis? *The Journal of Neuroscience : The Official Journal of the Society for Neuroscience*, *29*(34), 10588–10599. https://doi.org/10.1523/JNEUROSCI.2323-09.2009

Davidson, B. L., & McCray, P. B. (2011). Current prospects for RNA interference-based therapies. *Nature Reviews Genetics*, *12*(5), 329–340. https://doi.org/10.1038/nrg2968

Daya, S., & Berns, K. I. (2008). Gene therapy using adeno-associated virus vectors. *Clinical Microbiology Reviews*, *21*(4), 583–593. https://doi.org/10.1128/CMR.00008-08

Dayton, R. D., Wang, D. B., & Klein, R. L. (2012). The advent of AAV9 expands applications for brain and spinal cord gene delivery. *Expert Opinion on Biological Therapy*, *12*(6), 757–766. https://doi.org/10.1517/14712598.2012.681463

de Boer, A. G., van der Sandt, I. C. J., & Gaillard, P. J. (2003). The Role of Drug Transporters at the Blood-Brain Barrier. *Annual Review of Pharmacology and Toxicology*, *43*(1), 629–656. https://doi.org/10.1146/annurev.pharmtox.43.100901.140204

Deacon, R. M. J. (2013). Measuring motor coordination in mice. *Journal of Visualized Experiments : JoVE*, *75*, e2609. https://doi.org/10.3791/2609

Deacon, R. M. J., & Rawlins, J. N. P. (2006). T-maze alternation in the rodent. *Nature Protocols*, *1*(1), 7–12. https://doi.org/10.1038/nprot.2006.2

Decimo, I., Fumagalli, G., Berton, V., Krampera, M., & Bifari, F. (2012). Meninges: from protective membrane to stem cell niche. *American Journal of Stem Cells*, *1*(2), 92–105.

Dedovic, K., Duchesne, A., Andrews, J., Engert, V., & Pruessner, J. C. (2009). The brain and the stress axis: the neural correlates of cortisol regulation in response to stress. *NeuroImage*, *47*(3), 864–871. https://doi.org/10.1016/j.neuroimage.2009.05.074

Dehouck, M. P., Méresse, S., Delorme, P., Fruchart, J. C., & Cecchelli, R. (1990). An easier, reproducible, and mass-production method to study the blood-brain barrier in vitro. *Journal of Neurochemistry*, *54*(5), 1798–1801. https://doi.org/10.1111/j.1471-4159.1990.tb01236.x

Delaney, C., & Campbell, M. (2017). The blood brain barrier: Insights from development and ageing. *Tissue Barriers*, *5*(4), e1373897. https://doi.org/10.1080/21688370.2017.1373897

Deverman, B. E., Pravdo, P. L., Simpson, B. P., Kumar, S. R., Chan, K. Y., Banerjee, A., Wu, W.-L., Yang, B., Huber, N., Pasca, S. P., & Gradinaru, V. (2016). Cre-dependent selection yields AAV variants for widespread gene transfer to the adult brain. *Nature Biotechnology*, *34*(2), 204–209. https://doi.org/10.1038/nbt.3440

di Chiara, G. (1995). The role of dopamine in drug abuse viewed from the perspective of its role in motivation. *Drug and Alcohol Dependence*, *38*(2), 95–137. https://doi.org/10.1016/0376-8716(95)01118-i

Dion-Albert, L., Cadoret, A., Doney, E., Kaufmann, F. N., Dudek, K. A., Parise, L. F., Cathomas, F., Samba, N., Hudson, N., Lebel, M., Campbell, M., Turecki, G., Mechawar, N., & Menard, C. (2022). *Sex-specific blood-brain barrier alterations and vascular biomarkers underlie chronic stress responses in mice and human depression*. https://doi.org/10.1101/2021.04.23.441142

Dion-Albert, L., Cadoret, A., Doney, E., Kaufmann, F. N., Dudek, K. A., Daigle, B., Parise, L. F., Cathomas, F., Samba, N., Hudson, N., Lebel, M., Aardema, F., Ait Bentaleb, L., Beauchamp, J., Bendahmane, H., Benoit, E., Bergeron, L., Bertone, A., Bertrand, N., … Menard, C. (2022). Vascular and blood-brain barrier-related changes underlie stress responses and resilience in female mice and depression in human tissue. *Nature Communications*, *13*(1), 164. https://doi.org/10.1038/s41467-021-27604-x

Dohgu, S., Takata, F., Yamauchi, A., Nakagawa, S., Egawa, T., Naito, M., Tsuruo, T., Sawada, Y., Niwa, M., & Kataoka, Y. (2005). Brain pericytes contribute to the induction and up-regulation of blood-brain barrier functions through transforming growth factor-beta production. *Brain Research*, *1038*(2), 208–215. https://doi.org/10.1016/j.brainres.2005.01.027

Dominguez, E., Marais, T., Chatauret, N., Benkhelifa-Ziyyat, S., Duque, S., Ravassard, P., Carcenac, R., Astord, S., Pereira de Moura, A., Voit, T., & Barkats, M. (2011). Intravenous scAAV9 delivery of a codon-optimized SMN1 sequence rescues SMA mice. *Human Molecular Genetics*, *20*(4), 681–693. https://doi.org/10.1093/hmg/ddq514

Domino EF, & Luby ED. (1981). Abnormal mental states induced by phencyclidine as a model of schizophrenia. In Domino EF (Ed.), *PCP(phencyclidine): historical and current perspectives.* (pp. 401–418). Ann Arbor: NPP Books.

Dong, H.-W., Swanson, L. W., Chen, L., Fanselow, M. S., & Toga, A. W. (2009). Genomic-anatomic evidence for distinct functional domains in hippocampal field CA1. *Proceedings of the National Academy of Sciences of the United States of America*, *106*(28), 11794–11799. https://doi.org/10.1073/pnas.0812608106

dos Reis, M., Savva, R., & Wernisch, L. (2004). Solving the riddle of codon usage preferences: a test for translational selection. *Nucleic Acids Research*, *32*(17), 5036–5044. https://doi.org/10.1093/nar/gkh834

Dudek, K. A., Dion-Albert, L., Lebel, M., LeClair, K., Labrecque, S., Tuck, E., Ferrer Perez, C., Golden, S. A., Tamminga, C., Turecki, G., Mechawar, N., Russo, S. J., & Menard, C. (2020). Molecular adaptations of the blood–brain barrier promote stress resilience vs. depression. *Proceedings of the National Academy of Sciences*, *117*(6), 3326–3336. https://doi.org/10.1073/pnas.1914655117

Dudvarski Stankovic, N., Teodorczyk, M., Ploen, R., Zipp, F., & Schmidt, M. H. H. (2016). Microglia-blood vessel interactions: a double-edged sword in brain pathologies. *Acta Neuropathologica*, *131*(3), 347–363. https://doi.org/10.1007/s00401-015-1524-y

Duque, S., Joussemet, B., Riviere, C., Marais, T., Dubreil, L., Douar, A.-M., Fyfe, J., Moullier, P., Colle, M.-A., & Barkats, M. (2009). Intravenous administration of self-complementary AAV9 enables transgene delivery to adult motor neurons. *Molecular Therapy : The Journal of the American Society of Gene Therapy*, *17*(7), 1187–1196. https://doi.org/10.1038/mt.2009.71

el Hafny, B., Chappey, O., Piciotti, M., Debray, M., Boval, B., & Roux, F. (1997). Modulation of P-glycoprotein activity by glial factors and retinoic acid in an immortalized rat brain microvessel endothelial cell line. *Neuroscience Letters*, *236*(2), 107–111. https://doi.org/10.1016/s0304-3940(97)00679-4

Elahy, M., Jackaman, C., Mamo, J. C., Lam, V., Dhaliwal, S. S., Giles, C., Nelson, D., & Takechi, R. (2015). Blood-brain barrier dysfunction developed during normal aging is associated with inflammation and loss of tight junctions but not with leukocyte recruitment. *Immunity & Ageing : I & A*, *12*, 2. https://doi.org/10.1186/s12979-015-0029-9

Enerson, B. E., & Drewes, L. R. (2006). The Rat Blood-Brain Barrier Transcriptome. *Journal of Cerebral Blood Flow & Metabolism*, *26*(7), 959–973. https://doi.org/10.1038/sj.jcbfm.9600249

Engelhardt, B., & Liebner, S. (2014). Novel insights into the development and maintenance of the blood--brain barrier. *Cell and Tissue Research*, *355*(3), 687–699. https://doi.org/10.1007/s00441-014-1811-2

Everitt, B. J. (1990). Sexual motivation: a neural and behavioural analysis of the mechanisms underlying appetitive and copulatory responses of male rats. *Neuroscience and Biobehavioral Reviews*, *14*(2), 217–232. https://doi.org/10.1016/s0149-7634(05)80222-2

Fabricius, K., Helboe, L., Fink-Jensen, A., Wörtwein, G., & Steiniger-Brach, B. (2011). Pharmacological characterization of social isolation-induced hyperactivity. *Psychopharmacology*, *215*(2), 257–266. https://doi.org/10.1007/s00213-010-2128-9

Fantin, A., Vieira, J. M., Gestri, G., Denti, L., Schwarz, Q., Prykhozhij, S., Peri, F., Wilson, S. W., & Ruhrberg, C. (2010). Tissue macrophages act as cellular chaperones for vascular anastomosis downstream of VEGF-mediated endothelial tip cell induction. *Blood*, *116*(5), 829–840. https://doi.org/10.1182/blood-2009-12-257832

Farfara, D., Feierman, E., Richards, A., Revenko, A. S., MacLeod, R. A., Norris, E. H., & Strickland, S. (2019). Knockdown of circulating C1 inhibitor induces neurovascular impairment, glial cell activation, neuroinflammation, and behavioral deficits. *Glia*, *67*(7), 1359–1373. https://doi.org/10.1002/glia.23611

Faure, J.-B., Marques-Carneiro, J. E., Akimana, G., Cosquer, B., Ferrandon, A., Herbeaux, K., Koning, E., Barbelivien, A., Nehlig, A., & Cassel, J.-C. (2014). Attention and executive functions in a rat model of chronic epilepsy. *Epilepsia*, *55*(5), 644–653. https://doi.org/10.1111/epi.12549

Fava, M., & Davidson, K. G. (1996). DEFINITION AND EPIDEMIOLOGY OF TREATMENT-RESISTANT DEPRESSION. *Psychiatric Clinics of North America*, *19*(2), 179–200. https://doi.org/10.1016/S0193-953X(05)70283-5

Feder, A., Nestler, E. J., & Charney, D. S. (2009). Psychobiology and molecular genetics of resilience. *Nature Reviews. Neuroscience*, *10*(6), 446–457. https://doi.org/10.1038/nrn2649

Feder, N. (1971). Microperoxidase. An ultrastructural tracer of low molecular weight. *The Journal of Cell Biology*, *51*(1), 339–343. https://doi.org/10.1083/jcb.51.1.339

Fieschi, C., Lenzi, G. L., Zanette, E., Orzi, F., & Passero, S. (1980). Effects on EEG of the osmotic opening of the blood-brain barrier in rats. *Life Sciences*, *27*(3), 239–243. https://doi.org/10.1016/0024-3205(80)90143-5

Fiest, K. M., Sauro, K. M., Wiebe, S., Patten, S. B., Kwon, C.-S., Dykeman, J., Pringsheim, T., Lorenzetti, D. L., & Jetté, N. (2017). Prevalence and incidence of epilepsy: A systematic review and meta-analysis of international studies. *Neurology*, *88*(3), 296–303. https://doi.org/10.1212/WNL.0000000000003509

Fiorentino, M., Sapone, A., Senger, S., Camhi, S. S., Kadzielski, S. M., Buie, T. M., Kelly, D. L., Cascella, N., & Fasano, A. (2016). Blood-brain barrier and intestinal epithelial barrier alterations in autism spectrum disorders. *Molecular Autism*, *7*, 49. https://doi.org/10.1186/s13229-016-0110-z

Fone, K. C. F., & Porkess, M. V. (2008). Behavioural and neurochemical effects of post-weaning social isolation in rodents-relevance to developmental neuropsychiatric disorders. *Neuroscience and Biobehavioral Reviews*, *32*(6), 1087–1102. https://doi.org/10.1016/j.neubiorev.2008.03.003

Foust, K. D., Nurre, E., Montgomery, C. L., Hernandez, A., Chan, C. M., & Kaspar, B. K. (2009). Intravascular AAV9 preferentially targets neonatal neurons and adult astrocytes. *Nature Biotechnology*, *27*(1), 59–65. https://doi.org/10.1038/nbt.1515

Frey, B. N., Andreazza, A. C., Nery, F. G., Martins, M. R., Quevedo, J., Soares, J. C., & Kapczinski, F. (2007). The role of hippocampus in the pathophysiology of bipolar disorder. *Behavioural Pharmacology*, *18*(5–6), 419–430. https://doi.org/10.1097/FBP.0b013e3282df3cde

Friedman, A. (2011). Blood-brain barrier dysfunction, status epilepticus, seizures, and epilepsy: a puzzle of a chicken and egg? *Epilepsia*, *52 Suppl 8*, 19–20. https://doi.org/10.1111/j.1528-1167.2011.03227.x

Furtado, M. de A., Braga, G. K., Oliveira, J. A. C., del Vecchio, F., & Garcia-Cairasco, N. (2002). Behavioral, morphologic, and electroencephalographic evaluation of seizures induced by intrahippocampal microinjection of pilocarpine. *Epilepsia*, *43 Suppl 5*, 37–39. https://doi.org/10.1046/j.1528-1157.43.s.5.41.x

Furuse, M., Fujimoto, K., Sato, N., Hirase, T., Tsukita, S., & Tsukita, S. (1996). Overexpression of occludin, a tight junction-associated integral membrane protein, induces the formation of intracellular multilamellar bodies bearing tight junction-like structures. *Journal of Cell Science*, *109 (Pt 2)*, 429–435. https://doi.org/10.1242/jcs.109.2.429

Furuse, M., Fujita, K., Hiiragi, T., Fujimoto, K., & Tsukita, S. (1998). Claudin-1 and -2: novel integral membrane proteins localizing at tight junctions with no sequence similarity to occludin. *The Journal of Cell Biology*, *141*(7), 1539–1550. https://doi.org/10.1083/jcb.141.7.1539

Furuse, M., Sasaki, H., & Tsukita, S. (1999). Manner of interaction of heterogeneous claudin species within and between tight junction strands. *The Journal of Cell Biology*, *147*(4), 891–903. https://doi.org/10.1083/jcb.147.4.891

Gangarossa, G., Espallergues, J., Mailly, P., de Bundel, D., de Kerchove d'Exaerde, A., Hervé, D., Girault, J.-A., Valjent, E., & Krieger, P. (2013). Spatial distribution of D1R- and D2R-expressing medium-sized spiny neurons differs along the rostro-caudal axis of the mouse dorsal striatum. *Frontiers in Neural Circuits*, *7*, 124. https://doi.org/10.3389/fncir.2013.00124

Garbuzova-Davis, S., Haller, E., Saporta, S., Kolomey, I., Nicosia, S. v, & Sanberg, P. R. (2007). Ultrastructure of blood-brain barrier and blood-spinal cord barrier in SOD1 mice modeling ALS. *Brain Research*, *1157*, 126–137. https://doi.org/10.1016/j.brainres.2007.04.044

Garcia-Cairasco, N., Terra, V. C., & Doretto, M. C. (1993). Midbrain substrates of audiogenic seizures in rats. *Behavioural Brain Research*, *58*(1–2), 57–67. https://doi.org/10.1016/0166-4328(93)90090-d

Gaudet, D., Méthot, J., & Kastelein, J. (2012). Gene therapy for lipoprotein lipase deficiency. *Current Opinion in Lipidology*, *23*(4), 310–320. https://doi.org/10.1097/MOL.0b013e3283555a7e

Gautam, J., Zhang, X., & Yao, Y. (2016). The role of pericytic laminin in blood brain barrier integrity maintenance. *Scientific Reports*, *6*(1), 36450. https://doi.org/10.1038/srep36450

Gehne, N., Lamik, A., Lehmann, M., Haseloff, R. F., Andjelkovic, A. v, & Blasig, I. E. (2017). Cross-over endocytosis of claudins is mediated by interactions via their extracellular loops. *PloS One*, *12*(8), e0182106. https://doi.org/10.1371/journal.pone.0182106

Gerwien, H., Hermann, S., Zhang, X., Korpos, E., Song, J., Kopka, K., Faust, A., Wenning, C., Gross, C. C., Honold, L., Melzer, N., Opdenakker, G., Wiendl, H., Schäfers, M., & Sorokin, L. (2016). Imaging matrix metalloproteinase activity in multiple sclerosis as a specific marker of leukocyte penetration of the blood-brain barrier. *Science Translational Medicine*, *8*(364), 364ra152. https://doi.org/10.1126/scitranslmed.aaf8020

Geyer, M. A. (2006). The family of sensorimotor gating disorders: comorbidities or diagnostic overlaps? *Neurotoxicity Research*, *10*(3–4), 211–220. https://doi.org/10.1007/BF03033358

Geyer, M. A., & Braff, D. L. (1987). Startle habituation and sensorimotor gating in schizophrenia and related animal models. *Schizophrenia Bulletin*, *13*(4), 643–668. https://doi.org/10.1093/schbul/13.4.643

Giacomini, K. M., International Transporter Consortium, Huang, S.-M., Tweedie, D. J., Benet, L. Z., Brouwer, K. L. R., Chu, X., Dahlin, A., Evers, R., Fischer, V., Hillgren, K. M., Hoffmaster, K. A., Ishikawa, T., Keppler, D., Kim, R. B., Lee, C. A., Niemi, M., Polli, J. W., Sugiyama, Y., … Zhang, L. (2010). Membrane transporters in drug development. *Nature Reviews. Drug Discovery*, *9*(3), 215–236. https://doi.org/10.1038/nrd3028

Gibbons, L., Ozaki, E., Greene, C., Trappe, A., Carty, M., Coppinger, J. A., Bowie, A. G., Campbell, M., & Doyle, S. L. (2022). SARM1 Promotes Photoreceptor Degeneration in an Oxidative Stress Model of Retinal Degeneration. *Frontiers in Neuroscience*, *16*, 852114. https://doi.org/10.3389/fnins.2022.852114

Ginhoux, F., Greter, M., Leboeuf, M., Nandi, S., See, P., Gokhan, S., Mehler, M. F., Conway, S. J., Ng, L. G., Stanley, E. R., Samokhvalov, I. M., & Merad, M. (2010). Fate mapping analysis reveals that adult microglia derive from primitive macrophages. *Science (New York, N.Y.)*, *330*(6005), 841–845. https://doi.org/10.1126/science.1194637

Goddard, G. v, McIntyre, D. C., & Leech, C. K. (1969). A permanent change in brain function resulting from daily electrical stimulation. *Experimental Neurology*, *25*(3), 295–330. https://doi.org/10.1016/0014-4886(69)90128-9

Golden, S. A., Covington, H. E., Berton, O., & Russo, S. J. (2011). A standardized protocol for repeated social defeat stress in mice. *Nature Protocols*, *6*(8), 1183–1191. https://doi.org/10.1038/nprot.2011.361

Golden, S. A., Heshmati, M., Flanigan, M., Christoffel, D. J., Guise, K., Pfau, M. L., Aleyasin, H., Menard, C., Zhang, H., Hodes, G. E., Bregman, D., Khibnik, L., Tai, J., Rebusi, N., Krawitz, B., Chaudhury, D., Walsh, J. J., Han, M.-H., Shapiro, M. L., & Russo, S. J. (2016). Basal forebrain projections to the lateral habenula modulate aggression reward. *Nature*, *534*(7609), 688–692. https://doi.org/10.1038/nature18601

Gouveia, K., & Hurst, J. L. (2017). Optimising reliability of mouse performance in behavioural testing: the major role of non-aversive handling. *Scientific Reports*, *7*, 44999. https://doi.org/10.1038/srep44999

Graham, F. K. (1975). Presidential Address, 1974. The more or less startling effects of weak prestimulation. *Psychophysiology*, *12*(3), 238–248. https://doi.org/10.1111/j.1469-8986.1975.tb01284.x
Greenberg, P. E., Fournier, A.-A., Sisitsky, T., Simes, M., Berman, R., Koenigsberg, S. H., & Kessler, R. C. (2021). The Economic Burden of Adults with Major Depressive Disorder in the United States (2010 and 2018). *PharmacoEconomics*, *39*(6), 653–665. https://doi.org/10.1007/s40273-021-01019-4

Greene, C., & Campbell, M. (2016). Tight junction modulation of the blood brain barrier: CNS delivery of small molecules. *Tissue Barriers*, *4*(1), e1138017. https://doi.org/10.1080/21688370.2015.1138017

Greene, C., Hanley, N., & Campbell, M. (2019). Claudin-5: gatekeeper of neurological function. *Fluids and Barriers of the CNS*, *16*(1), 3. https://doi.org/10.1186/s12987-019-0123-z

Greene, C., Hanley, N., & Campbell, M. (2020). Blood-brain barrier associated tight junction disruption is a hallmark feature of major psychiatric disorders. *Translational Psychiatry*, *10*(1), 373. https://doi.org/10.1038/s41398-020-01054-3

Greene, C., Hanley, N., Reschke, C. R., Reddy, A., Mäe, M. A., Connolly, R., Behan, C., O'Keeffe, E., Bolger, I., Hudson, N., Delaney, C., Farrell, M. A., O'Brien, D. F., Cryan, J., Brett, F. M., Beausang, A., Betsholtz, C., Henshall, D. C., Doherty, C. P., & Campbell, M. (2022). Microvascular stabilization via blood-brain barrier regulation prevents seizure activity. *Nature Communications*, *13*(1), 2003. https://doi.org/10.1038/s41467-022-29657-y

Greene, C., Kealy, J., Humphries, M. M., Gong, Y., Hou, J., Hudson, N., Cassidy, L. M., Martiniano, R., Shashi, V., Hooper, S. R., Grant, G. A., Kenna, P. F., Norris, K., Callaghan, C. K., Islam, M. dN, O'Mara, S. M., Najda, Z., Campbell, S. G., Pachter, J. S., … Campbell, M. (2018). Dose-dependent expression of claudin-5 is a modifying factor in schizophrenia. *Molecular Psychiatry*, *23*(11), 2156–2166. https://doi.org/10.1038/mp.2017.156

Guo, Y., Singh, L. N., Zhu, Y., Gur, R. E., Resnick, A., Anderson, S. A., & Alvarez, J. I. (2020). Association of a functional Claudin-5 variant with schizophrenia in female patients with the 22q11.2 deletion syndrome. *Schizophrenia Research*, *215*, 451–452. https://doi.org/10.1016/j.schres.2019.09.014

Gur, R. E., Kohler, C. G., Ragland, J. D., Siegel, S. J., Lesko, K., Bilker, W. B., & Gur, R. C. (2006). Flat affect in schizophrenia: relation to emotion processing and neurocognitive measures. *Schizophrenia Bulletin*, *32*(2), 279–287. https://doi.org/10.1093/schbul/sbj041

Halliday, M. R., Rege, S. v, Ma, Q., Zhao, Z., Miller, C. A., Winkler, E. A., & Zlokovic, B. v. (2016). Accelerated pericyte degeneration and blood-brain barrier breakdown in apolipoprotein E4 carriers with Alzheimer's disease. *Journal of Cerebral Blood Flow and Metabolism : Official Journal of the International Society of Cerebral Blood Flow and Metabolism*, *36*(1), 216–227. https://doi.org/10.1038/jcbfm.2015.44

Hallmann, R., Horn, N., Selg, M., Wendler, O., Pausch, F., & Sorokin, L. M. (2005). Expression and function of laminins in the embryonic and mature vasculature. *Physiological Reviews*, *85*(3), 979–1000. https://doi.org/10.1152/physrev.00014.2004

Hallmann, R., Horn, N., Selg, M., Wendler, O., Pausch, F., & Sorokin, L. M. (2005). Expression and function of laminins in the embryonic and mature vasculature. *Physiological Reviews*, *85*(3), 979–1000. https://doi.org/10.1152/physrev.00014.2004

Han, H., Mann, A., Ekstein, D., & Eyal, S. (2017). Breaking Bad: the Structure and Function of the Blood-Brain Barrier in Epilepsy. *The AAPS Journal*, *19*(4), 973–988. https://doi.org/10.1208/s12248-017-0096-2

Haseloff, R. F., Dithmer, S., Winkler, L., Wolburg, H., & Blasig, I. E. (2015). Transmembrane proteins of the tight junctions at the blood-brain barrier: structural and functional aspects. *Seminars in Cell & Developmental Biology*, *38*, 16–25. https://doi.org/10.1016/j.semcdb.2014.11.004

Hawkins, B. T., & Davis, T. P. (2005). The blood-brain barrier/neurovascular unit in health and disease. *Pharmacological Reviews*, *57*(2), 173–185. https://doi.org/10.1124/pr.57.2.4

He, X. P., Wen, R., & McNamara, J. O. (2014). Impairment of kindling development in phospholipase Cγ1 heterozygous mice. *Epilepsia*, *55*(3), 456–463. https://doi.org/10.1111/epi.12536

Heidbreder, C. A., Weiss, I. C., Domeney, A. M., Pryce, C., Homberg, J., Hedou, G., Feldon, J., Moran, M. C., & Nelson, P. (2000). Behavioral, neurochemical and endocrinological characterization of the early social isolation syndrome. *Neuroscience*, *100*(4), 749–768. https://doi.org/10.1016/s0306-4522(00)00336-5

Henke, P. G. (1990). Hippocampal pathway to the amygdala and stress ulcer development. *Brain Research Bulletin*, *25*(5), 691–695. https://doi.org/10.1016/0361-9230(90)90044-z

Herculano-Houzel, S. (2014). The glia/neuron ratio: How it varies uniformly across brain structures and species and what that means for brain physiology and evolution. *Glia*, *62*(9), 1377–1391. https://doi.org/10.1002/glia.22683

Herculano-Houzel, S., Manger, P. R., & Kaas, J. H. (2014). Brain scaling in mammalian evolution as a consequence of concerted and mosaic changes in numbers of neurons and average neuronal cell size. *Frontiers in Neuroanatomy*, *8*. https://doi.org/10.3389/fnana.2014.00077

Herman, S. T. (2002). Epilepsy after brain insult: targeting epileptogenesis. *Neurology*, *59*(9 Suppl 5), S21-6. https://doi.org/10.1212/wnl.59.9_suppl_5.s21

Hermann, D. M., & ElAli, A. (2012). The abluminal endothelial membrane in neurovascular remodelling in health and disease. *Science Signalling*, *5*(236), re4. https://doi.org/10.1126/scisignal.2002886

Higashi, T., Tokuda, S., Kitajiri, S., Masuda, S., Nakamura, H., Oda, Y., & Furuse, M. (2013). Analysis of the "angulin" proteins LSR, ILDR1 and ILDR2--tricellulin recruitment, epithelial barrier function and implication in deafness pathogenesis. *Journal of Cell Science*, *126*(Pt 4), 966–977. https://doi.org/10.1242/jcs.116442

Hikida, T., Jaaro-Peled, H., Seshadri, S., Oishi, K., Hookway, C., Kong, S., Wu, D., Xue, R., Andradé, M., Tankou, S., Mori, S., Gallagher, M., Ishizuka, K., Pletnikov, M., Kida, S., & Sawa, A. (2007). Dominant-negative DISC1 transgenic mice display schizophrenia-associated phenotypes detected by measures translatable to humans. *Proceedings of the National Academy of Sciences of the United States of America*, *104*(36), 14501–14506. https://doi.org/10.1073/pnas.0704774104

Hinderer, C., Katz, N., Buza, E. L., Dyer, C., Goode, T., Bell, P., Richman, L. K., & Wilson, J. M. (2018). Severe Toxicity in Nonhuman Primates and Piglets Following High-Dose Intravenous Administration of an Adeno-Associated Virus Vector Expressing Human SMN. *Human Gene Therapy*, *29*(3), 285–298. https://doi.org/10.1089/hum.2018.015

Hitti, F. L., & Siegelbaum, S. A. (2014). The hippocampal CA2 region is essential for social memory. *Nature*, *508*(7494), 88–92. https://doi.org/10.1038/nature13028

Hladky, S. B., & Barrand, M. A. (2016). Fluid and ion transfer across the blood–brain and blood–cerebrospinal fluid barriers; a comparative account of mechanisms and roles. *Fluids and Barriers of the CNS*, *13*(1), 19. https://doi.org/10.1186/s12987-016-0040-3

Hodes, G. E., Pfau, M. L., Leboeuf, M., Golden, S. A., Christoffel, D. J., Bregman, D., Rebusi, N., Heshmati, M., Aleyasin, H., Warren, B. L., Lebonté, B., Horn, S., Lapidus, K. A., Stelzhammer, V., Wong, E. H. F., Bahn, S.,… Russo, S. J. (2014). Individual differences in the peripheral immune system promote resilience versus susceptibility to social stress. *Proceedings of the National Academy of Sciences of the United States of America*, *111*(45), 16136–16141. https://doi.org/10.1073/pnas.1415191111

Hoekstra, S., Bartz-Johannessen, C., Sinkeviciute, I., Reitan, S. K., Kroken, R. A., Løberg, E.-M., Larsen, T. K., Rettenbacher, M., Johnsen, E., & Sommer, I. E. (2021). Sex differences in antipsychotic efficacy and side effects in schizophrenia spectrum disorder: results from the BeSt InTro study. *Npj Schizophrenia*, *7*(1), 39. https://doi.org/10.1038/s41537-021-00170-3

Hoenig, K., Hochrein, A., Quednow, B. B., Maier, W., & Wagner, M. (2005). Impaired prepulse inhibition of acoustic startle in obsessive-compulsive disorder. *Biological Psychiatry*, *57*(10), 1153–1158. https://doi.org/10.1016/j.biopsych.2005.01.040

Hoffman, H. S., & Ison, J. R. (1980). Reflex modification in the domain of startle: I. Some empirical findings and their implications for how the nervous system processes sensory input. *Psychological Review*, *87*(2), 175–189.

Hoosain, F. G., Choonara, Y. E., Tomar, L. K., Kumar, P., Tyagi, C., du Toit, L. C., & Pillay, V. (2015). Bypassing P-Glycoprotein Drug Efflux Mechanisms: Possible Applications in Pharmacoresistant Schizophrenia Therapy. *BioMed Research International*, *2015*, 484963. https://doi.org/10.1155/2015/484963

Hoshi, Y., Uchida, Y., Tachikawa, M., Inoue, T., Ohtsuki, S., & Terasaki, T. (2013). Quantitative atlas of blood-brain barrier transporters, receptors, and tight junction proteins in rats and common marmoset. *Journal of Pharmaceutical Sciences*, *102*(9), 3343–3355. https://doi.org/10.1002/jps.23575

Huang, X., Hussain, B., & Chang, J. (2021). Peripheral inflammation and blood-brain barrier disruption: effects and mechanisms. *CNS Neuroscience & Therapeutics*, *27*(1), 36–47. https://doi.org/10.1111/cns.13569

Hudson, N., Celkova, L., Hopkins, A., Greene, C., Storti, F., Ozaki, E., Fahey, E., Theodoropoulou, S., Kenna, P. F., Humphries, M. M., Curtis, A. M., Demmons, E., Browne, A., Liddie, S., Lawrence, M. S., Grimm, C., Cahill, M. T., Humphries, P., Doyle, S. L., & Campbell, M. (2019). Dysregulated claudin-5 cycling in the inner retina causes retinal pigment epithelial cell atrophy. *JCI Insight*, *4*(15). https://doi.org/10.1172/jci.insight.130273

Hurley, J. v, Anderson, R. M., & Sexton, P. T. (1981). The fate of plasma protein which escapes from blood vessels of the choroid plexus of the rat--an electron microscope study. *The Journal of Pathology*, *134*(1), 57–70. https://doi.org/10.1002/path.1711340107

Ikemura, T. (1985). Codon usage and tRNA content in unicellular and multicellular organisms. *Molecular Biology and Evolution*, *2*(1), 13–34. https://doi.org/10.1093/oxfordjournals.molbev.a040335

Ikenouchi, J., Furuse, M., Furuse, K., Sasaki, H., Tsukita, S., & Tsukita, S. (2005). Tricellulin constitutes a novel barrier at tricellular contacts of epithelial cells. *The Journal of Cell Biology*, *171*(6), 939–945. https://doi.org/10.1083/jcb.200510043

Itoh, K., Ishihara, Y., Komori, R., Nochi, H., Taniguchi, R., Chiba, Y., Ueno, M., Takata-Tsuji, F., Dohgu, S., & Kataoka, Y. (2016). Levetiracetam treatment influences blood-brain barrier failure associated with angiogenesis and inflammatory responses in the acute phase of epileptogenesis in post-status epilepticus mice. *Brain Research*, *1652*, 1–13. https://doi.org/10.1016/j.brainres.2016.09.038

Ivanova, E., Corona, C., Eleftheriou, C. G., Stout, R. F., Körbelin, J., & Sagdullaev, B. T. (2022). AAV-BR1 targets endothelial cells in the retina to reveal their morphological diversity and to deliver Cx43. *The Journal of Comparative Neurology*, *530*(8), 1302–1317. https://doi.org/10.1002/cne.25277

Iwamoto, N., Higashi, T., & Furuse, M. (2014). Localization of Angulin-1/LSR and Tricellulin at Tricellular Contacts of Brain and Retinal Endothelial Cells in vivo. In *CELL STRUCTURE AND FUNCTION* (Vol. 39).
Jaaro-Peled, H. (2009). Gene models of schizophrenia: DISC1 mouse models. *Progress in Brain Research*, *179*, 75–86. https://doi.org/10.1016/S0079-6123(09)17909-8

Jäkel, S., & Dimou, L. (2017). Glial Cells and Their Function in the Adult Brain: A Journey through the History of Their Ablation. *Frontiers in Cellular Neuroscience*, *11*, 24. https://doi.org/10.3389/fncel.2017.00024

Janzer, R. C., & Raff, M. C. (n.d.). Astrocytes induce blood-brain barrier properties in endothelial cells. *Nature*, *325*(6101), 253–257. https://doi.org/10.1038/325253a0

Javitt, D. C., & Zukin, S. R. (1991). Recent advances in the phencyclidine model of schizophrenia. *The American Journal of Psychiatry*, *148*(10), 1301–1308. https://doi.org/10.1176/ajp.148.10.1301

Jin, J.-F., Zhu, L.-L., Chen, M., Xu, H.-M., Wang, H.-F., Feng, X.-Q., Zhu, X.-P., & Zhou, Q. (2015). The optimal choice of medication administration route regarding intravenous, intramuscular, and subcutaneous injection. *Patient Preference and Adherence*, *9*, 923–942. https://doi.org/10.2147/PPA.S87271

Jobe, P. C., Picchioni, A. L., & Chin, L. (1973). Role of brain norepinephrine in audiogenic seizure in the rat. *The Journal of Pharmacology and Experimental Therapeutics*, *184*(1), 1–10.

Jobson, D. D., Hase, Y., Clarkson, A. N., & Kalaria, R. N. (2021). The role of the medial prefrontal cortex in cognition, ageing and dementia. In *Brain Communications* (Vol. 3, Issue 3). Oxford University Press. https://doi.org/10.1093/braincomms/fcab125

Johnstone, M., Thomson, P. A., Hall, J., McIntosh, A. M., Lawrie, S. M., & Porteous, D. J. (2011). DISC1 in schizophrenia: genetic mouse models and human genomic imaging. *Schizophrenia Bulletin*, *37*(1), 14–20. https://doi.org/10.1093/schbul/sbq135

Jones, C. A., Watson, D., Fone, K., & Fone, K. (2011). *Themed Issue: Translational Neuropharmacology-Using Appropriate Animal Models to Guide Clinical Drug Development Animal models of schizophrenia Correspondence LINKED ARTICLES*. https://doi.org/10.1111/bph.2011.164.issue-4

Jones, D. L., & Mogenson, G. J. (1980). Nucleus accumbens to globus pallidus GABA projection: electrophysiological and iontophoretic investigations. *Brain Research*, *188*(1), 93–105. https://doi.org/10.1016/0006-8993(80)90559-4

Kadakia, A., Catillon, M., Fan, Q., Williams, G. R., Marden, J. R., Anderson, A., Kirson, N., & Dembek, C. (2022). The Economic Burden of Schizophrenia in the United States. *The Journal of Clinical Psychiatry*, *83*(6). https://doi.org/10.4088/JCP.22m14458

Kaidanovich-Beilin, O., Lipina, T., Vukobradovic, I., Roder, J., & Woodgett, J. R. (2011). Assessment of social interaction behaviors. *Journal of Visualized Experiments : JoVE*, *48*. https://doi.org/10.3791/2473

Kalinichev, M., Robbins, M. J., Hartfield, E. M., Maycox, P. R., Moore, S. H., Savage, K. M., Austin, N. E., & Jones, D. N. C. (2008). Comparison between intraperitoneal and subcutaneous phencyclidine administration in Sprague-Dawley rats: a locomotor activity and gene induction study. *Progress in Neuro-Psychopharmacology & Biological Psychiatry*, *32*(2), 414–422. https://doi.org/10.1016/j.pnpbp.2007.09.008

Kalueff, A. v, & Tuohimaa, P. (2004). Grooming analysis algorithm for neurobehavioural stress research. *Brain Research Protocols*, *13*(3), 151–158. https://doi.org/10.1016/j.brainresprot.2004.04.002

Kalueff, A. v, Aldridge, J. W., LaPorte, J. L., Murphy, D. L., & Tuohimaa, P. (2007). Analyzing grooming microstructure in neurobehavioral experiments. *Nature Protocols*, *2*(10), 2538–2544. https://doi.org/10.1038/nprot.2007.367

Kalueff, A. v, Stewart, A. M., Song, C., Berridge, K. C., Graybiel, A. M., & Fentress, J. C. (2016). Neurobiology of rodent self-grooming and its value for translational neuroscience. *Nature Reviews. Neuroscience*, *17*(1), 45–59. https://doi.org/10.1038/nrn.2015.8

Kandel E.R., Schwartz J.H, Jessell T.M, Siegelbaum S.A, Hudspeth A.J., & Mack S(Eds.). (2014). *Principles of Neural Science,*.

Kandratavicius, L., Balista, P. A., Lopes-Aguiar, C., Ruggiero, R. N., Umeoka, E. H., Garcia-Cairasco, N., Bueno-Junior, L. S., & Leite, J. P. (2014). Animal models of epilepsy: use and limitations. *Neuropsychiatric Disease and Treatment*, *10*, 1693–1705. https://doi.org/10.2147/NDT.S50371

Kandratavicius, L., Rosa-Neto, P., Monteiro, M. R., Guiot, M.-C., Assirati, J. A., Carlotti, C. G., Kobayashi, E., & Leite, J. P. (2013). Distinct increased metabotropic glutamate receptor type 5 (mGluR5) in temporal lobe epilepsy with and without hippocampal sclerosis. *Hippocampus*, *23*(12), 1212–1230. https://doi.org/10.1002/hipo.22160

Kandratavicius, L., Ruggiero, R. N., Hallak, J. E., Garcia-Cairasco, N., & Leite, J. P. (2012). Pathophysiology of mood disorders in temporal lobe epilepsy. *Revista Brasileira de Psiquiatria (Sao Paulo, Brazil : 1999)*, *34 Suppl 2*, S233-45. https://doi.org/10.1016/j.rbp.2012.08.003

Kealy, J., Greene, C., & Campbell, M. (2018). Blood-brain barrier regulation in psychiatric disorders. *Neuroscience Letters*. https://doi.org/10.1016/J.NEULET.2018.06.033

Keaney, J., & Campbell, M. (2015). The dynamic blood-brain barrier. *FEBS Journal*, *282*(21), 4067–4079. https://doi.org/10.1111/febs.13412

Kelley, A. E., Baldo, B. A., Pratt, W. E., & Will, M. J. (2005). Corticostriatal-hypothalamic circuitry and food motivation: integration of energy, action and reward. *Physiology & Behavior*, *86*(5), 773–795. https://doi.org/10.1016/j.physbeh.2005.08.066

Kelly, P. H., Seviour, P. W., & Iversen, S. D. (1975). Amphetamine and apomorphine responses in the rat following 6-OHDA lesions of the nucleus accumbens septi and corpus striatum. *Brain Research*, *94*(3), 507–522. https://doi.org/10.1016/0006-8993(75)90233-4

Kessler, R. C., Chiu, W. T., Demler, O., Merikangas, K. R., & Walters, E. E. (2005). Prevalence, severity, and comorbidity of 12-month DSM-IV disorders in the National Comorbidity Survey Replication. *Archives of General Psychiatry*, *62*(6), 617–627. https://doi.org/10.1001/archpsyc.62.6.617

Kettenmann H., & Ransom B. R. (2005). *The Concept of Neuroglia: A Historical Perspective.Oxford: Oxford University Press.*

Kharatishvili, I., Nissinen, J. P., McIntosh, T. K., & Pitkänen, A. (2006). A model of posttraumatic epilepsy induced by lateral fluid-percussion brain injury in rats. *Neuroscience*, *140*(2), 685–697. https://doi.org/10.1016/j.neuroscience.2006.03.012

Kim, B. J., Hancock, B. M., Bermudez, A., del Cid, N., Reyes, E., van Sorge, N. M., Lauth, X., Smurthwaite, C. A., Hilton, B. J., Stotland, A., Banerjee, A., Buchanan, J., Wolkowicz, R., Traver, D., & Doran, K. S. (2015). Bacterial induction of Snail1 contributes to blood-brain barrier disruption. *The Journal of Clinical Investigation*, *125*(6), 2473–2483. https://doi.org/10.1172/JCI74159

Kisanuki, Y. Y., Hammer, R. E., Miyazaki, J. ichi, Williams, S. C., Richardson, J. A., & Yanagisawa, M. (2001). Tie2-Cre transgenic mice: A new model for endothelial cell-lineage analysis in vivo. *Developmental Biology*, *230*(2), 230–242. https://doi.org/10.1006/dbio.2000.0106

Knowland, D., Arac, A., Sekiguchi, K. J., Hsu, M., Lutz, S. E., Perrino, J., Steinberg, G. K., Barres, B. A., Nimmerjahn, A., & Agalliu, D. (2014). Stepwise recruitment of transcellular and paracellular pathways underlies blood-brain barrier breakdown in stroke. *Neuron*, *82*(3), 603–617. https://doi.org/10.1016/j.neuron.2014.03.003

Knox, E. G., Aburto, M. R., Clarke, G., Cryan, J. F., & O'Driscoll, C. M. (2022). The blood-brain barrier in aging and neurodegeneration. In *Molecular Psychiatry* (Vol. 27, Issue 6, pp. 2659–2673). Springer Nature. https://doi.org/10.1038/s41380-022-01511-z

Koerber, J. T., Klimczak, R., Jang, J.-H., Dalkara, D., Flannery, J. G., & Schaffer, D. v. (2009). Molecular evolution of adeno-associated virus for enhanced glial gene delivery. *Molecular Therapy : The Journal of the American Society of Gene Therapy*, *17*(12), 2088–2095. https://doi.org/10.1038/mt.2009.184

Komada, M., Takao, K., & Miyakawa, T. (2008). Elevated plus maze for mice. *Journal of Visualized Experiments : JoVE*, *22*. https://doi.org/10.3791/1088

Kondratov, R. v, Kondratova, A. A., Gorbacheva, V. Y., Vykhovanets, O. v, & Antoch, M. P. (2006). Early aging and age-related pathologies in mice deficient in BMAL1, the core componentof the circadian clock. *Genes & Development*, *20*(14), 1868–1873. https://doi.org/10.1101/gad.1432206

Koob, G. F., & Volkow, N. D. (2010). Neurocircuitry of Addiction. *Neuropsychopharmacology*, *35*(1), 217–238. https://doi.org/10.1038/npp.2009.110

Körbelin, J., Dogbevia, G., Michelfelder, S., Ridder, D. A., Hunger, A., Wenzel, J., Seismann, H., Lampe, M., Bannach, J., Pasparakis, M., Kleinschmidt, J. A., Schwaninger, M., & Trepel, M. (2016). A brain microvasculature endothelial cell-specific viral vector with the potential to treat neurovascular and neurological diseases. *EMBO Molecular Medicine*, *8*(6), 609–625. https://doi.org/10.15252/emmm.201506078

Kraeuter, A.-K., Guest, P. C., & Sarnyai, Z. (2019). The Y-Maze for Assessment of Spatial Working and Reference Memory in Mice. *Methods in Molecular Biology (Clifton, N.J.)*, *1916*, 105–111. https://doi.org/10.1007/978-1-4939-8994-2_10

Krämer, S. D., Abbott, N. J., & Begley, D. J. (2001). Biological Models to Study Blood-Brain Barrier Permeation. In *Pharmacokinetic Optimization in Drug Research* (pp. 127–153). Verlag Helvetica Chimica Acta. https://doi.org/10.1002/9783906390437.ch9

Krause, G., Winkler, L., Mueller, S. L., Haseloff, R. F., Piontek, J., & Blasig, I. E. (2008). Structure and function of claudins. *Biochimica et Biophysica Acta*, *1778*(3), 631–645. https://doi.org/10.1016/j.bbamem.2007.10.018

Krause, G., Winkler, L., Piehl, C., Blasig, I., Piontek, J., & Müller, S. L. (2009). Structure and function of extracellular claudin domains. *Annals of the New York Academy of Sciences*, *1165*, 34–43. https://doi.org/10.1111/j.1749-6632.2009.04057.x

Krishnan, V., & Nestler, E. J. (2008). The molecular neurobiology of depression. *Nature*, *455*(7215), 894–902. https://doi.org/10.1038/nature07455

Kuhnline Sloan, C. D., Nandi, P., Linz, T. H., Aldrich, J. v., Audus, K. L., & Lunte, S. M. (2012). Analytical and Biological Methods for Probing the Blood-Brain Barrier. *Annual Review of Analytical Chemistry*, *5*(1), 505–531. https://doi.org/10.1146/annurev-anchem-062011-143002

Kwan, P., Schachter, S. C., & Brodie, M. J. (2011). Drug-Resistant Epilepsy. *New England Journal of Medicine*, *365*(10), 919–926. https://doi.org/10.1056/NEJMra1004418

Kwon, I., & Schaffer, D. v. (2008). Designer gene delivery vectors: molecular engineering and evolution of adeno-associated viral vectors for enhanced gene transfer. *Pharmaceutical Research*, *25*(3), 489–499. https://doi.org/10.1007/s11095-007-9431-0

Lamas, M., González-Mariscal, L., & Gutiérrez, R. (2002). Presence of claudins mRNA in the brain. Selective modulation of expression by kindling epilepsy. *Brain Research. Molecular Brain Research*, *104*(2), 250–254. https://doi.org/10.1016/s0169-328x(02)00328-5

Lapiz, M. D. S., Fulford, A., Muchimapura, S., Mason, R., Parker, T., & Marsden, C. A. (2003). Influence of postweaning social isolation in the rat on brain development, conditioned behavior, and

neurotransmission. *Neuroscience and Behavioral Physiology*, *33*(1), 13–29. https://doi.org/10.1023/a:1021171129766

Lasoń, W., Dudra-Jastrzębska, M., Rejdak, K., & Czuczwar, S. J. (2011). Basic mechanisms of antiepileptic drugs and their pharmacokinetic/pharmacodynamic interactions: an update. *Pharmacological Reports : PR*, *63*(2), 271–292. https://doi.org/10.1016/s1734-1140(11)70497-2

LeBleu, V. S., Macdonald, B., & Kalluri, R. (2007). Structure and function of basement membranes. *Experimental Biology and Medicine (Maywood, N.J.)*, *232*(9), 1121–1129. https://doi.org/10.3181/0703-MR-72

Leger, M., Quiedeville, A., Bouet, V., Haelewyn, B., Boulouard, M., Schumann-Bard, P., & Freret, T. (2013). Object recognition test in mice. *Nature Protocols*, *8*(12), 2531–2537. https://doi.org/10.1038/nprot.2013.155

Lein, E. S., Hawrylycz, M. J., Ao, N., Ayres, M., Bensinger, A., Bernard, A., Boe, A. F., Boguski, M. S., Brockway, K. S., Byrnes, E. J., Chen, L., Chen, L., Chen, T.-M., Chin, M. C., Chong, J., Crook, B. E., … Jones, A. R. (2007). Genome-wide atlas of gene expression in the adult mouse brain. *Nature*, *445*(7124), 168–176. https://doi.org/10.1038/nature05453

Leite, J. P., & Cavalheiro, E. A. (1995). Effects of conventional antiepileptic drugs in a model of spontaneous recurrent seizures in rats. *Epilepsy Research*, *20*(2), 93–104. https://doi.org/10.1016/0920-1211(94)00070-d

Leite, J. P., Nakamura, E. M., Lemos, T., Masur, J., & Cavalheiro, E. A. (1990). Learning impairment in chronic epileptic rats following pilocarpine-induced status epilepticus. *Brazilian Journal of Medical and Biological Research = Revista Brasileira de Pesquisas Medicas e Biologicas*, *23*(8), 681–683.

Leucht, S., Corves, C., Arbter, D., Engel, R. R., Li, C., & Davis, J. M. (2009). Second-generation versus first-generation antipsychotic drugs for schizophrenia: a meta-analysis. *Lancet (London, England)*, *373*(9657), 31–41. https://doi.org/10.1016/S0140-6736(08)61764-X

Lévesque, M., & Avoli, M. (2013). The kainic acid model of temporal lobe epilepsy. *Neuroscience and Biobehavioral Reviews*, *37*(10 Pt 2), 2887–2899. https://doi.org/10.1016/j.neubiorev.2013.10.011

Lewandowsky M. (1900). Zur Lehre von der Cerebrospinalflüssgkeit. *Z. Clin. Med. 40, 4*, 480–494.

Li, C., & Samulski, R. J. (2020). Engineering adeno-associated virus vectors for gene therapy. *Nature Reviews Genetics*, *21*(4), 255–272. https://doi.org/10.1038/s41576-019-0205-4

Li, G.-W., Burkhardt, D., Gross, C., & Weissman, J. S. (2014). Quantifying absolute protein synthesis rates reveals principles underlying allocation of cellular resources. *Cell*, *157*(3), 624–635. https://doi.org/10.1016/j.cell.2014.02.033

Liddelow, S. A. (2011). Fluids and barriers of the CNS: a historical viewpoint. *Fluids and Barriers of the CNS*, *8*(1), 2. https://doi.org/10.1186/2045-8118-8-2

Lieberman, J. A., Stroup, T. S., McEvoy, J. P., Swartz, M. S., Rosenheck, R. A., Perkins, D. O., Keefe, R. S. E., Davis, S. M., Davis, C. E., Lebowitz, B. D., Severe, J., Hsiao, J. K., & Clinical Antipsychotic Trials of Intervention Effectiveness (CATIE) Investigators. (2005). Effectiveness of antipsychotic drugs in patients with chronic schizophrenia. *The New England Journal of Medicine*, *353*(12), 1209–1223. https://doi.org/10.1056/NEJMoa051688

Liebner, S., Corada, M., Bangsow, T., Babbage, J., Taddei, A., Czupalla, C. J., Reis, M., Felici, A., Wolburg, H., Fruttiger, M., Taketo, M. M., von Melchner, H., Plate, K. H., Gerhardt, H., & Dejana, E. (2008). Wnt/beta-catenin signaling controls development of the blood-brain barrier. *The Journal of Cell Biology*, *183*(3), 409–417. https://doi.org/10.1083/jcb.200806024

Liebner, S., Kniesel, U., Kalbacher, H., & Wolburg, H. (2000). Correlation of tight junction morphology with the expression of tight junction proteins in blood-brain barrier endothelial cells. *European Journal of Cell Biology*, *79*(10), 707–717. https://doi.org/10.1078/0171-9335-00101

Lin, J. H., & Yamazaki, M. (2003). Role of P-glycoprotein in pharmacokinetics: clinical implications. *Clinical Pharmacokinetics*, *42*(1), 59–98. https://doi.org/10.2165/00003088-200342010-00003

Lindahl, P., Johansson, B. R., Levéen, P., & Betsholtz, C. (1997). Pericyte loss and microaneurysm formation in PDGF-B-deficient mice. *Science (New York, N.Y.)*, *277*(5323), 242–245. https://doi.org/10.1126/science.277.5323.242

Lippoldt, A., Kniesel, U., Liebner, S., Kalbacher, H., Kirsch, T., Wolburg, H., & Haller, H. (2000). Structural alterations of tight junctions are associated with loss of polarity in stroke-prone spontaneously hypertensive rat blood-brain barrier endothelial cells. *Brain Research*, *885*(2), 251–261. https://doi.org/10.1016/s0006-8993(00)02954-1

Lipska, B. K., & Weinberger, D. R. (1993). Delayed effects of neonatal hippocampal damage on haloperidol-induced catalepsy and apomorphine-induced stereotypic behaviors in the rat. *Brain Research. Developmental Brain Research*, *75*(2), 213–222. https://doi.org/10.1016/0165-3806(93)90026-7

Liu, H., Heath, S. C., Sobin, C., Roos, J. L., Galke, B. L., Blundell, M. L., Lenane, M., Robertson, B., Wijsman, E. M., Rapoport, J. L., Gogos, J. A., & Karayiorgou, M. (2002). Genetic variation at the 22q11 PRODH2/DGCR6 locus presents an unusual pattern and increases susceptibility to schizophrenia. *Proceedings of the National Academy of Sciences of the United States of America*, *99*(6), 3717–3722. https://doi.org/10.1073/pnas.042700699

Liu, H., Li, Y., Lu, S., Wu, Y., & Sahi, J. (2014). Temporal expression of transporters and receptors in a rat primary co-culture blood-brain barrier model. *Xenobiotica; the Fate of Foreign Compounds in Biological Systems*, *44*(10), 941–951. https://doi.org/10.3109/00498254.2014.919430

Loew, R., Heinz, N., Hampf, M., Bujard, H., & Gossen, M. (2010). Improved Tet-responsive promoters with minimized background expression. *BMC Biotechnology*, *10*. https://doi.org/10.1186/1472-6750-10-81

Löscher, W., & Friedman, A. (2020). Structural, Molecular, and Functional Alterations of the Blood-Brain Barrier during Epileptogenesis and Epilepsy: A Cause, Consequence, or Both? *International Journal of Molecular Sciences*, *21*(2), 591. https://doi.org/10.3390/ijms21020591

Löscher, W., & Potschka, H. (2005). Drug resistance in brain diseases and the role of drug efflux transporters. *Nature Reviews. Neuroscience*, *6*(8), 591–602. https://doi.org/10.1038/nrn1728

Löscher, W., & Potschka, H. (2005). Role of drug efflux transporters in the brain for drug disposition and treatment of brain diseases. *Progress in Neurobiology*, *76*(1), 22–76. https://doi.org/10.1016/j.pneurobio.2005.04.006

Löscher, W., & Schmidt, D. (2011). Modern antiepileptic drug development has failed to deliver: ways out of the current dilemma. *Epilepsia*, *52*(4), 657–678. https://doi.org/10.1111/j.1528-1167.2011.03024.x

Luissint, A.-C., Artus, C., Glacial, F., Ganeshamoorthy, K., & Couraud, P.-O. (2012). Tight junctions at the blood brain barrier: physiological architecture and disease-associated dysregulation. *Fluids and Barriers of the CNS*, *9*(1), 23. https://doi.org/10.1186/2045-8118-9-23

Maher, F. , V. S. J. , S. I. A. (1994). Glucose transporter proteins in brain. *The FASEB Journal*, *8*(13), 1003–1011.

Maldonado-Irizarry, C. S., & Kelley, A. E. (1995). Excitatory amino acid receptors within nucleus accumbens subregions differentially mediate spatial learning in the rat. *Behavioural Pharmacology*, *6*(5 And 6), 527–539.

Maldonado-Irizarry, C. S., Swanson, C. J., & Kelley, A. E. (1995). Glutamate receptors in the nucleus accumbens shell control feeding behavior via the lateral hypothalamus. *The Journal of Neuroscience : The Official Journal of the Society for Neuroscience*, *15*(10), 6779–6788.

Mandel, I., Paperna, T., Volkowich, A., Merhav, M., Glass-Marmor, L., & Miller, A. (2012). The ubiquitin-proteasome pathway regulates claudin 5 degradation. *Journal of Cellular Biochemistry*, *113*(7), 2415–2423. https://doi.org/10.1002/jcb.24118

Mandillo, S., Tucci, V., Hölter, S. M., Meziane, H., Banchaabouchi, M. al, Kallnik, M., Lad, H. v, Nolan, P. M., Ouagazzal, A.-M., Coghill, E. L., Gale, K., Golini, E., Jacquot, S., Krezel, W., Parker, A., Riet, F., Schneider, I., … Wurst, W. (2008). Reliability, robustness, and reproducibility in mouse behavioral phenotyping: a cross-laboratory study. *Physiological Genomics*, *34*(3), 243–255. https://doi.org/10.1152/physiolgenomics.90207.2008

Mansbach, R. S., & Geyer, M. A. (1989). Effects of phencyclidine and phencyclidine biologs on sensorimotor gating in the rat. *Neuropsychopharmacology : Official Publication of the American College of Neuropsychopharmacology*, *2*(4), 299–308. https://doi.org/10.1016/0893-133x(89)90035-3

Marchetti, L., & Engelhardt, B. (2020). Immune cell trafficking across the blood-brain barrier in the absence and presence of neuroinflammation. *Vascular Biology*, *2*(1), H1–H18. https://doi.org/10.1530/VB-19-0033

Marchi, N., Angelov, L., Masaryk, T., Fazio, V., Granata, T., Hernandez, N., Hallene, K., Diglaw, T., Franic, L., Najm, I., & Janigro, D. (2007). Seizure-promoting effect of blood-brain barrier disruption. *Epilepsia*, *48*(4), 732–742. https://doi.org/10.1111/j.1528-1167.2007.00988.x

Marchi, N., Cavaglia, M., Fazio, V., Bhudia, S., Hallene, K., and Janigro, D. (2004). Peripheral markers of blood-brain barrier damage. Clin. Chim. Acta 342, 1–12.

Maren, S., & Fanselow, M. S. (1995). Synaptic plasticity in the basolateral amygdala induced by hippocampal formation stimulation in vivo. *The Journal of Neuroscience : The Official Journal of the Society for Neuroscience*, *15*(11), 7548–7564.

Marescaux, C., Vergnes, M., Kiesmann, M., Depaulis, A., Micheletti, G., & Warter, J. M. (1987). Kindling of audiogenic seizures in Wistar rats: an EEG study. *Experimental Neurology*, *97*(1), 160–168. https://doi.org/10.1016/0014-4886(87)90290-1

Martinez, Z. A., Ellison, G. D., Geyer, M. A., & Swerdlow, N. R. (1999). Effects of sustained phencyclidine exposure on sensorimotor gating of startle in rats. *Neuropsychopharmacology : Official Publication of the American College of Neuropsychopharmacology*, *21*(1), 28–39. https://doi.org/10.1016/S0893-133X(98)00137-7

Masuda, S., Oda, Y., Sasaki, H., Ikenouchi, J., Higashi, T., Akashi, M., Nishi, E., & Furuse, M. (2011). LSR defines cell corners for tricellular tight junction formation in epithelial cells. *Journal of Cell Science*, *124*(Pt 4), 548–555. https://doi.org/10.1242/jcs.072058

Mathern, G. W., Adelson, P. D., Cahan, L. D., & Leite, J. P. (2002). Hippocampal neuron damage in human epilepsy: Meyer's hypothesis revisited. *Progress in Brain Research*, *135*, 237–251. https://doi.org/10.1016/s0079-6123(02)35023-4

Maurice, T., Hiramatsu, M., Itoh, J., Kameyama, T., Hasegawa, T., & Nabeshima, T. (1994). Behavioral evidence for a modulating role of sigma ligands in memory processes. I. Attenuation of dizocilpine (MK-801)-induced amnesia. *Brain Research*, *647*(1), 44–56. https://doi.org/10.1016/0006-8993(94)91397-8

McConnell, H. L., Kersch, C. N., Woltjer, R. L., & Neuwelt, E. A. (2017). The Translational Significance of the Neurovascular Unit. *The Journal of Biological Chemistry*, *292*(3), 762–770. https://doi.org/10.1074/jbc.R116.760215

McGonigle, P., & Ruggeri, B. (2014). Animal models of human disease: challenges in enabling translation. *Biochemical Pharmacology*, *87*(1), 162–171. https://doi.org/10.1016/j.bcp.2013.08.006

MEIRAGTX . *RE: MeiraGTx Announces Acquisition of Vector Neurosciences, Gains Phase 2 Gene Therapy Program for Parkinson's Disease*, New York, NY: (2018).

Meltzer, H., Vostanis, P., Ford, T., Bebbington, P., & Dennis, M. S. (2011). Victims of bullying in childhood and suicide attempts in adulthood. *European Psychiatry : The Journal of the Association of European Psychiatrists*, *26*(8), 498–503. https://doi.org/10.1016/j.eurpsy.2010.11.006

Ménard, C., Hodes, G. E., & Russo, S. J. (2016). Pathogenesis of depression: Insights from human and rodent studies. In *Neuroscience* (Vol. 321, pp. 138–162). Elsevier Ltd. https://doi.org/10.1016/j.neuroscience.2015.05.053

Ménard, C., Pfau, M. L., Hodes, G. E., & Russo, S. J. (2017). Immune and Neuroendocrine Mechanisms of Stress Vulnerability and Resilience. *Neuropsychopharmacology : Official Publication of the American College of Neuropsychopharmacology*, *42*(1), 62–80. https://doi.org/10.1038/npp.2016.90

Menard, C., Pfau, M. L., Hodes, G. E., Kana, V., Wang, V. X., Bouchard, S., Takahashi, A., Flanigan, M. E., Aleyasin, H., Leclair, K. B., Janssen, W. G., Labonté, B., Parise, E. M., Lorsch, Z. S., Golden, S. A., Heshmati, M., Tamminga, C., Turecki, G., Campbell, M., … Russo, S. J. (2017). Social stress induces neurovascular pathology promoting depression. *Nature Neuroscience*, *20*(12), 1752–1760. https://doi.org/10.1038/s41593-017-0010-3

Mendell, J. R., Al-Zaidy, S. A., Rodino-Klapac, L. R., Goodspeed, K., Gray, S. J., Kay, C. N., Boye, S. L., Boye, S. E., George, L. A., Salabarria, S., Corti, M., Byrne, B. J., & Tremblay, J. P. (2021). Current Clinical Applications of In Vivo Gene Therapy with AAVs. *Molecular Therapy : The Journal of the American Society of Gene Therapy*, *29*(2), 464–488. https://doi.org/10.1016/j.ymthe.2020.12.007

Meredith, G. E., Agolia, R., Arts, M. P., Groenewegen, H. J., & Zahm, D. S. (1992). Morphological differences between projection neurons of the core and shell in the nucleus accumbens of the rat. *Neuroscience*, *50*(1), 149–162. https://doi.org/10.1016/0306-4522(92)90389-j

Meredith, G. E., Blank, B., & Groenewegen, H. J. (1989). The distribution and compartmental organization of the cholinergic neurons in nucleus accumbens of the rat. *Neuroscience*, *31*(2), 327–345. https://doi.org/10.1016/0306-4522(89)90377-1

Mesli, S., Javorschi, S., Bérard, A. M., Landry, M., Priddle, H., Kivlichan, D., Smith, A. J. H., Yen, F. T., Bihain, B. E., & Darmon, M. (2004). Distribution of the lipolysis stimulated receptor in adult and embryonic murine tissues and lethality of LSR-/- embryos at 12.5 to 14.5 days of gestation. *European Journal of Biochemistry*, *271*(15), 3103–3114. https://doi.org/10.1111/j.1432-1033.2004.04223.x

Michelfelder, S., Lee, M.-K., deLima-Hahn, E., Wilmes, T., Kaul, F., Müller, O., Kleinschmidt, J. A., & Trepel, M. (2007). Vectors selected from adeno-associated viral display peptide libraries for leukemia cell-targeted cytotoxic gene therapy. *Experimental Hematology*, *35*(12), 1766–1776. https://doi.org/10.1016/j.exphem.2007.07.018

Milsted, A., Barna, B. P., Ransohoff, R. M., Brosnihan, K. B., & Ferrario, C. M. (1990). Astrocyte cultures derived from human brain tissue express angiotensinogen mRNA. *Proceedings of the National Academy of Sciences*, *87*(15), 5720–5723. https://doi.org/10.1073/pnas.87.15.5720

Miyake, N., Miyake, K., Yamamoto, M., Hirai, Y., & Shimada, T. (2011). Global gene transfer into the CNS across the BBB after neonatal systemic delivery of single-stranded AAV vectors. *Brain Research*, *1389*, 19–26. https://doi.org/10.1016/j.brainres.2011.03.014

Montagne, A., Barnes, S. R., Sweeney, M. D., Halliday, M. R., Sagare, A. P., Zhao, Z., Toga, A. W., Jacobs, R. E., Liu, C. Y., Amezcua, L., Harrington, M. G., Chui, H. C., Law, M., & Zlokovic, B. v. (2015). Blood-brain barrier breakdown in the aging human hippocampus. *Neuron*, *85*(2), 296–302. https://doi.org/10.1016/j.neuron.2014.12.032

Moons, C. P. H., van Wiele, P., & Odberg, F. O. (2004). To enrich or not to enrich: providing shelter does not complicate handling of laboratory mice. *Contemporary Topics in Laboratory Animal Science*, *43*(4), 18–21.

Morin-Brureau, M., Lebrun, A., Rousset, M.-C., Fagni, L., Bockaert, J., de Bock, F., & Lerner-Natoli, M. (2011). Epileptiform activity induces vascular remodeling and zonula occludens 1 downregulation in organotypic hippocampal cultures: role of VEGF signalling pathways. *The Journal of Neuroscience : The Official Journal of the Society for Neuroscience*, *31*(29), 10677–10688. https://doi.org/10.1523/JNEUROSCI.5692-10.2011

Morita, K., Sasaki, H., Furuse, M., & Tsukita, S. (1999). Endothelial claudin: claudin-5/TMVCF constitutes tight junction strands in endothelial cells. *The Journal of Cell Biology*, *147*(1), 185–194. https://doi.org/10.1083/jcb.147.1.185

Moser, M. B., & Moser, E. I. (1998). Functional differentiation in the hippocampus. *Hippocampus*, *8*(6), 608–619. https://doi.org/10.1002/(SICI)1098-1063(1998)8:6<608::AID-HIPO3>3.0.CO;2-7

Moser, M. B., Moser, E. I., Forrest, E., Andersen, P., & Morris, R. G. (1995). Spatial learning with a minislab in the dorsal hippocampus. *Proceedings of the National Academy of Sciences of the United States of America*, *92*(21), 9697–9701. https://doi.org/10.1073/pnas.92.21.9697

Müller, O. J., Kaul, F., Weitzman, M. D., Pasqualini, R., Arap, W., Kleinschmidt, J. A., & Trepel, M. (2003). Random peptide libraries displayed on adeno-associated virus to select for targeted gene therapy vectors. *Nature Biotechnology*, *21*(9), 1040–1046. https://doi.org/10.1038/nbt856

Münch, R. C., Janicki, H., Völker, I., Rasbach, A., Hallek, M., Büning, H., & Buchholz, C. J. (2013). Displaying high-affinity ligands on adeno-associated viral vectors enables tumor cell-specific and safe gene transfer. *Molecular Therapy : The Journal of the American Society of Gene Therapy*, *21*(1), 109–118. https://doi.org/10.1038/mt.2012.186

Murakami S, Takemoto T, & Shimizu S. (1953). Studies on the effective principles of Diagenea simplex Aq. I Separation of the effective fraction by liquid chromatography. *Journal of the Pharmaceutical Society of Japan 73.9*, 1026-1028.

Naso, M. F., Tomkowicz, B., Perry, W. L., & Strohl, W. R. (2017). Adeno-Associated Virus (AAV) as a Vector for Gene Therapy. *BioDrugs : Clinical Immunotherapeutics, Biopharmaceuticals and Gene Therapy*, *31*(4), 317–334. https://doi.org/10.1007/s40259-017-0234-5

Nestler, E. J., & Hyman, S. E. (2010). Animal models of neuropsychiatric disorders. In *Nature Neuroscience* (Vol. 13, Issue 10, pp. 1161–1169). Nature Publishing Group. https://doi.org/10.1038/nn.2647

Netser, S., Haskal, S., Magalnik, H., & Wagner, S. (2017). A novel system for tracking social preference dynamics in mice reveals sex- and strain-specific characteristics. *Molecular Autism*, *8*(1), 53. https://doi.org/10.1186/s13229-017-0169-1

Neuhaus, J. (1990). Orthogonal arrays of particles in astroglial cells: quantitative analysis of their density, size, and correlation with intramembranous particles. *Glia*, *3*(4), 241–251. https://doi.org/10.1002/glia.440030403

Neuwelt, E. A., Frenkel, E. P., Gumerlock, M. K., Braziel, R., Dana, B., & Hill, S. A. (1986). Developments in the diagnosis and treatment of primary CNS lymphoma: A prospective series. *Cancer*, *58*(8), 1609–1620. https://doi.org/10.1002/1097-0142(19861015)58:8<1609::AID-CNCR2820580805>3.0.CO;2-7

Neuwelt, E. A., Glasberg, M., Frenkel, E., & Barnett, P. (1983). Neurotoxicity of chemotherapeutic agents after blood-brain barrier modification: neuropathological studies. *Annals of Neurology*, *14*(3), 316–324. https://doi.org/10.1002/ana.410140310

Neuwelt, E. A., Specht, H. D., Howieson, J., Haines, J. E., Bennett, M. J., Hill, S. A., & Frenkel, E. P. (1983). Osmotic blood-brain barrier modification: clinical documentation by enhanced CT scanning and/or radionuclide brain scanning. *AJR. American Journal of Roentgenology*, *141*(4), 829–835. https://doi.org/10.2214/ajr.141.4.829

Nimmerjahn, A., Kirchhoff, F., & Helmchen, F. (2005). Resting microglial cells are highly dynamic surveillants of brain parenchyma in vivo. *Science (New York, N.Y.)*, *308*(5726), 1314–1318. https://doi.org/10.1126/science.1110647

Nishiura, K., Ichikawa-Tomikawa, N., Sugimoto, K., Kunii, Y., Kashiwagi, K., Tanaka, M., Yokoyama, Y., Hino, M., Sugino, T., Yabe, H., Takahashi, H., Kakita, A., Imura, T., & Chiba, H. (2017). PKA activation and endothelial claudin-5 breakdown in the schizophrenic prefrontal cortex. *Oncotarget*, *8*(55), 93382–93391. https://doi.org/10.18632/oncotarget.21850

Nitta, T., Hata, M., Gotoh, S., Seo, Y., Sasaki, H., Hashimoto, N., Furuse, M., & Tsukita, S. (2003). Size-selective loosening of the blood-brain barrier in claudin-5-deficient mice. *The Journal of Cell Biology*, *161*(3), 653–660. https://doi.org/10.1083/jcb.200302070

Nó, R. L. (1934). Studies on the structure of the cerebral cortex. II. Continuation of the study of the ammonic system. *Journal Für Psychologie Und Neurologie*, *46*, 113–175.

Nobis, A., Zalewski, D., & Waszkiewicz, N. (2020). Peripheral Markers of Depression. *Journal of Clinical Medicine*, *9*(12). https://doi.org/10.3390/jcm9123793

Oberheim, N. A., Tian, G.-F., Han, X., Peng, W., Takano, T., Ransom, B., & Nedergaard, M. (2008). Loss of astrocytic domain organization in the epileptic brain. *The Journal of Neuroscience : The Official Journal of the Society for Neuroscience*, *28*(13), 3264–3276. https://doi.org/10.1523/JNEUROSCI.4980-07.2008

Obermeier, B., Daneman, R., & Ransohoff, R. M. (2013). Development, maintenance and disruption of the blood-brain barrier. *Nature Medicine*, *19*(12), 1584–1596. https://doi.org/10.1038/nm.3407

Ohtsuki, S., Sato, S., Yamaguchi, H., Kamoi, M., Asashima, T., & Terasaki, T. (2007). Exogenous expression of claudin-5 induces barrier properties in cultured rat brain capillary endothelial cells. *Journal of Cellular Physiology*, *210*(1), 81–86. https://doi.org/10.1002/jcp.20823

Ohtsuki, S., Yamaguchi, H., Katsukura, Y., Asashima, T., & Terasaki, T. (2008). mRNA expression levels of tight junction protein genes in mouse brain capillary endothelial cells highly purified by magnetic cell sorting. *Journal of Neurochemistry*, *104*(1), 147–154. https://doi.org/10.1111/j.1471-4159.2007.05008.x

Oldendorf, W. H., & Brown, W. J. (1975). Greater number of capillary endothelial cell mitochondria in brain than in muscle. *Proceedings of the Society for Experimental Biology and Medicine. Society for Experimental Biology and Medicine (New York, N.Y.)*, *149*(3), 736–738. https://doi.org/10.3181/00379727-149-38889

Olney, J. W., & Farber, N. B. (1995). Glutamate receptor dysfunction and schizophrenia. *Archives of General Psychiatry*, *52*(12), 998–1007. https://doi.org/10.1001/archpsyc.1995.03950240016004

Osterloh, J. M., Yang, J., Rooney, T. M., Fox, A. N., Adalbert, R., Powell, E. H., Sheehan, A. E., Avery, M. A., Hackett, R., Logan, M. A., MacDonald, J. M., Ziegenfuss, J. S.,… Freeman, M. R. (2012). dSarm/Sarm1 is required for activation of an injury-induced axon death pathway. *Science (New York, N.Y.)*, *337*(6093), 481–484. https://doi.org/10.1126/science.1223899

Paolicelli, R. C., Bolasco, G., Pagani, F., Maggi, L., Scianni, M., Panzanelli, P., Giustetto, M., Ferreira, T. A., Guiducci, E., Dumas, L., Ragozzino, D., & Gross, C. T. (2011). Synaptic pruning by microglia is necessary for normal brain development. *Science (New York, N.Y.)*, *333*(6048), 1456–1458. https://doi.org/10.1126/science.1202529

Pardridge, W. M. (2005). The blood-brain barrier: bottleneck in brain drug development. *NeuroRx : The Journal of the American Society for Experimental NeuroTherapeutics*, *2*(1), 3–14. https://doi.org/10.1602/neurorx.2.1.3

Pardridge, W. M. (2009). Alzheimer's disease drug development and the problem of the blood-brain barrier. *Alzheimer's & Dementia : The Journal of the Alzheimer's Association*, *5*(5), 427–432. https://doi.org/10.1016/j.jalz.2009.06.003

Pardridge, W. M. (2010). Biopharmaceutical drug targeting to the brain. *Journal of Drug Targeting*, *18*(3), 157–167. https://doi.org/10.3109/10611860903548354

Parkinson, J. A., Willoughby, P. J., Robbins, T. W., & Everitt, B. J. (2000). Disconnection of the anterior cingulate cortex and nucleus accumbens core impairs Pavlovian approach behavior: further evidence for limbic cortical-ventral striatopallidal systems. *Behavioral Neuroscience*, *114*(1), 42–63.

Pauli, E., Hildebrandt, M., Romstöck, J., Stefan, H., & Blümcke, I. (2006). Deficient memory acquisition in temporal lobe epilepsy is predicted by hippocampal granule cell loss. *Neurology*, *67*(8), 1383–1389. https://doi.org/10.1212/01.wnl.0000239828.36651.73

Paxinos, G., & Franklin, K. B. J. (2001). *The mouse brain in stereotaxic coordinates: hard cover edition.*

Perry, W., Minassian, A., Feifel, D., & Braff, D. L. (2001). Sensorimotor gating deficits in bipolar disorder patients with acute psychotic mania. *Biological Psychiatry*, *50*(6), 418–424. https://doi.org/10.1016/s0006-3223(01)01184-2

Perry, W., Minassian, A., Lopez, B., Maron, L., & Lincoln, A. (2007). Sensorimotor gating deficits in adults with autism. *Biological Psychiatry*, *61*(4), 482–486. https://doi.org/10.1016/j.biopsych.2005.09.025

Perucca, E., French, J., & Bialer, M. (2007). Development of new antiepileptic drugs: challenges, incentives, and recent advances. *The Lancet Neurology*, *6*(9), 793–804. https://doi.org/10.1016/S1474-4422(07)70215-6

Phillips, M., Wang, C., & Johnson, K. M. (2001). Pharmacological characterization of locomotor sensitization induced by chronic phencyclidine administration. *The Journal of Pharmacology and Experimental Therapeutics*, *296*(3), 905–913.

Pinel, J. P., & Treit, D. (1978). Burying as a defensive response in rats. *Journal of Comparative and Physiological Psychology*, *92*(4), 708–712. https://doi.org/10.1037/h0077494

Piontek, J., Winkler, L., Wolburg, H., Müller, S. L., Zuleger, N., Piehl, C., Wiesner, B., Krause, G., & Blasig, I. E. (2008). Formation of tight junction: determinants of homophilic interaction between classic claudins. *FASEB Journal : Official Publication of the Federation of American Societies for Experimental Biology*, *22*(1), 146–158. https://doi.org/10.1096/fj.07-8319com

Pitkänen, A., & McIntosh, T. K. (2006). Animal models of post-traumatic epilepsy. *Journal of Neurotrauma*, *23*(2), 241–261. https://doi.org/10.1089/neu.2006.23.241

Pitkänen, A., Immonen, R. J., Gröhn, O. H. J., & Kharatishvili, I. (2009). From traumatic brain injury to posttraumatic epilepsy: what animal models tell us about the process and treatment options. *Epilepsia*, *50 Suppl 2*, 21–29. https://doi.org/10.1111/j.1528-1167.2008.02007.x

Pitkänen, A., Lukasiuk, K., Dudek, F. E., & Staley, K. J. (2015). Epileptogenesis. *Cold Spring Harbor Perspectives in Medicine*, *5*(10). https://doi.org/10.1101/cshperspect.a022822

Pletnikov, M. v, Ayhan, Y., Xu, Y., Nikolskaia, O., Ovanesov, M., Huang, H., Mori, S., Moran, T. H., & Ross, C. A. (2008). Enlargement of the lateral ventricles in mutant DISC1 transgenic mice. *Molecular Psychiatry*, *13*(2), 115. https://doi.org/10.1038/sj.mp.4002144

Pong, A. W., Geary, B. R., Engelstad, K. M., Natarajan, A., Yang, H., & de Vivo, D. C. (2012). Glucose transporter type I deficiency syndrome: epilepsy phenotypes and outcomes. *Epilepsia*, *53*(9), 1503–1510. https://doi.org/10.1111/j.1528-1167.2012.03592.x

Potkin, S. G., Kane, J. M., Correll, C. U., Lindenmayer, J.-P., Agid, O., Marder, S. R., Olfson, M., & Howes, O. D. (2020). The neurobiology of treatment-resistant schizophrenia: paths to antipsychotic resistance and a roadmap for future research. *Npj Schizophrenia*, *6*(1), 1. https://doi.org/10.1038/s41537-019-0090-z

Prinz, M., & Priller, J. (2014). Microglia and brain macrophages in the molecular age: from origin to neuropsychiatric disease. *Nature Reviews. Neuroscience*, *15*(5), 300–312. https://doi.org/10.1038/nrn3722

Pulver, A. E. (2000). Search for schizophrenia susceptibility genes. *Biological Psychiatry*, *47*(3), 221–230. https://doi.org/10.1016/s0006-3223(99)00281-4

Qiao, H., Noda, Y., Kamei, H., Nagai, T., Furukawa, H., Miura, H., Kayukawa, Y., Ohta, T., & Nabeshima, T. (2001). Clozapine, but not haloperidol, reverses social behavior deficit in mice during withdrawal from chronic phencyclidine treatment. *Neuroreport*, *12*(1), 11–15. https://doi.org/10.1097/00001756-200101220-00010

Raichle, M. E., & Gusnard, D. A. (2002). Appraising the brain's energy budget. *Proceedings of the National Academy of Sciences of the United States of America*, *99*(16), 10237–10239. https://doi.org/10.1073/pnas.172399499

Rapti, K., Louis-Jeune, V., Kohlbrenner, E., Ishikawa, K., Ladage, D., Zolotukhin, S., Hajjar, R. J., & Weber, T. (2012). Neutralizing antibodies against AAV serotypes 1, 2, 6, and 9 in sera of commonly used animal models. *Molecular Therapy : The Journal of the American Society of Gene Therapy*, *20*(1), 73–83. https://doi.org/10.1038/mt.2011.177

Reaves, D. K., Hoadley, K. A., Fagan-Solis, K. D., Jima, D. D., Bereman, M., Thorpe, L., Hicks, J., McDonald, D., Troester, M. A., Perou, C. M., & Fleming, J. M. (2017). Nuclear Localized LSR: A Novel Regulator of Breast Cancer Behavior and Tumorigenesis. *Molecular Cancer Research*, *15*(2), 165–178. https://doi.org/10.1158/1541-7786.MCR-16-0085-T

Rees, E., Kirov, G., Sanders, A., Walters, J. T. R., Chambert, K. D., Shi, J., Szatkiewicz, J., O'Dushlaine, C., Richards, A. L., Green, E. K., Jones, I., Davies, G., Legge, S. E., Moran, J. L., Pato, C., Pato, M., Genovese, G., Levinson, D., Duan, J., … Owen, M. J. (2014). Evidence that duplications of 22q11.2 protect against schizophrenia. *Molecular Psychiatry*, *19*(1), 37–40. https://doi.org/10.1038/mp.2013.156

Rempe, R. G., Hartz, A. M. S., Soldner, E. L. B., Sokola, B. S., Alluri, S. R., Abner, E. L., Kryscio, R. J., Pekcec, A., Schlichtiger, J., & Bauer, B. (2018). Matrix Metalloproteinase-Mediated Blood-Brain Barrier Dysfunction in Epilepsy. *The Journal of Neuroscience : The Official Journal of the Society for Neuroscience*, *38*(18), 4301–4315. https://doi.org/10.1523/JNEUROSCI.2751-17.2018

Rice, A. M., & McLysaght, A. (2017). Dosage-sensitive genes in evolution and disease. *BMC Biology*, *15*(1), 78. https://doi.org/10.1186/s12915-017-0418-y

Rist, R. J., Romero, I. A., Chan, M. W. K., Couraud, P.-O., Roux, F., & Abbott, N. J. (1997). F-Actin cytoskeleton and sucrose permeability of immortalised rat brain microvascular endothelial cell monolayers: effects of cyclic AMP and astrocytic factors. *Brain Research*, *768*(1–2), 10–18. https://doi.org/10.1016/S0006-8993(97)00586-6

Rist, R. J., Romero, I. A., Chan, M. W. K., Couraud, P.-O., Roux, F., & Abbott, N. J. (1997). F-Actin cytoskeleton and sucrose permeability of immortalised rat brain microvascular endothelial cell monolayers: effects of cyclic AMP and astrocytic factors. *Brain Research*, *768*(1–2), 10–18. https://doi.org/10.1016/S0006-8993(97)00586-6

Roberts, M. D., Gilpin, L., Parker, K. E., Childs, T. E., Will, M. J., & Booth, F. W. (2012). Dopamine D1 receptor modulation in nucleus accumbens lowers voluntary wheel running in rats bred to run high distances. *Physiology & Behavior*, *105*(3), 661–668. https://doi.org/10.1016/j.physbeh.2011.09.024

Roman-Goldstein, S., Clunie, D. A., Stevens, J., Hogan, R., Monard, J., Ramsey, F., & Neuwelt, E. A. (1994). Osmotic blood-brain barrier disruption: CT and radionuclide imaging. *AJNR. American Journal of Neuroradiology*, *15*(3), 581–590.

Roney, I. J., Rudner, A. D., Couture, J. F., & Kærn, M. (2016). Improvement of the reverse tetracycline transactivator by single amino acid substitutions that reduce leaky target gene expression to undetectable levels. *Scientific Reports*, *6*. https://doi.org/10.1038/srep27697

Ronzitti, G., Gross, D.-A., & Mingozzi, F. (2020). Human Immune Responses to Adeno-Associated Virus (AAV) Vectors. *Frontiers in Immunology*, *11*. https://doi.org/10.3389/fimmu.2020.00670

Ross, K. C., & Coleman, J. R. (2000). Developmental and genetic audiogenic seizure models: behavior and biological substrates. *Neuroscience and Biobehavioral Reviews*, *24*(6), 639–653. https://doi.org/10.1016/s0149-7634(00)00029-4

Rossa, J., Ploeger, C., Vorreiter, F., Saleh, T., Protze, J., Günzel, D., Wolburg, H., Krause, G., & Piontek, J. (2014). Claudin-3 and claudin-5 protein folding and assembly into the tight junction are controlled by non-

conserved residues in the transmembrane 3 (TM3) and extracellular loop 2 (ECL2) segments. *The Journal of Biological Chemistry*, *289*(11), 7641–7653. https://doi.org/10.1074/jbc.M113.531012

Roudnicky, F., Zhang, J. D., Kim, B. K., Pandya, N. J., Lan, Y., Sach-Peltason, L., Ragelle, H., Strassburger, P., Gruener, S., Lazendic, M., Uhles, S., Revelant, F., Eidam, O., Sturm, G., Kueppers, V., Christensen, K., Goldstein, L. D., Tzouros, M., Banfai, B., … Cowan, C. A. (2020). Inducers of the endothelial cell barrier identified through chemogenomic screening in genome-edited hPSC-endothelial cells. *Proceedings of the National Academy of Sciences of the United States of America*, *117*(33), 19854–19865. https://doi.org/10.1073/pnas.1911532117

Rubin, L. L., Hall, D. E., Porter, S., Barbu, K., Cannon, C., Horner, H. C., Janatpour, M., Liaw, C. W., Manning,
K., & Morales, J. (1991). A cell culture model of the blood-brain barrier. *The Journal of Cell Biology*, *115*(6), 1725–1735. https://doi.org/10.1083/jcb.115.6.1725

Rubin, R. D., Watson, P. D., Duff, M. C., & Cohen, N. J. (2014). The role of the hippocampus in flexible cognition and social behavior. *Frontiers in Human Neuroscience*, *8*, 742. https://doi.org/10.3389/fnhum.2014.00742

Saha, S., Chant, D., & McGrath, J. (2007). A systematic review of mortality in schizophrenia: is the differential mortality gap worsening over time? *Archives of General Psychiatry*, *64*(10), 1123–1131. https://doi.org/10.1001/archpsyc.64.10.1123

Saitou, M., Fujimoto, K., Doi, Y., Itoh, M., Fujimoto, T., Furuse, M., Takano, H., Noda, T., & Tsukita, S. (1998). Occludin-deficient embryonic stem cells can differentiate into polarized epithelial cells bearing tight junctions. *The Journal of Cell Biology*, *141*(2), 397–408. https://doi.org/10.1083/jcb.141.2.397

Saitou, M., Furuse, M., Sasaki, H., Schulzke, J. D., Fromm, M., Takano, H., Noda, T., & Tsukita, S. (2000). Complex phenotype of mice lacking occludin, a component of tight junction strands. *Molecular Biology of the Cell*, *11*(12), 4131–4142. https://doi.org/10.1091/mbc.11.12.4131

Salloway, S., Gur, T., Berzin, T., Tavares, R., Zipser, B., Correia, S., Hovanesian, V., Fallon, J., Kuo-Leblanc, V., Glass, D., Hulette, C., Rosenberg, C., Vitek, M., & Stopa, E. (2002). Effect of APOE genotype on microvascular basement membrane in Alzheimer's disease. *Journal of the Neurological Sciences*, *203–204*, 183–187. https://doi.org/10.1016/s0022-510x(02)00288-5

Sams-Dodd, F. (1995). Distinct effects of d-amphetamine and phencyclidine on the social behaviour of rats. *Behavioural Pharmacology*, *6*(1), 55–65.

Sams-Dodd, F., Lipska, B. K., & Weinberger, D. R. (1997). Neonatal lesions of the rat ventral hippocampus result in hyperlocomotion and deficits in social behaviour in adulthood. *Psychopharmacology*, *132*(3), 303–310. https://doi.org/10.1007/s002130050349

Saunders, N. R., Dreifuss, J.-J., Dziegielewska, K. M., Johansson, P. A., Habgood, M. D., Møllgård, K., & Bauer, H.-C. (2014). The rights and wrongs of blood-brain barrier permeability studies: a walk through 100 years of history. *Frontiers in Neuroscience*, *8*, 404. https://doi.org/10.3389/fnins.2014.00404

Saunders, N. R., Liddelow, S. A., & Dziegielewska, K. M. (2012). Barrier mechanisms in the developing brain. *Frontiers in Pharmacology*, *3*, 46. https://doi.org/10.3389/fphar.2012.00046

Sayin, U., Osting, S., Hagen, J., Rutecki, P., & Sutula, T. (2003). Spontaneous seizures and loss of axo-axonic and axo-somatic inhibition induced by repeated brief seizures in kindled rats. *The Journal of Neuroscience : The Official Journal of the Society for Neuroscience*, *23*(7), 2759–2768.

Schaffer, D. v, Koerber, J. T., & Lim, K. (2008). Molecular engineering of viral gene delivery vehicles. *Annual Review of Biomedical Engineering*, *10*, 169–194. https://doi.org/10.1146/annurev.bioeng.10.061807.160514

Scheffer, I. E., Berkovic, S., Capovilla, G., Connolly, M. B., French, J., Guilhoto, L., Hirsch, E., Jain, S., Mathern, G. W., Moshé, S. L., Nordli, D. R., Perucca, E., Tomson, T., Wiebe, S., Zhang, Y.-H., & Zuberi, S.

M. (2017). ILAE classification of the epilepsies: Position paper of the ILAE Commission for Classification and Terminology. *Epilepsia*, *58*(4), 512–521. https://doi.org/10.1111/epi.13709

Schinkel, A. H., Mayer, U., Wagenaar, E., Mol, C. A., van Deemter, L., Smit, J. J., van der Valk, M. A., Voordouw, A. C., Spits, H., van Tellingen, O., Zijlmans, J. M., Fibbe, W. E., & Borst, P. (1997). Normal viability and altered pharmacokinetics in mice lacking mdr1-type (drug-transporting) P-glycoproteins. *Proceedings of the National Academy of Sciences of the United States of America*, *94*(8), 4028–4033. https://doi.org/10.1073/pnas.94.8.4028

Schinkel, A. H., Smit, J. J., van Tellingen, O., Beijnen, J. H., Wagenaar, E., van Deemter, L., Mol, C. A., van der Valk, M. A., Robanus-Maandag, E. C., & te Riele, H. P. (1994). Disruption of the mouse mdr1a P-glycoprotein gene leads to a deficiency in the blood-brain barrier and to increased sensitivity to drugs. *Cell*, *77*(4), 491–502. https://doi.org/10.1016/0092-8674(94)90212-7

Schizophrenia Working Group of the Psychiatric Genomics Consortium. (2014). Biological insights from 108 schizophrenia-associated genetic loci. *Nature*, *511*(7510), 421–427. https://doi.org/10.1038/nature13595

Schlageter, K. E., Molnar, P., Lapin, G. D., & Groothuis, D. R. (1999). Microvessel organization and structure in experimental brain tumors: microvessel populations with distinctive structural and functional properties. *Microvascular Research*, *58*(3), 312–328. https://doi.org/10.1006/mvre.1999.2188

Schlingmann, B., Molina, S. A., & Koval, M. (2015). Claudins: Gatekeepers of lung epithelial function. *Seminars in Cell & Developmental Biology*, *42*, 47–57. https://doi.org/10.1016/j.semcdb.2015.04.009

Schroeter, M.L., Abdul-Khaliq, H., Krebs, M., Diefenbacher, A., and Blasig, I.E. (2008). Serum markers support disease-specific glial pathology in major depression. J. Affect. Disord. 111, 271–280.

Scoville, W. B., & Milner, B. (1957). Loss of recent memory after bilateral hippocampal lesions. *Journal of Neurology, Neurosurgery, and Psychiatry*, *20*(1), 11–21. https://doi.org/10.1136/jnnp.20.1.11

Seibenhener, M. L., & Wooten, M. C. (2015). Use of the Open Field Maze to measure locomotor and anxiety-like behavior in mice. *Journal of Visualized Experiments : JoVE*, *96*, e52434. https://doi.org/10.3791/52434

Seiffert, E., Dreier, J. P., Ivens, S., Bechmann, I., Tomkins, O., Heinemann, U., & Friedman, A. (2004). Lasting blood-brain barrier disruption induces epileptic focus in the rat somatosensory cortex. *The Journal of Neuroscience : The Official Journal of the Society for Neuroscience*, *24*(36), 7829–7836. https://doi.org/10.1523/JNEUROSCI.1751-04.2004

Sengillo, J. D., Winkler, E. A., Walker, C. T., Sullivan, J. S., Johnson, M., & Zlokovic, B. v. (2013). Deficiency in mural vascular cells coincides with blood-brain barrier disruption in Alzheimer's disease. *Brain Pathology (Zurich, Switzerland)*, *23*(3), 303–310. https://doi.org/10.1111/bpa.12004

Shibata, S. B., Yoshimura, H., Ranum, P. T., Goodwin, A. T., & Smith, R. J. H. (2017). Intravenous rAAV2/9 injection for murine cochlear gene delivery. *Scientific Reports*, *7*(1), 9609. https://doi.org/10.1038/s41598-017-09805-x

Shinozaki, H., & Konishi, S. (1970). Actions of several anthelmintics and insecticides on rat cortical neurones. *Brain Research*, *24*(2), 368–371. https://doi.org/10.1016/0006-8993(70)90122-8

Singh, V. K., & Seed, T. M. (2021). How necessary are animal models for modern drug discovery? In *Expert Opinion on Drug Discovery* (Vol. 16, Issue 12, pp. 1391–1397). Taylor and Francis Ltd. https://doi.org/10.1080/17460441.2021.1972255

Sobin, C., Kiley-Brabeck, K., & Karayiorgou, M. (2005). Lower prepulse inhibition in children with the 22q11 deletion syndrome. *The American Journal of Psychiatry*, *162*(6), 1090–1099. https://doi.org/10.1176/appi.ajp.162.6.1090

Sobue, K., Yamamoto, N., Yoneda, K., Hodgson, M. E., Yamashiro, K., Tsuruoka, N., Tsuda, T., Katsuya, H., Miura, Y., Asai, K., & Kato, T. (1999). Induction of blood-brain barrier properties in immortalized bovine

brain endothelial cells by astrocytic factors. *Neuroscience Research*, *35*(2), 155–164. https://doi.org/10.1016/s0168-0102(99)00079-6

Sofroniew, M. v, & Vinters, H. v. (2010). Astrocytes: biology and pathology. *Acta Neuropathologica*, *119*(1), 7–35. https://doi.org/10.1007/s00401-009-0619-8

Sohet, F., Lin, C., Munji, R. N., Lee, S. Y., Ruderisch, N., Soung, A., Arnold, T. D., Derugin, N., Vexler, Z. S., Yen, F. T., & Daneman, R. (2015). LSR/angulin-1 is a tricellular tight junction protein involved in blood–brain barrier formation. *Journal of Cell Biology*, *208*(6), 703–711. https://doi.org/10.1083/jcb.201410131

Srinivasan, B., Kolli, A. R., Esch, M. B., Abaci, H. E., Shuler, M. L., & Hickman, J. J. (2015). TEER measurement techniques for in vitro barrier model systems. *Journal of Laboratory Automation*, *20*(2), 107–126. https://doi.org/10.1177/2211068214561025

Stafstrom, C. E., & Carmant, L. (2015). Seizures and epilepsy: an overview for neuroscientists. *Cold Spring Harbor Perspectives in Medicine*, *5*(6). https://doi.org/10.1101/cshperspect.a022426

Stenger, C., Corbier, C., & T., F. (2012). Structure and Function of the Lipolysis Stimulated Lipoprotein Receptor. In *Chemical Biology*. InTech. https://doi.org/10.5772/34657

Stenman, J. M., Rajagopal, J., Carroll, T. J., Ishibashi, M., McMahon, J., & McMahon, A. P. (2008). Canonical Wnt signaling regulates organ-specific assembly and differentiation of CNS vasculature. *Science (New York, N.Y.)*, *322*(5905), 1247–1250. https://doi.org/10.1126/science.1164594

Stern L., G. R. (1918). Le passage dans le liquide céphalo-rachidien de substances introduites dans la circulation et leur action sur le système nerveux central chez les différentes espèces animales. . *R. C. R. d. Ia Soc. de Phys. et d'hist. Natur. de Genève 35*, 91–94.

Stern L., G. R. (1921). Recherches sur le liquide céphalo-rachidien. 1. Les rapports entre le liquide céphalo-rachidien et la circulation sanguine. . *Arch. Int. Physiol. 17*, 138–192.

Stewart, P. A., & Wiley, M. J. (1981). Developing nervous tissue induces formation of blood-brain barrier characteristics in invading endothelial cells: A study using quail-chick transplantation chimeras. *Developmental Biology*, *84*(1), 183–192. https://doi.org/10.1016/0012-1606(81)90382-1

Stoica, L., Ahmed, S. S., Gao, G., & Sena-Esteves, M. (2013). Gene transfer to the CNS using recombinant adeno-associated virus. *Current Protocols in Microbiology*, *Chapter 14*, Unit14D.5. https://doi.org/10.1002/9780471729259.mc14d05s29

Stupp, R., Mason, W. P., van den Bent, M. J., Weller, M., Fisher, B., Taphoorn, M. J. B., Belanger, K., Brandes, A. A., Marosi, C., Bogdahn, U., Curschmann, J., Janzer, R. C., Ludwin, S. K., Gorlia, T., Allgeier, A., Lacombe, D., Cairncross, J. G., Eisenhauer, E., & Mirimanoff, R. O. (2005). Radiotherapy plus Concomitant and Adjuvant Temozolomide for Glioblastoma. *New England Journal of Medicine*, *352*(10), 987–996. https://doi.org/10.1056/NEJMoa043330

Sun, Z.-Y., Wei, J., Xie, L., Shen, Y., Liu, S.-Z., Ju, G.-Z., Shi, J.-P., Yu, Y.-Q., Zhang, X., Xu, Q., & Hemmings, G. P. (2004). The CLDN5 locus may be involved in the vulnerability to schizophrenia. *European Psychiatry : The Journal of the Association of European Psychiatrists*, *19*(6), 354–357. https://doi.org/10.1016/j.eurpsy.2004.06.007

Sutula, T. P. (2004). Mechanisms of epilepsy progression: current theories and perspectives from neuroplasticity in adulthood and development. *Epilepsy Research*, *60*(2–3), 161–171. https://doi.org/10.1016/j.eplepsyres.2004.07.001

Swanson, L. W., & Cowan, W. M. (1977). An autoradiographic study of the organization of the efferent connections of the hippocampal formation in the rat. *The Journal of Comparative Neurology*, *172*(1), 49–84. https://doi.org/10.1002/cne.901720104

Sweeney, M. D., Sagare, A. P., & Zlokovic, B. v. (2018). Blood-brain barrier breakdown in Alzheimer disease and other neurodegenerative disorders. *Nature Reviews. Neurology*, *14*(3), 133–150. https://doi.org/10.1038/nrneurol.2017.188

Sweeney, M. D., Zhao, Z., Montagne, A., Nelson, A. R., & Zlokovic, B. v. (2019). Blood-Brain Barrier: From Physiology to Disease and Back. *Physiological Reviews*, *99*(1), 21–78. https://doi.org/10.1152/physrev.00050.2017

Swerdlow, N. R., Benbow, C. H., Zisook, S., Geyer, M. A., & Braff, D. L. (1993). A preliminary assessment of sensorimotor gating in patients with obsessive compulsive disorder. *Biological Psychiatry*, *33*(4), 298–301. https://doi.org/10.1016/0006-3223(93)90300-3

Swerdlow, N. R., Karban, B., Ploum, Y., Sharp, R., Geyer, M. A., & Eastvold, A. (2001). Tactile prepuff inhibition of startle in children with Tourette's syndrome: in search of an "fMRI-friendly" startle paradigm. *Biological Psychiatry*, *50*(8), 578–585. https://doi.org/10.1016/s0006-3223(01)01164-7

Swerdlow, N. R., Paulsen, J., Braff, D. L., Butters, N., Geyer, M. A., & Swenson, M. R. (1995). Impaired prepulse inhibition of acoustic and tactile startle response in patients with Huntington's disease. *Journal of Neurology, Neurosurgery, and Psychiatry*, *58*(2), 192–200. https://doi.org/10.1136/jnnp.58.2.192

Takeshita, Y., & Ransohoff, R. M. (2012). Inflammatory cell trafficking across the blood-brain barrier: chemokine regulation and in vitro models. *Immunological Reviews*, *248*(1), 228–239. https://doi.org/10.1111/j.1600-065X.2012.01127.x

Tang, F., Hartz, A. M. S., & Bauer, B. (2017). Drug-Resistant Epilepsy: Multiple Hypotheses, Few Answers. *Frontiers in Neurology*, *8*, 301. https://doi.org/10.3389/fneur.2017.00301

Tang, M., & Monani, U. R. (2021). Glut1 deficiency syndrome: New and emerging insights into a prototypical brain energy failure disorder. *Neuroscience Insights*, *16*, 26331055211011508. https://doi.org/10.1177/26331055211011507

Tang, M., Gao, G., Rueda, C. B., Yu, H., Thibodeaux, D. N., Awano, T., Engelstad, K. M., Sanchez-Quintero, M.-J., Yang, H., Li, F., Li, H., Su, Q., Shetler, K. E., Jones, L., Seo, R., McConathy, J., Hillman, E. M., Noebels, J. L., de Vivo, D. C., & Monani, U. R. (2017). Brain microvasculature defects and Glut1 deficiency syndrome averted by early repletion of the glucose transporter-1 protein. *Nature Communications*, *8*(1), 14152. https://doi.org/10.1038/ncomms14152

Tang, Y., Harrington, A., Yang, X., Friesel, R. E., & Liaw, L. (2010). The contribution of the Tie2+ lineage to primitive and definitive hematopoietic cells. *Genesis (New York, N.Y.: 2000)*, *48*(9), 563–567. https://doi.org/10.1002/dvg.20654

Tanimizu, T., Kenney, J. W., Okano, E., Kadoma, K., Frankland, P. W., & Kida, S. (2017). Functional Connectivity of Multiple Brain Regions Required for the Consolidation of Social Recognition Memory. *The Journal of Neuroscience : The Official Journal of the Society for Neuroscience*, *37*(15), 4103–4116. https://doi.org/10.1523/JNEUROSCI.3451-16.2017

Tashiro, T., Haruta, Y., Yanai, T., Ishii, H., & Todo, K. (1990). [A successful surgical case of ruptured thoracoabdominal aneurysm]. *Kyobu Geka. The Japanese Journal of Thoracic Surgery*, *43*(10), 839–842.

The Lancet Global Health. (2020). Mental health matters. *The Lancet. Global Health*, *8*(11), e1352. https://doi.org/10.1016/S2214-109X(20)30432-0

Thomas, A., Burant, A., Bui, N., Graham, D., Yuva-Paylor, L. A., & Paylor, R. (2009). Marble burying reflects a repetitive and perseverative behavior more than novelty-induced anxiety. *Psychopharmacology*, *204*(2), 361–373. https://doi.org/10.1007/s00213-009-1466-y

Thompson, C. L., Pathak, S. D., Jeromin, A., Ng, L. L., MacPherson, C. R., Mortrud, M. T., Cusick, A., Riley, Z. L., Sunkin, S. M., Bernard, A., Puchalski, R. B., Gage, F. H., Jones, A. R., Bajic, V. B., Hawrylycz, M. J., & Lein, E. S. (2008). Genomic anatomy of the hippocampus. *Neuron*, *60*(6), 1010–1021. https://doi.org/10.1016/j.neuron.2008.12.008

Thor, D. H., & Holloway, W. R. (1982). Social memory of the male laboratory rat. *Journal of Comparative and Physiological Psychology*, *96*(6), 1000–1006. https://doi.org/10.1037/0735-7036.96.6.1000

Toda, T., Parylak, S. L., Linker, S. B., & Gage, F. H. (2019). The role of adult hippocampal neurogenesis in brain health and disease. *Molecular Psychiatry*, *24*(1), 67–87. https://doi.org/10.1038/s41380-018-0036-2

Tomkins, O., Shelef, I., Kaizerman, I., Eliushin, A., Afawi, Z., Misk, A., Gidon, M., Cohen, A., Zumsteg, D., & Friedman, A. (2008). Blood-brain barrier disruption in post-traumatic epilepsy. *Journal of Neurology, Neurosurgery, and Psychiatry*, *79*(7), 774–777. https://doi.org/10.1136/jnnp.2007.126425

Tseng, K. Y., Chambers, R. A., & Lipska, B. K. (2009). The neonatal ventral hippocampal lesion as a heuristic neurodevelopmental model of schizophrenia. *Behavioural Brain Research*, *204*(2), 295–305. https://doi.org/10.1016/j.bbr.2008.11.039

Tsukita, S., & Furuse, M. (2000). The structure and function of claudins, cell adhesion molecules at tight junctions. *Annals of the New York Academy of Sciences*, *915*, 129–135. https://doi.org/10.1111/j.1749-6632.2000.tb05235.x

Tsukita, S., Furuse, M., & Itoh, M. (2001). Multifunctional strands in tight junctions. *Nature Reviews. Molecular Cell Biology*, *2*(4), 285–293. https://doi.org/10.1038/35067088

Turski, W. A., Cavalheiro, E. A., Schwarz, M., Czuczwar, S. J., Kleinrok, Z., & Turski, L. (1983). Limbic seizures produced by pilocarpine in rats: behavioural, electroencephalographic and neuropathological study. *Behavioural Brain Research*, *9*(3), 315–335. https://doi.org/10.1016/0166-4328(83)90136-5

Uchida, Y., Sumiya, T., Tachikawa, M., Yamakawa, T., Murata, S., Yagi, Y., Sato, K., Stephan, A., Ito, K., Ohtsuki, S., Couraud, P.-O., Suzuki, T., & Terasaki, T. (2019). Involvement of Claudin-11 in Disruption of Blood-Brain, -Spinal Cord, and -Arachnoid Barriers in Multiple Sclerosis. *Molecular Neurobiology*, *56*(3), 2039–2056. https://doi.org/10.1007/s12035-018-1207-5

Valzelli, L. (1973). The isolation syndrome in mice. *Psychopharmacologia*, *31*(4), 305–320. https://doi.org/10.1007/BF00421275

van der Plasse, G., Schrama, R., van Seters, S. P., Vanderschuren, L. J. M. J., & Westenberg, H. G. M. (2012). Deep brain stimulation reveals a dissociation of consummatory and motivated behaviour in the medial and lateral nucleus accumbens shell of the rat. *PloS One*, *7*(3), e33455. https://doi.org/10.1371/journal.pone.0033455

van Luijtelaar, E. L., & Coenen, A. M. (1986). Two types of electrocortical paroxysms in an inbred strain of rats. *Neuroscience Letters*, *70*(3), 393–397. https://doi.org/10.1016/0304-3940(86)90586-0

van Vliet, E. A., Aronica, E., & Gorter, J. A. (2015). Blood-brain barrier dysfunction, seizures and epilepsy. *Seminars in Cell & Developmental Biology*, *38*, 26–34. https://doi.org/10.1016/j.semcdb.2014.10.003

van Vliet, E. A., da Costa Araújo, S., Redeker, S., van Schaik, R., Aronica, E., & Gorter, J. A. (2007). Blood-brain barrier leakage may lead to progression of temporal lobe epilepsy. *Brain : A Journal of Neurology*, *130*(Pt 2), 521–534. https://doi.org/10.1093/brain/awl318

Vandamme, C., Adjali, O., & Mingozzi, F. (2017). Unraveling the Complex Story of Immune Responses to AAV Vectors Trial After Trial. *Human Gene Therapy*, *28*(11), 1061–1074. https://doi.org/10.1089/hum.2017.150

Vanlandewijck, M., He, L., Mäe, M. A., Andrae, J., Ando, K., del Gaudio, F., Nahar, K., Lebouvier, T., Laviña, B., Gouveia, L., Sun, Y., Raschperger, E., Räsänen, M., Zarb, Y., Mochizuki, N., Keller, A., Lendahl, U., & Betsholtz, C. (2018). A molecular atlas of cell types and zonation in the brain vasculature. *Nature*, *554*(7693), 475–480. https://doi.org/10.1038/nature25739

Vanlandewijck, M., Vanlandewijck, M., Lebouvier, T., Mäe, M. A., Nahar, K., & Betsholtz, C. (2018). Primary isolation of vascular cells from murine brain for single cell sequencing. *Protocol Exchange*. https://doi.org/10.1038/protex.2017.159

Veys, K., Fan, Z., Ghobrial, M., Bouché, A., García-Caballero, M., Vriens, K., Conchinha, N. V., Seuwen, A., Schlegel, F., Gorski, T., Crabbé, M., Gilardoni, P., Ardicoglu, R., Schaffenrath, J., Casteels, C., de Smet, G., Smolders, I., van Laere, K., Abel, E. D., … de Bock, K. (2020). Role of the GLUT1 Glucose Transporter in Postnatal CNS Angiogenesis and Blood-Brain Barrier Integrity. *Circulation Research*, *127*(4), 466–482. https://doi.org/10.1161/CIRCRESAHA.119.316463

Vincent, P., & Mulle, C. (2009). Kainate receptors in epilepsy and excitotoxicity. *Neuroscience*, *158*(1), 309–323. https://doi.org/10.1016/j.neuroscience.2008.02.066

Virgintino, D., Errede, M., Robertson, D., Capobianco, C., Girolamo, F., Vimercati, A., Bertossi, M., & Roncali, L. (2004). Immunolocalization of tight junction proteins in the adult and developing human brain. *Histochemistry and Cell Biology*, *122*(1), 51–59. https://doi.org/10.1007/s00418-004-0665-1

Voruganti, L., Cortese, L., Oyewumi, L., Cernovsky, Z., Zirul, S., & Awad, A. (2000). Comparative evaluation of conventional and novel antipsychotic drugs with reference to their subjective tolerability, side-effect profile and impact on quality of life. *Schizophrenia Research*, *43*(2–3), 135–145. https://doi.org/10.1016/s0920-9964(99)00154-1

Waldman, Y. Y., Tuller, T., Shlomi, T., Sharan, R., & Ruppin, E. (2010). Translation efficiency in humans: tissue specificity, global optimization and differences between developmental stages. *Nucleic Acids Research*, *38*(9), 2964–2974. https://doi.org/10.1093/nar/gkq009

Wang, Y., Rattner, A., Zhou, Y., Williams, J., Smallwood, P. M., & Nathans, J. (2012). Norrin/Frizzled4 signaling in retinal vascular development and blood brain barrier plasticity. *Cell*, *151*(6), 1332–1344. https://doi.org/10.1016/j.cell.2012.10.042

Watanabe, N., Yano, K., Tsuyuki, K., Okano, T., & Yamato, M. (2015). Re-examination of regulatory opinions in Europe: possible contribution for the approval of the first gene therapy product Glybera. *Molecular Therapy. Methods & Clinical Development*, *2*, 14066. https://doi.org/10.1038/mtm.2014.66

Weinberg, M. S., Samulski, R. J., & McCown, T. J. (2013). Adeno-associated virus (AAV) gene therapy for neurological disease. *Neuropharmacology*, *69*, 82–88. https://doi.org/10.1016/j.neuropharm.2012.03.004

Wen, H., Watry, D. D., Marcondes, M. C. G., & Fox, H. S. (2004). Selective decrease in paracellular conductance of tight junctions: role of the first extracellular domain of claudin-5. *Molecular and Cellular Biology*, *24*(19), 8408–8417. https://doi.org/10.1128/MCB.24.19.8408-8417.2004

White, K., Büning, H., Kritz, A., Janicki, H., McVey, J., Perabo, L., Murphy, G., Odenthal, M., Work, L. M., Hallek, M., Nicklin, S. A., & Baker, A. H. (2008). Engineering adeno-associated virus 2 vectors for targeted gene delivery to atherosclerotic lesions. *Gene Therapy*, *15*(6), 443–451. https://doi.org/10.1038/sj.gt.3303077

White, S. J., Nicklin, S. A., Büning, H., Brosnan, M. J., Leike, K., Papadakis, E. D., Hallek, M., & Baker, A. H. (2004). Targeted Gene Delivery to Vascular Tissue In Vivo by Tropism-Modified Adeno-Associated Virus Vectors. *Circulation*, *109*(4), 513–519. https://doi.org/10.1161/01.CIR.0000109697.68832.5D

Winkler, E. A., Nishida, Y., Sagare, A. P., Rege, S. v, Bell, R. D., Perlmutter, D., Sengillo, J. D., Hillman, S., Kong, P., Nelson, A. R., Sullivan, J. S., Zhao, Z., Meiselman, H. J., Wendy, R. B., Soto, J., Abel, E. D., Makshanoff, J., Zuniga, E., de Vivo, D. C., & Zlokovic, B. v. (2015). GLUT1 reductions exacerbate Alzheimer's disease vasculo-neuronal dysfunction and degeneration. *Nature Neuroscience*, *18*(4), 521–530. https://doi.org/10.1038/nn.3966

Winship, I. R., Dursun, S. M., Baker, G. B., Balista, P. A., Kandratavicius, L., Maia-de-Oliveira, J. P., Hallak, J., & Howland, J. G. (2019). An Overview of Animal Models Related to Schizophrenia. In *Canadian Journal of Psychiatry*(Vol. 64, Issue 1, pp. 5–17). SAGE Publications Inc. https://doi.org/10.1177/0706743718773728

Wolburg, H., & Lippoldt, A. (2002). Tight junctions of the blood-brain barrier: development, composition and regulation. *Vascular Pharmacology*, *38*(6), 323–337. https://doi.org/10.1016/s1537-1891(02)00200-8

Wu, N., Zhang, X., Jin, S., Liu, S., Ju, G., Wang, Z., Liu, L., Ye, L., & Wei, J. (2010). A weak association of the CLDN5 locus with schizophrenia in Chinese case-control samples. *Psychiatry Research*, *178*(1), 223. https://doi.org/10.1016/j.psychres.2009.11.019

Wu, X., Ding, Z., Fan, T., Wang, K., Li, S., Zhao, J., & Zhu, W. (2022). Childhood social isolation causes anxiety-like behaviors via the damage of blood-brain barrier in amygdala in female mice. *Frontiers in Cell and Developmental Biology*, *10*, 943067. https://doi.org/10.3389/fcell.2022.943067

Wu, Z., Asokan, A., & Samulski, R. J. (2006). Adeno-associated Virus Serotypes: Vector Toolkit for Human Gene Therapy. *Molecular Therapy*, *14*(3), 316–327. https://doi.org/10.1016/j.ymthe.2006.05.009

Wyse, C. A., & Coogan, A. N. (2010). Impact of aging on diurnal expression patterns of CLOCK and BMAL1 in the mouse brain. *Brain Research*, *1337*, 21–31. https://doi.org/10.1016/j.brainres.2010.03.113

Xu, S., Jiang, M., Liu, X., Sun, Y., Yang, L., Yang, Q., & Bai, Z. (2021). Neural Circuits for Social Interactions: From Microcircuits to Input-Output Circuits. *Frontiers in Neural Circuits*, *15*, 768294. https://doi.org/10.3389/fncir.2021.768294

Yalcin, I., Aksu, F., & Belzung, C. (2005). Effects of desipramine and tramadol in a chronic mild stress model in mice are altered by yohimbine but not by pindolol. *European Journal of Pharmacology*, *514*(2–3), 165–174. https://doi.org/10.1016/j.ejphar.2005.03.029

Yang, A. C., Stevens, M. Y., Chen, M. B., Lee, D. P., Stähli, D., Gate, D., Contrepois, K., Chen, W., Iram, T., Zhang, L., Vest, R. T., Chaney, A., Lehallier, B., Olsson, N., du Bois, H., Hsieh, R., Cropper, H. C., Berdnik, D., Li, L., … Wyss-Coray, T. (2020). Physiological blood-brain transport is impaired with age by a shift in transcytosis. *Nature*, *583*(7816), 425–430. https://doi.org/10.1038/s41586-020-2453-z

Ye, J., Coulouris, G., Zaretskaya, I., Cutcutache, I., Rozen, S., & Madden, T. L. (2012). Primer-BLAST: A tool to design target-specific primers for polymerase chain reaction. *BMC Bioinformatics*, *13*(1), 134. https://doi.org/10.1186/1471-2105-13-134

Yen, F. T., Roitel, O., Bonnard, L., Notet, V., Pratte, D., Stenger, C., Magueur, E., & Bihain, B. E. (2008). Lipolysis stimulated lipoprotein receptor: a novel molecular link between hyperlipidemia, weight gain, and atherosclerosis in mice. *The Journal of Biological Chemistry*, *283*(37), 25650–25659. https://doi.org/10.1074/jbc.M801027200

Vezzani, A., & Friedman, A. (2011). Brain inflammation as a biomarker in epilepsy. *Biomarkers in Medicine*, *5*(5), 607–614. https://doi.org/10.2217/bmm.11.61

Yuan, P., & Raz, N. (2014). Prefrontal cortex and executive functions in healthy adults: a meta-analysis of structural neuroimaging studies. *Neuroscience and Biobehavioral Reviews*, *42*, 180–192. https://doi.org/10.1016/j.neubiorev.2014.02.005

Zagórska-Swiezy, K., Litwin, J. A., Gorczyca, J., Pityński, K., & Miodoński, A. J. (2008). Arterial supply and venous drainage of the choroid plexus of the human lateral ventricle in the prenatal period as revealed by vascular corrosion casts and SEM. *Folia Morphologica*, *67*(3), 209–213.

Zhang, H., Yang, B., Mu, X., Ahmed, S. S., Su, Q., He, R., Wang, H., Mueller, C., Sena-Esteves, M., Brown, R., Xu, Z., & Gao, G. (2011). Several rAAV vectors efficiently cross the blood-brain barrier and transduce neurons and astrocytes in the neonatal mouse central nervous system. *Molecular Therapy : The Journal of the American Society of Gene Therapy*, *19*(8), 1440–1448. https://doi.org/10.1038/mt.2011.98

Zhang, X.Y., Xiu, M.H., Song, C., Chen, D.C., Wu, G.Y., Haile, C.N., Kosten, T.A., and Kosten, T.R. (2010). Increased serum S100B in never-medicated and medicated schizophrenic patients. J. Psychiatr. Res. 44, 1236–1240.

Zhou, Y., Wang, Y., Tischfield, M., Williams, J., Smallwood, P. M., Rattner, A., Taketo, M. M., & Nathans, J. (2014). Canonical WNT signaling components in vascular development and barrier formation. *The Journal of Clinical Investigation*, *124*(9), 3825–3846. https://doi.org/10.1172/JCI76431

Zhu, N., Wei, M., Yuan, L., He, X., Chen, C., Ji, A., & Zhang, G. (2022). Claudin-5 relieves cognitive decline in Alzheimer's disease mice through suppression of inhibitory GABAergic neurotransmission. *Aging*, *14*(8), 3554–3568. https://doi.org/10.18632/aging.204029

Zincarelli, C., Soltys, S., Rengo, G., & Rabinowitz, J. E. (2008). Analysis of AAV Serotypes 1–9 Mediated Gene Expression and Tropism in Mice After Systemic Injection. *Molecular Therapy*, *16*(6), 1073–1080. https://doi.org/10.1038/mt.2008.76

Zlokovic, B. v. (2008). The blood-brain barrier in health and chronic neurodegenerative disorders. *Neuron*, *57*(2), 178–201. https://doi.org/10.1016/j.neuron.2008.01.003